

**Monitoring and improving oxygenation of organs, cells, and tissue  
engineered grafts**

A DISSERTATION  
SUBMITTED TO THE FACULTY OF  
THE UNIVERSITY OF MINNESOTA

BY

Bradley Paul Weegman

IN PARTIAL FULFILLMENT OF THE REQUIREMENTS  
FOR THE DEGREE OF  
DOCTOR OF PHILOSOPHY

*Biophysical Sciences and Medical Physics*

Advisors:  
Michael Garwood  
&  
Klearchos K. Papas

December 2015

©2015 Bradley P. Weegman

## **ACKNOWLEDGEMENTS**

I have so much to be thankful for, I could write an entire thesis about all of my blessings.

I would first like to express my sincere gratitude and appreciation for the love and support of my darling wife Alison. She helps to keep me grounded, and has always been supportive and encouraging along my academic journey; I truly am blessed to have such a wonderful person in my life.

I would also like to thank my family for supporting me throughout my whole life, and especially my undergraduate and graduate studies. Specifically, I am grateful to my parents, Kathy and Larry Weegman, who have always provided helpful advice, guidance, and encouragement when I needed it. I am thankful that they gave me all of the tools I needed to succeed in the “real world” and the self-confidence to pursue my passions in life. I also want to thank my brother Greg and sister Julia who have always been available for moral support, and to help me keep things in perspective. I want to thank my family in-law as well, for their welcoming love and support during the past few years. My parents in law Drs. Betsey and Dave Siitari are impeccable role models and positive influences in my life. I also thank my numerous siblings in law; Kate, Andy, Steph, Brian, Bill, LeAnn, Erica, Ben, and Andrew, for their reassurance and playfully motivating banter.

I am especially thankful for the encouragement and support of all of my friends. I have the most incredibly accomplished group of friends, who not only celebrate each other's accomplishments, but also help to motivate success, and bring out the best in me. Thank you, Alyssa, Caleb, Chris, Dave, Jess, Liz, Marcus, Matt, Neal, Paige, and Tom.

I thank my committee members and scientific mentors who have helped guide me through my graduate career, Dr. Bruce Hammer, Dr. Tim O'Brien, Dr. Russel Ritenour, Dr. Raja Kandaswamy, Dr. Linda Tempelman, Dr. Michael Taylor, Dr. Efstathios Avgoustiniatos and Dr. Louis Kidder.

I especially thank my advisers Dr. Klearchos Papas and Dr. Michael Garwood. They have been positive role models, and inspired me to cultivate my true passion for science and medical research.

I want to thank all of the graduate students who have supported me, and served with me in the academic trenches of graduate school, especially Dr. Thomas M. Suszynski, Dr. William Earl Scott III, Dr. Garrett Swindlehurst, and last but not least, my partner at the Lions Islet Imaging Lab, Sam Aaron Einstein. Thank you for your moral support when I needed it, and for all of the laughs we have had in the lab. You are incredible colleagues, but even better friends; thank you.

Thank you to all of the lab-mates who have made the work described in this thesis possible.

**Papas Lab:**

Nichole Atchison  
Ryan Chaimberlain  
Christopher Chapman  
Eric Falde  
Joana Ferrer-Fabrega  
Varun Garg  
Becca Hooper  
C. Julia Vance  
Lou Kidder  
Varia Kircner  
Jenna Kitzmann (Miner)  
Bob Konz  
Conner Lyons  
Kristen Maynard  
Catherine Min  
Kate Mueller  
William Purvis  
Mike Rizzari  
Philip Rozak  
Chun Shan  
Kate Smith  
Brett Stanton  
Leah Steyn  
Tom Suszynski  
Garrett Swindlehurst  
Jikku Thomas  
Brad Weegman  
Gina Wildey

**Firpo Lab:**

Ben Becker  
Alex Carlson  
Zhaohui Geng  
Marjan Jahani  
Christen Volzke

**Wilson Wolf:**

John Wilson  
Dan

**Giner Inc.**

Linda Tempelman  
Nicole Mackenzie  
Simon Stone

**Others:**

Mike Taylor  
Kurt Albeck  
Steve Walsch  
Diana Freeman  
Brenda Koniar  
Henk-Jan Schuurman  
Greg Szot  
Mike Loughnane

**DIIT - Schulze Diabetes Institute :**

Janine Abouaish  
Taka Anazawa  
Jeff Ansite  
Balamurugan Appakalai  
Tom Gilmore  
Melanie Graham  
Bernhard Hering  
Minna Honkanen-Scott  
Lee Jones  
Suzie LaFreniere  
Gopal Loganathan  
Shuichiro Matsumoto  
Mike Murtaugh

**Garwood Lab and CMRR:**

Gregor Adriani  
Peter Andersen  
Andrew Berhow  
Curt Corum  
Ute Goerke  
Brian Hanna  
Michelle Hartwig  
Albert Jang  
Loretha King  
Naoharu Kobayashi  
Jeremy Kulesa  
Silvia Mangia  
Gosia Marjanska  
Shalom Michaeli  
Deb Morgan  
Gulin Oz  
Hattie Ring  
John Strupp  
Jennifer Taylor  
Kamil Ugurbil  
Lynn Utecht  
Nicole Wilkinson  
Jinjin Zhang

Luke Mutch  
Pratima Pakala  
Jamen Parkey  
Brian Perrault  
Sajjad Soltani  
Brett Sorge  
David Sutherland  
Tomo Tanaka  
Mukesh Tiwari  
Laura Vonhof  
Sandy White  
Josh Wilhelm  
Takeshi Yuasa

## **DEDICATION**

This thesis is dedicated to those who are living with diabetes every day,  
and to the families and friends who are affected by this terrible disease.

May this work be a step on the path to a cure.

## **ABSTRACT**

Oxygen is vital to the survival of many living things, and evolution has provided the human body with a complex cardiovascular system to ensure that all of the cells in the body are provided with adequate oxygen. Achieving adequate oxygen delivery remains of critical importance to the clinical management of many human diseases and has been the impetus for the development of many medical procedures and technologies. Despite much advancement in the understanding about oxygen delivery in the body, the current inability to attain life-sustaining levels of tissue oxygenation remains the major limitation for the emerging fields of cell, tissue, and organ replacement. There is a large body of research focused on developing methods to improve vascularization and oxygen supply for transplanted cells, tissues and organs, and this substantial challenge will require an interdisciplinary approach utilizing both engineering principles and a broad understanding of the physical science. The islet transplantation process can be divided into three critical steps: tissue procurement and preservation; isolation, culture and shipment; and graft transplantation and monitoring. To begin, whole organ oxygen consumption rate (WOCR) measurements are presented for the assessment of organ viability, followed by the description of new techniques for improving the efficacy of pancreas cooling during procurement, and the use of hypothermic machine perfusion (HMP) to improve pancreas preservation. These methods can be used to qualify biological tissue products and to evaluate and improve organ procurement and preservation. Next, HMP combined with silicon-rubber-membrane (SRM) culture systems are presented as techniques to improve the quality of tissues isolated from juvenile porcine pancreata, and advanced nutrient supplementation with suspension culture systems are shown to improve  $\beta$ -cell expansion. Finally,  $^{19}\text{F}$ -MRS oximetry techniques are presented for non-invasive oxygen monitoring of tissue-engineered grafts (TEGs), and these techniques are further applied to develop, implement, and validate a novel method for oxygen delivery to an implanted tissue-engineered islet grafts.

# **OVERVIEW TABLE OF CONTENTS**

<b>ACKNOWLEDGEMENTS</b> .....	<b>I</b>
<b>DEDICATION</b> .....	<b>IV</b>
<b>ABSTRACT</b> .....	<b>V</b>
<b>OVERVIEW TABLE OF CONTENTS</b> .....	<b>VI</b>
<b>DETAILED TABLE OF CONTENTS</b> .....	<b>VIII</b>
<b>LIST OF TABLES</b> .....	<b>XVII</b>
<b>LIST OF FIGURES</b> .....	<b>XVIII</b>
<b>CHAPTER 1 INTRODUCTION</b> .....	<b>1</b>
<b><u>DEVELOPMENT OF METHODS AND TECHNIQUES FOR IMPROVING ORGAN PROCUREMENT AND PRESERVATION</u></b>	
<b>CHAPTER 2 WHOLE ORGAN OXYGEN CONSUMPTION</b> .....	<b>12</b>
Continuous, Real-time Viability Assessment of Kidneys and Pancreas Based on Oxygen Consumption .....	13
<b>CHAPTER 3 IMPORVING PANCREAS PROCUREMENT</b> .....	<b>28</b>
Temperature Profiles of Different Cooling Methods in Porcine Pancreas Procurement ....	29
<b>CHAPTER 4 HYPOTHERMIC MACHINE PERFUSION TO IMPROVE ORGAN PRESERVATION</b> .....	<b>54</b>
Hypothermic Perfusion Preservation of Pancreas for islet grafts: validation using a split Lobe Porcine Model .....	55
<b><u>DEVELOPMENT OF METHODS AND TECHNIQUES FOR IMPROVING ISLET ISOLATION, CULTURE AND SHIPMENT</u></b>	
<b>CHAPTER 5 JUVENILE PORCINE ISLET CULTURE</b> .....	<b>67</b>
Plasticity and Aggregation of Juvenile Porcine Islets in Modified Culture for Xenotransplantation: Preliminary Observations .....	68
<b>CHAPTER 6 NUTRIET REGULATION AND SSB CULTURE</b> .....	<b>97</b>
Nutrient regulation by continuous feeding removes limitations on cell yield in the large-scale expansion of mammalian cell spheroids .....	98
<b><u>DEVELOPMENT OF METHODS AND TECHNIQUES FOR IMPROVING ORGAN PROCUREMENT AND PRESERVATION</u></b>	
<b>CHAPTER 7 <sup>19</sup>F-MRS FOR OXYGEN MEASUREMENT</b> .....	<b>125</b>
Development and validation of noninvasive magnetic resonance relaxometry for the <i>in vivo</i> assessment of tissue-engineered graft oxygenation. ....	126
<b>CHAPTER 8 OXYGENATION OF IMPLANTED TEGS</b> .....	<b>163</b>
Non-invasive monitoring of tissue-engineered islet grafts <i>in vivo</i> .....	165



Oxygen Delivery Improves Islet Graft Function <i>in vivo</i> .....	196
<b>CHAPTER 9 CONCLUSIONS AND FUTURE DIRECTIONS.....</b>	<b>224</b>
<b>REFERENCES.....</b>	<b>230</b>

**APPENDICES**

<b>APPENDIX A PORCINE PANCREAS ANATOMY.....</b>	<b>261</b>
Pig Pancreas Anatomy: Procurement, Preservation, and Islet Isolation .....	262
<b>APPENDIX B PERSUFFLATION IMPROVES PANCREAS PRESERVATION.....</b>	<b>287</b>
Pancreas oxygen persufflation increases ATP levels as shown by nuclear magnetic resonance .....	288
Supplemental Results and discussion of <sup>31</sup> P-MRS measurements with PSF.....	299
<b>APPENDIX C USING MRI TO IMPROVE ENZYME DISTRIBUTION .....</b>	<b>308</b>
Magnetic resonance imaging: A tool to monitor and optimize enzyme distribution during porcine pancreas distention for islet isolation.....	309
<b>APPENDIX D IMPROVING ISLET SHIPMENT.....</b>	<b>323</b>
Devices and methods for maintenance of temperature and pressure during islet shipment .....	324
<b>APPENDIX E QMS FOR IMPROVING ISLET PURIFICATION .....</b>	<b>338</b>
Improving purified porcine islet viability by continuous quadrupole magnetic sorting (QMS) .....	339
<b>APPENDIX F SUPPLEMENTAL REFERENCE FIGURES.....</b>	<b>359</b>
<b>APPENDIX G COPYRIGHT PERMISSIONS AND LICENSES .....</b>	<b>401</b>

# **DETAILED TABLE OF CONTENTS**

<b>ACKNOWLEDGEMENTS.....</b>	<b>I</b>
<b>DEDICATION .....</b>	<b>IV</b>
<b>ABSTRACT .....</b>	<b>V</b>
<b>OVERVIEW TABLE OF CONTENTS .....</b>	<b>VI</b>
<b>DETAILED TABLE OF CONTENTS.....</b>	<b>VIII</b>
<b>LIST OF TABLES .....</b>	<b>XVII</b>
<b>LIST OF FIGURES .....</b>	<b>XVIII</b>
<b>CHAPTER 1 INTRODUCTION .....</b>	<b>1</b>
Background .....	1
Overview and Thesis Organization .....	5
<b><u>DEVELOPMENT OF METHODS AND TECHNIQUES FOR IMPROVING ORGAN PROCUREMENT AND PRESERVATION</u></b>	
<b>CHAPTER 2 WHOLE ORGAN OXYGEN CONSUMPTION.....</b>	<b>12</b>
Continuous, Real-time Viability Assessment of Kidneys and Pancreas Based on Oxygen Consumption .....	13
Summary.....	13
Introduction .....	14
Materials and Methods.....	16
Porcine Kidney Procurement .....	16
Hypothermic Machine Perfusion and WOOCR Setup.....	16
Formalin Treatment of the Porcine Kidney .....	17
Results .....	18
Kidneys .....	19
Discussion.....	20
Conclusion .....	22
Supplementary Data: Kidney and Pancreas WOOCR .....	23
Introduction .....	23
Human and Porcine Pancreases Procurement.....	23
Kidney and Pancreas Supplementary Results and Discussion .....	24
<b>CHAPTER 3 IMPORVING PANCREAS PROCUREMENT.....</b>	<b>28</b>
Temperature Profiles of Different Cooling Methods in Porcine Pancreas Procurement ....	29

Summary.....	29
Introduction .....	30
Materials and Methods.....	32
Porcine Pancreas Procurement .....	32
Porcine Pancreas Cooling .....	33
Temperature Measurements.....	35
Histology .....	35
Statistical Analysis .....	36
Results .....	40
Discussion.....	49
Conclusion .....	53
<b>CHAPTER 4 HYPOTHERMIC MACHINE PERFUSION TO IMPROVE ORGAN PRESERVATION .....</b>	<b>54</b>
Hypothermic Perfusion Preservation of Pancreas for islet grafts: validation using a split Lobe Porcine Model .....	55
Summary.....	55
Introduction .....	56
Materials and Methods.....	58
Experimental Design.....	58
Procurement .....	58
Perfusion.....	58
Islet Isolation, Purification and Culture.....	59
Islet OCR/DNA.....	59
Islet morphology.....	60
Nude Mouse Bio-Assay .....	60
Results and Discussion.....	61
<b><u>DEVELOPMENT OF METHODS AND TECHNIQUES FOR IMPROVING ISLET ISOLATION, CULTURE AND SHIPMENT</u></b>	
<b>CHAPTER 5 JUVENILE PORCINE ISLET CULTURE.....</b>	<b>67</b>
Plasticity and Aggregation of Juvenile Porcine Islets in Modified Culture for Xenotransplantation: Preliminary Observations .....	68
Summary.....	68
Introduction .....	70
Materials and Methods.....	73

Ethics Statement:.....	73
Islet Isolation and Culture: .....	73
Islet Assessments: .....	74
Results .....	79
Discussion.....	88
Special Conditions for Culture of Juvenile Porcine Islets:.....	89
In vitro functional assessment:.....	90
In vivo functional assessment: .....	91
Observed pancreatite potential for regeneration:.....	92
Pancreatite size: .....	93
Advantages of the juvenile pancreas model .....	94
Conclusion .....	95
<b>CHAPTER 6 NUTRIET REGULATION AND SSB CULTURE .....</b>	<b>97</b>
Nutrient regulation by continuous feeding removes limitations on cell yield in the large-scale expansion of mammalian cell spheroids .....	98
Summary.....	98
Introduction .....	99
Materials and Methods.....	101
Cell Line and Maintenance .....	101
$\beta$ -TC6 Spheroid Formation .....	101
Experimental Culture Conditions .....	101
Continuous Feeding System.....	102
Spheroid Settling Rate Measurements .....	105
Cell Counts, Viability, and Glucose Concentration Measurements.....	105
Statistics.....	106
Results .....	107
$\beta$ -TC6 cell expansion in static and SSB cultures .....	107
Nutrient fluctuations in static and SSB cultures .....	107
Development of the continuous feeding (CF) culture system .....	108
Continuous feeding increased cell expansion.....	109
Continuous feeding could not maintain Physiological glucose levels .....	110
Adjusting feed rate can maintain physiological glucose levels in SSB culture.....	110

Predicted linear growth rate .....	111
Predicted medium replacement rate .....	111
Adjusted feed rate based on glucose levels .....	112
Discussion .....	120
Conclusion .....	123
<b><u>DEVELOPMENT OF METHODS AND TECHNIQUES FOR IMPROVING ORGAN PROCUREMENT</u></b>	
<b><u>AND PRESERVATION</u></b>	
<b>CHAPTER 7 <sup>19</sup>F-MRS FOR OXYGEN MEASUREMENT .....</b>	<b>125</b>
Development and validation of noninvasive magnetic resonance relaxometry for the <i>in vivo</i> assessment of tissue-engineered graft oxygenation. ....	126
Summary .....	126
Introduction .....	127
Materials and Methods .....	130
Comparison of PFC Compounds .....	130
TEG Construction .....	130
<sup>19</sup> F-MRS Acquisition .....	130
Calibration and Temperature Compensation .....	132
<sup>19</sup> F-MRS Calibration with TEGs .....	133
Validation of <sup>19</sup> F-MRS pO <sub>2</sub> Measurements in vitro .....	134
Perfusion Bioreactor .....	134
Animal Research .....	136
Validation of <sup>19</sup> F-MRS pO <sub>2</sub> Measurements in vivo .....	136
In vivo oximetry in Rats .....	136
Implants with DSO .....	137
Results .....	149
Discussion .....	155
Conclusion .....	161
<b>CHAPTER 8 OXYGENATION OF IMPLANTED TEGS .....</b>	<b>163</b>
Overview .....	164
Non-invasive monitoring of tissue-engineered islet grafts <i>in vivo</i> .....	165
Summary .....	165
Introduction .....	167
Materials and Methods .....	169

Engineering Model of Hypoxia .....	169
Animal Research.....	169
Tissue Engineered Graft (TEG) Construction .....	170
Experimental Conditions .....	171
Surgical Implantation and Ex-plantation of TEGs .....	172
Ex-plant Oxygen Consumption Rate (OCR) Measurements.....	172
<sup>19</sup> F-MRS Acquisition.....	173
<sup>19</sup> F-MRS Calibration .....	173
Measurement of in vivo TEG pO <sub>2</sub> .....	174
Histopathology and Immunohistochemistry .....	174
Serum C-peptide measurements .....	175
Statistical Analysis .....	176
Results .....	177
Engineering Model of Hypoxia .....	177
Ex-plant Oxygen Consumption Rate (OCR) Measurements.....	177
Histology and Immunohistochemistry .....	177
Measurement of in vivo TEG pO <sub>2</sub> .....	178
Serum C-peptide measurements .....	179
Discussion.....	186
Conclusions.....	195
Oxygen Delivery Improves Islet Graft Function <i>in vivo</i> .....	196
Summary.....	196
Introduction .....	198
Materials and Methods.....	200
Experimental Approach.....	200
Tissue Engineered Graft (TEG) Device Preparation.....	201
Perfusion Bioreactor .....	202
Animal Research.....	202
Implantation of TEG devices and DSO in vivo.....	202
<sup>19</sup> F-MRS Oxygen Measurements .....	205
Diabetic Rodent Model & Functional Measurements .....	205
Serum C-peptide.....	206

Histopathology and Immunohistochemistry .....	206
Statistical Analysis .....	207
Results .....	208
Oxygen measurements of TEGs with DSO in vitro .....	208
Oxygen measurements of TEGs with DSO in vivo. ....	208
Functional assessment of TEGs with DSO in diabetic rodents.....	209
Serum C-peptide measurements .....	209
Histology and Immunohistochemistry .....	210
Discussion.....	214
Conclusions.....	223
<b>CHAPTER 9 CONCLUSIONS AND FUTURE DIRECTIONS.....</b>	<b>224</b>
<b>REFERENCES.....</b>	<b>230</b>
<b><u>APPENDICES</u></b>	
<b>APPENDIX A PORCINE PANCREAS ANATOMY.....</b>	<b>261</b>
Pig Pancreas Anatomy: Procurement, Preservation, and Islet Isolation .....	262
Summary .....	262
Introduction .....	263
Materials and Methods.....	265
Surgical procedure .....	265
Pancreatic lobes .....	267
Arterial anatomy.....	268
Venous blood outflow (drainage) .....	269
Pancreatic duct .....	270
Statistical Analysis .....	270
Results .....	277
Discussion.....	282
<b>APPENDIX B PERSUFFLATION IMPROVES PANCREAS PRESERVATION.....</b>	<b>287</b>
Pancreas oxygen persufflation increases ATP levels as shown by nuclear magnetic resonance .....	288
Summary.....	288
Introduction .....	289
Materials and Methods.....	291

Procurements.....	291
Static Preservation (TLM) .....	291
Persufflation .....	291
<sup>31</sup> P-NMR Spectroscopy .....	292
MRI .....	292
Results .....	294
Discussion.....	298
Supplemental Results and discussion of <sup>31</sup> P-MRS measurements with PSF .....	299
Results: .....	299
Discussion:.....	300
<b>APPENDIX C USING MRI TO IMPROVE ENZYME DISTRIBUTION .....</b>	<b>308</b>
Magnetic resonance imaging: A tool to monitor and optimize enzyme distribution during porcine pancreas distention for islet isolation.....	309
Summary.....	309
Introduction .....	310
Materials and Methods.....	312
Procurement: .....	312
MRI: .....	312
Pancreas Distention:.....	313
Results .....	316
Discussion.....	319
Conclusions.....	322
<b>APPENDIX D IMPROVING ISLET SHIPMENT.....</b>	<b>323</b>
Devices and methods for maintenance of temperature and pressure during islet shipment .....	324
Summary.....	324
Introduction .....	325
Materials and Methods.....	326
Temperature Control Investigation.....	326
Pressure Control Investigation.....	327
Results .....	329
Discussion.....	335
Conclusion .....	337



<b>APPENDIX E QMS FOR IMPROVING ISLET PURIFICATION .....</b>	<b>338</b>
Improving purified porcine islet viability by continuous quadrupole magnetic sorting (QMS) .....	339
Summary .....	339
Introduction .....	341
Materials and Methods .....	344
Experimental design .....	344
Donors, procurement, and labeling .....	344
Digestion .....	345
Density Gradient Purification .....	345
QMS Purification .....	346
Isolation Outcomes and Islet Quality Assessment .....	347
Statistical Methods .....	347
Results .....	349
Discussion .....	352
Conclusion .....	357
<b>APPENDIX F SUPPLEMENTAL REFERENCE FIGURES.....</b>	<b>359</b>
Appendix F.1 : Organization.....	359
Appendix F.2 : Whole Organ Oxygen Consumption.....	360
Appendix F.3 : Improving Pancreas Procurement.....	361
Appendix F.4 Hypothermic Machine Perfusion to improve organ preservation .....	361
Appendix F.5 : Juvenile Porcine Islet Culture.....	361
Appendix F.6 : Nutrient Regulation and SSB Culture .....	362
Appendix F.7 : <sup>19</sup> F-MRS for Oxygen Measurement.....	364
Appendix F.8 : Oxygenation of implanted TEGs .....	373
Appendix F.A: Porcine Pancreas Anatomy .....	383
Appendix F.B: Persufflation Improves Pancreas Preservation .....	384
Appendix F.C: Using MRI to Improve Enzyme Distribution .....	392
Appendix F.D: Improving Islet Shipment .....	393
Appendix F.E: QMS for Improving Islet Purification .....	400
<b>APPENDIX G COPYRIGHT PERMISSIONS AND LICENSES .....</b>	<b>401</b>
Appendix G.1 : Permission for Published Manuscripts.....	401
Appendix G.2 : Referenced Theses Permissions .....	446

Appendix G.3 : Figures Reproduced with Permission ..... 447

## **LIST OF TABLES**

<b>Table 3.1: Surgical procurement data.....</b>	<b>48</b>
<b>Table 4.1: Islet Isolation and Quality Control (QC) Data.....</b>	<b>65</b>
<b>Table 5.1: Isolation and Culture Results .....</b>	<b>82</b>
<b>Table 8.1: Average Histology Scores .....</b>	<b>183</b>
<b>Table A.1: Porcine pancreas weights .....</b>	<b>280</b>
<b>Table A.2: Variations of the celiac trunk (CT) anatomy.....</b>	<b>280</b>
<b>Table A.3: Variations in posterior pancreatic artery (PPA) anatomy .....</b>	<b>281</b>
<b>Table A.4: Types of pancreatic ductal structure.....</b>	<b>281</b>

## LIST OF FIGURES

<b>Figure 1.1: Thesis Organization Flow Chart.....</b>	<b>6</b>
<b>Figure 1.2: Thesis Organization Diagram. ....</b>	<b>7</b>
<b>Figure 2.1: WOOCR perfusion system schematic .....</b>	<b>18</b>
<b>Figure 2.2: WOOCR results from porcine kidney .....</b>	<b>20</b>
<b>Figure 2.3: Damage from WIT and CIT is detected by WOOCR.....</b>	<b>25</b>
<b>Figure 2.4: WOOCR of porcine pancreas .....</b>	<b>26</b>
<b>Figure 2.5: WOOCR measures pancreas viability.....</b>	<b>27</b>
<b>Figure 3.1: Surgical Timeline.....</b>	<b>37</b>
<b>Figure 3.2: Effects of heparinization .....</b>	<b>38</b>
<b>Figure 3.3: Temperature probe placement.....</b>	<b>39</b>
<b>Figure 3.4: Procurement cooling method profiles.....</b>	<b>42</b>
<b>Figure 3.5: Combined Method D temperature profile .....</b>	<b>43</b>
<b>Figure 3.6: Cooling method comparison.....</b>	<b>44</b>
<b>Figure 3.7: Differences in histology sections.....</b>	<b>45</b>
<b>Figure 3.8: Histology and insulin staining images .....</b>	<b>46</b>
<b>Figure 3.9: Semi-quantitative histology comparison .....</b>	<b>47</b>
<b>Figure 4.1: Morphology and function of transplanted islets.....</b>	<b>63</b>
<b>Figure 4.2: Average OCR/DNA .....</b>	<b>64</b>
<b>Figure 5.1: Pancreatite plasticity micrographs .....</b>	<b>83</b>
<b>Figure 5.2: Juvenile porcine islet viability .....</b>	<b>84</b>
<b>Figure 5.3: Juvenile porcine islet immunohistochemistry.....</b>	<b>85</b>
<b>Figure 5.4: Nude mouse diabetes reversal .....</b>	<b>86</b>
<b>Figure 5.5 Insulin (A) and glucagon (B) staining in explanted pancreatite grafts.....</b>	<b>87</b>
<b>Figure 6.1: Culture in SSB.....</b>	<b>114</b>
<b>Figure 6.2: Glucose measurements in SSB cultures.....</b>	<b>115</b>
<b>Figure 6.3: Perfusion SSB diagram.....</b>	<b>116</b>
<b>Figure 6.4: Continuous feeding glucose and cell expansion .....</b>	<b>117</b>
<b>Figure 6.5: Glucose measurements with continuous feeding .....</b>	<b>118</b>
<b>Figure 6.6: Adjusted feed rates improve SSB cultures .....</b>	<b>119</b>
<b>Figure 7.1: PFCE and PFD spectra.....</b>	<b>139</b>

<b>Figure 7.2: Inversion recovery illustration</b> .....	140
<b>Figure 7.3: PFD Temperature probe calibration</b> .....	141
<b>Figure 7.4: Temperature compensation with PFD probe</b> .....	142
<b>Figure 7.5: Calibration and validation of <sup>19</sup>F-MRS</b> .....	143
<b>Figure 7.6: Schematic diagram of perfusion bioreactor</b> .....	144
<b>Figure 7.7: Perfusion bioreactor chamber viewed from the side</b> .....	145
<b>Figure 7.8: Perfusion bioreactor chamber viewed from the top</b> .....	146
<b>Figure 7.9: Bioreactor MRS Illustration</b> .....	147
<b>Figure 7.10: Validation of <sup>19</sup>F-MRS <i>in vivo</i></b> .....	148
<b>Figure 7.11: Oxygen measurements in bioreactor</b> .....	152
<b>Figure 7.12: Fiber optic (vs) <sup>19</sup>F-MRS oxygen measurements</b> .....	153
<b>Figure 7.13: Validation of <sup>19</sup>F-MRS methods <i>in vivo</i> with DSO</b> .....	154
<b>Figure 7.14: Preliminary oxygen measurements <i>in vivo</i></b> .....	155
<b>Figure 8.1: High islet densities decreases graft viability and function</b> .....	180
<b>Figure 8.2: High and Low islet density immunohistochemistry images</b> .....	181
<b>Figure 8.3: Vasculature in surrounding tissue</b> .....	182
<b>Figure 8.4: Overlaid <sup>19</sup>F (red) and <sup>1</sup>H (greyscale) MRI of subcutaneous TEG</b> .....	184
<b>Figure 8.5: Internal pO<sub>2</sub> of implanted TEG</b> .....	185
<b>Figure 8.6: Measuring oxygen in bioreactor with DSO</b> .....	211
<b>Figure 8.7: Internal pO<sub>2</sub> of TEGs with DSO</b> .....	212
<b>Figure 8.8: Blood glucose measurements of rats with TEGs (+/-) DSO</b> .....	213
<b>Figure A.1: The Lobes of a porcine pancreas</b> .....	272
<b>Figure A.2: Porcine Pancreas bridge communication</b> .....	273
<b>Figure A.3: Pig pancreas arterial anatomy</b> .....	274
<b>Figure A.4: Porcine pancreas variational vascular anatomy</b> .....	275
<b>Figure A.5: Ductal anatomy classification types</b> .....	276
<b>Figure B.1: Schematic of <sup>31</sup>P-MRS studies</b> .....	295
<b>Figure B.2: ATP spectra from rat, pig, and human pancreata</b> .....	296
<b>Figure B.3: MRI of persufflated pancreas</b> .....	297
<b>Figure B.4: Integration analysis of <sup>31</sup>P-MRS spectrum</b> .....	303
<b>Figure B.5: β-ATP/P<sub>i</sub> levels in human pancreata</b> .....	304
<b>Figure B.6: Measurements of ATP by <sup>31</sup>P-MRS in human pancreas with PSF</b> .....	305
<b>Figure B.7: PSF maintains ATP in human pancreata</b> .....	306

Figure B.8: $\beta$ -ATP/ $P_i$ measurements in porcine kidney .....	307
Figure C.1: Ductal MRI experimental setup .....	314
Figure C.2: Ductal MRI cannulation approaches .....	315
Figure C.3: Ductal contrast MRI of porcine pancreata lobes.....	317
Figure C.4: MRI detects ductal variants .....	318
Figure D.1: Temperature and pressure changes during shipment.....	331
Figure D.2: Temperature measurements in experimental containers .....	332
Figure D.3: Temperature measurements in ICR Shipping containers .....	333
Figure D.4: PRGSC maintains pressure .....	334
Figure E.1: Schematic diagram of continuous purification QMS system.....	348
Figure E.2: Juvenile porcine islet morphology and OCR/DNA.....	351
Figure E.3: Projected transplant outcomes using QMS .....	358
Figure F.2.1: Flow type fiber optic oxygen sensor .....	360
Figure F.6.1: Prototype outflow tubes v1.....	362
Figure F.6.2: Prototype outflow tubes v2.....	363
Figure F.7.1: Surface coil for $^{19}\text{F} - ^1\text{H}$ <i>in vitro</i> studies .....	364
Figure F.7.2: Surface coil for $^{19}\text{F} - ^1\text{H}$ <i>in vivo</i> studies .....	365
Figure F.7.3: Rat hammock v1 and v2 .....	366
Figure F.7.4: Rat hammock v2 mock-up .....	367
Figure F.7.5: Perfusion bioreactor picture .....	368
Figure F.7.6: TheraCyte devices with scale .....	369
Figure F.7.7: TheraCyte devices modified for <i>in vivo</i> cannulation.....	370
Figure F.7.8: TheraCyte with access port.....	371
Figure F.7.9: Fiber optic oxygen probe.....	372
Figure F.8.1: Picture of three-chamber TheraCyte modified for DSO.....	373
Figure F.8.2: Illustration of TheraCyte modified for DSO .....	374
Figure F.8.3: Picture with scale of DSO modified TheraCyte device.....	375
Figure F.8.4: Dual-channel harness and tether apparatus.....	376
Figure F.8.5: DSO manifold schematic diagram.....	377
Figure F.8.6: Pictures of custom assembled DSO manifold .....	378
Figure F.8.7: Animal cage lid modified for DSO .....	379
Figure F.8.8: Pictures of DSO harness and tether apparatus .....	380
Figure F.8.9: Dual-channel harness pictures.....	381

<b>Figure F.8.10: Dual-channel harness shown in position</b> .....	382
<b>Figure F.B.1: First pig/human organ persufflation preservation system</b> .....	384
<b>Figure F.B.2: Illustration of hypothetical ATP levels</b> .....	385
<b>Figure F.B.3: Two loop Surface coil for <sup>31</sup>P-MRS studies</b> .....	386
<b>Figure F.B.4: Water jacket schematic</b> .....	387
<b>Figure F.B.5: First-generation PSF organ container schematic</b> .....	388
<b>Figure F.B.6: First-generation organ container lid</b> .....	389
<b>Figure F.B.7: Picture of <sup>31</sup>P-MRS study experimental set-up</b> .....	390
<b>Figure F.B.8: Integration analysis of <sup>31</sup>P-MRS spectrum</b> .....	391
<b>Figure F.D.1: First generation Wilson Wolf SRM culture devices</b> .....	393
<b>Figure F.D.2: TheramSure and TCP temperature stabilizing materials</b> .....	394
<b>Figure F.D.3: Preparation of ThermaSure and TCP materials</b> .....	395
<b>Figure F.D.4: ThermoSafe and Red Box shipping containers</b> .....	396
<b>Figure F.D.5: Beverage container for temperature and pressure regulation</b> .....	397
<b>Figure F.D.6: Pressure regulated gyroscopic shipping container (PRGSC)</b> .....	398
<b>Figure F.D.7: PRGSC shown with SRM flask</b> .....	399

# Chapter 1 INTRODUCTION

## *Background*

Diabetes is a devastating disease, resulting in substantial humanitarian and economic suffering around the world. The international diabetes federation<sup>1</sup> reports that nearly 1 out of every 12 people (8.3%) in the world have diabetes and nearly half of those people remain undiagnosed. This disease afflicts more than 387 million people in the world today, and this number is expected to increase to over 500 million people during the next 20 years. The global economic impact is estimated to be 612 billion dollars, and accounts for more than 10% of all health care expenses in the world. The rate of diabetes in the United States is even worse with the CDC<sup>2</sup> reporting 9.3% of the U.S. population has diabetes. This amounts to nearly 30 million people with approximately 1.7 million new cases each year. These numbers do not account for the estimated 86 million Americans with “pre-diabetes” who are at high risk for developing diabetes during their lifetime. The economic burden in the United States alone is estimated to be more than 245 billion dollars per year. In the United States, diabetes is primarily managed by insulin injection, oral medication and lifestyle changes (eg. dietary management). Despite the extensive developments for improving treatment of this disease in the past decade, complications related to diabetes are still the 7<sup>th</sup> leading cause of death in the United States. Diabetes is still the primary cause of kidney failure, non-traumatic lower-limb amputations, and blindness in adults. Adults with diabetes in the U.S. are 1.7 times more likely to die from cardiovascular disease than adults without diabetes. This disease is clearly a systemic disease that affects every major organ system in the human body, and there is a growing need to improve treatment, optimize management, and to ultimately find a cure for diabetes.



A brief explanation of the disease itself is important for understanding the motivations of the work presented herein. The common disease called “diabetes” is medically termed “diabetes mellitus,” and is classified as a defect in carbohydrate metabolism that results in the inability of the body to regulate the concentration of glucose in the blood. The term diabetes mellitus originates from the Greek and Latin language and the translation is roughly “sweet urination” and describes frequent urination, and excessive sugar in the urine, which are defining symptoms of the disease. The medical explanations of these symptoms are beyond the scope of this work, but some basic terminology is needed to understand the challenges of diabetes treatment, and the subject matter discussed herein. People diagnosed with diabetes are classified into two primary “types” based on the pathophysiology and onset. Type 1 diabetes (T1D) is defined by the complete or near-complete autoimmune destruction of the insulin secreting “islet of Langerhans” or simply “islets” within the pancreas, and results in relatively rapid onset of hyperglycemia (or high-blood glucose levels) and the associated symptoms. Type 2 diabetes (T2D) is a bit more difficult to define, but is primarily characterized by a relatively gradual development of glucose intolerance that results from various other medical deficiencies (eg. insulin resistance). Regardless of the clinical pathophysiology, the resulting symptoms are similar, and are fundamentally caused by insufficient blood glucose regulation due to insufficient endocrine function of the pancreas. The hallmark condition resulting in disease progress is insufficient production of insulin. Insulin is a metabolic hormone produced by  $\beta$ -cells within a complex cluster of cells called the “islets of Langerhans,” which reside in the pancreas. When islets are destroyed by the immune system (eg. T1D) or can no longer meet the metabolic demand (eg. T2D), then blood glucose levels cannot be effectively regulated. The result is generally increased blood glucose concentrations (termed “hyperglycemia”) that are implicated in the majority of the complications related to diabetes.

As mentioned above, the primary medical treatments for diabetes are either oral or injected insulin therapy. This treatment became available following the discovery of insulin by Drs. Frederick Banting, and Charles Best in 1921<sup>3-5</sup>, and has successfully prevented the acute complications of hyperglycaemia that eventually leads to death. Many advances in the last century have allowed patients to live with diabetes; however as the current statistics demonstrate, diabetes still causes significant morbidity and mortality around the world. For people diagnosed with T1D, insulin therapy is a requirement, and most patients are burdened with the responsibility of measuring blood glucose and administering insulin injections 5 or more times each day. Even with diligent monitoring and care, patients become susceptible to hypoglycemic events, and the numerous chronic complications associated with hyperglycemia discussed above. For people undergoing intensive insulin administration (primarily T1D), the primary adverse event is severe hypoglycemia (low blood sugars)<sup>2,6,7</sup>, which can result in coma and death if not immediately treated. Despite recent advances in insulin administration technology like insulin pumps and continuous glucose sensing, insulin therapies cannot mimic the physiologic feedback-controlled regulation of blood glucose provided by native islets.

Pancreas transplantation was first pioneered by Drs. William Kelly, and Richard Lillehei in the 1960s, and the following developments indicated that pancreas transplantation could successfully normalize blood glucose levels. These observations initiated numerous investigations for treatments categorized as  $\beta$ -cell replacement. One such method developed was a less invasive technique for islet transplantation<sup>8,9</sup>, which entails isolation of islets from a surgically procured pancreas, and then transplantation of only the islets into a patient. Discussions of these procedures are included in the following chapters, but the promise of this basic technique is the basis for the work described herein. Briefly, a pancreas is procured from a donor, and then the islets, which make up only 2% of the entire pancreas, are subsequently isolated from the rest of the pancreatic

tissue (exocrine). Then islets are administered to a patient in such a way that they can function and alleviate the hypoglycemic condition. The pancreas can be procured from the patient himself or herself, which is termed autogeneic islet transplantation, or from another organ donor, which is termed allogeneic transplantation. Autogeneic islet transplantation is primarily performed for patients suffering from another disease called “pancreatitis.” In this case, the pancreas must be surgically removed to alleviate the symptoms of pancreatitis, and the islets are “salvaged” from the pancreas to be re-administered and hopefully preventing the subsequent development of diabetes. Allogeneic islet transplantation is currently being investigated for the treatment of severe T1D for patients with severe hypoglycemic unawareness. Methods and research developments for allogeneic islet transplantation are also discussed in the subsequent chapters of this thesis, but limitations in available donor organs will prevent the large-scale application of this promising therapy to the millions of people living with this disease. Because of this limitation, investigators have turned to alternative islet sources including xenogeneic sources (eg. islet from pigs), or stem-cell derived islets. Regardless of the source of  $\beta$ -cells used for therapy, many technical and medical advancements are required to extend access of this treatment to all of the patients that could benefit from  $\beta$ -cell replacement in general.

This thesis describes the development and application of technologies for the purpose of improving the outcomes and expanding access to  $\beta$ -cell replacement therapies (specifically islet transplantation).

## ***Overview and Thesis Organization***

In order to advance the development of islet transplantation for the treatment of diabetes the following chapters describe academic research studies to develop novel technologies and application of these technologies for improving islet transplantation. The chapters herein present original research studies previously described in publications included in whole or in part (with permission), or from unpublished studies that are in preparation for publication. The full reference to included publications and publications in press are included at the beginning of each chapter, and the associated co-authors are credited in the reference, and the acknowledgements section. Furthermore, additional related studies and co-authored manuscripts are included in the **Appendices A-E**.

The included studies are organized into three main categories, which coincide with critical stages of the islet transplantation process:

- 1. Development of assessment technologies and techniques for improving organ procurement and preservation**
- 2. Development of assessment technologies and techniques for improving islet isolation, culture and shipment**
- 3. Development of assessment technologies and techniques for improving tissue-engineered islet grafts post-transplant**

Each chapter or appendix is also identified as relating to: assessment and monitoring technologies, or improvement technologies, and the thesis organization scheme is outlined in **Figure 1.1** and **Figure 1.2** included below.

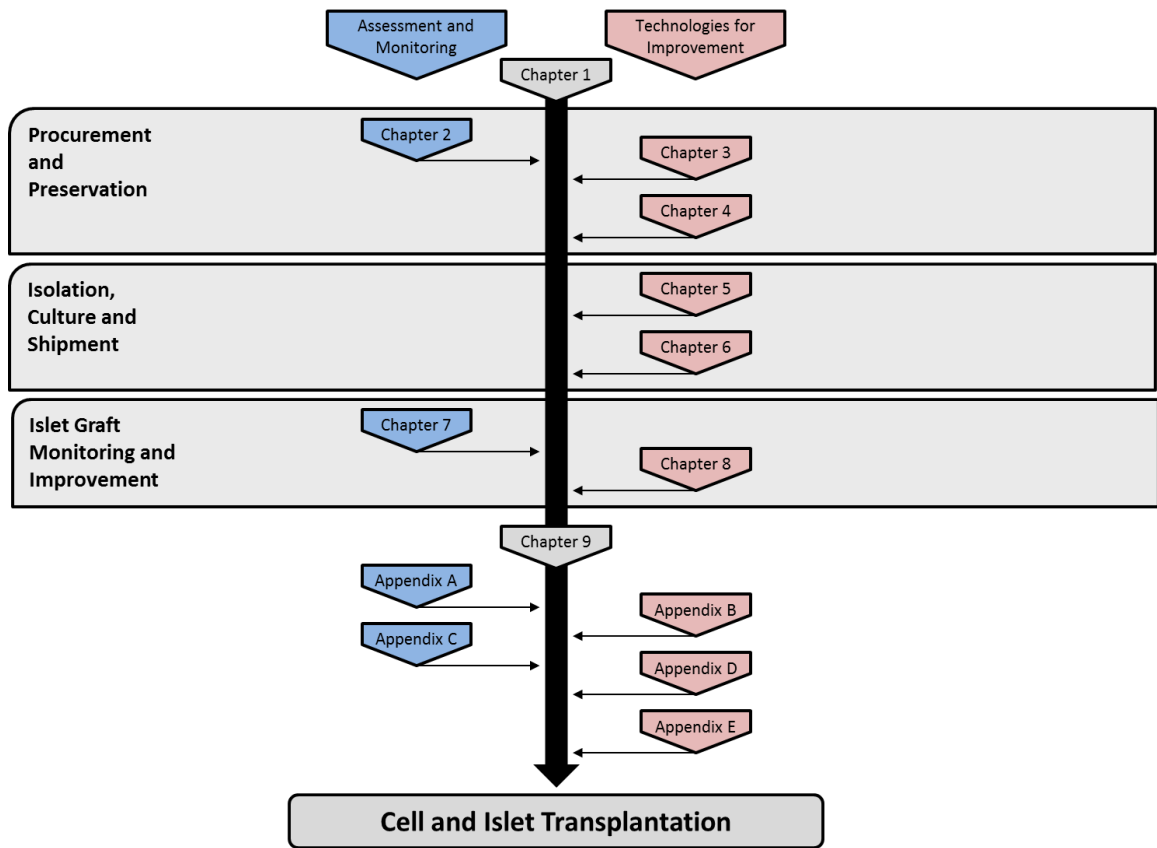
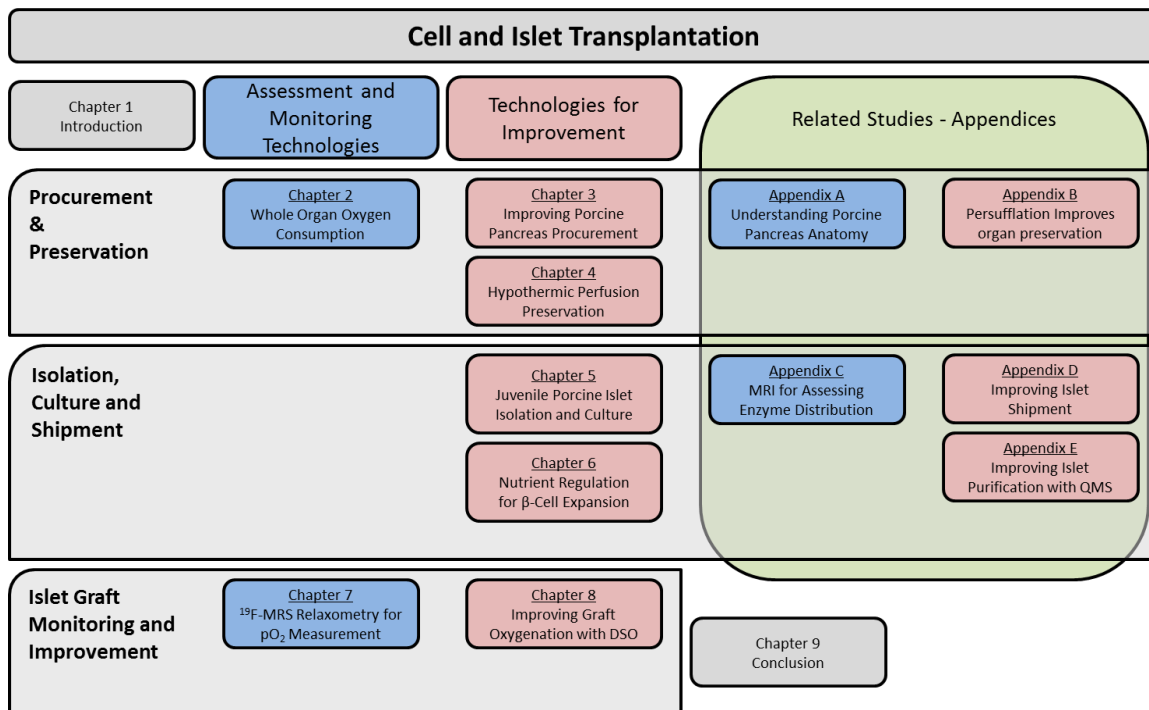


Figure 1.1: Thesis Organization Flow Chart.



**Figure 1.2: Thesis Organization Diagram.**

**The first section contains 3 chapters describing techniques for monitoring and improving organs during procurement and preservation.**

**Chapter 2** includes a published manuscript that describes the development of a novel technique for evaluating organ quality following procurement and during preservation. A method for measuring whole organ oxygen consumption rate (WOOOCR) is described and examined for quantitatively determining the viability of porcine kidneys and pancreata. This technique could be used for evaluating organs prior to solid organ transplantation or prior to processing for islet isolation, and could increase the use of organs from “marginal” donors by confirming viability prior to utilization. More recently, other investigators have described and applied this technique<sup>10</sup>, and filed a patent that describes this technique as a means of organ quality testing prior to transplantation<sup>11</sup>. However, others have found that oxygenation during HMP does not provide a benefit over HMP in regards to transplant outcomes<sup>12</sup>.

**Chapter 3** describes the development of techniques and methods for improving organ procurement. The included studies investigate the anatomical variability of porcine pancreata, and examine various pancreas procurement techniques for improving porcine pancreas quality prior to islet isolation. This study emphasizes the unique considerations for porcine pancreas procurement and the importance of pancreas cooling techniques used during procurement in a donation after cardiac death model.

**Chapter 4** describes studies investigating hypothermic liquid perfusion (HMP) to improve pancreas preservation prior to islet isolation. The presented studies include comparison of static cold preservation methods with HMP in a porcine pancreas model. This technique is shown to directly improve the quality of islets isolated from preserved pancreata compared to static preservation methods. This technique was adapted from kidney preservation methods and continues to be investigated for improving organ preservation<sup>12-14</sup>.

**The second section contains 2 chapters that present technologies for improving the isolation and culture of different  $\beta$ -cell sources.**

Error! Reference source not found. describes methods investigated for improving the process of islet isolation and the subsequent culture of isolated islets prior to transplantation. This chapter includes discussion of techniques to optimize enzyme distribution in pancreata prior to isolation, minimize liberated islet destruction during purification, promote islet survival during culture and shipment, and improve outcomes of juvenile porcine islet isolation.

**Chapter 6** describes a tangential study for improving the expansion and culture of an alternative  $\beta$ -cell source. These studies investigate the application of stirred suspension bioreactors and nutrient regulation for improving the expansion of  $\beta$ -cells *in vitro*. These techniques could support the development of alternative sources of  $\beta$ -cells for islet transplantation.

**The final section contains 2 chapters that describe techniques for monitoring and improving tissue engineered islet grafts post-transplant.**

**Chapter 7** describes the application of  $^{19}\text{F}$  magnetic resonance spectroscopy ( $^{19}\text{F}$ -MRS) to non-invasively measure oxygen partial pressures ( $\text{pO}_2$ ) *in vitro* and *in vivo* biological systems. These techniques are developed and validated for determining the oxygenation status of implantable tissue-engineered grafts (TEGs). Procedures, equipment and rigorous calibration studies are described for the application of this technique for non-invasively measuring  $\text{pO}_2$  *in vivo*. This technique is a valuable research tool for optimizing the oxygenation characteristics of implanted TEGs, and could translated into a reliable clinical tool for monitoring functional therapeutic TEGs.



**Chapter 8** describes the application of  $^{19}\text{F}$ -MRS techniques for monitoring the oxygenation of implanted tissue engineered grafts (TEGs) and a method for delivery of supplemental oxygen (DSO) to improve TEG oxygenation *in vivo*.

**The appendices included herein present additional related studies for monitoring and improving islet transplantation, and supplemental figures that were not included in the published articles.**

**Appendices A-E** include copies of published and unpublished co-authored manuscripts which relate to the work presented in the main chapters of the thesis.

**Appendix F** includes additional supportive figures that were not included in published drafts of manuscripts presented in the body of the thesis.

**Appendix G** includes copyright permission and license documents for reproduced figures and text within the body of the thesis.

**DEVELOPMENT OF METHODS AND TECHNIQUES**  
**FOR IMPROVING ORGAN PROCUREMENT AND**  
**PRESERVATION**

## Chapter 2 WHOLE ORGAN OXYGEN CONSUMPTION

Sections of this chapter are reproduced in whole, or in part from the following publications with permission:

**Weegman BP**, Kirchner VA, Scott WE 3rd, Avgoustiniatos ES, Suszynski TM, Ferrer-Fabrega J, Rizzari MD, Kidder LS, Kandaswamy R, Sutherland DE, Papas KK. “Continuous real-time viability assessment of kidneys based on oxygen consumption.” *Transplant Proc.* 2010 Jul-Aug;42(6):2020-3.

**Weegman BP**, Ferrer-Fabrega J, Scott III WE, Anazawa T, Avgoustiniatos ES, Yuasa T, Hammer BE, Loughnane MH, Hering BJ, Kandaswamy R, Sutherland DER, Suszynski TM, Papas KK, “Continuous, real-time viability assessment of pancreata based on oxygen consumption”. Abstract presented at the Joint CTS, IPITA, IXA, Conference, October 2009, Venice, Italy

License and agreement documentation is included in **Appendix G**.

**Acknowledgements:** The authors would like to thank Mike Taylor, Simona Baicu, Mike Loughnane, Kristen Maynard, Brian Perrault, Mel Graham, Luke Mutch, Takayuki Anazawa, Ichiro Matsumoto and Ron Joki for administrative and scientific support. Research funding provided by grants from the National Institutes of Health (NIH), National Institute of Diabetes and Digestive and Kidney Diseases (R43 DK070400), the Schott Foundation, the Carol Olson Memorial Diabetes Research Fund, the United Metal Traders, Inc., the Eunice L. Dwan Trust, the Iacocca Family Foundation and Tom and Meredith Olson

## **Continuous, Real-time Viability Assessment of Kidneys and Pancreas Based on Oxygen Consumption**

### ***Summary***

Current *ex vivo* quality assessment of donor organs is limited to vascular resistance measurements and histological analysis. New techniques for the assessment of organ quality prior to transplantation may further improve clinical outcomes while expanding the depleted deceased donor pool. We propose the measurement of whole organ oxygen consumption rate (WOOCR) as a method to assess the quality of kidneys in real-time prior to transplantation. Five ( $n = 5$ ) porcine kidneys were procured from non-heart-beating donors. The renal artery (RA) and renal vein (RV) were cannulated and the kidney was connected to a custom-made hypothermic machine perfusion (HMP) system equipped with an in-line oxygenator and fiber optic oxygen sensors. Kidneys were perfused at 8°C and the perfusion parameters and partial oxygen pressures ( $pO_2$ ) were measured to calculate WOOCR. Without an oxygenator in-line, the  $pO_2$  of the perfusion solution at the arterial inlet and venous outlet diminished to near 0 within minutes. However, once adequate oxygenation was provided a significant  $pO_2$  difference was observed and used to calculate the WOOCR. The WOOCR was consistently measured from healthy kidneys and results suggest that it can be used to differentiate between healthy and purposely damaged organs. Custom-made HMP systems equipped with an oxygenator and in-line oxygen sensors can be applied for WOOCR measurements. We suggest that WOOCR is a promising approach for the real-time quality assessment of kidneys, pancreas and potentially other organs during preservation prior to transplantation.

Furthermore, one human pancreas and 4 porcine pancreata were procured and cannulated in a similar fashion. WOOCR measurements in pancreata show large variability in viability upon arrival to the lab, suggesting large variabilities in organ quality due to procurement or preservation techniques.

## ***Introduction***

Renal transplantation is the definitive therapy for patients with end-stage renal disease, offering increased longevity and improved quality of life<sup>15</sup>. At present, one of the main challenges in the field of transplantation is that demand for donor organs far exceeds the available supply. To address this disparity, the field has promoted programs for living donation, the utilization of organs from expanded criteria donors, and donation after cardiac death (DCD)<sup>15</sup>. As an increasing number of marginal organs are used, organ quality assessment prior to transplantation has emerged as an important and urgent issue.

Current *ex vivo* quality assessment tools for donor kidneys are limited to histological analysis<sup>16</sup> and measurement of vascular resistance during perfusion<sup>17</sup>. The development of new, real-time, quantitative techniques for the assessment of organ quality *ex vivo* may potentially expand the already depleted donor kidney pool. We present a technique for the continuous, non-invasive measurement of whole organ oxygen consumption rate (WOOCR) as a method to assess the quality of organs during preservation and prior to transplantation. In addition to excluding organs that are unsuitable for transplantation, this method could allow for identification of healthy organs that would have otherwise been rejected as unsuitable.

The role of oxygen during organ preservation remains equivocal and even controversial. On one hand, there are concerns that the low levels of molecular oxygen dissolved in organ preservation solutions generate free radicals during prolonged storage, leading to the progressive tissue injury during the reperfusion phase<sup>18</sup>. On the other hand, studies have suggested that preservation-induced hypoxia causes depletion of high energy phosphate (i.e., ATP) and impairment of mitochondrial function that can be reversed by raising the pO<sub>2</sub> of the perfused medium<sup>19</sup>. Clearly, optimum HMP preservation will require a balance between these opposing effects. Under normal physiological conditions most viable tissues consume oxygen<sup>20</sup>. Consequently, determining

WOOCR could be useful for quantifying organ viability even when measurements are conducted during cold preservation (4-8 °C). Calculation of OCR has been applied before in the study of the heart<sup>21</sup>, the liver<sup>19</sup> and the kidney<sup>22-24</sup>. It has also been shown that OCR is a reliable and useful measure of pancreatic islet quality and can be used to predict islet transplant outcome<sup>25-27</sup>.

We present WOOCR as a method for use with a modified hypothermic machine perfusion (HMP) system. HMP has been shown to be an effective method of organ preservation and is becoming a standard of clinical practice for kidney preservation among organ procurement organizations (OPOs)<sup>28</sup>. Current clinical prototypes of HMP do not include oxygen sensors or an adequate oxygenation system to meet the oxygen demand of a viable kidney, even at cold temperatures. We propose two simple modifications to currently-available clinical perfusion devices, including (1) an in-line oxygenator with oxygen supply and (2) in-line fiber optic oxygen sensors, which are added to the HMP system without disturbing the organ. This setup provides the kidney with oxygenated perfusate and allows for real-time measurement of WOOCR.

## ***Materials and Methods***

### *Porcine Kidney Procurement*

Five porcine kidneys (n=7) were procured from non-heart-beating donors (NHBDs). Five minutes prior to sacrifice, animals received an intravenous injection of 50,000-100,000 U of heparin. Euthanasia was performed with a lethal injection of pentobarbital sodium. After sacrifice, the pig was eviscerated and the posterior wall of the aorta was incised longitudinally to expose the origin of the renal artery (RA) within the aortic lumen. RAs were individually cannulated and each kidney was flushed with 1 L of cold lactated Ringer's solution (LRS) and carefully dissected away from the viscera. Warm ischemia time was minimized to less than 10 minutes during the procurement. Each kidney was weighed after procurement and before HMP.

### *Hypothermic Machine Perfusion and WOOCR Setup*

Arterial and venous ends of each organ were cannulated and connected to the HMP system. In our custom-built HMP system, two fiber optic oxygen sensors (Instech Labs, Plymouth Meeting, PA) were placed in-line upstream of the RA and two were placed downstream of the renal vein (RV) for the measurement of arterial and venous  $pO_2$ , respectively. These sensors were specifically designed in collaboration with Instech Labs for these studies to provide accurate and reliable measurements of oxygen in a biological perfusion setting. Drawings of the sensors are included in **Appendix A** for reference. To provide maximum oxygenation without causing vascular damage, the flow rate was controlled between 100-200 mL/min and the temperature was maintained at 8°C for the duration of the perfusion. The WOOCR of a kidney was calculated using a mass balance equation where  $Q$  is the flow rate of perfusion (mL/min),  $pO_2$  is the partial pressure of oxygen (mm Hg),  $\alpha$  is the solubility of oxygen at a given temperature (mol/mL·mm Hg) and  $m$  is the mass of the kidney (grams).

$$OCR = \frac{Q \times (pO_{2Arterial} - pO_{2Arterial}) \times \alpha}{m} \quad 2.1$$

During perfusion of six (n = 6) kidneys, an oxygenator was incorporated into the setup to provide a steady supply of oxygenated preservation solution to the organ. **Figure 2.1** demonstrates the basic setup of the HMP system with in-line fiber optic oxygen sensors and the oxygenator. An oxygenator must be incorporated in order to provide a steady supply of the oxygenated preservation solution. This modification is integral for two reasons. First, if we assume that kidney is the only component extracting oxygen from the perfusion system, OCR of the kidney is similar to OCR of pancreatic islets (approximately 200 nmol/min per mg DNA<sup>25</sup>), and the oxygen delivery is not limited by the perfusion flow, than one liter of the preservation solution would be depleted of oxygen within minutes. Second, the delivery of constant concentration of oxygen will ensure an accurate measurement of OCR in steady state. Kidneys procured with or without WIT were preserved by HMP for up to 24 hours to generate a series of increasing organ damage, and WOOCR was measured for each condition.

#### Formalin Treatment of the Porcine Kidney

After a single porcine kidney was harvested and flushed with 1 L of cold LRS, the initial measurement was performed to establish WOOCR prior to a formalin treatment. Next, the kidney was flushed with 120 mL of 10% buffered formalin through the RA, followed by a flush with 120 mL of LRS to remove any remaining formalin. The new set of WOOCR data was collected 30 minutes after the formalin treatment.



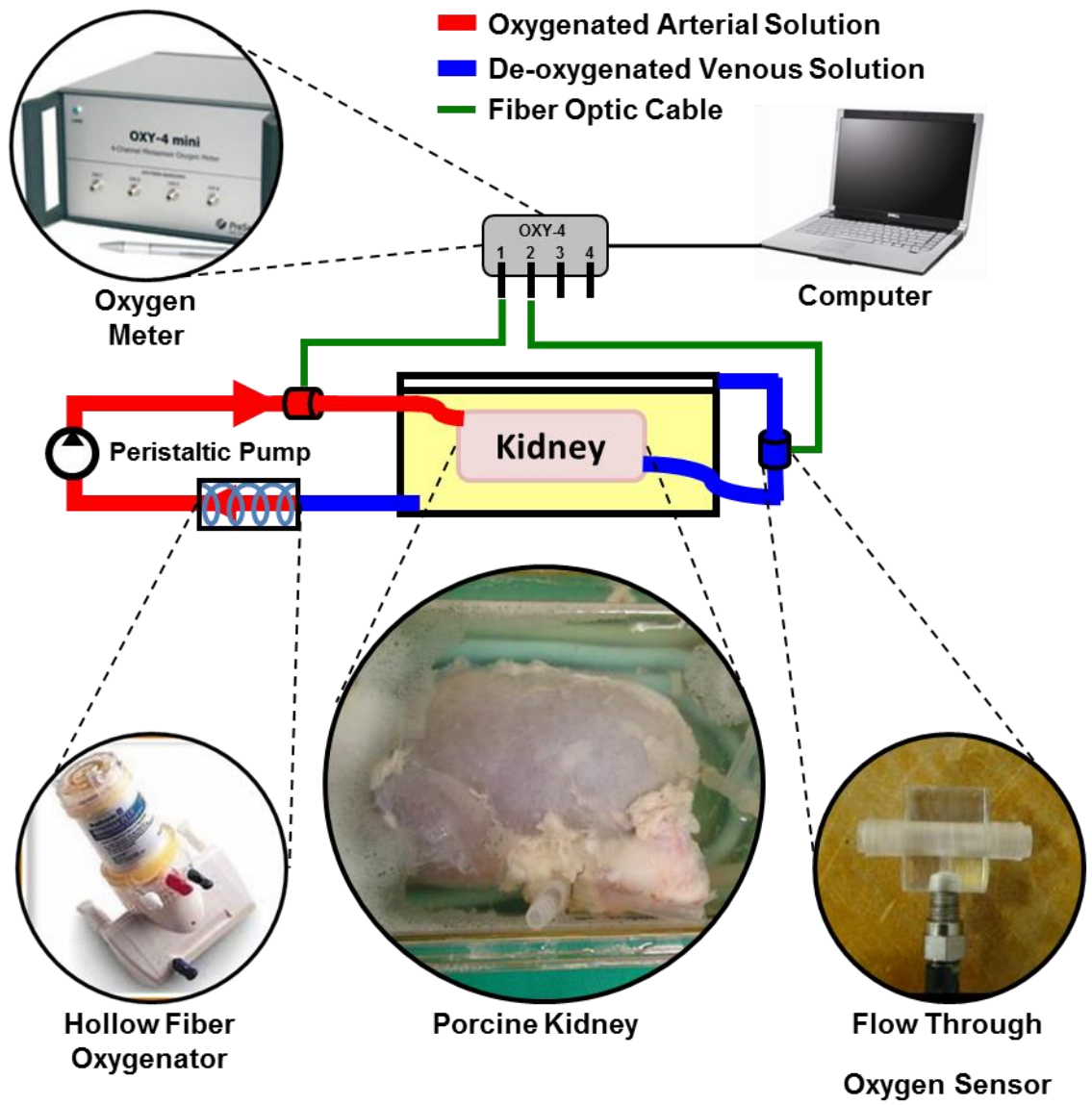


**Figure 2.1: WOOCR perfusion system schematic.** Diagram illustrating the perfusion circuit containing the in-line oxygenator and oxygen sensors.

## ***Results***

### **Kidneys**

As expected, without an oxygenator the measured pO<sub>2</sub> of the perfusate for both the RA and the RV approached zero within minutes while perfusing at 100 mL/min at 8°C. After incorporating an in-line oxygenator, the inlet (RA) pO<sub>2</sub> was maintained at approximately 150 mm Hg (in equilibrium with room air), but the outlet (RV) pO<sub>2</sub> still remained near zero. When the arterial pO<sub>2</sub> was elevated to more than 300 mm Hg (using an oxygen supply), the outlet pO<sub>2</sub> increased and a significant pO<sub>2</sub> drop that was not limited by the oxygen supply was measured between the RA and RV for every kidney (**Figure 2.1A**). The average WOO CR for presumably healthy kidneys on HMP with an in-line oxygenator was  $158 \pm 62$  nmol/min/g (n = 4, range = 92-229 nmol/min/g). These results (and our theoretical calculations) verify the requirement of an in-line oxygenator to provide an inlet pO<sub>2</sub> greater than 300 mm Hg for the adequate oxygenation of the entire organ and for the accurate measurement of WOO CR for the average porcine kidney. The viability of a kidney was observed to decrease markedly during 4 hours of HMP (**Figure 2.2B**), and a dramatic drop in the WOO CR of the kidney was observed after the formalin insult (17 nmol/min/g), when compared to the WOO CR of the same organ prior to formalin treatment (187 nmol/min/g, see **Figure 2.2C**).

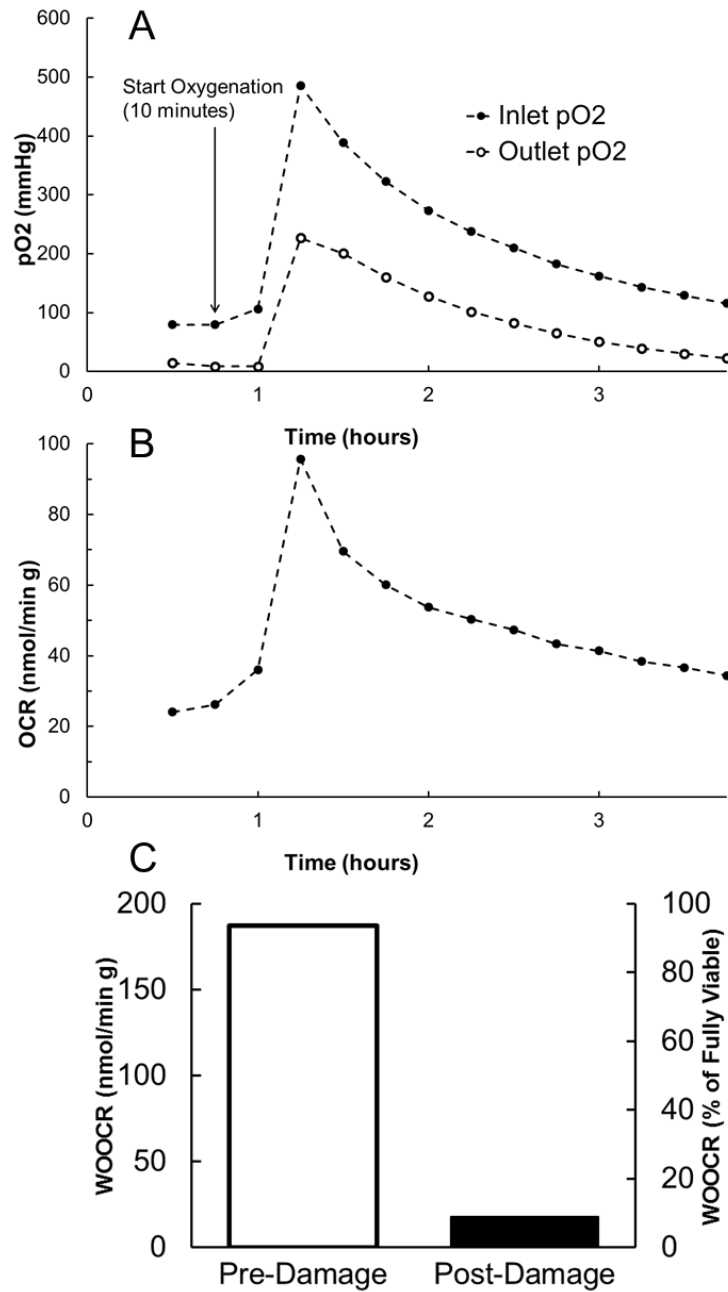


**Figure 2.2: WOOOCR results from porcine kidney.** Graph illustrating real-time measurements of pO<sub>2</sub> at the inlet (renal artery) and outlet (renal vein) of a machined perfused porcine kidney (A), and their time-dependent profiles over 3 hours of cold preservation; Note the need for active oxygenation of the perfusate medium at the inlet, as reflected by a pO<sub>2</sub> near zero until it was started. WOOOCR (normalized per gram) can be calculated for the same kidney from the pO<sub>2</sub> measurements (B). WOOOCR is negatively affected by lengthening ischemic time (B) or exposure to a caustic agent (C), in which WOOOCR measurements were obtained for a freshly procured porcine kidney (healthy) and after that same kidney was infused with 10% buffered formalin solution). Figure is adapted from published manuscript<sup>30</sup> to include supplementary parts A & B.

## ***Discussion***

Current clinical HMP systems are not equipped with oxygenators. Rapid depletion of oxygen from the reservoir containing non-oxygenated preservation solution subjects the organ to hypoxic conditions. A theoretical calculation demonstrates that one liter of LRS equilibrated with air would be depleted of its oxygen content in about 5 minutes by an average “healthy” adult porcine kidney undergoing HMP. The experimental results confirm that arterial and venous pO<sub>2</sub> values of the recycled perfusate (i.e., non-oxygenated) decreased to near zero after a few minutes of perfusion at 8°C. The results of this limited study clearly support the need for improved oxygen delivery in HMP systems during kidney preservation.

One solution is to use an in-line oxygenator which can supply a pO<sub>2</sub> of at least 300 mm Hg. Using a perfusion solution with a higher oxygen solubility could also improve oxygenation of tissue using a lower pO<sub>2</sub>. With adequate oxygenation, a significant pO<sub>2</sub> drop that was not limited by the oxygen supply (i.e., RV pO<sub>2</sub> was significantly higher than zero) was observed between the RA and RV of every organ, and an average WOOOCR value of presumably healthy kidneys on HMP was measured at 158 nmol/min/g. This value was similar to the OCR of healthy pancreatic tissue at 8°C (200 nmol/min/g)<sup>25</sup>.

Our results also indicate a significant variability in WOOOCR among freshly procured kidneys (range 92-229 nmol/min/g) that were harvested using our standardized technique. We hypothesize that the variability in WOOOCR among these organ can be correlated with the individual organ quality and may identify damaged organs *ex vivo* that otherwise would be undetected.

The difference between the WOOOCR in presumably healthy and damaged organs was supported by comparing the WOOOCR of a formalin-treated (damaged) kidney (17 nmol/min/g) to the WOOOCR of the same organ before treatment (187 nmol/min/g) or the average WOOOCR of all 4 untreated organs (158 nmol/min/g). Detection of any WOOOCR in the formalin-treated kidney

suggests the incomplete damage of the organ and reflects the OCR of the remaining viable tissue. The WOOCR of the kidney would be expected to approach zero if the amount of fixate and the duration of the fixation were increased.

## ***Conclusion***

Based on these data, we conclude that a real-time, non-invasive method for the measurement of WOOCR in conjunction with oxygenated HMP may be used to assess organ quality *ex vivo*. These measurements are feasible utilizing a modified clinical prototype of HMP system, and a protocol was developed describing how to implement WOOCR with the LifePort Kidney Transporter clinical HMP system. The role of oxygenation in organ preservation remains controversial<sup>18,19,29</sup>. The optimum HMP preservation will need to balance the potential damage that can occur with the generation of free radicals with the necessity to provide sufficient oxygen to sustain healthy tissues. Our future research will be directed towards further validation of the WOOCR method by correlating measurements to histological data, molecular profiles, and graft function following allogeneic transplantation in a large animal model.

## ***Supplementary Data: Kidney and Pancreas WOOCR***

### ***Introduction***

These expanded studies were not included in the published manuscript<sup>30</sup> because they were completed following publication but these studies follow the same protocols and procedures as described in the publication with minor modifications described below. After preliminary success with measuring WOOCR of porcine kidneys, the method was also expanded to include a small series of kidneys with varying warm and cold ischemia times to verify the sensitivity of the assay to individual organ viability.

Furthermore, these methods were adapted for a small proof of concept study to develop the WOOCR technique for use with pancreata. WOOCR was measured from a single human pancreas and small number of porcine pancreatic lobes (N=4) using adapted methods described below.

### ***Human and Porcine Pancreases Procurement***

A donor human pancreas was procured for research (n=1). In preparation, the spleen was removed and all of the arteries supplying the duodenum were ligated to prevent leakage. The splenic artery (SA) and the superior mesenteric artery (SMA) were cannulated and coupled using a Y splitter for connection to a peristaltic perfusion pump. One oxygen sensor was placed in-line upstream of the arteries to measure the ('arterial') oxygen partial pressure ( $pO_2$ ) of the perfusion solution and a second sensor was attached to the splenic vein (SV) which was also cannulated to measure the effluent (or 'venous')  $pO_2$ . The temperature was maintained at 8°C and the organ was perfused. The arterial and venous  $pO_2$ , the gross whole organ mass and the measured flow rate were used to calculate the OCR per gram tissue. Porcine pancreata with preserved vasculature were procured from a non-heart beating donor (n=4). The celiac trunk, SMA, and

portal vein were all cannulated and all leaks were ligated. The sensor placement, perfusion system and OCR calculation were the same as the human pancreas.

*Kidney and Pancreas Supplementary Results and Discussion*

Measurements from kidneys with increasing levels of procurement and preservation damage due to varying degrees of warm and cold ischemia are presented in **Figure 2.3**, and a decreasing trend in WOOCR was observed with increasing damage to the organ.

WOOCR measurements from a pancreas preserved by HMP for up to 20 hours are shown in **Figure 2.4** to decrease continuously during the preservation period. The average OCR value for all 5 organs measured at the time of arrival is 53 +/- 74 nmol/min/g, and individual measurements are shown in **Figure 2.5**. These findings illuminate a large variability in organ quality prior to long term cold storage, and demonstrate the sensitivity of the technique. More studies are required to develop baseline values for determination of donor organ viability.

These supplementary results support the original findings presented in the original manuscript<sup>30</sup> and confirm that WOOCR could be a valuable tool for evaluating the metabolic integrity and viability of kidneys and possibly pancreas for solid organ or islet transplantation.

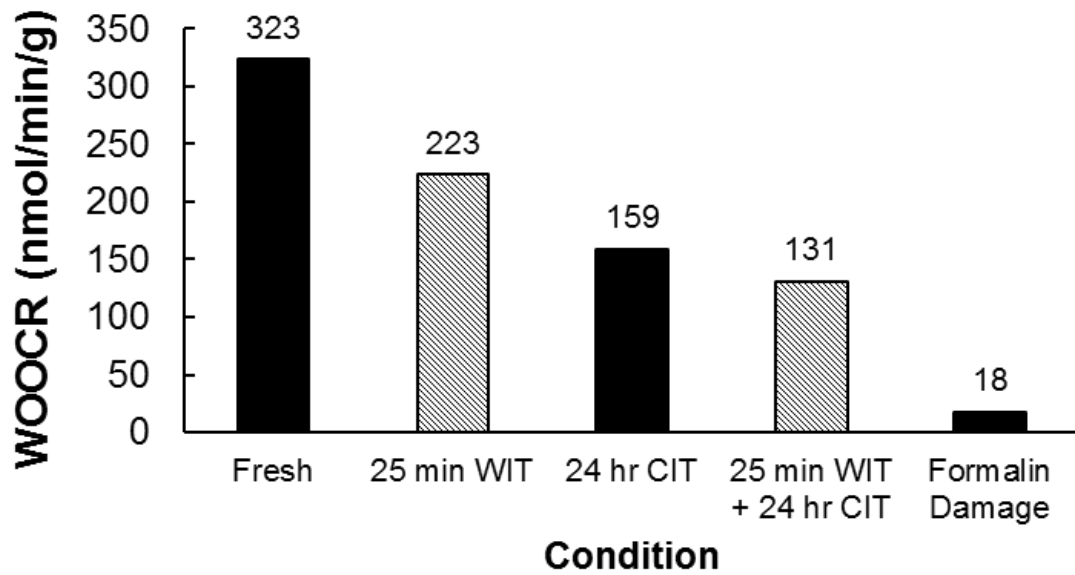


**Figure 2.3: Damage from WIT and CIT is detected by WOCR.** WOCR measurements from a fresh kidney, and measurements from kidneys that were exposed to a series of warm and cold ischemia during procurement and preservation. The fifth measurement shown is from a kidney damaged by formalin fixation. A clear decrease in WOCR is seen with increasing levels of organ damage. Figure is not included in original manuscript<sup>30</sup> but is included here to provide additional evidence.



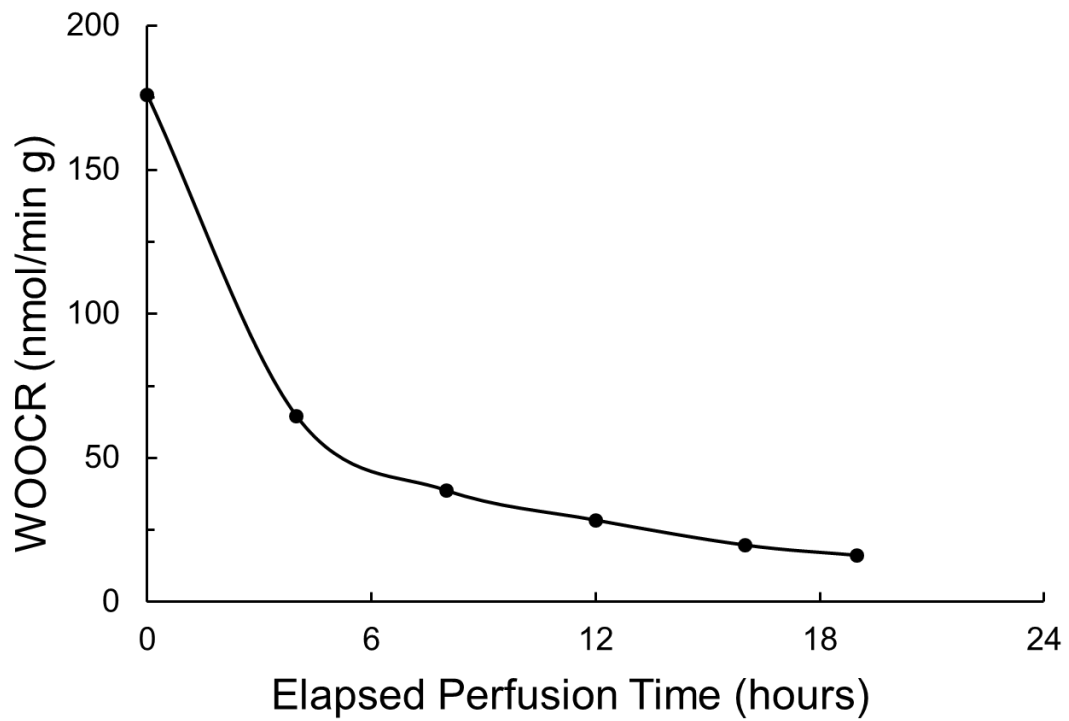


**Figure 2.4: WOOOCR of porcine pancreas.** WOOOCR measurements over time for a porcine pancreas, showing the WOOOCR decreasing as the organ is perfused with LRS. Results from pancreas were not included in original manuscript<sup>30</sup>, but are included here as supplementary data.

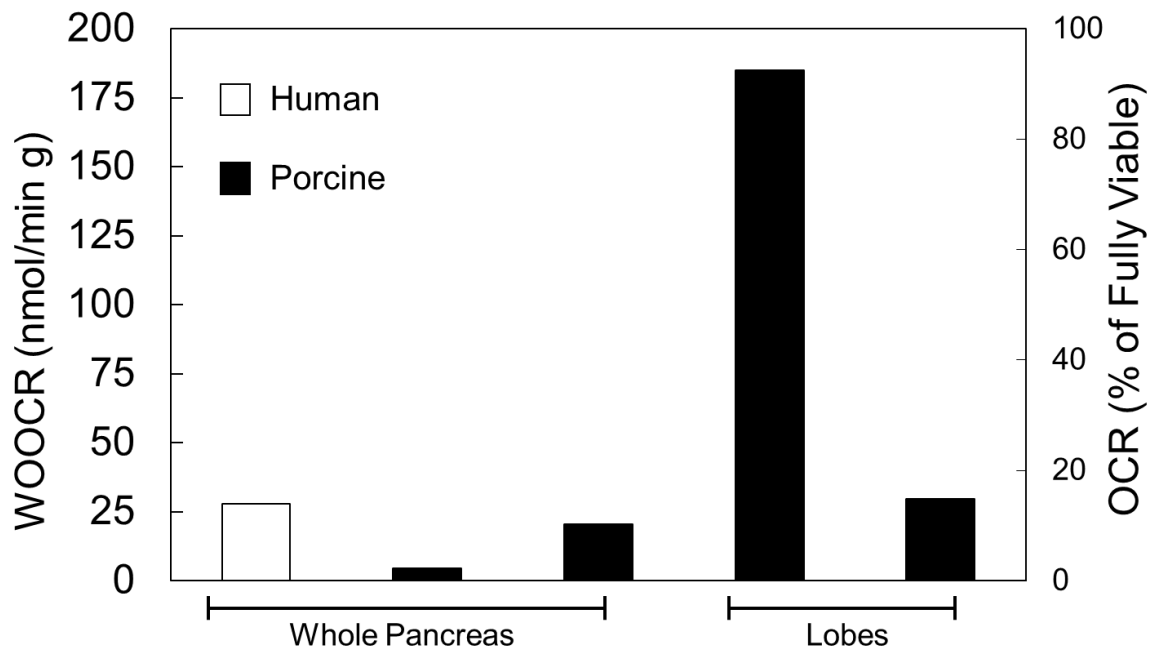


**Figure 2.5: WOCR measures pancreas viability.** Porcine pancreas (black) and human pancreas (white) WOCR values measured immediately upon arrival at the lab. Results from pancreas were not included in original manuscript<sup>30</sup>, but are included here as supplementary data.

## Chapter 3 IMPROVING PANCREAS PROCUREMENT

Sections of this chapter are reproduced in whole, or in part from the following publications with permission:

**Weegman BP**, Suszynski TM, Scott III WE, Ferrer-Fabrega J, Avgoustiniatos ES, Anazawa T, O'Brien TD, Rizzari MD, Karatzas T, Jie T, Sutherland DER, Hering BJ, Papas KK "Temperature Profiles of Different Cooling Methods in Porcine Pancreas Procurement", Xenotransplantation, July 2014

Supplementary **Figures 3.1, 3.2, 3.3, 3.5** and **3.8** were not included in the original published manuscript<sup>31</sup> but are included in the version presented here to provide additional clarity and supplemental information. References to these figures are also added to the text of the original published manuscript.

**Figure 3.7** is adapted from the originally published manuscript "**Figure 3**" to include additional images of the cooling strategies used for each histology section.

License and agreement documentation is included in **Appendix G**.

**Acknowledgements:** The authors would like to thank the Schott Foundation, the Minnesota Lions Diabetes Foundation, the Juvenile Diabetes Research Foundation (JDRF 5-2013-141), Giner Inc., the Schulze Diabetes Institute, and the NIH (P41 EB015894, and S10 RR025031) for supporting this research. The authors also thank Efstathios Avgoustiniatos, Louis Kidder, Kristen Maynard, Phillip Rozak, and Kate Mueller for assistance in manuscript preparation and review; A.N. Balamurugan and Melanie Graham for helpful discussions; and Shuichiro Matsumoto, Takayuki Anazawa, Thomas Gilmore, Brian Perrault, and Lucas Mutch for surgical assistance.

Research funding was also provided by grants from the National Institutes of Health (NIH), National Institute of Diabetes and Digestive and Kidney Diseases (R01DK068717, R44 DK070400 and R43 DK070400), the Iacocca Foundation, the Schott Foundation, and the Carol Olson Memorial Diabetes Research Fund.

## **Temperature Profiles of Different Cooling Methods in Porcine Pancreas Procurement**

### ***Summary***

Furthermore, the second study examines the effect of 4 different cooling *Methods* on core porcine pancreas temperature (n=24) and histopathology (n=16). All *Methods* involved surface cooling with crushed ice and chilled irrigation. *Method A*, which is the standard for porcine pancreas procurement, used only surface cooling. *Method B* involved an intravascular flush with cold solution through the pancreas arterial system. *Method C* involved an intraductal infusion with cold solution through the major pancreatic duct, and *Method D* combined all 3 cooling *Methods*. Temperature studies demonstrated that surface cooling alone (*Method A*) gradually decreased core pancreas temperature to < 10 °C after 30 minutes. Using an intravascular flush (*Method B*) improved cooling during the entire duration of procurement, but incorporating an intraductal infusion (*Method C*) rapidly reduced core temperature 15-20 °C within the first 2 minutes of cooling. Combining all methods (*Method D*) was the most effective at rapidly reducing temperature and providing sustained cooling throughout the duration of procurement, although the recorded WIT was not different between *Methods* ( $p=0.36$ ). Histological scores were different between the cooling *Methods* ( $p=0.02$ ) and the worst with *Method A*. There were differences in histological scores between *Methods A* and *C* ( $p=0.02$ ) and *Methods A* and *D* ( $p=0.02$ ), but not between *Methods C* and *D* ( $p=0.95$ ), which may highlight the importance of early cooling using an intraductal infusion. We found that surface cooling alone could not rapidly cool large (porcine or human) pancreata. Additional cooling with an intravascular flush and intraductal infusion results in improved core porcine pancreas temperature profiles during procurement and histopathology scores. These data may also have implications on human pancreas procurement since use of an intraductal infusion is not common practice.

## ***Introduction***

Widespread clinical application of islet transplantation is currently limited by the shortage of human organ donors<sup>32</sup>. Porcine islet xenotransplantation<sup>33-35</sup> provides an opportunity to obviate the inadequate supply of human organs by isolating islets from a practically-unlimited supply of porcine donors. Just as with human islet isolation, the outcome of porcine islet isolation is dependent on the quality of the donor pancreas<sup>36</sup>, which is in large part affected by the procurement and cooling methodologies used. This is especially true in porcine islet transplantation since the preservation periods are typically short and limit the negative impact that cold ischemia time may have on islet quality.

Donor porcine pancreata are frequently procured following cardiac death to save on the additional cost, complexity, and logistical challenges associated with performing a heart beating procurement with an adult porcine donor. However, donation after cardiac death (DCD) is accompanied by warm ischemia time (WIT), which is known to be detrimental to the quality of a donor pancreas<sup>37</sup>. The current procurement method involves dissecting the pancreas out as quickly as possible, while the core pancreas temperature is reduced by diffusion-based surface cooling with crushed ice and cold irrigation. The WIT is traditionally defined and recorded as the time from cardiac death until cooling is initiated. In a large organ, like a porcine or human-sized pancreas, diffusion-based cooling is not effective at rapidly reducing the core temperature below 8 °C and thus the WIT is underestimated. In this study, we evaluate 4 different methods of donor porcine pancreas cooling performed during the procurement: surface cooling alone (*Method A*), an intravascular arterial flush (*Method B*), an intraductal infusion (*Method C*), and combining an intravascular flush with an intraductal infusion (*Method D*). The primary outcome of this study was to establish temperature profiles for the core of the donor porcine pancreas for each of the cooling methods and to determine which cooling method most rapidly cools a large organ.

Secondary outcomes include correlating the cooling method that was employed with core pancreas tissue quality as assessed by histology. The main objective of this study was to optimize the DCD porcine pancreas cooling protocol used during procurement, which may also have implications on cooling protocols used during human pancreas procurements. .

## ***Materials and Methods***

### **Porcine Pancreas Procurement**

In this study, pancreata (n=94) were harvested following *en bloc* viscerectomy from DCD Landrace pigs. Subgroups of donor pancreata were designated for direct core pancreas temperature monitoring during procurement (n=24) and histological evaluation (n=16). All other donors (n=56) presented in this study were included to report statistics on the surgical procurement (e.g., mean WIT) but were used as part of other studies. All work involving animals was approved by the Institutional Animal Care and Use Committee at the University of Minnesota.

The porcine pancreas procurement methods used in this study are described in the previous section of this chapter, and have been described previously<sup>38</sup>. An illustrative timeline for the surgical procurement is included in **Figure 3.1**. Briefly, donors were given intravenous heparin (100,000 U bolus) 5 minutes prior to euthanasia, which was done via an overdose with sodium pentobarbital (Fatal Plus; Vortech Pharmaceuticals, Dearborn, MI) followed by exsanguination. Heparinization of the donor prior to euthanasia was found to be critical for effective removal of blood, and inadequate heparinization resulted in extensive thrombus formation in the vasculature that could not be flushed out. Examples of a pancreata from an inadequately heparinized donor, and a properly heparinized donor are included for reference in **Figure 3.2**. *En bloc* viscerectomy was performed and the abdominal viscera were transferred to a surgical dissection table. Care was taken to preserve the vasculature for all organ procurements regardless of cooling method used.

Different cooling methods were used for each pancreas during the remainder of the procurement. All cooling methods involved standard surface cooling with crushed ice and irrigation with chilled (refrigerated) lactated Ringers solution (LRS). Unless designated for surface cooling alone (*Method A*), organs were randomized to undergo enhanced cooling with additional methods

described below. Some of the organs underwent direct core pancreas temperature measurements throughout the procurement. Following organ cooling and dissection, each pancreas was massed and processed as indicated. If pancreas was designated for histological assessment (n=16), following procurement, the entire pancreas was flushed through the vasculature with 10% buffered formalin solution and biopsies from the core of the pancreas were taken for evaluation. If the pancreas was designated for islet isolation (n=18), the pancreas was placed on CPS and transported to the isolation facility.

### Porcine Pancreas Cooling

All donor pancreata were surface-cooled with crushed ice and chilled LRS. Pancreata were then randomized to undergo cooling using 1 of 4 cooling *Methods*:

#### **Method A**

This *Method* only involved surface cooling with crushed ice and irrigation with chilled LRS (n=8), with no additional cooling technique used. This was considered the standard cooling methodology used during DCD porcine pancreas procurement. Two or more liters of crushed ice and  $\geq 2$  liters of chilled LRS were applied to the surface of the donor pancreas throughout the duration of the procurement. Isotonic ice was used for organs designated for histology or islet isolation. Active cooling began as soon as the pancreas was located within the viscera (typically within 2 minutes of evisceration), and was completed at the time of total pancreatectomy.

#### **Method B**

This *Method* involved additional arterial intravascular flushing which was conducted as quickly as possible (typically between 1-3 minutes) following viscerectomy via cannulation of the aorta (*Method B1*, n=11) or individual cannulation of both the celiac trunk (CT) and superior mesenteric artery (SMA) (*Method B2*, n=10). For *Method B1*, the supraceliac aorta was flushed



anterogradely after the infrarenal aorta was clamped. For *Method B2*, all major branches from the CT that did not supply the pancreas and the intestinal branches from the SMA were ligated prior to flushing. *Method B1* was initially used during this study, which then evolved to *Method B2*. The methodology was changed because it was observed that substantial amounts of flush solution were lost through the numerous lumbar arteries, and needing to ligate these branches prolonged the procedure. It was determined that individually cannulating the CT and SMA did not increase WIT, so *Method B2* replaced *Method B1*. Regardless of which vessels were cannulated, 3-5L of heparinized (1,000 U/L) CPS (modified Cold Storage/Purification Stock Solution from Mediatech, Inc., Manassas, Va) or LRS were flushed at a rate of approximately 0.5L/min until flush effluent appeared clear of blood. CPS was used instead of LRS for pancreata designated for histology or islet isolation.

### **Method C**

This *Method* involved intraductal infusion of CPS (n=6). Following the viscerectomy, the head of the pancreas was quickly (typically 2-3 minutes) separated from the bowel, and the main pancreatic duct was identified and directly cannulated with an angiocatheter (18-20 gauge depending on size). After the catheter was placed, 60 mL of CPS was infused at a rate of 1 mL/sec.

### **Method D**

This *Method* combined an arterial intravascular flush (*Method B*) and an intraductal infusion (*Method C*) (n=59). Some of the pancreata were flushed via the aorta (n=4), but most via the CT and SMA (n=55). Immediately following transfer of the viscera to the surgical table, the vessels were cannulated and the flush was started. Next, the main pancreatic duct was located, cannulated, and infused as described above in *Method C*. Typically, 2 or more surgeons worked concurrently to expedite the cannulation and ligation procedures, and all cooling methods were

initiated within 4 minutes of viscerectomy. The total flush and infusion volumes of CPS or LRS, and flow rates were the same as used in *Methods B* and *C*.

### Temperature Measurements

As mentioned previously, some of the pancreata were designated for direct core pancreas temperature monitoring (n=24), and involved organs cooled by *Method A* (n=4), *Method B* (n=13), *Method C* (n=4) and *Method D* (n=3). Individual 33-gauge needle temperature probes were placed into the core of the distal splenic lobe, the proximal splenic lobe, the duodenal lobe and the connecting lobe<sup>38</sup> as soon as the viscera were transferred to the surgical table and the pancreas was identified. **Figure 3.3** shows the placement of the probes in the pancreas. Temperature measurements were recorded in real-time (every 30 seconds) and throughout the duration of the procurement. Care was taken to ensure that the probes remained within the core of the pancreas as the organ was dissected. The mass of each pancreas was recorded following procurement and the mass of the ductal infusion solution was subtracted for relevant pancreata. The temperature measurements were used to observe different trends in core temperature profiles between groups and to calculate the amount of energy removed from the donor pancreas during cooling. These energy values were calculated for each pancreas by multiplying the temperature change during a 10-minute period by the pancreas mass and an estimate of the specific heat of pancreas tissue. The specific heat for pancreas tissue was approximated assuming the pancreas has a density and thermal conductivity equal to that of water at the average observed temperature during the procurement. The average energy removed was also converted to a corresponding expected temperature drop ( $\Delta T$ ) for a representative and standardized 350-gram pancreas during the first 10 minutes of cooling.

### Histology

As mentioned previously, some of the pancreata were designated to undergo histological evaluation (n=16), and included organs cooled by *Method A* (n=4), *Method C* (n=4), and *Method D* (n=8). Histology was not done for any organ cooled by *Method B* due to budgetary constraints and also because significant differences in the histological scores between organs cooled by *Methods C* and *D* could be attributable to the use of an intravascular flush (which indirectly reflects the impact of *Method B*). Approximately 240 mL of chilled 10% buffered formalin solution was infused intravascularly following the surgical procurement, and multiple core biopsies were then taken and placed into formalin. The biopsies were then processed by embedding in paraffin, sectioning and staining with hematoxylin and eosin (HE). Histological evaluation was done in blinded fashion by an experienced histopathologist. Samples were systematically scored for the degree of necrosis and autolysis observed in each histological section; scoring was graded as follows: 0=none, 1≤10%, 2=11-25%, 3=26-50%, 4=50-75%, 5≥76%. Necrosis and/or autolysis was defined by the presence of nuclear pyknosis or karyorrhexis, cytoplasmic hypereosinophilia, loss of intercellular junctions, loss of tissue integrity, cellular lysis, dystrophic mineralization, and disintegration of tissue structures sometimes with associated extravasation of blood.

#### Statistical Analysis

All data were reported as mean values and standard errors. Overall differences between groups were compared using a one-way analysis of variance (ANOVA, if normally-distributed) or the Kruskal-Wallis test (if not normally-distributed). Mean values between all groups were compared using Tukey's multiple comparison post-test (if normally-distributed) or the Mann-Whitney test (if not normally-distributed). Statistical significance corresponded to *p*-values <0.05 using a 95% confidence interval. All statistical analyses were performed using Graphpad Prism Version 5.03 (Graphpad Software, Inc., La Jolla, CA).

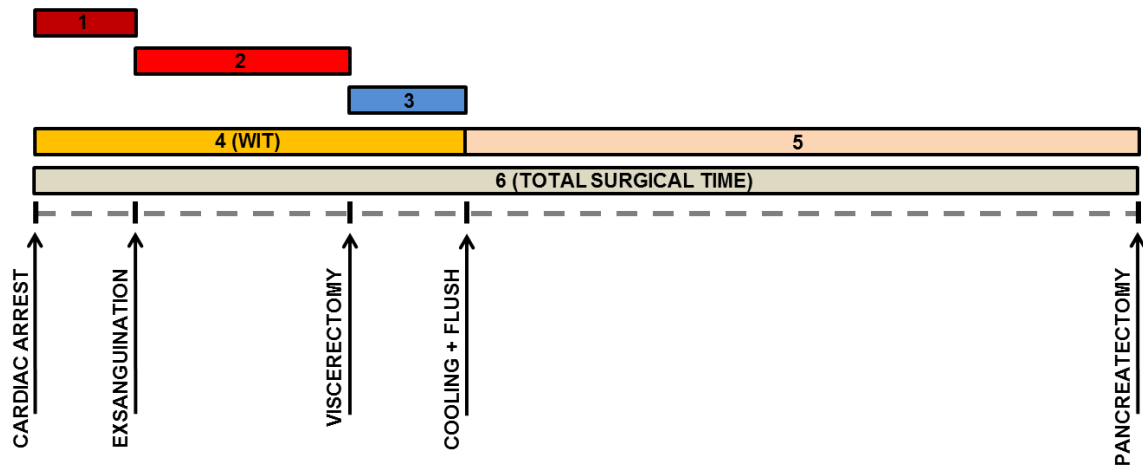


**Figure 3.1: Surgical Timeline.** Illustration depicting the relevant surgical times recorded during the porcine pancreas procurement. Time interval 4 marks the duration of time between cardiac arrest and the initiation of a cooling technique and is effectively the warm ischemia time (WIT). Time interval 6 represents the total pancreas preservation time.

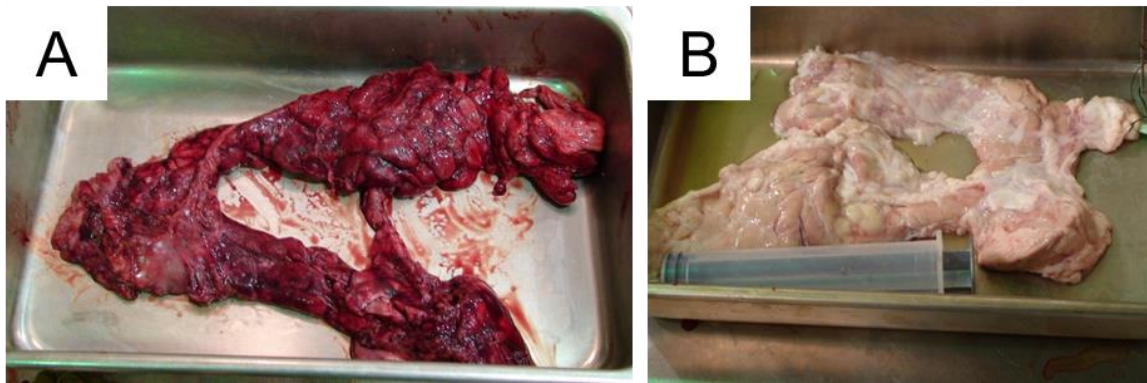


**Figure 3.2: Effects of heparinization.** Pictures of porcine pancreata illustrating the effects of (A) vascular blood clotting in a pancreas from a donor was not properly heparinized before euthanasia, and (B) minimal vascular clotting in the pancreas is observed when the donor is properly heparinized.

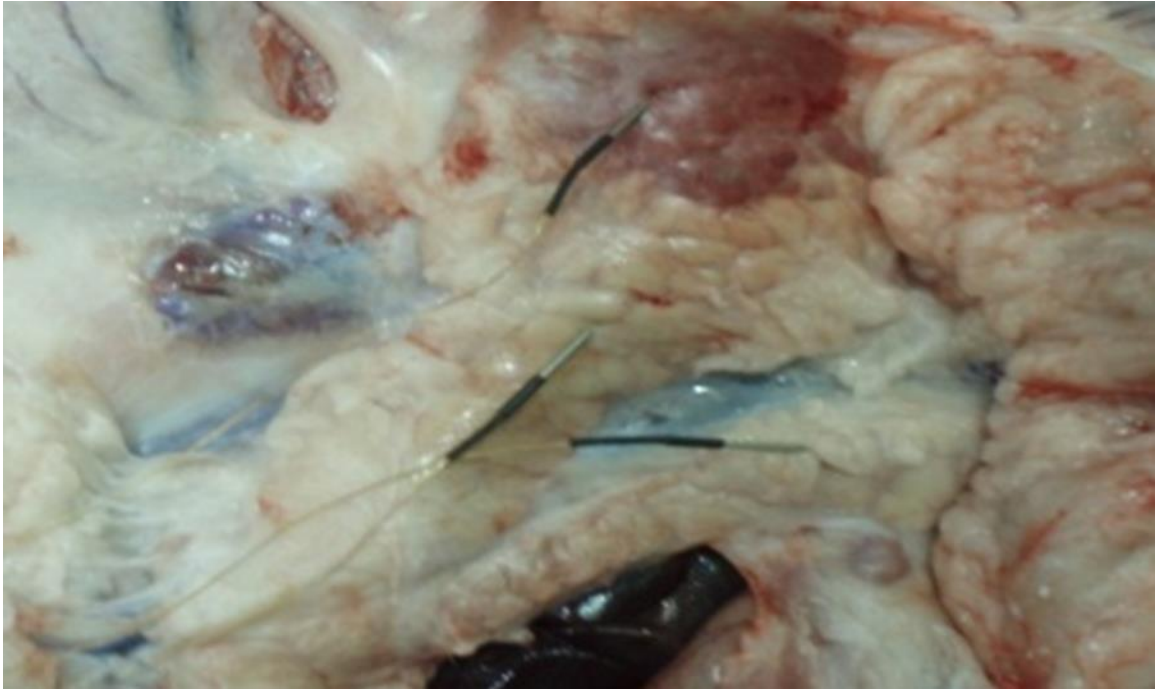


**Figure 3.3: Temperature probe placement.** Picture of needle temperature probes placed into a porcine pancreas during procurement. Probes were placed into the core of each lobe (duodenal, splenic and connecting) to monitor the temperature changes during procurements with different cooling methods.

## ***Results***

Donors had a mean age of  $22 \pm 2$  months (n=67) and a mean weight of  $505 \pm 10$  pounds (n=87), in those donors for which data was available. Mean time required to perform the en bloc viscerectomy was  $6.0 \pm 0.3$  minutes. Mean time to complete the arterial intravascular flush was  $31 \pm 1$  minutes. There were overall differences in the mean donor weight between Methods ( $p = 0.008$ ) and total procurement time ( $p < 0.001$ ), but no differences in the other metrics (Table 3.1). When comparing individual Methods, there were differences in the total procurement times between Method B1 and every other Method ( $p < 0.05$ ). This difference is likely explained by the increased time needed to ligate numerous lumbar arteries for organs procured using an arterial flush through the aorta (Method B1). This difference was not observed with Method B2 or D because these organs were primarily procured using direct intra-arterial flush via the CT and SMA. All other Methods took a statistically similar total procurement time ( $p > 0.05$ ). There were no differences in the recorded WIT between groups ( $p = 0.36$ ), and no difference when comparing Methods A and D ( $p = 0.50$ ), which represented the most different cooling methodologies.

The core temperature profiles were recorded for pancreata procured with each cooling Method and representative profiles are illustrated in Figure 3.4. The representative illustration was generated based on the actual data obtained from the recorded temperature profiles. Illustrative profiles were used to present this data because they accurately reflect the nature of the cooling observed with respect to the Method used. This interpretation of the data allows for direct visual comparison between cooling methods without the confounding differences that the organ variability introduces to the individual organ temperature measurements. Method A gradually decreased the core temperature over a 30 minute period. Method B decreased the organ temperature more rapidly than Method A. Method C decreased the core temperature of the pancreas rapidly ( $15\text{-}20$  °C during the first few minutes of cooling), but the rate of cooling

immediately slowed after completion of the intraductal infusion. Method D provided the most optimal cooling, including both rapid cooling in the first few minutes of the procurement and sustained cooling throughout the procurement.

When temperature data was used to calculate the average thermal energy removed during a 10 minute period and then standardized to a 350-gram pancreas, Method A removed an average of  $10 \pm 1.5$  kilojoules (KJ) of energy, which corresponded to a  $\Delta T$  of  $10^{\circ}\text{C}$ . Method B removed an average of  $18 \pm 2.8$  KJ of energy, corresponding to a  $\Delta T$  of  $22^{\circ}\text{C}$ . Method C removed an average of  $16.8 \pm 3.9$  KJ of energy, corresponding to a  $\Delta T$  of  $20^{\circ}\text{C}$ . Method D removed an average of  $34 \pm 4.8$  KJ of energy, corresponding to  $\Delta T$  of  $37^{\circ}\text{C}$ , and was the Method which provided the most rapid cooling (Figure 3.6). These calculations enabled more accurate comparisons between cooling Methods in the setting of confounding variables such as different starting core pancreas temperatures and organ masses.

Biopsies obtained from pancreata cooled with Method A exhibited moderate necrosis/autolysis, while biopsies from pancreata cooled with Method C exhibited mild necrosis/autolysis. Biopsies obtained from pancreata cooled with Method D exhibited the least (or minimal) necrosis/autolysis (Figure 3.7). Histological scores were overall different between the cooling Methods used ( $p=0.04$ ). When compared individually, there were differences in the histological scores between Methods A and C ( $p=0.03$ ) and Methods A and D ( $p=0.03$ ), but not between Methods C and D ( $p=0.91$ ) (Figure 3.9).



# Core Pancreas Cooling Profiles

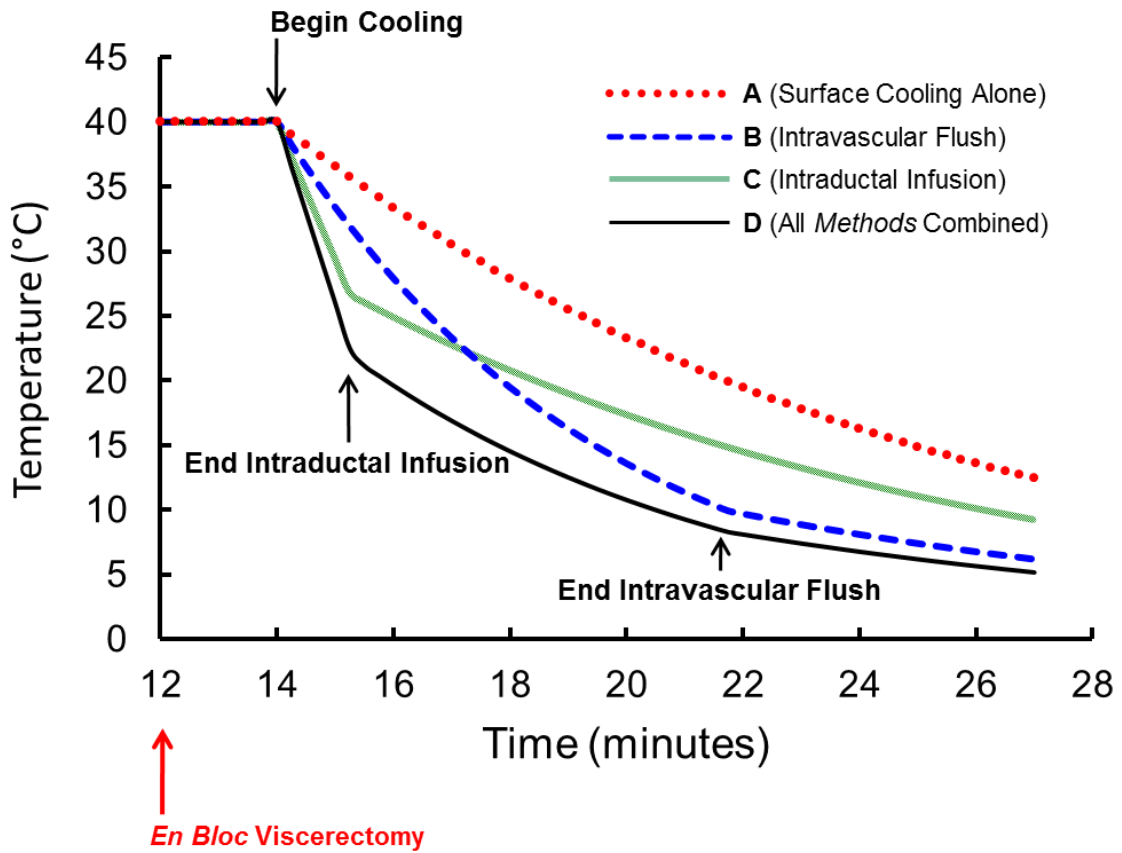


**Figure 3.4: Procurement cooling method profiles.** Illustration depicts the different core pancreas temperature profiles for each cooling *Method*: surface cooling alone (*Method A*, the current practice), intravascular (arterial) flush (*Method B*), intraductal infusion (*Method C*), and combined intravascular flush with intraductal infusion (*Method D*). Note the rapid cooling following an intraductal infusion of cold preservation solution (CPS), and the improved sustained cooling with an intravascular flush with CPS.

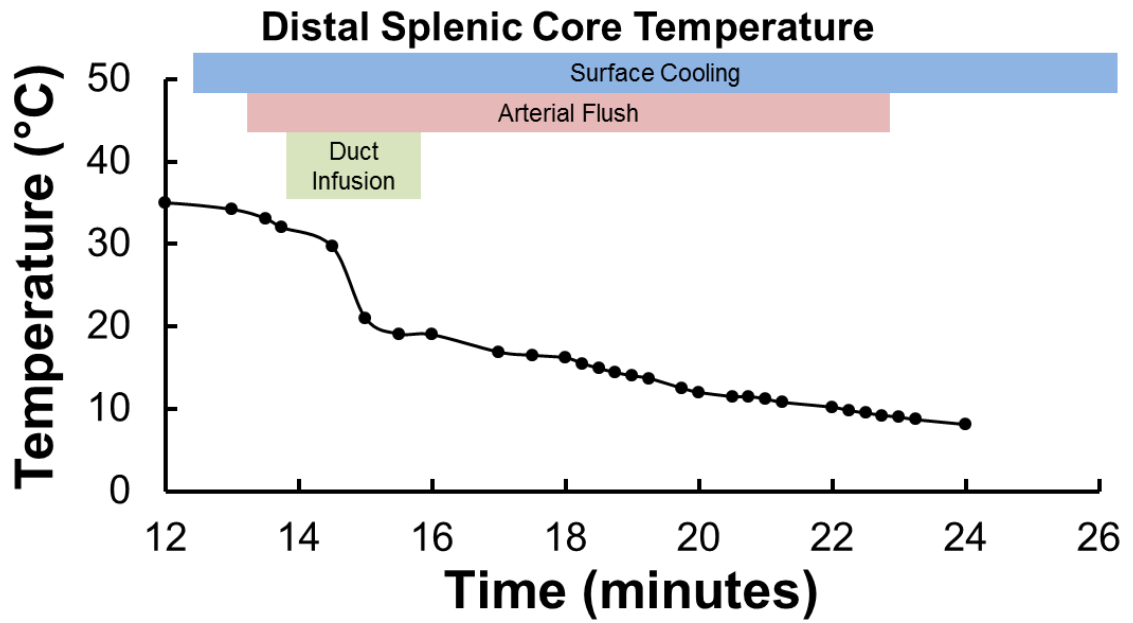


**Figure 3.5: Combined Method D temperature profile.** Representative core temperature measurements from the distal splenic lobe of a porcine pancreas cooled with Method D, which combines surface cooling with an arterial flush and a ductal injection.

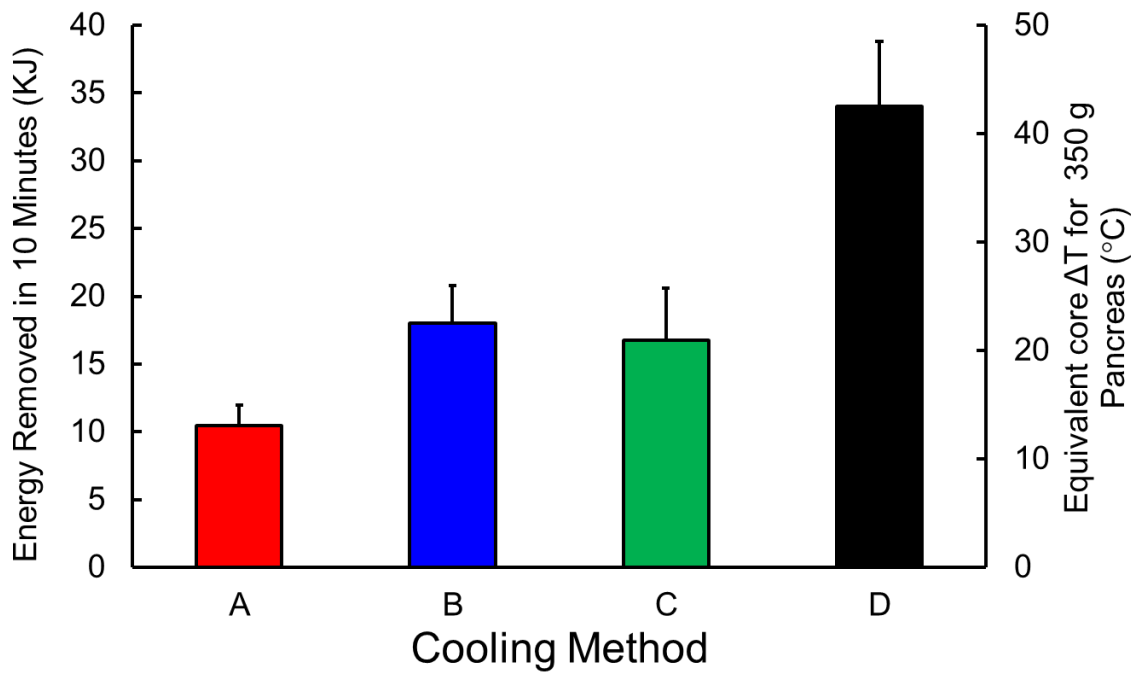


**Figure 3.6: Cooling method comparison.** Calculated average amount of energy removed and estimated core temperature drop ( $\Delta T$ ) during the first 10 minutes of cold ischemia time in a standardized 350-gram pancreas procured using surface cooling only (*Method A*, n=4), surface cooling and an intravascular flush (*Method B*, n=13), surface cooling and an intraductal infusion (*Method C*, n=4) and combined method with surface cooling, an intravascular flush, and an intraductal infusion (*Method D*, n=3).

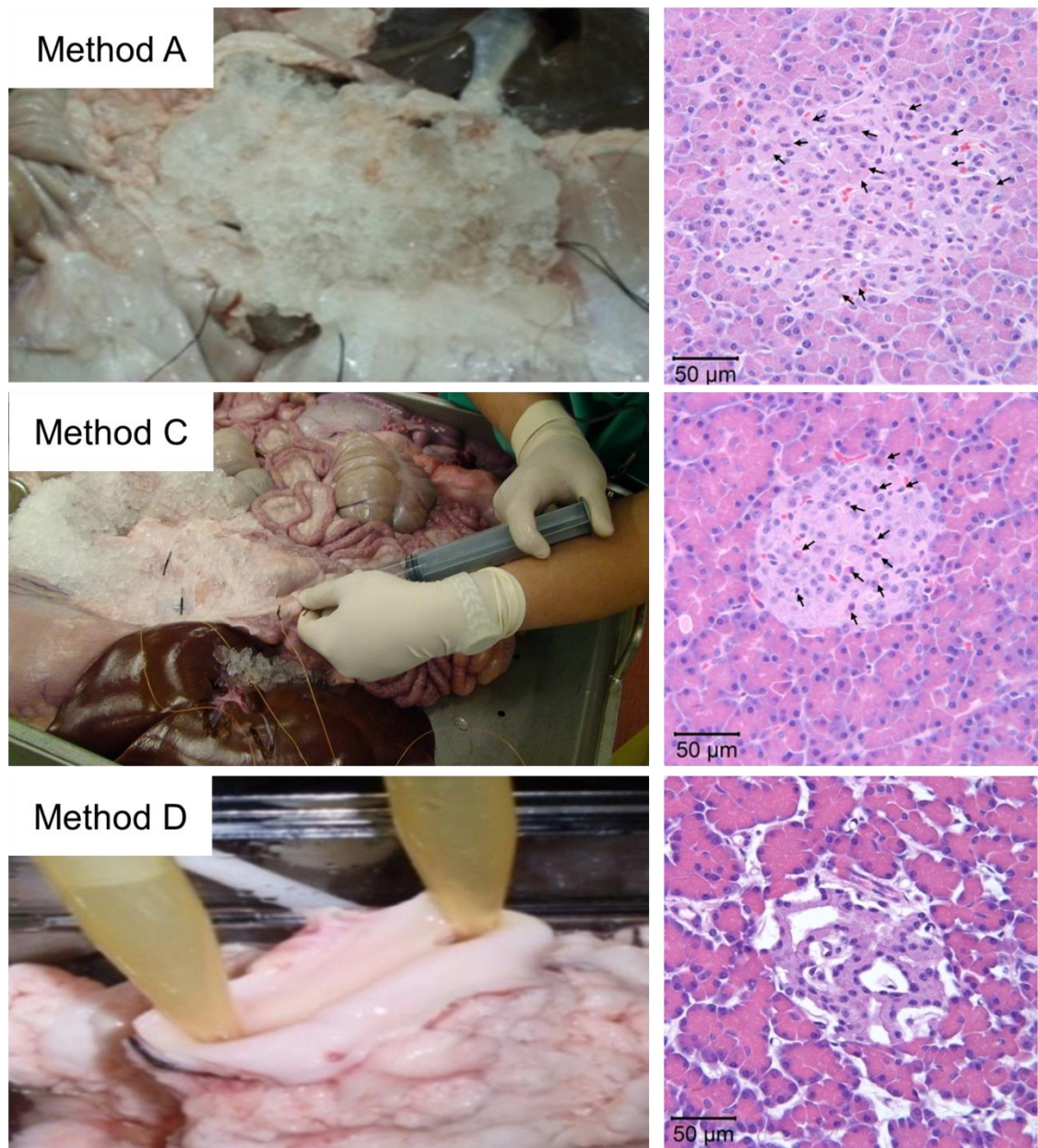


**Figure 3.7: Differences in histology sections.** Histology of biopsies taken from pancreata cooled by *Methods A, C* and *D*. Pancreatic tissue cooled using *Method A* exhibited moderate features of autolysis and many of the islet cells have partially condensed nuclear chromatin. Pancreatic tissue cooled using *Method C* showed mild autolysis, nuclear condensation or lysis and some islet cells exhibit cytoplasmic hyper-eosinophilia. Exocrine cells may present some pyknotic nuclei and cytoplasmic condensation. Pancreatic tissue cooled using *Method D* exhibited minimal autolysis. Very few of the islet cells appear exhibited cytoplasmic hyper-eosinophilia and nuclear pyknosis, and cell morphological details are more easily distinguishable with exocrine granules being well-preserved.

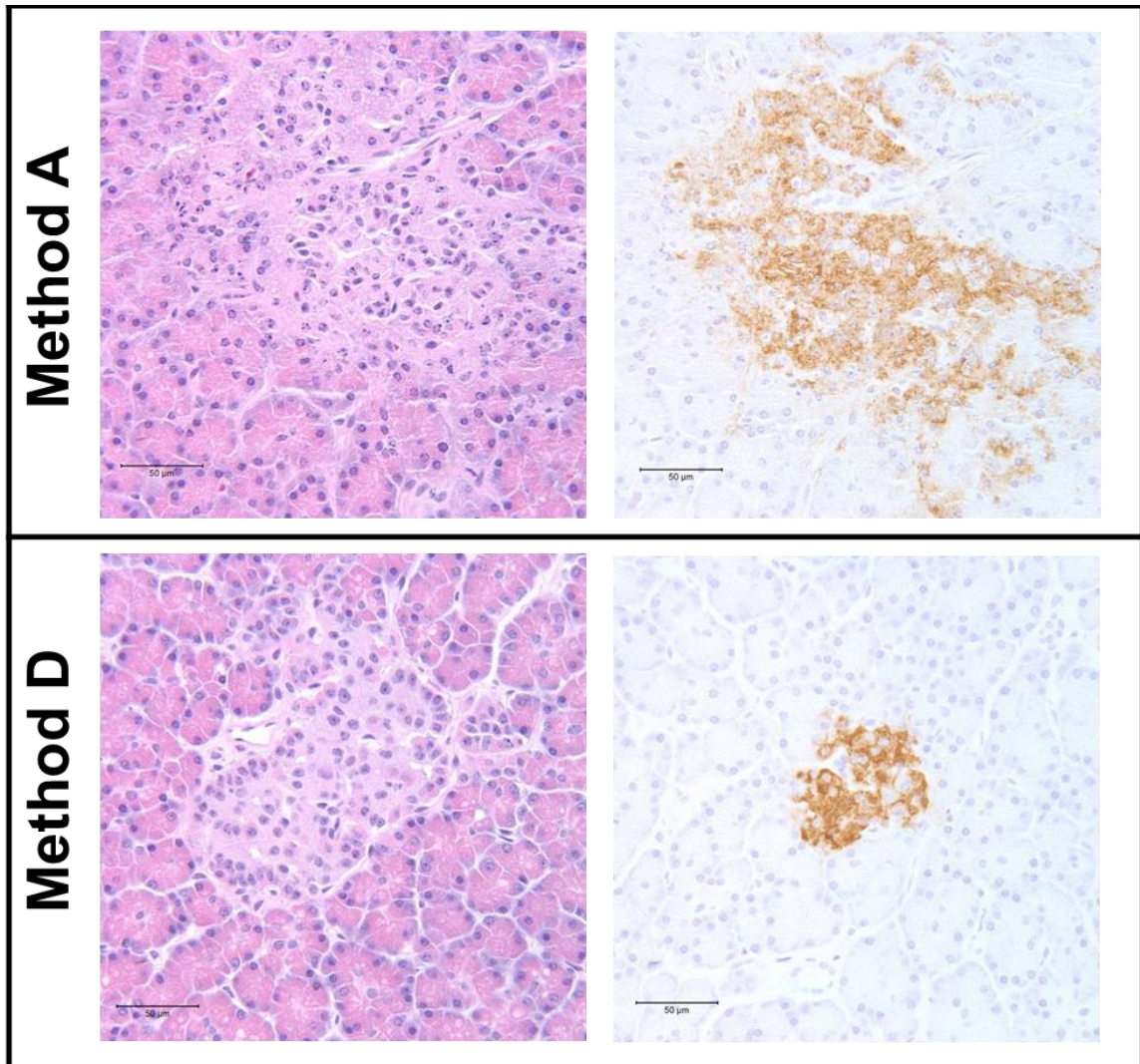


**Figure 3.8: Histology and insulin staining images.** Images of histological sections with hematoxylin and eosin stain (Left) and insulin stain (Right) of biopsies taken from a porcine pancreas. Images are from a pancreas cooled by Method A resulting in poorly-preserved regions of tissue (TOP) , and images from a pancreas cooled with Method D resulting in well-preserved tissue structures (BOTTOM).

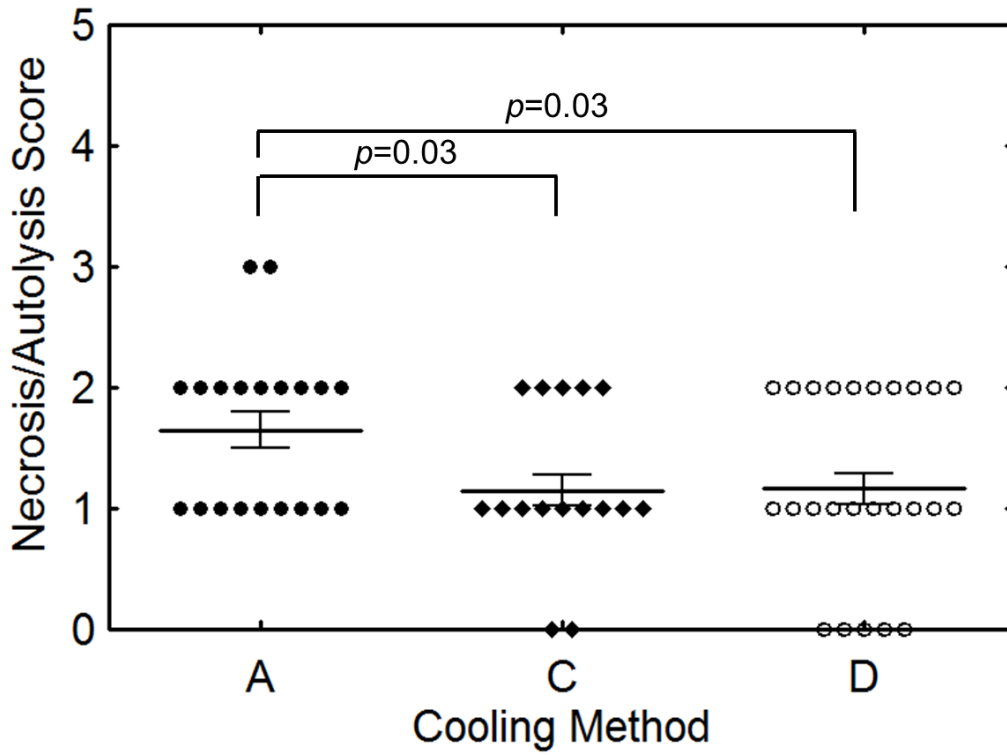


**Figure 3.9: Semi-quantitative histology comparison.** Plot of necrosis/autolysis scores from biopsies of pancreata cooled using *Methods A, C* and *D*. The scores were significantly worse in pancreata cooled only with surface cooling (*Method A*) as compared to pancreata cooled by intraductal infusion (*Method C*) or the combined approach (*Method D*). Lines and error bars represent the mean  $\pm$  standard errors.

**Table 3.1: Surgical procurement data**

	Cooling Method					p-value
	A	B		C	D	
		B1	B2			
Number	8	11	10	6	59	
Mean ( $\pm$ SE) donor weight (kg)	189.5 $\pm$ 14.3	206.9 $\pm$ 10.4	238.4 $\pm$ 18.4	215.6 $\pm$ 19.0	239.7 $\pm$ 5.3	0.008*
Mean ( $\pm$ SE) donor pancreas mass (g)	263.3 $\pm$ 30.1	371.9 $\pm$ 47.7	383.6 $\pm$ 66.1	234.0 $\pm$ 4.0	355.4 $\pm$ 20.0	0.358
WIT (min) <sup>a</sup>	11.7 $\pm$ 1.1	12.7 $\pm$ 2.6	10.8 $\pm$ 1.0	14.3 $\pm$ 2.1	13.0 $\pm$ 0.5	0.582
Procurement time (min) <sup>b</sup>	28.8 $\pm$ 1.8	39.4 $\pm$ 1.4	28.9 $\pm$ 3.0	24.6 $\pm$ 2.0	31.2 $\pm$ 0.9	< 0.001**

*Abbreviations:* SE, standard error (of the mean); WIT, warm ischemia time.

*Method A:* Surface cooling alone; *Method B1:* Arterial intravascular flush (supraceliac aorta); *Method B2:* Arterial intravascular flush (celiac trunk, superior mesenteric artery); *Method C:* Intraductal infusion; *Method D:* Combined method, including arterial intravascular flush and intraductal infusion.

<sup>a</sup>Traditional WIT defined as the duration of time from cardiac arrest to beginning of cooling intervention

<sup>b</sup>Defined as the duration of time from cardiac arrest to completion of pancreatectomy.

\* $p$ <0.05; \*\* $p$ <0.001

## ***Discussion***

Porcine islet xenotransplantation may offer an attractive alternative to human islet allotransplantation if an efficacious immunosuppressant protocol is developed<sup>35</sup> or if the xenoislets can be immunoisolated<sup>39</sup>. This would enable access to a practically-unlimited donor pancreas supply. Since the isolation procedure itself is expensive and time-consuming, optimizing isolation outcomes is imperative. Consequently, optimization of improved porcine pancreas procurement protocols is needed. There may be a substantial difference in the core organ temperature during procurement depending on the cooling method utilized, but also depending on the individual organ size (mass), shape, and condition. There were differences in the average pancreas mass in each group (**Table 3.1**), but these differences were not different between groups ( $p=0.36$ ), and are most likely explained by differences in donor mass or age. To effectively compare and interpret the efficacy of cooling methods, the heat removed during the first 10 minutes of cooling was calculated from the temperature data obtained for each individual organ. This calculation can account for the differences in the initial amount of thermal energy in each pancreas due to the observed variability in starting core pancreas temperature and organ mass. In this study, we found that additional cooling via the combination of an intravascular flush and an intraductal infusion of CPS reduced the core pancreas temperature much more rapidly than surface cooling alone. Surface cooling alone is incapable of quickly cooling a large organ (like a human or porcine pancreas). With surface cooling, heat transfer is very inefficient and highly variable, especially for larger organs since it relies on thermal diffusion from the surface of the organ. In many cases, it took as long as 30 minutes for a large pancreas to reach a core temperature of  $<15^{\circ}\text{C}$ . In these cases, the actual WIT is significantly underestimated. The deleterious effect of increased WIT on organ function following transplantation has been previously recognized<sup>40</sup>. Prolonged WIT has also been shown to be a critical factor affecting



successful islet isolation<sup>41</sup>. Tanioka *et al.* reported that periods of WIT >30 minutes result in significant reduction in islet yields and viability<sup>42</sup>.

Although variations in porcine pancreas anatomy and size can affect temperature profiles measured during and after procurement, we have demonstrated that intraductal infusion provided the most consistent and dramatic cooling during the first few minutes of the procedure and can be done quickly. Intraductal infusion was able to consistently cool the pancreas by >10°C during the first 2 minutes of cooling. As shown in Figure 1, a dramatic drop in core pancreas temperature was observed with both *Method C* and *Method D*. However, once the 60 mL of CPS was infused into the pancreatic duct, the rate of cooling was no better than with surface cooling alone. In contrast, the intravascular flush provided a sustained cooling of the pancreas throughout the duration of the procurement. When *Method C* was combined with intravascular flushing (*Method D*), core pancreas temperature could be reduced from 37°C to 15°C in 10 minutes. This dramatic improvement in cooling rate results from the substantial increase in the surface area available for heat transfer, which occurs with flushing CPS into the vasculature and instilling it into the ductal system. *Method D* leveraged both the immediate cooling of intraductal infusion and the sustained cooling of the intravascular flush without increasing the time of procurement when compared with *Method A* ( $p=0.31$ ). Detailed studies focused on the effects of pancreas size and shape on cooling method heat transfer would considerably improve our understanding of these methods, and could potentially suggest further optimized methods for improved organ cooling.

Other factors during procurement and beyond WIT may affect the success of subsequent islet isolation. Increased pancreatic edema has been shown to correlate with decreased islet yields for human islet isolation<sup>43</sup>. However, there is some conflicting evidence in the literature which suggests that some edema may improve islet recovery<sup>44</sup>. This may explain why the use of hypothermic machine perfusion (via the CT and SMA) has been associated with greater porcine

islet yields as compared to static cold storage<sup>45</sup>. We were concerned that flushing and instilling fluid into the pancreas may cause edema, which would be problematic. In our study, no obvious gross pancreatic edema was observed.

In addition to improved cooling, the intravascular flush, either via the supraceliac aorta or directly through the CT and SMA, appeared to completely clear the intravascular space of residual blood (see histology from pancreas cooled by *Method D* in **Figure 3.7**). When combined with adequate heparinization, the finding of intrapancreatic blood or clotting is unlikely. This is of particular importance for islet isolation, because the presence of intravascular thrombi within the pancreas has been shown to diminish islet yield<sup>46</sup>. The number of recovered islets following enzymatic digestion correlates inversely with the blood content in the porcine pancreas<sup>47</sup>.

Our results indicate that there is a correlation between the rate of core pancreas cooling and histological outcomes. Histological scores of the islet tissue sections were compared, and as expected, *Method A*, *C*, and *D* resulted in moderate, mild and minimal autolysis observed, respectively. The necrosis/autolysis score and necrosis/autolysis score per pancreas also inversely correlated with the rate of cooling, and there were differences between *Methods A* and *C* ( $p=0.02$ ) and *Methods A* and *D* ( $p=0.02$ ). Histological studies were not conducted for *Method B*, because of budgetary constraints and because differences between *Method C* and *D* could be in part attributable to the use of an intravascular flush with *Method D*. Interestingly, there were no differences in the necrosis and autolysis score when comparing samples cooled by *Methods C* and *D* ( $p=0.95$ ). This may suggest that the addition of a selective intravascular flush, though able to clear blood and facilitate sustained cooling of the organ, may provide less benefit as indicated by histology. This study compared the histological necrosis/autolysis score between *Methods* as an early indicator of tissue damage. Tissue biopsies were collected and fixed immediately following completion of the procurement and represent a snap-shot of the tissue quality up to the time of

tissue fixation. Although beyond the scope of this study, there may be further divergence in tissue quality following transplantation and reperfusion. However, the observation that combined cooling involving an intraductal infusion may have implications for human pancreas procurement, where an intraductal infusion is not standard practice but may be beneficial<sup>48,49</sup>.

Porcine DCD donors were used to compare cooling methods in this study, but the temperature profiles and energy calculation results can offer insights into cooling methods used for human DCD and donation after brain death (DBD) procurements. DCD organs are being utilized in higher numbers due to an increasing demand for donor organs and improved organ preservation. Enhanced organ cooling may enable even more higher-quality DCD organs to be used for islet isolation. Analysis of the temperature data suggests that it could be advantageous to include an intraductal infusion during human pancreas procurements. For solid pancreas transplant the benefits of the improved cooling would have to be weighed against the potential increased risk of contamination associated with cannulation of the pancreatic duct. For human islet isolation, ductal cannulation is already necessary for the infusion of enzyme, therefore, the added risk of bacterial contamination may be minimal. In these studies, the risk of contamination is reduced during the cannulation of the duct by avoiding an enterotomy.

Improved cooling results in better porcine islet yields and quality, and these results (from a subset of pancreata studied herein) have been published previously<sup>39</sup>. It was reported that when pancreata were cooled with both intravascular flush and intraductal infusion, purified islet yields, and the number of islet equivalents per gram pancreas increased by >150% compared to surface cooling alone. The fractional viability (measured by the oxygen consumption rate normalized to DNA content) of islets after 7 days in culture was also significantly improved for pancreata procured using combined cooling. The rapid, early cooling resulting from using an intraductal infusion may have an effect on islet isolation outcomes<sup>48-51</sup>. Noguchi *et al.* found that islet yields

were improved, islet apoptosis was reduced and ATP levels in the pancreatic tissue were higher in human pancreata procured with an intraductal infusion prior to cold storage<sup>51</sup>. Similarly, Matsumoto *et al.* reported that islet yields and quality were higher in those human pancreata undergoing an intraductal infusion<sup>48</sup>. In contrary, Nakanishi *et al.* showed no improvement in rat islet yield and quality<sup>49</sup>, which highlights that the greatest benefit of an intraductal infusion may be with larger (human or porcine) pancreata. Cold ischemia time (CIT) is a factor that impacts islet yield after isolation<sup>43</sup>. In the present study, CITs recorded for pancreata selected for islet isolation<sup>38</sup> were found to be comparable with CITs recorded for all pancreata cooled by *Methods A, C or D* of this study (data not shown).

## ***Conclusion***

In conclusion, using a combined cooling method (*Method D*) can consistently cool the core of the pancreas, in sharp contrast to standard surface cooling alone (*Method A*) which is ineffective at rapidly reducing the core temperature in DCD porcine pancreata and resulted in poorer histological outcomes. In our study, intraductal infusion improved initial organ cooling, but is limited by the volume of CPS that can be used and does not contribute to sustained organ cooling. Alternatively, an intravascular flush can be performed continuously and should be done as it provides sustained cooling during the entire duration of the procurement. Combined surface, intravascular and intraductal cooling, appears to be the optimized and most consistent cooling *Method*. These data also may have implications on human pancreas procurement since intraductal infusion of CPS is not common practice, and should be studied further.

## Chapter 4 HYPOTHERMIC MACHINE PERFUSION TO IMPROVE ORGAN PRESERVATION

Sections of this chapter are reproduced in whole, or in part from the following publications with permission:

**Weegman BP**, Taylor MJ, Baicu SC, Scott WE 3rd, Mueller KR, Kitzmann JP, Rizzari MD, Papas KK “Hypothermic Perfusion Preservation of Pancreas for islet grafts: validation using a split Lobe Porcine Model.” Cell Medicine: part B Cell Transplantation, January 2012

License and agreement documentation is included in **Appendix G**.

**Acknowledgements:** The authors would like to thank the Schott Foundation, the Minnesota Lions Diabetes Foundation, the Juvenile Diabetes Research Foundation (JDRF 5-2013-141), Giner Inc., the Schulze Diabetes Institute, and the NIH (P41 EB015894, and S10 RR025031) for supporting this research. We gratefully acknowledge Dr. Henk Schuurman for his critical reading of the manuscripts. This work was funded in part by a grant from the NIH (R44DK076326), the National Center for Research Resources (U42 RR016598), National Institutes of Health (NIH), National Institute of Diabetes and Digestive and Kidney Diseases (R43 DK070400), the Schott Foundation, and the Carol Olson Memorial Diabetes Research Fund. We would also like to thank Dr L. Guenther and Dr T. Tanaka for help with early technique development; K. Albeck for technical assistance and manufacturing preservation containers; B. Perrault for surgical assistance; and Dr. K.S. Maynard, D. Duderio, G. Wildey, M.L. Graham, L. Mutch, and H. Nelson for administrative assistance.

## **Hypothermic Perfusion Preservation of Pancreas for islet grafts: validation using a split Lobe Porcine Model**

### ***Summary***

HPP is being investigated for extended pancreas preservation in light of the beneficial effects reported for other organs. The present pilot study aimed to establish the potency of porcine islets isolated from pancreata after 24-hour of HPP at 4-8°C. The study design included a split-lobe pancreas model that permitted paired comparisons of islets isolated from 24-hour HPP splenic lobes with non-perfused, fresh control duodenal/connecting lobes stored at 4°C for <3h. Prior to transplantation, islet viability was assessed in vitro using the ratio of oxygen consumption rate to DNA (OCR/DNA) assay and correlated with subsequent in vivo function by transplantation in diabetic immunodeficient mice. The OCR/DNA (mean  $\pm$ SD) measured after 7 days culture and immediately prior to transplantation for islets from the 24-hour HPP group was  $269 \pm 19$  nmol/min/mg DNA, which was higher but not statistically different to the mean of  $236 \pm 43$  for the counterpart control group. All four nude mice transplanted with islets from the 24-hour HPP group showed diabetes reversal, compared with 5 of 6 transplants from the control group. In conclusion, islets isolated from adult porcine pancreata after 24-hour HPP exhibited high viability as measured by OCR/DNA and were able to consistently reverse diabetes in a nude mouse bioassay.

## ***Introduction***

The field of islet transplantation for the treatment of Type I diabetes is currently in the phase of clinical trials at several centers around the world<sup>52,53</sup>. The growing recognition that islet transplantation is becoming a viable proposition for clinical therapy has led to an increasing demand for high quality islets for both research and clinical procedures. Moreover, the potential for xenotransplantation to relieve the demand on an inadequate supply of human pancreases will also depend upon the efficiency of techniques for isolation of islets from alternative sources, of which the pig is highly favored for a number of compelling reasons<sup>54</sup>. Islets are highly vulnerable to irreversible damage after prolonged ischemia, in part because they do not possess the enzymatic machinery necessary (LDH $\alpha$ ) for ATP generation under anaerobic conditions<sup>55-61</sup> and cold ischemia of the cadaveric pancreas is detrimental to islet yield<sup>62-67</sup>. In vitro studies have shown a significant reduction in insulin release in response to a glucose challenge even after short periods of conventional static cold storage in UW solution<sup>63</sup>. These observations have been seen in clinical practice as there have been no reports of successful single-donor islet transplants with prolonged cold storage beyond 10 hours, which is still regarded as the safe limit of cold ischemia<sup>64</sup>. Furthermore, Ryan et al have provided evidence of the detrimental impact of cold ischemia on post-transplant islet function<sup>68</sup>.

In light of the recent resurgence of clinical interest in hypothermic perfusion preservation (HPP) of organs, notably for marginal and expanded criteria organs<sup>28</sup> we have recently applied the state-of-the-art technology to pancreas perfusion as a prelude to islet isolation<sup>44,69</sup>. It was recently reported that, by comparison with conventional static cold storage, hypothermic machine perfusion preservation allows safe storage of juvenile pig pancreases for 24 hours with excellent in vitro structure and function of islets isolated from the perfused pancreata. The present study reports the outcome of a pilot study to validate these in vitro findings using expanded quality

assessment including oxygen consumption rate (OCR) analysis<sup>25-27</sup> and in vivo transplantation in immunodeficient “nude” mice.



## ***Materials and Methods***

### ***Experimental Design***

This study was designed to validate, in an adult pig model, the recent findings of Taylor et al<sup>44,69</sup> concerning the functional integrity of islets prepared from the pancreata of juvenile pigs after 24-hour HPP. To this end, the study assessed the outcome of 10 nude mouse transplants using islets derived from 3 adult pig pancreas perfusions compared with 3 paired fresh islet isolations. This was achieved using our previously established split-lobe porcine pancreas model as described below<sup>38</sup>.

### ***Procurement***

Pancreata were procured from adult (1-2 years old) Landrace pigs using a deceased after cardiac death DCD donor model involving total viscerectomy followed by en bloc pancreatectomy. All animal care and handling complied with policies and approval of the Institutional Animal Care and Use Committee (IACUC) of the University of Minnesota. Following procurement, the pancreas was divided into two segments for use in paired isolation outcomes. The first segment consisted of the connecting and duodenal lobes<sup>38</sup>, which were processed for islet isolation with the least cold ischemia time (CIT) possible (< 3 hours). The second segment consisted of the splenic lobe procured with the entire vascular network which was then prepared for HPP according to the technique of Taylor and Baicu<sup>44,69</sup>. The splenic lobe was selected for perfusion, as this lobe in contrast to the connecting and duodenal lobes has the vasculature available for perfusion. In our experience with porcine islet isolation, the yields and quality of islets are similar for the connecting, duodenal and splenic lobes, so that a different outcome based on differences in lobes is not expected.

### ***Perfusion***

Both the splenic artery and the celiac trunk attached to the splenic lobe were cannulated using a SealRing™ cannula (10mm x 35mm. Organ Recovery Systems, Itasca, IL) and connected to a LifePort® Kidney Transporter pulsatile perfusion machine (Organ Recovery Systems, Itasca, IL) as described previously<sup>44,69</sup>. All arterial vessel leaks were identified and ligated. The lobe was then perfused for 24 hours with a systolic pressure of 10mmHg, while the pancreas was immersed in cold perfusion solution (KPS-1, Organ Recovery Systems) controlled between 4-8°C.

#### Islet Isolation, Purification and Culture

Islets were isolated from both segments of each pancreas using identical conventional techniques involving collagenase digestion in a modified Ricordi chamber (BioRep Technologies, Miami, FL) as previously described<sup>33,44</sup>. In brief, the pancreas segment was chopped into pieces and digested at 35-37 °C using Liberase MTF enzyme (Roche, Indianapolis, IN) at a concentration of 150-167 µg/ml. Islets were purified after isolation using established standard continuous Ficoll gradient separation with a COBE 2991 (Gambro BCT, Lakewood, CO). After purification, islets were cultured between 4 and 12 hours and then assessed using OCR and DNA quantitation<sup>25-27</sup>. Subsequently, islets were cultured in ME199 media at 37°C, for 7-8 days. After the culture period, islets were again assessed using OCR and DNA quantitation as well as gross morphology using dithizone staining. Aliquots were taken for mouse transplants at this time.

#### Islet OCR/DNA

Islet viability was assessed by measuring the OCR/DNA of the purified islets using a sealed chamber fiber optic oxygen sensing system (Instech Labs, Newton, MA) as described elsewhere<sup>25-27</sup>. For this analysis, 5,000 islet equivalents (IE) were allocated immediately after purification and again after 7 days of culture. Islets were suspended in a non-supplemented, nutrient rich ME199 and sealed in stainless steel chambers. The oxygen partial pressure inside the chamber was recorded and the consumption rate was calculated based on the rate of oxygen

depletion from the chamber. The DNA quantity in each chamber was determined using the Quant-iT Picogreen dsDNA kit (Molecular Probes, Eugene, OR).

#### Islet morphology

Islet samples stained with dithizone for counting were also scored for morphology on a 10-point scale. The total score was calculated by summing 5 categories, each evaluated on a 2-point scale: 1) shape (3D), with more points awarded to more spherical islets; 2) border (2D), with more points awarded to well-rounded islets; 3) integrity, with more points awarded to more solid/compact islets; 4) presence of single cells, with more points awarded to preparations with less single cells; 5) diameter, with more points awarded for larger diameter islets.

#### Nude Mouse Bio-Assay

Diabetes was induced in nude mice using a 240 mg/kg dose of streptozotocin injected intravenously, following recommendations of the Clinical Islet Transplant (CIT) consortium regarding procedures for the mouse bioassay in testing human islet cell preparations (150-240 mg/kg)<sup>70</sup>. The mice were confirmed diabetic after blood glucose levels were maintained above 500 mg/dL for 2 days. Islets were then transplanted beneath the kidney capsule and distributed along the surface of one side of the kidney. Diabetes is considered to be reversed when blood glucose measurements were less than 200 mg/dL on two or more consecutive days. After about 4 weeks the grafts were explanted by nephrectomy to ensure that blood glucose levels in animals that had diabetes reversal returned to diabetic levels. Two mice were transplanted with 2000 IE after seven days in culture for each pancreas lobe with the exception of the last splenic lobe due to a sub-critical mass of islets surviving at 7 days to justify transplantation. A total of 10 mice were transplanted, 4 with islets from 24-hour HPP lobes and 6 with islets from controls.

## ***Results and Discussion***

Islet yields (<1000IEQ/g) were typically lower than our experience previously for the adult pig model. This is attributed, in part, to the decision to switch to the new Liberase MTF enzyme preparation, to conform to current clinical practice and the phasing out of the Liberase PI product used in prior studies. Moreover, this pilot study was undertaken before the optimal concentration of Liberase MTF was determined for this model on the basis that the study design included internal controls for each pancreas by virtue of the split-lobe model. The mean ( $\pm$ SEM) yields from the control and the 24-hour HPP were not statistically significantly different (see **Table 4.1**;  $p = 0.4$ ) in the small population of tests in this pilot study. Furthermore, as shown in **Table 4.1**, the purity and yields of islets were more than adequate to satisfy the principal objective of this pilot validation study by allowing measurement of viability based on OCR/DNA and in vivo islet function based on transplantation outcome in mice and a paired comparison of these parameters between experimental perfused lobes and non-perfused controls.

With respect to viability assessed by the OCR/DNA assay, **Table 4.1** shows that the OCR/DNA value of islets at day 7 was comparable between the groups and that the pre-transplantation OCR/DNA values all exceeded the acceptable threshold of 175 nm/min/mg DNA currently used as a release criterion for transplantation of porcine islets in non-human primates<sup>71</sup> (Papas et al unpublished observations). **Figure 4.1** further shows the averaged OCR/DNA data for the two groups immediately after isolation and after 7 days of culture. In both cases, there was no statistically significant difference between the 24-hour HPP islets and the controls. Moreover, **Figure 4.1** shows that the freshly isolated islets from both groups demonstrated mean OCR/DNA ratios >100 nm/min/mg DNA but failed to meet the pre-determined “release criteria” derived in earlier studies for correlating the OCR/DNA index with transplantation outcome. In sharp contrast, islets from both groups exceeded this threshold after 7-days culture. This is actually

reflecting the clearance of dead tissue (DNA) originally present post-isolation and reflected in less than 100% IE recovery. Culture clears dead islet tissue (that did not survive the isolation process) while viable tissue is maintained therefore viability (OCR/DNA) increases. Most importantly, the recovery and viability of islets from the 24-hour HPP pancreata, which was not significantly different to controls, was further corroborated by the transplantation outcome as shown in **Figure 4.2**. Here the individual and mean data for the nude mice transplants shows that all 4 mice receiving islets of the HPP group reversed diabetes: the efficacy of the islets was proven by the return to the diabetic state after graftectomy. Mice receiving islets from the control group showed diabetes reversal in 5 out of 6 cases.

Islets are highly sensitive to ischemia such that various modes of pancreas preservation are currently under investigation. It is generally assumed that using conventional preservation media, pancreata do not survive periods of 24-hour cold ischemia with insufficient yields in islet manufacturing. The present results give a strong indication that 24-hour HPP provides sufficient protection for adult porcine pancreata so that islets in sufficient quantity and of high quality can be prepared. 24 hours HPP of adult porcine pancreas yielded high quality islets with a robust in vitro viability (based on OCR/DNA) that was equal to non-perfused fresh controls and exceeded the established threshold set as a release criterion for transplantation in non-human primates. The in vivo functional quality of the islets derived from 24-hour HPP pancreas was sufficient to reverse diabetes consistently in a nude mouse bioassay. Hypothermic perfusion preservation (HPP) is now favored as the method of choice for clinical kidney preservation when applied to marginal or expanded criteria organs that have suffered a warm ischemic insult<sup>28,72</sup>. HPP is also under investigation for pancreas preservation and this study set out to validate recent findings that 24-hour HPP is tolerated in a porcine model<sup>44,69</sup>.

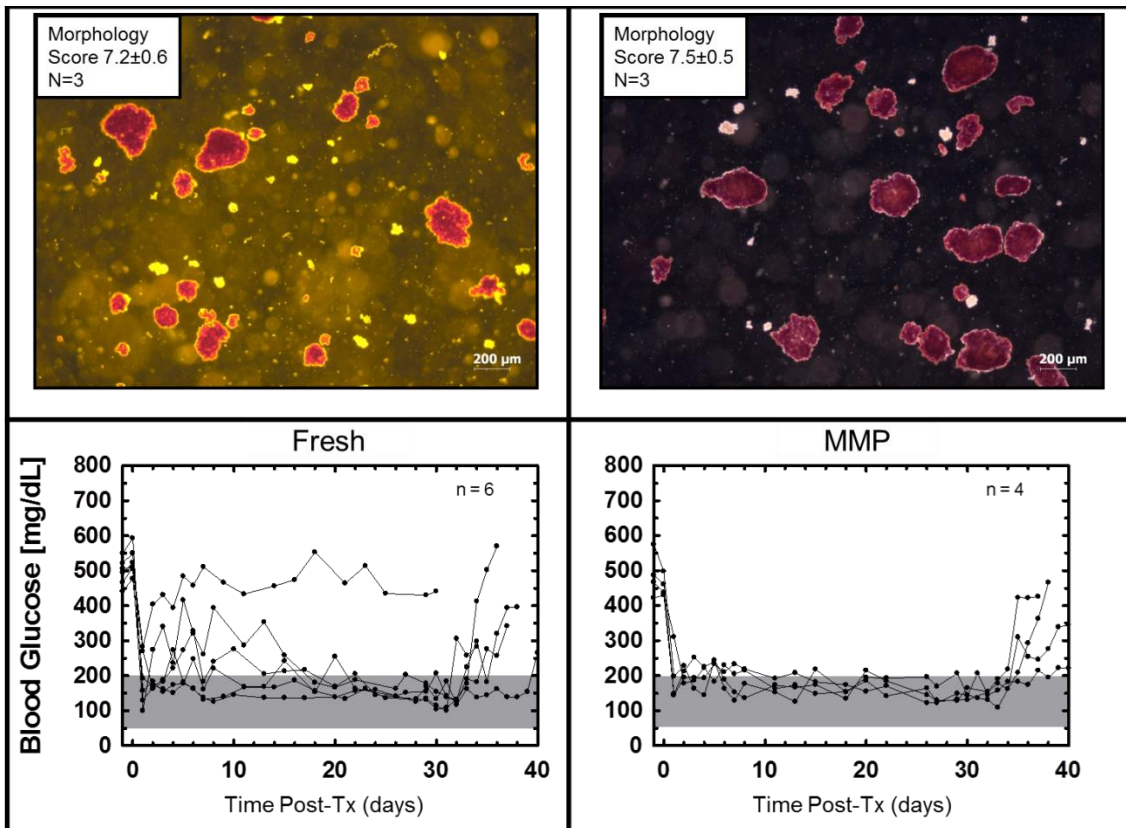


**Figure 4.1: Morphology and function of transplanted islets.** Upper panels show brightfield micrographs of dithizone-stained islet aliquots immediately prior to transplantation: Panel A shows representative islets from the control group which was assigned a mean morphology score of  $7.2 \pm 0.6$  ( $n=3$ ); Panel B shows islets from the HPP group with a mean morphology score of  $7.5 \pm 0.5$  ( $n=3$ ). Lower panels show individual blood glucose levels for mice transplanted on Day 7 for each condition. The number of animals in which diabetes was reversed is indicated. In animals that reversed diabetes after islet transplantation, the effect of the transplant was proven by graftectomy 4 weeks after transplantation followed by an increase in blood glucose confirming the diabetic state.

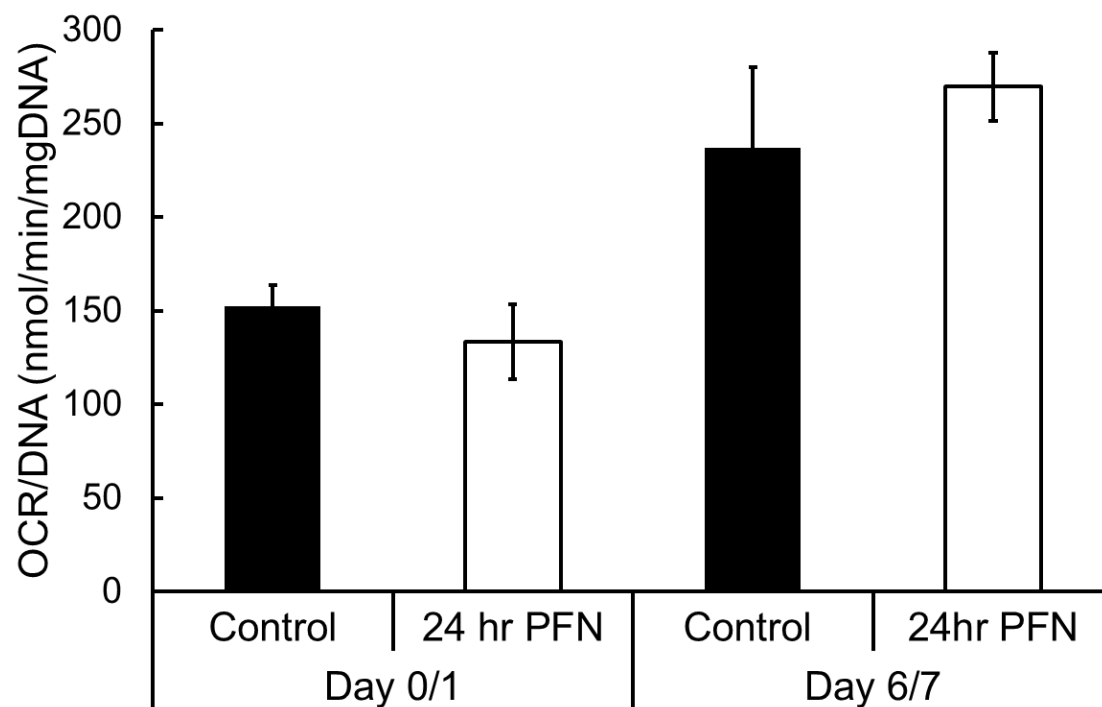


**Figure 4.2: Average OCR/DNA.** OCR/DNA of isolated porcine islets by condition for Day 0/1, and Day 7. Error bars represent the standard error of the mean.

**Table 4.1: Islet Isolation and Quality Control (QC) Data**

Pancreas	Lobe	IEQ/g	Purity %	Day 7 Recovery (%)*	Pre-transplant (Day 7) OCR/DNA (ng/min/mgDNA)
1	Conn/Duod (Control)	592	90	61	269
	Splenic (24-hr HPP)	128	95	57	279
2	Conn/Duod (Control)	661	95	27	187
	Splenic (24-hr HPP)	721	90	88	248
3	Conn/Duod (Control)	858	85	56	253
	Splenic (24-hr HPP)	497	90	63	281

IEQ, islet equivalent; OCR, oxygen consumption rate; conn, connecting lobes; duod, duodenal lobe; HPP, hypothermic perfusion preservation.  
\*Based on IEQ/DNA



**DEVELOPMENT OF METHODS AND TECHNIQUES**  
**FOR IMPROVING ISLET ISOLATION, CULTURE**  
**AND SHIPMENT**

## Chapter 5 JUVENILE PORCINE ISLET CULTURE

Sections of this chapter are reproduced in whole, or in part from the following publications with permission:

Manuscripts in Preparation:

**Weegman BP**, Taylor MJ, Baicu SC, Mueller KR, O'Brien TD, Wilson J, Papas KK, "Plasticity and Aggregation of Juvenile Porcine Islets in Modified Culture for Xenotransplantation: Preliminary Observations." In Press, December 2015

License and agreement documentation is included in **Appendix G**.

**Acknowledgements:** The authors would like to thank the Schott Foundation, the Minnesota Lions Diabetes Foundation, the Juvenile Diabetes Research Foundation (JDRF 5-2013-141), Giner Inc., the Schulze Diabetes Institute, and the NIH (P41 EB015894, and S10 RR025031) for supporting this research.

We thank William G. Purvis and Jennifer P. Kitzmann for graphical and editorial assistance and Samuel A. Stein for technical assistance with MRI imaging. This work was supported by the NIH, National Institute of Diabetes and Digestive and Kidney Diseases Grant Numbers R01DK068717 and R44 DK070400, as well as The Carol Olson Memorial Diabetes Research Fund, The Iacocca Foundation, and The Schott Foundation.

The authors acknowledge Kurt Albreck of Donovan Specialties (Osseo, Minn), Denice Dudero, Laurie Macleod, Dr Kristen Maynard, Heather Nelson, William E. Scott III, and Christine Vincent from the Diabetes Institute for Immunology and Transplantation at the UMN.

The research described here was supported in part by grants from US National Institute of Health (R44DK065508-02 - MJT, R44 DK076326-0 & 5 R44DK076326-03- MJT, and R44DK069865 - JW) and The Richard M. Schulze Family Foundation. The authors gratefully acknowledge the assistance of Elizabeth Greene with the preparation of the figures, and Dr. Melanie Graham with the analysis of the nude mouse bioassay results.

## **Plasticity and Aggregation of Juvenile Porcine Islets in Modified Culture for Xenotransplantation: Preliminary Observations**

### ***Summary***

Diabetes is a major health problem worldwide and there is substantial interest in developing xenogeneic islet transplantation as a potential treatment. The potential to relieve the demand on an inadequate supply of human pancreata is dependent upon the efficiency of techniques for isolating and culturing islets from the source pancreata. Porcine islets are favored for xenotransplantation, but mature pigs (>2 years) present logistic and economic challenges and young pigs (3-6 months) have not yet proven to be an adequate source. In this study, islets were isolated from 20 juvenile porcine pancreata (~3 months; 25 kg Yorkshire pigs) immediately following procurement, or after 24 hours of hypothermic machine perfusion preservation. The resulting islet preparations were characterized using a battery of tests during culture in silicone rubber membrane flasks. Islet biology assessment included oxygen consumption, insulin secretion, histopathology and *in vivo* function. Islet yields were highest from HMP preserved pancreata (2242±449 IEQ/g). All preparations comprised a high proportion (>90%) of small islets (<100 µm), and purity was on average 63±6%. Morphologically, islets appeared as clusters on day-0, loosely disaggregated structures at day-1, and transitioned to aggregated structures comprising both exocrine and endocrine cells by day-6. Histopathology confirmed both insulin and glucagon staining in cultures and grafts excised after transplantation in mice. Nuclear staining (Ki67) confirmed mitotic activity consistent with the observed plasticity of these structures. Metabolic integrity was demonstrated by oxygen consumption rates = 175±16 nmol/min/mg DNA and physiological function was intact by glucose stimulation after 6-8 days in culture. *In vivo* function was confirmed with blood glucose control achieved in nearly 50% (8/17) transplants. Preparation and culture of juvenile porcine islets as a source for islet transplantation requires specialized conditions. These immature islets undergo plasticity in culture and form fully

functional multi-cellular structures. Further development of this method for culturing immature porcine islets is expected to generate small pancreatic tissue-derived organoids termed “pancreatites” as a therapeutic product from juvenile pigs for xenotransplantation and diabetes research.

## ***Introduction***

A recent report on worldwide markets and emerging technologies for tissue engineering and regenerative medicine emphasizes the alarming statistics concerning the rapidly growing worldwide problem of Diabetes as an estimated 366 million cases that will be diagnosed in the next 20 years<sup>73</sup>. Type 1 diabetes accounts for 5-10% of all diagnosed cases but 27% of Type 2 diabetes also require insulin. Therefore, about a third of all diabetics could potentially benefit from a cell-based therapy that restores insulin production, particularly one that is minimally invasive such as isolated islet infusion into a heterotopic site (especially if this can be accomplished without the need for systemic immunosuppression). This situation clearly demonstrates a major clinical/commercial impact for new technologies that provide desperately needed improved methods of pancreas preservation to produce better yields of high quality islets.

Ever since the first experimental attempts to ameliorate Type 1 diabetes by transplantation of allograft donor islets the field has been challenged by the need for improved methods of retrieving and/or obtaining islets from donor pancreata. There is a considerable worldwide effort to further develop the concept for treating Type 1 diabetes by transplanting islets, but clinical application of the techniques developed in animal models is fraught with many challenges. The source of the islets remains a primary concern, and isolation from donor pancreata demands resolution of questions concerning the source, supply, and condition of the donor organs. Reliance upon an adequate supply of human organs for this purpose is considered limited, such that alternative sources are actively being sought<sup>74,75</sup>.

Various mammals are considered potential candidates for xenogeneic islet transplantation. Of these, pigs are considered the donor species of choice for xenogeneic islet transplantation for a number of compelling reasons. Pigs share many physiological similarities to humans and porcine insulin has demonstrated clinical efficacy for many years. Pigs are raised as a food source and

provide an ethical source of donor islets by being housed in a controlled environment to ensure safety for porcine islet xenotransplantation<sup>33,76</sup>. However, experiences in many laboratories over the past decades show that isolation of porcine islets appears to be more difficult<sup>54,77-80</sup> compared with the isolation of human<sup>81</sup>, bovine<sup>82</sup>, or rodent islets<sup>83</sup>. For example, porcine islets are less compact and tend to fragment during the isolation procedure and during prolonged periods of in vitro culture<sup>84,85</sup>. Moreover, the age, and even the strain, of the donor pig has been documented by several groups to markedly influence the islet isolation process, with young, so-called market size pigs ( $\leq 6$  months old) proving to be particularly difficult as a source of transplantable islets<sup>80,85-88</sup>. Islets from adult pigs ( $> 2$  years old) offered higher yields, and retained better morphology during the isolation process and culture, in association with higher functional properties after transplantation<sup>87</sup>. Despite the challenge encountered by many groups attempting to isolate islets from young pigs, donor pigs of market weight ( $< 50$  kg  $\leq 6$  months old) are preferred to retired breeders ( $> 200$  kg  $\geq 2$  years old) due to their abundance and relative cost efficiency with lower animal and husbandry costs. They are much easier to handle than  $> 200$  kg adults and more suitable to meet regulatory guidelines for donor tissue for xenotransplantation<sup>80,85-87,89,90</sup>. If the supply of islet cells could be augmented by culturing and improving the therapeutic capacity of donated islets from more readily available sources (such as young pigs), these new sources would provide sufficient material to become a new treatment for insulin-dependent diabetes, assuming immunological issues (rejection) are eventually addressed.

Preservation of the pancreas prior to islet isolation is also a critical step in the procedure and we have recently described a technique for 24h hypothermic machine perfusion (HMP) of pancreata that facilitates islet isolation from young pigs<sup>44,45,69</sup>. The research described here combines this technology with a culture method involving silicone-rubber membrane (SRM), gas-permeable flasks<sup>91</sup> (<http://www.wilsonwolf.com/>), in an attempt to develop a system for culture and

shipping of these fragile juvenile porcine islets for research and possible future xenotransplantation. In so doing, the immature porcine islets were observed to undergo plasticity during 7 days in culture resulting in larger aggregate structures comprising both endocrine and exocrine cells. For convenience, we refer to these aggregates as “pancreatites” to reflect their apparent structure as small pancreatic tissue-derived organoids, not previously described to our knowledge.

## ***Materials and Methods***

### **Ethics Statement:**

For the respective work at each institution, the Medical University of South Carolina (Department of Comparative Medicine) Institutional Animal Care and Use Committee (pigs) or the University of Minnesota Institutional Animal Care and Use Committee (mice) approved all studies with animals as described in this manuscript. Every effort was made to minimize suffering, and all studies complied with the USDA Animal Welfare Act Regulations, the Public Health Service Policy on Humane Care and Use of Laboratory Animals, and the recommendations in the Guide for the Care and Use of Laboratory Animals (NIH).

### **Islet Isolation and Culture:**

Islets were isolated by conventional collagenase (Roche MTF) digestion of juvenile porcine pancreata (2-3 month old, 25-30 kg Yorkshire pigs) either between 2-3 hours after procurement (Fresh), or after 24 hours of hypothermic machine perfusion (HMP) using the methods we have previously reported<sup>44,45,69</sup>. Briefly, pancreata preserved by HMP were perfused using the Lifeport Kidney Transporter and KPS1 perfusion solution both from Organ Recovery Systems (Itasca, IL). The liberated islet tissue was purified by Optiprep density-gradient separation (Sigma-Aldrich, St Louis, MO), and cultured for up to 7 days at 37 °C. The isolation and culture protocols were identical for both Fresh and HMP pancreata. ME199 medium (Mediatech, Herndon, VA) was used for the duration of the culture period, and modified based on our experience with the addition of an anti-oxidant, 50 mM Trolox (Roche, Basel, Switzerland), a broad spectrum anti-apoptotic agent, Quinoline-Val-Asp-DifluoroPhenoxyethylketone (Q-VD-OPH, 10 μM from MP Biomedical, Santa Ana, California) and 10% porcine serum (Gibco, Life Technologies, Carlsbad, CA)<sup>92</sup>. The isolation product was then characterized using a battery of tests at various time points during culture in SRM flasks (Wilson Wolf, New Brighton, MN). Islet



morphology was assessed daily by phase contrast microscopy (Olympus IX70 inverted microscope) in the presence of dithizone stain, and the dynamic cell morphology was recorded in digital micrographs. Viability, functional status, and islet biology were assessed using established islet quality assays at various time points during the culture period, including measurements of oxygen consumption rate normalized to DNA (OCR/DNA), static insulin secretion (Glucose-stimulated insulin secretion: GSIS), immunohistochemistry, and confocal microscopy. Extended quality assessment entailed shipment of pancreatite structures overnight by standard courier to the laboratories of our collaborators at the University of Minnesota (UMN, Minneapolis, MN) and Yale University (New Haven, CT). For these shipments, we used the shipping version of the Wilson-Wolf silicone membrane flasks <sup>91</sup>, using a temperature controlled shipping system <sup>93</sup>. Perfusion insulin release measurements were done at Yale as previously reported <sup>94</sup>, and post shipment evaluation and diabetic nude mice transplantation was done at the UMN. The extended assessments at Yale, and UMN did not compare Fresh vs HMP pancreatitis due to limited data sets. All data is reported as the mean and the standard error of the mean, with statistical comparisons between two groups using a two-tailed unpaired t-test, and comparison between multiple groups using one-way repeated measures ANOVA and Tukey's multiple comparison post-test.

#### Islet Assessments:

**Islet quantification:** Following islet isolation and purification, the total number of islets was determined using standard published techniques <sup>85,95</sup>. A volume of 50µl of the purified prep was added to 2 ml of dithizone stain inside a 35x10 mm tissue dish with grid. Thus, islet tissue clusters were stained in contrast to exocrine tissue and then counted and converted to islet equivalents (IE) according to standard convention <sup>85,95</sup>. Counting the pancreatites using the conventional method was challenging given the co-localized nature of stained and unstained

tissues in each sample. To ameliorate observer bias, all counts were performed in duplicate by two independent observers, and reported values are averages of both counts. The purity of the islet preparation was also assessed by comparing dithizone-stained tissue to unstained exocrine tissue.

**OCR/DNA:** The OCR/DNA assay is a measure of isolated islet functional viability, and is used as a predictor of islet function in-vivo<sup>25-27,96</sup>. Oxygen consumption rate measurements of the islets were done on the same day as isolation, after 7 days in culture, and after shipment to the University of Minnesota (Day 8). Designated islet samples (~5,000 IEQ/sample), were collected, washed, and suspended in Dulbecco's modified Eagle's medium (Mediatech, Herndon, VA) containing 4.5 g/L L-glutamine and supplemented with 100 U/ml penicillin, 100 µg/ml streptomycin, 10 mM HEPES without serum. Each islet suspension was divided into three or more 200 µL titanium chambers. The chambers were sealed and maintained at 37°C. The time-dependent oxygen partial pressures (pO<sub>2</sub>) within the chambers were recorded over time using a fluorescent-based fiber optic oxygen sensor (Micro Oxygen Uptake System, FO=SYSZ-P250; Instech Laboratories, Plymouth Meeting, PA). The OCR was then calculated as previously described<sup>26</sup>. The cell suspensions were then carefully removed from the chambers and processed for DNA quantification as described below.

**DNA Quantification:** Islet samples analyzed by the OCR assays were subsequently sampled for quantification of DNA content. To measure DNA content, islet samples were diluted in an aqueous cell lysis solution of 1M ammonium hydroxide (Fisher Scientific, Pittsburgh, PA) and 3.4 mM Triton X-100 (Sigma-Aldrich, St Louis, MO), and sonicated to ensure adequate cell lysis. DNA content was determined using the Quant-iT PicoGreen dsDNA kit (Molecular Probes, Eugene, OR) as per manufacturer's instructions. Fluorescence readings were taken on a SpectraMax M5 microplate reader (Molecular Devices, Sunnyvale, CA)

**Islet Insulin Content and Stimulated Secretion Assay:** Islet insulin release upon exposure to low and high glucose concentrations was determined following an initial recovery of 1 hour at 37 °C in low, 2 mM, glucose (in RPMI-1640, Gibco, Life Technologies, Carlsbad, CA) solution. Consecutive 30 minute islet incubation periods (37 °C water bath shaker) in 2.5 mM, 16.7 mM and then 2.5 mM glucose solution, respectively, were performed, each followed by careful supernatant removal and freezing (0.5 mL), and islet resuspension in the next glucose concentration solution. A total of 12 x 1.5 mL conical tubes, each containing 25 IEQ in 1 mL glucose solution were employed. Gravity driven sedimentation of islets was used prior to supernatant removal. The insulin content of frozen supernatants and samples was determined using Insulin Porcine EIA kits (Alpco Diagnostics, Windham, NH) and normalized to islet equivalents.

**Histology, Immunohistochemistry, and Confocal Microscopy:** Islet samples containing 1,000-2,000 IEQ were collected from cultures 7-8 days following isolation. The samples were immediately fixed in 10% buffered formalin (Fisher Scientific, Pittsburgh, PA) for at least 24 hours and then transferred to a 70% ethanol solution. Fixed samples were embedded in paraffin and sectioned at 4 µm, and stained with hematoxylin and eosin. For insulin, glucagon, and Ki67 immunohistochemical staining, sections were cut at 4 µm, de-paraffinized, and rehydrated, followed by incubation with 3% hydrogen peroxide to quench endogenous peroxidase activity. Following appropriate antigen retrieval, sections were incubated with the primary antibody (guinea pig anti-swine insulin, 1:300 dilution, cat.#A0564, Dako, Carpinteria, CA; rabbit anti-human glucagon, cat.#NB120-1846 Novus Biologicals, Littleton, CO; mouse anti-human Ki67 monoclonal antibody clone MiB-1, 1:50 dilution, cat. #M7240, Dako. Antigen detection was done with anti-rabbit polymer, EnVision, Dako, and color visualization was done using DAB, Dako. The same protocols were used for examining explanted graft tissues. Double

immunofluorescence staining for insulin/cytokeratins was done on formalin fixed, paraffin-embedded sections cut at 4  $\mu\text{m}$ . For insulin labeling, sections were first deparaffinized, rehydrated, and incubated with guinea pig anti-swine insulin (Dako) for 60 minutes. Next sections were incubated in the dark with FITC-conjugated, goat anti-guinea pig immunoglobulin (NOVUS, cat # NB7397) for 60 minutes. Sections were next incubated with antibodies to wide spectrum cytokeratin (Rabbit anti-cytokeratin, cat.#Z0622, Dako) followed by incubation in the dark with Streptavidin-AlexaFluor-594 (Invitrogen, cat # 21207) for 60 minutes. Finally, nuclear staining was done using TOPRO-3 (Molecular Probes, Eugene, OR). Labeled sections were examined with a Biorad laser confocal microscope.

**Nude Mouse Bioassay:** Islets from six different preparations were shipped to the University of Minnesota for implantation into diabetic nude mice (n=17). Mice (CrI:NU-Foxn1nu mice from Charles River Laboratories, Wilmington, MA) were rendered diabetic by a 240 mg/kg intraperitoneal injection of streptozotocin (Zanosar)<sup>71</sup>. After diabetes establishment (hyperglycemia) was confirmed, and based upon our previous experience using this model a dose of 2,000 IEQ of islets were transplanted into the renal subcapsular space of each mouse, and blood glucose and body weights were observed for between 30-60 days. The standard 30 day follow-up period was extended for a sub-group (n=8) of these implants because it was suspected that these under-developed pancreatite structures may continue to mature in-vivo and may offer delayed graft function. In some animals, the observation period was extended if the glucose levels were observed to decrease following transplant but had not yet reached the critical conclusive levels. Mice were considered to be diabetic when three consecutive blood glucose measurements of >300 mg/dL were observed, and a graft was considered functional upon a return to stable glycemic control when three consecutive blood glucose measurements were <200 mg/dL during the observation period. Mice with functioning grafts were nephrectomized following the

observation period to ensure that blood glucose measurements returned to diabetic levels, after which the mice were euthanized<sup>26,71,97</sup>.

## ***Results***

Yields and purities for both fresh and HMP islets are reported in **Table 5.1**, along with culture recoveries and insulin data. The average purified islet yield per gram of digested tissue was notably higher for islets isolated from HMP organs when compared to islets isolated from fresh controls with a 57% improvement observed for these studies, but due to the limited number of isolations studied and large variability this difference was not statistically significant ( $p=0.285$ ). Following culture for one week, pancreatites from both conditions demonstrated to be fully functional in terms of insulin secretion in response to glucose challenge (**Table 5.1**). When compared using a two tailed unpaired t-test; average yield, average purity, culture duration, culture recovery, insulin stimulation index and insulin content were not different between groups ( $p>0.05$ ). These observations were consistent with our recently published findings describing islet isolation from juvenile porcine pancreas after 24-hr hypothermic machine perfusion preservation<sup>44,45,69</sup>. Islets isolated from HMP and Fresh pancreata exhibited similar behavior in culture and yielded comparable functional outcomes (OCR/DNA, immunohistochemistry, nude mouse transplants); therefore, the results reported on these aspects represent the observations of islets from both groups.

As illustrated in **Figure 5.1A**, islet preparations from both Fresh and HMP pancreata comprised a high proportion (>90%) of small islets (<100  $\mu\text{m}$ ) immediately following isolation. The dithizone stained islets appeared as “grape-like” clusters on Day 0. **Figure 5.1** also shows the plasticity observed during subsequent post-isolation culture of the immature islets. The term “plasticity” is used according to the definition of the ability of a biological system to be altered into different shapes and/or behavior according to varying environmental conditions. Each panel in **Figure 5.1 (A-E)** shows the typical appearance of the  $\beta$ -cells (stained red with dithizone) and exocrine (unstained grey-brown) at various time points during 1 week of culture post-isolation, and after

shipment (**Figure 5.1G**). The gross morphology of the islets was observed to change during the first 24-48 hours in culture. (Compare the looser more fragmented nature of the Day 1 cultured islets in **Figure 5.1B**, with the “grape-like” clusters of islets on day 0 immediately post-isolation in **Figure 5.1A**).

During the initial 48 hours of culture, the islets appeared to disaggregate to form strings of cells and then they associated with residual non-dithizone stained tissue (**Figure 5.1B-C**). The most significant observation is the transition of the tissue from this loosely disaggregated appearance at 24 hours (Day 1) to more condensed aggregated structures comprising both exocrine and endocrine cells by Days 4-7 (**Figure 5.1D-E**).

The pancreatite structures shipped to Yale University maintained their structural integrity, and demonstrated dynamic insulin secretory responses to a standard panel of secretagogues as described in a previous publication<sup>94</sup>. Moreover, pancreatite samples shipped to University of Minnesota (n=5) retained their morphology and their metabolic capability as demonstrated by the oxygen consumption measurements, which were not significantly different to the pre-shipment values (**Figure 5.2**). The OCR/DNA (mmol/min/mgDNA) was measured to be = 134±19 at Day 0; 159±25 on Day 7 (pre-shipment) and 175±16 on Day 8 (post-shipment), and analysis by one way ANOVA (p=0.3391) with Tukey’s multiple comparisons post-test concluded that no significant differences were observed between time-points.

Upon arrival in Minnesota, immunohistochemistry of the tissue showed cells with insulin or glucagon immunoreactivity among cells in the cultured aggregates (**Figure 5.3A&B** respectively). Nuclear staining for Ki67-MiB confirmed mitotic activity within the cell aggregates during culture (**Figure 5.3C**), and within the graft post-transplant (**Figure 5.4B** inset). These observations suggest that the formation of pancreatites was not simply due to aggregation but also due to growth by cell division, and possibly maturation in culture and *in vivo*. Confocal

microscopy of double immunofluorescently stained pancreatites showed strong, non-overlapping staining for insulin and wide spectrum cytokeratins indicating the presence of both beta cells and ductal epithelial cells within the tissue (**Figure 5.4D**).

The pancreatites maintained metabolic integrity, demonstrated by oxygen consumption rates ( $175 \pm 16$  nmol/min/mgDNA), and physiological function, confirmed by both static and previously published dynamic glucose stimulation<sup>94</sup>. Furthermore, *in vivo* function was examined by transplantation under the kidney capsule in nude mice. **Figure 5.4A** shows the average blood glucose measurements for the 8 animals that achieved glycemic control (blood glucose levels  $\leq 200$  mg/dL for 3 consecutive days), as well as the average blood glucose measurements of the 9 animals that did not (shown separately for clarity). Glycemic control was achieved in 8/17 mice (47%) on average 25 days post transplantation (for these mice) with 7 animals achieving control 10 or more days following transplant (**Figure 5.4B**). Post-explant glucose measurements were excluded from this figure due to variable explant timing, but all animals returned to hyperglycemic state ( $\geq 3$  consecutive BG measurements  $\geq 300$  mg/dL) following graft explant. The average mass of all animals was observed to decrease by 0.3 grams from the time of transplant until nephrectomy or euthanasia which is not statistically significant ( $p=0.3722$  for paired student t-test comparing starting mass and final mass), and no animal was observed to lose more than 10% of starting body mass. Histopathology of explanted grafts confirmed persistent islet tissue within the graft and sections showed strong insulin and glucagon staining (**Figure 5.5**). Furthermore, continued mitotic activity was observed within the graft as indicated by Ki67-MiB staining, and a representative image is shown as an inset in **Figure 5.4B**.



**Table 5.1: Isolation and Culture Results**

	<b>Fresh Control (n=9)</b>	<b>HMP [KPS1] (n=11)</b>
<b>Islet Yield (IEQ/g, Day 0)</b>	1425±610	2242±449*
<b>Purity (Day 0)</b>	69.2±7.6	63.8±6.1
<b>Total Culture Time (days)</b>	6.7±0.1	5.7±0.6
<b>End-Culture Recovery (% of Day 0)</b>	71.7±12.5	75.5±14.2
<b>End Culture Stimulation Index</b>	6.54±1.19	5.26±0.77
<b>End Culture Insulin Content (ng/IEQ)</b>	2.55±0.33	2.10±0.28*

\*difference is significant (p<0.05)

HMP = Hypothermic Machine Perfusion, IEQ = Islet Equivalent

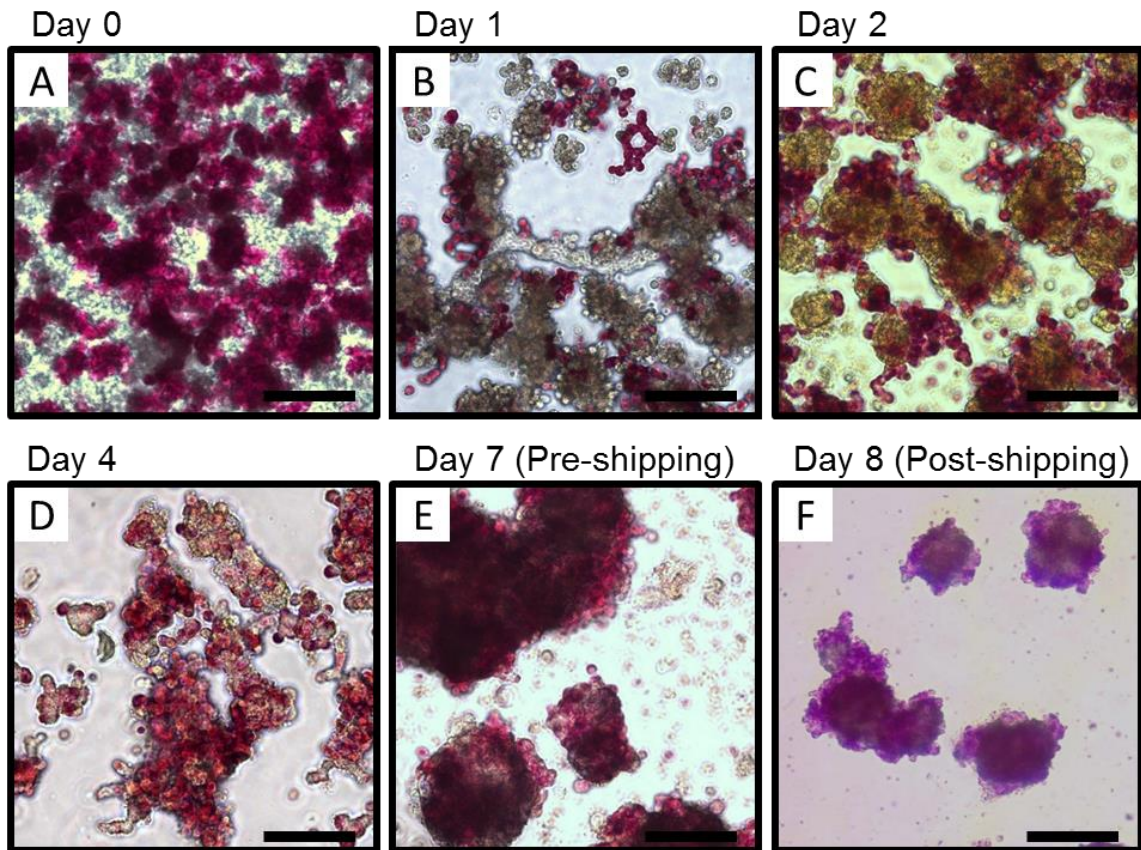


**Figure 5.1: Pancreatite plasticity micrographs.** Micrographs demonstrating the plasticity of pancreatite structures during 7 days of culture, and after shipment. Phase contrast micrographs of dithizone-stained (red) islet cultures at critical times in culture (A-E) and after shipment (F). Exocrine tissue remains unstained (light grey/yellow). Day 0 purified islets (A) show the familiar irregular shape of “grape-like” islet clusters. During the first 24 hours in culture (B), the islets appear to disaggregate into strings of loosely clustered islets associated with the residual exocrine tissue. Between 2 and 4 days of culture (C&D), this process continues and the clusters become larger and more condensed aggregate structures comprising both exocrine and endocrine cells. By 7 days, the larger re-aggregated structures, which we termed “pancreatites,” were clearly more dense and compact. The final panel (F) shows that the pancreatites remained morphologically intact following ambient shipment to Minnesota in Wilson-Wolf flasks. Scale bars represent 100  $\mu\text{m}$ .

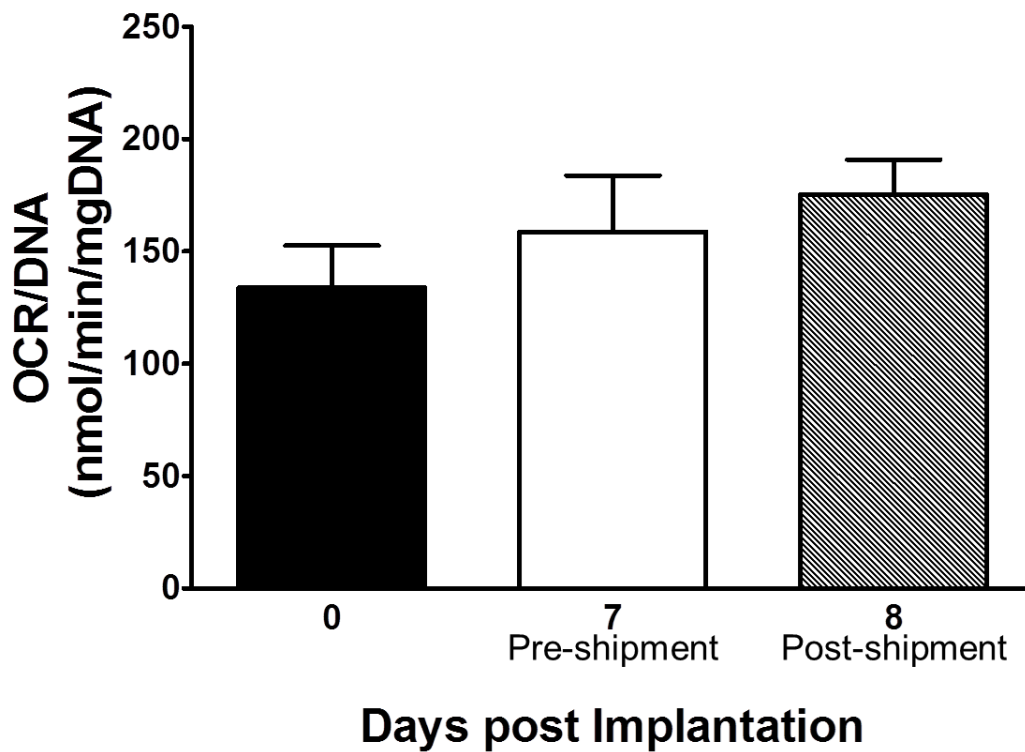


**Figure 5.2: Juvenile porcine islet viability.** OCR/DNA was  $134 \pm 19$  at Day 0;  $159 \pm 25$  on Day 7 (pre-shipment) and  $175 \pm 16$  nmol/min/mgDNA on Day 8 (post shipment) The viability of the pancreatites improved in culture, and was on average  $18 \pm 14\%$  higher but not significantly different post-shipment compared to pre-shipment.

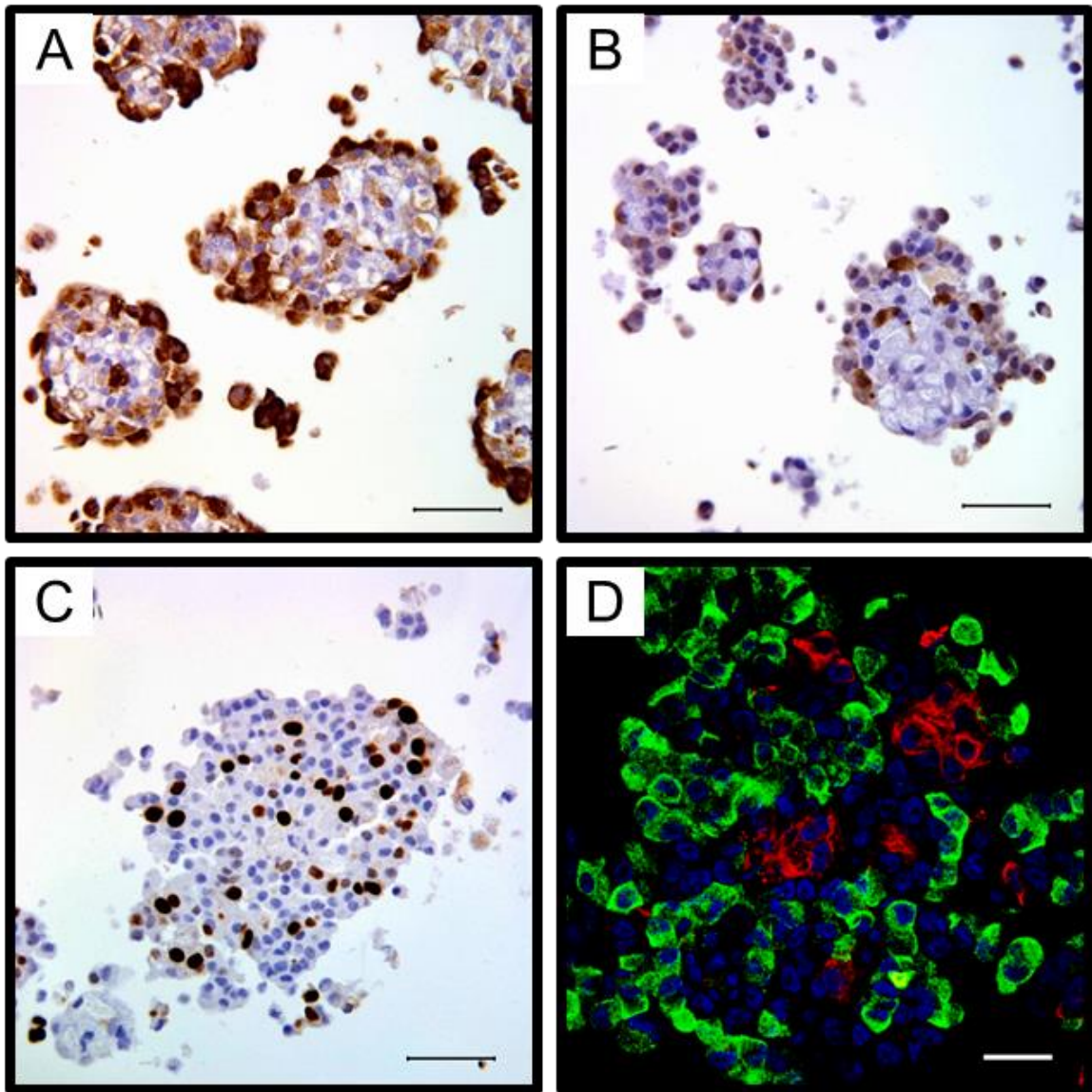


**Figure 5.3: Juvenile porcine islet immunohistochemistry.** Immunohistochemistry staining of 7-day cultured pancreatite tissue shows staining for islet markers and proliferation markers. Upon arrival at Minnesota, pancreatites showed strong staining of both insulin (A) and glucagon (B) from the islets. Ki67-MiB nuclear staining (C) shows mitotic activity in these structures providing evidence of cell proliferation. Confocal microscopy of double immunofluorescently stained pancreatites (D) showed staining for insulin and wide spectrum cyokeratins indicating the presence of both beta cells and ductal epithelial cells within the tissue.

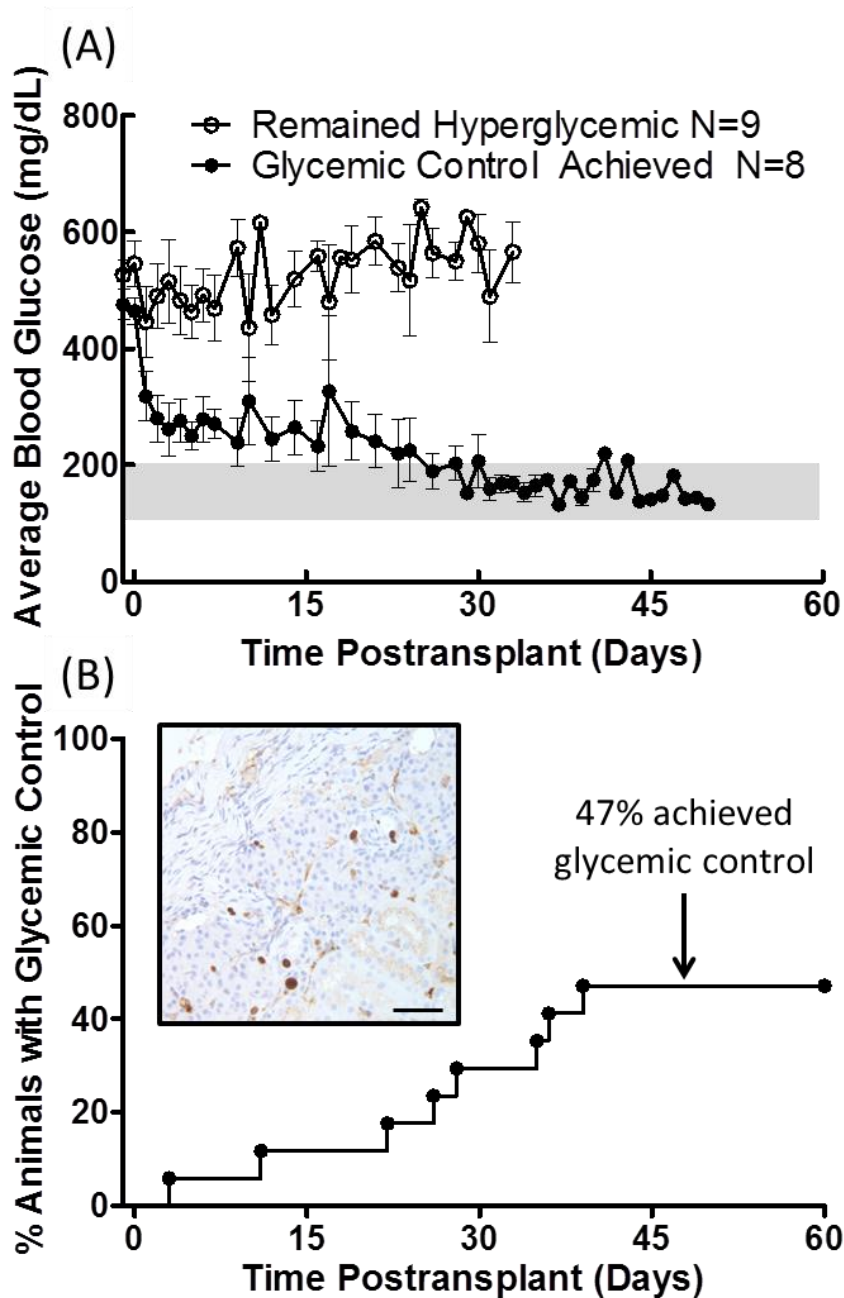


**Figure 5.4: Nude mouse diabetes reversal.** Mean blood glucose measurements (A) and diabetes reversal rate plot (B) from diabetic nude mice. Data from mice that received a renal sub-capsular transplant of pancreatitis shipped to Minnesota for assessment. Blood glucose data shown is grouped by outcome; 8 of 17 animals achieved glycemic control after an average of 25 days. Blood glucose measurements following explant are not shown for clarity due to differing points of euthanasia, although all animals reverted to hyperglycemia following explanation of the graft. Achievement of glycemic control was defined as three consecutive blood glucose measurements  $\leq 300$  mg/dL following transplant. The delayed control of blood glucose levels is suspected to reflect possible generation of a critical mass of insulin-secreting cells by neogenesis as evidenced by the positive Ki67-MiB immunostaining in the explanted grafts [inset].

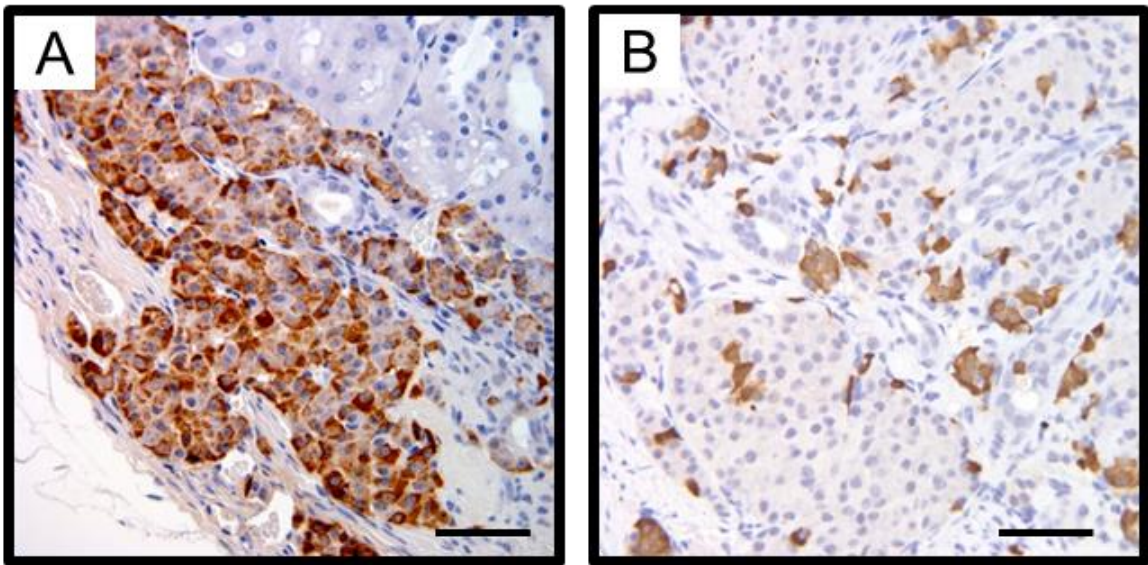


**Figure 5.5 Insulin (A) and glucagon (B) staining in explanted pancreatite grafts.** Sections from explanted grafts show strong staining for both insulin (A) and glucagon (B), which confirms the preservation of endocrine cell phenotypes within these pancreatites *in vivo*. Future studies with co-localized staining to investigate the mitotic activity observed in these grafts will further illuminate the behavior and plasticity of these pancreatites *in vivo*.

## ***Discussion***

Clinical trials are underway at several centers around the world to assess the efficacy of implantation of functional pancreatic islet cells as a potentially curative treatment for Type 1 diabetes<sup>52,53</sup>. Nevertheless, the limited availability of donor human pancreata means that clinical islet transplantation may not reach its full potential without reliance upon alternative sources of islets. Porcine islets are favored for xenotransplantation for a variety of reasons<sup>54</sup> but mature pigs (>2 years old) present logistic and economic challenges and young pigs (3-6 months) have not yet proved to be an adequate source. As discussed by several investigators, experiences in many laboratories over several decades show that isolation of porcine islets appears more difficult than other mammals including human, and the economically-favored juvenile pig has proved even more problematic due to poor yields and extreme fragility of the immature islets<sup>87,98-100</sup>. Despite some reports for the successful isolation of islets from young market pigs (4-6 months old) the studies did not involve culturing the islets<sup>100</sup>, which remains a significant challenge. For example, Rijkeljkhuizen et al report 80% attrition of adult porcine islets after 1 day culture<sup>99</sup>. More recently, Lakey's group has reported successful post-isolation culturing of partially digested pancreatic fragments from infant pigs (<4 weeks old)<sup>101</sup>. This model produces small numbers of islets compared with conventional models using older pigs, but the study demonstrates a robust capacity for continued *in vitro* development in culture thus supporting the basic premise of our study.

Preservation of the pancreas prior to islet isolation is also a critical step in the procedure and we have recently described a technique for 24hour hypothermic machine perfusion (HMP) of pancreas that facilitates islet isolation from young pigs<sup>44,45,69</sup>. The research described here combines this technology with an effective culture method involving silicone-membrane, gas-permeable flasks, in an attempt to develop a system for culture and shipping of juvenile porcine

islets for research and possible future xenotransplantation. This contrasts sharply with conventional culture of porcine islets from pigs of any age, especially juvenile, which have proved to be too fragile and labile in culture to be of practical utility<sup>84,86,87,99</sup>.

*Special Conditions for Culture of Juvenile Porcine Islets:*

An important achievement of the studies reported here is the successful isolation and culture of juvenile porcine islets, which are notoriously difficult to establish and maintain in culture<sup>86,87,99</sup>. Until the introduction of the use of gas permeable culture flasks<sup>91</sup> (Wilson Wolf Manufacturing, MN) our experience was the same as many in the field in that islets from young market-size pigs are very difficult to maintain in culture. Conventional culture in regular flasks led to the demise of the islets within 12-24 hours of culture. Even the purest preparations resulted in disappearance of islets within the first 24 hours as reported previously by other investigators<sup>84,86,99</sup>.

Although considerable attention has been given to the formulation of media for islet culture as reviewed by Clayton<sup>102</sup> and London and Murdoch et al.<sup>103</sup>, very little attention was given to the role of oxygen transport until the introduction of gas permeable substrates in the form of silicone rubber membrane flasks<sup>91</sup>. Islet density and aggregation have been shown to negatively impact islet survival in culture such that a marked improvement was demonstrated by increasing external pO<sub>2</sub> and culturing on a SRM<sup>91</sup>. This new technology was therefore introduced in this study to complement changes to the culture medium and islet isolation after hypothermic machine perfusion<sup>44,69,104</sup>.

The ME199 medium was specially modified for porcine islet culture through the addition of various supplements and porcine serum<sup>92</sup>. Using this scheme, it was observed that the juvenile islets did not behave the same as conventional cultures of adult pig islets, or even human islets. As described above the immature porcine islets underwent plasticity during 7 days in culture resulting in larger, re-aggregated structures. This contrasts markedly with the typical behavior of



islets from adult species, which maintain their islet individuality and post-isolation structure throughout conventional tissue culture. In cultures of adult islets, the contaminating exocrine tissue tends to disintegrate and disappear by autolysis leaving an even purer preparation of individual islets<sup>98</sup>. In contrast, the tissue from juvenile pigs appeared to re-aggregate into larger new structures comprising endocrine and exocrine cells in coexistence, hence the term “pancreatite”. Confocal double-staining (**Figure 5.3D**) clearly demonstrated the heterogeneous aggregated tissue character, and confirmed the presence of both beta cells and ductal epithelial cells in the structures after 7 days in culture.

For convenience, we refer to these aggregates as “pancreatites” to reflect their apparent structure as small pancreatic tissue-derived organoids, not previously described to our knowledge. These preliminary observations have been achieved by combining previously reported developments for modified preservation solutions and juvenile porcine islet isolation after HMP, with the use of SRM flasks. This phenomenological discovery of pancreatite formation using the combined technologies has been generated without specific knowledge of the relative contributions of each of the component systems. Hence, this new phenomenon provides the basis for further research to employ this combination of technologies for the synergistic development of “pancreatites” as a potentially new solution for generating a therapeutic product from juvenile pigs for xenotransplantation and diabetes research.

*In vitro functional assessment:*

The pancreatite cultures were monitored daily for one week to observe these changes in morphology, and were assessed at critical points for quality by OCR/DNA, Insulin secretion, histopathology, and immunohistochemistry. The islet tissue function was also tested *in vivo* by nude mouse bioassay. The OCR/DNA results showed high tissue viability following culture ( $159 \pm 25$  nmol/min/mgDNA), and this viability was maintained following shipment to the

University of Minnesota ( $175 \pm 16$  nmol/min/mgDNA). These observations are consistent with reports in literature using similar shipping methods<sup>105</sup>. The OCR/DNA assay in conjunction with the total transplanted OCR dose has been shown to be an accurate predictor of diabetes reversal in nude mice transplanted with human islets. The viability level of the pancreatite structures was comparable with high-viability human islets reported in literature<sup>26</sup>, and sufficiently higher than the reported minimum OCR/DNA boundary (150 nm/min/mgDNA) required to reverse diabetes in mice with rat islets<sup>96</sup>. This comparison can only be considered as a reference because as discussed above, these preparations exhibit notable morphological and functional differences between adult pig islets, and are also different from observations with human, or rat islets. These differences, along with the limited reports in literature warranted a brief examination of these structures *in vivo*, and suggest a need for further studies examining the viability and function of these pancreatites.

*In vivo functional assessment:*

Further examination of the pancreatite functionality was assessed with a limited number of nude mouse transplants (n=17). The average blood glucose of all the animals shown in **Figure 5.4A** (separated into reversed and not reversed groups) demonstrates a gradual decrease in average fasting blood glucose levels with reversal glycemic control achieved on average 25 days post transplantation. Despite strong staining for insulin and glucagon in culture, (**Figure 5.3A-B** respectively) delayed function was observed in 7 of the 8 animals that reversed diabetes. These animals gained glycemic control 10 or more days following transplant as shown in **Figure 5.4B**. This is likely due to an inadequate functional beta cell mass immediately following transplant with possible islet neogenesis contributing to the primary graft function after 10 or more days *in vivo*. These results are consistent with the findings of Korbitt et al. describing the delayed graft function of neonatal porcine islet cell (NIC) aggregate transplants in nude mice<sup>106</sup>. Neonatal pigs

represent a much earlier stage of development (1-3 days old) compared to juvenile pigs used in our studies (1-3 months old). His studies found a dose-dependent return to normoglycemia in nude mice transplanted with NIC aggregates, and reported 100% achieved normoglycemia after 8 weeks for grafts with 2,000 aggregates<sup>106</sup>. However, only 30% of these animals achieved normoglycemia after 4 weeks, suggesting that pancreatite grafts may offer expedited graft function compared to NIC grafts. It should also be noted that these *in vivo* results are highly dependent on the initial amount of grafted tissue (eg. islet dose), and more rigorous methods for quantification of pancreatite tissue (eg. DNA) or total beta cell mass would allow for a better understanding of the dose-dependent nature of glycemic control. Future studies to parallel these findings, which extend the transplant follow-up period of mice with pancreatite grafts, would provide a valuable comparison of these two similar cell-sources. Furthermore, pancreatites exhibited notable staining for Ki67-MiB in culture (**Figure 5.3C**) and in explanted grafts (**Figure 5.4B** Inset), indicating an elevated level of mitotic activity. Separate sections from explanted grafts were also stained for insulin and glucagon (**Figure 5.5**) to confirm the presence of endocrine islet tissue in the explanted graft. Strong staining for both hormones indicated that the endocrine phenotypes of these pancreatite cells were maintained *in vivo*. This finding supports the hypothesis of *in vivo* islet neogenesis, but quantitative morphometric analysis and co-localization with insulin staining would be required to confirm this mechanism.

*Observed pancreatite potential for regeneration:*

Over the past decade, significant advances have been made in developmental biology of the pancreas and other endoderm-derived organs. Studies on islet morphogenesis show that the majority of islet cells are formed in late gestation by the process of neogenesis from precursor cells. The changes observed in the early periods of our juvenile porcine islet culture system closely resembles the budding of islet cells from the ducts and re-organization to form clusters,

during the process of islet morphogenesis seen both *in vitro* and *in vivo*<sup>107-109</sup>. Bonner-Weir et al. among others have reviewed the plasticity of adult pancreatic cells and the ultimate feasibility of *in vivo* neogenesis<sup>74,75,107</sup>. *In vitro* differentiation of stem/progenitor cells into  $\beta$ -cells is being pursued as an important approach to generate a reliable and replenishable source of  $\beta$ -cells. Pancreatic ductal cell lines and primary ductal cells have been successfully differentiated into insulin-expressing cells by *in vitro* approaches, including treatment with growth factors (e.g. EGF, Gastrin, exendin), expression of pancreatic transcription factors, and aggregation<sup>107</sup>. The aggregation and plasticity of the pancreatic cell cultures derived in our preliminary studies using juvenile porcine pancreas is consistent with this approach and is remarkably complementary to the parallel studies of Bonner-Weir et al. For example, her group has shown that discarded digested pancreatic tissue from human islet isolations can be successfully processed to expand and differentiate the ductal cells over a period of 3-4 weeks *in vitro* to cultivate human islet buds consisting of cytokeratin-19 positive duct cells and hormone positive islet cells<sup>110</sup>. On the basis of these findings it may be important to extend the culture period of the juvenile porcine islets to 28 days to parallel Bonner-Weir's studies using human tissue. Since it is now believed that *in vitro* neogenesis may recapitulate development of the embryonic pancreas, the system we propose to develop using immature porcine pancreatic tissue will not only be an important, readily available and economically viable source of therapeutic material, but will also generate a new model to identify potential markers of neogenesis and to determine the molecular mechanisms underlying the process.

#### Pancreatite size:

The notable growth or size change of these structures is demonstrated by our observations in Figure 1. In our 2010 study of HMP of juvenile pig pancreas we included an analysis of the size distribution of the islets in the purified preps showing that >90% of the young pig islets fall

within the range 50-100  $\mu\text{m}$  and very rarely were any islets found with diameters greater than 200  $\mu\text{m}$  <sup>44</sup>. In contrast the micrographs here (**Figure 5.1**) shows that most of the pancreatite structures are much bigger (>100  $\mu\text{m}$ ) and often substantially larger as illustrated by the large (387  $\mu\text{m}$ ) structure in **Figure 5.1E**. It is likely that the changing size, morphology, and cellular composition of the pancreatite structures gave rise to some error in the estimate of “islet equivalents” for the purpose of tissue quantification. The reported data is based upon the usual convention of counting individual islets that are primarily composed of dithizone stained endocrine cells only, while these pancreatites were composed of both exocrine and endocrine cells. This complication undoubtedly led to an overestimate of the islet mass transplanted in the nude mouse assay and may in part be responsible for the delayed graft function observed in some recipients as noted above. This is also consistent with the observations in several other studies involving the transplantation of adult pig islets in which the numbers of IEQ transplanted show considerable variation and range 10-fold from 1000 IEQ/mouse to 10,000 IEQ/mouse. Moreover, the time-to-normoglycemia showed considerable variance often taking > 50 days <sup>99</sup>. Hence achieving glycemic control in 47% (8 of 17 transplanted mice) in this study is comparable with reports in the literature for adult pig islets as discussed by Rijkkelijkhuizen <sup>99</sup>. Further extended studies will necessitate a titration of the pancreatite dose in the transplanted mice to resolve this issue of the critical Beta-cell mass within the pancreatites necessary for achieving glycemic control.

#### Advantages of the juvenile pancreas model

A variety of strategies are currently being investigated to deliver regulatory factors to pancreatic cells, *in vitro*, aimed at increasing  $\beta$ -cell mass for transplantation. Trans-differentiation of  $\alpha$ -cells into  $\beta$ -cells is another approach that has merit for *in vivo* regeneration and neogenesis <sup>107</sup>. The processes of neogenesis of  $\beta$ -cells *in vitro* are currently inefficient for adult human cells and do not generate sufficient  $\beta$ -cell mass to normalize hyperglycemia <sup>107</sup>. In contrast, we demonstrate

here preliminary data showing that the pancreatite cell clusters derived from juvenile porcine pancreas are able to reverse diabetes in a diabetic nude mouse model (**Figure 5.4**). The association of multiple cell types in the formation of the pancreatite cell clusters is another important characteristic with potential therapeutic benefit since there is mounting evidence for improved transplantation outcome using impure islet preparations containing non-endocrine cells, notably ductal epithelial cells <sup>111</sup>. In the broad context of processing tissue to generate a readily available cost-effective product for therapeutic treatment of diabetes, the novel “pancreatite” structures derived from juvenile pigs is potentially an innovative solution to the inevitable deficiency of supply of human tissue.

The delayed return to glycemic control, which took on average 25 days, may be an indication of the generation of a critical mass of insulin-secreting cells by cell division as evidenced by the positive Ki67-MiB staining in the explanted grafts (**Figure 5.4B** inset). There is insufficient evidence in this preliminary study however, which did not include a rigorous correlation of insulin immunostaining co-localized with the evident Ki67 staining, to fully support this hypothesis. Nevertheless, the phenomenological appearance of strong insulin, glucagon and Ki67 staining in the explants supports the notion of on-going islet development and maturation in the graft and provides encouragement for further more in depth studies to test this hypothesis.

## ***Conclusion***

The pancreatites (pancreatic cell aggregates) derived from the preservation, isolation, and culture of juvenile porcine pancreas tissue using the described techniques could provide an unlimited source of  $\beta$ -cells to integrate into a reproducible, economic and safe system for therapeutic and research applications. Moreover, the model we propose here meets the stringent economic demands that have emerged in the healthcare marketplace, and could be a cost-efficient alternative to standard management of diabetes <sup>112</sup>. We conclude from these preliminary

observations that immature islets isolated from juvenile porcine pancreas form cellular aggregates comprising both exocrine and endocrine cells in modified tissue culture. This phenomenon has not previously been reported to our knowledge presumably because of the notorious difficulty of maintaining juvenile pig islets in conventional tissue culture.

## Chapter 6 NUTRIET REGULATION AND SSB CULTURE

Sections of this chapter are reproduced in whole, or in part from the following publications with permission:

**Weegman BP**, Nash P, Carlson AL, Voltzke KJ, Geng Z, Jahani M, Becker BB, Papas KK, Firpo MT “Nutrient regulation by continuous feeding removes limitations on cell yield in the large-scale expansion of mammalian cell spheroids” PLoS ONE, 2013, May;8(10):e76611

**Weegman BP**, Nash P, Carlson AL, Voltzke KJ, Geng Z, Jahani M, Becker BB, Papas KK, Firpo MT “Nutrient regulation by continuous feeding for large-scale expansion of mammalian cells in spheroids.” In Press, Journal of Visualized Experiments, In Press November 2014

License and agreement documentation is included in **Appendix G**.

**Acknowledgements:** The authors would like to thank the Schott Foundation, the Minnesota Lions Diabetes Foundation, the Juvenile Diabetes Research Foundation (JDRF 5-2013-141), Giner Inc., the Schulze Diabetes Institute, and the NIH (P41 EB015894, and S10 RR025031) for supporting this research. The authors thank Michael Garwood and Sam Stein for their helpful comments, and Kristen M. Maynard for assistance with manuscript preparation.



## **Nutrient regulation by continuous feeding removes limitations on cell yield in the large-scale expansion of mammalian cell spheroids**

### ***Summary***

Cellular therapies are emerging as a standard approach for the treatment of several diseases. However, realizing the promise of cellular therapies across the full range of treatable disorders will require large-scale, controlled, reproducible culture methods. Bioreactor systems offer the scale-up and monitoring needed, but standard stirred bioreactor cultures do not allow for the real-time regulation of key nutrients in the medium. In this study,  $\beta$ -TC6 insulinoma cells were aggregated and cultured for 3 weeks as a model of manufacturing a mammalian cell product. Cell expansion rates and medium nutrient levels were compared in static, stirred suspension bioreactors (SSB), and continuously fed (CF) SSB. While SSB cultures facilitated increased culture volumes, no increase in cell yields were observed, partly due to limitations in key nutrients, which were consumed by the cultures between feedings, such as glucose. Even when glucose levels were increased to prevent depletion between feedings, dramatic fluctuations in glucose levels were observed. Continuous feeding eliminated fluctuations and improved cell expansion when compared with both static and SSB culture methods. Further improvements in growth rates were observed after adjusting the feed rate based on calculated nutrient depletion, which maintained physiological glucose levels for the duration of the expansion. Adjusting the feed rate in a continuous medium replacement system can maintain the consistent nutrient levels required for the large-scale application of many cell products. Continuously fed bioreactor systems combined with nutrient regulation can be used to improve the yield and reproducibility of mammalian cells for biological products and cellular therapies and will facilitate the translation of cell culture from the research lab to clinical applications.

## ***Introduction***

Cell replacement therapies in humans require the production of large-scale culture of viable, functioning cells. Reproducibility of cell product, and optimal cell yield and function all depend on the presence of appropriate levels of key nutrients, and sub-toxic levels of cell waste products<sup>113,114</sup>. For research purposes, mammalian cells are typically cultured in static culture and propagated by passaging at regular intervals, with supplemental medium changes as needed. This method is limited by the requirement for frequent manipulations, which results in variability of culture conditions and increased risk of contamination<sup>115–118</sup>. Further, these culture methods are time intensive and require trained technicians to maintain large-scale cultures. Stirred suspension bioreactors (SSB) can be used as an alternative to static cell culture for microorganism cultures to increase culture volume and density, and decrease handling<sup>119</sup>. This approach has been applied to mammalian cells, including pluripotent stem cells<sup>120–129</sup>. However, SSB cultures still require interventions for medium changes, exhibit fluctuations in nutrient and waste product levels, and provide limited information about culture status. A perfusion system can be used to address these challenges by continuous infusion and removal of medium, but parameters such as calculating feed rate based on real-time cell requirements must be established<sup>130–133</sup>.

In this study, SSB culture was used to expand an insulinoma cell line with many beta cell features intact,  $\beta$ -TC6 cells<sup>134–138</sup>, to increase culture scale and improve cell expansion rates without compromising viability. These cells, like most mammalian cells, are dependent on a key nutrient, glucose, for energy production<sup>139</sup>. In addition, beta cells are sensitive to chronic high levels of glucose<sup>103</sup>. For this study,  $\beta$ -TC6 cells were allowed to form spheroids in culture approximating islet cluster sizes in vivo, and then allocated to either static or SSB culture conditions. While stirred bioreactors allowed the increase of culture volume by more than 10-fold, a continuous

feeding perfusion bioreactor system<sup>127-130,140</sup> was required to both maintain stable culture conditions, and maintain cell growth.

## ***Materials and Methods***

### ***Cell Line and Maintenance***

The  $\beta$ -TC6 cells were provided by the ATCC (Manassas, VA). In preparation for the study, they were cultured, passaged, and cryopreserved according to provider instructions in Dulbecco's Modified Eagles Medium (DMEM, Invitrogen, Carlsbad, CA), with 4 mM L-glutamine, 4.5 g/L glucose and 1 mM sodium pyruvate (all from Invitrogen). Cells were passaged at a ratio of 1:3 every 3-4 days.

### ***$\beta$ -TC6 Spheroid Formation***

This technique is described in literature<sup>127-130,140-143</sup>, and was slightly modified to accommodate spheroid formation of  $\beta$ -TC6 cells. For all conditions,  $\beta$ -TC6 cells were first cultured and expanded in adherent cultures described above, until enough cells were obtained to reach the required (total n=12) numbers for 250 ml stirred bioreactors (Corning, Corning, NY). The cells were collected by gentle trypsinization (0.25% (w/v) Trypsin- 0.53 mM EDTA, Invitrogen) at room temperature aided by mechanical agitation for 2-3 minutes, and seeded into bioreactors at a density of  $1.32 \times 10^6 \pm 5.7\%$  cells/mL in 200ml culture medium. Cells were then cultured in the bioreactors without feeding for 3 days at 37°C, with 5% CO<sub>2</sub>, 100% relative humidity, and stir rate of 70 rpm to allow spheroids to form. No significant proliferation was observed during the three day spheroid formation period. After spheroid formation, each bioreactor was allocated to a specific culture condition.

### ***Experimental Culture Conditions***

After spheroid formation, spheroids were divided among three culture methods: static culture, stirred suspension bioreactor (SSB) culture, and continuously fed SSB culture. Cultures were compared at three different glucose concentrations (1.0 g/L, 2.75 g/L, and 4.5 g/L) to represent

the range between physiological glucose (approximately 0.7 g/L) and standard  $\beta$ -TC6 culture medium (4.5g/L). **Static Culture:** Spheroids from the initial bioreactor cultures were transferred to 10cm diameter cell culture dishes (Nunc, Rochester, NY) containing 10 ml of culture medium. Parallel cultures were established for each glucose concentration; 100% medium exchange was done every 3 days by collecting the spheroids in 50 ml conical tubes (Falcon, San Jose, CA). The spheroids were gently pelleted using a refrigerated centrifuge at 4°C and 52.1xG. Culture medium was aspirated and pellets were re-suspended in fresh medium and placed back into culture. **Stirred Suspension Bioreactor Culture (SSB):** Stirred bioreactors remained in bioreactor conditions identical to spheroid formation cultures for the duration of the 21-day culture. Medium was replenished by performing a 100% medium exchange every three days. For media changes, cultures were removed from the bioreactor and processed as for static cultures above. Fresh medium was then added to re-establish the 200ml culture volume. **Continuously Fed SSB Culture:** Stirred bioreactors identical to the SSB condition were adapted with a lid designed for this study to provide connection to a continuous feed. The feeding system, described in detail below, was designed to maintain stable culture conditions by continuously adding fresh medium at a regulated rate, and removing waste medium at the same rate. Initially, continuously fed SSB cultures had the same medium replacement rate as the SSB and static cultures with 100% of the medium replaced every three days. Fresh medium was constantly added at an average rate of 0.046 ml/min (200ml/3 days) and removed at the same average rate to maintain a consistent culture volume. Later experiments utilized a variable feed rate to maintain nutrient levels based on the rate of cell usage.

#### Continuous Feeding System

The continuous feeding system design was based on systems described in literature<sup>127-130,144-146</sup>. Briefly, the system consists of five primary components: a media reservoir, peristaltic pump,

stirred bioreactor, waste reservoir, and custom designed tubing/sampling set. The medium reservoir consisted of a 1L glass bottle (Corning), the waste reservoir was a 2L glass bottle (Corning), and the stirred bioreactor was a 250 ml volume glass reactor (Corning). A Masterflex digital peristaltic pump with an 8 channel pump head (Cole Parmer, Vernon Hills, IL) was used to control medium exchange. Reservoir and bioreactor lids were manufactured from hard plastic (Delran, Dupont, Wilmington, DE) with stainless steel pipe pass-through ports providing ventilation through sterile filters, and allowing for medium transfer between reservoirs and bioreactor. The bioreactor lid contained additional pass-through ports for optional instrumentation and monitoring probes (eg. oxygen monitor). The bioreactor lid also contained a novel outflow tube (OT) fabricated from porous glass aeration tubes that had an average pore size range of 40  $\mu\text{m}$  to 60  $\mu\text{m}$ , and a pore density of 40%. The OT pore size was chosen to remove only medium and cell debris, leaving cell aggregates in culture.

Custom autoclavable perfusion tubing sets were assembled from polyvinylidene fluoride (PVDF) tubing connectors and PharMed BPT Tubing (PharMedCorp, Westlake, OH). The tubing set consisted of three parts: a feed line, a waste line, and a sample line. The feed line was assembled using L/S 14 tubing for the primary lengths with a disposable L/S 13 section spliced in the middle as a replaceable “pump section.” This line connected to the fresh medium reservoir stored inside a refrigerator to reduce soluble factor degradation, passed through the pump head, and terminated at the feed port of the stirred bioreactor inside a NuAire (Princeton, MN) cell culture incubator. The second line for bioreactor waste removal was similar to the feed line but consisted of L/S 16 tubing for its primary lengths, and L/S 14 tubing for the replaceable “pump section.” The tubing diameters used for the waste line were larger to allow removal of medium from the bioreactor at the same rate as fed conditions to avoid significant culture volume changes, and to avoid the possibility of media overflows. The same tubing diameters could not be used to accomplish this

task because any small variability in the tubing quality could result in a removal rate that was slower than the feed rate. Effectively, the waste line was pumping at a higher speed than the feed line because of the larger diameter tubing, and the volume in the reactor was controlled by setting the OT to the appropriate level.

The system functions by continuously pumping medium into the bioreactor, resulting in a rise in the level of medium in the bioreactor until reaching the height of the OT. The medium is removed through the OT, leaving the cell spheroids in culture, until the medium level falls below the bottom of the OT. This method of volume control with continuous feeding is used in many large-scale culture applications used to generate cell products<sup>144,145</sup>. The system is designed to be simple without the need for specialized sensors and automation systems to control pump speeds. The medium level in the bioreactors fluctuates slightly because the surface tension of the media allows the outflow tube to remove medium briefly from the bioreactor after the average medium level is below the bottom of the tube. This small variability in culture volume does not exceed 6% of the total culture volume, and did not appear to adversely affect the spheroids during culture. To avoid vapor lock or pressure build up inside the sealed vessels, sterile vents were added to allow sterile air exchange. This was also important for allowing gas exchange between the incubator (5% CO<sub>2</sub>) environment and the bioreactor, which is necessary to maintain the correct pH.

The final component of the tubing set was a sample collection assembly. Briefly, it consisted of three short (~6 cm) L/S 14 tubing lengths connected together with a T-type PVDF connector, and two small hose clamps on two of the tubing lengths. One of the clamped lengths contained a sterile gas filter for gas venting, and the other was used for connection to a sterile sampling syringe. The third end was connected to a stainless steel sample connector attached on the lid of the bioreactor. This entire assembly was autoclavable and connected to the bioreactor for the

duration of the experiment. The assembly was used to collect a sterile sample from the bioreactor as needed without disturbing the continuous feed process.

#### Spheroid Settling Rate Measurements

In order to ensure cell clusters were not being removed by the continuous feeding system, the settling rate of  $\beta$ -TC6 spheroids were measured by observing their descent in a large diameter plastic pipette.  $\beta$ -TC6 cells were cultured in SSB bioreactors to form spheroids as described above. After 3 days of culture, 30 ml samples of the spheroid suspension were gently pipetted to distribute evenly in suspension and placed in a large diameter 25 ml pipette, and the time for all of the spheroids to settle 5 cm was recorded. This was repeated three times for each of the three separate samples, and the data was averaged and used to determine the linear settling rate of the cells.

#### Cell Counts, Viability, and Glucose Concentration Measurements

Samples were collected from each bioreactor every three days before a medium change. For static and SSB culture methods all cells were collected as described above, and samples were taken from the cell suspension for cell counts and medium glucose measurements. Samples were collected using a wide orifice pipette to carefully suspend the spheroids and remove a representative sample, which consisted of no more than 2% of the total culture. Continuously fed SSB cultures were sampled using a specialized sampling port. For all culture methods, cells were dissociated by incubation for 2 minutes in trypsin-EDTA (0.25% (w/v) Trypsin- 0.53 mM EDTA, Invitrogen), and counted in triplicate using a standard hemocytometer with trypan blue staining<sup>147</sup>. Cell viability was calculated by recording live (unstained) cells, and dead (stained) cells independently (viability % = live cells / total cells). Cell growth rates are reported as a fold expansion percentage, calculated by dividing the live cell count after 21 days of culture to the original cell count at the beginning of the culture (Day 0). Glucose levels were measured in



triplicate using a blood glucose meter (One Touch Ultra, Johnson & Johnson, New Brunswick, New Jersey), and single use test-strips (one touch ultra-strips). Both the fresh medium and waste medium were tested for glucose concentration, and measurements lower than 20 mg/dL (detectable threshold of the meter), although undetectable, were plotted as 20mg/dL.

### Statistics

All data are reported as the mean +/- the standard error of the mean for at least three discrete measurements. Cell counts and glucose measurements were done in triplicate, and the two tailed un-paired student-t test was used to compare conditions. A p value < 0.05 was considered significantly different.

## ***Results***

### ***$\beta$ -TC6 cell expansion in static and SSB cultures***

In order to determine whether clusters of  $\beta$ -TC6 cells could be scaled up simply by increasing culture volume in a stirred suspension bioreactor. Static and SSB cultures were compared directly for cell yield and growth rate over a 3 week culture period. Although the SSB culture offers benefits when compared with static culture, **Figure 6.1** demonstrates that there was no improvement in cellular expansion when compared to static cultures. The batch fed method had the same fold expansion over 21 days, and offered no significant improvement in growth rate compared with the static culture method.

### ***Nutrient fluctuations in static and SSB cultures***

As glucose is a key nutrient in cell culture, and glucose concentrations above normal are toxic to  $\beta$  cells over time in vivo [38], high and low levels of glucose were investigated as a limiting reagent for growth rate in static and SSB cultures with regular (3 day) medium changes. Static and SSB cultures were compared using standard medium with high glucose (4.5 g/L) as well as intermediate (2.75 g/L), and low (physiological) glucose (1.0 g/L) medium. Measurements were taken every 3 days, and it was found that static cultures experienced significant fluctuations in glucose levels (**Figure 6.2a**), which may limit cellular expansion and could diminish cellular viability and function. However, similar fluctuations were observed in the SSB cultures (**Figure 6.2b**), which may explain the similarities in cell expansion rates demonstrated in **Figure 1** for static and SSB cultures. These results were consistent with the observation that no differences were observed in cell yields between static and SSB cultures (**Figure 6.2c**).

To determine whether the high levels of glucose observed when using standard medium or the fluctuations themselves were responsible for the limited cell expansion, cultures with different glucose concentrations were compared over the three week period. Culture medium with lower

glucose concentrations could not maintain physiological glucose levels, and resulted in undetectable levels after 15 days of culture. Glucose measurements from  $\beta$ -TC6 spheroids using high (4.5 g/L) glucose medium resulted in super-physiological glucose levels for the duration of the 21 day culture period. Medium with intermediate (2.75 g/L), and low (1.0 g/L) glucose concentrations fluctuated between super-physiological and sub-physiological glucose concentrations, and resulted in levels below the detection threshold after 15 and 21 days of culture for SSB and static culture methods respectively. Despite maintaining glucose levels closer to the physiological range [39] in both culture methods by feeding with reduced glucose medium, **Figure 6.2c** illustrates that cell expansion was not improved, and was actually slightly reduced when compared to the standard (high glucose) cultures, although only the intermediate glucose SSB culture was significant ( $p=0.027$ ). The cell expansion was statistically similar between the static and SSB cultures at each glucose level. Thus, fluctuations in glucose levels are likely contributing to the limitation of cell expansion.

#### Development of the continuous feeding (CF) culture system

To eliminate glucose fluctuations, a continuous feeding stirred suspension bioreactor system, shown in **Figure 6.3**, was assembled, that continuously replenished medium in the culture system with no manual manipulation during the culture period<sup>131,132</sup>. The perfusion circuit regulated the addition of refrigerated medium to the bioreactor while removing medium through the outflow tube at the same rate. The total culture volume was maintained by adjusting the depth of the outflow tube inside the bioreactor. The outflow tube illustrated in **Figure 6.3b**, allowed the removal of waste medium from the bioreactor without removing the cell spheroids using a fritted glass filter tube with small pores (40-60 $\mu$ m) that prevent the spheroids from being removed. The pore density was high (>40%) and the surface area was large, so that the linear flow velocity through each pore does not exceed the measured settling velocity of the spheroids. The linear

flow velocity ( $V_p$ ) through a pore was calculated using **Equation 6.1** below by dividing the maximum volumetric flow rate through the outflow tube ( $Q$ ) divided by the total pore area calculated by multiplying the pore surface density ( $\rho_T$ ) by the bottom surface area of the outflow tube ( $A_T$ ).

$$V_p = \frac{Q}{\rho_T \times A_T} \quad 6.1$$

The average settling velocity for the spheroids measured after three days of SSB spheroid formation was observed to be  $2.53 \pm 0.26$  cm/min, which is more than ten times the calculated average linear medium velocity through a single pore (0.17 cm/min). This difference ensured that spheroids near the outflow tube were not pulled into the pores of the tube because they settled (due to gravity) much faster than the flow rate pulled them in. This design also ensured that the outflow tube would not become obstructed with spheroids.

#### Continuous feeding increased cell expansion

Eliminating the nutrient fluctuations allowed greater cell expansion. The continuously fed culture was fed at a constant rate equivalent to the other culture methods, replacing 100% of the medium every three days. All cultures were fed with the same high glucose (~500 mg/dL) medium. **Figure 6.4a** shows that continuous feeding at a constant rate eliminated the glucose fluctuations observed when using static or SSB culture methods, but resulted in a super-physiological concentration of glucose in the culture medium for the duration of the culture period. Eliminating these nutrient fluctuations resulted in the general improvement in cell expansion observed in **Figure 6.4b**. Spheroid size was compared on day 6 and day 21 for all conditions. The average sizes on day 6 were  $0.20 \pm 0.01$  mm,  $0.17 \pm 0.01$  mm,  $0.18 \pm 0.01$  mm for static, SSB, and CF-SSB respectively. The average sizes after 21 days of culture were  $0.14 \pm 0.02$  mm,  $0.12 \pm 0.01$  mm, and  $0.28 \pm 0.04$  mm for the same conditions. Average spheroid sizes were

not significantly different between culture methods for all conditions after 6 days of culture ( $p > 0.08$ ), while the spheroids in the CF condition were significantly larger than either static or SSB cultures ( $p < 0.02$ ) after 21 days of culture. The larger size of the spheroids in the CF culture group is consistent with our cell count data, suggesting a higher growth rate for cells in the CF group. The average viability for all days and all culture conditions was  $96.23 \pm 0.85\%$ , and no differences were observed when comparing culture conditions or culture time points. This suggests that increased cell yields are primarily the result of increased growth rate, rather than reduced cell death following reduction of glucose fluctuations.

#### *Continuous feeding could not maintain Physiological glucose levels*

Although the continuous feeding system eliminated the glucose fluctuations and improved the cell expansion, physiological levels could not be maintained using the recommended culture medium. In order to reduce the average glucose concentration in the culture, media with low or intermediate glucose levels were used. The continuous feeding system replaced medium in the culture at a rate of 100% medium change every three days. **Figure 6.5** shows that using feed medium with decreased glucose concentration cannot maintain physiological levels for the duration of the 21 day culture period. Further, the glucose levels for the CF culture using the ATCC recommended high glucose culture medium stayed super-physiological for the entire 21 day expansion period, while the intermediate and low glucose medium cultures dropped to sub-physiological glucose levels by the 15<sup>th</sup> day of culture, and this may explain the slightly reduced expansion for these conditions.

#### *Adjusting feed rate can maintain physiological glucose levels in SSB culture*

Continuously fed cultures with a constant feed rate were not able to maintain a physiological glucose level during the 21 day culture period. In order to maintain a more constant culture environment, an algorithm was developed to adjust the feed rate by incorporating data obtained

from regular culture samples. The algorithm incorporated the predicted growth rate based on current cell counts, the predicted medium replacement rate based on historical glucose consumption measurements, and the adjusted feed rate based on current medium glucose measurements. Adjusting the feed rate based on this algorithm in a continuously fed SSB culture improved the cell expansion by 25% (**Figure 6.6a**) compared to the constant feeding method and the glucose level in the medium was maintained near physiological levels for the duration of the 21 day culture (**Figure 6.6b**).

Predicted linear growth rate

**Equation 6.2** represents a linear approximation that was used to predict growth in culture. Previous spheroid culture data was fit, and a linear approximation most closely resembled the growth profile of the  $\beta$ -TC6 spheroids. This equation was used to predict the cell number every three days of culture. The equation calculates the predicted cell count ( $N_2$ ) by adding the cell count on the day of sampling ( $N_1$ ) to the linear growth rate approximated by fitting previous growth data ( $R_G=1.26 \times 10^8$  cells/day), which is multiplied by the culture period ( $t_2-t_1$ ).

$$N_2 = N_1 + R_G \times (t_2 - t_1) \quad 6.2$$

Predicted medium replacement rate

To predict the feed rate that was needed to replace the glucose consumed during culture, **Equation 6.3** incorporated the predicted cell growth to calculate the glucose consumption during the culture period. The feed rate ( $R_F$ ) was calculated by assuming that it should equal the estimated glucose consumption of the entire culture and dividing by the glucose concentration in the feed medium ( $C_F$ ). This equation used the cellular glucose consumption rate ( $R_1=1.25 \times 10^{-10}$  mg/cell/min), which was calculated by averaging the consumption rate empirically measured in previous SSB cultures over a 21 day culture period. The cellular consumption rate was multiplied

by a weighted average of the cell number counted in a sample ( $N_1$ ) and the predicted cell number ( $N_2$ ) from **Equation 6.2** to approximate the glucose consumption during the culture periods. The weighted average weights  $N_1$  two times over the predicted cell number in the average to increase the influence of the experimentally obtained data specific to each culture. This consumption rate was then divided by the glucose concentration ( $C_F$ ) in the feed medium (4.5 g/dL for these experiments) to obtain the predicted medium replacement rate needed to maintain a constant glucose concentration in culture.

$$R_F = \frac{R_1 \times \frac{2N_1 + N_2}{3}}{C_F} \quad 6.3$$

*Adjusted feed rate based on glucose levels*

In order to incorporate actual glucose levels observed during culture, **Equation 6.4** was added to provide a feedback control system. This adjusted the predicted culture medium replacement rate to account for the measured glucose levels in the culture medium on each sample day. The glucose adjusted feed rate (GAFR) is the rate that medium was actually replaced in the culture. This equation incorporated a unit-less engineering feedback control constant ( $X$ ) ranging from 0-1 (value of 0.5 used for these experiments). It could be adjusted to change the amplitude of the feedback control with a smaller “ $X$ ” causing less control, and larger “ $X$ ” cause more control.  $C_1$  was the glucose concentration measured in the culture medium on the sample day, and  $C_D$  was the desired medium glucose concentration (100 mg/dL). The difference between  $C_1$  and  $C_D$  was divided by  $C_D$  to obtain a ratio describing the deviation from the desired glucose concentration, which was then multiplied by the control constant. The final value was subtracted from 1 to obtain the adjustment factor used to adjust the predicted medium replacement rate found in **Equation 6.3** ( $R_F$ ). This adjustment decreased the feed rate when the glucose levels were higher than the desired concentration, and increased the feed rate when glucose levels were lower than

the desired concentration. The effects of the feedback control are shown in **Figure 6.6**, where the calculated feed rate was plotted on the right hand axis. A large spike in the feed rate as calculated by the growth rate prediction part of the equation was observed on the 9<sup>th</sup> day of culture, that was “corrected” downward by the feedback control on the 12<sup>th</sup> day when the glucose levels in the medium were measured to be increasing above the desired concentration.

$$GAFR = \left[ 1 - X \left( \frac{C_1 - C_D}{C_D} \right) \right] R_F \quad 6.4$$



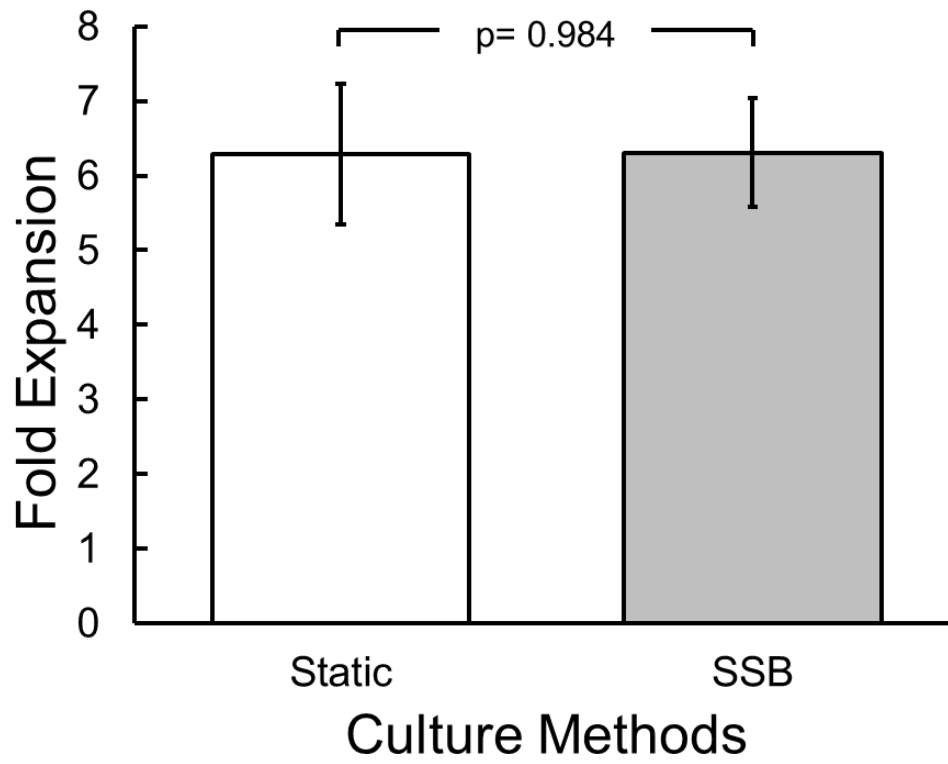


**Figure 6.1: Culture in SSB.** Fold expansion of  $\beta$ -TC6 spheroids after twenty one days compared stirred suspension bioreactor to static culture using standard high glucose medium.

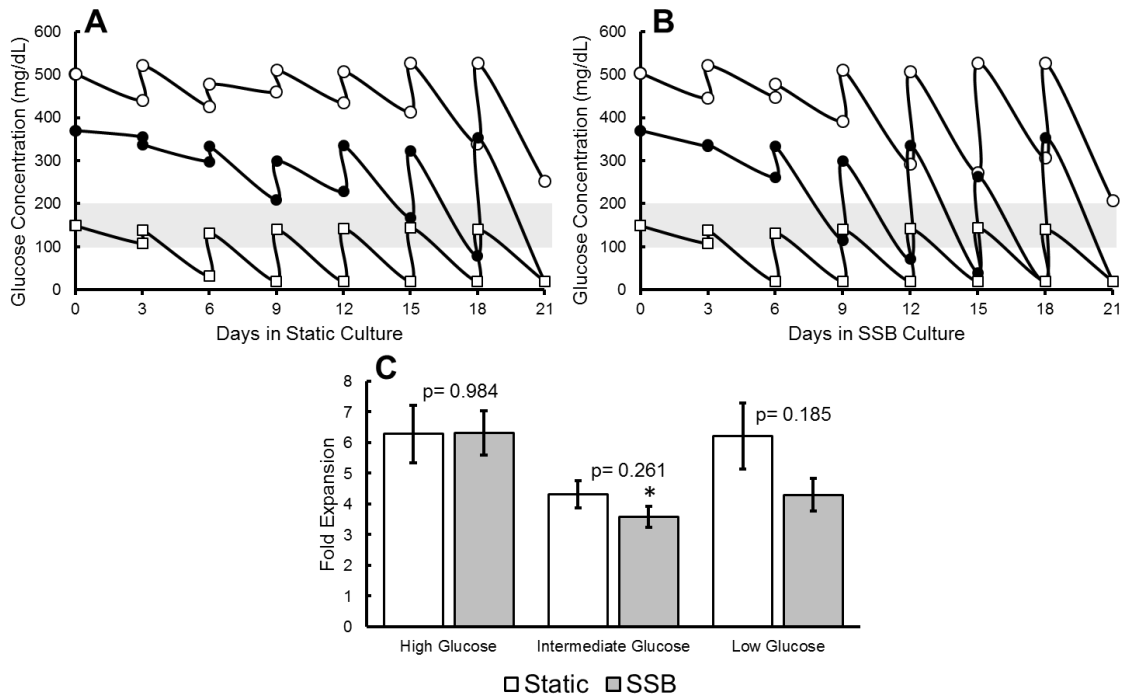


**Figure 6.2: Glucose measurements in SSB cultures.** Glucose measurements from  $\beta$ -TC6 cell spheroids cultured in (A) Static cultures, and (B) stirred suspension bioreactors using high (4.5g/L), intermediate (2.75g/L), and low (1.0g/L) glucose medium, as depicted by their position on the Y axis. The physiological glucose range is indicated by the grey bar. Error bars for glucose measurements are too small to be visible on the scale shown (Standard Error  $\leq$  4% for all measurements). (C) No difference was seen comparing static to SSB cultures with any of the glucose levels. Comparison of expansion of  $\beta$ -TC6 spheroid cultures indicated that changing the glucose in the medium to achieve levels closer to the physiological range did not significantly improve cell expansion. (\* indicates a p value of 0.027 compared with the same culture method using high glucose medium.) SSB: stirred suspension bioreactor.

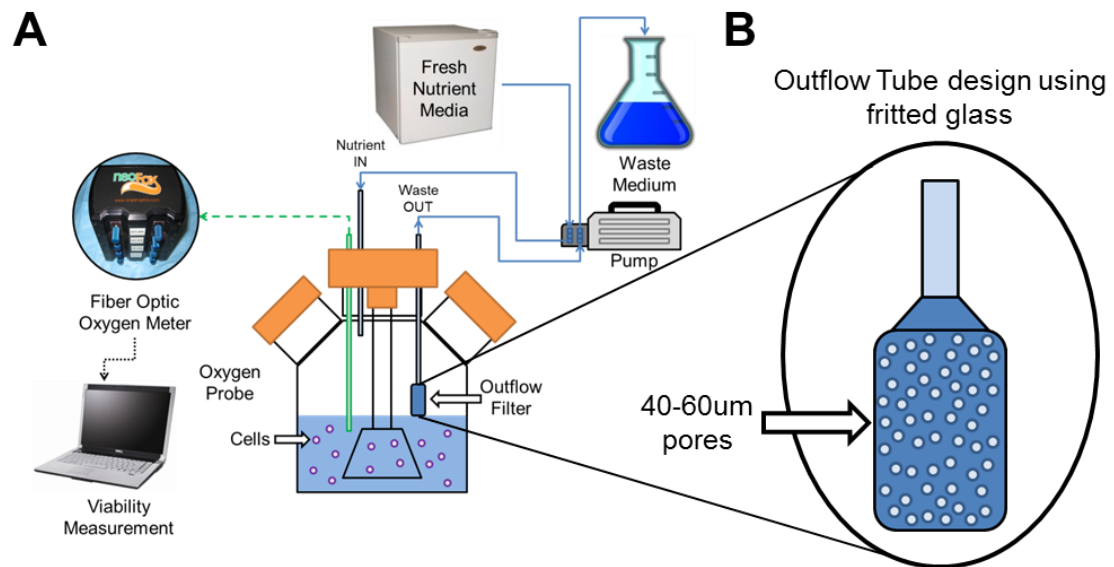


**Figure 6.3: Perfusion SSB diagram.** (A) Schematic diagram of continuous feeding perfusion circuit with fresh medium, perfusion pump, outflow tube, and waste medium. Solid blue lines are medium connections, dashed green lines are fiber optic connections, and dotted black lines are electronic connections. (B) Exploded illustration of outflow tube showing small pores, which do not allow spheroids to pass through, but allow the removal of waste medium. The continuous feeding system was designed to help improve consistency of nutrient and supplement concentrations making  $\beta$ -TC6 cell culture parameters more stable and controlled.

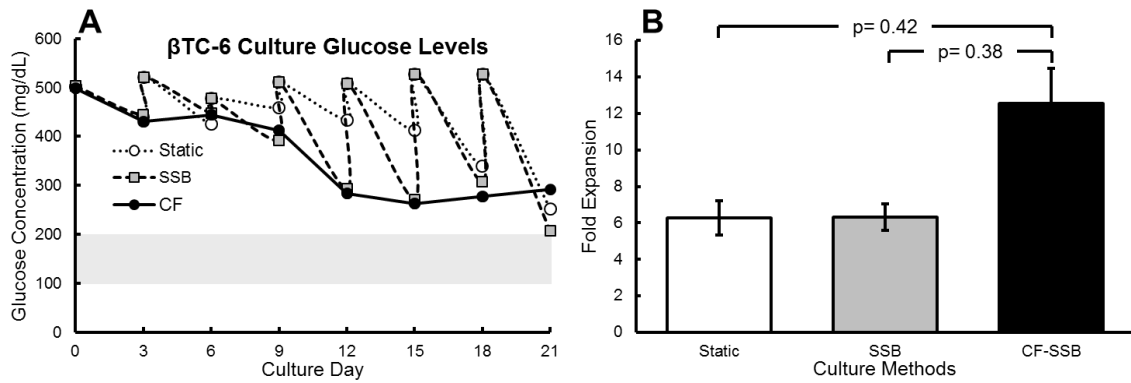


**Figure 6.4: Continuous feeding glucose and cell expansion.** (A) Glucose measurements for  $\beta$ -TC6 spheroid culture medium using static, SSB, and CF-SSB culture methods and feeding with standard high glucose medium. The physiological glucose range is indicated by the grey bar. Error bars for glucose measurements are too small to be visible on the scale shown (Standard Error  $\leq$  4% for all measurements). (B) Fold Expansion of  $\beta$ -TC6 spheroids over 21 days of culture comparing static, SSB, and CF culture methods. SSB: stirred suspension bioreactor. CF: Continuously fed stirred suspension bioreactor.

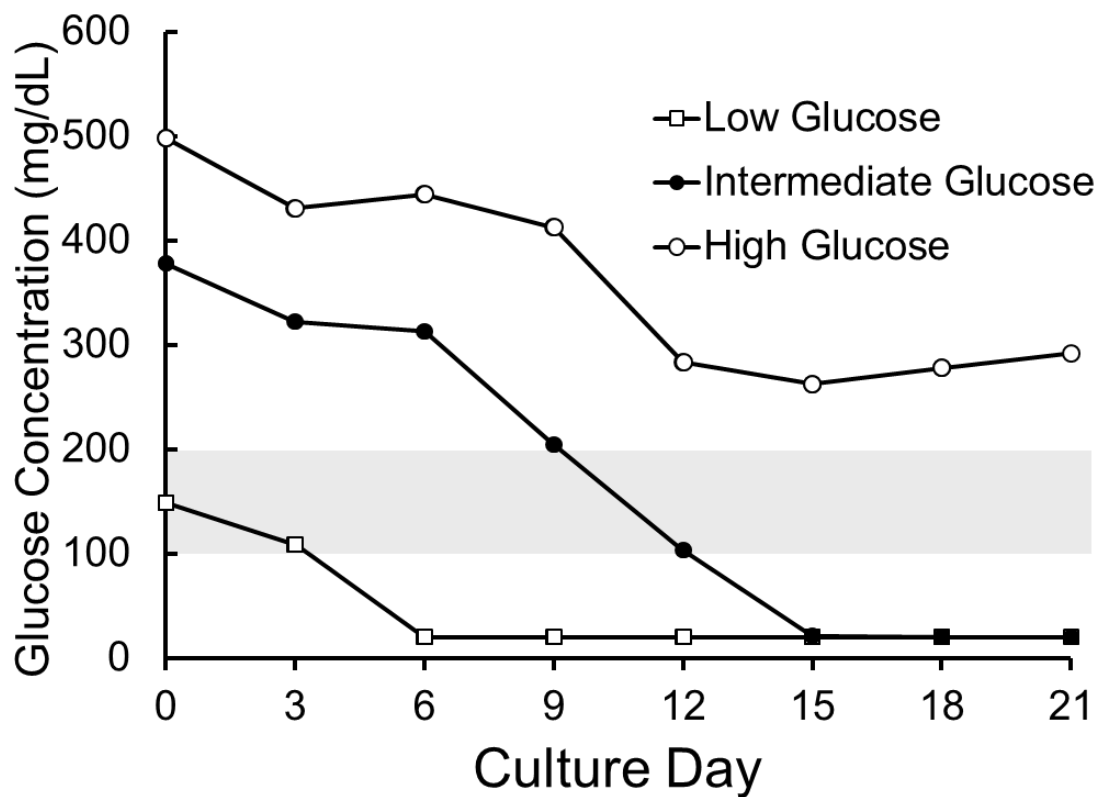


**Figure 6.5: Glucose measurements with continuous feeding.** Culture medium glucose measurements from continuous fed cultures with high, intermediate, or low glucose medium during 21 days of expansion. The physiological glucose range is indicated by the grey bar.

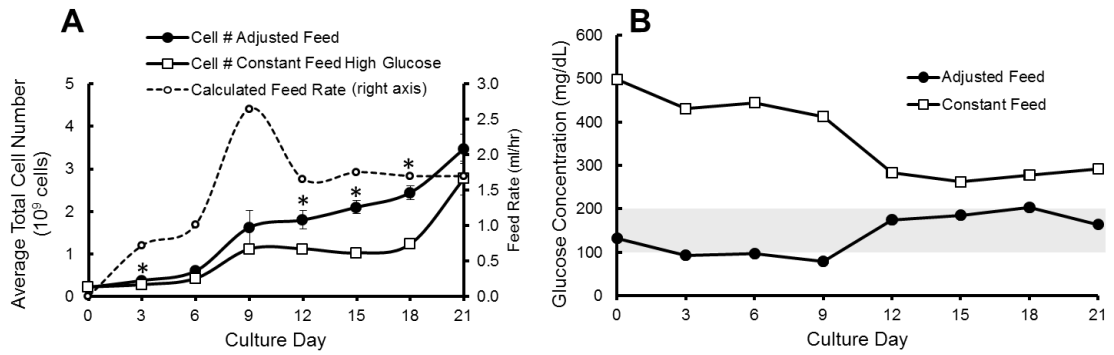


**Figure 6.6: Adjusted feed rates improve SSB cultures.** (A) Cell counts comparing constant feed rate to adjusted feed rate from the same cultures (\* represents a p value < 0.05 indicating a significant difference in culture expansion). (B) Average culture medium glucose levels from 21 day constant feeding, and adjusted feeding bioreactor cultures. The physiological glucose range is indicated by the grey bar. Error bars for glucose measurements are too small to be visible on the scale shown (Standard Error  $\leq$  4% for all measurements).

## ***Discussion***

Cell therapies are the subject of intense research activity, and are becoming a realistic treatment option for many human diseases<sup>148-151</sup>. Many cell therapies will require the large-scale culture and monitoring of mammalian cells, as well as defined and validated culture conditions. Large-scale bioreactors provide an established approach from bio-pharmaceutical applications and culture of microorganisms that can be applied to the culture of mammalian cells with specific modifications to address this challenge. Mammalian cell culture techniques use static culture in disposable dishes for most research applications. Simply scaling up from static cultures to SSB methods still requires medium changes at regular intervals that result in dramatic changes in the cell culture environment. Cells are dosed with high concentrations of nutrients and growth factors at these batch-style medium changes to ensure survival between changes. During the culture intervals, cells experience steadily decreasing nutrient levels and increasing waste products. To address these issues in this study, glucose measurements were made to estimate degrading and consumed nutrients in the medium that spike immediately following medium change, and drop significantly over time, resulting in a constantly changing environment for the cells over the culture period. This study demonstrated that glucose levels fluctuated dramatically in the static and SSB culture of  $\beta$ -TC6 beta cell line, with 100% medium changes every 3 days. During cell expansion, when the cell density was greatest, glucose concentrations dropped as much as 275 mg/dL over three days. Although the glucose concentration never dropped to a physiological level during the 21 day culture period when culturing with DMEM high glucose medium (450 mg/dL) that is standard for the  $\beta$ -TC6 cell line, these fluctuations limited cell yield. The SSB medium glucose levels dropped at a similar rate with static cultures, and were nearly identical after 21 days of culture in static and SSB conditions.

Most cells experience environments *in vivo* that are more stable than cell culture conditions, with regulated levels of nutrients, and the constant processing and removal of cellular waste products. In this case, fluctuations in nutrient levels were sufficient to limit cell expansion. One strategy to improve the continuity of culture conditions is to increase the frequency of medium changes, decreasing nutrient level fluctuations and buildup of waste. Despite the improvements this approach would bring to nutrient and waste levels, for large-scale and long-term mammalian cell cultures, the time and cost associated with frequent batch-style medium changes make this approach impractical. The data presented in this study suggest that use of a stirred suspension bioreactor with growth adjusted continuous medium replacement can both maintain controlled culture conditions and improve culture outcomes without significant impact on cell viability. The increase in cell number and spheroid size, along with the consistent viability levels among culture groups suggest that CF culture conditions support increased growth rates in these cultures. Spheroids in static cultures were slightly larger than those in a SSB cultures, likely due to observed agglomerations under static conditions.

The adjusted feed algorithm used for these studies incorporated the linear growth rate of the cells in a spheroid, assumed a constant and average glucose consumption rate for all of the cells in culture, and included a feedback control system to account for the variability of individual cultures. A linear growth rate was used based on observed data from suspended  $\beta$ -TC6 cell spheroid cultures, but exponential growth, or more complex growth profiles could be used for various cell types. Glucose consumption and feeding can be generalized to a number of key nutrients in the medium. The glucose consumption used for these calculations were assumed to be constant and the same rate for each cell in the culture, but more complex glucose consumption relationships could be used in the same algorithm for cultures that contain more than one cell type or cell types that change during the culture period, such as differentiating stem cells. These



techniques could also be used in conjunction with other advanced culture technologies including encapsulation, or micro-carrier surface cultures for adherent cells to improve cell growth rates. Any empirically determined glucose consumption profile specific to a cell type could be used to determine the needed medium replacement rate. In this study, the average glucose consumption rates observed in all conditions were similar to the rates observed in surface attached cultures suggesting that spheroid formation itself did not affect the glucose consumption of individual cells. The feedback adjustment system for this algorithm is a simple control that incorporates the scaled difference between the observed glucose levels and the desired glucose levels in the culture medium. More complex adjustment systems could be implemented to provide tighter culture control. The effects of this simple control system were apparent after nine days of culture (**Figure 6.6a**), when the predicted growth rate and glucose consumption rates were not able to maintain physiological levels on their own. The feedback control parameter was able to account for the increasing glucose concentrations in the culture, and adjust the predicted glucose replacement rate, decreasing it to account for the real-time observed glucose concentrations despite the increasing cell numbers. Furthermore, more complex cellular models tied to feedback control systems<sup>152,153</sup> could be used to help regulate other culture parameters such as pH, dissolved oxygen concentration, and temperature. The adjusted feed system could be incorporated into a fully automated culture system<sup>125,133</sup> and the feed rate could be adjusted based on more frequent sampling measurements which would further improve the control of nutrient levels in the medium. The automated system could control any culture parameters making mammalian cell cultures more consistent and production more reproducible.

Federal regulatory bodies have decided that mammalian cellular products for implantation or other cell therapy will be held to a similar standard as other transplant therapies. The industry is focused on developing and providing completely defined culture media<sup>154-156</sup> and working to meet

these guidelines. Cell culture and manufacturing parameters will need to be controlled, monitored and recorded to ensure the efficacy and reproducibility of cellular products. As new products translate from the research lab into the clinic, the challenges of scale-up and production will be a significant barrier to implementation. As cell therapies are emerging as a treatment option for many human diseases, it is essential that culture parameters for cellular products are clearly defined, controlled, and monitored during the manufacturing process. Continuous medium replacement can reduce or eliminate fluctuations in critical nutrients observed in both static and stirred suspension bioreactor cultures. Incorporating an adjusted feed rate algorithm can further improve the control of culture conditions and can maintain near physiological nutrient levels for an extended culture period.

### ***Conclusion***

The continuous feed system maintains glucose levels in the physiological range, when adjusted for cell growth and glucose consumption rate. Maintenance of glucose levels and removal of waste products continually supported cell expansion while maintaining viability. These systems could be adapted for expansion and differentiation of other cell types, including pluripotent stem cells, in addition to their utility for therapeutic mammalian cell spheroid culture.

**DEVELOPMENT OF METHODS AND TECHNIQUES**  
**FOR IMPROVING ORGAN PROCUREMENT AND**  
**PRESERVATION**

## Chapter 7 **<sup>19</sup>F-MRS FOR OXYGEN MEASUREMENT**

Sections of this chapter are reproduced in whole, or in part from the following publications with permission:

Presented Abstracts:

**Weegman BP**, Einstein SA, Steyn LV, Suszynski TM, Firpo MT, Graham ML, Janecek J, Eberly LE, Garwood M, Papas KK, “Continuous oxygen delivery improves oxygenation of tissue-engineered islet grafts in vivo as measured with fluorine-19 magnetic resonance spectroscopy” Abstract accepted for a mini-oral presentation at the Joint IPITA-IXA-CTS Congress, November 2015, Melbourne, AUS

**Weegman BP**, Einstein SA, Purvis W, Steyn LV, Stanton JB, Kitzmann JP, Mueller KR, Limesand SW, Suszynski TM, Firpo MT, Graham ML, Janecek J, Eberly LE, Garwood M, Papas KK “Non-Invasive Monitoring of Hypoxia and Viability Assessment of Implanted High-Cell-Density Tissue-Engineered Grafts” Accepted for a poster presentation at The Nineteenth Annual Hilton Head Regenerative Medicine Workshop, May 2015, Hilton Head, SC, USA

Manuscripts in Preparation:

Einstein SA, **Weegman BP**, Suszynski TM, Firpo MT, Papas KK, Garwood M, “Development and validation of noninvasive magnetic resonance relaxometry for the *in vivo* assessment of tissue-engineered graft oxygenation.”

License and agreement documentation is included in **Appendix G**.

**Acknowledgements:** The authors would like to thank the Schott Foundation, the Minnesota Lions Diabetes Foundation, the Juvenile Diabetes Research Foundation (JDRF 5-2013-141), Giner Inc., the Schulze Diabetes Institute, and the NIH (P41 EB015894, and S10 RR025031) for supporting this research.

## **Development and validation of noninvasive magnetic resonance relaxometry for the *in vivo* assessment of tissue-engineered graft oxygenation.**

### ***Summary***

This chapter describes a  $^{19}\text{F}$  magnetic resonance spectroscopy ( $^{19}\text{F}$ -MRS) method for non-invasive evaluation of oxygen levels ( $\text{pO}_2$ ) within implanted TEGs. Our early studies and literature have identified perfluoro-15-crown-5-ether (PFCE) as the optimal choice for *in vivo* oximetry, and we developed robust oxygen and temperature calibration data sets using this compound.  $^{19}\text{F}$ -MRS methods were validated *in vitro* with a temperature and oxygen regulating bioreactor, and *in vivo* by implanting into a dorsal subcutaneous pocket of Lewis rats (Charles River, Wilmington, MA). Fiber optic fluorescence-quenching sensors (Ocean Optics, Dunedin, FL) were used to simultaneously measure oxygen levels *in vitro* and *in vivo*, and  $^{19}\text{F}$ -MRS data were collected for all animals using a 16.4 T horizontal-bore magnet (Agilent Technologies, Santa Clara, CA). The  $\text{pO}_2$  within TEGs were determined using the fluorine spin-lattice relaxation rate,  $R_1$  ( $=1/T_1$ ), and the established calibration between  $R_1$  and  $\text{pO}_2$ . PFCE within the TEG was detected with sufficient signal to noise (SNR), and oxygen was measured non-invasively both *in vitro* and *in vivo*. Fiber optic (FO) oxygen sensor measurements *in vivo* reporting single point oxygen pressures were on average 11 mmHg higher than  $^{19}\text{F}$ -MRS measurements ( $p < 0.05$ ), which represent an average pressure within the scaffold.  $^{19}\text{F}$ -MRS could be a valuable tool for the non-invasive assessment of oxygenation within an implanted macro-encapsulated TEG. The average  $\text{pO}_2$ , provided by the MRS method, is a more robust measurement of the overall graft oxygen status when compared to FO single point measurements. Further studies investigating local oxygen delivery systems and relating  $\text{pO}_2$  measurements with changes in TEG status or condition are described in **Chapter 8**.

## ***Introduction***

Tissue engineering is an emerging field, and implantable tissue-engineered grafts (TEGs) have the potential to treat numerous debilitating diseases. Pancreatic islet transplantation (ITx) is a potential cure for type 1 diabetes, but favorable long-term outcomes are inconsistent, and the liver may not be the optimal site. Macro-encapsulation of islets within a TEG could offer many advantages, however oxygenation is a critical limitation for the development of large-scale and high-cell density implanted TEGs<sup>57,157</sup>. Islets are especially sensitive to prolonged exposure to hypoxia, which has been shown to decrease graft viability and function<sup>59</sup>. Oxygen limitations are a critically important consideration for the development of large-scale implantable TEGs, and a tool for non-invasive monitoring of the oxygen partial pressure (pO<sub>2</sub>) could be used to improve graft development and potentially monitor graft viability post-implant.

Eppendorf needle probes, utilizing polarographic techniques, remain the gold standard for *in vivo* oxygen measurements. These needle probes, however, remain invasive, MR-unsafe, and only measure the oxygen at a single point necessitating multiple measurements to map the average oxygenation of a given volume. Luminescence-based fiber optical (FO) sensors are an MR-compatible oxygen-measurement technique providing equivalent results when compared with Eppendorf probes while remaining invasive and limited to single-point measurements.

Magnetic Resonance Spectroscopy (MRS) is a useful tool for observing real-time biological changes in a non-invasive way. The nuclear spin relaxation mechanisms of some biocompatible fluorine compounds (perfluorocarbons, PFCs) are sensitive to dissolved oxygen concentrations, and fluorine-19 nuclear magnetic resonance spectroscopy (<sup>19</sup>F-MRS) can be used to quantify the oxygenation status of a TEG. Highly substituted fluorine molecules have demonstrated to be useful for the measurement of oxygen concentration *in vitro* and *in vivo*<sup>158-173</sup>, but have had limited clinical applications due to high levels of uncertainty and difficulty with molecule

delivery to target tissues<sup>174</sup>. <sup>19</sup>F itself has many qualities that make it an ideal nuclear target for oxygen measurements *in vivo*. Specifically <sup>19</sup>F has a relatively large magnetic moment, and this provides a relatively high sensitivity (similar to <sup>1</sup>H). Furthermore, there is very little background <sup>19</sup>F signal in the body, due to its relative scarcity in biological systems, and this allows for detection of relatively small amounts of fluorine without background interference.

The observed spin-lattice relaxation rate constant ( $R_1$ ) of the <sup>19</sup>F nuclei is established to have a linear relationship to the local oxygen concentration<sup>158,159,175-177</sup>. Relaxation in the context of MRS describes the physical phenomena of the change in magnetization that occurs following nuclear spin excitation in the presence of a magnetic field. Two basic relaxation mechanisms are observed in magnetic resonance (MR); they are defined as the transverse (spin-spin) relaxation time and the longitudinal (spin-lattice) relaxation time. The transverse relaxation time is defined by a decay constant ( $T_2$ ) and it describes the exponential return of excited magnetization to the lowest energy state (thermal equilibrium). This is sometimes called “spin-lattice” relaxation because the decay occurs as the individual spins lose energy to the surrounding “lattice.” This mechanism is strongly influenced by the temperature and local oxygen concentration (due to its quadrupolar nature), which results in an associated change in the relaxation rate constant ( $R_1=1/T_1$ ). The details of this physical process are described by Parhami and Fung<sup>158</sup> among others<sup>175,176</sup>. The transverse relaxation time is defined by a second time constant ( $T_2$ ) and it describes exponential decay of MR signal caused by the loss of spin coherence or “de-phasing” following spin excitation. This complex relaxation mechanism is also influenced by numerous physical and chemical interactions, and in our hands has been less reliable for these purposes, nevertheless, this mechanism should be explored further in future work.

Perfluorocarbons (PFCs) are used for biological oxygen measurements using <sup>19</sup>F-MRS, and perfluoro-15-crown-5-ether (PFCE) is the preferred choice due to reasonable biocompatibility,

high oxygen solubility, and optimal signal intensity<sup>161,168,170,172,178-181</sup>. Researchers have developed *in vitro*, and *in vivo* MRS methods for the determination of oxygen concentrations within microcapsules loaded with cells<sup>161,168-170</sup>, and our lab has used similar methods for determination of TEG viability *in vitro*<sup>182</sup>. This study expands these methods for non-invasive measurement of oxygen concentrations within a bio-artificial pancreas (TEG) constructs implanted in rats.



## ***Materials and Methods***

### *Comparison of PFC Compounds*

Various PFC materials were tested for oxygen and temperature sensitivity using neat compounds. An extensive literature review supported these findings<sup>159–162,168,183–185</sup>, and PFCE was chosen for the following studies due to the high oxygen sensitivity and large number of equivalent <sup>19</sup>F (N=20). The large number of equivalent <sup>19</sup>F atoms resulted in much higher relative signal intensities for a single resonance when using the same amount of PFC chemical. Perfluorodecalin (PFD) was also used for development of an implantable temperature probe that was used for some preliminary *in vitro* studies due to the abundant availability and established biocompatibility.

### *TEG Construction*

TEG construction is described in detail in **Chapter 8**. Briefly, Model TEGs were prepared by loading encapsulation devices with an oxygen sensitive matrix. Fluorine-loaded fibrin gels were prepared with 75 µl of porcine plasma (Sigma Aldrich, St. Louise, MO, USA) that was emulsified with 75 µl of perfluoro-15-crown-5-ether (Exfluor Research Corporation, Round Rock, TX, USA). The mixture was emulsified by manual agitation, injected into a 40 µl TheraCyte device (TheraCyte, Inc. Laguna Hills, CA) using a 250 µl precision syringe (Hamilton), and then cross-linked with 5% v/v bovine thrombin solution. The thrombin solution was made by diluting concentrated topical thrombin solution (GenTrac Inc., Middleton, WI) in PBS++. The cell access port was trimmed short, and sealed with adhesive (Dermabond, Ethicon Inc., Somerville, NJ, USA). These grafts were used for calibration as well as *in vitro* and *in vivo* validation studies.

### *<sup>19</sup>F-MRS Acquisition*

<sup>19</sup>F-MRS spectra were acquired with a 16.4 Tesla MR system (Agilent Technologies, Santa Clara, CA, USA) using a custom-built single-loop surface coil tuned to 656.8 MHz. Pictures of equipment developed and designed for use in these studies are included in **Appendix A**. An inversion-recovery pulse sequence was used to measure the spin-lattice relaxation rate, R<sub>1</sub>. Adiabatic half-passage (at60ph0) and adiabatic inversion pulses (invpat10) were used to ensure a uniform flip angle. At the beginning of each study, the coil was tuned and the samples were placed into the bore of the magnet. PFC resonance was confirmed to ensure hardware functionality, and the iso-center was located by performing a 1D profile and adjusting the sample position to center the maximum signal intensity within the bore. First and second order shims were manually adjusted to achieve maximal signal intensity and to minimize the spectral line-width for the desired resonance. Representative spectra from two PFCs studied (PFCE, and PFD) are presented in **Figure 7.1**. For each scan, the magnetization recovery was interrogated after 10 different inversion-recovery delays (0.05, 0.1, 0.15, 0.25, 0.5, 0.75, 1, 2, 4, and 5 seconds), each spectral array was integrated (integralWater3), and integrations were fit to **Equation 6.4** using 3-parameter non-linear regression with GraphPad Prism software (v5, Graphpad Software Inc., La Jolla, CA, USA).

$$M_z(t) = M_{z,eq} \left( 1 - 2 \cdot e^{-t/T_1} \right) + C \quad 7.1$$

Representative integration data and fit-curve are shown in **Figure 7.2** (spectral lines are included for illustrative purposes). **Equation 6.4** is the solution to the time (t) dependent Bloch equation for the longitudinal magnetization, M<sub>z</sub>(t), during an inversion-recovery pulse sequence when TR >> T<sub>1</sub> and TE << T<sub>2</sub>. To achieve the most robust measurement of T<sub>1</sub>, three parameters are fit with regression: M<sub>z,eq</sub> (the equilibrium magnetization), T<sub>1</sub> (the spin-lattice relaxation time constant), and C (a fitting constant).  $M_z = A \cdot \left( 1 - 2e^{-R_1 \cdot t} \right) + B$ . Each condition was measured in

replicate (n=6) with a TR of at least 5 x T<sub>1</sub> seconds (6 seconds was used for most studies using PFCE).

#### Calibration and Temperature Compensation

A small pilot study was done using a PFD loaded temperature probe. Pictures of the probe used are included in **Appendix A** for reference. PFD (~2 ml) were sealed in a 1.5 mm diameter glass NMR tube to ensure that oxygen cannot diffuse into or out of the sealed tube. A method for temperature compensation was initially investigated using the developed PFD temperature probe to compensate for any temperature changes encountered during the course of the study. A temperature calibration curve using the PFD probe was generated. The PFD probe was tested to ensure that it was not sensitive to oxygen by a same bubbling technique described in the calibration section below, and confirming that PFD-R<sub>1</sub> did not change. The R<sub>1</sub> of the PFD probe was measured by <sup>19</sup>F-MRS under 4 temperature conditions confirmed by MRI compatible thermocouple. The results were fit to **Equation 7.2** assuming a linear relationship between R<sub>1</sub> and temperature (T), and the line is shown in **Figure 7.3**.

$$R_1 = A \cdot T + B \quad 7.2$$

The same technique was used to determine the temperature sensitivity of neat PFCE using 6 different temperatures confirmed by MRI compatible thermocouple, and the curve is presented in **Figure 7.4A**. Due to the relatively small change in the oxygen sensitivity with changing temperature (see **Figure 7.5**), the room-air (pO<sub>2</sub> ≈ 150 mmHg) condition was used for the PFCE temperature curve. The PFD temperature probe was used for a brief series of experiments where the probe was included during oxygen calibration of PFCE loaded TEG. The R<sub>1</sub> of PFD in the temperature probe was used with the calibration line presented in **Figure 7.3** to determine the temperature of the sample. The calculated temperature was then used along with the PFCE

temperature calibration fit (**Figure 7.4A**) to determine the difference in the calculated PFCE  $R_1$  and the  $R_1$  at 37 °C in room-air. This difference was then subtracted from the measured sample PFCE- $R_1$ , and then fit on the oxygen sensitivity curve for PFCE at 37 °C presented in **Figure 7.4B** to calculate the temperature-adjusted  $pO_2$  of the sample. Temperature control and measurement using an MRS compatible thermocouple during *in vitro* and *in vivo* studies were greatly improved during the development of these methods. The multi-parametric calibration fit equation described below was used along with thermocouple temperature measurements instead of the PFD MRS temperature probe for all future studies. This approach was found to be equally reproducible, more practical, more time efficient. These factors expedited the collection of  $^{19}F$ -MRS data for *in vivo* applications, which was an important consideration when transitioning to studies in living animals.

#### *$^{19}F$ -MRS Calibration with TEGs*

TEGs were prepared as described above and placed into a 50 ml conical tube filled with phosphate buffered saline with calcium and magnesium (PBS++). The vial was placed in the center of a custom-built surface coil and inserted into a 16.4 T MR system (Varian Inc., Palo Alto, CA). The sample was then bubbled with a gas of known oxygen concentration for 30 minutes while the temperature was held constant with a circulating water bath, and forced-air heater. A fiber optic oxygen probe (Ocean Optics, Dunedin, FL) was inserted into the TEG for comparisons to the  $^{19}F$ -MRS measured  $pO_2$ .  $R_1$  was then measured with an inversion-recovery sequence utilizing adiabatic pulses. Measurements were made for five different  $pO_2$ s (0, 38, 76, 114, and 160 mmHg) at three different temperatures (21, 37, and 45 degrees C). The  $R_1$  was assumed to be a function of the  $pO_2$ , temperature (T) shown in **Equation 7.3** and four calibration constants (A, B, C, and D).  $R_1$  measurements were fit to the multi-parametric calibration equation using a Levenberg–Marquardt algorithm (OriginLab, Northampton, MA). **Equation 7.4** is the

same equation solved for  $pO_2$  to illustrate the linear relationship with  $R_1$  with a given constant temperature. The oxygen curves for each temperature investigated are presented in **Figure 7.5A**.

$$R_1 = A \cdot pO_2 + B \cdot T + C(pO_2 \cdot T) + D \quad 7.3$$

$$pO_2 = R_1 \cdot \frac{-1}{A + (C \cdot T)} + \frac{B \cdot T + D}{A + (C \cdot T)} \quad 7.4$$

#### Validation of $^{19}F$ -MRS $pO_2$ Measurements in vitro

As described in the calibration section above, FO oxygen probes were used in conjunction with  $^{19}F$ -MRS to compare the two techniques. The FO oxygen probe was inserted into the central compartment of the TEG and measurements were obtained simultaneously in the same samples using both methods. A correlation plot comparing both methods is shown in **Figure 7.5B**. Furthermore, in vitro studies were performed using a perfusion bioreactor system with controlled temperatures and oxygen to confirm that  $^{19}F$ -MRS methods could be used to monitor the kinetic changes in oxygen when exogenous oxygen is delivered to the TEG itself.

#### Perfusion Bioreactor

*In vitro* studies were conducted using a perfusion bioreactor system, which continuously perfused with porcine islet culture medium (ME199 based, Mediatech Inc.) around a TEG modified for delivery of supplemental oxygen (DSO). TEGs devices with DSO were used for these *in vitro*  $^{19}F$ -MRS oxygen measurement studies without porcine islets, and placed inside a perfusion bioreactor chamber. Detailed analysis and discussion of the DSO system and *in vivo* studies using these devices is described in **Chapter 8**. The bioreactor perfusion circuit illustrated in **Figure 7.6** was composed of a perfusion-chamber to contain the TEG, a peristaltic pump to circulate culture medium, a gas exchanger to control dissolved oxygen levels in the perfusion medium, and a heat-exchanging system to control the ambient temperature in the chamber. The perfusion chamber

design, illustrated in **Figure 7.7** and **Figure 7.8**, was instrumented with FO oxygen and temperature probes to confirm the  $pO_2$  and temperature of the perfusion medium. The bioreactor containing a TEG was placed inside a 16.4 T MRS system (Agilent Technologies, Santa Clara, CA, USA) to obtain baseline oxygen measurements prior to beginning perfusion. An illustration of the experimental set-up is also included in **Figure 7.9**, which includes a picture of the perfusion chamber and the 16.4 T scanner (note that islets were not used for these studies, but are included in the figure for illustrative purposes). The perfusion medium was de-oxygenated ( $pO_2 = 30 \pm 5$  mmHg) to simulate the low external oxygen levels observed *in vivo*, and the reactor was maintained at  $37 \pm 2$  °C by heating the perfusion medium with a water-bath and heat exchanger. The conditions within the bioreactor are also described in **Figure 7.8** and **Figure 7.9**. Following acquisition of the baseline oxygen measurements, the perfusion medium was circulated at 30 ml/min while the  $pO_2$  and temperature of the perfusion medium was continuously monitored using MR compatible oxygen and temperature probes. Non-invasive measurements of the  $pO_2$  inside the TEG were obtained every 1-5 minutes with  $^{19}F$ -MRS for the duration of the study. After a steady-state  $pO_2$  was observed in the TEG, suggesting acclimation to the surrounding perfusion medium, DSO was initiated. DSO was achieved by delivering oxygen-supplemented gas to the internal compartment of the TEG within the bioreactor at a flow rate of 2 ml/min with two different target oxygen pressures. The first phase delivered gas with a  $pO_2 = 380$  mmHg, which was continued until a steady state  $pO_2$  in the TEG was observed. Then the  $pO_2$  of the delivered gas was increased to 760 mmHg in the second phase until a second steady state  $pO_2$  was observed inside the TEG. Finally, DSO was stopped and oxygen measurements were continued until the  $pO_2$  inside the TEG decayed down to the external  $pO_2$  of the perfusion medium ( $\sim 30$  mmHg). These studies were repeated 5 times to confirm the reproducibility and reliability of the DSO system.

### Animal Research

All animal research presented herein was approved and overseen by the University of Minnesota Institute for Animal Care and Use Committee (IACUC), the University of California IACUC, or the University of Arizona IACUC. This study was designed to minimize the pain and suffering of animals used for the study, and the three R's were observed. These techniques were developed, refined and tested *in vitro* and in deceased animals to minimize the number of animals used to obtain quantitative and significant results. The body weight, and general well-being of each animal was monitored for the duration of the studies described, and no adverse events were noted.

### Validation of $^{19}\text{F}$ -MRS $p\text{O}_2$ Measurements *in vivo*

A small group of *in vivo* validation studies were used in the context of measuring oxygen of implanted TEG in rats. Details of the implant preparation, surgical procedures, and global study design are described in **Chapter 8**. The  $^{19}\text{F}$ -MRS  $p\text{O}_2$  measurements of a subset of TEGs with porcine islets (n=3) and control TEGs (n=3) were validated with an FO oxygen probe *in vivo*. These devices were equipped with an additional access port (**Figure 7.10**). These rats were followed for up to 29 days; on the day of scanning rats were anesthetized and a catheter was transcutaneously inserted into the access port. A previously calibrated FO oxygen probe was then threaded through the catheter into the TEG and the rat was inserted into the MR system. FO  $p\text{O}_2$  was measured simultaneously with the MR  $p\text{O}_2$  measurement technique. Furthermore, additional rats (N=3) were equipped with DSO systems and implanted with TEGs modified for DSO.  $^{19}\text{F}$ -MRS methods were used to monitor the improvement of TEG oxygenation *in vivo* by measuring the  $p\text{O}_2$  in implants after 24 hours of DSO. DSO was then stopped for > 24 hours and measurements were repeated, and compared to implants without DSO.

### *In vivo oximetry in Rats*

A series of rats (N=9) were implanted with a PFCE loaded TEG. On the day of implantation, rats were anesthetized with inhalation isoflurane using a respirator and vaporizer. Details of the device loading and surgical procedure are described in **Chapter 8**. Briefly, TEGs were prepared by loading them with a PFCE fibrin matrix, and were subcutaneously implanted on the dorsal side of Lewis rats. Animals were divided into three groups with three animals in each group. Each group was assigned a critical terminal time-point (1, 7, 15 days post-implantation) when  $^{19}\text{F}$ -MRS was used to measure the internal  $\text{pO}_2$  of the implanted TEG prior to euthanasia. On the day of measurement, rats were anesthetized with inhalation isoflurane. The rats were immobilized onto a holder with the device centered over the custom-built surface coil. The rat holder and coil were designed for use with rats in the 16.4 T MRS system, and pictures of these equipment are included for reference in **Appendix A**. The holder was inserted into a 16.4 T MRS system and scanned while anesthesia depth was continuously monitored and adjusted as needed. Rat body temperature was maintained at  $37 \pm 0.2$  °C as measured with a rectal thermocouple and regulated with a forced air heater. Six  $R_1$  measurements were made with an inversion-recovery sequence utilizing adiabatic pulses. The  $R_1$  of each measurement was converted to a  $\text{pO}_2$  using the previously determined multi-parametric calibration. *In vivo*  $\text{pO}_2$  was measured 1, 4 and 15 days post-implantation.

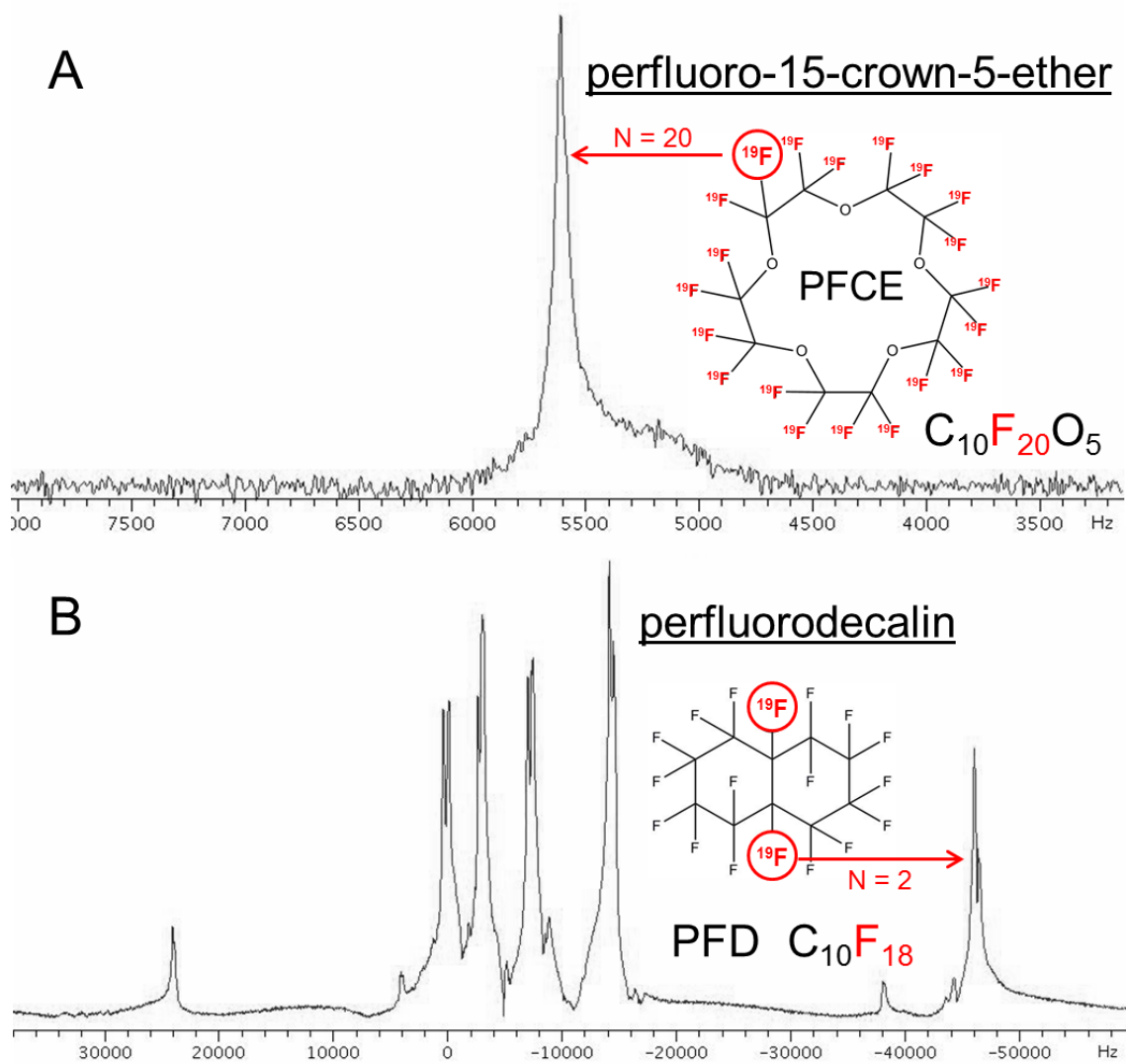
#### Implants with DSO

A small group of animals (N=3) were fitted with harness and tether apparatus for two weeks to allow for acclimation prior to implantation with a TEG modified for DSO. The TEGs were modified to include cannulas for trans-cutaneous oxygen delivery and by including an internal compartment to allow for continuous DSO *in vivo*. Briefly, the 40  $\mu\text{l}$  TheraCyte device previously described<sup>186-191</sup> was modified by adding two additional internal membranes to create a three chamber device with an internal oxygen compartment, and two distinct cell compartments

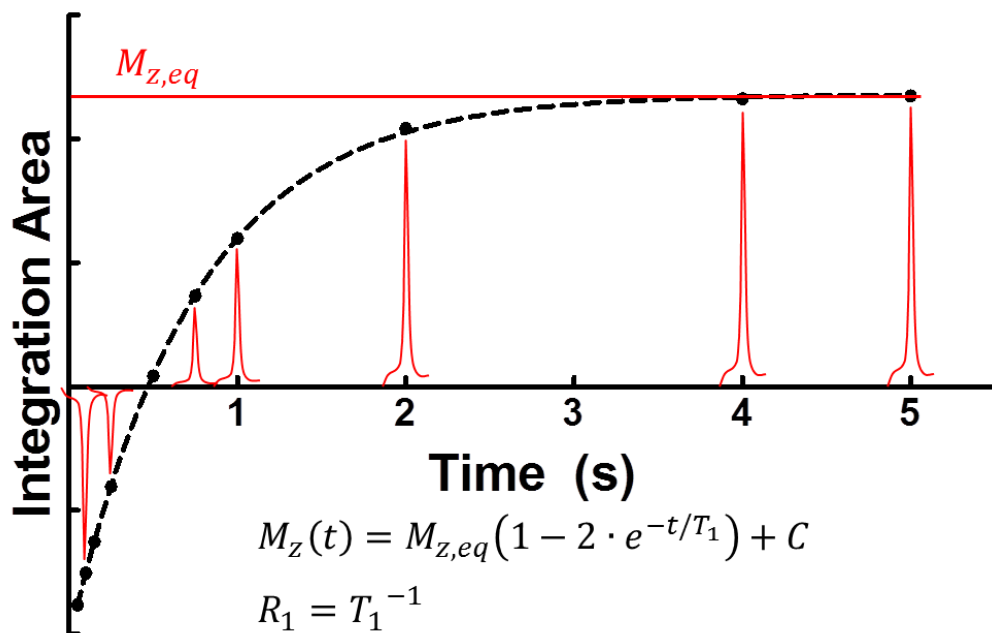


on either side of the central oxygen compartment. Furthermore, three additional access ports were added to the device to access each compartment. Two access ports on the longitudinal ends provide access to the central compartment to allow for oxygen gas infusion and effusion. Two more ports are situated on the transverse sides of the device with one port providing access to a cell compartment on top and the second port providing access to the cell compartment on the bottom. TEGs for DSO were prepared by loading the cell-compartments of the modified devices with a PFCE-plasma gel emulsion (no islets) as described above.

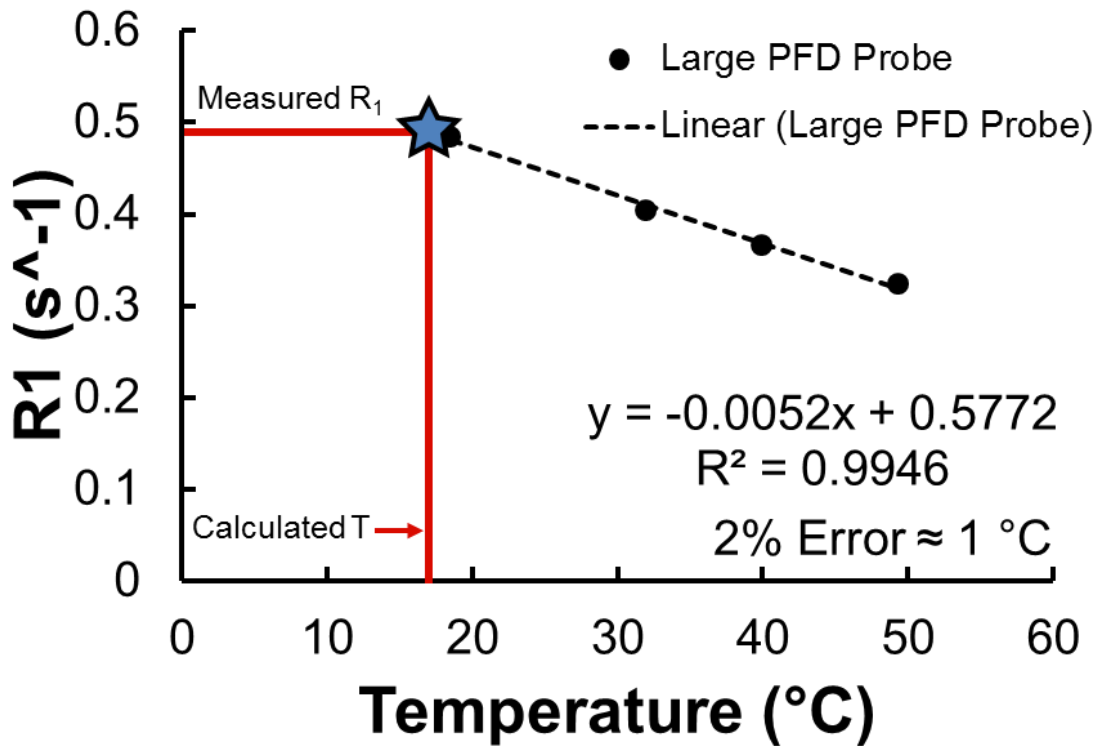
The TEGs were then implanted in the subcutaneous space as described above leaving oxygen compartment access cannulas protruding through the incision for attachment to dual-channel harness and tether apparatus (Instech Laboratories, Plymouth Meeting, PA, USA). The harness and tether apparatus contains a swivel, and counter-balance system to allow for animal movement around the cage, and normal feeding, drinking, and grooming behaviors. The tether system was connected through the cage top to an oxygen generating system previous described (Giner Inc., Auburndale, MA, USA) and a specialized manifold to regulate and monitor the delivery of oxygen gas to the implanted devices. Pure humidified oxygen gas (760 mmHg) was continuously delivered through the harness and tether apparatus to the modified TEG for the duration of the study with limited disconnection to monitor animal weights and well-being. Extended sections of tubing were used to continue DSO during MRS procedures.



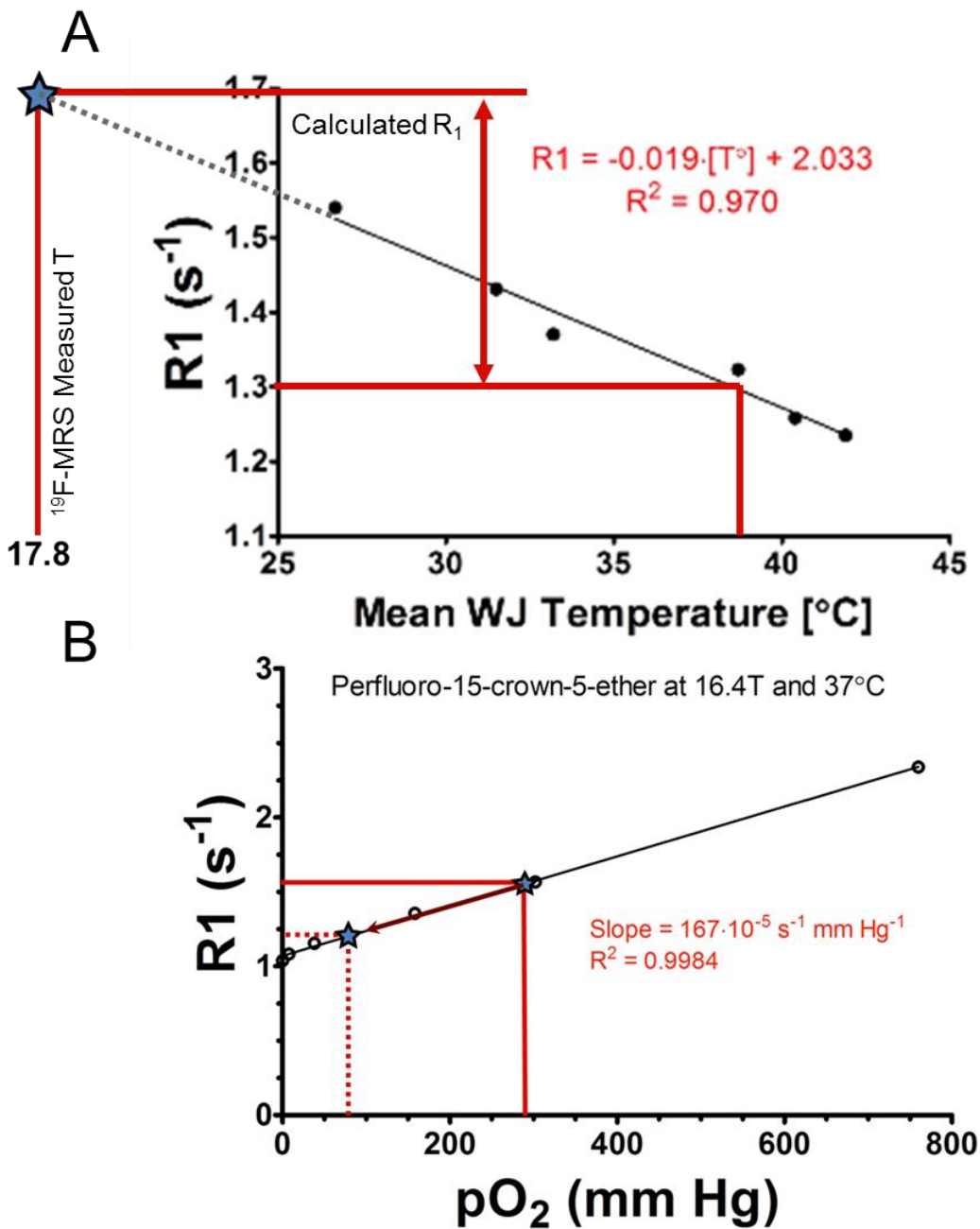
**Figure 7.1: PFCE and PFD spectra.** Example spectra from perfluoro-15-crown-5-ether (PFCE) and perfluorodecalin (PFD) collected at 16.4 T. PFCE has 20 equivalent  $^{19}F$  atoms generating a single resonance, while PFD has 5 distinct resonances with added J-coupled splitting. The peak used for oxygen measurements has two equivalent  $^{19}F$  atoms as is illustrated in the figure (red arrow).



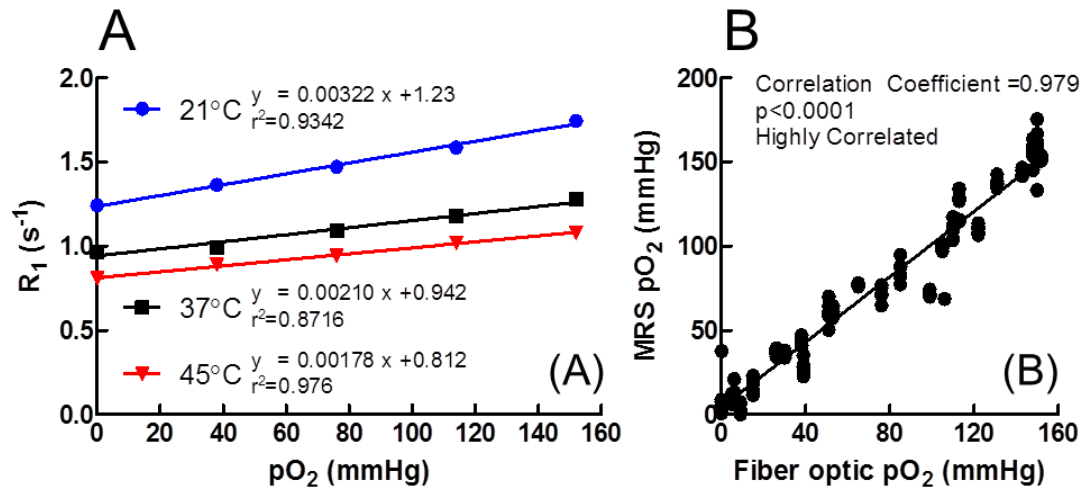
**Figure 7.2: Inversion recovery illustration.** Example inversion recovery results from pefluro-15-crown-5-ether (PFCE). The plotted points (N=10) represent the relative integral area of each time-delayed point collected during the inversion recovery sequence. Spectral lines are included for illustrative purposes (red), and the equation for the fitting curve (dotted black) is included for reference.



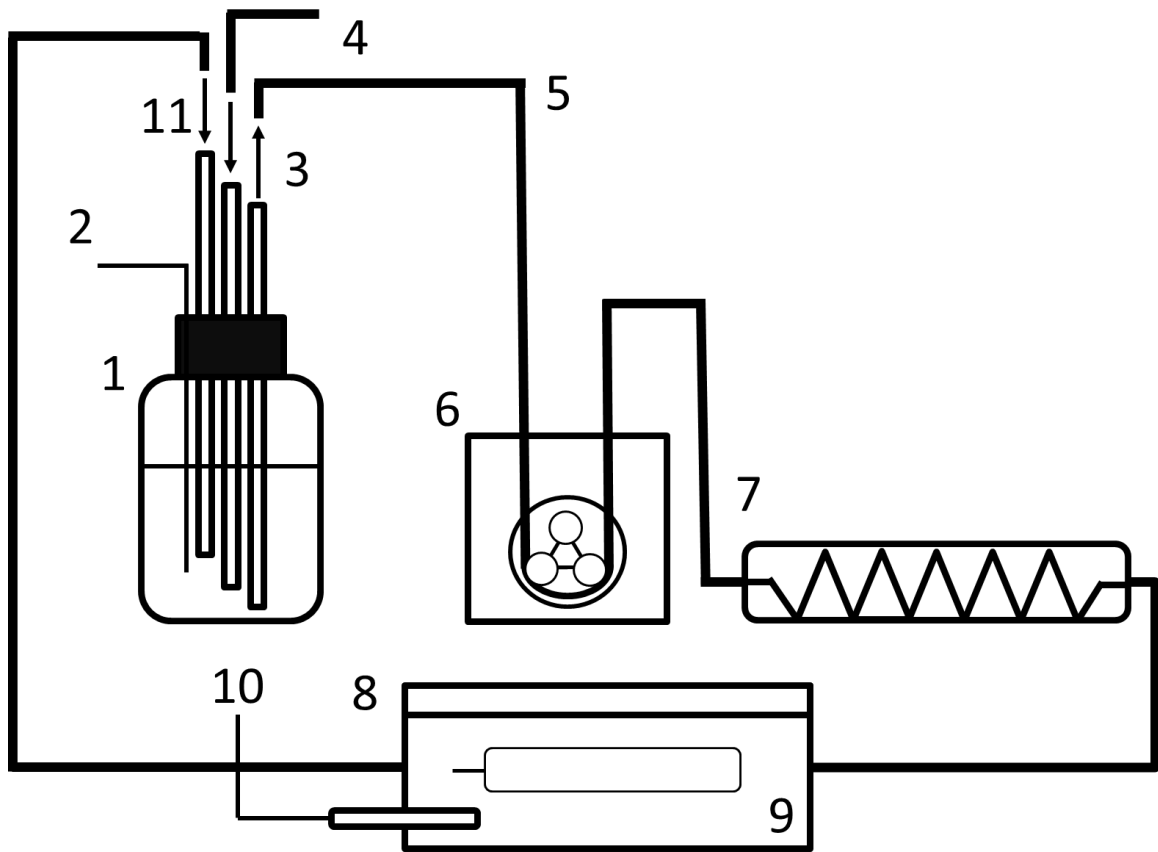
**Figure 7.3: PFD Temperature probe calibration.** Temperature calibration of perfluorodecalin (PFD) loaded temperature probe. This probe was developed to non-invasively measure the temperature of the probe using <sup>19</sup>F-MRS. The measured R1 of the PFD within a sealed glass tube was used with this calibration line to determine the local temperature of the probe for a small set of preliminary studies. A linear relationship between R1 and temperature was confirmed.



**Figure 7.4: Temperature compensation with PFD probe.** Preliminary temperature and oxygen calibration lines for perfluoro-15-crown-5-ether (PFCE). A) The temperature measured using the perfluorodecalin probe was used to establish the change in  $R_1$  that was due to the change in temperature when compared to the 37 °C  $R_1$ . B) The oxygen calibration line of PFCE at 37 °C. The measured  $R_1$  of the sample was then adjusted based on the  $R_1$  difference determined with the temperature calibration. This method was successfully used to compensate for sample temperature variability and successfully determined the  $\text{pO}_2$  of the sample.

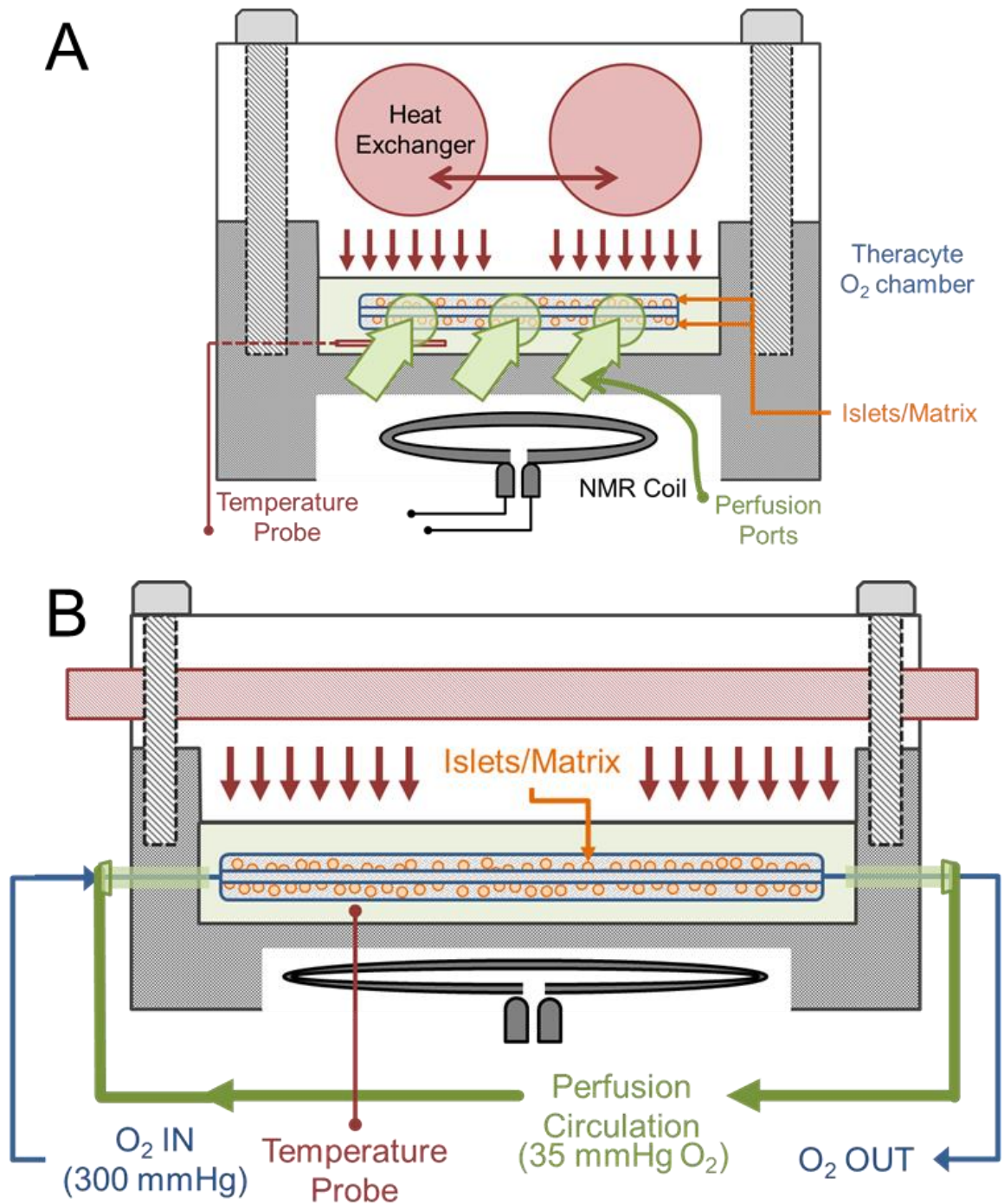


**Figure 7.5: Calibration and validation of <sup>19</sup>F-MRS.** In vitro oxygen calibration and validation of perfluoro-15-crown-5-ether using <sup>19</sup>F-MRS relaxation rate ( $R_1$ ) and fiber optic oxygen sensors. (A) Calibration of  $R_1$  results shown for PFCE-fibrin loaded TheraCyte devices at various oxygen levels at three temperatures (21 °C, 37 °C and 45 °C) measured in 16.4 T MRS system. These values were used to generate the multi-parametric non-linear calibration coefficients used for all of the studies described. (B) Correlation plot of <sup>19</sup>F-MRS in vitro oxygen measurements against fiber optic (FO) fluorescent lifetime oxygen measurements showing a highly correlated relationship between the MRS measurements and FO measurements. These results validate the success of a robust and reliable calibration that accounts for temperature variability observed during a measurement.



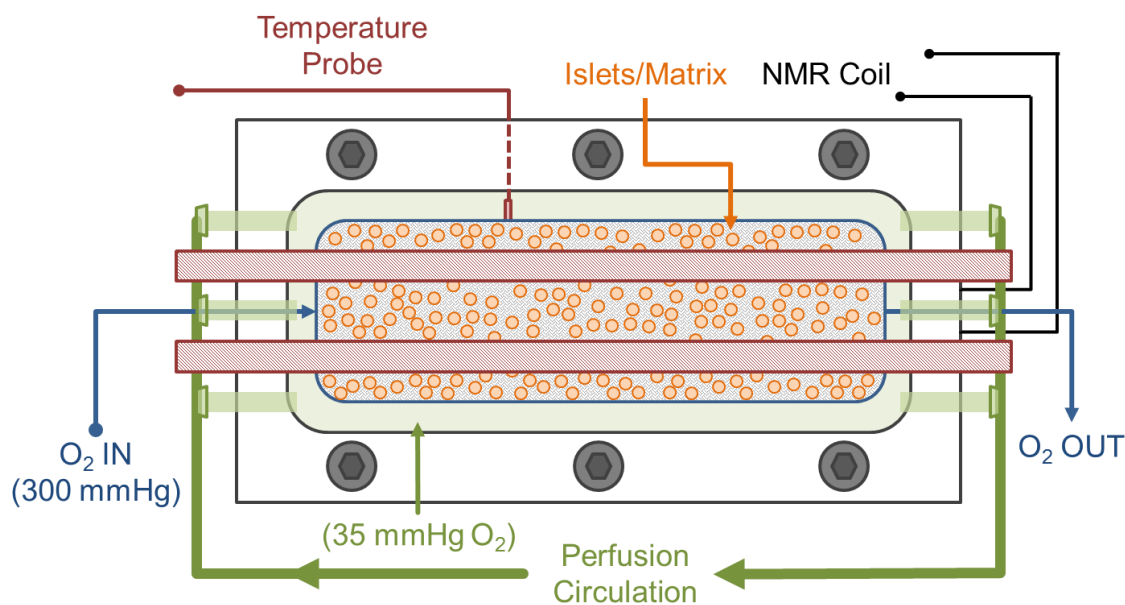
- |  |                               |
|--|-------------------------------|
| 1. Medium reservoir, high glucose DMEM | 7. Heat exchanger             |
| 2. Temperature probe                   | 8. Bioreactor                 |
| 3. Medium outlet                       | 9. TheraCyte                  |
| 4. Gas flow into medium                | 10. In-line temperature probe |
| 5. Masterflex tubing                   | 11. Medium return             |
| 6. Peristaltic pump, Instech           |                               |

Figure 7.6: Schematic diagram of perfusion bioreactor.



**Figure 7.7: Perfusion bioreactor chamber viewed from the side.** A) diagram showing the end view of the chamber, and emphasizing the individual components and the positioning of the tissue engineered graft. The heat exchanger was built into the lid to provide direct temperature regulation of the internal compartment of the chamber. The MRS surface coil was positioned directly beneath the bioreactor to obtain maximum sensitivity. B) Side view of the chamber.





**Figure 7.8: Perfusion bioreactor chamber viewed from the top.** The illustration highlights the individual components of the chamber as the external conditions controlled by the oxygenation and temperature regulation components of the bioreactor system. The temperature was regulated to  $37 \pm 2$  °C using the heat-exchanger and measured with the included temperature probe. The oxygen concentration within the chamber (outside of the tissue engineered graft) was controlled by continuously circulating deoxygenated medium (30 mmHg) through the chamber. The oxygen concentration within the chamber was monitored using an MR compatible oxygen probe to confirm the stability of the hypoxic environment.

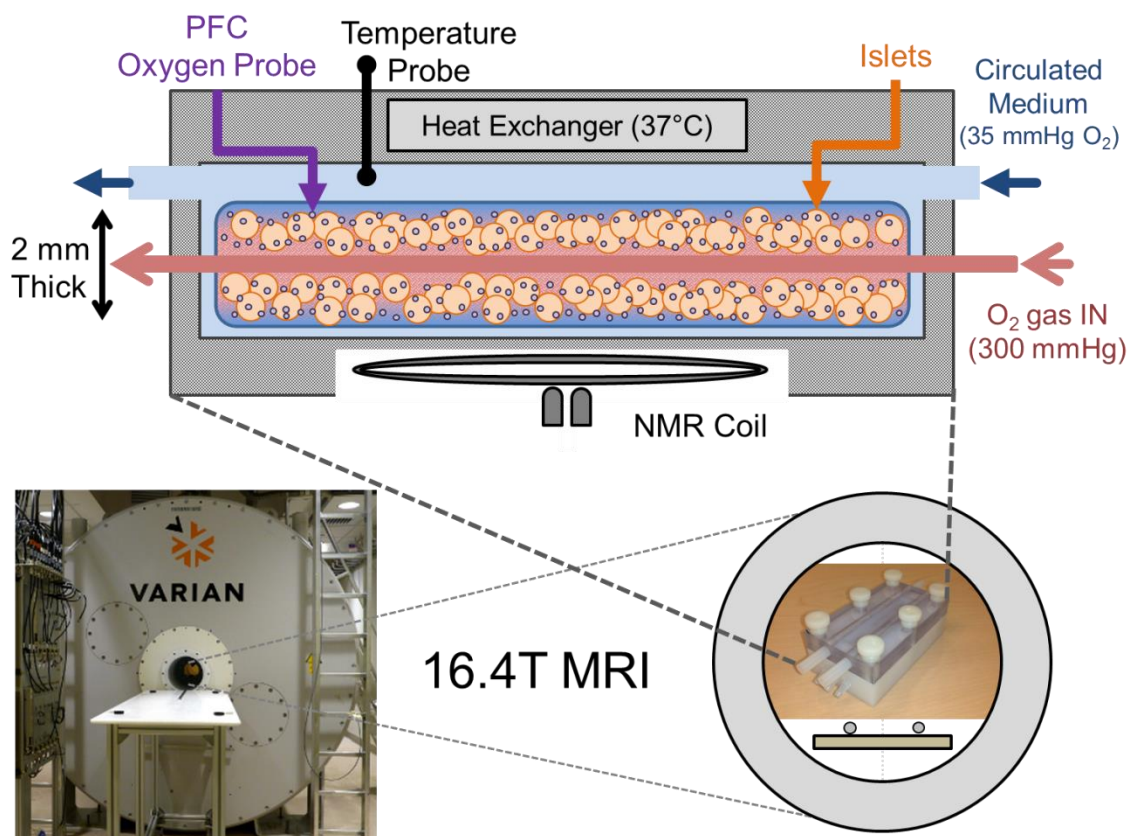


**Figure 7.9: Bioreactor MRS Illustration.** Diagram, illustration, and picture of the bioreactor chamber inside the 16.4 T MRS system. The chamber was connected to the bioreactor using long sections of tubing and then positioned over the surface coil and inserted in the scanner. Temperature and oxygen levels in the chamber were controlled and monitored for in vitro validation studies while <sup>19</sup>F-MRS was used to measure the internal pO<sub>2</sub> within the tissue engineered graft. Oxygen was delivered at 380 mmHg, and 760 mmHg to the internal compartment of the TEG to observe the kinetic changes of the pO<sub>2</sub> within the TEG under these conditions.

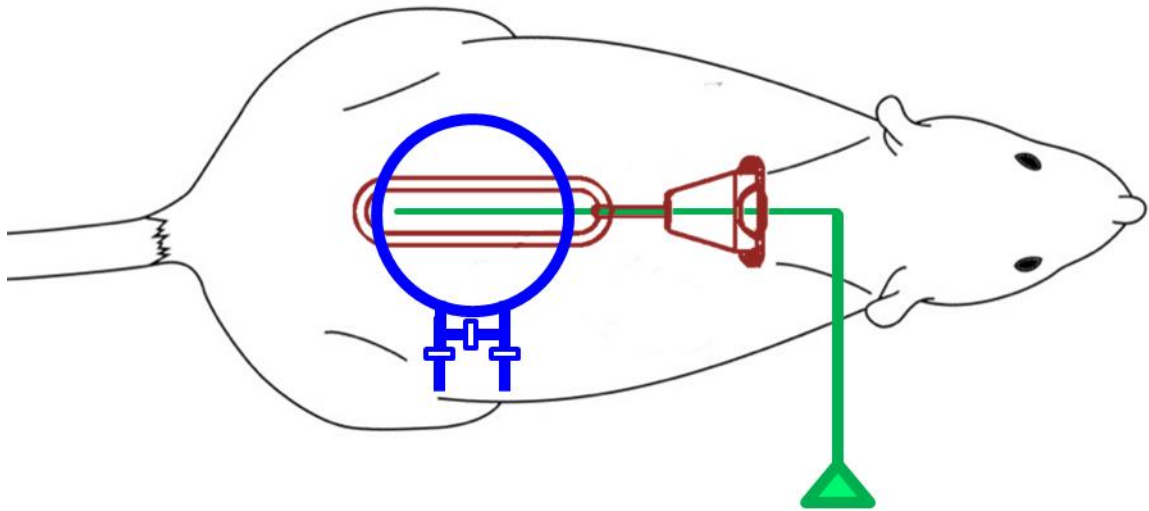


**Figure 7.10: Validation of  $^{19}\text{F}$ -MRS *in vivo*.** Illustration of TheraCyte Implant with access port (Red) in the subcutaneous pocket on the dorsal side of a Lewis rat. For fiber optic measurements the 250  $\mu\text{m}$  thin-fiber oxygen probe (green) was inserted through the skin and the access port into the central portion of the cell compartment of the TheraCyte implant. The  $^{19}\text{F}$ -MRS coil (blue) was placed on the back-side of the anesthetized rat to detect the  $^{19}\text{F}$ -MRS signal for the PFCE within.

## ***Results***

The SNR of PFCE loaded TEGs was sufficient to measure the  $T_1$  relaxation time, and example spectra, and inversion recovery fit are presented in **Figure 7.1** and **Figure 7.2**. PFCE and PFD  $R_1$  were found to be directly proportional to  $pO_2$  with the slope and intercept dependent on temperature (**Figure 7.5A**). A linear relationship between  $R_1$  and temperature was also found for both PFCE and PFD. A PFD temperature probe confirmed that temperature has a profound effect on the measurement of  $pO_2$  with  $^{19}F$ -MRS. The independent MR temperature probe can be used to measure large temperature differences successfully (**Figure 7.3**), and these results can be used to compensate for the changing temperature without requiring independent calibration data sets for every temperature measured (**Figure 7.4**). Compensation for temperature with  $^{19}F$ -MRS oxygen measurements dramatically improves measurement accuracy, but a separate  $^{19}F$ -MRS temperature probe was not necessary when MR compatible thermocouples could be used to measure temperature accurately, and temperature was adequately controlled in the MRS system. A multiparametric calibration equation containing  $R_1$ ,  $pO_2$ , and temperature was successfully extrapolated (**Equation 7.4**), and used for all future *in vitro* and *in vivo* oxygen measurements. With adequate temperature control and measurement,  $^{19}F$ -MRS oxygen measurements correlated well ( $p < 0.0001$ ) with FO oxygen measurements *in vitro* (**Figure 7.5B**). These data validate  $^{19}F$ -MRS as a robust and reliable measurement technique *in vitro*.

Non-invasive oxygen measurements from TEGs in a bioreactor show significantly increased internal  $pO_2$  for implants with DSO. A group of 5 TEG devices were prepared for *in vitro* oxygen measurements with DSO by placing TEGs inside a temperature regulated perfusion bioreactor (**Figure 7.6**, **Figure 7.7**, **Figure 7.8**). A continuous series of  $^{19}F$ -MRS oxygen measurements acquired from TEGs inside a bioreactor are presented in **Figure 7.11**. The results demonstrate that optimal DSO was achieved with delivery of either 380 or 760 mmHg enriched oxygen gas,

and implants equilibrated to a steady-state internal  $pO_2$  in  $\leq 20$  minutes regardless of the  $pO_2$  of the delivered gas. The external  $pO_2$  of each TEG was controlled to simulate the hypoxic  $pO_2$  levels previously observed *in vivo*. The hypoxic external environment was verified by continuous fiber-optic probe measurements ( $34 \pm 6$  mmHg), and confirmed with  $^{19}F$ -MRS measurements when the internal  $pO_2$  of each TEG acclimated to the external  $pO_2$  within an hour after beginning perfusion. The average internal  $pO_2$  of all TEGs reached  $64 \pm 4\%$  of the delivered  $pO_2$  regardless of the DSO concentration. TEG implants achieved average steady-state internal  $pO_2$  measurements of  $207 \pm 22$  mmHg and  $469 \pm 40$  mmHg for DSO with  $pO_2 = 380$  mmHg and 760 mmHg respectively. After steady-state measurements, DSO was stopped to record the internal  $pO_2$  decay as the TEG returned to ambient external oxygen. Oxygen measurements were fit with a mono-exponential decay function yielding an average characteristic time-constant ( $\tau$ ) of  $15 \pm 1$  minutes.

*In vivo* validation using simultaneous FO oxygen probe and  $^{19}F$ -MRS methods for measuring  $pO_2$  showed that FO probes consistently measured significantly higher oxygen levels than  $^{19}F$ -MRS methods when compared using a two-tailed paired student t-test, and the results are presented in **Figure 7.12**. The  $pO_2$  measured with FO oxygen probes were on average 11 mmHg higher than  $^{19}F$ -MRS measurements, but all measurements indicated similar hypoxic oxygen conditions *in vivo*. The variability of FO probe measurements was greater than  $^{19}F$ -MRS measurements, and the standard deviations were 15 and 13 mmHg respectively for these techniques.

Delivery of supplemental oxygen (DSO) was successfully achieved and sustained for at least 24 hours in a subset (N=3) of animals for preliminary examination. These animals received DSO to the internal compartment of a modified control TEG (no islets) for 24 or more hours, and then internal TEG  $pO_2$  was determined using MRS methods. The average internal  $pO_2$ , presented in **Figure 7.13**, was observed to be significantly higher ( $p < 0.0001$ ) for animals that received DSO *in*

*in vivo* when compared to the TEGs which did not receive DSO, achieving  $532 \pm 35$  mmHg one day following implantation. After DSO was stopped, the average  $pO_2$  returned to low-levels ( $pO_2 = 26 \pm 21$  mmHg) that were not significantly different from the values observed without DSO ( $p=0.56$ ).

$^{19}F$ -MRS was used to measure the internal  $pO_2$  of implanted TEGs after 1, 8, and 15 days following implantation, and the results are presented in **Figure 7.14**. Oxygen levels started high one day following implantation, and then decreased to hypoxic levels for the following measurements. The  $pO_2$  one day following implantation was elevated with an average of  $69 \pm 22$  mmHg and decreased to  $16 \pm 3$  and  $0 \pm 10$  mmHg after 8 and 15 days post implantation respectively. This study was expanded to include more time-points and higher numbers of animals, and those results are presented and discussed in **Chapter 8**. The implications of the data presented here suggest that  $^{19}F$ -MRS can successfully be used to track the  $pO_2$  changes within implanted TEGs over time.

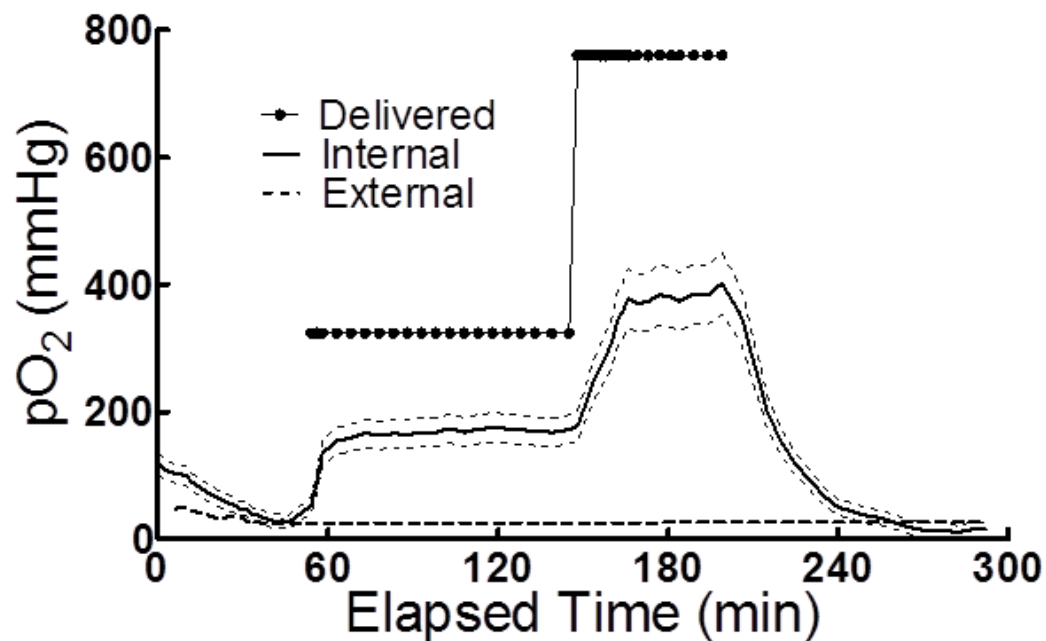


**Figure 7.11: Oxygen measurements in bioreactor.** Time series of oxygen levels measured in a typical bioreactor using <sup>19</sup>F-MRS. Oxygen levels were allowed to equilibrate with the surrounding medium, and then delivery of supplemental oxygen (DSO) was initiated at 300 mmHg and then increased to 760 mmHg and then followed by stopping DSO. The pO<sub>2</sub> decay after stopping DSO was also quantified and the decay constant was measured to be an average of 15±1 minutes.

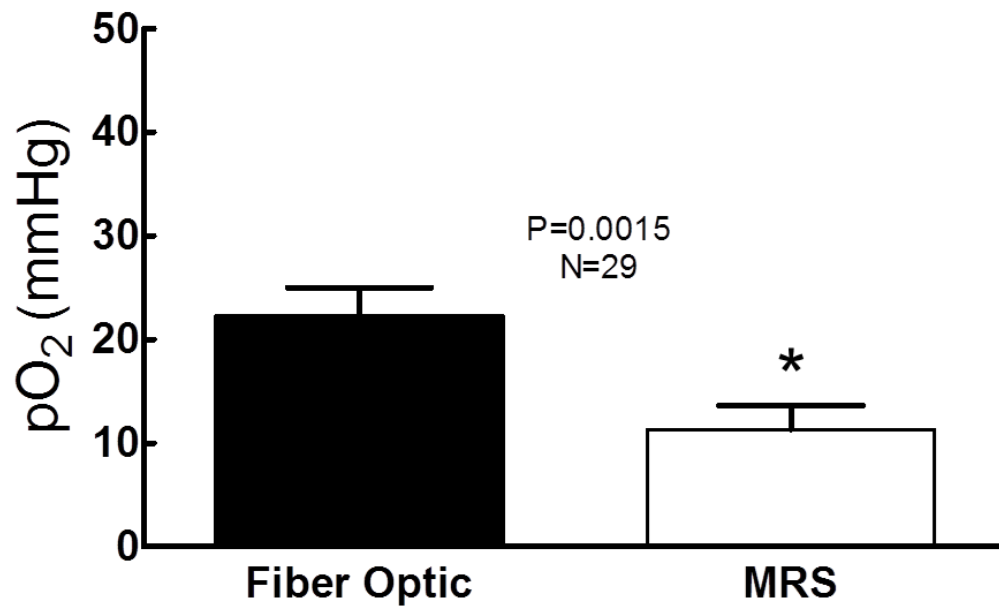


**Figure 7.12: Fiber optic (vs) <sup>19</sup>F-MRS oxygen measurements.** Comparison of <sup>19</sup>F-MRS and fiber optic (FO) oxygen measurements *in vivo*. Average oxygen partial pressure measured in subcutaneous implants over 30 days using FO oxygen sensors and <sup>19</sup>F-MRS method. Oxygen levels measured with both methods were less than venous blood oxygen concentration (40 mmHg), but there was a significant difference between methods with the FO probes measuring an average of 11 mmHg higher than the <sup>19</sup>F-MRS method (\* indicates significant difference P<0.05).



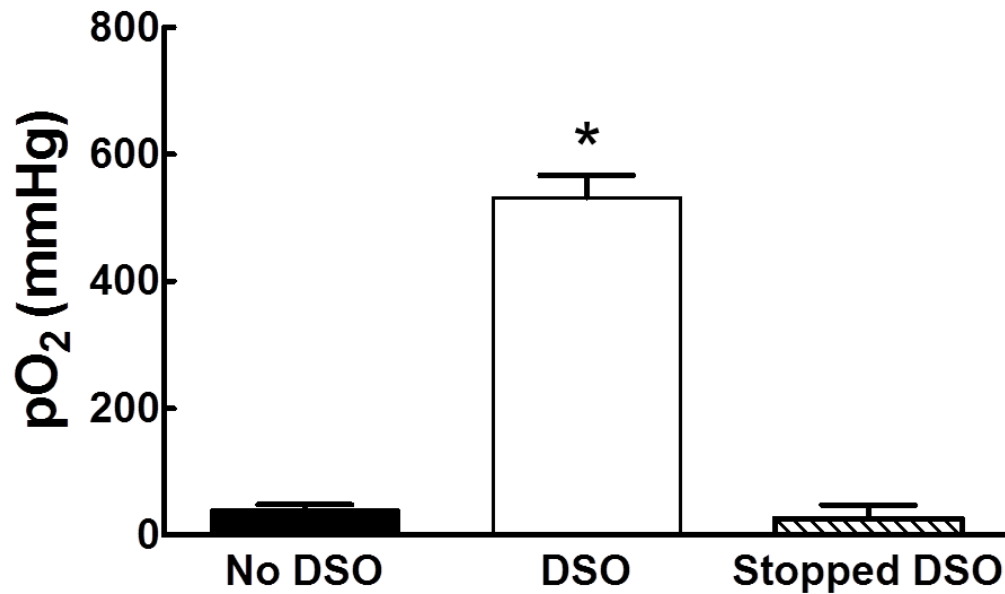


**Figure 7.13: Validation of <sup>19</sup>F-MRS methods *in vivo* with DSO.** Delivery of supplemental oxygen (DSO) increases <sup>19</sup>F-MRS measured oxygen partial pressures in bioartificial pancreas devices tested *in vivo*. Average <sup>19</sup>F-MRS oxygen partial pressures measured in devices subcutaneously implanted in rats with, and without DSO. Oxygen was delivered at 760 mmHg continuously following implantation, and then assessed by <sup>19</sup>F-MRS. For a subset of animals (N=3), oxygen delivery was stopped for at least 24 hours, and then re-assessed showing a return to ambient oxygen partial pressures seen without oxygen delivery. (\* indicates a significant difference,  $p < 0.05$ , when compared to the control, No DSO, condition).

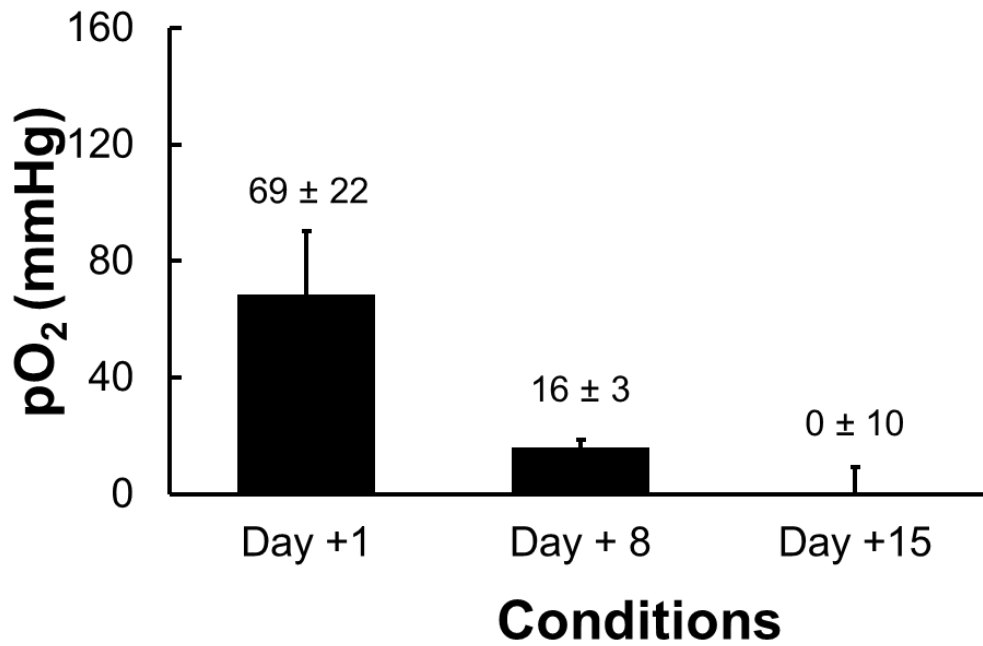


**Figure 7.14: Preliminary oxygen measurements *in vivo*.** Series of  $^{19}F$ -MRS oxygen measurements of TEG *in vivo* at 1, 8, and 15 days post implantation. Oxygen levels within implanted TEGs start at elevated levels ( $69 \pm 22$  mmHg), but decrease to hypoxic levels ( $< 20$  mmHg) measured after 8 and 15 days following implantation.

## ***Discussion***

To develop a better understanding of the oxygen available to subcutaneous implanted TEGs, we developed a method for non-invasive oxygen measurements within TEGs *in vivo* using  $^{19}\text{F}$ -MRS. Traditional oxygen sensors for oxygen measurement *in vivo* use Clark electrodes<sup>57,174,192</sup>, or fiber optic fluorescence quenching probes. Traditional polarographic, “Clark type,” electrodes suffer from inaccuracy due to the consumptive nature during operation, and both conventional methods are mechanically invasive. The traditional “needle” type probes require mechanical disturbance of the sampled tissue, and may actually introduce oxygen to the system during the measurement procedure. These traditional sensors also provide a single point measurement at the tip of the probe itself, and thus multiple mechanically disruptive measurements are required to obtain an average  $\text{pO}_2$  measurement with high levels of confidence. There are some reports using a photoacoustic lifetime imaging methods<sup>193,194</sup> for oxygen measurement, but these methods are only applicable for very superficial measurements in tissues.  $^{19}\text{F}$ -MRS methods overcome many of these limitations, and offer a sensitive, accurate, and non-invasive method for oxygen measurements *in vivo*.

Our lab has investigated  $^{19}\text{F}$ -MRS methods for functional graft assessment *in vitro*<sup>182</sup>, and others have explored similar methods for measuring oxygen levels *in vivo* using raw perfluorocarbons (PFC)<sup>172</sup>, PFC lipid emulsions<sup>163,179,195–197</sup>, or PFC loaded alginate beads<sup>161,168–170,172,183</sup>, but none have attempted to measure the average localized oxygen concentration within a macro-encapsulation device *in vivo*. Our methods were optimized and adapted for measurements within macro-encapsulated TEGs using an ultra-high field 16.4T MRS system for optimal signal intensities. We examined a number of PFC compounds and chose to use PFCE due to the reported biocompatibility<sup>172,180,181</sup> and large number of equivalent fluorine atoms which provide an intense signal at a single resonance (singlet). We also used PFD to test a dedicated  $^{19}\text{F}$ -MRS

temperature sensor for simultaneous determination of temperature with oxygen. Example spectra are presented in **Figure 7.1**.

Our experiences with *in vitro* studies (**Figure 7.2-Figure 7.5**) and reports in literature<sup>159,174,177,198</sup> document the sensitivity of <sup>19</sup>F-MRS relaxation rates to both oxygen and temperature, yet many reports using <sup>19</sup>F-MRS for oxygen measurement do not address this multi-parametric physical nature. Controlling and even measuring the body temperature of anesthetized animals inside an MRS system can be technically challenging, but due to the high sensitivity of <sup>19</sup>F-MRS relaxation rates to both oxygen and temperature, temperature must be considered to achieve a high-level of oxygen measurement accuracy.

To account for the relaxation effects of both oxygen and temperature, we chose to perform detailed and robust multi-parametric oxygen and temperature calibrations using control TEGs loaded with a PFCE impregnated plasma gel matrix<sup>199</sup>. We fit this oxygen-temperature data set using established numerical methods to derive the calibration constants used for these studies<sup>159,174</sup>. Despite these complex calibrations, the oxygen measurements are still susceptible to errors in temperature measurement, and <sup>19</sup>F-MRS methods for oximetry would greatly benefit from improved temperature measurement techniques, especially if the temperature measurements could be localized to the area of interest. An MRS method to locally measure temperature *in vivo* would be an ideal complement to <sup>19</sup>F-MRS oximetry, and development in this area would greatly improve the sensitivity and accuracy of the described methods. A PFD loaded temperature probe was developed, and used for temperature compensation for a small number of *in vitro* experiments. This method was able to compensate for large temperature variabilities observed during the study, but the two-parameter calibration method used with an MRS compatible thermocouple achieved sufficient accuracy. This method was used for all future *in vitro* and *in vivo* studies due to the relative simplicity, and reliable results observed. Despite these findings, an

internal temperature standard could provide significant improvements in measurement accuracy when temperature is difficult to control or measure. High accuracy and precision in calibration were achieved by measuring  $R_1$  using a surface coil, a standard inversion recovery pulse sequence with adiabatic pulses, and a two-parameter fit accounting for temperature sensitivity. These measurements were correlated with measurements from FO oxygen probes, and a high correlation was observed with the correlation coefficient was 0.979. These results suggested that  $^{19}\text{F}$ -MRS methods could reliably measure the  $\text{pO}_2$  of *in vitro* samples with a high level of accuracy.

The next objective was to validate these methods further by approximating the *in vivo* environment using a bioreactor and novel DSO methods to increase the local oxygen concentration inside a modified TEG device. The design of this complex bioreactor system is described in **Figure 7.6** through **Figure 7.9**, and **Figure 7.11** shows the representative oxygen measurements from a series of 5 studies with this bioreactor.  $^{19}\text{F}$ -MRS methods were able to detect significantly elevated  $\text{pO}_2$  levels within a TEG device, despite the surrounding hypoxic environment. The perfusion bioreactor was used to maintain physiologic temperature and to provide a controlled external environment that would simulate the hypoxic environment. The  $\text{pO}_2$  and temperature of the perfusion medium inside the bioreactor was continuously monitored using MRS compatible temperature and oxygen sensors to ensure controlled conditions were maintained throughout the study.  $^{19}\text{F}$ -MRS methods were used to measure the average  $\text{pO}_2$  within TEG non-invasively during a series of changing internal and external oxygen conditions. The studies began by measuring the starting  $\text{pO}_2$  within the TEG before any controlled conditions were initiated. The observed average  $\text{pO}_2$  initially began at  $123 \pm 19$  mmHg, which was only slightly different from the ambient humidified atmospheric  $\text{pO}_2$  (152 mmHg). The deviation from the atmospheric level is explained primarily by the variability in starting temperature (36.7-42.8 °C), which was difficult to regulate before perfusion was started. When the perfusion circuit was

started, deoxygenated culture medium was continuously circulated to maintain a constant hypoxic external condition (average measured  $pO_2 = 34 \pm 6$  mmHg) for the TEG inside the bioreactor. The internal  $pO_2$  of the TEG shown in **Figure 7.11** was observed to acclimate to the surrounding perfusion medium within the first hour following initiation of perfusion, and an average steady state  $pO_2$  of  $38 \pm 3$  mmHg was observed prior to beginning DSO. DSO was tested at two different oxygen concentrations (50% or 380 mmHg, and 100% or 760 mmHg), and the  $pO_2$  time-series of the delivered gas is presented in **Figure 7.11**. The initial  $pO_2$  tested for DSO was 380 mmHg, and the measured internal  $pO_2$  of TEGs rose quickly to an average of  $207 \pm 22$  mmHg. The  $pO_2$  of DSO was then switched to 760 mmHg, and the internal  $pO_2$  again quickly rose up to an average of  $469 \pm 40$  mmHg. At the completion of the study, DSO was stopped and the  $pO_2$  decay to equilibrium with the surrounding  $pO_2$  was observed. Further analysis and discussions of DSO and oxygen kinetics within a TEG with DSO are included in **Chapter 8**. These results clearly demonstrate that  $^{19}F$ -MRS methods can be used to measure changes of internal TEG  $pO_2$ , and could be used to non-invasively study the kinetic effects of interventions (such as DSO) on implanted TEG.

Validation studies were continued with a small series of animals ( $n=6$ ) that received TEG devices that were modified with an addition of an access-port to allow for insertion of a FO oxygen probe. This modification allowed for simultaneous  $pO_2$  measurement using the FO oxygen probe and  $^{19}F$ -MRS at various time-points. A paired comparison between FO oxygen measurements and  $^{19}F$ -MRS measurements indicated a significant difference in the measured *in vivo*  $pO_2$  within implanted TEGs. This difference is significant, but both measurement techniques confirm a hypoxic oxygen level within the TEG *in vivo*. It is important to recognize some critical differences between the FO oxygen probe measurements and  $^{19}F$ -MRS methods. The FO oxygen probe provides a single-point measurement of  $pO_2$  within the TEG, while  $^{19}F$ -MRS provides a

volume average measurement of the internal  $pO_2$ . This difference makes the FO probe method susceptible to local variabilities in oxygen levels, and probe placement is critical to results measured with these kinds of probes. It is also important to note that the FO probe requires invasive intrusion into the TEG itself to obtain a reliable oxygen measurement. The probe has to be inserted into the central compartment of the TEG, and this certainly disturbs the condition of the tissues/cells within the TEG. The probe itself is also likely introducing some oxygen to the TEG during the insertion process as it will be acclimated to atmospheric  $pO_2$ , and opens access to the external environment during the insertion procedure, which will likely contribute to measurement error. Measurements with the FO oxygen probe had slightly higher standard deviations when compared to  $^{19}F$ -MRS methods. Despite the differences observed with these *in vivo* studies,  $^{19}F$ -MRS can clearly provide reliable and reproducible measurements of internal TEG  $pO_2$ , and may offer significant advantages over traditional invasive oxygen measurement techniques.

As described above and in **Chapter 8** for further confirmation of  $^{19}F$ -MRS oxygen measurement methods *in vivo*, the TheraCyte device was modified to provide for a separate central oxygen chamber, and additional access ports to allow for continuous delivery of supplemental oxygen (DSO) to the TEG *in vivo*.  $^{19}F$ -MRS measurements suggest a dramatic increase in available oxygen in the TEGs with DSO, and the results are reported in **Figure 7.13**. Discussion of the DSO system and the development of a functional bio-artificial pancreas is limited here because this topic is not the primary focus of these studies. However, a limited number of preliminary proof-of-concept studies were done in 3 animals implanted with these TEGs modified for oxygen delivery. The implants were prepared in a similar way to the standard TEGs, but contained two chambers loaded with the PFCE-matrix material on either side of the central oxygen chamber, and did not contain any islets or other cells. These TEGs were implanted like others in the

subcutaneous space of Lewis rats, and connected by transcutaneous cannulas to the DSO system. Oxygen gas (100%) was generated using an electrochemical oxygen generator, and continuously delivered to the implanted TEGs through a harness and tether system for 24 hours. After this period of acclimation, DSO was continued during the  $^{19}\text{F}$ -MRS procedure, and the average internal  $\text{pO}_2$  was measured for each implant. After these initial measurements, DSO was stopped for at least 24 hours for these animals, and then  $^{19}\text{F}$ -MRS oxygen measurements were repeated. The oxygen levels observed during DSO reached an average internal  $\text{pO}_2$  of  $532\pm 34$  mmHg, and then returned to ambient tissue oxygen levels ( $26\pm 21$  mmHg) when DSO was ceased for at least 24 hours. The results of these preliminary studies suggest that  $^{19}\text{F}$ -MRS oxygen measurements can be used to measure the oxygenation of therapeutically relevant macro-encapsulated TEGs *in vivo*. These measurements can be used to optimize these types of interventions, and to determine the optimal parameters for DSO.

Finally to confirm that  $^{19}\text{F}$ -MRS methods can reliably monitor changing oxygen conditions based on physiological changes *in vivo*, 9 animals were implanted with TEGs and oxygen levels were measured after 1, 8 and 15 days. These limited studies are expanded for discussions of *in vivo* oxygen availability in **Chapter 8**, but these preliminary studies demonstrated that  $^{19}\text{F}$ -MRS methods can be used to track changes of oxygenation status that occur due to natural physiological changes in graft oxygen environment.

## ***Conclusion***

In conclusion, a robust two-parameter calibration was successfully developed to account for temperature changes that are encountered during oxygen measurement studies, and this method improves the reliability of the measured  $\text{pO}_2$  *in vivo*. Rigorous validations of  $^{19}\text{F}$ -MRS method *in vitro* using a bioreactor and *in vivo* using Lewis rats confirmed reliable measurements of internal TEG  $\text{pO}_2$ , and that these methods can detect both natural physiological changes in oxygen



environment as well as interventional change in oxygenation by using DSO. Application of these techniques are used to study the natural progression of oxygenation within TEG *in vivo*, and to evaluate the success of DSO for increasing internal oxygenation of implanted TEG for up to 29 days, and these studies are described in **Chapter 8**.

## Chapter 8 OXYGENATION OF IMPLANTED TEGs

Sections of this chapter are reproduced in whole, or in part from the following publications with permission:

Presented Abstracts:

**Weegman BP**, Einstein SA, Steyn LV, Suszynski TM, Firpo MT, Graham ML, Janecek J, Eberly LE, Garwood M, Papas KK, “Continuous oxygen delivery improves oxygenation of tissue-engineered islet grafts in vivo as measured with fluorine-19 magnetic resonance spectroscopy” Abstract accepted for a mini-oral presentation at the Joint IPITA-IXA-CTS Congress, November 2015, Melbourne, AUS

Manuscripts in Preparation:

**Weegman BP**, Einstein SA, Steyn LV, Avgoustiniatos ES, Suszynski TM, Firpo MT, Graham ML, Janecek J, Eberly LE, Papas KK, Garwood M, “Non-invasive monitoring of hypoxia in tissue-engineered islet grafts in vivo using fluorine-19 magnetic resonance spectroscopy” Intended for submission December 2015

**Weegman BP**, Steyn LV, Einstein SA, Garwood M, Papas KK, “Delivery of Supplemental Oxygen Alleviates Hypoxia and Improves Function of Encapsulated Islet Grafts: Measurements with <sup>19</sup>F- Magnetic Resonance Spectroscopy” Intended for submission December 2015

License and agreement documentation is included in **Appendix G**.

**Acknowledgements:** The authors would like to thank the Schott Foundation, the Minnesota Lions Diabetes Foundation, the Juvenile Diabetes Research Foundation (JDRF 5-2013-141), Giner Inc., the Schulze Diabetes Institute, and the NIH (P41 EB015894, and S10 RR025031) for supporting this research.

## ***Overview***

Islet transplantation (ITx) offers a minimally invasive alternative to pancreas transplantation, and shows promise as a possible cure for type 1 diabetes, but widespread application of this therapy is still inhibited by numerous barriers. Due to persistent challenges and limitations, there has been a recent resurgence of interest in developing a bio-artificial pancreas (BAP) construct based on augmenting islet transplantation by applying tissue-engineering approaches. Adequate oxygenation within tissue engineered grafts (TEGs) is critical, as both hypoxia and anoxia are detrimental to islet function and survival. This chapter includes a comprehensive discussion of the oxygenation challenges associated with development of a functional TEG, and uses methods described in **Chapter 7** to examine and improve oxygenation of TEG devices implanted in rats. This chapter is broken into two sections based on two manuscripts in preparation. The first section describes the use of  $^{19}\text{F}$ -MRS methods to monitor the internal  $\text{pO}_2$  of implanted TEGs for up to 29 days. The findings of this study re-enforce the findings of earlier studies and confirm that an implanted TEGs will suffer from a severely hypoxic environment *in vivo*, and that this condition is further strained by the presence of islets at high-densities. A model predicts that the hypoxic condition observed will severely compromise graft viability and function unless oxygenation is improved. The second section investigates a novel method for delivery of supplemental oxygen (DSO) to a TEG device, and evaluates the improvement in oxygenation using non-invasive  $^{19}\text{F}$ -MRS techniques. DSO was found to dramatically-increase the oxygenation of TEG devices *in vivo* for up to 29 days, and a feasibility study in diabetic nude rats suggest that DSO could promote long-term survival of high-islet density and functional tissue engineered BAP devices.

## **Non-invasive monitoring of tissue-engineered islet grafts *in vivo***

### ***Summary***

Tissue engineering is an essential component within the field of regenerative medicine, and implantable tissue-engineered grafts (TEGs) have the potential to treat numerous debilitating diseases. Oxygen limitations are a critically important consideration for the development of large-scale implantable TEGs, and a tool for non-invasive monitoring of the oxygen partial pressure ( $pO_2$ ) could be used to improve graft development and potentially monitor graft viability post-implant. TEGs with high cell-densities inevitably fail *in vivo* due to oxygen limitations, and viability and function of islets are predicted to decrease with increasing islet densities. Methods for non-invasive oxygen measurement are described in **Chapter 7**, and this study applies these  $^{19}F$ -MRS techniques for the non-invasive measurement of  $pO_2$  within macro-encapsulated TEGs *in vivo*. We examined the oxygen concentration within TEGs with or without porcine islets for 29 days following subcutaneous implantation in Lewis rats.

A model predicting viability and function of TEGs loaded with various islet densities was developed, and the predictions were verified by measuring explant viability of TEGs loaded with variable islet densities. TEGs were constructed by injecting an emulsion of perfluoro-15-crown-5-ether and porcine plasma into a 40- $\mu$ L TheraCyte<sup>TM</sup> immunoisolation device (TheraCyte, Inc. Laguna Hills, CA), which was then cross-linked using 5% v/v bovine thrombin solution making a fluorine loaded fibrin scaffold. Control TEGs (no cells, N=6), or TEGs seeded with porcine islet cells (N=6) were implanted into a dorsal subcutaneous pocket of Lewis rats (Charles River, Wilmington, MA).  $^{19}F$ -MRS data were collected as described in **Chapter 7** at critical time-points after 1, 4, 8, 15, 22 and 29 days following implantation.

The model and experimental findings demonstrate a strong inverse-correlation between islet density and graft function and viability when the graft maintained in a hypoxic *in vivo*

environment. The mean  $pO_2$  measured by  $^{19}F$ -MRS began at  $39\pm 9$  mmHg for controls and  $27\pm 6$  mmHg for porcine islet-loaded TEGs on the first day following implantation, and decreased to  $\leq 10$  mmHg and remained at low levels up to 29 days. These preliminary results indicate that the subcutaneously implanted TEGs become hypoxic within 1 week post-implantation, and this suggests that supplemental oxygenation may be required to sustain cells and tissues at high densities in these implants. Further studies described in the next section explore local oxygen delivery systems, and correlate  $pO_2$  measurements with changes in TEG viability both pre- and post-transplantation.

## ***Introduction***

Islet transplantation remains an experimental treatment despite its potential to be a minimally invasive cure for type 1 diabetes<sup>200,201</sup>. Despite recent improvements, only 50% of patients achieve insulin independence at five years post-transplant<sup>53,200,202–208</sup>. Intraportal delivery of islets to the sinusoids of the liver may be suboptimal and lead to loss of graft function or graft death. Factors leading to graft function and viability losses in the liver include blood-mediated reactions resulting in inflammation and thrombus formation<sup>209,210</sup>, recurrent autoimmunity<sup>211</sup>, immunosuppression cytotoxicity<sup>212–214</sup>, and poor oxygenation<sup>215–220</sup>. Additionally, cells transplanted into the liver are irretrievable and difficult to monitor<sup>221–223</sup>. Due to these persistent challenges and limitations, there has been a recent resurgence of interest in developing a bio-artificial pancreas construct<sup>157,224–226</sup>.

Extrahepatic islet transplantation using tissue-engineered grafts (TEGs) may alleviate many of these barriers, but there is a plethora of considerations when designing such a device. One approach is to protect from the immune system by imposing a physical immunological barrier using a macro-encapsulation device<sup>39,186,189,225–228</sup>. TEGs that incorporate an immunoisolating or encapsulation device may reduce or eliminate the need for systemic immunosuppression post islet transplantation, but increase the challenges associated with oxygen and nutrient diffusion within such a device<sup>129,132,157,190,229</sup>. Transplanting cells inside such a TEG also allows the graft to be retrievable and more accessible for graft assessment *in vivo*. Previous efforts to develop a bioartificial pancreas have failed to translate clinically<sup>39,129,131,132,229,230</sup>, but with recent developments in stem cell technologies<sup>231–235</sup> and the promise of scalable alternative  $\beta$ -cell sources<sup>79,236–238</sup>, there is a renewed interest in developing a bioartificial pancreas<sup>157</sup>. The implantation site for such a device is also a critical question and must ensure proper access to nutrients and allow for kinetically sufficient secretory responses<sup>188</sup>. Many extrahepatic sites have

been considered and even investigated<sup>239–242</sup>, but little is known about the local pO<sub>2</sub> at these alternative prospective sites.

Maintaining adequate oxygenation within TEGs is critical, as both hypoxia and anoxia are detrimental to islet function and survival<sup>59,130,192,243–246</sup>. Islets are highly vascularized in vivo<sup>245,246</sup>, and even short-term hypoxia can permanently impair islet function<sup>192,243</sup>. Colten, Chhabra, and Yang have recently provided comprehensive reviews examining many of these subjects in detail<sup>157,224,242</sup>. These reviews summarize recent work that highlights the importance of oxygen for such implantable devices, and demonstrates the limitations of these implants and a need for improved oxygenation. Oxygenation is especially challenging when using high cell densities, which create significant diffusion-reaction limitations within a graft<sup>157</sup>. Monitoring the oxygenation status of TEGs, therefore is crucial, especially in the early post-transplant period before potential revascularization. Additionally, this assessment of TEGs may detect oxygenation-altering events such as cell proliferation, inflammation, cell death, and fibrous capsule formation. Finally, quantitative measurements of oxygenation could allow for the real-time estimation of cell and tissue viability<sup>182</sup>.

Magnetic Resonance Spectroscopy (MRS) is a useful tool for observing real-time biological changes in a non-invasive way. Detailed methods and background of this technique are included in **Chapter 7**, and the studies described in this chapter expand and apply these techniques for non-invasive measurement of oxygen concentrations within a tissue engineered graft (TEG) constructs implanted in rats. Furthermore, a model for describing the harmful effects of hypoxia on islet graft viability and function is presented, and validated by explant TEG viability measurements *ex vivo*.

## ***Materials and Methods***

### ***Engineering Model of Hypoxia***

A diffusion-reaction oxygen transport model was developed based on the size and shape of the dimensions of the devices described in this study using methods previously described<sup>227,229,247–250</sup>. Briefly, Comsol Multiphysics software (Comsol Inc., Stockholm, Sweden) was used to develop a finite-element model describing the steady state 1D diffusion-reaction condition within a macro-encapsulating TEG device (described below). The TEG is modeled as a thin-slab of oxygen consuming tissue surrounded by the device membranes. Oxygen diffusion into the device is described by the permeability of the membranes and the pO<sub>2</sub> differential between the inside and outside of the implant<sup>251</sup>. Transport of oxygen through the consuming tissue is governed by the diffusion through the tissue and the oxygen consumption rate (OCR) of the tissue<sup>229</sup>. The model was used to determine the steady state spatial oxygen concentrations within the central tissue of TEGs with various islet densities, and these oxygen concentrations were used to estimate the fractional viability and function of the tissue within the central compartment of the device. The model used an external oxygen pressure of 30 mmHg based on reports of in vivo tissue oxygen pressures in literature<sup>57,161,168,169,183,251,252</sup>, and an OCR of highly viable islets of 300 nmol/min/mg DNA<sup>96</sup>. Islets were considered anoxic (non-viable) if the steady state pO<sub>2</sub> was < 0.1 mmHg<sup>59</sup>, and islets were considered non-functional if the steady state pO<sub>2</sub> was < 10 mmHg<sup>59</sup>.

### ***Animal Research***

All animal research presented herein was approved and overseen by the University of Minnesota Institute for Animal Care and Use Committee (IACUC), the University of California IACUC, or the University of Arizona IACUC. This study was designed to minimize the pain and suffering of animals used for the study, and the three R's were observed. These techniques were developed, refined and tested in vitro and in deceased animals to minimize the number of animals used to



obtain quantitative and significant results. The body weight, and general well-being of each animal was monitored for the duration of the studies described, and no adverse events were noted.

#### Tissue Engineered Graft (TEG) Construction

TEG constructs were composed of isolated islets of Langerhans suspended in a matrix and protected within a clinically established macro-encapsulating immunoisolation device (TheraCyte Inc., Laguna Hills, CA, USA) which is well described and studied in literature<sup>187-191,253</sup>. Briefly, the device was completely fabricated using plastic (PTFE) membranes designed for flexibility and biocompatibility, and a single PE100 access port to an internal cell compartment. TEGs were prepared using human islets for implantation followed by in vitro explant viability assessments, and with porcine islets for in vivo oxygen measurements. All procedures for implantation were done using sterile technique and sterile materials and reagents.

Human islets were isolated at the University of California, San Francisco, cultured at 22 °C in supplemented CMRL culture medium for up to 14 days, and shipped to the University of Arizona in 10 cm<sup>2</sup> G-Rex devices (Wilson Wolf Manufacturing, New Brighton, MN, USA). Islets were quantified by DNA content<sup>25,26,254,255</sup> and allocated in various doses; ranging from 500-8000 islet equivalents (IE) per device. Each dose was then allowed to settle at the bottom of a tube (gentle pellet), the supernatant was removed, and the islets were re-suspended in 5-20 µl of sterile 1 % sodium alginate solution. The islet suspension was then drawn into a 100 µl precision syringe (Hamilton, Reno, NV, USA) and injected into the cell compartment of a 4.5 or 20 µl TheraCyte device. The TEG was then submerged in a 1.2 mM of calcium chloride solution (PBS++) for 20-30 minutes to cross-link the alginate, and transported in sterile PBS++ solution to the surgical suite for implantation.

Porcine islets were isolated from porcine donors at the Schulze Diabetes Institute at the University of Minnesota. Islets were cultured at 37 °C in 10 cm<sup>2</sup> G-Rex devices using

supplemented ME199 culture medium for up to 14 days prior to use for this study. For these implants, 10,000 IE were quantified by DNA content assay (Quant-iT PicoGreen dsDNA Assay Kit, Life Technologies, Carlsbad, CA, USA) and collected into a centrifuge tube on the day of implantation. The islets were allowed to settle at the bottom of the tube (gentle pellet) and the supernatant was carefully removed. The islets were re-suspended in 75  $\mu$ l of porcine plasma (Sigma Aldrich, St. Louise, MO, USA) and then mixed with 75  $\mu$ l of perfluoro-15-crown-5-ether (Exflur Research Corporation, Round Rock, TX, USA) by manually agitating the tube. This emulsion was drawn into a 250  $\mu$ l precision syringe (Hamilton), injected into a 40  $\mu$ l TheraCyte device and then cross-linked with 5% v/v bovine thrombin solution. The thrombin solution was made by diluting concentrated topical thrombin solution (GenTrac Inc., Middleton, WI) in phosphate buffered saline with calcium and magnesium. The cell access port was trimmed short, and sealed with adhesive (Dermabond, Ethicon Inc., Somerville, NJ, USA). The implant has a functional surface area of 6.5 cm<sup>2</sup> (two flat sides) resulting in an effective islet surface density of 1,500 IE/cm<sup>2</sup>. Additional TEGs were prepared in the same manner, without islets to act as controls and for calibration purposes.

### Experimental Conditions

A total of 34 TEGs were prepared in a sterile manner for implantation. TEGs (N=19) loaded with various doses of human islets were implanted in the subcutaneous space of 7 non-diabetic nude rats (Athymic nude mutant, Hsd:RH-Foxn1<sup>tmu</sup>, Harlan Laboratories, Inc, Indianapolis, IN, USA) for ex-plant viability assessment. Each rat received between 2 and 4 implants into the subcutaneous space, and after 7 days the implants were removed for explant viability assessment. Porcine islet loaded TEGs (N=6), and control TEGs (N=6) were implanted in the subcutaneous space of non-diabetic Lewis rats (RT1<sup>1</sup>, Charles River Laboratories International, Inc., Wilmington, MA, USA) for <sup>19</sup>F-MRS oxygen measurements. For <sup>19</sup>F-MRS studies, only one

implant was used for each animal, and implants were monitored for 29 days, and then explanted for histopathology assessments. A small set (N=3) of control TEGs were prepared in the same manner and implanted in the peritoneal cavity of three non-diabetic Lewis rats for  $^{19}\text{F}$ -MRS measurements.

#### *Surgical Implantation and Ex-plantation of TEGs*

On the day of implantation, rats were anesthetized with inhalation isoflurane using a respirator and vaporizer. The surgical sites were shaved with an electric clipper, and the skin was surgically prepped with chlorhexidine or equivalent antiseptic. For subcutaneous implants, a 1.5 cm incision was made in the skin on the dorsal side, just inferior to the scapulae, and perpendicular to, but symmetric across the medial line. Using gentle blunt dissection, a small pocket was created adjacent to the vertebral column just large enough to accommodate one or more devices snugly. The pocket was rinsed and lubricated with saline, and the device(s) were tucked into the pocket. For peritoneal implants, a 1.5 cm incision was made through the skin and abdominal lining to expose the peritoneum. The TEG implant was gently tucked in the peritoneal space, and then tacked to the abdominal lining using permanent sutures to hold it in place. The abdominal lining and the incisions were closed with absorbable suture in a normal fashion using at least two layers and taking care to make sure the device components were not directly below the incision. Surgical glue was applied over the closed incision as a barrier. NSAIDs (meloxicam 1 mg/kg) were administered by subcutaneous injection to minimize pain and inflammation for 3 or more days following surgery. Animals were monitored daily during recovery for up to 14 days until the incision was fully healed. After completion of the study, animals were euthanized by inhalation of 100%  $\text{CO}_2$  for 5 or more minutes until death was confirmed. The TEGs were then surgically removed and used for ex-pant OCR evaluation or histopathology analysis.

#### *Ex-plant Oxygen Consumption Rate (OCR) Measurements*

Implants containing various doses of human islets were implanted in rats for 7 days and then ex-planted for oxygen consumption measurements. The OCR of each ex-planted TEG was measured using a method similar to methods described in literature for the assessment of free islet viability. Briefly, after ex-plant, the TEGs were surgically recovered following euthanasia, and prepared by removing any surrounding tissue that had adhered to the outer surface of the device. The implant was then placed into a modified OCR chamber<sup>25</sup> and filled with air-saturated cell culture medium (supplemented DMEM). The chamber was sealed and the pO<sub>2</sub> of the medium was monitored until an adequate linear slope was observed. The slope was used to calculate the OCR, which was then normalized, by the number of IE loaded into each device to calculate the individual graft viability (OCR/IE). The viability values were grouped based on the surface density of islets loaded into each device, and the relative average OCR/IE is reported as a percentage (%) of the control, low-density ( $\leq 500$  IE/cm<sup>2</sup>) condition.

#### <sup>19</sup>F-MRS Acquisition

The relaxation rate constant ( $R_1$ ) was measured from implanted TEGs using a 16.4 Tesla, horizontal bore, magnetic resonance imaging system (Agilent Technologies, Santa Clara, CA, USA). Detailed methods are described in **Chapter 7**. Briefly, a custom-built single-loop surface coil with a 1.5 cm radius was used as a transceiver and tuned to <sup>19</sup>F resonance frequency (656.8 MHz). The coil was positioned on the surface of the skin covering the implanted TEG to obtain the highest possible signal intensity. An inversion-recovery pulse sequence with adiabatic pulses was used to measure  $R_1$ . The inversion-recovery curve was fit to the Bloch equation solution for the longitudinal magnetization using 3-parameter non-linear regression with Graphpad-Prism software (Graphpad Software Inc., La Jolla, CA, USA). Each  $R_1$  was measured in replicate (n=6) with a repetition time of 6 seconds (Ensuring complete relaxation between repetitions).

#### <sup>19</sup>F-MRS Calibration

Detailed methods are described in **Chapter 7**, but briefly, control TEGs without cells were prepared as described above and placed into a 50 ml conical tube (source) filled with phosphate buffered saline (with calcium and magnesium). The vial was placed in the center of a custom-built surface coil and inserted into a 16.4 T MRS system. The sample was then bubbled with a gas of known oxygen concentration for 30 minutes while the temperature was held constant. A fiber optic oxygen probe (source) was inserted into the TEG to verify the  $pO_2$ .  $R_1$  was then measured with an inversion-recovery sequence utilizing adiabatic pulses. Measurements were made for five different  $pO_2$ s (0, 38, 76, 114, and 160 mmHg) at three different temperatures (21, 37, and 45 degrees C). The  $R_1$  was assumed to be a function of the  $pO_2$ , temperature, and four fitting constants (A, B, C, and D).  $R_1$  measurements were fit to the multi-parametric calibration equation using a Levenberg–Marquardt algorithm (OriginLab, Northampton, MA).

#### Measurement of in vivo TEG $pO_2$

On the day of measurement, rats were anesthetized with inhalation isoflurane. The rats were immobilized onto a holder with the device centered over the custom-built surface coil. The holder was inserted into a 16.4 T MRS system and scanned while anesthesia depth was continuously monitored and adjusted as needed. Rat body temperature was maintained at 37 +/- 0.2 degrees C as measured with a rectal thermocouple and regulated with a forced air heater. Six  $R_1$  measurements were made with an inversion-recovery sequence utilizing adiabatic pulses. The  $R_1$  of each measurement was converted to a  $pO_2$  using the previously determined multi-parametric calibration. In vivo  $pO_2$  was measured 1, 4, 8, 15, 22, and 29 days post-implantation.

#### Histopathology and Immunohistochemistry

Ex-planted TEGs were fixed in 10% buffered formalin for  $\geq 24$  hours, and then transferred to 70% ethanol solution. The TEGs containing various densities of human islets explanted from nude rats after seven days were carefully embedded in paraffin wax and sectioned into 5  $\mu$ m

sections and then stained for DNA (DAPI, source), insulin (stain, source), and caspase-3 (stain, source). Micrographs of immune-stained sections were collected, and composite images were colored and assembled (red = insulin, green = caspase 3, blue = DAPI). TEGs containing porcine islets were ex-planted from Lewis rats after 29 days, fixed as described, and prepared for histology. Three 5  $\mu$ m sections from different locations of each ex-plant were histologically examined to assess the degree of vascularity, the extent of foreign body reaction present, and the extent of fibrosis in the adhered tissue surrounding the TEG. The internal contents of the TEG were also examined to determine the extent of necrosis and autolysis of tissue within the cell compartment. The degree of vascularity in the surrounding tissue of each TEG was scored in a blinded manner by an experienced pathologist on a scale from 0-3. Vascularity scores indicate the following tissue condition: 3 = well vascularized; 2 = moderate vascularity; 1 = minimal vascularity; 0 = avascular. The degree of foreign body reaction (FBR) was scored from 0-6 by examining the degree of inflammatory cell infiltrate comprised of multinucleated inflammatory giant cells, macrophages, and the lack of lymphocytes and plasma cells. The following scores indicated the extent of FBR: 6 = severe; 5 = moderate-severe; 4 = moderate; 3 = mild-moderate; 2 = mild; 1 = minimal; 0 = none. The degree of fibrosis was scored using the same scale but examined based on the density of fibrosis in the surrounding tissue.

#### *Serum C-peptide measurements*

Blood samples were collected from the tail vein of anesthetized animals implanted with porcine islet containing TEGs for measurement of systemic porcine C-peptide concentrations. After 15 and 29 days following implantation (at the same MRS assessment time-points during the study), 200  $\mu$ l blood samples were drawn from the lateral tail vein of each animal using a 25-gauge needle attached to a 1-ml syringe. Blood samples were collected into serum separator tubes (BD Microtainer SST, Franklin Lakes, NJ, USA ) containing 2  $\mu$ l of aprotinin (Sigma Aldrich, St.

Louise, MO, USA), and then spun (300 x gravity) in a chilled centrifuge (4°C) for 10 minutes. The serum was then removed from the tube and stored at -80°C for storage prior to assay. Serum C-peptide (porcine) was measured using a porcine C-peptide ELISA (Merckodia, Uppsala, Sweden).

### Statistical Analysis

Average values are reported as the mean value and the standard error of the mean (SEM). Weighted-means and error values are reported for oxygen measurements due to large variabilities observed with some of the oxygen measurements. The weighted means are calculated by weighting each oxygen measurement by the inverse of the error in the measurement squared. This method is considered superior to the arithmetic mean for increasing the confidence in average values of these kinds of data. Statistical comparisons were done using Graphpad-Prism software or SAS (version 9.2) analysis package. When comparisons between mean values of multiple groups are compared, a one-way analysis of variance (ANOVA) is used to determine if any statistical differences exist between groups, and a Tukey's post-test is used to compare individual groups. A repeated measures two-way ANOVA is used to compare differences between groups with the time-series of oxygen measurements. For nonparametric data (histology scores), the two-tailed Mann-Whitney rank sum test was used to compare two groups. Differences are considered significant if  $p < 0.05$ .

## ***Results***

### ***Engineering Model of Hypoxia***

The diffusion reaction model results are presented in **Figure 8.1A**, showing a predicted decrease in graft viability (% of tissue) at high islet densities ( $\geq 4000$  IE/cm<sup>2</sup>) in the thin macro-encapsulated TEG device with only 57% viability of the graft when the density is 8,000 IE/cm<sup>2</sup>. At this high-density approximately 52,000 IE are loaded in each 40  $\mu$ l TEG. The model predicts a more dramatic drop in graft function with increasing islet densities with 84% of the total functional capacity (% functional tissue) for the low-density condition of 500 IE/cm<sup>2</sup>, and only 13% predicted function for high-density TEGs with 8,000 IE/cm<sup>2</sup>.

### ***Ex-plant Oxygen Consumption Rate (OCR) Measurements***

Viability measurements of ex-planted TEGs suggest a more dramatic effect on viability than the engineering model predicts. TEGs with various islet densities were implanted in nude rats for 7 days, and were then ex-planted and assessed for viability by measuring the total graft OCR. TEGs were grouped based on islet density, and the average measured viabilities are expressed as a percentage of the average viability of low-density control grafts ( $< 500$  IE/cm<sup>2</sup>) in **Figure 8.1B**. The average viability (measured by OCR) of ex-planted grafts drops to only 25 $\pm$ 12% of the low-density (control, N=7) TEGs when the density is increased to between 500-1,000 IE/cm<sup>2</sup> (N=3). As the model predicts, the measured viability (viable tissue %) decreases with increasing islet density, but exhibits a more pronounced decrease in viability at moderate densities with only 14 $\pm$ 2% average viability for grafts with 1,000-2,000 IE/cm<sup>2</sup> (N=7) , and 7 $\pm$ 4% average viability for grafts with  $\geq 2,000$  IE/cm<sup>2</sup> (N=2).

### ***Histology and Immunohistochemistry***



Explanted TEGs with high-densities ( $\geq 2000$  IE/cm<sup>2</sup>) of human islets exhibited elevated caspase-3 activation based on immunohistochemical staining when compared to low-density (500 IE/cm<sup>2</sup>) TEGs. Representative images shown in **Figure 8.2** of low-density (500 IE/cm<sup>2</sup>, **Figure 8.2A**) and high-density (4,000 IE/cm<sup>2</sup>, **Figure 8.2B**) implants show the strong staining for caspase-3 indicating increased activation of apoptotic pathways. The caspase stain is also localized to the insulin-stained tissue within the graft. TEGs from oxygen measurement studies contained porcine islets loaded at a moderate density (1,500 IE/cm<sup>2</sup>) and were explanted after 30 days in vivo.

Histological examination (hematoxylin and eosin staining) of the ex-plants indicated no significant differences in the vascularity ( $p=0.72$ ) or the fibrosis ( $p=0.92$ ) of the adherent tissue surrounding the TEGs when comparing implants with and without porcine islets. All of the implants had moderate-well vascularization (scores range from 2-3), and exhibited only mild-moderate levels of fibrosis. **Figure 8.3** includes representative images and sections of the adherent tissue surrounding explanted TEGs, and similar vascular structures with the presence of red blood cells were clearly identified embedded within the vascularization membrane of all TEGs. The degree of foreign body reaction was however significantly higher ( $p=0.03$ ) for implants containing porcine islets. The average histology scores for all conditions are reported in **Table 8.1**. Examination of the internal compartments of the TEGs showed remaining eosinophilic material in all ex-plants indicating some remaining fibrin scaffold, however very little cellular tissue remained in the devices that originally contained porcine islets. No inflammatory cell infiltration was observed within the internal chamber of the TEGs suggesting that the immunoisolation chamber remained intact in vivo for up to 29 days.

#### Measurement of in vivo TEG pO<sub>2</sub>

The average pO<sub>2</sub> values within TEGs in vivo were observed to be less than 40 mmHg at all time-points examined for both conditions. <sup>19</sup>F-MRS signal with good signal-to-noise ratio (SNR = 100-

500) was obtained from the PFCE-matrix within all implanted TEGs investigated. A representative example of a fused image from  $^{19}\text{F}$  and  $^1\text{H}$ -MRI presented in **Figure 8.4** clearly demonstrates that the  $^{19}\text{F}$  signal originates from within the TEG device, and no signal was present outside of the graft. A time-series of average internal  $^{19}\text{F}$ -MRS  $\text{pO}_2$  measurements were successfully obtained from implanted TEGs containing only the matrix or 10,000 IE of porcine islets at 1, 4, 8, 15, 22, and 29 days following implantation. These results are summarized in **Figure 8.5**. The measured  $\text{pO}_2$  within TEGs containing porcine islets were consistently and significantly lower ( $p=0.0470$ ) than control TEGs which only contained the control matrix. The average internal  $\text{pO}_2$  of control TEGs one day following implantation was  $39\pm 9$  mmHg and decreased to very low levels ( $\leq 10$  mmHg) for all remaining time-points. In a similar way, TEGs containing porcine islets were observed to have an internal  $\text{pO}_2$  of  $27\pm 6$  mmHg after one day *in vivo*, which then decreased to very low levels ( $\leq 10$  mmHg) for all remaining time-points. The  $\text{pO}_2$  within TEGs was significantly higher ( $p<0.0001$ ) on the first day following implantation than any of the following days for both conditions.

#### Serum C-peptide measurements

For all animals tested, porcine C-peptide levels in rat serum were below detectible levels ( $\leq 0.2$  ng/ml) after 15 and 29 days *in vivo*.

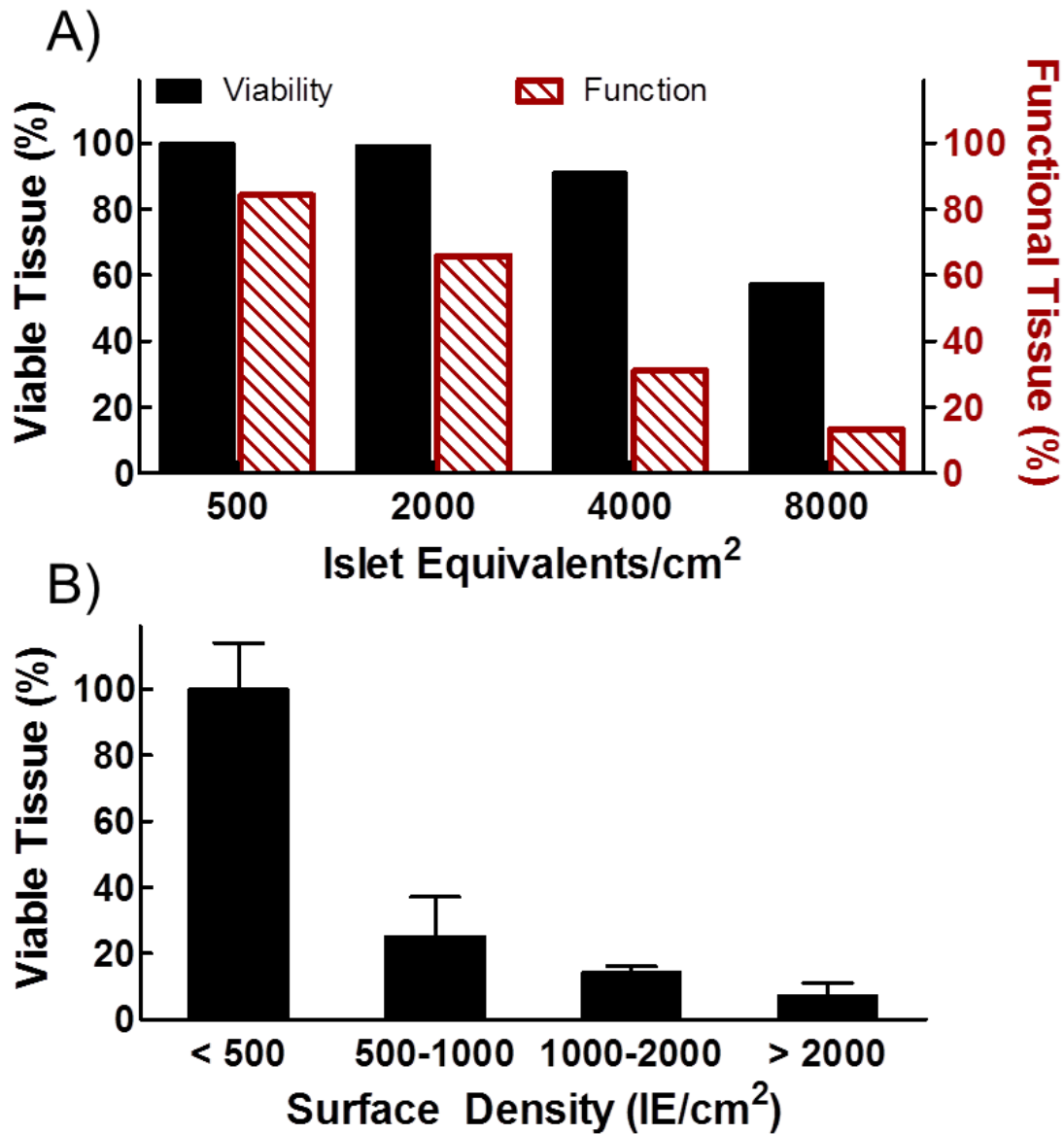
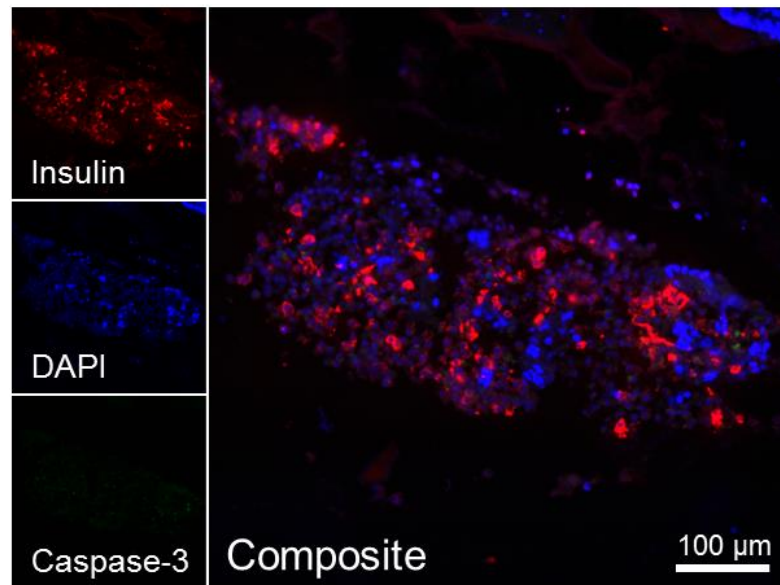


**Figure 8.1: High islet densities decreases graft viability and function.** Mathematical estimates and explant measurements of graft viability loss, and functional impairment for tissue engineered islet grafts. (A) Theoretical calculations suggest that TEGs with high islet densities will suffer from hypoxia causing a significant decrease in islet viability, and a more pronounced decrease in islet function. Islet viability and function decrease with increasing islet densities. (B) Viability measurements of islets in explanted TEGs loaded with different densities show an even more dramatic decline in OCR (viability) with increasing islet density than predicted by theoretical models. Plotted values are normalized to control TEGs implanted with  $\leq 500$  IE/cm<sup>2</sup> and bars indicate the mean + standard error of the mean percentage. (\* indicates  $p < 0.05$  for post-test when compared to low density controls, while all other values are not significantly different from each other.)

A) 500 IE/cm<sup>2</sup>



B) 4000 IE/cm<sup>2</sup>

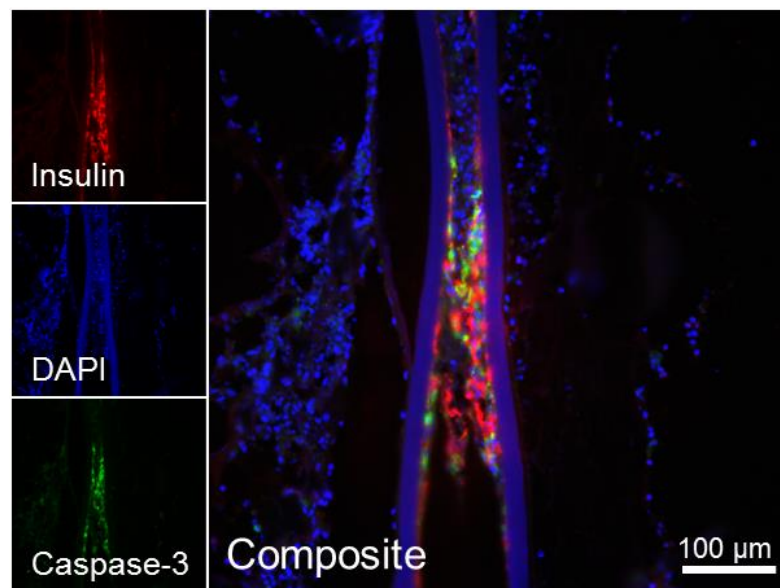


**Figure 8.2: High and Low islet density immunohistochemistry images.** Ex-planted TEG immunohistochemistry staining (representative images) comparing TEGs with (A) low 500 IE/cm<sup>2</sup> and (B) high 4000 IE/cm<sup>2</sup> islet densities show DAPI (blue), insulin (red), and increased caspase-3 (green) activation with high islet densities. Caspase-3 staining (green) is co-localized with insulin staining in TEGs with high islet densities, and this indicates that these beta cells have activated apoptotic pathways. TEGs were implanted subcutaneously in nude rats and ex-planted after 7 days for assessment.

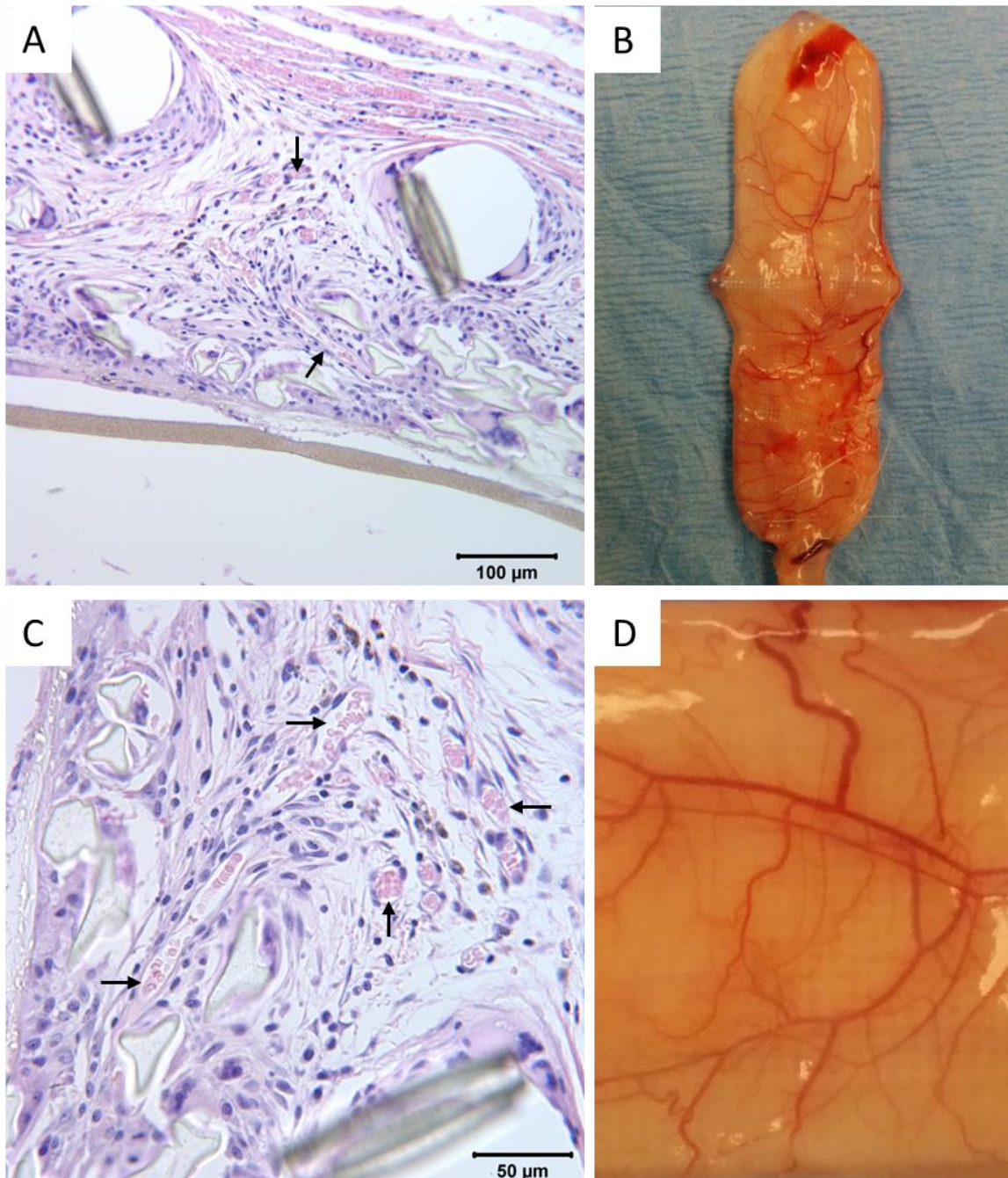


**Figure 8.3: Vasculature in surrounding tissue.** (A-C) Representative histology sections of tissue surrounding the explanted TEG after 29 days in vivo. Clear vascular structures (arrows) are visible in the tissue immediately surrounding and adhered to the vascularization membrane of the TEG. Red blood cells are also clearly seen inside the vascular tracks that are formed in the newly remodeled tissue. (B-D) Representative pictures of explanted TEGs prior to fixation with vascular network clearly incorporated in the adherent tissue surrounding the TEGs.

**Table 8.1: Average Histology Scores**

	Vascularity (0-3)	FBR* (0-6)	Fibrosis (0-6)
No cells	2.3	2.7	2.3
Porcine Islets	2.5	3.8	2.3
P-values	0.72	0.029	0.92

\*FBR = foreign body reaction,  $p \leq 0.05$  is significant

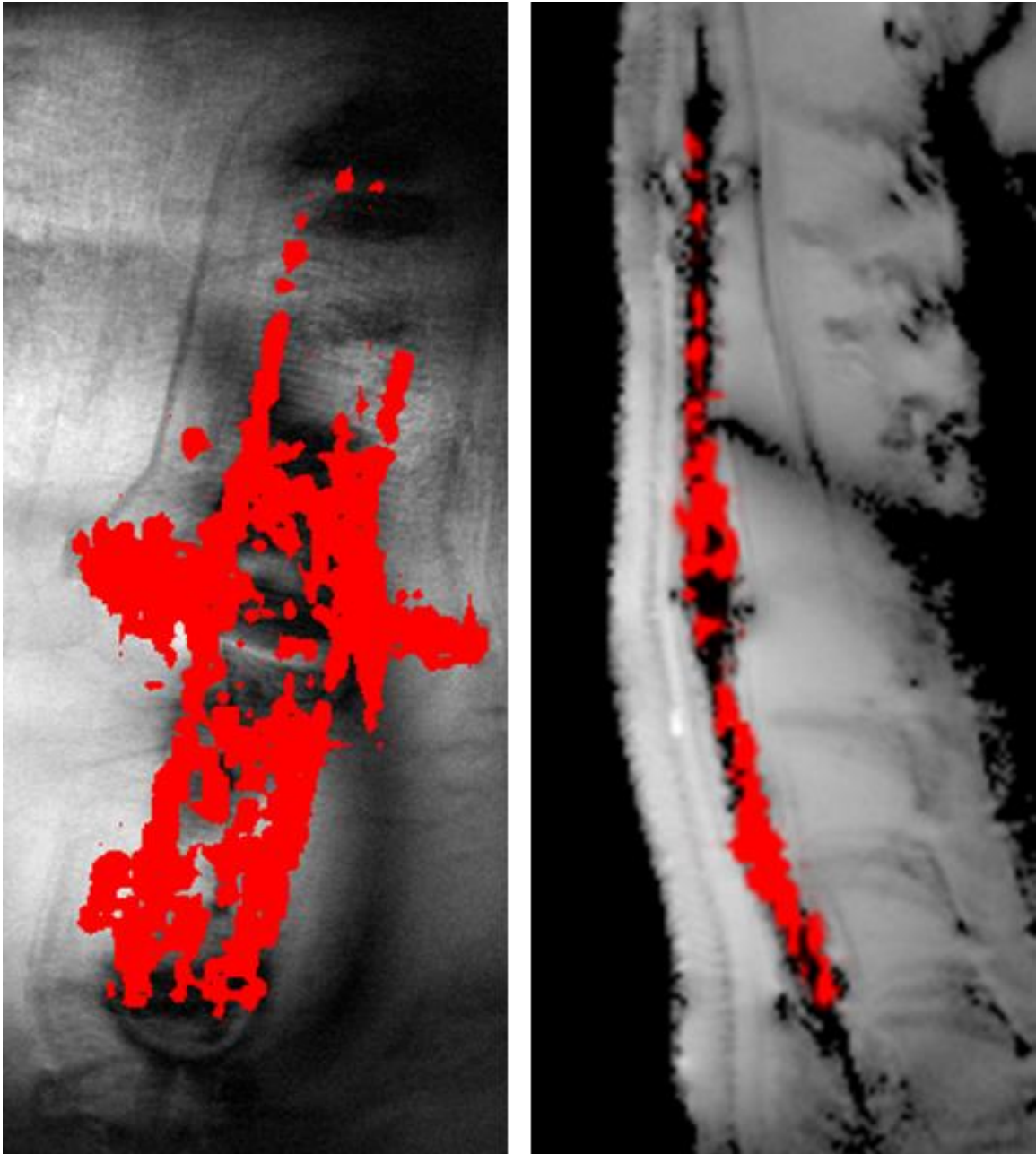


**Figure 8.4: Overlaid  $^{19}\text{F}$  (red) and  $^1\text{H}$  (greyscale) MRI of subcutaneous TEG. PFCE is distributed throughout the TEG *in vivo* and strong signal is present within the device, while no signal is detected outside of the device suggesting that the PFCE is adequately contained within the TEG.**

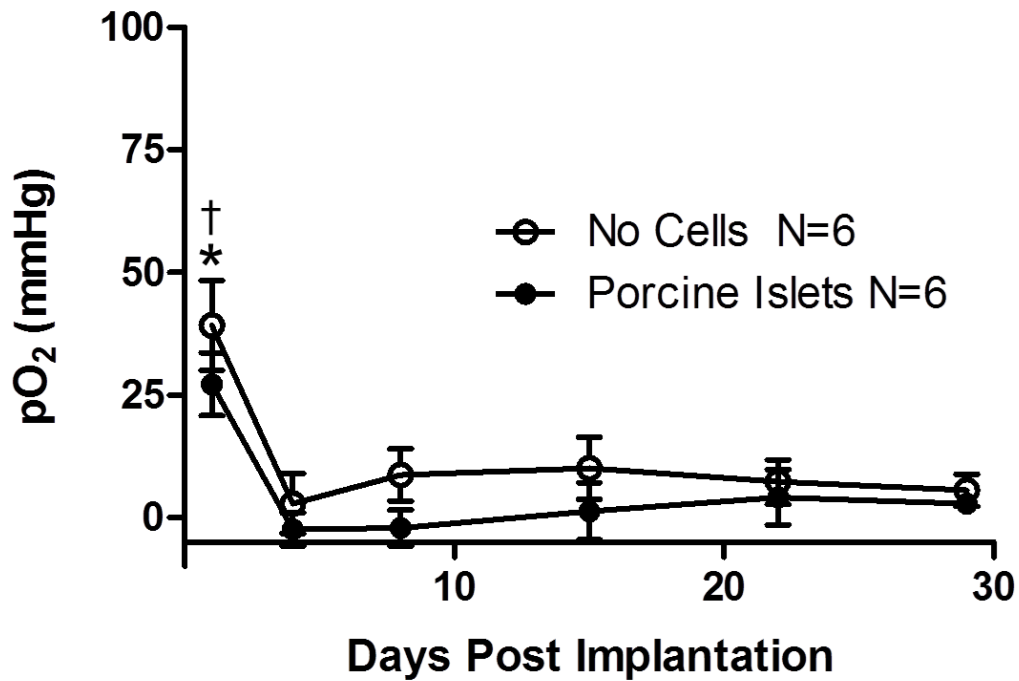


**Figure 8.5: Internal pO<sub>2</sub> of implanted TEG.** Time-course plots of oxygen partial pressures measured inside subcutaneous implanted TEGs followed for 30 days using non-invasive <sup>19</sup>F MRS method. Average pO<sub>2</sub> in TEGs containing control scaffolds (N=6) or scaffolds seeded with 10,000 IE of porcine islets (N=6) were measured at each time point (1, 4, 8, 15, 22, and 29 days post implantation). Oxygen levels in implants containing porcine islets were consistently and significantly lower than implants without cells (\*, p=0.0470), and were significantly higher (†, p<0.0001) on the first day following implantation than any of the following days for both conditions.



## ***Discussion***

Many researchers have previously described the challenges of oxygenation for tissue-engineered grafts (TEG), especially if such a graft requires high-cell densities for therapeutic or practical reasons<sup>157,224,242</sup>. In this report, these challenges were first examined by developing a model to predict the oxygenation of a macro-encapsulated islet graft, and then the effects on islet viability and function were predicted to examine implants with various islet densities. Next, the findings of the model were experimentally tested by implanting TEGs with various islet densities in nude rats for 7 days, and then measured the viability of the ex-planted devices using oxygen consumption rate measurements. Finally, <sup>19</sup>F-MRS methods were used to non-invasively measure the internal pO<sub>2</sub> of implanted TEGs with and without islets.

Other reports in literature have examined the effects of hypoxia and anoxia on pancreatic islet viability and function<sup>59,60,130,192,243–246,256</sup>, and some have reported results from diffusion-reaction models that predict oxygen limitations in macro-encapsulated TEGs<sup>227,229,247–250</sup>. We developed a 1D diffusion-reaction model to evaluate the viability and function of a macro-encapsulated islet grafts with various islet densities with the results shown in **Figure 8.1A**. The model demonstrates that as the islet density increases, the fractional viability and fractional function of a TEG decreases. Islet function is more dramatically affected by islet density because islet function is compromised at pO<sub>2</sub> ≤ 10 mmHg<sup>59</sup>, while viability is not compromised until oxygen levels fall below 0.1 mmHg<sup>59</sup>. These results suggest that thin devices with high-oxygen permeability are required to prevent hypoxic damage to encapsulated tissues, and that low islet densities are needed to ensure adequate islet function. To accommodate TEGs with such low islet densities (≤500 IE/cm<sup>2</sup>), very large implants would be required to achieve the surface area needed for adequate oxygenation, and this large-size would be impractical for implantation in humans. Literature suggests that oxygen levels of tissues *in vivo* are below venous oxygen levels (40

mmHg)<sup>257,258</sup>, and our model assumed an external pO<sub>2</sub> of 30 mmHg to be consistent with these reports<sup>252</sup>. With this low-level of surrounding tissue oxygen, high-densities of islets within a reasonably sized device will suffer from hypoxia *in vivo* as well as greatly decreased function (**Figure 8.1A**).

To examine these findings experimentally, a series of TEGs containing various densities of human islets were implanted in nude rats and then explanted 7 days later for viability assessment using the OCR assay and evaluation by immunohistochemistry. The results of explant OCR measurements reported in **Figure 8.1B** support the model findings that TEG viability decreases with increasing islet density, but the experimental observations indicate a more pronounced drop in viability starting at moderate densities and a profound drop in viability at high islet densities. These findings suggested that the encapsulated islet grafts were suffering from a more-harsh environment than the model assumes. Representative ex-plant immunohistochemistry micrographs shown in **Figure 8.2** further support the findings of the model, and the experimental viability measurements. After 7 days *in vivo*, TEGs with low islet densities ( $\leq 500$  IE/cm<sup>2</sup>) showed strong insulin staining of islet tissue inside the cell compartment of the immunoisolation device indicating that  $\beta$ -cells can survive in this environment for up to 7 days *in vivo*. However, TEGs with high islet densities ( $\geq 4,000$  IE/cm<sup>2</sup>) also showed some insulin staining in surviving islet tissue; these implants also exhibited strong staining for caspase-3. The insulin staining with the strong co-localized caspase-3 staining suggests increased activation of apoptosis pathways in the islet tissue. When combined, the results from the predictive model of hypoxia, the experimental measurement of ex-plant viability, and the confirmatory results from immunohistochemical examination suggest that TEGs with high islet densities suffer from catastrophic and possibly irreversible damage within the sub-cutaneous environment. Furthermore, these results indicate that oxygen limitations may in-fact be more severe than our initial model presumed. More

detailed examination of literature provided only limited reports of direct oxygen measurements of *in vivo* tissues<sup>56,57,161,168–170,183</sup>.

To gain a better understanding of the oxygen available to subcutaneous implanted TEGs, we developed a method for non-invasive oxygen measurements within TEGs *in vivo* using <sup>19</sup>F-MRS. Traditional oxygen sensors for oxygen measurement *in vivo* use Clark electrodes<sup>57,174,192</sup>, or fiber optic fluorescence quenching probes. Traditional polarographic, “Clark type,” electrodes suffer from inaccuracy due to the consumptive nature during operation, and both conventional methods are mechanically invasive. The traditional “needle” type probes require mechanical disturbance of the sampled tissue, and may actually introduce oxygen to the system during the measurement procedure. These traditional sensors also provide a single point measurement at the tip of the probe itself, and thus multiple mechanically disruptive measurements are required to obtain an average pO<sub>2</sub> measurement with high levels of confidence. There are some reports using a photoacoustic lifetime imaging methods<sup>193,194</sup> for oxygen measurement, but these methods are only applicable for very superficial measurements in tissues. <sup>19</sup>F-MRS methods overcome many of these limitations, and offer a sensitive, accurate, and non-invasive method for oxygen measurements *in vivo*.

Our lab has investigated <sup>19</sup>F-MRS methods for functional graft assessment *in vitro*<sup>182</sup>, and others have explored similar methods for measuring oxygen levels *in vivo* using raw perfluorocarbons (PFC)<sup>172</sup>, PFC lipid emulsions<sup>163,179,195–197</sup>, or PFC loaded alginate beads<sup>161,168–170,172,183</sup>, but none have attempted to measure the average localized oxygen concentration within a macro-encapsulation device *in vivo*. Our methods were optimized and adapted for measurements within macro-encapsulated TEGs using an ultra-high field 16.4 T MRS system for optimizing signal-to-noise ratio. Our experiences with *in vitro* studies and reports in literature<sup>159,174,177,198</sup> document the sensitivity of <sup>19</sup>F-MRS relaxation rates to both oxygen and temperature, yet many reports using

<sup>19</sup>F-MRS for oxygen measurement do not address this multi-parametric physical nature. Controlling and even measuring the body temperature of anesthetized animals inside an MRS system can be technically challenging, but due to the high sensitivity of these methods, temperature must be considered to achieve a high-level of measurement accuracy. To account for the relaxation effects of both oxygen and temperature, we chose to perform detailed and robust multi-parametric oxygen and temperature calibrations using control TEGs loaded with a PFCE impregnated plasma gel matrix<sup>199</sup>. We fit this oxygen-temperature data set using established numerical methods to derive the calibration constants used for these studies<sup>159,174</sup>. Despite these complex calibrations, the oxygen measurements are still susceptible to errors in temperature measurement, and <sup>19</sup>F-MRS methods for oximetry would greatly benefit from improved temperature measurement techniques, especially if the temperature measurements could be localized to the area of interest. An MRS method to locally measure temperature *in vivo* would be an ideal complement to <sup>19</sup>F-MRS oximetry, and development in this area would greatly improve the sensitivity and accuracy of the described methods. We chose to use PFCE due to the reported biocompatibility<sup>172,180,181</sup>, and large number of equivalent fluorine atoms, which provide an intense signal at a single resonance (singlet). Six control TEGs were prepared without any islets for subcutaneous implantation in rats to examine the ambient oxygen availability without the confounding factor of oxygen consumption. Six more functional TEGs each containing 10,000 porcine IE (1,500 IE/cm<sup>2</sup>) were implanted in the subcutaneous space to examine any changes in average oxygen levels when functional islet tissue is present in the graft. Furthermore, a small set (N=3) of control TEGs without islets were implanted in the peritoneal space to determine if the peritoneal space offered a more favorable oxygen environment.

Oxygen measurements from these implant studies, presented in **Figure 8.5**, indicate that *in vivo* TEGs are far more hypoxic than predicted by our diffusion-reaction model. Oxygen levels in

control TEGs (no islets) started at  $39\pm 9$  mmHg one day following implantation, but then decreased to  $\leq 10$  mmHg for all remaining time-points. These very low levels of available oxygen in the subcutaneous space dramatically affect the results from the diffusion-reaction model. The model assumed an external  $pO_2$  of 30 mmHg and the results predicted a modest decrease in viability at moderate islet densities and a more profound decrease in graft function. The trend of decreasing viability with increasing islet density predicted in the model was supported by the ex-plant OCR viability measurement; however, the explant measurements predicted a much more dramatic drop in viability at moderate densities. The control TEG measurements of available oxygen *in vivo* suggested that the external oxygen availability in the subcutaneous space is much lower than assumed in the model with an average available  $pO_2$  of 6.8 mmHg after the first day. With this low-oxygen availability confirmed, the predictions change, and the model suggest a more dramatic drop in islet viability at moderate densities and a profound drop in graft function. These adjusted model results are in strong agreement with the ex-plant viability measurements (**Figure 8.1B**), and predict an extremely hypoxic environment within TEGs with moderate and high islet densities. The profoundly hypoxic condition within these TEGs result in dramatic effects on islet graft viability and function, and better explain the observations from ex-plant viability measurements. TEGs implanted in the peritoneum had a similar  $pO_2$  trend and a similar hypoxic environment as subcutaneous TEGs during the 29-day measurement period. The maximum  $pO_2$  of peritoneal implanted TEGs was  $3\pm 7$  mmHg after the first day *in vivo*.

Measured average internal  $pO_2$  in TEGs containing porcine islets were significantly lower than observed in control subcutaneous implanted TEGs (without islets) at all time-points investigated. These results are anticipated due to the increased oxygen consumption of the islet tissue within the graft causing further decreases in  $pO_2$  when compared to the ambient oxygen availability. TEGs with porcine islets had a maximum average internal  $pO_2$  of  $4\pm 5$  mmHg after the first day *in*

*in vivo*, and all average pO<sub>2</sub> values were lower than values observed in control TEGs. Due to the very low oxygen levels (near zero) observed in some implants containing porcine islets, and the natural variability in the measurement techniques, the application of the established calibration curve occasionally yielded mildly negative pO<sub>2</sub> values. These SEM for these measurements included zero, and the values were not statistically different from a measurement of zero oxygen ( $p \geq 0.05$ ). As previously discussed, the <sup>19</sup>F-MRS measurement method is susceptible to variability in the absolute temperature of the TEG and the uncertainty in the measurement of the temperature using the rectal probe. Therefore, the analysis herein interprets such values to be near zero pO<sub>2</sub> and “immeasurably-low” such that the oxygen levels are in-fact lower than the error of the measurement method.

These results suggest a critical need for improved oxygenation in macro-encapsulated TEGs to support the high-cell densities needed for therapeutic applications. These studies investigate applications of TEGs for islet transplantation, but these observations are pertinent to the entire field of tissue engineering. Many engineered tissues for the treatment of human disease will require development of complex tissues with high cell densities (near native cell densities) to provide a therapeutic benefit. Oxygenation is a critical challenge facing the field of tissue engineering, and specifically for encapsulation approaches that do not allow complete re-vascularization of tissues. These challenges are recognized in recent reviews in the field<sup>157,224,242</sup>, and some have had marginal success with approaches for increasing oxygenation of implanted TEGs<sup>226,227,259–266</sup>. To address the oxygen limitations observed in our TEG system, an exogenous oxygen delivery system was developed by the Klearchos Papas lab at the University of Arizona.

As described above in **Chapter 7** and in more detail in the next section, the TheraCyte device was modified to provide for a separate central oxygen chamber, and additional access ports to allow for continuous delivery of supplemental oxygen (DSO) to the TEG *in vivo*. <sup>19</sup>F-MRS

measurements suggest a dramatic increase in available oxygen in the TEGs with DSO, and the results were reported in **Figure 7.13**. The results of these preliminary studies suggest that a continuous DSO system could be used to improve the oxygenation of therapeutically relevant macro-encapsulated TEGs, which require high islet densities.

The oxygen levels of implanted TEGs were monitored for a 29-day period to examine the kinetics of oxygen concentrations, and the  $pO_2$  on the first day following implantation was observed to be significantly higher than all of the future time-points studied. No other significant differences between time-points were found; however, a predictable trend in oxygen availability was observed for both TEG varieties. For both conditions, the oxygen levels started at the highest levels observed on the first day following implantation, and these high levels are likely due to the continued presence of oxygen in the TEGs and surrounding surgical fluid at this early time-point. A second phase is characterized by a dramatic decrease in  $pO_2$  observed on the fourth day following implantation with oxygen levels reaching near-zero levels at this time-point. This dramatic drop in oxygen is expected due to the early recruitment of highly-metabolic inflammatory cells to the site of tissue damage (surgical site). These cells migrate to the surface of the TEG, and begin the regenerative process to repair the tissues damaged during the surgery, and to respond to the newly implanted device. As the regenerative process continues, the cellular tissues grow closer to the TEG, and actually grow into the outer membrane of the TEG causing an average decrease in local oxygen availability. The third-phase in the trend occurs from 8-22 days following implantation when a moderate and gradual increase of  $pO_2$  is observed. This modest increase in  $pO_2$  can be explained by vascular formation in the adherent tissue surrounding the implanted TEG. However, this vascular formation does not significantly improve TEG oxygenation, and cannot alleviate the hypoxic condition suffered by the encapsulated islet graft. In the final phase, TEG oxygen levels appear to reach a steady-state with minimal change from

22-29 days following implantation. These trends in oxygen levels are not statistically significant, but they are consistent with the general regenerative process that occurs following a surgical insult to tissue and implanted materials. Deviations in this predictable trajectory could be indicative of catastrophic or interventional events, and with further development, these temporally repeated measurements could provide a functional tool for non-invasive examination of TEGs.

The same TEGs used for oxygen measurements were ex-planted after 29 days, and processes with the surrounding adhered tissue to examine the engraftment by histopathology. The surrounding tissue was scored in a blinded fashion by an experienced histopathologist to assess the degree of vascularity, the extent of foreign body reaction, and formation of fibrosis in the surrounding tissue with the results presented in **Table 8.1**. The results suggest that the surrounding tissue in both grafts that contain porcine islets and grafts without islets had developed a moderate level of vascular formation with average scores of 2.5 and 2.3 respectively with no significant differences observed for this metric. The adherent tissues surrounding implanted TEGs exhibited only mild fibrosis with the same average score of 2.3 for both conditions of TEGs. The extent of the foreign body reaction was significantly higher for implants that contained porcine islets; however, the response was only moderate for these implants with an average score of 3.8. These results are consistent with previous reports using similar TEGs<sup>157,248,251</sup>, and moderate levels of fibrosis and foreign body reactions are expected with these materials<sup>267-269</sup>. The increase in the foreign body reaction observed in TEGs that contained porcine islets can also be expected using an immunocompetent animal model like the Lewis rats used for these studies. The TheraCyte device has been reported to effectively protect allogeneic grafts<sup>186,191</sup>, but it has not proven to be effective for protecting xenogeneic grafts<sup>228,269</sup>. The presence of xenogeneic islet tissue within the TEG is expected to cause an elevated inflammatory response despite the immunoprotective



capacity of the device, and this likely explains the increased scores for these TEGs. Histological examination of the internal cellular compartments of the explanted TEGs showed remnant amounts of eosinophilic material (PFCE-fibrin matrix) in all devices, but only minimal surviving islet tissue remained in porcine islet loaded TEGs after 29 days *in vivo*. These findings are consistent with the measured oxygen levels and suggest that the severely hypoxic environment may be causing complete loss of the islet graft after 29 days. The results are also likely confounded by the xenogeneic response, as the TheraCyte has not been effective for protecting xenogeneic grafts<sup>228,269</sup>. Systemic porcine C-peptide levels were also measured on day 15, and 29 for animals that received TEGs with porcine islets, and no detectible levels were observed in any of the animals adding further support to the hypothesis of early graft failure and death due to the severely hypoxic environment within the TEGs.

## ***Conclusions***

Oxygenation is a critical barrier to the success of any highly cellular implantable tissue engineered graft (TEG). Hypoxic stress is suspected to be the primary cause of TEG failure for encapsulated grafts that do not accommodate direct vascularization or re-vascularization of tissue. Our model describing a macro-encapsulated TEG demonstrates that adequate oxygenation is not possible *in vivo* with high islet densities, and that graft viability and function will be severely limited without intervention. Oxygen consumption measurements and immunohistochemical examination of ex-planted TEG conclude that hypoxic conditions *in vivo* have harmful effects on graft viability and function, and that TEGs with moderate islet densities suffer from dramatic losses in viability after 7 days. To examine the oxygenation status of implanted TEGs, <sup>19</sup>F-MRS methods were successfully developed to measure pO<sub>2</sub> non-invasively. The developed <sup>19</sup>F-MRS method is robust, accurate, and reproducible; and can be used to track the oxygenation status of TEGs for long durations post-implantation (up to 29 days). Oxygen measurements of control TEGs in rats showed that the subcutaneous and peritoneal spaces are severely hypoxic environments that cannot support the oxygen requirements of a TEG with high islet densities. The same measurements in TEGs containing porcine islets further support these conclusions, and demonstrate that external graft vascularization in the first 29 days is not sufficient to promote graft survival. However, delivery of supplemental oxygen could alleviate the hypoxic condition and promote TEG survival *in vivo*. In conclusion, further development of novel methods for improving oxygenation *in vivo* are needed to support the function of macro-encapsulated TEGs, and innovative non-invasive assessment techniques, like <sup>19</sup>F-MRS, are critical to the development and validation of various oxygenation approaches.

## Oxygen Delivery Improves Islet Graft Function *in vivo*

### *Summary*

Macro-encapsulation and immunoisolation to create a tissue engineered bio-artificial pancreas (BAP) could allow for islets and beta-cells from alternative sources to be implanted in diabetic patients to restore glycemic control without the need for immunosuppression. However, oxygenation remains a critical limitation for the application of tissue engineered grafts (TEGs) that contain therapeutic cell doses at practical cell-densities. This study describes the development of a non-invasive method for the measurement of internal oxygen partial pressures ( $pO_2$ ) using fluorine-19 magnetic resonance spectroscopy ( $^{19}F$ -MRS) within an implanted TEG, with and without the *in situ* delivery of supplemental oxygen (DSO). TEGs were constructed using a TheraCyte immunoisolation device (TheraCyte, Inc. Laguna Hills, CA) modified to allow for DSO. TEGs were prepared with or without porcine islets (20,000 islet equivalents) suspended within a matrix containing perfluoro-15-crown-5-ether (PFCE) as an oxygen probe for  $^{19}F$ -MRS measurements. TEGs with and without DSO were implanted into a dorsal subcutaneous pocket in non-diabetic Lewis rats (Charles River, Wilmington, MA). The internal  $pO_2$  was monitored periodically for 29 days *in vivo* using the methods described in **Chapter 7**. A small feasibility study implanting TEG devices in diabetic rats with or without DSO was done to examine the functional impact of DSO. Blood glucose measurements were done to evaluate graft function. As described in the previous section of this chapter, without DSO, the average *in vivo*  $pO_2$  was severely hypoxic at all time-points investigated for both conditions. TEGs with DSO *in vivo* achieved  $pO_2 > 300$  mmHg the first day after implantation, which remained elevated for up to 29 days in islet loaded and islet-free TEGs. Functional outcomes (BG levels) suggest that DSO supports prolonged high-islet density graft function for up to 30 days. Non-invasive  $^{19}F$ -MRS can be used for the accurate measurement of  $pO_2$  within an implanted TEG. DSO successfully

increased the internal  $pO_2$  of implants with and without islets, and supported prolonged graft function in diabetic nude rats.

## ***Introduction***

Islet transplantation (ITx) offers a minimally invasive alternative to pancreas transplantation, and shows promise as a possible cure for type 1 diabetes<sup>200,201</sup>, but widespread application of this therapy is still inhibited by numerous barriers. Despite recent improvements with single-donor ITx at some centers, the five-year insulin independence rate is only 50%, and many cases still require more than one transplant to achieve insulin independence<sup>53,200,202–208</sup>. Furthermore, due to the insurmountable shortage in available donor pancreata, this therapy is currently limited to select patients with severe hypoglycemic unawareness<sup>53,207,242</sup>. To expand access to this promising therapy, many are investigating methods to improve donor pancreas quality<sup>20,31,37,44,45,50,69,104,270–273</sup>, optimize isolation processes<sup>36,274–277</sup>, and optimize the use of immunosuppressive drugs<sup>200,204,207,208</sup>. Despite these improvements, the limited source of allogeneic donor islet tissue will never be sufficient to treat the growing population suffering from diabetes. Investigators have turned to xenogeneic<sup>76,89,90,238,278–280</sup> and stem-cell sources to alleviate this shortage, but these sources introduce further challenges related to long-term immune protection and physiological islet function. There has been limited success with xenogeneic porcine islet transplantation in animal models<sup>33,34,281–290</sup>, but aggressive immunosuppression protocols are needed to prevent rejection, which increases patient risk and has been shown to harm to islet grafts<sup>212–214</sup>. There have also been promising advances toward development of functional stem-cell derived islets<sup>231–235</sup>, but concerns remain about the increased risk and safety of these sources.

Macro-encapsulation approaches to create a tissue engineered bioartificial pancreas (BAP) could offer physical immunoprotection and containment of transplanted islet tissue addressing concerns for the use of both xenogeneic and stem-cell derived sources. Various encapsulation techniques have been investigated, and some success has been achieved with small doses of islets in animal models, but scaling these devices to therapeutic sizes for humans is not practical. Tissue

engineered grafts (TEGs) which contain high-densities of islet tissue suffer from severe hypoxic stress resulting in graft failure and limited function after only a few days *in vivo*. Extensive discussion of previous efforts and detailed explanations of these challenges are described in the recent reviews of Colten, Chhabra, and Yang<sup>157,224,242</sup>. Various approaches for increasing oxygenation of macro-encapsulated implants have been investigated, and results suggest that revascularization alone will not support sufficient oxygen transport, and continuous oxygenation will be required for these approaches<sup>226,227,259–266</sup>. To evaluate various oxygenation strategies, and to optimize methods for oxygen delivery; a robust method for non-invasive oxygen measurement is needed. Our lab<sup>182</sup> and others<sup>161,163,168–170,172,179,183,195–197</sup> have successfully applied <sup>19</sup>F-MRS methods for non-invasive measurements of oxygen within implanted TEG devices, and the results confirmed a persistent hypoxic environment *in vivo*. The non-invasive nature of these methods can provide accurate and reliable measurements of oxygen partial pressures (pO<sub>2</sub>) *in vivo*, without disrupting the surrounding tissue or the integrity of the implanted device.

These studies evaluate the feasibility and functionality of a macro-encapsulated islet graft employing a method for delivery of supplemental oxygen (DSO) to alleviate hypoxia *in vivo*. High islet density grafts were implanted in the subcutaneous space of rats and supplemented with exogenous oxygen delivery while periodic non-invasive oxygen measurements were obtained by <sup>19</sup>F-MRS.

## ***Materials and Methods***

### ***Experimental Approach***

The work presented herein represents the results of collaborative projects done at the University of Minnesota (UMN), and the University of Arizona (UA). To examine the effects of continuous oxygen delivery on the success of encapsulated islet grafts, these studies test the efficiency and function of a TEG being developed at the UA intended for future clinical application. To determine the efficacy of oxygen delivery, Fluorine-19 magnetic resonance spectroscopy (<sup>19</sup>F-MRS) methods were used to measure the internal oxygen partial pressure (pO<sub>2</sub>) of TEG devices non-invasively in vitro and in vivo. All <sup>19</sup>F-MRS oxygen measurement studies were done at the UMN. A series of 5 TEG devices modified for DSO were prepared without islets for in vitro studies using <sup>19</sup>F-MRS measurements to validate successful delivery of oxygen to TEGs within a perfusion bioreactor. A second series of TEGs with DSO were implanted in 12 non-diabetic Lewis rats (RT1<sup>l</sup>, Charles River Laboratories International, Inc., Wilmington, MA, USA) with 6 of the rats receiving implants containing 20,000 porcine islet equivalents (PIEs), and 6 receiving control implants containing only an oxygen sensitive hydrogel-matrix. The internal pO<sub>2</sub> of implanted TEGs were monitored for up to 29 days. Furthermore, a series of 6 rats were implanted with control TEGs (no islets) that did not receive oxygen to compare against ambient available oxygen levels. For preliminary assessment of graft survival and function in vivo, a small number of TEGs with (N=2) and without DSO (N=6) were loaded with 24,000 PIE and implanted in diabetic nude rats (athymic nude mutant, Hsd:RH-Foxn1<sup>tmu</sup>, Harlan Laboratories, Inc, Indianapolis, IN, USA). Graft function and survival were evaluated by measuring daily blood glucose levels in diabetic animals, and histological examination of all explants. Furthermore, blood samples were collected from all animals that received porcine islets porcine C-peptide

measurements as secondary measure of graft function *in vivo*. All studies with diabetic animals were conducted at the UA.

#### Tissue Engineered Graft (TEG) Device Preparation

A modified TEG was built by adapting the clinically-established TheraCyte (TheraCyte Inc., Laguna Hills, CA, USA) device<sup>186-191</sup> to allow for continuous DSO *in vivo*. All studies with DSO used these modified devices, while studies without DSO used an un-modified 40- $\mu$ l TheraCyte device. Briefly, for TEGs with DSO, the 40- $\mu$ l device was modified to include a central chamber that allowed for direct delivery of oxygen gas to the internal aspect of the device, and additional ports were added for access to this central oxygen chamber. The TheraCyte device is originally constructed by sandwiching two PTFE immunoisolation membranes to form an internal cellular chamber, which is surrounded by two vascularizing membranes that provide structural support and improved vascularization of the device surface *in vivo*. A single access port allowed for loading of the internal cell compartment. The modified device was constructed with two additional PTFE immunoisolation membranes layered on top of each other, which created two distinct cellular chambers on either side of a central oxygen chamber. Additional access ports were included with two ports on the longitudinal end to provide access to the central oxygen chamber, and two lateral ports to provide individual access to each cell-chamber. One of the DSO access ports provided for oxygen gas flow into the central chamber (inlet), while the other port allowed gas to flow back-out of the device (outlet). The access port design and cannula attachments are included in **Appendix A**. This approach was intended to accommodate constant flow of oxygen-rich gas through the modified device, which provided for continuous replenishment of oxygen within the device.

To prepare TEGs, porcine islets (if included) were suspended in a hydrogel-matrix and injected into the cell compartments of each device (the total dose was split between both cell



compartments for TEGs with DSO). Porcine islets were isolated at the University of Minnesota, and cultured for up to 14 days prior to use for this study. All islet doses were quantified by DNA content assay (Quant-iT PicoGreen dsDNA Assay Kit, Life Technologies, Carlsbad, CA, USA). For  $^{19}\text{F}$ -MRS oxygen measurement studies, the hydrogel-matrix was composed of perfluoro-15-crown-5-ether (PFCE,  $^{19}\text{F}$  oxygen probe, Exflur Research Corporation, Round Rock, TX, USA) emulsified in porcine plasma (Sigma Aldrich, St. Louise, MO, USA) which was cross-linked using 5% v/v solution of topical bovine thrombin (GenTrac Inc., Middleton, WI) following injection into the device. For diabetic rodent studies, the matrix was composed of a 5% alginate solution, which was cross-linked using a 1.2 mM calcium chloride solution following injection into the device. Additional TEGs were prepared using the same methods without islets for bioreactor studies, control implants, and for  $^{19}\text{F}$ -MRS oxygen calibrations.

#### Perfusion Bioreactor

In vitro studies were conducted using a perfusion bioreactor system, which continuously perfused with porcine islet culture medium (ME199 based, Mediatech Inc.) around a TEG modified for DSO. These methods are described in detail in **Chapter 7** TEG devices with DSO were prepared as described for in vitro  $^{19}\text{F}$ -MRS oxygen measurement studies without porcine islets, and placed inside a perfusion bioreactor chamber.

#### Animal Research

The Institute for Animal Care and Use Committee (IACUC) at the University of Minnesota (UMN) and the University of Arizona (UA) reviewed and approved all animal studies described herein. Animal welfare was carefully monitored daily during all studies.

#### Implantation of TEG devices and DSO in vivo.

A total of 26 rats were implanted with subcutaneous TEG devices, and the surgical implantation procedure was similar for all animals presented in this study with minor differences for animals which did not receive DSO. Two or more weeks prior to surgery, animals designated to receive TEGs with DSO were fitted with a vascular access harness and tether apparatus (Instech Laboratories, Plymouth Meeting, PA, USA) to allow for sufficient acclimation to restraint. The harness and tether apparatus consisted of a flexible-silicon adjustable harness, which provided a sterile access port on the back of the animal. A tether assembly attached securely to the access port and consisted of plastic cannulas protected by a flexible stainless steel spring that extended out the top of the cage to a swivel and counter-balance assembly, which provided for minimal restraint of natural feeding, drinking, and grooming behaviors. Animals were monitored daily during the acclimation period and for the duration of the study to ensure animal welfare. Body weights along with any signs of distress were recorded and complications were documented and remedied if necessary throughout the study. All animals successfully acclimated to the restraint during the two-week period.

In preparation for surgery, the harness was removed, and anesthesia was induced with 3% isoflurane and maintained at 1.5% isoflurane during the procedure using a small animal respirator system. Animal temperature was maintained using a warming pad, and monitored using a rectal temperature probe. The surgical site, on the dorsal side, was shaved and prepared using chlorhexidine antiseptic swabs. A 1.5 cm incision through the skin was made in a transverse direction on the dorsal side, inferior the scapulae and symmetric across the medial line. Gentle blunt dissection was used to create a small pocket under the skin and adjacent to the vertebral column to accommodate the modified TEG device. After rinsing the pocket with sterile saline, the TEG device was gently tucked into the space leaving the DSO cannula extending out of the incision (for TEGs with DSO). The incision was closed using at least two layers in a normal

fashion around the cannula using absorbable sutures, and then sealed by applying a light coat of surgical sealant (Dermabond, Ethicon Inc., Somerville, NJ, USA). Care was taken to ensure that the implant components did not put pressure on the incision, and to ensure that DSO transcutaneous cannulas were not obstructed during closure. A new sterile harness was then re-fitted, and oxygen gas flow for DSO was confirmed by manual injection through the harness. Anesthesia was then stopped and the animal was allowed to recover completely on the surgical warming pad prior to returning the animal to the cage and attaching to the tether apparatus. Upon returning to the cage, DSO was immediately initiated (when applicable), and oxygen-rich (650 mmHg) gas was continuously delivered at a target flow rate of 1.5 ml/min for the duration of the study. DSO was only stopped for brief periods (1-2 minutes) when animals were disconnected from the tether apparatus for daily monitoring and examination. TEGs without DSO (N=12) were implanted using the same surgical approach, but non-modified TharaCyte devices were used, transcutaneous cannulas were omitted, and animals were not restrained via the harness and tether apparatus.

The DSO system was composed of an electrochemical oxygen generator (EOG, Giner Inc., Auburndale, MA, USA) along with a specialized DSO regulating manifold. The EOG system generated a constant stream of humidified pure oxygen gas (760 mmHg), which flowed directly to the DSO manifold. The manifold was designed using a series of gauges and valves to independently monitor and control the pressure and flow of oxygen-rich gas to each TEG. The outlet side of the manifold was connected to external connections in the animal cage lids, and provided oxygen to the tether apparatus. Extended DSO tubing was used to continue DSO during <sup>19</sup>F-MRS measurement procedures. Gas flow through each TEG was confirmed daily by measuring flow through the manifold, and confirming a continuous stream of gas leaving the implanted TEG through the outlet cannula.

For diabetic animals that achieved blood glucose control, the TEG was surgically removed after 30 days using the same surgical techniques that were used for implantation. Animals were then allowed to recover and were monitored for up to 5 days to observe a return to diabetic state. Upon completion of each study, animals were euthanized by inhalation of 100% CO<sub>2</sub> for 5 or more minutes until death was confirmed. The TEGs were then surgically removed and processed for explant histopathology analysis.

#### *<sup>19</sup>F-MRS Oxygen Measurements*

Oxygen measurements were obtained using methods previously described by our group and in **Chapter 7**. Briefly, the <sup>19</sup>F relaxation rates of control TEG (without cells and without DSO) devices were measured *in vitro* at 6 controlled pO<sub>2</sub> levels (0, 38, 76, 114, 160, and 760 mmHg) and at three different temperatures (21, 37, and 45 °C) to generate calibration curves using a 16.4 Tesla MRS system. All <sup>19</sup>F R<sub>1</sub> measurements were obtained using an inversion recovery sequence with adiabatic pulses and a custom-made surface coil tuned to the <sup>19</sup>F resonance frequency (656.8 MHz). The calibration data was fit to a multi-parametric calibration equation using regression methods to generate the needed calibration constants that relate R<sub>1</sub> to pO<sub>2</sub> and temperature. The calibration constants were then used to determine the bulk average oxygen concentration within TEG implants based on <sup>19</sup>F-R<sub>1</sub> and temperature measurements. For *in vivo* studies, animals were anesthetized by isoflurane inhalation and were immobilized on an MRS bed with the TEG centered over the custom-built coil. The animal was inserted in the 16.4 T MRS scanner, and body temperature was maintained at 37±0.2 mmHg using a forced-air heater. The average internal pO<sub>2</sub> of each TEG device was measured by <sup>19</sup>F-MRS after 1, 4, 8, 15, and 29 days following implantation. Oxygen measurements from TEGs for *in vitro* in bioreactors described above were measured in the same way.

#### *Diabetic Rodent Model & Functional Measurements*

TEGs containing  $25,000 \pm 1000$  PIE with or without DSO were implanted in diabetic nude rats, and function was assessed by measuring non-fasting daily blood glucose levels. Diabetes was chemically induced in nude rats by intraperitoneal injection of a 60 mg/kg dose of streptozotocin (Zanostar) reconstituted in fresh sterile citrate buffer (10 mM, pH 4.5). Following induction, blood glucose (BG) measurements were recorded at the same time every day from diabetic animals using a blood glucose meter (True track glucose monitoring system, NIPRO Diagnostics, Fort Lauderdale, FL, USA). For each animal, the tail was pricked at the tip using a sharp lancet, and a small drop of blood was collected on the test-strip of the glucose meter. Induction was considered successful after measuring 3 consecutive daily BG levels of  $>300$  mg/dL. After 6-7 days, TEG devices with or without DSO were implanted in diabetic rats as described above. After implantation BG measurements were continued daily to monitor graft function.

#### Serum C-peptide

Samples of blood were collected from the tail vein of animals with TEGs containing porcine islets during anesthesia prior to  $^{19}\text{F}$ -MRS oxygen measurements. Blood samples were processed for porcine C-peptide content by centrifuging (300 x gravity) blood in serum separator tubes containing 2  $\mu\text{l}$  aprotinin (Sigma Aldrich, St. Louise, MO, USA) for 10 minutes. The separated serum was collected and porcine C-peptide levels were measured by ELISA (Mercodia, Uppsala, Sweden).

#### Histopathology and Immunohistochemistry

At the completion of each study, the TEG devices were explanted, and then fixed in a 10% buffered formalin solution for  $\geq 24$  hours, and then transferred to 70% ethanol for long-term storage. Sections from three separate locations in each TEG were embedded in paraffin, and stained for histopathology with hematoxylin and eosin, to assess the extent of fibrosis, vascularity, and foreign body reaction in the adhered tissue surrounding the TEG. An experienced

histopathologist scored each section in a blinded manner for each metric. The degree of vascularity was scored on a scale from 0-3; 3 = well vascularized; 2 = moderate vascularity; 1 = minimal vascularity; 0 = avascular. The foreign body reaction (FBR) and degree of fibrosis were scored in a similar way from 0-6: 6 = severe; 5 = moderate-severe; 4 = moderate; 3 = mild-moderate; 2 = mild; 1 = minimal; 0 = none.

#### Statistical Analysis

Statistical comparisons were made between all groups with sufficient replicates, and average values are reported as the mean value with the standard error of the mean (SEM). Graphpad-Prism software or SAS version 9.2 analysis package was used for statistical analysis. A one-way analysis of variance (ANOVA) is used for comparisons between multiple groups, and a Tukey's post-test is used to compare individual groups. A two-way repeated measures ANOVA was used for comparing time-series data (BG, and oxygen measurements). The two-tailed Mann-Whitney rank sum test was used to compare groups of non-parametric data (histology scores). Differences were considered significant if  $p < 0.05$ .

## ***Results***

### *Oxygen measurements of TEGs with DSO in vitro*

Non-invasive oxygen measurements from TEGs in a bioreactor show significantly increased internal  $pO_2$  for implants with DSO. These results are presented in **Chapter 7**, but included here as well for comparing in the context of *in vivo* oxygen delivery. A continuous series of  $^{19}F$ -MRS oxygen measurements acquired from TEGs inside a bioreactor are presented in **Figure 8.6**, which is reproduced from **Figure 7.11**. The results demonstrate that optimal DSO was achieved with delivery of either 380 or 760 mmHg enriched oxygen gas, and implants equilibrated to a steady-state internal  $pO_2$  in  $\leq 20$  minutes regardless of the  $pO_2$  of the delivered gas. The external  $pO_2$  of each TEG was controlled to simulate the hypoxic  $pO_2$  levels previously observed *in vivo*. The hypoxic external environment was verified by continuous fiber-optic probe measurements ( $34 \pm 6$  mmHg), and confirmed with  $^{19}F$ -MRS measurements when the internal  $pO_2$  of each TEG acclimated to the external  $pO_2$  within an hour after beginning perfusion. The average internal  $pO_2$  of all TEGs reached  $64 \pm 4\%$  of the delivered  $pO_2$  regardless of the DSO concentration. TEG implants achieved average steady-state internal  $pO_2$  measurements of  $207 \pm 22$  mmHg and  $469 \pm 40$  mmHg for DSO with  $pO_2 = 380$  mmHg and 760 mmHg respectively. After steady-state measurements, DSO was stopped to record the internal  $pO_2$  decay as the TEG returned to ambient external oxygen. Oxygen measurements were fit with a mono-exponential decay function yielding an average characteristic time-constant ( $\tau$ ) of  $15 \pm 1$  minutes.

### *Oxygen measurements of TEGs with DSO in vivo.*

DSO was also very successful *in vivo* and highly elevated internal  $pO_2$  levels were measured one day after implantation in non-diabetic immunocompetent rats (shown graphically in **Figure 7.13** from **Chapter 7**). TEGs receiving 760 mmHg DSO without islets achieved an average internal  $pO_2 = 556 \pm 19$  mmHg (N=9) while implants containing 20,000 PIE achieved  $370 \pm 49$  mmHg

(N=4). When DSO was stopped for a sub-set (N=3) of implanted TEGs without islets, the internal pO<sub>2</sub> decreased to an average of 22±2 mmHg which is not significantly different than the oxygen concentrations observed in TEGs without DSO. Measurements presented in **Figure 8.7** from critical time-points during the 29-day study period show that the average internal pO<sub>2</sub> inside implanted TEGs starts at a high level on the first day following implantation, and then decreases until 15 days after implantation when an apparent steady-state is reached. The internal pO<sub>2</sub> of TEGs with porcine islets (N=6) were significantly lower (p<0.05) than control TEGs without islets (N=6) at every time-point investigated with an average overall difference of 186±23 mmHg. All TEGs with DSO had a significantly higher average internal pO<sub>2</sub> than implants that did not receive DSO (p<0.05), and results from implants without DSO are reproduced here from **Figure 8.5** for direct comparison.

*Functional assessment of TEGs with DSO in diabetic rodents.*

A TEG with DSO demonstrated improved graft function when compared to TEGs without DSO. Results from BG measurements demonstrated that sustained diabetes reversal was achieved in an animal that received a TEG implant with DSO. **Figure 8.8** shows that a subcutaneous implanted TEG with DSO effectively regulated BG levels in a diabetic rodent; which were significantly lower (p<0.05) than animals who received TEGs without DSO. BG levels were quickly normalized (≤200 mg/dL) and sustained for 30 days with DSO, while levels remained elevated (>300 mg/dL) when TEGs did not receive DSO.

*Serum C-peptide measurements*

Porcine C-peptide was detected in the serum of non-diabetic Lewis rats both 1 and 4 days following implantation of TEGs with DSO that contained 20,000 PIE. The average detected porcine C-peptide was 0.1±0.4 ng/ml on the first day after implantation, which increased to



0.4±0.08 ng/ml on the fourth day; however, there was no detectible porcine C-peptide ( $\leq 0.05$  ng/ml) in serum for any following time-points investigated.

#### *Histology and Immunohistochemistry*

Histology of TEGs explanted from non-diabetic Lewis rats used for  $^{19}\text{F}$ -MRS studies, showed minor differences in the surrounding adherent tissue of implants with and without DSO. Tissue surrounding TEGs with DSO had slightly lower levels of vascularity, and slightly higher levels of FBR than TEGs without DSO after 30 days in vivo, and these differences were significant ( $p < 0.05$ ). There were no significant differences in fibrosis of the surrounding tissue between groups, and there were no significant differences between implants with or without porcine islets. With or without DSO, the internal cell-compartments of TEGs containing porcine islets implanted in Lewis rats contained only scattered fragments of islet tissue after 30 days in vivo.

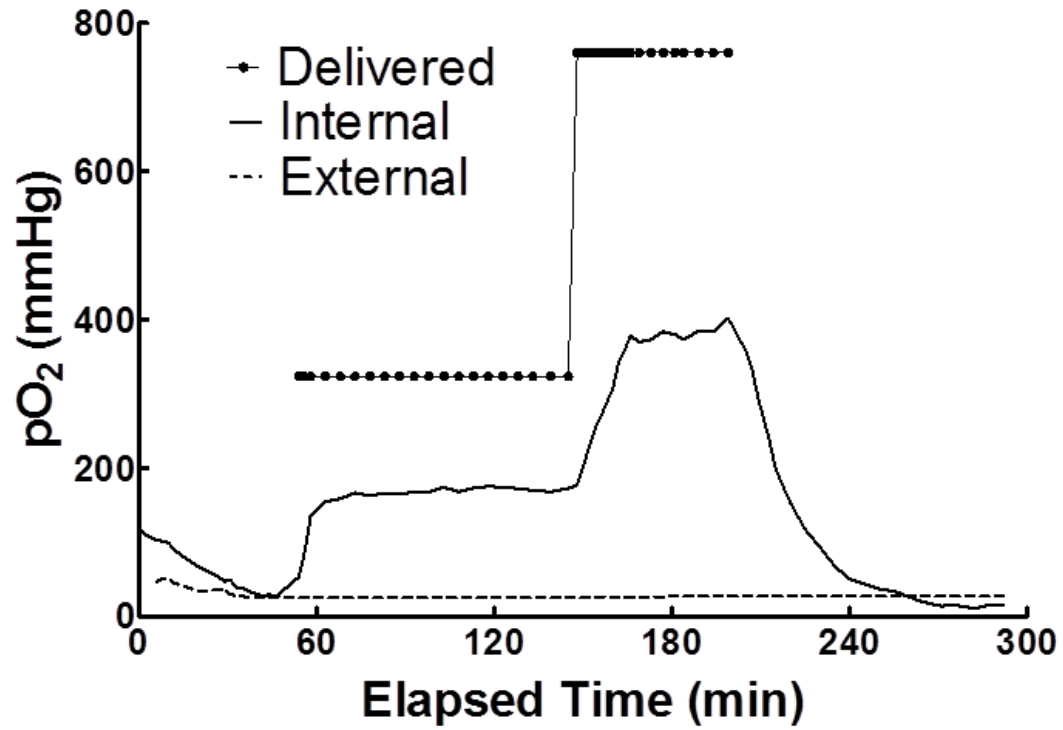


**Figure 8.6: Measuring oxygen in bioreactor with DSO.** Reproduction of figure **Figure 7.11** Oxygen levels in a typical bioreactor with DSO at 300 mmHg and then 760 mmHg followed by observed pO<sub>2</sub> decay without DSO.

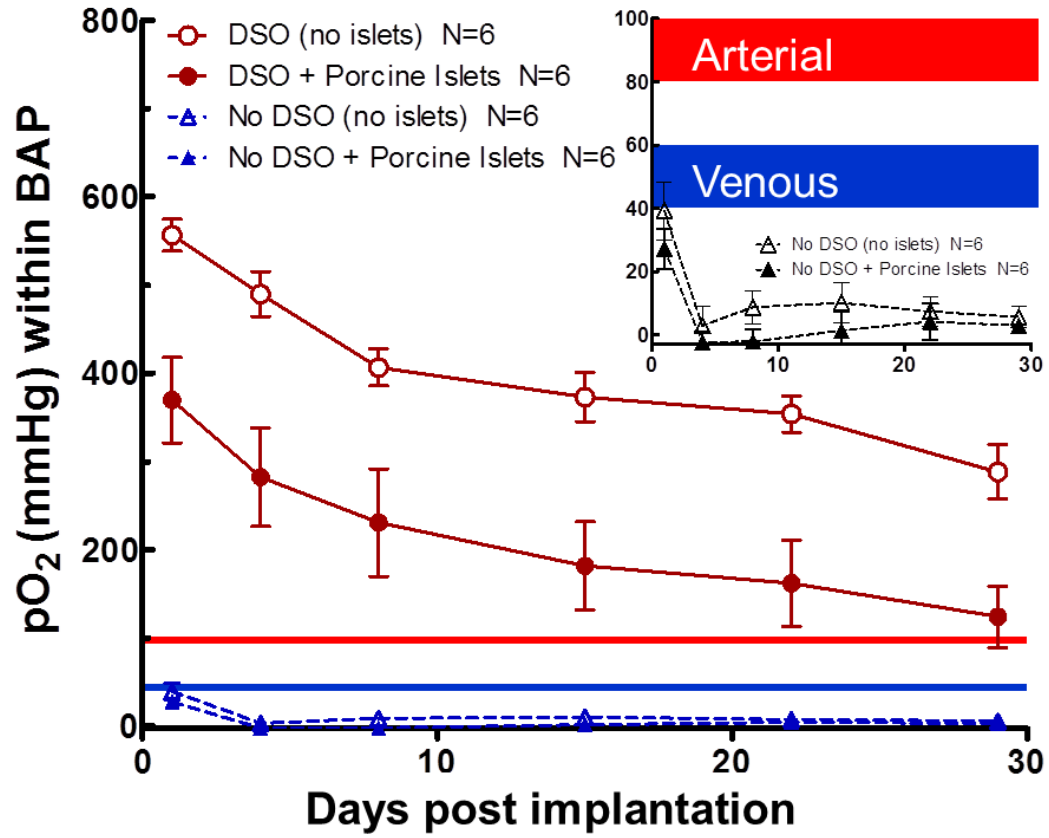


**Figure 8.7: Internal pO<sub>2</sub> of TEGs with DSO.** <sup>19</sup>F-MRS oxygen measurements within TEGs implanted for 29 days with and without DSO. The measurements without DSO (inset) are much lower than arterial (red-bar) or venous (blue-bar) pO<sub>2</sub>.

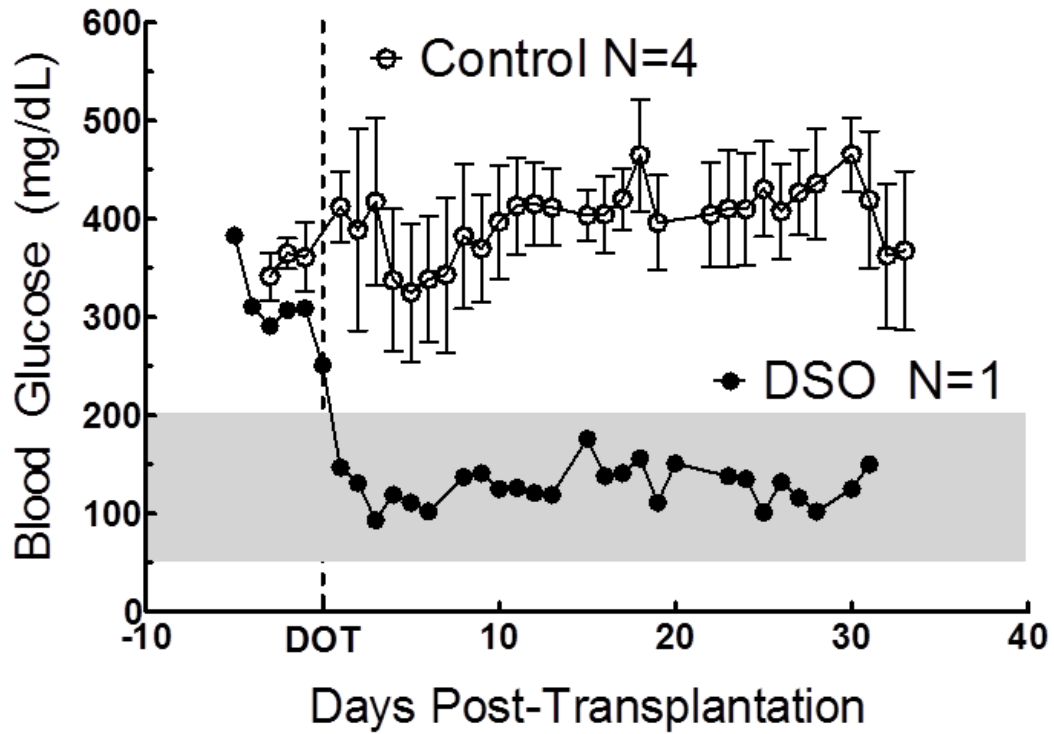


**Figure 8.8: Blood glucose measurements of rats with TEGs (+/-) DSO.** Blood glucose (BG) measurements from the rat implanted with a TEG containing 25,000±1000 porcine islet equivalents modified for DSO demonstrating diabetes reversal, and graft function for up to 30 days. In contrast, rats implanted with control TEGs (no DSO) never achieved diabetes reversal, and remained hyperglycemic for the duration of the study.

## ***Discussion***

Macro-encapsulation of an islet (or  $\beta$ -cell) graft for immune protection has been extensively investigated over the past two decades with limited success<sup>39,186,189,225–228</sup>. Macro-encapsulation solutions to create a TEG as a possible “bio-artificial pancreas” offer the promise of reducing the need for potent and harmful immunosuppressive drugs, and provide a contained vessel to investigate the use of alternative  $\beta$ -cell sources such as porcine islets, or stem-cell-derived islets. However, the success of TEGs in small animals has not translated to large-animal systems due to the large doses of functional tissue needed for effective therapy. When small-animal approaches are scaled-up to accommodate the large tissue doses needed for treatment in large-animals, a very high islet density is needed to maintain a reasonably sized implant. With these high islet densities, oxygen limitations within the TEG create a stressful hypoxic environment that decreases overall graft viability, and limits proper islet function<sup>59,60,130,192,243–246,256,291</sup>.

Recent efforts focused on improving graft oxygenation have demonstrated promising results by frequent injection of oxygen directly into the TEG device<sup>226,227,259–266</sup>. We are investigating a similar approach by developing an implantable system for continuous delivery of supplemental oxygen (DSO) to an immunoisolating TEG. The approach presented herein describes a novel proof-of-concept method for continuous DSO using an electrochemical oxygen generator to deliver oxygen-rich gas to a central compartment of a modified TheraCyte device. For these studies, we use non-invasive <sup>19</sup>F-MRS methods to examine the changes in the average internal pO<sub>2</sub> of TEGs receiving DSO *in vitro* and *in vivo*, and briefly investigated the therapeutic function of high-islet-density TEGs with DSO in diabetic nude rats.

The first objective was to determine if the novel DSO methods could significantly increase the local oxygen concentration inside a modified TEG device *in vitro*. **Figure 8.6** is reproduced from **Figure 7.11** shows the representative oxygen measurements from a series of 5 studies, and they

clearly show that despite the surrounding hypoxic environment, DSO can achieve significantly elevated  $pO_2$  within a TEG device. A perfusion bioreactor was used to maintain physiologic temperature and to provide a controlled external environment that would simulate the hypoxic environment observed in earlier *in vivo* implant studies described in the previous section. The  $pO_2$  and temperature of the perfusion medium inside the bioreactor was continuously monitored using MRS compatible temperature and oxygen sensors to ensure controlled conditions were maintained throughout the study.  $^{19}F$ -MRS methods previously developed in our lab <sup>182</sup> and described in **Chapter 7** were used to measure the average  $pO_2$  within TEG devices non-invasively during a series of changing internal and external oxygen conditions. The studies began by measuring the starting  $pO_2$  within the TEG before any controlled conditions were initiated. The observed average  $pO_2$  initially began at  $123 \pm 19$  mmHg, which was only slightly different from the ambient humidified atmospheric  $pO_2$  (152 mmHg). The deviation from the atmospheric level is explained primarily by the variability in starting temperature (36.7-42.8 °C), which was difficult to regulate before perfusion was started. When the perfusion circuit was started, deoxygenated culture medium was continuously circulated to maintain a constant hypoxic external condition (average measured  $pO_2 = 34 \pm 6$  mmHg) for the TEG inside the bioreactor. The internal  $pO_2$  of the TEG shown in **Figure 8.6** was observed to acclimate to the surrounding perfusion medium within the first hour following initiation of perfusion, and an average steady state  $pO_2$  of  $38 \pm 3$  mmHg was observed prior to beginning DSO.

DSO was tested at two different oxygen concentrations (50% or 380 mmHg, and 100% or 760 mmHg), and the  $pO_2$  time-series of the delivered gas is also presented in **Figure 8.6**. The initial  $pO_2$  tested for DSO was 380 mmHg, and the measured internal  $pO_2$  of TEGs rose quickly to an average of  $207 \pm 22$  mmHg. The  $pO_2$  of DSO was then switched to 760 mmHg, and the internal  $pO_2$  again quickly rose up to an average of  $469 \pm 40$  mmHg. The kinetic and steady state oxygen

concentrations measured inside the TEG are governed by the basic equations of diffusion dominated mass transport, and the steady-state solution for this simple geometry is a linear  $pO_2$  gradient within each segment of the TEG device. The perfusion bioreactor maintained a constant external  $pO_2$  and continuous DSO maintained a constant internal  $pO_2$ , and therefore, the gradient within each cell-compartment is predicted to be linear between these two controlled conditions. For the purpose of this analysis, the gradients within the membranes themselves are considered negligible because the diffusional distances are very small compared to the thickness of the loaded cell compartment. Under this assumption, the average  $pO_2$  of this linear gradient across the thickness of the cell-compartment is simply the average value between the internal and external  $pO_2$  for this case. The predicted internal  $pO_2$  of *in vitro* TEGs would be 207 and 396 mmHg for DSO with 50% and 100% oxygen respectively. The  $^{19}F$ -MRS technique measures the average “bulk” oxygen concentration of the PFCE-loaded fibrin-matrix that is contained inside the cell compartments of the TEG device modified for DSO. The measured results agree strongly with the expected values, but the measured oxygen with DSO of 760 mmHg was 76 mmHg higher than the expected value. This difference is likely due to the thicker external membrane on the outside of the device causing an increased diffusional barrier resulting in higher internal oxygen concentrations within the device. This difference is more apparent with steeper oxygen gradients during DSO with 760 mmHg. These results confirmed that continuous DSO could successfully increase the internal  $pO_2$  of TEG devices despite a hypoxic external environment, and that the immunoisolation membranes do not present a significant diffusional barrier to oxygen delivery from within the device. The internal  $pO_2$  can also be controlled and adjusted to optimal levels by manipulating the oxygen concentration of the DSO gas. The success of these initial *in vitro* tests encouraged further testing and development of the continuous DSO system *in vivo*.

The DSO system was further examined with a series of implant studies to investigate the oxygenation of control TEGs without islets, and functional TEGs with high densities of porcine islets. The average internal  $pO_2$  of TEG devices implanted in non-diabetic Lewis rats was measured at critical time-points for a 29 day period to observe the efficiency of oxygenation with DSO, and to track any changes during the healing and remodeling processes. **Figure 7.13** from **Chapter 7** from the previous section shows the average internal  $pO_2$  of implanted control TEG devices the day after implantation with and without DSO. The oxygen measurements of implants without DSO from previous studies are included with permission in the figure to provide context for the average ambient oxygen concentrations within TEGs without DSO. TEGs with DSO achieved significantly elevated  $pO_2$  levels compared to implants without DSO after one day *in vivo*, and TEGs with DSO containing porcine islets had significantly lower  $pO_2$  levels than control implants without porcine islets. The TEGs containing porcine islets were expected to have a lower oxygen concentration when compared to controls because the presence of highly-metabolic islets will consume oxygen in the cell compartment resulting in a lower average concentration. DSO was stopped for at least 24 hours for a small group of animals implanted with control TEGs (N=3), and the measured internal  $pO_2$  levels returned to hypoxic levels that were not significantly different than implants without DSO. The observed return to hypoxic  $pO_2$  levels suggest that continuous DSO may be needed to sustain sufficient oxygenation.

The internal  $pO_2$  levels of implanted TEGs with DSO were measured at various time points for up to 29 days. The time-course of oxygen levels for control and porcine islet loaded TEGs with DSO are presented in **Figure 8.7** along with measurements from control TEGs without DSO reproduced with permission from previous section. The internal  $pO_2$  for both control and porcine islet loaded TEGs began at highly elevated levels one day after implantation, and then gradually decreased to an apparent steady-state internal  $pO_2$  over the next 29 days. It is clear that



continuous DSO can achieve significantly elevated oxygen levels for up to 29 days *in vivo* for both control and porcine islet loaded TEGs. The lowest average oxygen level observed for TEGs with DSO was  $124\pm 35$  mmHg after 29 days *in vivo*, which is higher than the minimum reported value of 60 mmHg needed to maintain islet viability and function without a necrotic core<sup>157</sup>. TEGs loaded with porcine islets had significantly lower internal  $pO_2$  levels than control TEGs, and these implants had higher variability in the measured internal oxygenation as well (indicated by the larger error-bars for mean values). Porcine islet tissue consumes oxygen within the cell compartments of loaded TEGs and results in lower average internal  $pO_2$  levels. The islet loading procedure and differences between individual islet preparations likely result in the increase variability of  $pO_2$  levels observed in these implants. Non-invasive oxygen measurements using  $^{19}F$ -MRS may provide a means for individual graft assessment. In a future clinical setting, these measurements could be used to specifically optimize the DSO system for each individual TEG to ensure adequate oxygenation despite intrinsic graft variability.

It is also apparent that the measured  $pO_2$  levels in control TEGs after one day *in vivo* were much higher than the expected values predicted and observed during *in vitro* studies, with  $556\pm 18$  mmHg observed compared to the expected 396 mmHg. Control TEGs without islets *in vivo* were expected to have a similar average internal  $pO_2$  as the TEGs tested in the bioreactor because the steady-state oxygen concentration is still determined by the same diffusion-dominated transport. This observed difference on the first day following surgery is likely due to transiently increased external  $pO_2$  following implantation of the TEG. The external  $pO_2$  in the bioreactor was controlled at a constant hypoxic level by continuously circulating deoxygenated perfusion medium around the implant. By controlling the external  $pO_2$  within the bioreactor, the oxygen gradient within the TEG was able to quickly reach a steady state with a predictable average  $pO_2$ . The controlled environment within the bioreactor is not reflective of the highly variable and

changing environment surrounding the TEG during the healing and remodeling process following surgical implantation. Immediately following implantation, the TEG would be surrounded by surgical fluid, and the surrounding tissue would be kept at a distance until the fluid is absorbed. This condition increases the diffusional distance, so that the  $pO_2$  gradient extends from the highest level at the inside of the TEG until it reaches the lowest point in the surrounding tissue. Extending the gradient across a greater distance would result in a smaller gradient within the TEG, and a higher average  $pO_2$  within the cell compartment. This increased diffusional distance could explain the higher oxygen levels on the first day following implantation of the TEG. As the healing process begins at the implant site and the surrounding tissues starts to remodel and grow closer to the implant surface. The gradient distances gets shorter, and the gradient gets steeper resulting in a lower average  $pO_2$  within the cell compartment until the tissue has adhered very closely to the surface of the TEG. As the tissue grows closer to the TEG, and vasculature begins to form on the surface of the vascularizing membrane, the system approaches an equilibrium condition that is similar to the bioreactor case where the external  $pO_2$  remains constant. The observed changes in  $pO_2$  are consistent with the progression and timing of the healing process<sup>189,267-269,292</sup>.

The average  $pO_2$  within the cell compartments of control TEGs with DSO approached an apparent steady-state of  $288 \pm 31$  mmHg during the 29 day period studied. Interestingly, this value is much lower than the expected value for DSO with 100% oxygen (396 mmHg). The EOG system generates 100% oxygen (760 mmHg), but oxygen was lost within the manifold, tubing, and tether system so that the  $pO_2$  of the gas entering the device was measured at  $652 \pm 8$  mmHg. Even if this lower DSO  $pO_2$  is taken into account, the expected steady state  $pO_2$  would be 342 mmHg, which is still 54 mmHg higher than the observed value. For all of the previous estimates of average internal  $pO_2$ , the oxygen gradients within the immunoisolation membranes themselves

were ignored because the permeability of the membranes is relatively high<sup>188,190,253,293</sup>, and the membranes are much thinner than the material within the cell compartments. The permeability of the immunoisolation membranes within the TEG have been shown to change over-time *in vivo*<sup>188,190,293</sup>, and this may have significant effects on the transport of oxygen within the device itself. It is also observed that the internal pO<sub>2</sub> levels of TEGs that contain porcine islets are on average 186±23 mmHg lower than the levels observed in control TEGs at every time-point studied. A significant difference between conditions is expected due to the oxygen consumption of the islets within the cell compartments of the devices, but more complex models that consider the diffusion and reaction effects are required to estimate the magnitude of this difference. This estimation is also made increasingly complex when considering the progression of immunological responses and potential proliferation or degeneration of cells within the device. Many others have examined such models by employing finite-element techniques and then investigating a series of assumed conditions to help determine the functional and practical limits of tissue engineered systems<sup>157,248–251,294</sup>. Complex analyses of these models, and consideration of material and physiological kinetics are beyond the scope of the discussion here, but acknowledgement of these complex interactions highlight the importance and value of direct oxygen measurements. Direct experimental observations of TEG oxygenation by <sup>19</sup>F-MRS can provide valuable information for refining predictive models, improving TEG design, and optimizing DSO specifications. Furthermore, with continued development, these techniques may offer a non-invasive method for periodic observation for individual clinically implanted therapeutic TEG devices.

TEG devices with DSO used for <sup>19</sup>F-MRS oxygen studies were explanted at the end of the study period (29 days), and processed for histology to examine the adherent tissue surrounding the devices. Furthermore, a small set of TEGs were implanted in diabetic nude rats to examine the functional effects of DSO on the encapsulated islet grafts. Only minor differences were observed

in the tissue surrounding the explanted devices from Lewis rats. The adherent tissue surrounding all of TEGs studied were moderately well vascularized after 29 days but TEGs with DSO had slightly less vascularization than previously studied TEGs without DSO. Slightly higher levels of foreign body reaction were also observed in the tissue surrounding TEGs with DSO, but only mild-moderate levels were present in any of the explanted devices. There were no differences observed between control TEGs and TEGs that contained porcine islets, and all TEGs exhibited only mild-moderate levels of fibrosis. Despite the positive histopathology of the tissue surrounding the explanted TEG devices, assessment of the internal cell compartments showed that only scattered fragments of islet tissue remained after 29 days in Lewis rats. Previous reports concluded that the Theracyte device alone was unable to protect a xenogeneic graft against rejection <sup>269</sup>, and the histology, and porcine C-peptide results reported herein agree with these earlier findings. Increasing the average internal pO<sub>2</sub> by incorporating a system for DSO successfully alleviated the hypoxic condition within the TEG as confirmed by <sup>19</sup>F-MRS measurements, but this did not appear to improve the immunoprotective capability of the encapsulation system. Measurements of porcine C-peptide in serum samples from these rats suggest that grafts were no longer functional after 4 days, and this is typical of the rejection observed in previous xenogeneic islet transplant studies <sup>269</sup>. Histology also confirmed that very few islets remained within the cell compartment despite DSO; however, there were some surviving islets. These findings present a notable difference compared to TEGs without DSO from previous studies that had no detectible islet tissue remaining after 29 days.

The <sup>19</sup>F-MRS measurements suggest that DSO improves oxygenation within TEG devices *in vivo*, but xenogeneic grafts were not functional for more than 4 days in immunocompetent Lewis rats. The results from these studies in non-diabetic Lewis rats prompted preliminary investigations with a small set of diabetic nude rats, to eliminate the effects of xenogeneic rejection and test the

functional capacity of TEGs with DSO. For these early feasibility studies, 5 diabetic Lewis rats were implanted with TEG devices and one were modified for DSO. The TEGs were loaded with  $25,000 \pm 1000$  porcine IE, and graft function was evaluated by testing BG levels for up to 30 days. The TEGs were also explanted after 30 days and examined by immunohistochemistry to evaluate the contents of the cell compartments. The BG measurements presented in **Figure 8.8** show that a TEG with DSO was able to reverse diabetes and achieve glucose control for up to 30 days while TEGs without DSO were not. The TEG with DSO was successfully able to regulate BG levels for up to 30 days.  $^{19}\text{F}$ -MRS measurements showed that the internal compartments of implanted TEG devices returned to hypoxic conditions within one day after stopping DSO, and prolonged hypoxia (>24 hours) has been shown to inhibit islet graft function, and cause irreversible damage to isolated islets<sup>59,60,130,192,243–246,256,291</sup>. These findings are consistent with the observations in diabetic nude rats that demonstrate prolonged graft survival with DSO, and subsequent graft failure when DSO was discontinued. More studies are needed to study the functional effects of DSO in allogeneic islet transplant models, but observations from this preliminary investigation with diabetic nude animals suggest that continuous DSO may alleviate hypoxic stresses and enable long-term survival of encapsulated islet grafts loaded with a therapeutic dose of islets.

## ***Conclusions***

In summary, continuous DSO can improve oxygenation of macro-encapsulated islet TEGs to promote long-term graft survival *in vivo*, and this approach could be used to create a functional and feasible BAP device for the treatment of diabetes. Non-invasive oxygen measurements using <sup>19</sup>F-MRS confirm that continuous DSO can regulate and increase internal oxygen concentrations within implanted TEG devices, and this enables immunoisolation of therapeutic doses of islets within a practically-sized macro-encapsulation device. Although studies in Lewis rats confirmed that this model could not sufficiently prevent xenograft rejection, a feasibility study in diabetic nude rats demonstrated that continuous DSO might enable long-term survival of TEG devices loaded with therapeutically relevant doses of islets. It is clear that <sup>19</sup>F-MRS is a valuable tool for the continued development, and potentially for non-invasive monitoring and real-time optimization of implanted tissue engineered devices. These promising results suggest that this approach for non-invasive monitoring, and continuous DSO to an encapsulation device is a critical first step toward the development of a functional BAP for the treatment of diabetes.

## Chapter 9 CONCLUSIONS AND FUTURE DIRECTIONS

Islet transplantation offers real promise as a cure for type 1 diabetes, and further development defining alternative  $\beta$ -cell sources, improving islet isolation processing, and overcoming immune barriers will expand access to this therapy in the future. The work presented herein describes developments for monitoring and improving the quality of organs, tissues and cells.

### **Development of assessment technologies and techniques for improving organ procurement and preservation.**

The first section includes three chapters describing unique approaches for evaluating the quality of organs, improving the organ procurement process, and improving the preservation of organs following procurement. First, in **Chapter 2**, a novel quantitative method using whole organ oxygen consumption rate (WOOOCR) measurements was presented for organ quality assessment, which could provide a reliable method for qualifying organs prior to transplantation, and could be applied to expand the availability of marginal organs for solid organ transplantation or islet isolation. This technique could also be used as a research tool for evaluating organ preservation methods, and guide improvements in this field. This technique was shown to reliably quantify the viability of porcine kidneys and pancreata during hypothermic machine perfusion, and minor adaptations could extend the application to other organs such as heart, liver, or lungs. This technique also holds promise for incorporation with comprehensive clinical organ preservation systems (such as clinical HMP devices) for the in-line and real time viability assessment of organs for transplantation<sup>10,11</sup>. In **Chapter 3**, a study examining techniques for improving organ cooling during the procurement procedure is presented. These studies aimed to improve the procurement of pancreata from porcine donors as an alternative source of islets for possible xenogeneic transplantation. A related study of the anatomic variability of porcine pancreata is

included in **Appendix A**, and in **Chapter 3** the anatomic information was used to evaluate various techniques to ensure optimal pancreas cooling during procurement from a porcine donation after cardiac death model. A combined cooling approach was devised that used surface cooling in conjunction with arterial flushing and a ductal infusion to minimize warm ischemia time and improve blood clearance. These methods could be used to improve the quality of organs procured from porcine or human donors specifically in the case of donation after cardiac death. Next in **Chapter 4**, hypothermic machine perfusion (HMP) was shown to improve organ quality and extend preservation time when compared to cold storage techniques. HMP was studied by paired comparison against static cold storage in a model for extended preservation time using split-lobe porcine pancreata. HMP was shown to improve the viability and quality of isolated porcine islets when pancreatic lobes were preserved for 24 hours. A related study included in **Appendix B** describes a novel method for gaseous oxygen perfusion (persufflation, PSF) PSF for extending preservation of both human and porcine pancreata. This technique was shown to improve pancreatic ATP levels<sup>271</sup>, as well as improve isolated islet viability, histology, and morphology when compared to static cold storage methods<sup>270</sup>. These advanced preservation techniques could be applied to extend preservation time of pancreata procured for islet isolation, and may improve the quality of islets isolated from preserved pancreata. The developed PSF technique is currently being investigated for this purpose in a clinical setting in our lab.

#### **Development of assessment technologies and techniques for improving islet isolation, culture and shipment**

The second section focuses on technologies for improving islet and cell culture process. The islet isolation process has many steps and each step offers an opportunity for improvement. **Chapter 5** describes the use of HMP and advanced silicon rubber membrane (SRM) devices for improving the isolation and culture of juvenile porcine islets. Juvenile porcine islets offer many logistical



benefits compared to adult porcine islets, but isolation and culture of these fragile islets has historically proven challenging. By utilizing advanced organ preservation techniques, HMP, and an advanced culture system with SRM have shown to improve isolation outcomes, and islet recovery in culture. With further development, this approach could provide a reliable source of islets from juvenile porcine donors, and may offer a valuable option for an alternative islet source needed for the eventual success of xenotransplantation. **Chapter 6** presented advanced culture techniques for improving the reliable expansion of pancreatic  $\beta$ -cells. This method uses continuous nutrient regulation scheme with stirred suspension bioreactors that can successfully regulate glucose levels during the culture of renewable  $\beta$ -cells. These methods were shown to significantly improve cell-yield during culture, and could be adapted for the expansion of renewable  $\beta$ -cell lines or stem cell derived islets for therapeutic applications.

Enzyme delivery or pancreas “distension” is the first step of the isolation protocol, and in **Appendix C**, supplementary investigations for improving enzyme distribution by evaluating infusion techniques using contrast-enhanced magnetic resonance imaging (MRI) are presented. The ductal anatomy of porcine pancreata presented in **Appendix A** suggested the possibility for improving the distension process, and MRI was used to evaluate three different techniques enzyme administration in porcine pancreata. MRI imaging of these three techniques confirmed that the standard approach for enzyme delivery is incapable of delivering enzyme consistently and uniformly to all pancreatic regions given the large variability in porcine ductal anatomy. These methods could be used to make further improvements in the distension step of the isolation process, and could help identify a more robust method for uniform enzyme delivery in porcine pancreata.

The next steps in the islet isolation protocol are digestion and purification. To supplement this work, **Appendix E** describes a method for combining these steps by using eliminating the density

gradient purification step in favor of using a quadrupole magnetic separation (QMS) method for continuous purification of digested pancreatic tissue. This method employs the use of iron oxide particles<sup>295</sup> and a specially developed magnetic separator to continuously-separate isolated islets during the collection phase of digestion. This method decreases isolated islet exposure to the toxic environment following digestion, and decreases the overall duration of the isolation procedure. Porcine islets separated by QMS had significantly improved morphology and viability when compared to islets purified using standard techniques. QMS offers the possibility of improving the quality of isolated porcine islets, and could be adapted for use during human islet isolation to improve islet viability. Improving islet viability may decrease the amount of islets needed to reverse diabetes, and could possibly improve the graft success rates for autogeneic and single-donor allogeneic islet transplantation.

Islet isolation is an incredibly complex procedure, and only a limited number of centers have had success using this technique. The proposed model for this therapy would utilize a select number of islet isolation centers that distribute islets to numerous treatment centers for transplantation. This model requires validated methods for islet shipment, and verification of islet quality following shipment. Supplemental studies included in **Appendix D** describe the development of improved shipping techniques for maintaining temperature and pressure during islet shipment. This method was shown to allow for sufficient temperature and pressure regulation during shipments up to 24 hours under harsh environmental conditions. Using these techniques, isolated islets could be reliably shipped overnight anywhere within the US without the risk of exposure to harmful temperature or pressure fluctuations.

## **Development of assessment technologies and techniques for improving tissue-engineered islet grafts post-transplant**

The final section focuses on the development of a technique for non-invasive monitoring of tissue engineered islet grafts, and application of that technique to evaluate and improve oxygen delivery to implanted grafts. In **Chapter 7**,  $^{19}\text{F}$  magnetic resonance spectroscopy techniques were adapted for non-invasive measuring the internal oxygen concentration of implantable tissue engineered grafts (TEGs). This non-invasive method for graft assessment was developed for the purpose of investigating and optimizing alternate implant sites, as well as defining and optimizing implant parameters. The developed protocols were validated against established fiber optic oxygen probes *in vitro* using a temperature and oxygen regulating bioreactor, and *in vivo* by measuring oxygen of implanted TEGs in rats.  $^{19}\text{F}$ -MRS offers many benefits compared to traditional probes for measuring oxygen *in vivo*, and could be a valuable research tool for evaluating the oxygenation status of various designs of TEGs. This non-invasive approach could also be adapted for simultaneous use with other MRI techniques or for use with portable magnetic resonance equipment, which could provide a real-time assessment technique for clinical implanted TEGs. **Chapter 8** is the final chapter that presents original scientific research and describes the application of  $^{19}\text{F}$ -MRS techniques to determine the oxygen levels of implanted TEGs containing porcine islets. These techniques were further used to evaluate a bioartificial pancreas system that uses delivery of supplemental oxygen for improving oxygenation *in vivo*. Oxygen levels were confirmed to be severely hypoxic within implanted TEGs, and inclusion of porcine islets proved to decrease internal  $\text{pO}_2$  further. DSO was able to increase the internal  $\text{pO}_2$  of therapeutic TEGs containing a high-density of porcine islets for up to 29 days *in vivo*. These techniques could be used to optimize the design of TEG devices and improve graft survival *in vivo*. Further

developments result in a clinically relevant tool for this a non-invasive monitoring of functional implanted TEG devices for the treatment of diabetes.

In conclusion, the studies presented herein describe the development of novel techniques for evaluating and improving the oxygenation of organs, tissues, and cells for improving the treatment of diabetes with  $\beta$ -cell replacement therapies. Continued development of these described methods could contribute to the advancement of islet transplantation technologies including the development of a functional TEG device. Furthermore, these innovations will be valuable to improving treatment of diabetes and expanding access to  $\beta$ -cell replacement therapies.

## **REFERENCES**

1. International Diabetes Federation, I. *IDF Diabetes Atlas, 6th Edn.*; Brussels, Belgium, 2014.
2. Centers for Disease Control and Prevention, C. *National Diabetes Statistics Report: Estimates of Diabetes and Its Burden in the United States*; Atlanta, GA, 2014.
3. Banting, F. G.; Best, C. H.; Collip, J. B.; Campbell, W. R.; Fletcher, A. A. Pancreatic Extracts in the Treatment of Diabetes Mellitus. *Canadian Medical Association Journal* **1922**, *12*, 141–146.
4. Banting, F. G. Early Work on Insulin. *Science (New York, N.Y.)* **1937**, *85*, 594–596.
5. Bliss, M. The Discovery of Insulin. *Univ. Chicago Press* **1982**.
6. Klein, R.; Klein, B. E.; Moss, S. E.; Davis, M. D.; DeMets, D. L. Glycosylated Hemoglobin Predicts the Incidence and Progression of Diabetic Retinopathy. *JAMA : the journal of the American Medical Association* **1988**, *260*, 2864–2871.
7. *The Effect of Intensive Treatment of Diabetes on the Development and Progression of Long-Term Complications in Insulin-Dependent Diabetes Mellitus. The Diabetes Control and Complications Trial Research Group.*; 1993; vol329.
8. Sutherland, D. E. Pancreas and Islet Transplantation. II. Clinical Trials. *Diabetologia* **1981**, *20*, 435–50.
9. Shapiro, A. M.; Lakey, J. R.; Ryan, E. A.; Korbitt, G. S.; Toth, E.; Warnock, G. L.; Kneteman, N. M.; Rajotte, R. V *Islet Transplantation in Seven Patients with Type 1 Diabetes Mellitus Using a Glucocorticoid-Free Immunosuppressive Regimen.*; 2000; vol343.
10. Bunegin, L.; Tolstykh, G. P.; Gelineau, J. F.; Cosimi, a B.; Anderson, L. M. Oxygen Consumption during Oxygenated Hypothermic Perfusion as a Measure of Donor Organ Viability. *ASAIO journal (American Society for Artificial Internal Organs : 1992)* **2013**, *59*, 427–32.
11. Anderson, L. M.; Judson, J. A. Methods and Systems for Assessing the Suitability of an Organ for Transplant. US9155297 B2 **2015**.
12. Gallinat, A.; Paul, A.; Efferz, P.; Lüer, B.; Swoboda, S.; Hoyer, D.; Minor, T.; Lu, B. Role of Oxygenation in Hypothermic Machine Perfusion of Kidneys from Heart Beating Donors. *Transplantation* **2012**, *94*, 1–5.
13. Gallinat, A.; Paul, A.; Efferz, P.; Lüer, B.; Kaiser, G.; Wohlschlaeger, J.; Treckmann, J.; Minor, T. Hypothermic Reconditioning of Porcine Kidney Grafts by Short-Term Preimplantation Machine Perfusion. *Transplantation* **2012**, *93*, 787–93.
14. Cobert, M. L.; Merritt, M. E.; West, L. M.; Ayers, C.; Jessen, M. E.; Peltz, M. Metabolic Characteristics of Human Hearts Preserved for 12 Hours by Static Storage, Antegrade Perfusion, or Retrograde Coronary Sinus Perfusion. *Journal of Thoracic and Cardiovascular Surgery* **2014**, *148*, 2310–2315.e1.
15. Knoll, G. Trends in Kidney Transplantation over the Past Decade. *Drugs* **2008**, *68*, 3–10.
16. Reznik, O. N.; Bagnenko, S. F.; Loginov, I. V.; Iljina, V. a.; Ananyev, a. N.; Eremich, S. V.; Moysyuk, Y. G. Machine Perfusion as a Tool to Select Kidneys Recovered From Uncontrolled Donors After Cardiac Death. *Transplantation Proceedings* **2008**, *40*, 1023–

1026.

17. Snoeijs, M. G. J.; Buurman, W. a.; Christiaans, M. H. L.; Hooff, J. P. Van; Goldschmeding, R.; Suylen, R. J. Van; Peutz-Kootstra, C. J.; Heurn, L. W. E. Van Histological Assessment of Preimplantation Biopsies May Improve Selection of Kidneys from Old Donors after Cardiac Death. *American Journal of Transplantation* **2008**, *8*, 1844–1851.
18. Kim, J.; Seok, Y. M.; Jung, K.; Park, K. M.; Kim, J.; Ym, S.; K-j, J.; Km, P. Reactive Oxygen Species / Oxidative Stress Contributes to Progression of Kidney Fibrosis Following Transient Ischemic Injury in Mice. **2009**, 461–470.
19. Dutkowski, P.; Furrer, K.; Tian, Y.; Graf, R.; Clavien, P.-A. Novel Short-Term Hypothermic Oxygenated Perfusion (HOPE) System Prevents Injury in Rat Liver Graft from Non-Heart Beating Donor. *Annals of surgery* **2006**, *244*, 968–976; discussion 976–977.
20. Papas, K. K.; Hering, B. J.; Gunther, L.; Rappel, M. J.; Colton, C. K.; Avgoustiniatos, E. S. Pancreas oxygenation is limited during preservation with the two-layer method. In *Transplantation Proceedings*; 2005; vol37, pp. 3501–3504.
21. Stowe, D. F.; Camara, a. K. S.; Heisner, J. S.; Aldakkak, M.; Harder, D. R. Low-Flow Perfusion of Guinea Pig Isolated Hearts With 26??C Air-Saturated Lifer Solution for 20 Hours Preserves Function and Metabolism. *Journal of Heart and Lung Transplantation* **2008**, *27*, 1008–1015.
22. Levy, M. N. Oxygen Consumption and Blood Flow in the Hypothermic, Perfused Kidney. *The American journal of physiology* **1959**, *197*, 1111–1114.
23. Stubenitsky, B. M.; Booster, M. M.; Brasile, L.; Green, E. M.; Haisch, C. E.; Singh, H. K.; Jacobs, R. W.; Kootstra, G. II: Ex Vivo Viability Testing of Kidneys after Postmortem Warm Ischemia. *ASAIO journal (American Society for Artificial Internal Organs : 1992)* **2015**, *46*, 62–64.
24. Crane, N. J.; Pinto, P. a; Hale, D.; Gage, F. a; Tadaki, D.; Kirk, A. D.; Levin, I. W.; Elster, E. a Non-Invasive Monitoring of Tissue Oxygenation during Laparoscopic Donor Nephrectomy. *BMC surgery* **2008**, *8*, 8.
25. Papas, K. K.; Pisania, A.; Wu, H.; Weir, G. C.; Colton, C. K. A Stirred Microchamber for Oxygen Consumption Rate Measurements with Pancreatic Islets. *Biotechnology and bioengineering* **2007**, *98*, 1071–1082, PMID: PMC2859188.
26. Papas, K. K.; Colton, C. K.; Nelson, R. A.; Rozak, P. R.; Avgoustiniatos, E. S.; Scott, W. E.; Wildey, G. M.; Pisania, A.; Weir, G. C.; Hering, B. J. Human Islet Oxygen Consumption Rate and DNA Measurements Predict Diabetes Reversal in Nude Mice. *American Journal of Transplantation* **2007**, *7*, 707–713, PMID: PMC2857994.
27. Papas, K. K.; Suszynski, T. M.; Colton, C. K. Islet Assessment for Transplantation. *Current opinion in organ transplantation* **2009**, *14*, 674–682.
28. Taylor, M. J.; Baicu, S. C. Current State of Hypothermic Machine Perfusion Preservation of Organs: The Clinical Perspective. *Cryobiology* **2010**, *60*, S20–35.
29. Treckmann, J.; Nagelschmidt, M.; Minor, T.; Saner, F.; Saad, S.; Paul, A. Function and Quality of Kidneys after Cold Storage, Machine Perfusion, or Retrograde Oxygen Persufflation: Results from a Porcine Autotransplantation Model. *Cryobiology* **2009**, *59*, 19–23.

30. Weegman, B. P.; Kirchner, V. A.; Scott, W. E.; Avgoustiniatos, E. S.; Suszynski, T. M.; Ferrer-Fabrega, J.; Rizzari, M. D.; Kidder, L. S.; Kandaswamy, R.; Sutherland, D. E. R.; Papas, K. K. Continuous real-time viability assessment of kidneys based on oxygen consumption. In *Transplantation Proceedings*; Elsevier Inc., 2010; vol42, pp. 2020–2023.
31. Weegman, B. P.; Suszynski, T. M.; Scott, W. E.; Ferrer Fábrega, J.; Avgoustiniatos, E. S.; Anazawa, T.; O'Brien, T. D.; Rizzari, M. D.; Karatzas, T.; Jie, T.; Sutherland, D. E. R.; Hering, B. J.; Papas, K. K. Temperature Profiles of Different Cooling Methods in Porcine Pancreas Procurement. *Xenotransplantation* **2014**, *21*, 574–81, PMID: PMC2947552.
32. Shapiro, A. Strategies Towards Single-Donor Islets of Langerhans Transplantation. *Current opinion in organ transplantation* **2011**, *16*, 627–631.
33. Hering, B. J.; Wijkstrom, M.; Graham, M. L.; Hårdstedt, M.; Aasheim, T. C.; Jie, T.; Ansite, J. D.; Nakano, M.; Cheng, J.; Li, W.; Moran, K.; Christians, U.; Finnegan, C.; Mills, C. D.; Sutherland, D. E.; Bansal-Pakala, P.; Murtaugh, M. P.; Kirchoff, N.; Schuurman, H.-J. Prolonged Diabetes Reversal after Intraportal Xenotransplantation of Wild-Type Porcine Islets in Immunosuppressed Nonhuman Primates. *Nature medicine* **2006**, *12*, 301–303.
34. Cardona, K.; Korbitt, G. S.; Milas, Z.; Lyon, J.; Cano, J.; Jiang, W.; Bello-Laborn, H.; Hacquoil, B.; Strobert, E.; Gangappa, S.; Weber, C. J.; Pearson, T. C.; Rajotte, R. V.; Larsen, C. P. Long-Term Survival of Neonatal Porcine Islets in Nonhuman Primates by Targeting Costimulation Pathways. *Nature medicine* **2006**, *12*, 304–6.
35. Thompson, P.; Badell, I. R.; Lowe, M.; Turner, a; Cano, J.; Avila, J.; Azimzadeh, a; Cheng, X.; Pierson, R. N.; Johnson, B.; Robertson, J.; Song, M.; Leopardi, F.; Strobert, E.; Korbitt, G.; Rayat, G.; Rajotte, R.; Larsen, C. P.; Kirk, a D. Alternative Immunomodulatory Strategies for Xenotransplantation: CD40/154 Pathway-Sparing Regimens Promote Xenograft Survival. *American journal of transplantation: official journal of the American Society of Transplantation and the American Society of Transplant Surgeons* **2012**, *12*, 1765–75.
36. Nano, R.; Clissi, B.; Melzi, R.; Calori, G.; Maffi, P.; Antonioli, B.; Marzorati, S.; Aldrighetti, L.; Freschi, M.; Grochowicki, T.; Socci, C.; Secchi, a; Carlo, V. Di; Bonifacio, E.; Bertuzzi, F. Islet Isolation for Allograft Transplantation: Variables Associated with Successful Islet Yield and Graft Function. *Diabetologia* **2005**, *48*, 906–12.
37. Ridgway, D.; Manas, D.; Shaw, J.; White, S. Preservation of the Donor Pancreas for Whole Pancreas and Islet Transplantation. *Clinical transplantation* **2010**, *24*, 1–19.
38. Ferrer, J.; Scott, W. E.; Weegman, B. P.; Suszynski, T. M.; Sutherland, D. E. R.; Hering, B. J.; Papas, K. K. Pig Pancreas Anatomy: Implications for Pancreas Procurement, Preservation, and Islet Isolation. *Transplantation* **2008**, *86*, 1503–1510, PMID: PMC2704055.
39. Grundfest-Broniatowski, S. F.; Tellioglu, G.; Rosenthal, K. S.; Kang, J.; Erdodi, G.; Yalcin, B.; Cakmak, M.; Drazba, J.; Bennett, A.; Lu, L.; Kennedy, J. P. A New Bioartificial Pancreas Utilizing Amphiphilic Membranes for the Immunoisolation of Porcine Islets: A Pilot Study in the Canine. *ASAIO journal (American Society for Artificial Internal Organs : 1992)* **2009**, *55*, 400–5.
40. Denecke, C.; Yuan, X.; Ge, X.; Kim, I. K.; Bedi, D.; Boenisch, O.; Weiland, A.; Jurisch, A.; Kotsch, K.; Pratschke, J.; Reutzel-Selke, A.; Tullius, S. G. Synergistic Effects of Prolonged Warm Ischemia and Donor Age on the Immune Response Following Donation

- after Cardiac Death Kidney Transplantation. *Surgery* **2013**, *153*, 249–61.
41. Lakey, J. R. T.; Kneteman, N. M.; Rajotte, R. V.; Wu, D. C.; Bigam, D.; Shapiro, a M. J. Effect of Core Pancreas Temperature during Cadaveric Procurement on Human Islet Isolation and Functional Viability. *Transplantation* **2002**, *73*, 1106–10.
  42. Tanioka, Y.; Hering, B. J.; Sutherland, D. E.; Kronson, J. W.; Kuroda, Y.; Gilmore, T. R.; Aasheim, T. C.; Rusten, M. C.; Leone, J. P. Effect of Pancreatic Warm Ischemia on Islet Yield and Viability in Dogs. *Transplantation* **1997**, *64*, 1637–41.
  43. Kaddis, J. S.; Danobeitia, J. S.; Niland, J. C.; Stiller, T.; Fernandez, L. a Multicenter Analysis of Novel and Established Variables Associated with Successful Human Islet Isolation Outcomes. *American journal of transplantation : official journal of the American Society of Transplantation and the American Society of Transplant Surgeons* **2010**, *10*, 646–56.
  44. Taylor, M. J.; Baicu, S.; Greene, E.; Vazquez, A.; Brassil, J. Islet Isolation from Juvenile Porcine Pancreas after 24-H Hypothermic Machine Perfusion Preservation. *Cell transplantation* **2010**, *19*, 613–628.
  45. Taylor, M. J.; Baicu, S.; Leman, B.; Greene, E.; Vazquez, A.; Brassil, J. Twenty-Four Hour Hypothermic Machine Perfusion Preservation of Porcine Pancreas Facilitates Processing for Islet Isolation. *Transplantation proceedings* **2008**, *40*, 480–482.
  46. Liu, X.; Matsumoto, S.; Okitsu, T.; Iwanaga, Y.; Noguchi, H.; Yonekawa, Y.; Nagata, H.; Kamiya, H.; Ueda, M.; Hatanaka, N.; Miyakawa, S.; Kobayashi, N.; Song, C. Analysis of Donor- and Isolation-Related Variables From Non-Heart-Beating Donors (NHBDs) Using the Kyoto Islet Isolation Method. *Cell Transplantation* **2008**, *17*, 649–656.
  47. Wright, M. J.; Cavanagh, T. J.; Fetterhoff, T. J.; Wile, K. J. Effect of Blood Content on Porcine Pancreatic Dissociation and Islet Yield. *Transplantation proceedings* **1994**, *26*, 3442.
  48. Matsumoto, S.; Noguichi, H.; Shimoda, M.; Ikemoto, T.; Naziruddin, B.; Jackson, A.; Tamura, Y.; Olson, G.; Fujita, Y.; Chujo, D.; Takita, M.; Kobayashi, N.; Onaca, N.; Levy, M. Seven Consecutive Successful Clinical Islet Isolations with Pancreatic Ductal Injection. *Cell transplantation* **2010**, *19*, 291–7.
  49. Nakanishi, W.; Imura, T.; Inagaki, A.; Nakamura, Y.; Sekiguchi, S.; Fujimori, K.; Satomi, S.; Goto, M. Ductal Injection Does Not Increase the Islet Yield or Function after Cold Storage in a Vascular Perfusion Model. *PloS one* **2012**, *7*, e42319.
  50. Anazawa, T.; Balamurugan, a N.; Papas, K. K.; Avgoustiniatos, E. S.; Ferrer, J.; Matsumoto, S.; Sutherland, D. E. R.; Hering, B. J. Improved Method of Porcine Pancreas Procurement with Arterial Flush and Ductal Injection Enhances Islet Isolation Outcome. *Transplantation proceedings* **2010**, *42*, 2032–5.
  51. Noguchi, H.; Ueda, M.; Hayashi, S.; Kobayashi, N.; Okitsu, T.; Iwanaga, Y.; Nagata, H.; Nakai, Y.; Matsumoto, S. Ductal Injection of Preservation Solution Increases Islet Yields in Islet Isolation and Improves Islet Graft Function. *Cell transplantation* **2008**, *17*, 69–81.
  52. Alejandro, R.; Barton, F. B.; Hering, B. J.; Wease, S. 2008 Update from the Collaborative Islet Transplant Registry. *Transplantation* **2008**, *86*, 1783–1788.
  53. Shapiro, A. M. J.; Ricordi, C.; Hering, B. J.; Auchincloss, H.; Lindblad, R.; Robertson, R. P.; Secchi, A.; Brendel, M. D.; Berney, T.; Brennan, D. C.; Cagliero, E.; Alejandro, R.; Ryan, E. A.; DiMercurio, B.; Morel, P.; Polonsky, K. S.; Reems, J.; Bretzel, R. G.;



- Bertuzzi, F.; Froud, T.; Kandaswamy, R.; Sutherland, D. E. R.; Eisenbarth, G.; Segal, M.; Preiksaitis, J.; Korbitt, G. S.; Barton, F. B.; Viviano, L.; Seyfert-Margolis, V.; Bluestone, J.; Lakey, J. R. T. International Trial of the Edmonton Protocol for Islet Transplantation. *The New England journal of medicine* **2006**, *355*, 1318–1330.
54. O'Neil, J. J.; Stegemann, J. P.; Nicholson, D. T.; Gagnon, K. A.; Solomon, B. A.; Mullan, C. J. The Isolation and Function of Porcine Islets from Market Weight Pigs. *Cell transplantation* **2001**, *10*, 235–246.
  55. Belzer, F. O.; Ploeg, R. J.; Knechtle, S. J.; D'Alessandro, A. M.; Pirsch, J. D.; Kalayoglu, M. M.; Sollinger, H. W. Clinical Pancreas Preservation and Transplantation. *Transplantation proceedings* **1994**, *26*, 550–551.
  56. Carlsson, P. O.; Palm, F.; Andersson, A.; Liss, P. Chronically Decreased Oxygen Tension in Rat Pancreatic Islets Transplanted under the Kidney Capsule. *Transplantation* **2000**, *69*, 761–766.
  57. Carlsson, P. O.; Palm, F.; Andersson, A.; Liss, P. Markedly Decreased Oxygen Tension in Transplanted Rat Pancreatic Islets Irrespective of the Implantation Site. *Diabetes* **2001**, *50*, 489–495.
  58. Delmonico, F. L.; Jenkins, R. L.; Auchincloss, H.; Etienne, T. J.; Russell, P. S.; Monaco, A. B.; Cosimi, A. B. Procurement of a Whole Pancreas and Liver from the Same Cadaveric Donor. *Surgery* **1989**, *105*, 718–723.
  59. Dionne, K. E.; Colton, C. K.; Yarmush, M. L. Effect of Hypoxia on Insulin Secretion by Isolated Rat and Canine Islets of Langerhans. *Diabetes* **1993**, *42*, 12–21.
  60. Papas, K. K.; Colton, C. K.; Gounarides, J. S.; Roos, E. S.; Jarema, M. A.; Shapiro, M. J.; Cheng, L. L.; Cline, G. W.; Shulman, G. I.; Wu, H.; Bonner-Weir, S.; Weir, G. C. NMR Spectroscopy in Beta Cell Engineering and Islet Transplantation. *Annals of the New York Academy of Sciences* **2001**, *944*, 96–119.
  61. Tanioka, Y.; Sutherland, D. E. R.; Kuroda, Y.; Suzuki, Y.; Matsumoto, I.; Deai, T. Preservation of Dog Pancreas before Islet Isolation with the Two-Layer Method. *Transplantation Proceedings* **1998**, *30*, 3419–3420.
  62. Benhamou, P. Y.; Watt, P. C.; Mullen, Y.; Ingles, S.; Watanabe, Y.; Nomura, Y.; Hober, C.; Miyamoto, M.; Kenmochi, T.; Passaro, E. P. Human Islet Isolation in 104 Consecutive Cases. Factors Affecting Isolation Success. *Transplantation* **1994**, *57*, 1804–1810.
  63. Gotoh, M.; Maki, T.; Satomi, S.; Porter, J.; Monaco, A. P. Immunological Characteristics of Purified Pancreatic Islet Grafts. *Transplantation* **1986**, *42*, 387–390.
  64. Hering, B. J.; Ricordi, C. Islet Transplantation for Patients with Type 1 Diabetes. *Graft* **1999**, *2*, 12.
  65. Ketchum, R. J.; Nicolae, M.; Jahr, H.; Friedman, A.; Naji, A.; Barker, C. F.; Brayman, K. L. Analysis of Donor Age and Cold Ischemia Time as Factors in Cadaveric Human Islet Isolation. *Transplantation proceedings* **1994**, *26*, 596–597.
  66. Lakey, J. R.; Rajotte, R. V.; Warnock, G. L.; Kneteman, N. M. Human Pancreas Preservation prior to Islet Isolation. Cold Ischemic Tolerance. *Transplantation* **1995**, *59*, 689–694.
  67. Robertson, G. S.; Chadwick, D.; Thirdborough, S.; Swift, S.; Davies, J.; James, R.; Bell, P. R.; London, N. J. Human Islet Isolation--a Prospective Randomized Comparison of

- Pancreatic Vascular Perfusion with Hyperosmolar Citrate or University of Wisconsin Solution. *Transplantation* **1993**, *56*, 550–553.
68. Ryan, E. a; Lakey, J. R.; Rajotte, R. V; Korbitt, G. S.; Kin, T.; Imes, S.; Rabinovitch, a; Elliott, J. F.; Bigam, D.; Kneteman, N. M.; Warnock, G. L.; Larsen, I.; Shapiro, a M. Clinical Outcomes and Insulin Secretion after Islet Transplantation with the Edmonton Protocol. *Diabetes* **2001**, *50*, 710–9.
  69. Taylor, M.; Baicu, S. Hypothermic perfusion of pancreas: emphasis on preservation prior to islet isolation. In *Methods in Bioengineering: Organ Preservation and Reengineering*; Uygun, K.; Lee, C. Y., Eds.; Artech House: Norwood, 2011; pp. 85–103.
  70. Clinical Islet Transplant Study *Purified Human Pancreatic Islets, In Vivo Islets Function*; A04; Iowa City, 2008.
  71. Graham, M. L.; Janecek, J. L.; Kittredge, J. A.; Hering, B. J.; Schuurman, H. The Streptozotocin-Induced Diabetic Nude Mouse Model: Differences between Animals from Different Sources. *Comparative medicine* **2011**, *61*, 356–360.
  72. Moers, C.; Smits, J. M.; Maathuis, M.-H. J.; Treckmann, J.; Gelder, F. van; Napieralski, B. P.; Kasterop-Kutz, M. van; Heide, J. J. H. van der; Squifflet, J.-P.; Heurn, E. van; Kirste, G. R.; Rahmel, A.; Leuvenink, H. G. D.; Paul, A.; Pirenne, J.; Ploeg, R. J. Machine Perfusion or Cold Storage in Deceased-Donor Kidney Transplantation. *The New England journal of medicine* **2009**, *360*, 7–19.
  73. InteLab Corporation *Report I601, Worldwide Markets and Emerging Technologies for Tissue Engineering and Regenerative Medicine*; Mission Viejo, 2013.
  74. Bonner-Weir, S.; Weir, G. C. New Sources of Pancreatic Beta-Cells. *Nature biotechnology* **2005**, *23*, 857–861.
  75. Inada, A.; Bonner-Weir, S.; Toschi, E. How Can We Get More Beta Cells? *Current Diabetes Reports* **2006**, *6*, 96–101.
  76. Hering, B. J.; Cooper, D. K. C.; Cozzi, E.; Schuurman, H.-J.; Korbitt, G. S.; Denner, J.; O’Connell, P. J.; Vanderpool, H. Y.; Pierson, R. N. The International Xenotransplantation Association Consensus Statement on Conditions for Undertaking Clinical Trials of Porcine Islet Products in Type 1 Diabetes-- Executive Summary. *Xenotransplantation* **2009**, *16*, 196–202.
  77. Finke, E.; Marchetti, P.; Falqui, L.; Swanson, C.; McLear, M.; Olack, B.; Scharp, D.; Lacy, P. Large Scale Isolation, Function, and Transplantation of Islets of Langerhans from the Adult Pig Pancreas. *Transplantation proceedings* **1991**, *23*, 772–773.
  78. Giannarelli, R.; Marchetti, P.; Villani, G.; Carlo, A. di; Cosimi, S.; Andreozzi, M.; Cruschelli, L.; Masiello, P.; Coppelli, A.; Navalesi, R. Preparation of Pure, Viable Porcine and Bovine Islets by a Simple Method. *Transplantation proceedings* **1994**, *26*, 630–631.
  79. Marchetti, P.; Finke, E. H.; Gerasimidi-Vazeou, A.; Falqui, L.; Scharp, D. W.; Lacy, P. E. Automated Large-Scale Isolation, in Vitro Function and Xenotransplantation of Porcine Islets of Langerhans. *Transplantation* **1991**, *52*, 209–213.
  80. Toso, C.; Brandhorst, D.; Oberholzer, J.; Triponez, F.; Buhler, L.; Morel, P. Isolation of Adult Porcine Islets of Langerhans. *Cell Transplant.* **2000**, *9*, 297–305.
  81. Kenmochi, T.; Miyamoto, M.; Une, S.; Nakagawa, Y.; Moldovan, S.; Navarro, R. A.; Benhamou, P. Y.; Brunicardi, F. C.; Mullen, Y. Improved Quality and Yield of Islets

- Isolated from Human Pancreata Using a Two-Step Digestion Method. *Pancreas* **2000**, *20*, 184–190.
82. Figliuzzi, M.; Zappella, S.; Morigi, M.; Rossi, P.; Marchetti, P.; Remuzzi, A. Influence of Donor Age on Bovine Pancreatic Islet Isolation. *Transplantation* **2000**, *70*, 1032–1037.
  83. Shapiro, A. M.; Hao, E.; Rajotte, R. V.; Kneteman, N. M. High Yield of Rodent Islets with Intraductal Collagenase and Stationary Digestion--a Comparison with Standard Technique. *Cell transplantation* *5*, 631–638.
  84. Ricordi, C.; Finke, E. H.; Lacy, P. E. A Method for the Mass Isolation of Islets from the Adult Pig Pancreas. *Diabetes* **1986**, *35*, 649–653.
  85. Bertera, S.; Marigliano, M.; Bottino, R.; Trucco, M. Pancreatic Islet Isolation from Swine. In *Methods in bioengineering : cell transplantation*; Soto-Gutierrez, A.; Navarro-Alvarez, N.; Fox, I. J., Eds.; Artech House: Boston, 2011; pp. 77–99.
  86. Dufrane, D.; Goebbels, R.; Fdilal, I.; Guiot, Y.; Gianello, P. Impact of Porcine Islet Size on Cellular Structure and Engraftment after Transplantation: Adult versus Young Pigs. *Pancreas* **2005**, *30*, 138–147.
  87. Bottino, R.; Balamurugan, A. N.; Smetanka, C.; Bertera, S.; He, J.; Rood, P. P. M.; Cooper, D. K. C.; Trucco, M. Isolation Outcome and Functional Characteristics of Young and Adult Pig Pancreatic Islets for Transplantation Studies. *Xenotransplantation* **2007**, *14*, 74–82.
  88. Jay, T. R.; Heald, K. A.; Carless, N. J.; Topham, D. E.; Downing, R. The Distribution of Porcine Pancreatic Beta-Cells at Ages 5, 12 and 24 Weeks. *Xenotransplantation* **1999**, *6*, 131–140.
  89. Schuurman, H.-J. The International Xenotransplantation Association Consensus Statement on Conditions for Undertaking Clinical Trials of Porcine Islet Products in Type 1 Diabetes--Chapter 2: Source Pigs. *Xenotransplantation* **2009**, *16*, 215–222.
  90. Cozzi, E.; Tallacchini, M.; Flanagan, E. B.; Pierson, R. N.; Sykes, M.; Vanderpool, H. Y. The International Xenotransplantation Association Consensus Statement on Conditions for Undertaking Clinical Trials of Porcine Islet Products in Type 1 Diabetes-Chapter 1: Key Ethical Requirements and Progress toward the Definition of an International Reg. *Xenotransplantation* **2009**, *16*, 196–202.
  91. Papas, K. K.; Avgoustiniatos, E. S.; Tempelman, L. A.; Weir, G. C.; Colton, C. K.; Pisania, A.; Rappel, M. J.; Friberg, A. S.; Bauer, A. C.; Hering, B. J. High-density culture of human islets on top of silicone rubber membranes. In *Transplantation Proceedings*; 2005; vol37, pp. 3412–3414.
  92. Campbell, L. H.; Taylor, M. J.; Brockbank, K. G. M. Development of Pancreas Storage Solutions: Initial Screening of Cytoprotective Supplements for  $\beta$ -Cell Survival and Metabolic Status after Hypothermic Storage. *Biopreservation and biobanking* **2013**, *11*, 12–18.
  93. Rozak, P. R.; Weegman, B. P.; Avgoustiniatos, E. S.; Wilson, J. R.; Welch, D. P.; Hering, B. J.; Papas, K. K. Devices and Methods for Maintenance of Temperature and Pressure during Islet Shipment. *Transplantation proceedings* **2008**, *40*, 407–410, PMID: PMC2799926.
  94. Mueller, K. R.; Balamurugan, A. N.; Cline, G. W.; Pongratz, R. L.; Hooper, R. L.; Weegman, B. P.; Kitzmann, J. P.; Taylor, M. J.; Graham, M. L.; Schuurman, H.-J.; Papas,

- K. K. Differences in Glucose-Stimulated Insulin Secretion in Vitro of Islets from Human, Nonhuman Primate, and Porcine Origin. *Xenotransplantation* **2013**, *20*, 75–81.
95. Ricordi, C.; Hering, B. J.; Londo, N. J. Islet Isolation Assessment. In *Pancreatic islet cell transplantation, 1892-1992 : One century of transplantation for diabetes*; Ricordi, C., Ed.; R.G. Landes: Austin, Texas, 1992; pp. 132–142.
  96. Papas, K. K.; Colton, C. K.; Qipo, A.; Wu, H.; Nelson, R. a; Hering, B. J.; Weir, G. C.; Koulmanda, M. Prediction of Marginal Mass Required for Successful Islet Transplantation. *Journal of investigative surgery : the official journal of the Academy of Surgical Research* **2010**, *23*, 28–34.
  97. Loganathan, G.; Graham, M. L.; Radosevich, D. M.; Soltani, S. M.; Tiwari, M.; Anazawa, T.; Papas, K. K.; Sutherland, D. E. R.; Hering, B. J.; Balamurugan, A. N. Factors Affecting Transplant Outcomes in Diabetic Nude Mice Receiving Human, Porcine, and Nonhuman Primate Islets: Analysis of 335 Transplantations. *Transplantation* **2013**, *95*, 1439–1447.
  98. Bonner-Weir, S.; Davalli, A. M.; Scaglia, L.; Hollister, J.; Weir, G. C. Myths about the Structure and Function of Porcine Islets. *Xenotransplantation* **1995**, *2*, 207–212.
  99. Rijkeljkhuizen, J. K. R. A.; Burg, M. P. M. van der; Töns, A.; Terpstra, O. T.; Bouwman, E. Pretransplant Culture Selects for High-Quality Porcine Islets. *Pancreas* **2006**, *32*, 403–407.
  100. Krickhahn, M.; Bühler, C.; Meyer, T.; Thiede, A.; Ulrichs, K. The Morphology of Islets within the Porcine Donor Pancreas Determines the Isolation Result: Successful Isolation of Pancreatic Islets Can Now Be Achieved from Young Market Pigs. *Cell transplantation* **2002**, *11*, 827–838.
  101. Lamb, M.; Laugenour, K.; Liang, O.; Alexander, M.; Foster, C. E.; Lakey, J. R. T. In Vitro Maturation of Viable Islets From Partially Digested Young Pig Pancreas. *Cell Transplantation* **2014**, *23*, 263–272.
  102. Clayton, H. A.; London, N. J. Survival and Function of Islets during Culture. *Cell transplantation* **1996**, *5*, 1–12; discussion 13–17, 19.
  103. Murdoch, T. B.; McGhee-Wilson, D.; Shapiro, A. M. J.; Lakey, J. R. T. Methods of Human Islet Culture for Transplantation. *Cell transplantation* **2004**, *13*, 605–617.
  104. Weegman, B. P.; Taylor, M. J.; Baicu, S. C.; Scott, W. E.; Mueller, K. R.; Kitzmann, J. D.; Rizzari, M. D.; Papas, K. K. Hypothermic Perfusion Preservation of Pancreas for Islet Grafts: Validation Using a Split Lobe Porcine Model. *Cell medicine* **2012**, *2*, 105–110, PMID: PMC3786062.
  105. Kitzmann, J. P.; Pepper, A. R.; Gala-Lopez, B.; Pawlick, R.; Kin, T.; O’Gorman, D.; Mueller, K. R.; Gruessner, A. C.; Avgoustiniatos, E. S.; Karatzas, T.; Szot, G. L.; Posselt, A. M.; Stock, P. G.; Wilson, J. R.; Shapiro, A. M.; Papas, K. K. Human Islet Viability and Function Is Maintained during High-Density Shipment in Silicone Rubber Membrane Vessels. *Transplantation proceedings* **2014**, *46*, 1989–1991.
  106. Korbitt, G. S.; Elliott, J. F.; Ao, Z.; Smith, D. K.; Warnock, G. L.; Rajotte, R. V. Large Scale Isolation, Growth, and Function of Porcine Neonatal Islet Cells. *Journal of Clinical Investigation* **1996**, *97*, 2119–2129.
  107. Juhl, K.; Bonner-Weir, S.; Sharma, A. Regenerating Pancreatic Beta-Cells: Plasticity of Adult Pancreatic Cells and the Feasibility of in-Vivo Neogenesis. *Current opinion in*

- organ transplantation* **2010**, *15*, 79–85.
108. Bouwens, L. Islet Morphogenesis and Stem Cell Markers. *Cell biochemistry and biophysics* **2004**, *40*, 81–88.
  109. Dodge, R.; Loomans, C.; Sharma, A.; Bonner-Weir, S. Developmental Pathways during in Vitro Progression of Human Islet Neogenesis. *Differentiation; research in biological diversity* **2009**, *77*, 135–147.
  110. Bonner-Weir, S.; Taneja, M.; Weir, G. C.; Tatarkiewicz, K.; Song, K. H.; Sharma, A.; O’Neil, J. J. In Vitro Cultivation of Human Islets from Expanded Ductal Tissue. *Proceedings of the National Academy of Sciences of the United States of America* **2000**, *97*, 7999–8004.
  111. Webb, M. A.; Dennison, A. R.; James, R. F. The Potential Benefit of Non-Purified Islets Preparations for Islet Transplantation. *Biotechnology & genetic engineering reviews* **2012**, *28*, 101–114.
  112. Beckwith, J.; Nyman, J. a; Flanagan, B.; Schrover, R.; Schuurman, H.-J. A Health-Economic Analysis of Porcine Islet Xenotransplantation. *Xenotransplantation* **2010**, *17*, 233–242.
  113. Reuveny, S.; Velez, D.; Macmillan, J. D.; Miller, L. Factors Affecting Cell Growth and Monoclonal Antibody Production in Stirred Reactors. *Journal of immunological methods* **1986**, *86*, 53–9.
  114. Tarleton, R. L.; Beyer, A. M. Medium-Scale Production and Purification of Monoclonal Antibodies in Protein-Free Medium. *BioTechniques* **1991**, *11*, 590–3.
  115. Dazey, B.; Duchez, P.; Letellier, C.; Vezon, G.; Ivanovic, Z. Cord Blood Processing by Using a Standard Manual Technique and Automated Closed System “Sepax” (Kit CS-530). *Stem cells and development* **2005**, *14*, 6–10.
  116. Gastens, M. H.; Goltry, K.; Prohaska, W.; Tschöpe, D.; Stratmann, B.; Lammers, D.; Kirana, S.; Götting, C.; Kleesiek, K. Good Manufacturing Practice-Compliant Expansion of Marrow-Derived Stem and Progenitor Cells for Cell Therapy. *Cell transplantation* **2007**, *16*, 685–96.
  117. Naing, M. W.; Williams, D. J. Three-Dimensional Culture and Bioreactors for Cellular Therapies. *Cytotherapy* **2011**, *13*, 391–9.
  118. Stacey, G. N. *Cancer Cell Culture*; Cree, I. A., Ed.; Methods in Molecular Biology; Humana Press: Totowa, NJ, 2011; vol731.
  119. Sharma, S.; Raju, R.; Sui, S.; Hu, W.-S. Stem Cell Culture Engineering - Process Scale up and Beyond. *Biotechnology journal* **2011**, *6*, 1317–29.
  120. Nieden, N. I. zur; Cormier, J. T.; Rancourt, D. E.; Kallos, M. S. Embryonic Stem Cells Remain Highly Pluripotent Following Long Term Expansion as Aggregates in Suspension Bioreactors. *Journal of biotechnology* **2007**, *129*, 421–32.
  121. Kehoe, D. E.; Jing, D.; Lock, L. T.; Tzanakakis, E. S.; Ph, D. Scalable Stirred-Suspension Bioreactor Culture. *Tissue engineering Part A* **2010**, *16*, 405–21.
  122. Krawetz, R.; Taiani, J. T.; Liu, S.; Meng, G.; Li, X.; Kallos, M. S.; Rancourt, D. E. Large-Scale Expansion of Pluripotent Human Embryonic Stem Cells in Stirred-Suspension Bioreactors. *Tissue engineering. Part C, Methods* **2010**, *16*, 573–82.

123. Shafa, M.; Sjonnesen, K.; Yamashita, A.; Liu, S.; Michalak, M.; Kallos, M. S.; Rancourt, D. E. Expansion and Long-Term Maintenance of Induced Pluripotent Stem Cells in Stirred Suspension Bioreactors. *Journal of tissue engineering and regenerative medicine* **2012**, *6*, 462–72.
124. Oh, S. K. W.; Chen, A. K.; Mok, Y.; Chen, X.; Lim, U.-M.; Chin, A.; Choo, A. B. H.; Reuveny, S. Long-Term Microcarrier Suspension Cultures of Human Embryonic Stem Cells. *Stem cell research* **2009**, *2*, 219–30.
125. Olmer, R.; Lange, A.; Selzer, S.; Kasper, C.; Haverich, A.; Martin, U.; Zweigerdt, R. Suspension Culture of Human Pluripotent Stem Cells in Controlled, Stirred Bioreactors. *Tissue engineering. Part C, Methods* **2012**, *18*, 772–84.
126. Baptista, R. P.; Fluri, D. a; Zandstra, P. W. High Density Continuous Production of Murine Pluripotent Cells in an Acoustic Perfused Bioreactor at Different Oxygen Concentrations. *Biotechnology and bioengineering* **2013**, *110*, 648–55.
127. Papas, K. K. Characterization of the Metabolic and Secretory Behavior of Suspended Free and Entrapped ART-20 Spheroids in Fed-Batch and Perfusion Cultures, Georgia Institute of Technology, Atlanta GA, 1992.
128. Papas, K. K.; Constantinidis, I.; Sambanis, A. Cultivation of Recombinant, Insulin-Secreting AtT-20 Cells as Free and Entrapped Spheroids. *Cytotechnology* **1993**, *13*, 1–12.
129. Sambanis, A.; Papas, K. K.; Flanders, P. C.; Long, R. C.; Kang, H.; Constantinidis, I. Towards the Development of a Bioartificial Pancreas: Immunoisolation and NMR Monitoring of Mouse Insulinomas. *Cytotechnology* **1994**, *15*, 351–63.
130. Papas, K. K.; Long, R. C.; Constantinidis, I.; Sambanis, A. Role of ATP and Pi in the Mechanism of Insulin Secretion in the Mouse Insulinoma betaTC3 Cell Line. *The Biochemical journal* **1997**, *326* ( Pt 3, 807–14.
131. Papas, K. K.; Long, R. C.; Sambanis, A.; Constantinidis, I. Development of a Bioartificial Pancreas: I. Long-Term Propagation and Basal and Induced Secretion from Entrapped betaTC3 Cell Cultures. *Biotechnology and bioengineering* **1999**, *66*, 219–30.
132. Papas, K. K.; Long, R. C.; Sambanis, A.; Constantinidis, I. Development of a Bioartificial Pancreas: II. Effects of Oxygen on Long-Term Entrapped betaTC3 Cell Cultures. *Biotechnology and bioengineering* **1999**, *66*, 231–7.
133. Hu, W. S. Cell Culture Process Monitoring and Control—a Key to Process Optimization. *Cytotechnology* **1994**, *14*, 155–6.
134. Knaack, D.; Fiore, D. M.; Surana, M.; Leiser, M.; Laurance, M.; Fusco-DeMane, D.; Hegre, O. D.; Fleischer, N.; Efrat, S. Clonal Insulinoma Cell Line That Stably Maintains Correct Glucose Responsiveness. *Diabetes* **1994**, *43*, 1413–7.
135. Poitout, V.; Stout, L. E.; Armstrong, M. B.; Walseth, T. F.; Sorenson, R. L.; Robertson, R. P. Morphological and Functional Characterization of Beta TC-6 Cells—an Insulin-Secreting Cell Line Derived from Transgenic Mice. *Diabetes* **1995**, *44*, 306–13.
136. Poitout, V.; Olson, L. K.; Robertson, R. P. Insulin-Secreting Cell Lines: Classification, Characteristics and Potential Applications. *Diabetes & metabolism* **1996**, *22*, 7–14.
137. Suzuki, R.; Okada, N.; Miyamoto, H.; Yoshioka, T.; Sakamoto, K.; Oka, H.; Tsutsumi, Y.; Nakagawa, S.; Miyazaki, J.; Mayumi, T. Cyotomedical Therapy for Insulinopenic Diabetes Using Microencapsulated Pancreatic Beta Cell Lines. *Life sciences* **2002**, *71*,

- 1717–29.
138. Skelin, M.; Rupnik, M.; Cencic, A. Pancreatic Beta Cell Lines and Their Applications in Diabetes Mellitus Research. *Altex* **2010**, *27*, 105–13.
  139. Masters, J. R.; Stacey, G. N. Changing Medium and Passaging Cell Lines. *Nature protocols* **2007**, *2*, 2276–84.
  140. Woodside, S. M.; Bowen, B. D.; Piret, J. M. Mammalian Cell Retention Devices for Stirred Perfusion Bioreactors. *Cytotechnology* **1998**, *28*, 163–75.
  141. Liu, H.; Liu, X.-M.; Li, S.-C.; Wu, B.-C.; Ye, L.-L.; Wang, Q.-W.; Chen, Z.-L. A High-Yield and Scaleable Adenovirus Vector Production Process Based on High Density Perfusion Culture of HEK 293 Cells as Suspended Aggregates. *Journal of bioscience and bioengineering* **2009**, *107*, 524–9.
  142. Zhi, Z.; Liu, B.; Jones, P. M.; Pickup, J. C. Polysaccharide Multilayer Nanoencapsulation of Insulin-Producing Beta-Cells Grown as Pseudoislets for Potential Cellular Delivery of Insulin. *Biomacromolecules* **2010**, *11*, 610–6.
  143. Lock, L. T.; Laychock, S. G.; Tzanakakis, E. S. Pseudoislets in Stirred-Suspension Culture Exhibit Enhanced Cell Survival, Propagation and Insulin Secretion. *Journal of biotechnology* **2011**, *151*, 278–86.
  144. Serra, M.; Brito, C.; Sousa, M. F. Q.; Jensen, J.; Tostões, R.; Clemente, J.; Strehl, R.; Hyllner, J.; Carrondo, M. J. T.; Alves, P. M. Improving Expansion of Pluripotent Human Embryonic Stem Cells in Perfused Bioreactors through Oxygen Control. *Journal of Biotechnology* **2010**, *148*, 208–215.
  145. Gálvez, J.; Lecina, M.; Solà, C.; Cairó, J.; Gòdia, F. Optimization of HEK-293S Cell Cultures for the Production of Adenoviral Vectors in Bioreactors Using on-Line OUR Measurements. *Journal of biotechnology* **2012**, *157*, 214–22.
  146. Trabelsi, K.; Majoul, S.; Rourou, S.; Kallel, H. Development of a Measles Vaccine Production Process in MRC-5 Cells Grown on Cytodex1 Microcarriers and in a Stirred Bioreactor. *Applied microbiology and biotechnology* **2012**, *93*, 1031–40.
  147. Marchenko, S.; Flanagan, L. Counting Human Neural Stem Cells. *Journal of visualized experiments : JoVE* **2007**, 262.
  148. Eve, D. J.; Fillmore, R.; Borlongan, C. V.; Sanberg, P. R. Stem Cells Have the Potential to Rejuvenate Regenerative Medicine Research. *Medical science monitor: international medical journal of experimental and clinical research* **2010**, *16*, RA197–217.
  149. Hsiao, L.-C.; Carr, C.; Chang, K.-C.; Lin, S.-Z.; Clarke, K. Review Article: Stem Cell-Based Therapy for Ischemic Heart Disease. *Cell transplantation* **2012**.
  150. Oldershaw, R. a. Cell Sources for the Regeneration of Articular Cartilage: The Past, the Horizon and the Future. *International journal of experimental pathology* **2012**, *93*, 389–400.
  151. Coppi, P. De Regenerative Medicine for Congenital Malformations. *Journal of pediatric surgery* **2013**, *48*, 273–80.
  152. Tziampazis, E.; Sambanis, A. Modeling of Cell Culture Processes. *Cytotechnology* **1994**, *14*, 191–204.
  153. Sidoli, F. R.; Mantalaris, A.; Asprey, S. P. Modelling of Mammalian Cells and Cell

- Culture Processes. *Cytotechnology* **2004**, *44*, 27–46.
154. Yim, R. Administrative and Research Policies Required to Bring Cellular Therapies from the Research Laboratory to the Patient's Bedside. *Transfusion* **2005**, *45*, 144S–58S.
  155. Fink, D. W. FDA Regulation of Stem Cell-Based Products. *Science (New York, N.Y.)* **2009**, *324*, 1662–3.
  156. Moos, M. Stem-Cell-Derived Products: An FDA Update. *Trends in pharmacological sciences* **2008**, *29*, 591–3.
  157. Colton, C. K. Oxygen Supply to Encapsulated Therapeutic Cells. *Adv. Drug Deliv. Rev.* **2014**, *67-68*, 93–110.
  158. Parhaml, P.; Fung, B. M. Fluorine-19 Relaxation Study of Perfluoro Chemicals as Oxygen Carriers. *Journal of Physical Chemistry* **1983**, *87*, 1928–1931.
  159. Mason, R. P.; Shukla, H.; Antich, P. P. In Vivo Oxygen Tension and Temperature: Simultaneous Determination Using <sup>19</sup>F NMR Spectroscopy of Perfluorocarbon. *Magnetic resonance in medicine : official journal of the Society of Magnetic Resonance in Medicine / Society of Magnetic Resonance in Medicine* **1993**, *29*, 296–302.
  160. Noth, U.; Morrissey, S. P.; Deichmann, R.; Adolf, H.; Schwarzbauer, C.; Lutz, J.; Haase, A. In Vivo Measurement of Partial Oxygen Pressure in Large Vessels and in the Reticuloendothelial System Using Fast <sup>19</sup>F-MRI. *Magnetic Resonance in Medicine* **1995**, *34*, 738–745.
  161. Noth, U.; Grohn, P.; Jork, A.; Zimmermann, U.; Haase, A.; Lutz, J. <sup>19</sup>F-MRI In Vivo Determination of the Partial Oxygen Pressure in Perfluorocarbon-Loaded Alginate Capsules Implanted Into the Peritoneal Cavity and Different Tissues. *Magnetic Resonance in Medicine* **1999**, *42*, 1039–1047.
  162. Shukla, H. P.; Mason, R. P.; Bansal, N.; Antich, P. P. Regional Myocardial Oxygen Tension: <sup>19</sup>F. 827–833.
  163. Dardzinski, B. J.; Sotak, C. H. Rapid Tissue Oxygen Tension Mapping Using <sup>19</sup>F Inversion-Recovery Echo- Planar Imaging of Perfluoro-15-Crown-5-Ether. *Magnetic Resonance in Medicine* **1994**, *32*, 88–97.
  164. Boudewijn, B. P. J.; Heerschap, A.; Simonetti, A. W.; Rijken, P. F. J. W.; Peters, H. P. W.; Siben, G.; Kogel, A. J. Van Der Characterization and Validation of Noninvasive Oxygen Tension Measurements in Human Glioma Xenografts by <sup>19</sup>F-MR Relaxometry. *International Journal of Radiation Oncology Biology Physics* **1999**, *44*, 649–658.
  165. Duong, T. Q.; Kim, S. G. In Vivo MR Measurements of Regional Arterial and Venous Blood Volume Fractions in Intact Rat Brain. *Magnetic resonance in medicine : official journal of the Society of Magnetic Resonance in Medicine / Society of Magnetic Resonance in Medicine* **2000**, *43*, 393–402.
  166. Duong, T. Q.; Iadecola, C.; Kim, S. G. Effect of Hyperoxia, Hypercapnia, and Hypoxia on Cerebral Interstitial Oxygen Tension and Cerebral Blood Flow. *Magnetic Resonance in Medicine* **2001**, *45*, 61–70.
  167. Helmer, K. G.; Han, S.; Sotak, C. H. On the Correlation between the Water Diffusion Coefficient and Oxygen Tension in RIF-1 Tumors. *NMR in Biomedicine* **1998**, *11*, 120–130.
  168. Gross, J. D.; Long, R. C.; Constantinidis, I.; Sambanis, A. Monitoring of Dissolved



- Oxygen and Cellular Bioenergetics within a Pancreatic Substitute. *Biotechnology and Bioengineering* **2007**, *98*, 261–270.
169. Goh, F.; Sambanis, A. In Vivo Noninvasive Monitoring of Dissolved Oxygen Concentration within an Implanted Tissue-Engineered Pancreatic Construct. *Tissue engineering. Part C, Methods* **2011**, *17*, 887–894.
  170. Goh, F.; Long, R.; Simpson, N.; Sambanis, A. Dual Perfluorocarbon Method to Noninvasively Monitor Dissolved Oxygen Concentration in Tissue Engineered Constructs in Vitro and in Vivo. *Biotechnology Progress* **2011**, *27*, 1115–1125.
  171. McNab, J. a.; Yung, a. C.; Kozlowski, P. Tissue Oxygen Tension Measurements in the Shionogi Model of Prostate Cancer Using <sup>19</sup>F MRS and MRI. *Magnetic Resonance Materials in Physics, Biology and Medicine* **2004**, *17*, 288–295.
  172. Mignon, L.; Magat, J.; Schakman, O.; Marbaix, E.; Gallez, B.; Jordan, B. F. Hexafluorobenzene in Comparison with Perfluoro-15-Crown-5-Ether for Repeated Monitoring of Oxygenation Using <sup>19</sup>F MRI in a Mouse Model. *Magnetic resonance in medicine : official journal of the Society of Magnetic Resonance in Medicine / Society of Magnetic Resonance in Medicine* **2013**, *69*, 248–54.
  173. Fan, X.; River, J. N.; Zamora, M.; Al-Hallaq, H. a.; Karczmar, G. S. Effect of Carbogen on Tumor Oxygenation: Combined Fluorine-19 and Proton MRI Measurements. *International Journal of Radiation Oncology Biology Physics* **2002**, *54*, 1202–1209.
  174. Kodibagkar, V. D.; Wang, X.; Mason, R. P. Physical Principles of Quantitative Nuclear Magnetic Resonance Oximetry. *Frontiers in bioscience : a journal and virtual library* **2008**, *13*, 1371–1384.
  175. Reid, R. S.; Koch, C. J.; Castro, M. E.; Lunt, J. a; Treiber, E. O.; Boisvert, D. J.; Allen, P. S. The Influence of Oxygenation on the <sup>19</sup>F Spin-Lattice Relaxation Rates of Fluosol-DA. *Physics in medicine and biology* **1985**, *30*, 677–686.
  176. Mason, R. P.; Nunnally, R. L.; Antich, P. P. Tissue Oxygenation: A Novel Determination Using <sup>19</sup>F Surface Coil NMR Spectroscopy of Sequestered Perfluorocarbon Emulsion. *Magnetic resonance in medicine : official journal of the Society of Magnetic Resonance in Medicine / Society of Magnetic Resonance in Medicine* **1991**, *18*, 71–79.
  177. Mason, R. P. Non-Invasive Physiology: <sup>19</sup>F NMR of Perfluorocarbons. *Artificial cells, blood substitutes, and immobilization biotechnology* **1994**, *22*, 1141–1153.
  178. Waiczies, H.; Lepore, S.; Janitzek, N.; Hagen, U.; Seifert, F.; Ittermann, B.; Purfürst, B.; Pezzutto, A.; Paul, F.; Niendorf, T.; Waiczies, S. Perfluorocarbon Particle Size Influences Magnetic Resonance Signal and Immunological Properties of Dendritic Cells. *PloS one* **2011**, *6*, e21981.
  179. Lemaire, L.; Bastiat, G.; Franconi, F.; Lautram, N.; Duong Thi Dan, T.; Garcion, E.; Saulnier, P.; Benoit, J. P. Perfluorocarbon-Loaded Lipid Nanocapsules as Oxygen Sensors for Tumor Tissue pO<sub>2</sub> Assessment. *European journal of pharmaceuticals and biopharmaceutics : official journal of Arbeitsgemeinschaft für Pharmazeutische Verfahrenstechnik e.V* **2013**, *84*, 479–86.
  180. Flaim, S. F. Pharmacokinetics and Side Effects of Perfluorocarbon-Based Blood Substitutes. *Artificial cells, blood substitutes, and immobilization biotechnology* **1994**, *22*, 1043–1054.
  181. Mattrey, R. F. The Potential Role of Perfluorochemicals (PFCs) in Diagnostic Imaging.

- Artificial cells, blood substitutes, and immobilization biotechnology* **1994**, 22, 295–313.
182. Suszynski, T. M.; Avgoustiniatos, E. S.; Stein, S. a; Falde, E. J.; Hammer, B. E.; Papas, K. K. Assessment of Tissue-Engineered Islet Graft Viability by Fluorine Magnetic Resonance Spectroscopy. *Transplantation proceedings* **2011**, 43, 3221–5.
  183. Lutz, J.; Nöth, U.; Morrissey, S. P.; Adolf, H.; Deichmann, R.; Haase, A. Measurement of Oxygen Tensions in the Abdominal Cavity and in the Skeletal Muscle Using <sup>19</sup>F-MRI of Neat PFC Droplets. *Advances in experimental medicine and biology* **1997**, 428, 569–572.
  184. McGovern, K. A.; Schoeniger, J. S.; Wehrle, J. P.; Ng, C. E.; Glickson, J. D. Gel-Entrapment of Perfluorocarbons: A Fluorine-19 NMR Spectroscopic Method for Monitoring Oxygen Concentration in Cell Perfusion Systems. *Magnetic resonance in medicine : official journal of the Society of Magnetic Resonance in Medicine / Society of Magnetic Resonance in Medicine* **1993**, 29, 196–204.
  185. Holland, S. K.; Kennan, R. P.; Schaub, M. M.; D'Angelo, M. J.; Gore, J. C. Imaging Oxygen Tension in Liver and Spleen by <sup>19</sup>F NMR. *Magnetic resonance in medicine : official journal of the Society of Magnetic Resonance in Medicine / Society of Magnetic Resonance in Medicine* **1993**, 29, 446–458.
  186. Sweet, I. R.; Yanay, O.; Waldron, L.; Gilbert, M.; Fuller, J. M.; Tupling, T.; Lernmark, A.; Osborne, W. R. a Treatment of Diabetic Rats with Encapsulated Islets. *Journal of Cellular and Molecular Medicine* **2008**, 12, 2644–2650.
  187. Sörenby, A. K.; Kumagai-Braesch, M.; Sharma, A.; Hultenby, K. R.; Wernerson, A. M.; Tibell, A. B. Preimplantation of an Immunoprotective Device Can Lower the Curative Dose of Islets to that of Free Islet Transplantation: Studies in a Rodent Model. *Transplantation* **2008**, 86, 364–366.
  188. Rafael, E.; Wernerson, A.; Arner, P.; Tibell, A. In Vivo Studies on Insulin Permeability of an Immunoisolation Device Intended for Islet Transplantation Using the Microdialysis Technique. *European Surgical Research* **1999**, 31, 249–258.
  189. Rafael, E.; Wu, G. S.; Hultenby, K.; Tibell, A.; Wernerson, A. Improved Survival of Macroencapsulated Islets of Langerhans by Preimplantation of the Immunoisolating Device: A Morphometric Study. *Cell Transplantation* **2003**, 12, 407–412.
  190. Rafael, E.; Wernerson, a; Arner, P.; Wu, G. S.; Tibell, a In Vivo Evaluation of Glucose Permeability of an Immunoisolation Device Intended for Islet Transplantation: A Novel Application of the Microdialysis Technique. *Cell transplantation* **1999**, 8, 317–26.
  191. Tibell, A.; Rafael, E.; Wennberg, L.; Nordenström, J.; Bergström, M.; Geller, R. L.; Loudovaris, T.; Johnson, R. C.; Brauker, J. H.; Neuenfeldt, S.; Wernerson, A. Survival of Macroencapsulated Allogeneic Parathyroid Tissue One Year after Transplantation in Nonimmunosuppressed Humans. *Cell Transplantation* **2001**, 10, 591–599.
  192. Lau, J.; Henriksnäs, J.; Svensson, J.; Carlsson, P.-O. Oxygenation of Islets and Its Role in Transplantation. *Current opinion in organ transplantation* **2009**, 14, 688–693.
  193. Shao, Q.; Morgounova, E.; Jiang, C.; Choi, J.; Bischof, J.; Ashkenazi, S. In Vivo Photoacoustic Lifetime Imaging of Tumor Hypoxia in Small Animals. *Journal of biomedical optics* **2013**, 18, 076019.
  194. Ashkenazi, S. Photoacoustic Lifetime Imaging of Dissolved Oxygen Using Methylene Blue. *Journal of biomedical optics* **2014**, 15, 040501.

195. Winter, P. M. Perfluorocarbon Nanoparticles: Evolution of a Multimodality and Multifunctional Imaging Agent. *Scientifica* **2014**, *2014*, 746574.
196. Shi, Y.; Oeh, J.; Eastham-Anderson, J.; Yee, S.; Finkle, D.; Peale Jr, F. V; Ross, J.; Hedehus, M.; Bruggen, N. Van; Venook, R.; Ross, S.; Sampath, D.; Carano, R. a D. Mapping In Vivo Tumor Oxygenation within Viable Tumor by F19-MRI and Multispectral Analysis. *Neoplasia* **2013**, *15*, 1241–1250.
197. Giraudeau, C.; Djemai, B.; Ghaly, M. A.; Boumezbeur, F.; Mériaux, S.; Robert, P.; Port, M.; Robic, C.; Bihan, D. Le; Lethimonnier, F.; Valette, J. High Sensitivity 19F MRI of a Perfluorooctyl Bromide Emulsion: Application to a Dynamic Biodistribution Study and Oxygen Tension Mapping in the Mouse Liver and Spleen. *NMR in Biomedicine* **2012**, *25*, 654–660.
198. Berkowitz, B. A.; Handa, J. T.; Wilson, C. A. Perfluorocarbon Temperature Measurements Using 19F NMR. *NMR in biomedicine* *5*, 65–68.
199. Maillard, E.; Juszczak, M. T.; Clark, A.; Hughes, S. J.; Gray, D. R. W.; Johnson, P. R. V Perfluorodecalin-Enriched Fibrin Matrix for Human Islet Culture. *Biomaterials* **2011**, *32*, 9282–9.
200. Ramesh, A.; Chhabra, P.; Brayman, K. L. Pancreatic Islet Transplantation in Type 1 Diabetes Mellitus: An Update on Recent Developments. *Current diabetes reviews* **2013**, *9*, 294–311.
201. Cogger, K.; Nostro, M. C. Recent Advances in Cell Replacement Therapies for the Treatment of Type 1 Diabetes. *Endocrinology* **2015**, *156*, 8–15.
202. Froud, T.; Ricordi, C.; Baidal, D. a; Hafiz, M. M.; Ponte, G.; Cure, P.; Pileggi, A.; Poggioli, R.; Ichii, H.; Khan, A.; Ferreira, J. V; Pugliese, A.; Esquenazi, V. V; Kenyon, N. S.; Alejandro, R. Islet Transplantation in Type 1 Diabetes Mellitus Using Cultured Islets and Steroid-Free Immunosuppression: Miami Experience. *American journal of transplantation : official journal of the American Society of Transplantation and the American Society of Transplant Surgeons* **2005**, *5*, 2037–46.
203. Barton, F. B.; Rickels, M. R.; Alejandro, R.; Hering, B. J.; Wease, S.; Naziruddin, B.; Oberholzer, J.; Odorico, J. S.; Garfinkel, M. R.; Levy, M.; Pattou, F.; Berney, T.; Secchi, A.; Messinger, S.; Senior, P. a; Maffi, P.; Posselt, A.; Stock, P. G.; Kaufman, D. B.; Luo, X.; Kandeel, F.; Cagliero, E.; Turgeon, N. a; Witkowski, P.; Najj, A.; O’Connell, P. J.; Greenbaum, C.; Kudva, Y. C.; Brayman, K. L.; Aull, M. J.; Larsen, C.; Kay, T. W. H.; Fernandez, L. a; Vantyghem, M. C.; Bellin, M.; Shapiro, a M. J. Improvement in Outcomes of Clinical Islet Transplantation: 1999-2010. *Diabetes Care* **2012**, *35*, 1436–1445.
204. Shapiro, A.; Lakey, J.; Ryan, E.; Baker, S. 2007 Update on Allogeneic Islet Transplantation from the Collaborative Islet Transplant Registry (CITR). *Cell Transplantation* **2009**, *18*, 753–767.
205. Bellin, M. D.; Kandaswamy, R.; Parkey, J.; Zhang, H.-J.; Liu, B.; Ihm, S. H.; Ansite, J. D.; Witson, J.; Bansal-Pakala, P.; Balamurugan, a N.; Papas, K. K.; Papas, K.; Sutherland, D. E. R.; Moran, a; Hering, B. J. Prolonged Insulin Independence after Islet Allotransplants in Recipients with Type 1 Diabetes. *American journal of transplantation : official journal of the American Society of Transplantation and the American Society of Transplant Surgeons* **2008**, *8*, 2463–70.

206. White, S. a.; Shaw, J. a.; Sutherland, D. E. Pancreas Transplantation. *The Lancet* **2009**, *373*, 1808–1817.
207. Ryan, E. a.; Paty, B. W.; Senior, P. a.; Bigam, D.; Alfadhli, E.; Kneteman, N. M.; Lakey, J. R. T.; Shapiro, a. M. J. Five-Year Follow-up after Clinical Islet Transplantation. *Diabetes* **2005**, *54*, 2060–2069.
208. Bellin, M. D.; Barton, F. B.; Heitman, a; Harmon, J. V; Kandaswamy, R.; Balamurugan, a N.; Sutherland, D. E. R.; Alejandro, R.; Hering, B. J. Potent Induction Immunotherapy Promotes Long-Term Insulin Independence after Islet Transplantation in Type 1 Diabetes. *American journal of transplantation: official journal of the American Society of Transplantation and the American Society of Transplant Surgeons* **2012**, *12*, 1576–83.
209. Davalli, a M.; Ogawa, Y.; Ricordi, C.; Scharp, D. W.; Bonner-Weir, S.; Weir, G. C. A Selective Decrease in the Beta Cell Mass of Human Islets Transplanted into Diabetic Nude Mice. *Transplantation* **1995**, *59*, 817–820.
210. Moberg, L.; Johansson, H.; Lukinius, a.; Berne, C.; Foss, a.; Källen, R.; Østraat; Salmela, K.; Tibell, a.; Tufveson, G.; Elgue, G.; Nilsson Ekdahl, K.; Korsgren, O.; Nilsson, B. Production of Tissue Factor by Pancreatic Islet Cells as a Trigger of Detrimental Thrombotic Reactions in Clinical Islet Transplantation. *Lancet* **2002**, *360*, 2039–2045.
211. Huurman, V. a L.; Hilbrands, R.; Pinkse, G. G. M.; Gillard, P.; Duinkerken, G.; Linde, P. van de; Meer-Prins, P. M. W. van der; Versteeg-van der Voort Maarschalk, M. F. J.; Verbeeck, K.; Alizadeh, B. Z.; Mathieu, C.; Gorus, F. K.; Roelen, D. L.; Claas, F. H. J.; Keymeulen, B.; Pipeleers, D. G.; Roep, B. O. Cellular Islet Autoimmunity Associates with Clinical Outcome of Islet Cell Transplantation. *PLoS ONE* **2008**, *3*.
212. Desai, N. M.; Goss, J. a; Deng, S.; Wolf, B. a; Markmann, E.; Palanjian, M.; Shock, A. P.; Feliciano, S.; Brunicaardi, F. C.; Barker, C. F.; Naji, A.; Markmann, J. F. Elevated Portal Vein Drug Levels of Sirolimus and Tacrolimus in Islet Transplant Recipients: Local Immunosuppression or Islet Toxicity? *Transplantation* **2003**, *76*, 1623–1625.
213. Paty, B. W.; Harmon, J. S.; Marsh, C. L.; Robertson, R. P. Inhibitory Effects of Immunosuppressive Drugs on Insulin Secretion from HIT-T15 Cells and Wistar Rat Islets. *Transplantation* **2002**, *73*, 353–357.
214. Laugharne, M.; Cross, S.; Richards, S.; Dawson, C.; Ilchyshyn, L.; Saleem, M.; Mathieson, P.; Smith, R. Sirolimus Toxicity and Vascular Endothelial Growth Factor Release from Islet and Renal Cell Lines. *Transplantation* **2007**, *83*, 1635–1638.
215. Mattsson, G.; Jansson, L.; Carlsson, P. O. Decreased Vascular Density in Mouse Pancreatic Islets after Transplantation. *Diabetes* **2002**, *51*, 1362–1366.
216. Olsson, R.; Olerud, J.; Pettersson, U.; Carlsson, P. O. Increased Numbers of Low-Oxygenated Pancreatic Islets after Intraportal Islet Transplantation. *Diabetes* **2011**, *60*, 2350–2353.
217. Lau, J.; Carlsson, P.-O. Low Revascularization of Human Islets When Experimentally Transplanted into the Liver. *Transplantation* **2009**, *87*, 322–325.
218. Carlsson, P. O.; Palm, F.; Mattsson, G. Low Revascularization of Experimentally Transplanted Human Pancreatic Islets. *Journal of Clinical Endocrinology and Metabolism* **2002**, *87*, 5418–5423.
219. Arteel, G. E.; Thurman, R. G.; Yates, J. M.; Raleigh, J. a Evidence That Hypoxia Markers Detect Oxygen Gradients in Liver: Pimonidazole and Retrograde Perfusion of Rat Liver.

- British journal of cancer* **1995**, 72, 889–895.
220. Suszynski, T. M.; Avgoustiniatos, E. S.; Papas, K. K. Intraportal Islet Oxygenation. *Journal of Diabetes Science and Technology* **2014**.
  221. Medarova, Z.; Moore, A. MRI as a Tool to Monitor Islet Transplantation. *Nature reviews. Endocrinology* **2009**, 5, 444–452.
  222. Chen, X.; Kaufman, D. B. Bioluminescent Imaging of Transplanted Islets. *Methods in Molecular Biology* **2009**, 574, 75–85.
  223. Wang, P.; Schuetz, C.; Vallabhajosyula, P.; Medarova, Z.; Tena, A.; Wei, L.; Yamada, K.; Deng, S.; Markmann, J. F.; Sachs, D. H.; Moore, A. Monitoring of Allogeneic Islet Grafts in Nonhuman Primates Using MRI. *Transplantation* **2015**, 00, 1.
  224. Yang, H. K.; Yoon, K.-H. Current Status of Encapsulated Islet Transplantation. *Journal of Diabetes and its Complications* **2015**, 29, 737–743.
  225. Ludwig, B.; Zimerman, B.; Steffen, a; Yavriants, K.; Azarov, D.; Reichel, a; Vardi, P.; German, T.; Shabtay, N.; Rotem, a; Evron, Y.; Neufeld, T.; Mimon, S.; Ludwig, S.; Brendel, M. D.; Bornstein, S. R.; Barkai, U. A Novel Device for Islet Transplantation Providing Immune Protection and Oxygen Supply. *Hormone and metabolic research = Hormon- und Stoffwechselforschung = Hormones et métabolisme* **2010**, 42, 918–22.
  226. Ludwig, B.; Reichel, A.; Steffen, A.; Zimerman, B.; Schally, A. V.; Block, N. L.; Colton, C. K.; Ludwig, S.; Kersting, S.; Bonifacio, E.; Solimena, M.; Gendler, Z.; Rotem, A.; Barkai, U.; Bornstein, S. R. Transplantation of Human Islets without Immunosuppression. *Proceedings of the National Academy of Sciences of the United States of America* **2013**, 110, 19054–8.
  227. Barkai, U.; Weir, G. C.; Colton, C. K.; Ludwig, B.; Bornstein, S. R.; Brendel, M. D.; Neufeld, T.; Bremer, C.; Leon, A.; Evron, Y.; Yavriants, K.; Azarov, D.; Zimermann, B.; Maimon, S.; Shabtay, N.; Balyura, M.; Rozenshtein, T.; Vardi, P.; Bloch, K.; Vos, P. de; Rotem, A. Enhanced Oxygen Supply Improves Islet Viability in a New Bioartificial Pancreas. *Cell transplantation* **2013**, 22, 1463–76.
  228. Yang, Z.; Chen, M.; Fialkow, L. B.; Ellett, J. D.; Wu, R.; Nadler, J. L. Survival of Pancreatic Islet Xenografts in NOD Mice with the Theracyte Device. *Transplantation Proceedings* **2002**, 34, 3349–3350.
  229. Tziampazis, E.; Sambanis, A. Tissue Engineering of a Bioartificial Pancreas: Modeling the Cell Environment and Device Function. *Biotechnology progress* **1995**.
  230. Mikos, a G.; Papadaki, M. G.; Kouvroukoglou, S.; Ishaug, S. L.; Thomson, R. C. Mini-Review: Islet Transplantation to Create a Bioartificial Pancreas. *Biotechnology and bioengineering* **1994**, 43, 673–7.
  231. Bose, B.; Katikireddy, K. R.; Shenoy P, S. *Regenerative Medicine for Diabetes: Differentiation of Human Pluripotent Stem Cells into Functional ??-Cells in Vitro and Their Proposed Journey to Clinical Translation*; 1st ed.; Elsevier Inc., 2014; vol95.
  232. Li, W.; Nakanishi, M.; Zumsteg, A.; Shear, M.; Wright, C.; Melton, D. a.; Zhou, Q. In Vivo Reprogramming of Pancreatic Acinar Cells to Three Islet Endocrine Subtypes. *Elife* **2014**, 2014, 1–20.
  233. Li, W.; Cavelti-Weder, C.; Zhang, Y.; Clement, K.; Donovan, S.; Gonzalez, G.; Zhu, J.; Stemann, M.; Xu, K.; Hashimoto, T.; Yamada, T.; Nakanishi, M.; Zhang, Y.; Zeng, S.;

- Gifford, D.; Meissner, A.; Weir, G.; Zhou, Q. Long-Term Persistence and Development of Induced Pancreatic Beta Cells Generated by Lineage Conversion of Acinar Cells. *Nature biotechnology* **2014**, *32*, 1223–1230.
234. Lee, S.-H.; Hao, E.; Savinov, A. Y.; Geron, I.; Strongin, A. Y.; Itkin-Ansari, P. Human Beta-Cell Precursors Mature into Functional Insulin-Producing Cells in an Immunoisolation Device: Implications for Diabetes Cell Therapies. *Transplantation* **2009**, *87*, 983–991.
235. Kroon, E.; Martinson, L. a.; Kadoya, K.; Bang, A. G.; Kelly, O. G.; Eliazar, S.; Young, H.; Richardson, M.; Smart, N. G.; Cunningham, J.; Agulnick, A. D.; D'Amour, K. a.; Carpenter, M. K.; Baetge, E. E. Pancreatic Endoderm Derived from Human Embryonic Stem Cells Generates Glucose-Responsive Insulin-Secreting Cells in Vivo. *Nature biotechnology* **2008**, *26*, 443–452.
236. Aoki, T.; Hui, H.; Umehara, Y.; LiCalzi, S.; Demetriou, A. a.; Rozga, J.; Perfetti, R. Intrasplenic Transplantation of Encapsulated Genetically Engineered Mouse Insulinoma Cells Reverses Streptozotocin-Induced Diabetes in Rats. *Cell Transplantation* **2005**, *14*, 411–421.
237. Simpson, N. E.; Khokhlova, N.; Oca-Cossio, J. a.; McFarlane, S. S.; Simpson, C. P.; Constantinidis, I. Effects of Growth Regulation on Conditionally-Transformed Alginate-Entrapped Insulin Secreting Cell Lines in Vitro. *Biomaterials* **2005**, *26*, 4633–4641.
238. Rood, P. P. M.; Buhler, L. H.; Bottino, R.; Trucco, M.; Cooper, D. K. C. Pig-to-Nonhuman Primate Islet Xenotransplantation: A Review of Current Problems. *Cell Transplantation* **2006**, *15*, 89–104.
239. Merani, S.; Toso, C.; Emamaullee, J.; Shapiro, a. M. J. Optimal Implantation Site for Pancreatic Islet Transplantation. *British Journal of Surgery* **2008**, *95*, 1449–1461.
240. Cantarelli, E.; Piemonti, L. Alternative Transplantation Sites for Pancreatic Islet Grafts. *Current Diabetes Reports* **2011**, *11*, 364–374.
241. Rajab, A. Islet Transplantation: Alternative Sites. *Current Diabetes Reports* **2010**, *10*, 332–337.
242. Chhabra, P.; Brayman, K. L. Overcoming Barriers in Clinical Islet Transplantation: Current Limitations and Future Prospects. *Current Problems in Surgery* **2014**, *51*, 49–86.
243. Sekine, N.; Cirulli, V.; Regazzi, R.; Brown, L. J.; Gine, E.; Tamarit-Rodriguez, J.; Girotti, M.; Marie, S.; MacDonald, M. J.; Wollheim, C. B.; Rutter, G. a. Low Lactate Dehydrogenase and High Mitochondrial Glycerol Phosphate Dehydrogenase in Pancreatic Beta-Cells: Potential Role in Nutrient Sensing. *Journal of Biological Chemistry* **1994**, *269*, 4895–4902.
244. Bonner-Weir, S. Morphological Evidence for Pancreatic Polarity of Beta-Cell within Islets of Langerhans. *Diabetes* **1988**, *37*, 616–621.
245. Bonner-Weir, S. The microvasculature of the pancreas, with emphasis on that of the islets of Langerhans. In *The pancreas: biology, pathobiology, and disease.*; Go, V. L. W., Ed.; Raven Press: New York, 1993; pp. 759–768.
246. Lifson, N.; Kramlinger, K. G.; Mayrand, R. R.; Lender, E. J. Blood Flow to the Rabbit Pancreas with Special Reference to the Islets of Langerhans. *Gastroenterology* **1980**, *79*, 466–473.

247. Colton, C. K. Engineering Challenges in Cell- Encapsulation Technology. *Most* **1996**, *14*, 158–162.
248. Colton, C. K. Challenges in the Development of Immunoisolation Devices. In *Principles of Tissue Engineering*; Robert Lanza, R. L. and J. P. V., Ed.; Elsevier, 2014; pp. 543–562.
249. Avgoustiniatos, E. S.; Colton, C. K. Design Considerations in Immunoisolation. In *Principles of Tissue Engineering*; R.P. Lanza, R. Langer, and W. L. C., Ed.; R.G. Landes Company: Austin, Texas, 1997; pp. 333–346.
250. Avgoustiniatos, E. S.; Wu, H.; Colton, C. K. Engineering Challenges in Immunoisolation Device Development. In *Principles of Tissue Engineering*; Lanza, R. P.; Langer, R.; Vacanti, J., Eds.; Academic Press: San Diego, 2000; pp. 331–350.
251. Avgoustiniatos, E. S.; Colton, C. K. Effect of External Oxygen Mass Transfer Resistances on Viability of Immunoisolated Tissue. *Annals of the New York Academy of Sciences* **1997**, *831*, 145–167.
252. Intaglietta, M.; Johnson, P. C.; Winslow, R. M. Microvascular and Tissue Oxygen Distribution. *Cardiovascular research* **1996**, *32*, 632–643.
253. Neuenfeldt, S.; Daugird, J.; Brauker, J.; Geller, L.; Fredericksen, S.; Jones, M.; Loudovaris, T.; Maryanov, D.; Shors, S. United States Patent 5,964,261 **1999**.
254. Pisania, A.; Papas, K. K.; Powers, D. E.; Rappel, M. J.; Omer, A.; Bonner-Weir, S.; Weir, G. C.; Colton, C. K. Enumeration of Islets by Nuclei Counting and Light Microscopic Analysis. *Laboratory investigation; a journal of technical methods and pathology* **2010**, *90*, 1676–1686.
255. Suszynski, T. M.; Wildey, G. M.; Falde, E. J.; Cline, G. W.; Maynard, K. S.; Ko, N.; Sotiris, J.; Naji, A.; Hering, B. J.; Papas, K. K. The ATP/DNA Ratio Is a Better Indicator of Islet Cell Viability than the ADP/ATP Ratio. *Transplantation proceedings* **2008**, *40*, 346–50, PMID: PMC2804259.
256. Giuliani, M.; Moritz, W.; Bodmer, E.; Dindo, D.; Kugelmeier, P.; Lehmann, R.; Gassmann, M.; Groscurth, P.; Weber, M. Central Necrosis in Isolated Hypoxic Human Pancreatic Islets: Evidence for Postisolation Ischemia. *Cell Transplantation* **2005**, *14*, 67–76.
257. Huber, F. L.; Latshang, T. D.; Goede, J. S.; Bloch, K. E. Does Venous Blood Gas Analysis Provide Accurate Estimates of Hemoglobin Oxygen Affinity? *Annals of Hematology* **2013**, *92*, 517–521.
258. Wang, W.; Vadgama, P. O<sub>2</sub> Microsensors for Minimally Invasive Tissue Monitoring. *Journal of the Royal Society, Interface / the Royal Society* **2004**, *1*, 109–117.
259. Ludwig, B.; Rotem, a.; Schmid, J.; Weir, G. C.; Colton, C. K.; Brendel, M. D.; Neufeld, T.; Block, N. L.; Yavriyants, K.; Steffen, a.; Ludwig, S.; Chavakis, T.; Reichel, a.; Azarov, D.; Zimmermann, B.; Maimon, S.; Balyura, M.; Rozenshtein, T.; Shabtay, N.; Vardi, P.; Bloch, K.; Vos, P. de; Schally, a. V.; Bornstein, S. R.; Barkai, U. Improvement of Islet Function in a Bioartificial Pancreas by Enhanced Oxygen Supply and Growth Hormone Releasing Hormone Agonist. *Proceedings of the National Academy of Sciences* **2012**, *109*, 5022–5027.
260. Khattak, S. F.; Chin, K.; Bhatia, S. R.; Roberts, S. C. Enhancing Oxygen Tension and Cellular Function in Alginate Cell Encapsulation Devices through the Use of Perfluorocarbons. *Biotechnology and bioengineering* **2007**, *96*, 156–66.

261. Wu, H.; Avgoustiniatos, E. S.; Swette, L.; Bonner-Weir, S.; Weir, G. C.; Colton, C. K. In situ electrochemical oxygen generation with an immunoisolation device. In *Annals of the New York Academy of Sciences*; 1999; vol875, pp. 105–125.
262. Bloch, K.; Papismedov, E.; Yavriyants, K.; Vorobeychik, M.; Beer, S.; Vardi, P. Immobilized Microalgal Cells as an Oxygen Supply System for Encapsulated Pancreatic Islets: A Feasibility Study. *Artificial Organs* **2006**, *30*, 715–718.
263. Neufeld, T.; Ludwig, B.; Barkai, U.; Weir, G. C.; Colton, C. K.; Evron, Y.; Balyura, M.; Yavriyants, K.; Zimmermann, B.; Azarov, D.; Maimon, S.; Shabtay, N.; Rozenshtein, T.; Lorber, D.; Steffen, A.; Willenz, U.; Bloch, K.; Vardi, P.; Taube, R.; Vos, P. de; Lewis, E. C.; Bornstein, S. R.; Rotem, A. The Efficacy of an Immunisolating Membrane System for Islet Xenotransplantation in Minipigs. *PLoS ONE* **2013**, *8*.
264. Ward, C. L.; Corona, B. T.; Yoo, J. J.; Harrison, B. S.; Christ, G. J. Oxygen Generating Biomaterials Preserve Skeletal Muscle Homeostasis under Hypoxic and Ischemic Conditions. *PLoS ONE* **2013**, *8*.
265. Pedraza, E.; Coronel, M. M.; Fraker, C. a.; Ricordi, C.; Stabler, C. L. Preventing Hypoxia-Induced Cell Death in Beta Cells and Islets via Hydrolytically Activated, Oxygen-Generating Biomaterials. *Proceedings of the National Academy of Sciences* **2012**, 1–6.
266. Pedraza, E.; Brady, A.-C.; Fraker, C. a.; Stabler, C. L. Synthesis of Macroporous Poly(dimethylsiloxane) Scaffolds for Tissue Engineering Applications. *Journal of Biomaterials Science, Polymer Edition* **2012**, 1–16.
267. Padera, R. F.; Colton, C. K. Time Course of Membrane Neovascularization. *Biomaterials* **1996**, *17*, 277–284.
268. Brauker, J. H.; Carr-Brendel, V. E.; Martinson, L. A.; Crudele, J.; Johnston, W. D.; Johnson, R. C. Neovascularization of Synthetic Membranes Directed by Membrane Microarchitecture. *Journal of Biomedical Materials Research* **1995**, *29*, 1517–1524.
269. Brauker, J.; Martinson, L. a; Young, S. K.; Johnson, R. C. Local Inflammatory Response around Diffusion Chambers Containing Xenografts. Nonspecific Destruction of Tissues and Decreased Local Vascularization. *Transplantation* **1996**, *61*, 1671–1677.
270. Scott, W. E.; O'Brien, T. D.; Ferrer-Fabrega, J.; Avgoustiniatos, E. S.; Weegman, B. P.; Anazawa, T.; Matsumoto, S.; Kirchner, V. A.; Rizzari, M. D.; Murtaugh, M. P.; Suszynski, T. M.; Aasheim, T.; Kidder, L. S.; Hammer, B. E.; Stone, S. G.; Tempelman, L. a; Sutherland, D. E. R.; Hering, B. J.; Papas, K. K. Persufflation Improves Pancreas Preservation When Compared with the Two-Layer Method. *Transplantation proceedings* **2010**, *42*, 2016–9, PMID: PMC2956134.
271. Scott, W. E.; Weegman, B. P.; Ferrer-Fabrega, J.; Stein, S. a; Anazawa, T.; Kirchner, V. a; Rizzari, M. D.; Stone, J.; Matsumoto, S.; Hammer, B. E.; Balamurugan, a N.; Kidder, L. S.; Suszynski, T. M.; Avgoustiniatos, E. S.; Stone, S. G.; Tempelman, L. a; Sutherland, D. E. R.; Hering, B. J.; Papas, K. K. Pancreas Oxygen Persufflation Increases ATP Levels as Shown by Nuclear Magnetic Resonance. *Transplantation proceedings* **2010**, *42*, 2011–5, PMID: PMC2947552.
272. Noguchi, H.; Levy, M. F.; Kobayashi, N.; Matsumoto, S. Pancreas Preservation by the Two-Layer Method: Does It Have a Beneficial Effect Compared with Simple Preservation in University of Wisconsin Solution? *Cell Transplantation* **2009**, *18*, 497–503.
273. Hering, B. J.; Matsumoto, I.; Sawada, T.; Nakano, M.; Sakai, T.; Kandaswamy, R.;



- Sutherland, D. E. R. Impact of Two-Layer Pancreas Preservation on Islet Isolation and Transplantation. *Transplantation* **2002**, *74*, 1813–6.
274. Balamurugan, a N.; Loganathan, G.; Bellin, M. D.; Wilhelm, J. J.; Harmon, J.; Anazawa, T.; Soltani, S. M.; Radosevich, D. M.; Yuasa, T.; Tiwari, M.; Papas, K. K.; McCarthy, R.; Sutherland, D. E. R.; Hering, B. J. A New Enzyme Mixture to Increase the Yield and Transplant Rate of Autologous and Allogeneic Human Islet Products. *Transplantation* **2012**, *93*, 693–702.
275. Taylor, M. J.; Baicu, S. Cryo-Isolation: A Novel Method for Enzyme-Free Isolation of Pancreatic Islets Involving in Situ Cryopreservation of Islets and Selective Destruction of Acinar Tissue. *Transplantation proceedings* **2011**, *43*, 3181–3.
276. Taylor, M. J.; Baicu, S. Non-Enzymatic Cryogenic Isolation of Therapeutic Cells: Novel Approach for Enzyme-Free Isolation of Pancreatic Islets Using In Situ Cryopreservation of Islets and Concurrent Selective Freeze Destruction of Acinar Tissue. *Cell transplantation* **2013**.
277. Shenkman, R. M.; Chalmers, J. J.; Hering, B. J.; Kirchoff, N.; Papas, K. K. Quadrupole Magnetic Sorting of Porcine Islets of Langerhans. *Tissue engineering. Part C, Methods* **2009**, *15*, 147–56.
278. Cooper, D. K.; Koren, E.; Oriol, R. Clinical Potential of Xenotransplantation. *Transplantation proceedings* **1994**, *26*, 1331–1332.
279. Taniguchi, S.; Cooper, D. K. C. Clinical Xenotransplantation: Past, Present and Future. *Ann. R. Coll. Surg. Engl.* **1997**, *79*, 13–19.
280. Park, C.-G.; Bottino, R.; Hawthorne, W. J. Current Status of Islet Xenotransplantation. *International journal of surgery (London, England)* **2015**, 6–11.
281. Cardona, K.; Milas, Z.; Strobert, E.; Cano, J.; Jiang, W.; Safley, S. a.; Gangappa, S.; Hering, B. J.; Weber, C. J.; Pearson, T. C.; Larsen, C. P. Engraftment of Adult Porcine Islet Xenografts in Diabetic Nonhuman Primates through Targeting of Costimulation Pathways. *American Journal of Transplantation* **2007**, *7*, 2260–2268.
282. Sun, Y.; Ma, X.; Zhou, D.; Vacek, I.; Sun, A. M. Normalization of Diabetes in Spontaneously Diabetic Cynomolgus Monkeys by Xenografts of Microencapsulated Porcine Islets without Immunosuppression. *Journal of Clinical Investigation* **1996**, *98*, 1417–1422.
283. Dufrane, D.; Goebbels, R.-M.; Gianello, P. Alginate Macroencapsulation of Pig Islets Allows Correction of Streptozotocin-Induced Diabetes in Primates up to 6 Months without Immunosuppression. *Transplantation* **2010**, *90*, 1054–1062.
284. Lowe, M.; Badell, I. R.; Thompson, P.; Martin, B.; Leopardi, F.; Strobert, E.; Price, a. a.; Abdulkerim, H. S.; Wang, R.; Iwakoshi, N. N.; Adams, a. B.; Kirk, a. D.; Larsen, C. P.; Reimann, K. a. A Novel Monoclonal Antibody to CD40 Prolongs Islet Allograft Survival. *American Journal of Transplantation* **2012**, *12*, 2079–2087.
285. Thompson, P.; Cardona, K.; Russell, M.; Badell, I. R.; Shaffer, V.; Korbitt, G.; Rayat, G. R.; Cano, J.; Song, M.; Jiang, W.; Strobert, E.; Rajotte, R.; Pearson, T.; Kirk, a. D.; Larsen, C. P. CD40-Specific Costimulation Blockade Enhances Neonatal Porcine Islet Survival in Nonhuman Primates. *American Journal of Transplantation* **2011**, *11*, 947–957.
286. Major, E. O. Progressive Multifocal Leukoencephalopathy in Patients on Immunomodulatory Therapies. *Annual review of medicine* **2010**, *61*, 35–47.

287. Hawthorne, W. J.; Salvaris, E. J.; Phillips, P.; Hawkes, J.; Liuwantara, D.; Burns, H.; Barlow, H.; Stewart, a. B.; Peirce, S. B.; Hu, M.; Lew, a. M.; Robson, S. C.; Nottle, M. B.; D'Apice, a. J. F.; O'Connell, P. J.; Cowan, P. J. Control of IBMIR in Neonatal Porcine Islet Xenotransplantation in Baboons. *American Journal of Transplantation* **2014**, *14*, 1300–1309.
288. Bottino, R.; Wijkstrom, M.; Windt, D. J. van der; Hara, H.; Ezzelarab, M.; Murase, N.; Bertera, S.; He, J.; Phelps, C.; Ayares, D.; Cooper, D. K. C.; Trucco, M. Pig-to-Monkey Islet Xenotransplantation Using Multi-Transgenic Pigs. *American Journal of Transplantation* **2014**, *14*, 2275–2287.
289. Thompson, P.; Badell, I. R.; Lowe, M.; Cano, J.; Song, M.; Leopardi, F.; Avila, J.; Ruhil, R.; Strobert, E.; Korbitt, G.; Rayat, G.; Rajotte, R.; Iwakoshi, N.; Larsen, C. P.; Kirk, a. D. Islet Xenotransplantation Using Gal-Deficient Neonatal Donors Improves Engraftment and Function. *American Journal of Transplantation* **2011**, *11*, 2593–2602.
290. Windt, D. J. Van Der; Bottino, R.; Casu, a.; Campanile, N.; Smetanka, C.; He, J.; Murase, N.; Hara, H.; Ball, S.; Loveland, B. E.; Ayares, D.; Lakkis, F. G.; Cooper, D. K. C.; Trucco, M. Long-Term Controlled Normoglycemia in Diabetic Non-Human Primates after Transplantation with hCD46 Transgenic Porcine Islets. *American Journal of Transplantation* **2009**, *9*, 2716–2726.
291. Sekine, N.; Cirullis, V.; Regazzi, R.; Brown, L. J.; Ginen, E.; Tamarit-rodrigued, J.; Girotti, M.; Marie, S.; Macdonaldg, M. J.; Wollheim, C. B.; Rutted, G. A. Low Lactate Dehydrogenase and High Mitochondrial Glycerol Phosphate Dehydrogenase in Pancreatic P-Cells. **1994**, *269*, 4895–4902.
292. Sörenby, A. K.; Kumagai-Braesch, M.; Sharma, A.; Hultenby, K. R.; Wernerson, A. M.; Tibell, A. B. Preimplantation of an Immunoprotective Device Can Lower the Curative Dose of Islets to that of Free Islet Transplantation: Studies in a Rodent Model. *Transplantation* **2008**, *86*, 364–6.
293. Larsson, H.; Courivaud, F.; Rostrup, E.; Hansen, a Concurrent Measurement of Brain Perfusion, Blood Volume and Blood Brain Barrier Permeability Using Dynamic Contrast Enhanced T1 -Weighted MRI. *Proceedings 17th Scientific Meeting, International Society for Magnetic Resonance in Medicine* **2009**, *584*, 1485.
294. Colton, C. K. Implantable biohybrid artificial organs. In *Cell Transplantation*; 1995; vol4, pp. 415–436.
295. Rizzari, M. D.; Suszynski, T. M.; Kidder, L. S.; Stein, S. A.; O'Brien, T. D.; Sajja, V. S. K.; Scott, W. E.; Kirchner, V. A.; Weegman, B. P.; Avgoustiniatos, E. S.; Todd, P. W.; Kennedy, D. J.; Hammer, B. E.; Sutherland, D. E. R.; Hering, B. J.; Papas, K. K. Surgical Protocol Involving the Infusion of Paramagnetic Microparticles for Preferential Incorporation within Porcine Islets. *Transplantation proceedings* **2010**, *42*, 4209–12, PMID: PMC3035915.
296. Fiorina, P.; Secchi, A. Pancreatic Islet Cell Transplant for Treatment of Diabetes. *Endocrinology and Metabolism Clinics of North America* **2007**, *36*, 999–1013.
297. Hogan, A.; Pileggi, A.; Ricordi, C. Transplantation: Current Developments and Future Directions; the Future of Clinical Islet Transplantation as a Cure for Diabetes. *Frontiers in bioscience : a journal and virtual library* **2008**, *13*, 1192–1205.
298. Hering, B. J.; Ansite, J. D.; Eckman, P. M.; Parkey, J.; Hunter, D. W.; Sutherland, D. E. R.

- Single-Donor, Marginal-Dose Islet Transplantation in Patients with Type 1 Diabetes. *JAMA: the journal of ...* **2005**, *293*, 830–836.
299. Frank, A.; Deng, S.; Huang, X.; Velidedeoglu, E.; Bae, Y.-S.; Liu, C.; Abt, P.; Stephenson, R.; Mohiuddin, M.; Thambipillai, T.; Markmann, E.; Palanjian, M.; Sellers, M.; Naji, A.; Barker, C. F.; Markmann, J. F. Transplantation for Type I Diabetes: Comparison of Vascularized Whole-Organ Pancreas with Isolated Pancreatic Islets. *Annals of surgery* **2004**, *240*, 631–640; discussion 640–643.
300. Keymeulen, B.; Gillard, P.; Mathieu, C.; Movahedi, B.; Maleux, G.; Delvaux, G.; Ysebaert, D.; Roep, B.; Vandemeulebroucke, E.; Marichal, M.; Veld, P. In 't; Bogdani, M.; Hendrieckx, C.; Gorus, F.; Ling, Z.; Rood, J. van; Pipeleers, D. Correlation between Beta Cell Mass and Glycemic Control in Type 1 Diabetic Recipients of Islet Cell Graft. *Proc Natl Acad Sci U S A* **2006**, *103*, 17444–9.
301. Badet, L.; Benhamou, P. Y.; Wojtuszczyński, A.; Baertschiger, R.; Milliat-Guittard, L.; Kessler, L.; Penformis, A.; Thivolet, C.; Renard, E.; Bosco, D.; Morel, P.; Morelon, E.; Bayle, F.; Colin, C.; Berney, T. Expectations and Strategies Regarding Islet Transplantation: Metabolic Data from the GRAGIL 2 Trial. *Transplantation* **2007**, *84*, 89–96.
302. Kin, T.; Murdoch, T. B.; Shapiro, a. M. J.; Lakey, J. R. T. Estimation of Pancreas Weight from Donor Variables. *Cell Transplantation* **2006**, *15*, 181–185.
303. Matsumoto, S.; Zhang, G.; Qualley, S.; Clever, J.; Tombrello, Y.; Strong, D. M.; Reems, J. a. Analysis of Donor Factors Affecting Human Islet Isolation with Current Isolation Protocol. *Transplantation Proceedings* **2004**, *36*, 1034–1036.
304. Ponte, G. M.; Pileggi, A.; Messinger, S.; Alejandro, A.; Ichii, H.; Baidal, D. a.; Khan, A.; Ricordi, C.; Goss, J. a.; Alejandro, R. Toward Maximizing the Success Rates of Human Islet Isolation: Influence of Donor and Isolation Factors. *Cell Transplantation* **2007**, *16*, 595–607.
305. Sakuma, Y.; Ricordi, C.; Miki, a.; Yamamoto, T.; Pileggi, a.; Khan, a.; Alejandro, R.; Inverardi, L.; Ichii, H. Factors That Affect Human Islet Isolation. *Transplantation Proceedings* **2008**, *40*, 343–345.
306. Mellert, J.; Hering, B. J.; Liu, X.; Brandhorst, D.; Brandhorst, H.; Pfeffer, F.; Federlin, K.; Bretzel, R. G.; Hopt, U. T. Critical Islet Mass for Successful Porcine Islet Autotransplantation. *Journal of molecular medicine (Berlin, Germany)* **1999**, *77*, 126–129.
307. Jensen, S. L.; Kühl, C.; Nielsen, O. V.; Holst, J. J. Isolation and Perfusion of the Porcine Pancreas. *Scandinavian journal of gastroenterology. Supplement* **1976**, *37*, 57–61.
308. Shokouh-Amiri, M. H.; Rahimi-Saber, S.; Andersen, H. O. Segmental Pancreatic Autotransplantation in the Pig. *Transplantation* **1989**, *47*, 42–44.
309. Morel, P.; Kaufmann, D. B.; Matas, a J.; Tzardis, P.; Field, M. J.; Lloveras, J. K.; Sutherland, D. E. Total Pancreatectomy in the Pig for Islet Transplantation. Technical Alternatives. *Transplantation* **1991**, *52*, 11–15.
310. Skjennald, A. Anatomy of the Liver and Pancreas in the Domestic Swine, with Special Reference to Vascular Structures. *Scand J Gastroenterol* **1982**, *17*, 16–31.
311. Traverso, L. W.; MacFarlane, S. Pancreas Autotransplantation--Unsuitability of the Swine as a Model. *Transplantation* **1987**, *44*, 450–451.

312. Turégano-Fuentes, F.; Garcia-Menéndez, C.; Larrad-Jiménez, a; Domínguez-Comesaña, E.; Sanz-Sánchez, M.; Pérez-Gallardo, a The Feasibility of Porcine Pancreas Autotransplantation--a Case for Controversy. *Transplantation* **1990**, *49*, 1028–1029.
313. Scott, W. E.; Matsumoto, S.; Tanaka, T.; Avgoustiniatos, E. S.; Graham, M. L.; Williams, P. C.; Tempelman, L. a.; Sutherland, D. E.; Hering, B. J.; Hammer, B. E.; Papas, K. K. Real-Time Noninvasive Assessment of Pancreatic ATP Levels During Cold Preservation. *Transplantation Proceedings* **2008**, *40*, 403–406.
314. Sabat, M.; Godlewska, E.; Kinasiewicz, J.; Urbanowicz, a.; Orłowski, T. Assessment of Some Porcine Strains as Donors of Islets of Langerhans. *Transplantation Proceedings* **2003**, *35*, 2343–2344.
315. Dufrane, D.; D'hoore, W.; Goebbels, R. M.; Saliez, A.; Guiot, Y.; Gianello, P. Parameters Favouring Successful Adult Pig Islet Isolations for Xenotransplantation in Pig-to-Primate Models. *Xenotransplantation* **2006**, *13*, 204–214.
316. Ricordi, C.; Soggi, C.; Davalli, A. M.; Staudacher, C.; Baro, P.; Vertova, A.; Sassi, I.; Gavazzi, F.; Pozza, G.; Carlo, V. Di Isolation of the Elusive Pig Islet. *Surgery* **1990**, *107*, 688–694.
317. Soggi, C.; Ricordi, C.; Davalli, A. M.; Staudacher, C.; Baro, P.; Vertova, A.; Freschi, M.; Gavazzi, F.; Braghi, S.; Pozza, G. Selection of Donors Significantly Improves Pig Islet Isolation Yield. *Hormone and metabolic research. Supplement series* **1990**, *25*, 32–34.
318. Kim, J. H.; Kim, H. II; Lee, K. W.; Yu, J. E.; Kim, S. H.; Park, H. S.; Park, C. G.; Ihm, S. H.; Ha, J.; Kim, S. J.; Lee, H. K.; Ahn, C.; Park, K. S. Influence of Strain and Age Differences on the Yields of Porcine Islet Isolation: Extremely High Islet Yields from SPF CMS Miniature Pigs. *Xenotransplantation* **2007**, *14*, 60–66.
319. Prabhakaran, S.; Hering, B. J. What Strain of Pig Should Be Used? *Xenotransplantation* **2008**, *15*, 83–86.
320. Kirchhof, N.; Hering, B. J.; Geiss, V.; Federlin, K.; Bretzel, R. G. Evidence for Breed-Dependent Differences in Porcine Islets of Langerhans. *Transplantation proceedings* **1994**, *26*, 616–617.
321. Ulrichs, K.; Bosss, M.; Heiser, A.; Eckstein, V.; Wacker, H.; Thiede, A.; Muller-Ruchhoitz, W. Histomorphological Characteristics of the Porcine Pancreas as a Basis for the Isolation of Islets of Langerhans. *Xenotransplantation* **1995**, *2*, 176–187.
322. Calne, R. Y.; Sells, R. A.; Marshall, V. C.; Millard, P. R.; Herbertson, B. M.; Hadjiyannakis, E. J.; Dunn, D. C.; Robson, A. J.; Davis, D. R. Multiple Organ Grafts in the Pig. Techniques and Results of Pancreatic, Hepatic, Cardiac, and Renal Allografts. *The British journal of surgery* **1972**, *59*, 969–977.
323. König, H. E.; Liebich, H.-G.; Bragulla, H. (Hermann) *Veterinary Anatomy of Domestic Mammals : Textbook and Colour Atlas*; König, H. E.; Liebich, H. G., Ed.; 3rd ed.; Stuttgart ; New York : Schattauer, 2004.
324. Kumagai, N.; O'Neil, J. J.; Barth, R. N.; LaMattina, J. C.; Utsugi, R.; Moran, S. G.; Yamamoto, S.; Vagefi, P. a; Kitamura, H.; Kamano, C.; Sachs, D. H.; Yamada, K. Vascularized Islet-Cell Transplantation in Miniature Swine. I. Preparation of Vascularized Islet Kidneys. *Transplantation* **2002**, *74*, 1223–1230.
325. Gänger, K. H.; Mettler, D.; Höflin, F.; Ruchti, C.; Minnig, E.; Böss, H. P.; Schilt, W. Experimental Pancreaticosplenic Composite Transplantation in the Pig. Operative

- Technique and Assessment of Graft Function. *European surgical research. Europäische chirurgische Forschung. Recherches chirurgicales europeennes* **1987**, *19*, 323–328.
326. Shokouh-Amiri, M. H.; Rahimi-Saber, S.; Andersen, H. O.; Jensen, S. L. Pancreas Autotransplantation in Pig with Systemic or Portal Venous Drainage. Effect on the Endocrine Pancreatic Function after Transplantation. *Transplantation* **1996**, *61*, 1004–1009.
327. Schröder, T.; Rämö, O. J.; Joffe, S. N. Laser Pancreatectomy. *Research in Experimental Medicine* **1988**, *188*, 227–233.
328. Zhang, Z. Da; Han, F. H.; Meng, L. X. Establishment of a Pig Model with Enteric and Portal Venous Drainage of Pancreatoduodenal Transplantation. *World Journal of Gastroenterology* **2005**, *11*, 5475–5479.
329. Gäbel, H.; Brynner, H.; Heding, L.; Säve-Söderbergh, J.; Wedel, N.; Lundholm, K. Pancreas Transplantation in Streptozotocin-Diabetic Juvenile Pigs. Evaluation of Function among Duct-Ligated, Duct-Occluded, and Nonligated Allografts. *Transplantation* **1983**, *36*, 609–614.
330. Swindle, M. M. *Comparative Anatomy of the Pig*; Columbia, 2008.
331. Pitkäranta, P.; Kivisaari, L.; Nordling, S.; Saari, A.; Schröder, T. Experimental Chronic Pancreatitis in the Pig. *Scandinavian journal of gastroenterology* **1989**, *24*, 987–992.
332. Shapiro, A. M. J.; Ricordi, C.; Hering, B. Edmonton's Islet Success Has Indeed Been Replicated Elsewhere [7]. *Lancet* **2003**, *362*, 1242.
333. Hiraoka, K.; Kuroda, Y.; Suzuki, Y.; Fujino, Y.; Tanioka, Y.; Matsumoto, S.; Sakai, T.; Kandaswamy, R.; Sutherland, D. E. R. Outcomes in clinical pancreas transplantation with the two-layer cold storage method versus simple storage in University of Wisconsin solution. In *Transplantation Proceedings*; 2002; vol34, pp. 2688–2689.
334. Tsujimura, T.; Kuroda, Y.; Avila, J. G.; Kin, T.; Oberholzer, J.; Shapiro, a M. J.; Lakey, J. R. T. Influence of Pancreas Preservation on Human Islet Isolation Outcomes: Impact of the Two-Layer Method. *Transplantation* **2004**, *78*, 96–100.
335. Matsumoto, S.; Zhang, G.; Qualley, S.; Clever, J.; Tombrello, Y.; Strong, D. M.; Reems, J. a. The effect of two-layer (University of Wisconsin solution/ perfluorochemical) preservation method on clinical grade pancreata prior to islet isolation and transplantation. In *Transplantation Proceedings*; 2004; vol36, pp. 1037–1039.
336. Tsujimura, T.; Kuroda, Y.; Avila, J. G.; Kin, T.; Churchill, T. a.; Shapiro, a M. J.; Lakey, J. R. T. Resuscitation of the Ischemically Damaged Human Pancreas by the Two-Layer Method prior to Islet Isolation. *Transplantation proceedings* **2003**, *35*, 2461–2.
337. Ricordi, C.; Fraker, C.; Szust, J.; Al-Abdullah, I.; Poggioli, R.; Kirlew, T.; Khan, A.; Alejandro, R. Improved Human Islet Isolation Outcome from Marginal Donors Following Addition of Oxygenated Perfluorocarbon to the Cold-Storage Solution. *Transplantation* **2003**, *75*, 1524–1527.
338. Matsumoto, S.; Kuroda, Y. Perfluorocarbon for Organ Preservation before Transplantation. *Transplantation* **2002**, *74*, 1804–1809.
339. Avgoustiniatos, E. S.; Hering, B. J.; Papas, K. K. The Rat Pancreas Is Not an Appropriate Model for Testing the Preservation of the Human Pancreas with the Two-Layer Method. *Transplantation* **2006**, *81*, 1471–1472; author reply 1472.

340. Kin, T.; Mirbolooki, M.; Salehi, P.; Tsukada, M.; O’Gorman, D.; Imes, S.; Ryan, E. a; Shapiro, a M. J.; Lakey, J. R. T. Islet Isolation and Transplantation Outcomes of Pancreas Preserved with University of Wisconsin Solution versus Two-Layer Method Using Preoxygenated Perfluorocarbon. *Transplantation* **2006**, *82*, 1286–1290.
341. Caballero-Corbalan, J.; Eich, T.; Foss, A.; Felldin, M.; Kallen, R.; Lundgren, T.; Salmela, K.; Tibell, A.; Tufveson, G.; Korsgren, O. WORLD TRANSPLANT CONGRESS 2006 ORAL ABSTRACTS. In *American Journal of Transplantation*; 2006; vol6, pp. 65–472.
342. Caballero-Corbalán, J.; Eich, T.; Lundgren, T.; Foss, A.; Felldin, M.; Källen, R.; Salmela, K.; Tibell, A.; Tufveson, G.; Korsgren, O.; Brandhorst, D. No Beneficial Effect of Two-Layer Storage Compared with UW-Storage on Human Islet Isolation and Transplantation. *Transplantation* **2007**, *84*, 864–869.
343. Kuhn-Régnier, F.; Fischer, J. H.; Jeschkeit, S.; Switkowski, R.; Bardakcioglu, Ö.; Sobottke, R.; Vivie, E. R. De Coronary Oxygen Persufflation Combined with HTK Cardioplegia Prolongs the Preservation Time in Heart Transplantation. *European Journal of Cardio-thoracic Surgery* **2000**, *17*, 71–76.
344. Fischer, J. H.; Kuhn-Régnier, F.; Jeschkeit, S.; Switkowski, R.; Bardakcioglu, O.; Sobottke, R.; Rainer de Vivie, E. Excellent Recovery after Prolonged Heart Storage by Preservation with Coronary Oxygen Persufflation: Orthotopic Pig Heart Transplantations after 14-Hr Storage. *Transplantation* **1998**, *66*, 1450–1459.
345. Yotsumoto, G.; Jeschkeit-Schubbert, S.; Funcke, C.; Kuhn-Régnier, F.; Fischer, J. H. Total Recovery of Heart Grafts of Non-Heart-Beating Donors after 3 Hours of Hypothermic Coronary Oxygen Persufflation Preservation in an Orthotopic Pig Transplantation Model. *Transplantation* **2003**, *75*, 750–756.
346. Tolba, R. H.; Schildberg, F. a; Schnurr, C.; Glatzel, U.; Decker, D.; Minor, T. Reduced Liver Apoptosis after Venous Systemic Oxygen Persufflation in Non-Heart-Beating Donors. *Journal of investigative surgery : the official journal of the Academy of Surgical Research* **2006**, *19*, 219–227.
347. Saad, S.; Minor, T.; Kötting, M.; Fu, Z. X.; Hagn, U.; Paul, A.; Nagelschmidt, M. Extension of Ischemic Tolerance of Porcine Livers by Cold Preservation Including Postconditioning with Gaseous Oxygen. *Transplantation* **2001**, *71*, 498–502.
348. Minor, T.; Akbar, S.; Tolba, R.; Dombrowski, F. Cold Preservation of Fatty Liver Grafts: Prevention of Functional and Ultrastructural Impairments by Venous Oxygen Persufflation. *Journal of hepatology* **2000**, *32*, 105–111.
349. Rolles, K.; Foreman, J.; Pegg, D. E. A Pilot Clinical Study of Retrograde Oxygen Persufflation in Renal Preservation. *Transplantation* **1989**, *48*, 339–342.
350. Rolles, K.; Foreman, J.; Pegg, D. E. Preservation of Ischemically Injured Canine Kidneys by Retrograde Oxygen Persufflation. *Transplantation* **1984**, *38*, 102–106.
351. Treckmann, J. W.; Paul, A.; Saad, S.; Hoffmann, J.; Waldmann, K. H.; Broelsch, C. E.; Nagelschmidt, M. Primary Organ Function of Warm Ischaemically Damaged Porcine Kidneys after Retrograde Oxygen Persufflation. *Nephrology Dialysis Transplantation* **2006**, *21*, 1803–1808.
352. Minor, T.; Klauke, H.; Isselhard, W. Improved preservation of the small bowel by luminal gas oxygenation: Energetic status during ischemia and functional integrity upon reperfusion. In *Transplantation Proceedings*; 1997; vol29, pp. 2994–2996.

353. Arias-Mendoza, F.; Brown, T. R. In Vivo Measurement of Phosphorous Markers of Disease. *Disease markers* **2004**, *19*, 49–68.
354. Dobbins, R. L.; Malloy, C. R. Measuring in-Vivo Metabolism Using Nuclear Magnetic Resonance. *Current opinion in clinical nutrition and metabolic care* **2003**, *6*, 501–509.
355. Horn, M. Cardiac Magnetic Resonance Spectroscopy: A Window for Studying Physiology. *Methods in molecular medicine* **2006**, *124*, 225–248.
356. Barnard, M. L.; Changani, K. K.; Taylor-Robinson, S. D. The Role of Magnetic Resonance Spectroscopy in the Assessment of Kidney Viability. *Scandinavian journal of urology and nephrology* **1997**, *31*, 487–492.
357. Davidson, B. R.; Barnard, M. L.; Changani, K. K.; Taylor-Robinson, S. D. Liver Transplantation: Current and Potential Applications of Magnetic Resonance Spectroscopy. *Liver transplantation and surgery: official publication of the American Association for the Study of Liver Diseases and the International Liver Transplantation Society* **1997**, *3*, 481–493.
358. Khan, S. a; Cox, I. J.; Hamilton, G.; Thomas, H. C.; Taylor-Robinson, S. D. In Vivo and in Vitro Nuclear Magnetic Resonance Spectroscopy as a Tool for Investigating Hepatobiliary Disease: A Review of H and P MRS Applications. *Liver international: official journal of the International Association for the Study of the Liver* **2005**, *25*, 273–281.
359. Gillies, R. J.; Morse, D. L. In Vivo Magnetic Resonance Spectroscopy in Cancer. *Annual review of biomedical engineering* **2005**, *7*, 287–326.
360. Yoshikawa, T.; Suzuki, Y.; Kanashiro, M.; Li, S.; Goto, T.; Tanaka, T.; Kakinoki, K.; Sakai, T.; Tanioka, Y.; Fujino, Y.; Kuroda, Y. Objective and Rapid Assessment of Pancreas Graft Viability Using <sup>31</sup>P-Nuclear Magnetic Resonance Spectroscopy Combined with Two-Layer Cold Storage Method. *Transplantation* **2004**, *78*, 78–82.
361. Siech, M.; Sotak, C. H.; Letko, G.; Davis, M. A. A Method for in Vivo Assessment of Reversible Rat Pancreatic Ischemia Using <sup>31</sup>P NMR Spectroscopy at 2.0 Tesla. *Magnetic resonance imaging* **1995**, *13*, 463–469.
362. Kuroda, Y.; Kawamura, T.; Suzuki, Y.; Fujiwara, H.; Yamamoto, K.; Saitoh, Y. A New, Simple Method for Cold Storage of the Pancreas Using Perfluorochemical. *Transplantation* **1988**, *46*, 457–460.
363. Hering, B. J.; Walawalkar, N. Pig-to-Nonhuman Primate Islet Xenotransplantation. *Transplant Immunology* **2009**, *21*, 81–86.
364. Abrahante, J. E.; Martins, K.; Papas, K. K.; Hering, B. J.; Schuurman, H. J.; Murtaugh, M. P. Microbiological Safety of Porcine Islets: Comparison with Source Pig. *Xenotransplantation* **2011**, *18*, 88–93.
365. Kim, H.-I.; Lee, S.-Y.; Jin, S. M.; Kim, K. S.; Yu, J. E.; Yeom, S.-C.; Yoon, T. W.; Kim, J. H.; Ha, J.; Park, C.-G.; Kim, S.-J. Parameters for Successful Pig Islet Isolation as Determined Using 68 Specific-Pathogen-Free Miniature Pigs. *Xenotransplantation* **2009**, *16*, 11–8.
366. London, N. J.; Swift, S. M.; Clayton, H. a Isolation, Culture and Functional Evaluation of Islets of Langerhans. *Diabetes & metabolism* **1998**, *24*, 200–7.
367. Gotoh, M.; Ohzato, H.; Porter, J.; Maki, T.; Monaco, A. P. Crucial Role of Pancreatic

- Ductal Collagenase Injection for Isolation of Pancreatic Islets. *Hormone and metabolic research. Supplement series* **1990**, 25, 10–6.
368. Kin, T.; Shapiro, a M. J.; Lakey, J. R. T. Pancreas Divisum: A Study of the Cadaveric Donor Pancreas for Islet Isolation. *Pancreas* **2005**, 30, 325–327.
369. Ichii, H.; Sakuma, Y.; Pileggi, A.; Fraker, C.; Alvarez, A.; Montelongo, J.; Szust, J.; Khan, A.; Inverardi, L.; Naziruddin, B.; Levy, M. F.; Klintmalm, G. B.; Goss, J. a.; Alejandro, R.; Ricordi, C. Shipment of Human Islets for Transplantation. *American Journal of Transplantation* **2007**, 7, 1010–1020.
370. Beckwith, J.; Nyman, J. a; Flanagan, B.; Schrover, R.; Schuurman, H.-J. A Health Economic Analysis of Clinical Islet Transplantation. *Clinical transplantation* **2012**, 26, 23–33.
371. Balamurugan, A. N.; Bottino, R.; Giannoukakis, N.; Smetanka, C. Prospective and Challenges of Islet Transplantation for the Therapy of Autoimmune Diabetes. *Pancreas* **2006**, 32, 231–43.
372. Abdelli, S.; Ansite, J.; Roduit, R.; Borsello, T. Intracellular Stress Signaling Pathways Activated during Human Islet Preparation and Following Acute Cytokine Exposure. *Diabetes* **2004**, 53, 2815–2823.
373. Rosenberg, L.; Wang, R.; Paraskevas, S.; Maysinger, D. Structural and Functional Changes Resulting from Islet Isolation Lead to Islet Cell Death. *Surgery* **1999**, 126, 393–8.
374. Balamurugan, a N.; He, J.; Guo, F.; Stolz, D. B.; Bertera, S.; Geng, X.; Ge, X.; Trucco, M.; Bottino, R. Harmful Delayed Effects of Exogenous Isolation Enzymes on Isolated Human Islets: Relevance to Clinical Transplantation. *American journal of transplantation: official journal of the American Society of Transplantation and the American Society of Transplant Surgeons* **2005**, 5, 2671–81.
375. Bottino, R.; Balamurugan, a N.; Tse, H.; Thirunavukkarasu, C.; Ge, X.; Profozich, J.; Milton, M.; Ziegenfuss, A.; Trucco, M.; Piganelli, J. D. Response of Human Islets to Isolation Stress and the Effect of Antioxidant Treatment. *Diabetes* **2004**, 53, 2559–68.
376. Loganathan, G.; Dawra, R. K.; Pugazhenthii, S.; Guo, Z.; Soltani, S. M.; Wiseman, A.; Sanders, M. a; Papas, K. K.; Velayutham, K.; Saluja, A. K.; Sutherland, D. E. R.; Hering, B. J.; Balamurugan, a N. Insulin Degradation by Acinar Cell Proteases Creates a Dysfunctional Environment for Human Islets Before/after Transplantation: Benefits of  $\alpha$ -1 Antitrypsin Treatment. *Transplantation* **2011**, 92, 1222–30.
377. Heuser, M.; Wolf, B.; Vollmar, B.; Menger, M. D. Exocrine Contamination of Isolated Islets of Langerhans Deteriorates the Process of Revascularization after Free Transplantation. *Transplantation* **2000**, 69, 756–61.
378. Gray, D. W. The Role of Exocrine Tissue in Pancreatic Islet Transplantation. *Transplant international: official journal of the European Society for Organ Transplantation* **1989**, 2, 41–5.
379. Jahr, H.; Bretzel, R. G.; Wacker, T.; Weinand, S.; Brandhorst, H.; Brandhorst, D.; Lau, D.; Hering, B. J.; Federlin, K. Toxic Effects of Superoxide, Hydrogen Peroxide, and Nitric Oxide on Human and Pig Islets. *Transplantation proceedings* **1995**, 27, 3220–1.
380. Jahr, H.; Pfeiffer, G.; Hering, B. J.; Federlin, K.; Bretzel, R. G. Endotoxin-Mediated Activation of Cytokine Production in Human PBMCs by Collagenase and Ficoll. *Journal*



- of molecular medicine (Berlin, Germany)* **1999**, 77, 118–20.
381. Salvalaggio, P. R. O.; Deng, S.; Ariyan, C. E.; Millet, I.; Zawalich, W. S.; Basadonna, G. P.; Rothstein, D. M. Islet Filtration: A Simple and Rapid New Purification Procedure That Avoids Ficoll and Improves Islet Mass and Function. *Transplantation* **2002**, 74, 877–9.
  382. Scharp, D. W.; Kemp, C. B.; Knight, M. J.; Ballinger, W. F.; Lacy, P. E. The Use of Ficoll in the Preparation of Viable Islets of Langerhans from the Rat Pancreas. *Transplantation* **1973**, 16, 686–9.
  383. Davies, J. E.; James, R. F.; London, N. J.; Robertson, G. S. Optimization of the Magnetic Field Used for Immunomagnetic Islet Purification. *Transplantation* **1995**, 59, 767–71.
  384. London, N. J.; Toomey, P.; Contractor, H.; Thirdborough, S. T.; James, R. F.; Bell, P. R. The Effect of Osmolality and Glucose Concentration on the Purity of Human Islet Isolates. *Transplantation proceedings* **1992**, 24, 1002.
  385. Davies, J. E.; Winoto-Morbach, S.; Ulrichs, K.; James, R. F.; Robertson, G. S. A Comparison of the Use of Two Immunomagnetic Microspheres for Secondary Purification of Pancreatic Islets. *Transplantation* **1996**, 62, 1301–6.
  386. Fujioka, T.; Terasaki, P. I.; Heintz, R.; Merideth, N.; Lanza, R. P.; Zheng, T. L.; Soon-Shiong, P. Rapid Purification of Islets Using Magnetic Microspheres Coated with Anti-Acinar Cell Monoclonal Antibodies. *Transplantation* **1990**, 49, 404–7.
  387. Pinkse, G. G. M.; Steenvoorde, E.; Hogendoorn, S.; Noteborn, M.; Terpstra, O. T.; Bruijn, J. a; Heer, E. De Stable Transplantation Results of Magnetically Retracted Islets: A Novel Method. *Diabetologia* **2004**, 47, 55–61.
  388. Kennedy, D. J.; Todd, P.; Logan, S.; Becker, M.; Papas, K. K.; Moore, L. R. Engineering Quadrupole Magnetic Flow Sorting for the Isolation of Pancreatic Islets. *Journal of Magnetism and Magnetic Materials* **2007**, 311, 388–395.
  389. Shenkman, R. M.; Godoy-Silva, R.; Papas, K. K.; Chalmers, J. J. Effects of Energy Dissipation Rate on Islets of Langerhans: Implications for Isolation and Transplantation. *Biotechnology and bioengineering* **2009**, 103, 413–23.
  390. Suszynski, T. M.; Rizzari, M. D.; Kidder, L. S.; Mueller, K.; Chapman, C. S.; Kitmann, J. P.; Pongratz, R. L.; Cline, G. W.; Todd, P. W.; Kennedy, D. J.; O'Brien, T. D.; Avgoustiniatos, E. S.; Schuurman, H.-J.; Papas, K. K. Paramagnetic Microparticles Do Not Elicit Islet Cytotoxicity with Co-Culture or Host Immune Reactivity after Implantation. *Xenotransplantation* **2011**, 18, 239–44.
  391. Ricordi, C.; Lacy, P. E.; Finke, E. H.; Olack, B. J.; Scharp, D. W. Automated Method for Isolation of Human Pancreatic Islets. *Diabetes* **1988**, 37, 413–20.
  392. Swanson, C. J.; Olack, B. J.; Goodnight, D.; Zhang, L.; Mohanakumar, T. Improved Methods for the Isolation and Purification of Porcine Islets. *Human immunology* **2001**, 62, 739–49.
  393. Burg, M. P. van der; Basir, I.; Bouwman, E. No Porcine Islet Loss during Density Gradient Purification in a Novel Iodixanol in University of Wisconsin Solution. *Transplantation proceedings* **1998**, 30, 362–3.
  394. Sajja, V. S. K.; Hanley, T. R.; Gapsis, H.; Guernsey, B.; Kennedy, D. J.; Taylor, M. J.; Papas, K. K.; Todd, P. W. Application of Magnetic Particle Tracking Velocimetry to Quadrupole Magnetic Sorting of Porcine Pancreatic Islets. *Biotechnology and*

*bioengineering* **2011**, *108*, 2107–17.

395. Morini, S.; Braun, M.; Onori, P.; Cicalese, L.; Elias, G.; Gaudio, E.; Rastellini, C. Morphological Changes of Isolated Rat Pancreatic Islets: A Structural, Ultrastructural and Morphometric Study. *Journal of anatomy* **2006**, *209*, 381–92.
396. Robertson, R. P. Islet Transplantation as a Treatment for Diabetes - a Work in Progress. *The New England journal of medicine* **2004**, *350*, 694–705.
397. Bruno W. Volk, K. F. W. Quantitative Studies of the Islets of Nondiabetic Patients. In *The Diabetic Pancreas*; Volk, B. W.; Arquilla, E. R., Eds.; Plenum Medical: Boston, MA, 1985; pp. 117–125.
398. Korc, M. Normal function of endocrine pancreas. In *The Pancreas: Biology, Pathobiology, and Disease*; Raven Press: New York, 1993; pp. 751–758.
399. Weir, G. C.; Bonner-weir, S.; Leahy, J. L. Perspectives in Diabetes Islet Mass and Function in Diabetes and Transplantation. **1990**, *39*, 401–405.

# **APPENDICES**

## Appendix A PORCINE PANCREAS ANATOMY

Sections of this chapter are reproduced in whole, or in part from the following publications with permission:

Ferrer J, Scott WE 3rd, **Weegman BP**, Suszynski TM, Sutherland DE, Hering BJ, Papas KK. “Pig pancreas anatomy: implications for pancreas procurement, preservation, and islet isolation.” *Transplantation*. 2008 Dec 15;86(11):1503-10.

License and agreement documentation is included in **Appendix G**.

**Acknowledgements:** The authors would like to thank the Schott Foundation, the Minnesota Lions Diabetes Foundation, the Juvenile Diabetes Research Foundation (JDRF 5-2013-141), Giner Inc., the Schulze Diabetes Institute, and the NIH (P41 EB015894, and S10 RR025031) for supporting this research.

The authors also thank Efstathios Avgoustiniatos, Louis Kidder, Kristen Maynard, Phillip Rozak, and Kate Mueller for assistance in manuscript preparation and review; A.N. Balamurugan and Melanie Graham for helpful discussions; and Shuichiro Matsumoto, Takayuki Anazawa, Thomas Gilmore, Brian Perrault, and Lucas Mutch for surgical assistance.

Research funding was also provided by grants from the National Institutes of Health (NIH), National Institute of Diabetes and Digestive and Kidney Diseases (R01DK068717 and R43 DK070400), the Iacocca Foundation, the Schott Foundation, and the Carol Olson Memorial Diabetes Research Fund.

## **Pig Pancreas Anatomy: Procurement, Preservation, and Islet Isolation**

### ***Summary***

To investigate the anatomy, pancreata were removed by *en bloc* viscerectomy from 65 female Landrace pigs. The results from anatomical studies showed that 15% of organs exhibited inconsistent vascular branching from the celiac trunk. All organs had uniform patterns of branching at the superior mesenteric artery. The superior and inferior mesenteric veins (IMV) merged to become the portal vein in all but one case in which the IMV drained into the splenic vein. 97% of pancreata had three lobes: duodenal (DL), connecting (CL), and splenic (SL); 39% demonstrated ductal communication between the CL and the other two lobes; 50% had ductal communication only between the CL and DL; and 11% presented other types of ductal delineation. Accounting for the variations in vascular and ductal anatomy, as detailed in this study, will facilitate development of protocols for preservation, optimal enzyme administration, and pancreas distention and digestion, and ultimately lead to substantial improvements in isolation outcomes.

## ***Introduction***

Islet transplantation (ITx) is a promising treatment option for selected patients with type 1 diabetes<sup>296,297</sup>. Increasing evidence demonstrates the ability of human islet allografts to consistently restore normoglycemia and insulin independence in immunosuppressed recipients without the procedural risks associated with vascularized pancreas transplantation<sup>9,53,202,298–301</sup>. Technical and immunological challenges, however, remain prior to larger scale, cost-effective application of ITx. Technical challenges relate to the limited human islet supply from cadavers and to the low islet yield and quality associated with donor brain death and long cold-ischemia times during organ procurement, storage, and transportation<sup>302–305</sup>.

The use of islets isolated from pig pancreata, a source with an unlimited supply<sup>238</sup>, will have a marked impact as it will enable the application of ITx to a larger segment of the population in need. The recent achievement of long-term diabetes reversal after porcine islet xenotransplantation in non-human primates (NHP) demonstrated the potential of islet xenotransplantation in humans<sup>33,34</sup>.

In addition to addressing safety concerns, clinical use of porcine islets will also require the development and implementation of protocols that maximize the viable islet yield per donor pig pancreas<sup>54,306</sup>. Consistent isolation of large numbers of high-quality islets from porcine donors is dependent on advances in organ procurement, organ preservation, and islet isolation, all of which will benefit from detailed knowledge of the porcine pancreatic anatomy<sup>307–309</sup>. Even though studies of porcine pancreatic anatomy have been previously published<sup>310</sup>, the detailed information needed for optimizing pancreas preservation and ductal perfusion is unavailable. Since variations in porcine anatomy have been reported as limiting in these studies<sup>311,312</sup>, it is important to establish an understanding of the extent and implications of such anatomical variations of the pig pancreas in the context of pancreas procurement, pancreas preservation, and islet isolation.

The first goal of this investigation was to gain a detailed understanding of the porcine pancreas vascular anatomy to facilitate the development and implementation of improved procurement and perfusion-based preservation techniques. The second goal was to develop a better understanding of the ductal branching structure and gain critical knowledge to facilitate the development of improved techniques for ductal enzyme loading for optimal pancreas distention prior to islet isolation.

## ***Materials and Methods***

A total of 65 female Landrace non-heart beating donor pigs were pancreatectomized in order to study the vascular and ductal anatomy of the pancreas. The age of the animals was between 6 and 24 months. The mean weight was  $452 \pm 99$  lbs, with a range between 248 and 680 lbs. All experiments were conducted according to the rules and regulations of the Institutional Animal Care and Use Committee of the University of Minnesota. Animals were heparinized, sacrificed by sodium pentobarbital overdose, and then, following the cessation of heart rhythm completely bled out and eviscerated. All of the internal organs were placed onto a procurement table. The pancreas was then removed by *en bloc* viscerectomy to study the pancreatic lobes and general anatomy. The vasculature was studied *in situ* by dissecting and identifying all the vessels that supply the pancreas, allowing for the investigation of perfusion-based preservation techniques. The pancreatic vascular supply and ductal drainage systems were studied following organ procurement by the infusion of colored 0.9% NaCl saline (**Figure A.1**).

### *Surgical procedure*

1. Once all the internal organs were out of the pig abdominal cavity, the greater omentum was incised.
2. The peritoneum that covers the surface of the viscera was opened and the tail of the pancreas (distal splenic lobe (SL)) was dissected from its posterior attachments starting laterally adjacent to the spleen. The upper and lower margins of the pancreatic tail were freed of their mesenteric attachments. The tail of the pancreas was isolated and the spleen was then mobilized.
3. The distal splenic artery and vein were divided to the left of the pancreas.



4. With the splenic artery as a landmark, the celiac trunk (CT) was located and dissected to completely expose the upper part of the abdominal aorta.
5. The tail and distal portions of the body (proximal SL) of the pancreas were mobilized to the junction of the splenic vein, superior mesenteric vein (SMV), and portal vein (PV).
6. The posterior attachments of the pancreas and all tissues between the splenic artery and the junction of the splenic vein and PV were divided.
7. The dissection between the left adrenal gland and the pancreas was later determined to provide more rapid access to the CT, the superior mesenteric artery (SMA), and the aorta, which was isolated by sectioning of the fibromuscular extensions of the diaphragmatic crura and the abdominal lymphatic duct.
8. Dissection continued along the superior margin of the pancreas. The left gastric artery (LGA) was divided at its origin from the splenic artery. The body of the pancreas wraps the PV with a large anterior and thin posterior ring, termed the “portal ring”.
9. After dissecting the hepatoduodenal ligament, the common bile duct (which enters proximally into the duodenum on the major duodenal papilla, about 2–5 cm from the pylorus) was cut off at its entrance into the duodenum, and the proper hepatic and gastroduodenal arteries were ligated.
10. The body of the pancreas and the connecting lobe (CL) were dissected free from the PV by ligating the vascular branches between them.
11. The head of the pancreas (duodenal lobe (DL)) was then dissected and mobilized to the right of the aorta. The head of the pancreas is in a C-shape with respect to the duodenum and is attached to the second, third, and fourth parts of the duodenum. The duodenum

was pulled up and the pancreas was dissected free from the right portion of the PV and the infrahepatic vena cava.

12. The pancreas was then carefully separated from the pancreaticoduodenal vascular arcade so that the pancreatic branches of this vessel could be individually ligated.
13. The main pancreatic duct opens about 20 cm distally into the second (descending) portion of the duodenum. The peritoneum on the right side and behind the lower part of the duodenum was subsequently incised and the transverse colonic ligament was sharply dissected to expose the SMA and the SMV.
14. The right part of the CT, the SMA, and the aorta were then isolated.
15. The inferior pancreatic artery was also ligated, after the dissection of the SMA in the root of the aorta, about 2 cm caudal to the CT.
16. The pancreas was excised by dissection and individual ligation and division of the small vessels from the SMA to the pancreas.
17. The portal ring around the PV was dissected free from the surrounding structures.
18. The proximal and distal duodenum were ligated and transected.
19. The inferior and anterior aspect of the gland is attached to the mesocolon, which had to be transected to remove the organ completely in finishing the total pancreatectomy.
20. The pancreas was ready to be removed after sectioning of the portal ring and after transection of the vasculature.

### Pancreatic lobes

The pancreas is composed of three lobes featuring a nodular surface with irregular margins (**Figure A.1** and **Figure A.2**). The “splenic” lobe (corresponding to the tail and body in the

human pancreas) is situated posteriorly and is attached to the spleen and the stomach. The “duodenal” lobe (corresponding to the head of the pancreas) is located adjacent to the duodenum while the “connecting” lobe (corresponding to the uncinate process) is an extension of the pancreas which is attached to the anterior aspect of the portal vein. There is a “bridge” of pancreatic tissue serving as an anatomical connection between the splenic and connecting lobes.

### Arterial anatomy

The abdominal aorta is retroperitoneal. The viscera had to be moved aside and the parietal peritoneum had to be removed to locate the aorta. The aorta was immediately dissected from the rest of the tissue. The CT was the first branch off the abdominal aorta infra-diaphragmatically and branched into the splenic artery, the LGA, and the common hepatic artery, as is common in the human (**Figure A.3a**). These arteries were immediately identified and transected distally to the pancreas. The splenic artery was the first branch identified, dissected, and tied. The posterior or dorsal pancreatic artery (PPA) is a small pancreatic branch originating from the splenic or hepatic artery and was next identified along the upper border of the pancreas. In some cases the PPA can have its origin more proximal off of the splenic artery, but distal to the celiac trifurcation. In some animals, more than one PPA were identified with large variability in size. The other two main branches from the CT were then identified. The first was the LGA, which runs parallel to the left gastric vein to supply the stomach, and the other was the common hepatic artery which supplies the liver with arterial blood. The proper hepatic artery and common bile duct were ligated and divided. The gastroduodenal artery arises from the hepatic artery before its bifurcation into the right and left hepatic artery. The pyloric region of the gastroduodenal artery exhibits two branches that supply the duodenal lobe of the pancreas: (1) the superior pancreaticoduodenal artery and (2) the right gastroepiploic (or gastromental) artery. The superior pancreaticoduodenal artery supplies the descending duodenum in addition to the DL. This artery

anastomoses with the inferior pancreaticoduodenal artery that originates from the SMA. The pancreaticoduodenal vascular arcade runs between the pancreas and the duodenum, and also extends branches to both organs.

Caudal to the CT was the SMA and the renal arteries (found by following the abdominal aorta to the level of the kidneys). The SMA and the SMV were isolated at the lower edge of the pancreas on the left side of the PV. The SMA gives branches (jejunal arteries, right colic artery, middle colic artery, and ileocolic artery) that supply the distal part of the descending duodenum to the proximal part of the ascending colon. The CL, the bridge, and the inferior aspect of the SL are vascularized by an arterial branch, the inferior pancreatic artery, which emerges from the inferior pancreaticoduodenal arterial arcade (**Figure A.3b**).

In order to study which lobes are supplied by which main arteries, the aorta was cut open longitudinally and then the CT and the SMA were cannulated separately. Then, colored saline was infused through them to highlight (by introducing visible contrast) the distribution of the arterial blood supply. Once the infusion was completed, the vascular anatomy was mapped by recording the regions supplied by the CT and SMA, respectively, and by dissecting to determine the borders of these regions. The differently-colored saline infusions were surprisingly visible, even to the naked eye. The normal pig pancreatic anatomy along with the major variants are presented in **Figure A.4a** and **Figure A.4b** respectively.

#### *Venous blood outflow (drainage)*

The PV collects the blood from stomach, pancreas, intestine, and spleen. The PV, on its way from the root of the mesentery to the liver, penetrates the pancreas at an acute angle so that it lies caudally on the ventral surface and rostrally on the dorsal surface of the pancreas. The PV has two branches which drain into it, the splenic vein and the SMV. The splenic vein drains the body

and tail of the pancreas and it is partly surrounded by pancreatic tissue. Veins draining blood from the stomach (left gastric vein, left gastroepiploic vein) also come out into the splenic vein.

The SMV passes through the portal ring receiving the inferior pancreaticoduodenal vein. The inferior mesenteric vein (IMV) usually flows into the SMV, which would be considered an unusual variation in the human anatomy. Small branches drain the CL into the SMV. The gastroduodenal vein empties into the SMV immediately before its junction with the splenic vein. The gastroduodenal vein receives small veins from the DL. Peripherally, the gastroduodenal vein receives the superior pancreaticoduodenal vein which anastomoses with the inferior pancreaticoduodenal vein.

#### Pancreatic duct

Following dissection, the pancreas was removed from the viscera utilizing an *en bloc* style procurement technique and placed onto a cooled dissection tray for trimming. The next step was the cannulation of the pancreatic papilla. In some cases, the pancreatic duct was cannulated *in situ* during the dissection of the viscera. Ductal anatomy was investigated by infusing colored saline into the main pancreatic duct (**Figure A.1**) while clamping access to the CL (position 1 in **Figure A.2**) and tracing the color change. Next, the CL was infused with a differently colored saline solution while access to the DL was clamped off (position 2 in **Figure A.2**). The pancreas was then further dissected to determine the extent of ductal communication between the lobes. A classification scheme for the different types of pancreatic ductal networks was designed by observing the ductal anatomy (**Figure A.5**).

#### Statistical Analysis

We performed a descriptive analysis of the number of cases reporting median and extreme, average, and standard deviation (SD). For statistical analyses, we used the Statistical Package for Social Sciences program (SPSS Inc, Chicago, USA).

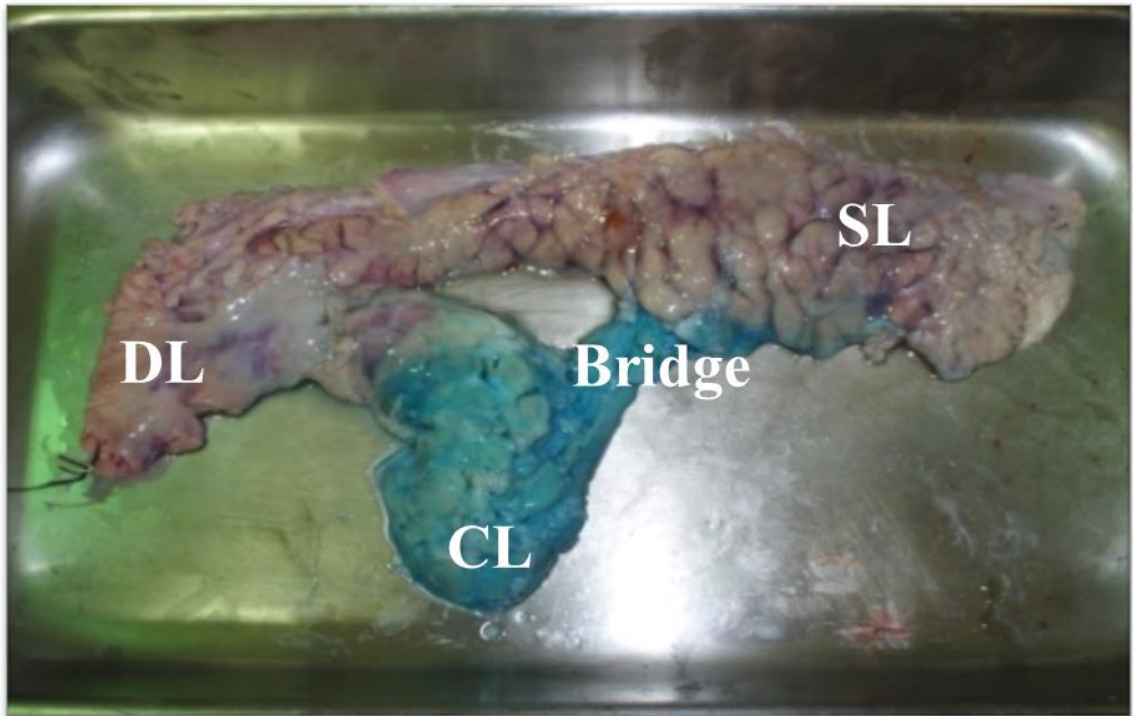


**Figure A.1: The Lobes of a porcine pancreas.** The divisions between the lobes were determined by flushing the arterial system with preservation solution that contained a food-grade dye. Different colors were used for different arteries. For this pancreas, the celiac trunk was flushed with red dye, and the superior mesenteric artery was flushed with blue dye.

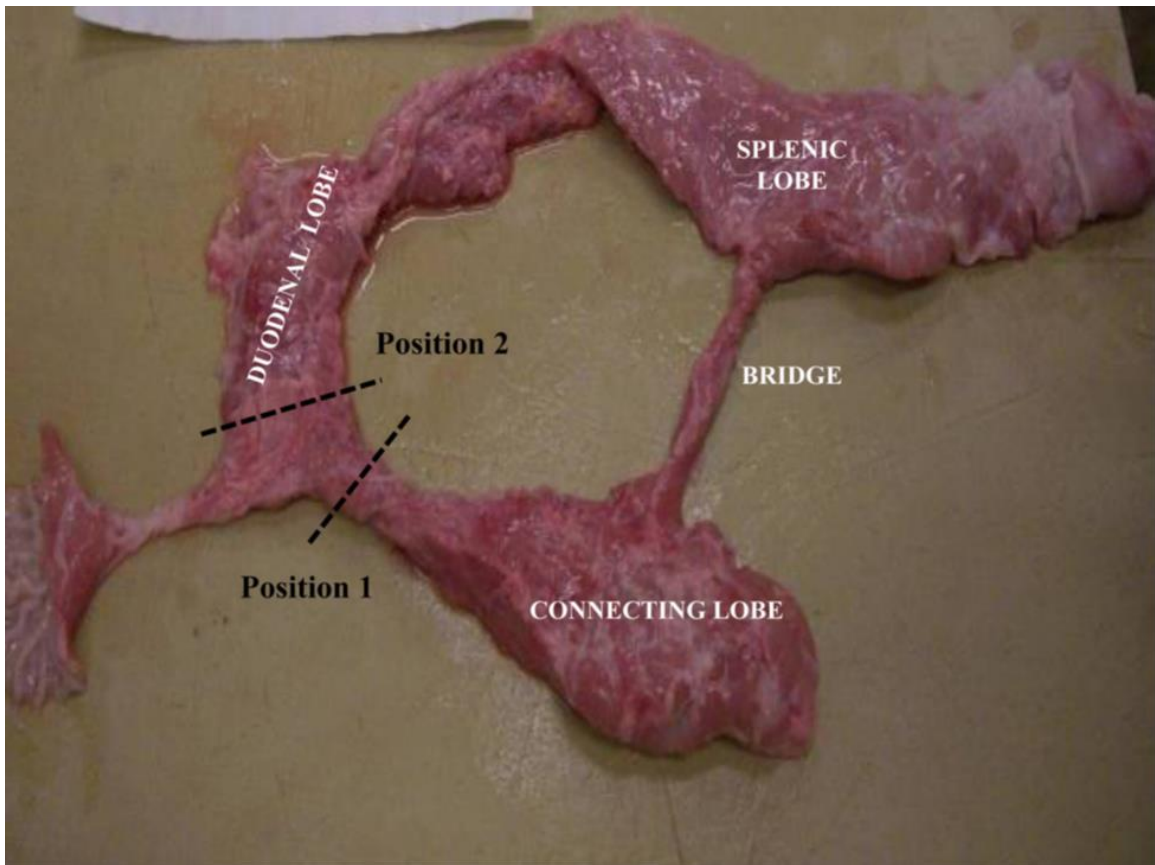


**Figure A.2: Porcine Pancreas bridge communication.** Photograph of an excised pig pancreas exhibiting normal anatomy with the duodenal, splenic, and connecting lobes, as well as the bridge. Ductal connections were obstructured with a clamp to determine if there was ductal communication through the “bridge” portion between the splenic lobe and the connecting lobe. Position 1: Dotted lines indicate the positioning of the clamp restricting flow to the connecting lobe. Position 2: Dotted lines indicate the positioning of the clamp restricting flow to the duodenal lobe.



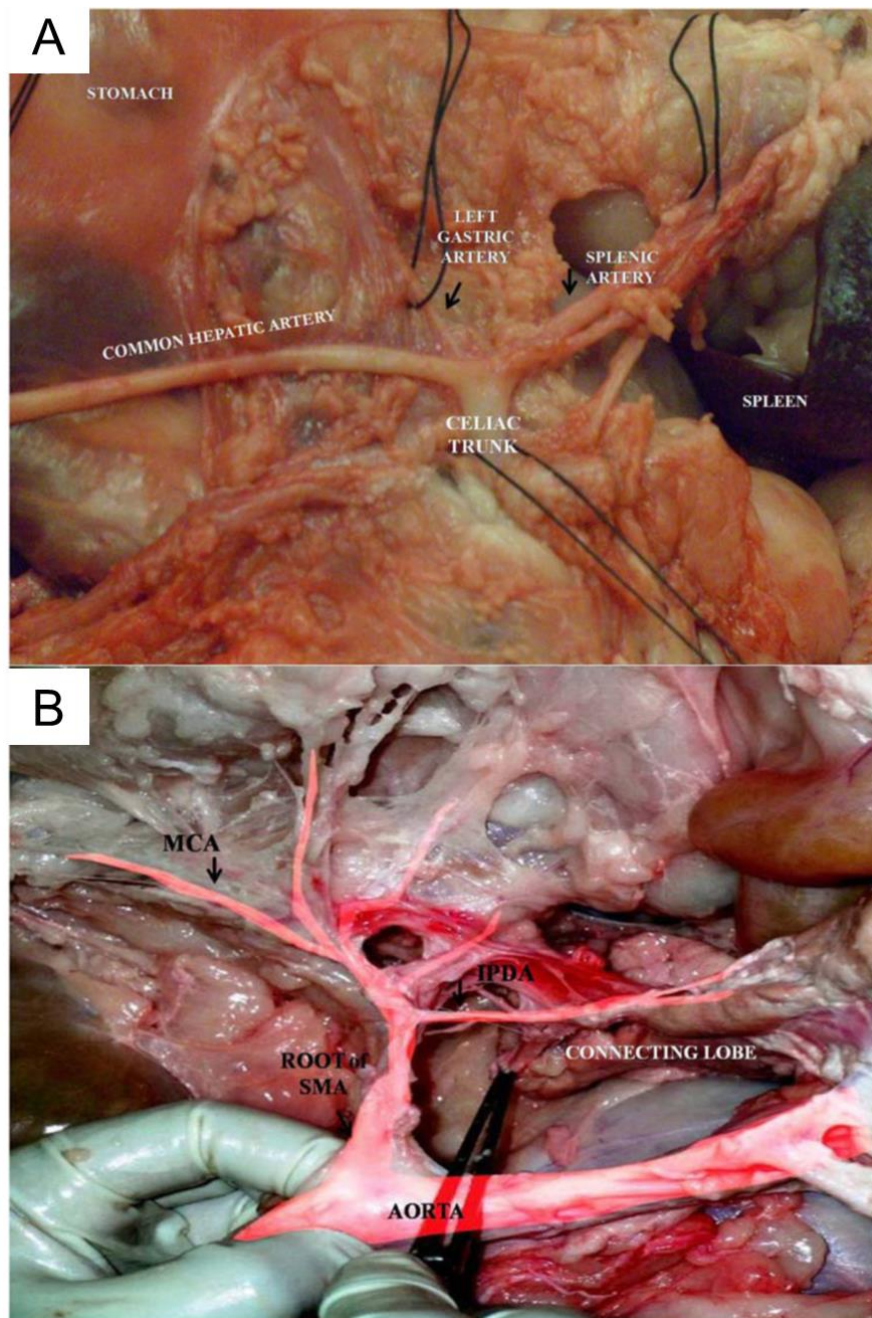


**Figure A.3: Pig pancreas arterial anatomy.** (A) Celiac trunk and the main branches (splenic artery, hepatic artery, and left gastric artery). (B) Arterial system (superior mesenteric artery with distal branches). The branch of SMA to pancreas (inferior pancreaticoduodenal artery) is distributed mainly in the connecting lobe. SMA, superior mesenteric artery; IPDA, inferior pancreaticoduodenal artery; MCA, middle colic artery.

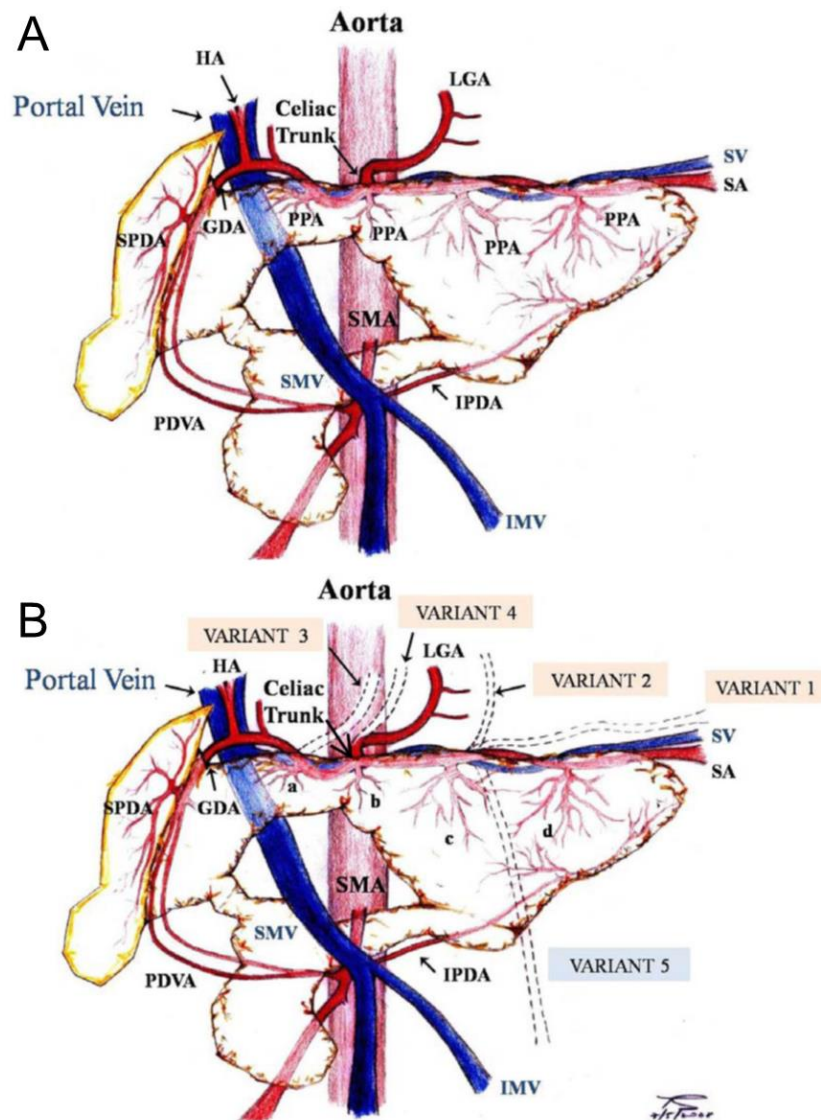
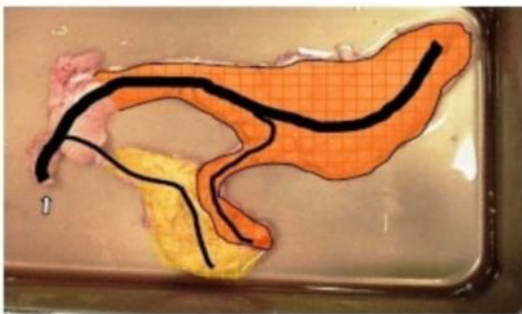


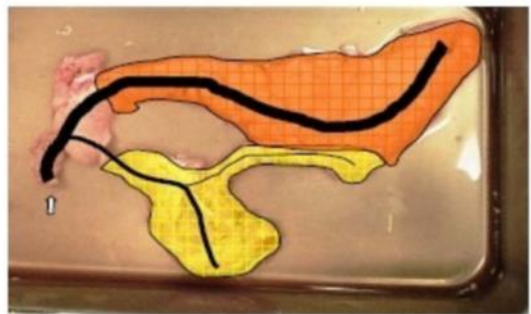
**Figure A.4: Porcine pancreas variational vascular anatomy.** Diagram of (A) normal vascular pancreatic anatomy and (B) the major variants of vascular pancreatic anatomy.

(A) GDA: Gastroduodenal artery; HA: Hepatic artery; IMV: Inferior mesenteric vein; IPDA: Inferior pancreaticoduodenal artery; LGA: Left gastric artery; PDVA: Pancreaticoduodenal vascular arcade; PPA: Posterior pancreatic artery; SA: Splenic artery; SMA: Superior mesenteric artery; SMV: Superior mesenteric vein; SPDA: Superior pancreaticoduodenal artery; SV: Splenic vein. (B) (a) Posterior pancreatic artery from the hepatic artery; (b) Posterior pancreatic artery from the celiac trunk; (c) Posterior pancreatic artery from the proximal splenic artery; (d) Posterior pancreatic artery from the distal splenic artery. GDA: Gastroduodenal artery; HA: Hepatic artery; IMV: Inferior mesenteric vein; IPDA: Inferior pancreaticoduodenal artery; LGA: Left gastric artery; PDVA: Pancreaticoduodenal vascular arcade; SA: Splenic artery; SMA: Superior mesenteric artery; SMV: Superior mesenteric vein; SPDA: Superior pancreaticoduodenal artery; SV: Splenic vein. VARIANT 1: “Accessory” splenic artery travelling along with the splenic artery; VARIANT 2: LGA from the splenic artery; VARIANT 3: LGA from the common hepatic artery; VARIANT 4: LGA from the CT; VARIANT 5: Inferior mesenteric vein draining into the splenic vein.

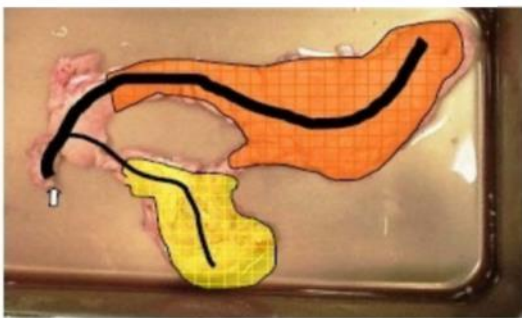
Type A



Type B



Type C



Type X

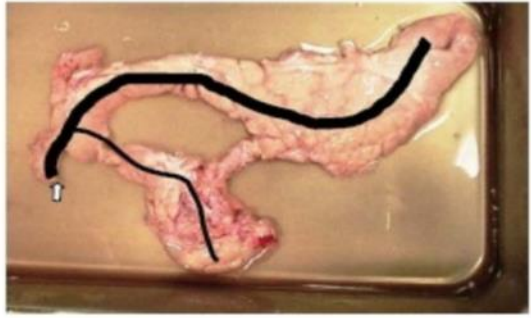


**Figure A.5: Ductal anatomy classification types.** Illustrations of the different ductal variational anatomies. Type A drains some of the connecting lobe through the bridge and splenic lobe into the primary duct. Type B drains part of the splenic lobe through the bridge and connecting lobe into the primary duct. Type C has no drainage through the bridge. Type X describes all other ductal anatomies that do not fit into categories A, B or C.

## ***Results***

The pig pancreas is a retroperitoneal organ, with comparable anatomical orientation and localization to the human. However, there are significant differences between the pig and human pancreas with respect to the number and distribution of the pancreatic lobes. In our series, 63 of the 65 porcine pancreata examined (97%), exhibited the three lobes (duodenal, splenic, and connecting) that we considered the normal representation of the pancreas in the porcine model (**Figure A.2**). One pancreas presented no “bridging tissue” between the SL and the CL, and another case exhibited a “ring-shaped” pancreas (the portal vein ran parallel to the duodenum and both were covered by the DL). A third pancreas that had the three expected lobes also contained an additional piece or elongation of pancreas tissue extending from the SL. After the pig pancreas was removed and trimmed each organ was weighed. The mean weight of the whole trimmed gland was  $347\pm 103$  g, with a range from 190 to 698 g. The mean weight of the different lobes was: duodenal,  $75\pm 9$  g (68–85); splenic,  $246\pm 50$  g (188–308); connecting,  $84\pm 17$  g (71–114) (**Table A.1**).

The arterial and venous vasculature was studied in 61 animals. It was observed that 51 pigs (84%) exhibited normal branching from the CT. We found variations in CT anatomy in 10 cases (**Table A.2**, **Figure A.4b**). All pigs exhibited traditional branching at the SMA, sending branches to the CL of the pancreas (inferior pancreaticoduodenal artery). However, one displayed a branch below the SMA that supplied the bowel and another presented additional branches from the SMA towards the colon without variation in the pancreatic supply. Another pig had a branch to the bowel that came off the SMA before the pancreatic branches. Anatomical findings related to the PPA were very diverse and are shown in **Table A.3** (**Figure A.4b**). It was found that the PPA most commonly branches from the hepatic artery (54%).

After inserting the cannulas into the root of the CT and the SMA, and infusing each one with different colors, it became apparent that the CT supplied the entire DL and the majority of the SL. The SMA supplied the CL, the bridge, and the inferior aspect of the SL.

The venous outflow occurred through the PV as a result of the merging of the splenic vein and SMV. The splenic vein typically traveled around the superior and posterior aspect of the pancreas and drained the body and the tail (SL). The rest of the pancreas was drained by branches coming from the SMV and the PV. In the cases we examined, the SMV and IMV merged to become the PV in all but one pig; the exception was the IMV draining into the splenic vein, as is the traditional case in humans (**Figure A.4b**). The left gastric vein drained into the splenic vein in all studied cases.

The pancreatic ductal network was traced by differential colored saline infusions in 36 pancreata (**Table A.4**). Fourteen of the 36 pigs (39%) of the pigs exhibited ductal communication between the CL and the other two lobes. Eleven pigs (31%) exhibited ductal communication only from the SL to the CL with the clamp in position 1 (**Figure A.5**, type A). In one case (2.8%) the communication only existed from the CL to the SL when the clamp was in position 2 (**Figure A.5**, type B). In two cases (5.6%), the colored infusion illustrated that the whole organ could be infused through from both communications, with the clamp in either position (Type A + B). Eighteen pigs (50%) of the pigs exhibited no ductal communication between the SL and CL, but featured communications solely from the DL (Type C). We classified a type X (neither type A, B, or C) ductal anatomy in four cases (11.1%). In this category, one pig exhibited no anatomical connection between the SL and CL (bridge atresia); another pig exhibited two separate ducts (one for the DL and SL, and the other for the CL); and in two pigs, the pancreata exhibited minimal ductal communication between the CL and distal SL after the initial infusion and clamping off of

the connection between the DL and SL. After clamping off the connection between the DL and CL, the infused colored saline flowed into the DL and the proximal SL.

**Table A.1: Porcine pancreas weights**

<b>Partition</b>	<b>Mean Weight (grams)</b>	<b>Weight Range (grams)</b>
<b>Whole Gland</b>	347.39±103.71	190-698
<b>Duodenal</b>	75±8.88	68-85
<b>Splenic</b>	246.26±49.6	188-307.50
<b>Connecting</b>	84.16±17.17	70.50-114

**Table A.2: Variations of the celiac trunk (CT) anatomy**

<b>VARIATIONS CELIAC TRUNK ANATOMY</b>	<b>n =10</b>
"Accessory" splenic artery traveling along with the splenic	1/10
Left gastric artery from the splenic artery	3/10
Left gastric artery from the common hepatic artery	2/10
Two left gastric arteries, one from the CT and another from splenic artery	2/10
Two left gastric arteries from the root of the CT	1/10
No CT. Hepatic and splenic arteries from aorta and LGA from splenic artery	1/10

**Table A.3: Variations in posterior pancreatic artery (PPA) anatomy**

<b>POSTERIOR PANCREATIC ARTERY</b>	<b>N</b>	<b>%</b>
Splenic artery	6	21.42
Hepatic artery	15	53.57
Splenic and Hepatic	6	21.42
Root celiac trunk	1	3.57
<b>Total</b>	<b>28</b>	<b>100</b>

**Table A.4: Types of pancreatic ductal structure**

<b>TYPE PANCREATIC DUCT</b>	<b>N</b>	<b>%</b>
<b>A</b>	11	30.6
<b>B</b>	1	2.8
<b>A + B</b>	2	5.6
<b>C</b>	18	50
<b>X</b>	4	11.1
<b>Total</b>	<b>36</b>	<b>100</b>



## ***Discussion***

There is a lack of literature describing the detailed anatomy of the pig pancreas. Comprehensive knowledge of the pig pancreatic anatomy is essential for improvements in pancreas procurement, preservation, and islet isolation protocols<sup>45,313</sup>. It has been reported that the pancreatic anatomy may vary from donor to donor<sup>314</sup> and several studies<sup>80,315</sup> have demonstrated the importance of pig strain on islet isolation outcome. Although the use of different breeds was considered, it was decided to focus on Landrace pigs, as this breed is considered to be the most suitable donor for islet isolation<sup>316-318</sup>. Recent literature<sup>319-321</sup> suggests that this breed is desirable for use in xenotransplantation since isolations yield large numbers of islets and pancreata contain a high islet volume density (3.4%) when compared to other breeds (1-2%). For this reason the investigation was focused on understanding the anatomy of the Landrace breed in detail. Krickhahn et al<sup>100</sup> demonstrated that pancreatic islet size may be an important parameter influencing islet yield after isolation and this may be dependent on the strain of the pig.

The present study provides more detailed information about the distribution of the lobes in the pancreas and demonstrates that almost 97% of pancreata exhibited three lobes. One pancreas presented no bridge and another case exhibited a “ring” shaped pancreas. It is important to recognize these kinds of variations if the porcine pancreas is to be used as a source of islets for clinical xenotransplantation. It is critical to understand the functional relationship between pancreatic ducts and drained pancreatic tissue for proper infusion of digestive enzymes and the subsequent isolation of islets. A lack of anatomical knowledge can result in poor or incomplete distension and digestion of the gland. In the 1970s, Calne et al<sup>322</sup> had described two lobes attached near the duodenum to the body of the pancreas. Other authors<sup>323</sup> divided the pig pancreas into three parts, but named these parts differently as compared to our study: body of the pancreas (corpus pancreatis), right lobe of the pancreas (lobus pancreatis dexter), left lobe of the pancreas

(lobus pancreatis sinister). Kumagai et al<sup>324</sup> described the pancreas as consisting of the tail, body, head, and the bridge lobes. Gänger et al<sup>325</sup>, described the pig donor operation to obtain duodenopancreaticosplenic specimen for experimental transplantation. They located the orifice of pancreatic duct in the distal tip of the uncinate process, which corresponds to a duodenal lobe according to our nomenclature. Our data provides a reliable system to classify the pancreatic lobes and the variants in the anatomy eliminating inconsistency in the naming and distribution of the lobes described in the literature; this is an important point with major implications in the field of pig islet isolation and xenotransplantation.

The present study has demonstrated 10 variations related to the CT anatomy and normal branching coming from the SMA. The distribution and disposition of the PPA were unpredictable (**Table A.3**). The most common origin of the PPA in the series of Morel et al<sup>309</sup> was from the splenic artery along the upper border of the pancreas. They found that only 2 pigs exhibited a major pancreatic artery coming from the hepatic artery, but a small arterial branch from the splenic artery was also observed. Shokouh-Amiri MH et al<sup>308</sup> had classified the variations in arterial blood supply of the porcine pancreas with three types as they related to the major pancreatic artery (PPA in our study). Nonetheless, they found a PPA arising from the root of the CT. They concluded that segmental pancreatic autotransplantation was technically possible in all animals regardless of the type of arterial supply if the anatomy of the vasculature is known adequately. In contrast, Traverso and McFarlane<sup>311</sup>, based on the description of variations in the arterial blood supply to the body and tail of the pancreas, concluded that the pig is unsuitable for pancreatic autotransplantation studies.

Some authors<sup>326</sup> used the tail of the pancreas for various experiments, to minimize complexities associated with variations in the anatomy of the head of the pancreas. To develop a pig model either for whole or segmental pancreas transplantation, the arterial anatomy of the pancreas must

be precisely mapped out. The blood supply of the pancreas is provided by the celiac and superior mesenteric arteries. The DL of the pancreas receives its blood supply from the superior pancreaticoduodenal artery, which is in all cases a branch of the gastroduodenal artery. In contrast with this finding, Schröder et al<sup>327</sup>, described the origin of the superior pancreaticoduodenal artery from the splenic artery. The SL is supplied by the splenic artery and the inferior pancreaticoduodenal artery which branches off from the SMA and also supplies the CL and the bridge as well.

After the abdominal aorta was opened through the anterior wall and cannulas were placed into the CT and SMA, the organ was infused with colored saline. It was observed that the color was distributed homogenously throughout the whole gland. The finding demonstrated that CT and SMA cannulation is a suitable technique to sufficiently perfuse the pancreas and could be used in other experiments related to pancreas preservation. In fact, Zhang et al<sup>328</sup> used the pig model for pancreaticoduodenal transplantation and the donors were perfused via the abdominal aorta without clamping the portal venous outflow. Gäbel et al<sup>329</sup>, used the entire pancreas with intact vascular supply to get a graft from a pig donor to transplant in a pig recipient. The organ was perfused via the CT only with no mention of the SMA. These authors described early graft failure caused by concomitant acute pancreatic necrosis, probably followed by vascular complications. To avoid these kinds of complications, it could be very useful to dissect the CT and the SMA selectively to ensure good perfusion of the entire pancreas, even if you use it for islet transplantation or for a vascularized graft for pancreas transplantation.

In our study, as well as in others<sup>308,309</sup>, few variations were found in the venous drainage of the pancreas. In only one pig the IMV drained into the splenic vein instead of the SMV.

The impetus to study the pancreatic ductal system was to better understand the ductal branching structure for the purpose of applying the knowledge to the development of enzyme perfusion and

pancreatic distention techniques within the context of the pig model. All but one pancreas exhibited only one main pancreatic duct. Only in one case we found two separate ducts, one for the DL and SL and the other for the CL. There are some discrepancies in the literature. König-Liebich<sup>323</sup> described the dual origin of the pancreas as arising from dorsal and ventral primordial buds, stating that some species have two pancreatic ducts, and the pig is one of them. The accessory pancreatic duct enters the duodenum at the minor duodenal papilla located distal to the major duodenal papilla<sup>310</sup>. On the other hand, Swindle<sup>330</sup> asserted that the pancreas is related to the proximal duodenum with a single pancreatic duct entering the duodenal lumen distal to the common bile duct. Morel et al<sup>309</sup> in a series of 49 Yorkshire pigs, found one pancreatic duct emerging from the lower right part of the pancreatic head, draining into the second part of the duodenum. Only in one instance of this study was an accessory duct found draining the connecting lobe into the third part of the duodenum. Pitkaranta et al<sup>331</sup>, developed an experimental model of chronic pancreatitis in the pig. They observed a papilla obstruction failure rate of 30%, suggesting the presence of an accessory duct. However, our data do not support these findings.

Even though the pancreatic ductal system and its variability remain the Achilles' heel in islet isolation, the detailed anatomy described here helps to overcome the difficulties associated with complete distention of the gland. Understanding the variable ductal distribution facilitates simple adaptation of technical distention protocols to make the process more efficient and effective.

In conclusion, the vascular anatomy of the pig pancreas makes it suitable for perfusion via the suprarenal aorta, as is the case in humans. The knowledge of the variations in the anatomy in the vascular supply could help to develop successful new models of whole or segmental pig pancreas preservation and transplantation and islet isolation and transplantation<sup>45,313</sup>. However, the ductal anatomy can be highly variable, with branching from the connecting lobe being extremely

inconsistent. If cannulation is not carefully performed, one portion of the organ may not be properly distended with proteolytic enzymes, resulting in a substantial loss of the islets present in this portion. Careful consideration of all these anatomical findings is likely to facilitate less variable and more economical pig islet isolation for research studies and therapeutic purposes.

## **Appendix B PERSUFFLATION IMPROVES PANCREAS PRESERVATION**

Sections of this chapter are reproduced in whole, or in part from the following publications with permission:

Scott WE 3rd, **Weegman BP**, Ferrer-Fabrega J, Stein SA, Anazawa T, Kirchner VA, Rizzari MD, Stone J, Matsumoto S, Hammer BE, Balamurugan AN, Kidder LS, Suszynski TM, Avgoustiniatos ES, Stone SG, Tempelman LA, Sutherland DE, Hering BJ, Papas KK. "Pancreas oxygen persufflation increases ATP levels as shown by nuclear magnetic resonance." *Transplant Proc.* 2010 Jul-Aug;42(6):2011-5.

Some additional methods details are included in this adaptation of the published manuscript<sup>271</sup>, and some supplemental results and discussion are included in a separate section at the end.

Referenced Thesis:

Scott III, William Earl. (2012). Application of NMR in the characterization of existing and development of new methods for pancreas preservation. Retrieved from the University of Minnesota Digital Conservancy, <http://purl.umn.edu/143984>

License and agreement documentation is included in **Appendix G**.

**Acknowledgements:** The authors thank Dr. T.C. Aasheim, Dr. L. Guenther, and Dr. T. Tanaka for help with early technique development; P.C. Williams, K. Albeck, and S. Walsch for technical assistance with the manufacturing of MR-compatible preservation containers; B. Perrault for surgical assistance; and Dr. K.S. Maynard, D. Dudero, G. Wildey, M.L. Graham, L. Mutch, and H. Nelson for administrative assistance. Research funding provided by a grant from the National Center for Research Resources (U42 RR016598), National Institutes of Health (NIH), National Institute of Diabetes and Digestive and Kidney Diseases (R43 DK070400), NIH, the Schott Foundation, and the Carol Olson Memorial Diabetes Research Fund

## **Pancreas oxygen persufflation increases ATP levels as shown by nuclear magnetic resonance**

### ***Summary***

Islet transplantation is a promising treatment for type 1 diabetes. It is important to maximize viable islet yield due to a shortage of suitable human pancreata, high cost and the large dose of islets currently required for long-term diabetes reversal. Traditional methods of pancreas preservation have been identified as suboptimal with oxygenation thought to be one of the key areas for improvement. One method of delivering oxygen throughout the organ, persufflation (PSF), is explored here. Human pancreata were obtained by a combined pancreas-liver procurement from brain-dead donors. Porcine pancreata were procured by *en bloc* viscerectomy from heparinized non-heart beating donors. Porcine pancreata were divided with lobes either preserved by TLM or PSF. Following procurement, organs were transported to a 1.5 T magnet for  $^{31}\text{P}$ -NMR spectroscopy to investigate their bio-energetic status by measuring the ratio of ATP-to-inorganic phosphate (ATP: $\text{P}_i$ ) and by assessing PSF homogeneity by MRI. Prior studies have shown that TLM can effectively raise ATP: $\text{P}_i$  levels in rat pancreata. When a similar study was attempted in the larger porcine model, ATP: $\text{P}_i$  levels decreased to almost undetectable levels. When human or porcine organs were persufflated, ATP: $\text{P}_i$  was elevated to levels similar to those observed in the rat model. MRI showed that pancreatic tissue was homogeneously filled with gas. Methods developed for human and porcine pancreas PSF oxygen delivery throughout the organ. This elevates ATP levels during preservation and may improve current islet isolation outcomes while enabling the use of marginal donors, expanding the donor pool.

## ***Introduction***

Islet transplantation is an emergent treatment alternative for type 1 diabetes<sup>9,332</sup>. Currently, clinical islet allotransplantation is limited by a shortage in suitable donor organs, loss of islets throughout the islet manufacturing and engraftment process, as well as by the high cost and the large dose of islets required for long-term diabetes reversal. Islets may be predisposed to death before or during isolation due to improper handling of the organ during procurement and/or suboptimal cold preservation (CP) during transport. Significant research effort has focused on investigating the efficacy of the two-layer method (TLM), the present state-of-the-art for pancreas preservation<sup>333–338</sup>. In the late nineties, many centers reported improvements in islet isolation outcome using TLM for CP. These improvements were attributed to an increase in tissue ATP due to enhanced tissue oxygenation with TLM compared to the previously used CP in University of Wisconsin (UW) solution alone<sup>3–8</sup>. However, recent studies have suggested that TLM is not able to oxygenate large portions of human or porcine pancreata during CP<sup>20,339</sup>. In addition, several large retrospective analyses have found no significant improvement in isolation outcomes for pancreata stored with TLM when compared to pancreata stored on UW solution alone<sup>340–342</sup>. Therefore, it is of great importance to develop novel methods of preservation, which can better oxygenate large organs throughout CP. One such preservation method investigated here is persufflation (PSF), or vascular gas perfusion. PSF has been investigated in the heart, liver and kidney, but until now not reported for pancreas preservation<sup>343–352</sup>. This method is investigated in more detail in the next section; however, it is equally important to develop methods for evaluating the efficacy of preservation methods. Current methods of organ viability assessment are limited to examination of donor records, histopathology assessment,<sup>16</sup> or visual and manual inspection. These methods are not definitive or quantitative, and thus require very large groups to make scientific comparisons. In **Chapter 2**, we presented a method for measuring solid organ viability



using whole organ oxygen consumption rate (WOOOCR)<sup>30</sup>, and in this section, we introduce another method for solid organ viability measurement. To evaluate the viability of organs and to compare preservation methods, we developed equipment and techniques for non-invasive organ assessment using <sup>31</sup>P magnetic resonance spectroscopy (<sup>31</sup>P-MRS). <sup>31</sup>P-MRS is an established technique for monitoring the amount of ATP present relative to inorganic phosphate (P<sub>i</sub>) in tissues. <sup>31</sup>P-MRS has been extensively used to study tumor biology, bioenergetics as well as metabolism and the health status of organs, such as the heart, brain, kidney, liver, and recently, the pancreas<sup>313,353-361</sup>. The non-invasive nature of <sup>31</sup>P-MRS and its ability to provide information in real time make it an effective and powerful tool for monitoring the bio-energetic status of pancreata during CP.

Hypoxia experienced during CP has been shown to cause depletion of ATP in organs, and results in impairment of mitochondrial function<sup>19</sup>. There is evidence that this effect can be reversed by raising the pO<sub>2</sub> in perfused medium<sup>19</sup>. The hypothesis presented herein is illustrated in **Appendix F**. We predict that ATP levels will not be detectable in large organs preserved by TLM and that levels are expected to rise when oxygen is introduced by briefly exposing the organ to PSF. Furthermore, we predict organs that are continuously oxygenated by PSF during preservation will maintain higher levels of metabolic function resulting in maintenance of ATP levels during preservation. ATP levels in all CP organs are expected to decrease during the preservation period indicating general loss of organ viability during the preservation period. The large size of porcine and human organs will prevent sufficient oxygen diffusion to the center of the organ. The majority of the organ will not be adequately oxygenated during TLM preservation<sup>339</sup>. To assess the efficacy of preservation of large organs, we compared the ATP:Pi ratios of organs preserved with TLM compared with PSF. We also compare these data with that collected from our previous study of murine pancreata<sup>313</sup>.

## ***Materials and Methods***

### *Procurements*

Rat pancreata were investigated as detailed by Scott WE et al<sup>313</sup>. All procedures using laboratory animals were approved by the University of Minnesota IACUC. Pig pancreata and kidneys were procured by *en bloc* viscerectomy from heparinized non-heart beating Landrace donors as detailed by Ferrer J, et al<sup>38</sup>. Organs were then preserved either with TLM or by PSF. All procedures using laboratory animals were approved by the University of Minnesota IACUC. Human pancreata were procured by a combined pancreas-liver procurement from brain-dead donors. In short, after the adequate exposure was obtained through a cruciate abdominal incision, the preliminary dissection was performed with intact donor circulation. Once the donor was fully heparinized, the distal aortic cannula was inserted with the infusion of the chilled preservation solution after the encircled supraceliac aorta was cross-clamped. It was left up to the liver team to decide whether portal venous infusion should be performed through cannulation of the inferior mesenteric vein. The venous system was decompressed via venotomy. The organs remained *in situ* until the cold infusion was complete. The pancreas was harvested either *en bloc* with the liver and separated on the back table or the research pancreas was removed once the clinical organs were harvested. Research consent was obtained from all donor families before procurement.

### *Static Preservation (TLM)*

Lobes preserved by TLM were preserved as previously described<sup>362</sup>. In brief, lobes were suspended halfway between 1 L of CP solution and perfluorodecalin, which was pre-oxygenated for 1 hour prior to preservation by bubbling with 99% oxygen gas. Preservation was performed in specially constructed vessels composed of magnetic resonance (MR)-compatible materials. Drawings and pictures of this equipment are included in **Appendix F**.

### *Persufflation*

PSF methods and outcomes are discussed in more detail in the next section, but briefly, all persufflated organs were oxygenated by pumping 20 ml/min of 40% humidified gaseous O<sub>2</sub> to both the superior mesenteric artery and either the splenic artery (human) or celiac trunk (pig) utilizing an electrochemical oxygen concentrator (EOG, Giner Inc, Newton, MA). Following procurement, organs were transported to an MRI facility and <sup>31</sup>P-MRS was performed on a 1.5 T magnet to investigate their bio-energetic status by measuring the ratio of ATP to inorganic phosphate (ATP:P<sub>i</sub>).

### *<sup>31</sup>P-NMR Spectroscopy*

For the pig and human organs, <sup>31</sup>P-MRS was done in the 1.5 T magnet by placing a surface coil tuned to 25.85 MHz as close to the organ as possible. A diagram and images of the coil are shown in **Appendix F**. Each critical peak in the <sup>31</sup>P-MRS spectrum was analyzed with an NMR analysis package (ACD 1D-NMR software) to determine the relative integral areas of each peak. The areas of the α-, β-, and γ-ATP peaks were compared with the area of the inorganic phosphate (P<sub>i</sub>) peak to compare the bio-energetic status of the organs. A schematic of how organs were placed into the magnet and maintained during preservation is included in **Appendix F**. The organ was cannulated as described, and the cannulas were connected access points on an MRI safe organ container. Long sections (approximately 10 meters) of tubing were used to connect the EOG to the organ container to achieve PSF inside the MRI system, and during MRS acquisition as needed. The organ was maintained at hypothermic temperatures (< 8 °C) by placing the organ container inside a specially constructed MRI safe heat exchanger, which was cooled using a standard refrigerated circulating water bath. These custom components are described in more detail in **Appendix F**.

### *MRI*

All proton imaging ( $^1\text{H}$ -MRI) was done at 1.5 T in a birdcage coil tuned to 63.85 MHz. Assessment of the homogeneity of PSF was done by observing the presence of gas in the vasculature by the negative contrast it develops during MRI.

## ***Results***

<sup>1</sup>H-MRI images of PSF organs typically exhibited the presence of negative contrast (indicating the presence of gas in the vasculature) in 90% of the tissue. Representative images from a PSF pancreas and a pancreas that exhibited significant gas leakage are shown in **Figure B.3A and B**. Also shown in **Figure B.3C** is a well PSF porcine kidney showing typical vascular branching structure and a non-PSF kidney that exhibited no negative contrast. As previously reported, rat pancreata exposed to TLM exhibited high levels of ATP:P<sub>i</sub><sup>313</sup> (**Figure B.2A**). When we investigated porcine pancreata preserved with TLM, ATP levels dropped to nearly undetectable levels (**Figure B.2B**). These data were similar to data collected from porcine organs preserved in preservation solution alone. This suggests the inability of TLM to adequately supply the majority of the pancreas with oxygen in larger organs, such as from pigs or humans. However, when we investigated human pancreata undergoing PSF, we observed elevated ATP:P<sub>i</sub> levels similar to those observed from the rat model preserved by TLM (**Figure B.2C**). When PSF was abruptly stopped and the pancreas was exposed to static preservation alone, ATP:P<sub>i</sub> quickly decreased to undetectable levels, similar to those observed from porcine organs preserved by TLM. This observation confirms that PSF was responsible for the elevated β-ATP:Pi observed during preservation, and that <sup>31</sup>P-MRS can detect and quantify changes in ATP levels of large organs when oxygen is provided by PSF.

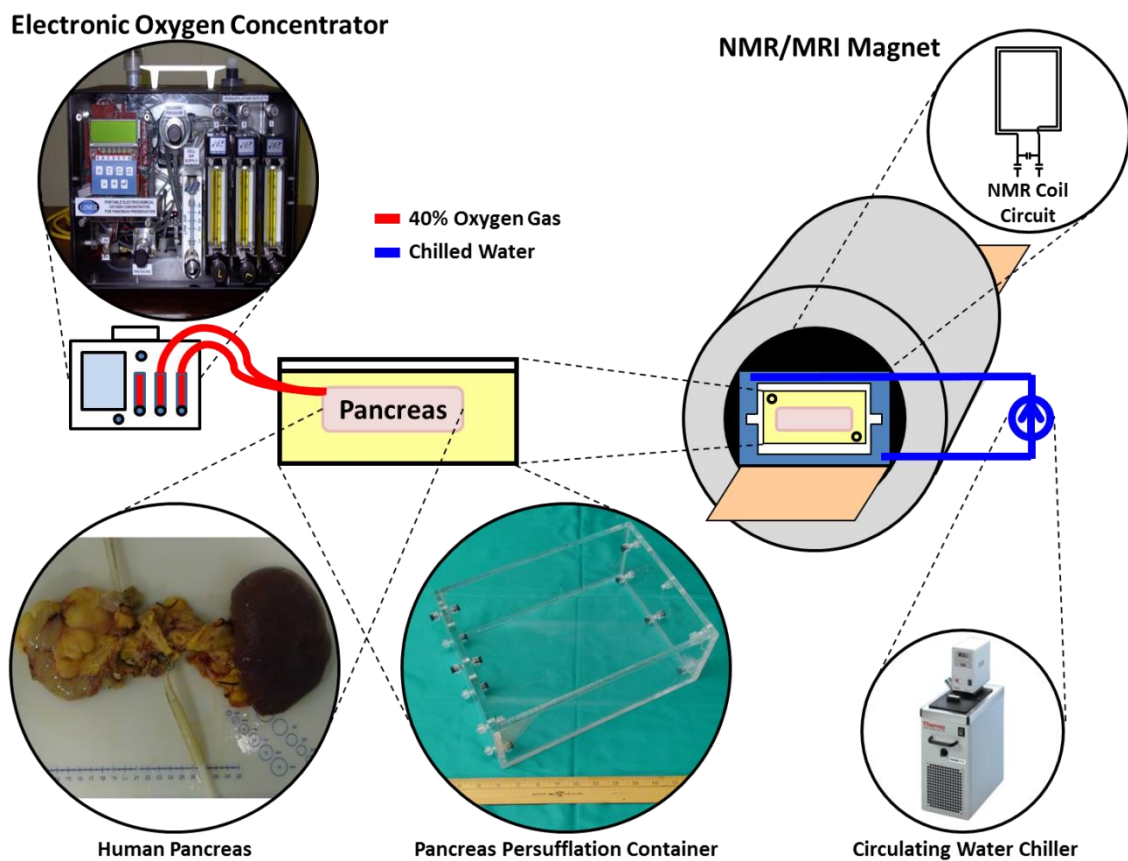


**Figure B.1: Schematic of  $^{31}\text{P}$ -MRS studies.** Diagram illustrating how the pancreas was placed into the magnet during data acquisition.

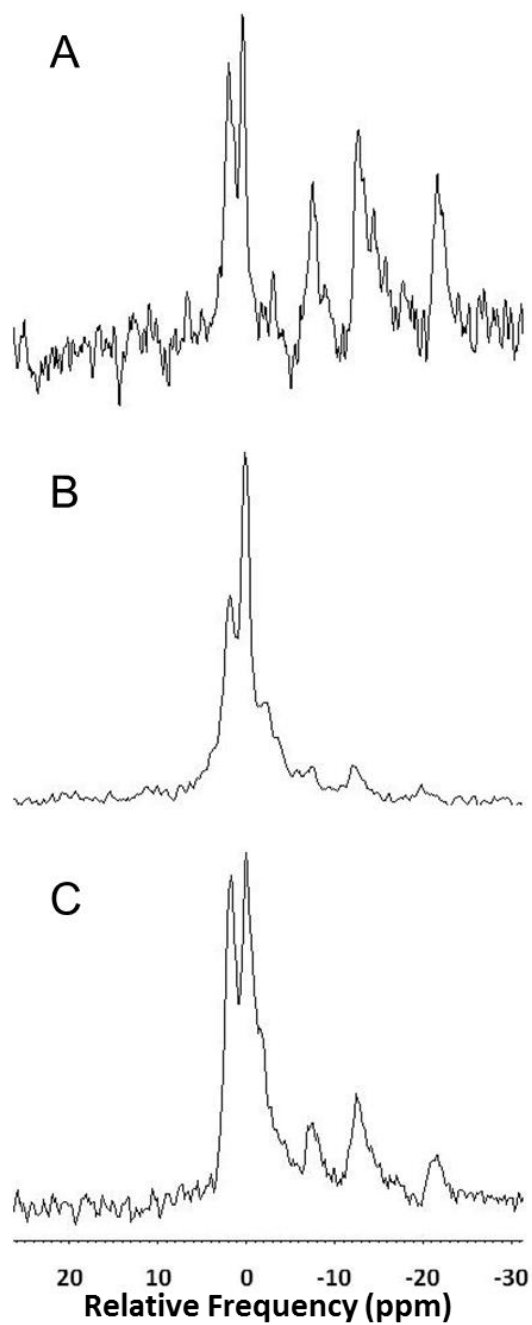


**Figure B.2: ATP spectra from rat, pig, and human pancreata.**  $^{31}\text{P}$ -NMR spectra acquired from a) a rat pancreas preserved by the Two-Layer Method (TLM); b) a porcine pancreas preserved by TLM; c) a persufflated human pancreas. Peak numbering corresponds to: (1) phosphomonoester, (2) inorganic phosphate, (3) phosphodiester, (4)  $\gamma$ -ATP, (5)  $\alpha$ -ATP, and (6)  $\beta$ -ATP.

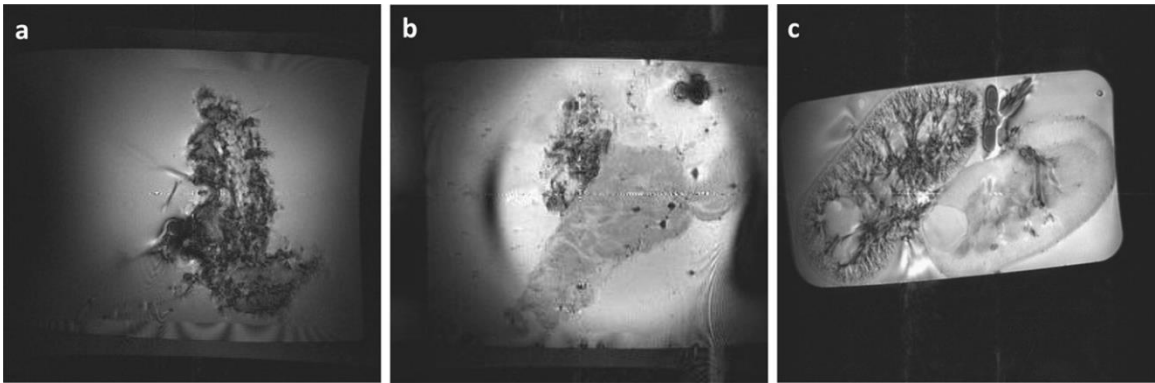


**Figure B.3: MRI of persufflated pancreas.** Gradient echo MRI of a) a well persufflated pancreas with gas filling the vasculature indicated by dark regions. This is typical of what was observed in general. b) A pancreas with poor persufflation which had a large arterial gas leak. c) A well persufflated kidney (left) and a non-persufflated kidney (right). The persufflated kidney shows typical vascular branching(dark regions).



## ***Discussion***

In this paper we utilized a  $^{31}\text{P}$ -MRS method to evaluate the metabolic status of organs undergoing CP, and to non-invasively assess the efficacy of different preservation protocols (i.e., TLM, PSF) in maintaining ATP levels (a direct reflection of respiration and a measure of organ health and viability) in rat, porcine, and human organs. Previous investigation demonstrated that, in the rat pancreas model, CP with TLM results in dramatically improved ATP levels<sup>313</sup>. To study the impact of TLM, CP methods were investigated in porcine pancreata and the TLM was compared with a novel method of pancreas preservation, PSF, in pig and human models. ATP levels were consistently low for all large organs preserved by static methods, such as TLM. However, ATP levels of human and porcine pancreata undergoing PSF were consistently higher than those observed from organs exposed to static preservation, approaching levels observed from the smaller rat pancreata preserved by TLM. This is due to the improved oxygenation the tissue experiences during PSF by providing humidified oxygen directly into the bulk of the solid organ through the extensive, native and intact vasculature. This delivery method circumvents the problem of limited oxygen diffusion into the core of larger organs (such as human or porcine pancreata) associated with the static methods of preservation. MRI results support that PSF can actively supply most of the pancreas with gaseous oxygen during cold preservation.

## **Supplemental Results and discussion of $^{31}\text{P}$ -MRS measurements with PSF**

### ***Results:***

A series of  $^{31}\text{P}$ -MRS measurements were obtained from a small set of (N=4) individual human research pancreata during PSF immediately upon arrival to the lab. A representative spectrum from a human pancreas oxygenated by PSF with individual peak assignment and analysis is shown in **Figure B.4**. The resulting spectra from each organ were analyzed by identifying each critical peak and then fit assuming a lorentzian shape. The individual peak areas were calculated and then ATP levels are reported as ratios of ATP: $\text{P}_i$ . The results presented in **Figure B.5** show variability in the initial  $\beta$ -ATP: $\text{P}_i$  upon arrival, which appears to correspond to the amount of warm ischemia time (WIT) recorded in the donor records. One pancreas which was indicated to have no WIT did not fit this trend, and showed lower  $\beta$ -ATP: $\text{P}_i$  levels than expected.  $^{31}\text{P}$ -MRS measurements for one pancreas were continued for a 24 hour CP period, and the  $\beta$ -ATP: $\text{P}_i$  results are plotted in **Figure B.6**. PSF was started as soon as the pancreas arrived at the lab to obtain the initial “base-line” ATP levels, and PSF was continued for up to 24 hours. PSF was stopped between 8-12 hours to observe any decrease in ATP when oxygenation was stopped. Almost immediately following succession of PSF, the ATP levels were observed to drop significantly. When PSF was resumed, the  $\beta$ -ATP: $\text{P}_i$  then increased to approximately 50% of the initial base-line measurement.

The  $\beta$ -ATP levels proved to be more sensitive to oxygenation status than the total ATP ( $\alpha+\beta+\gamma$ ), and  $\beta$ -ATP: $\text{P}_i$  is reported for these studies with CP organs for this reason. Representative total ATP data from the same pancreas is also included in **Figure B.6** to illustrate this observation. Furthermore, additional human pancreata preserved with PSF were examined using  $^{31}\text{P}$ -MRS (N=4), and the complete data set is included in **Figure B.7**. These results show the maintenance

of ATP levels in organs with continuous PSF (n=7), and again, a single human pancreas with interrupted PSF showing the dramatic drop in ATP when oxygenation is stopped.

A single porcine kidney was examined in a similar study, and  $^{31}\text{P}$ -MRS measurements were collected during CP with continuous PSF for up to 80 hours. The results are presented in **Figure B.8**. For this kidney, PSF also stopped for a brief period between 7-9 hours of CP, and the  $\beta$ -ATP: $\text{P}_i$  levels also quickly decreased to near-zero, and recovered to approximately 50% of the initial measurement when PSF was resumed. Measured  $\beta$ -ATP: $\text{P}_i$  continued to fluctuate and generally decreased during the 80 hour CP time, but maintained 27% of initial levels at the end of the study.

### ***Discussion:***

The implications of the early studies in rats were that improved oxygenation provided by the TLM allowed for increased aerobic metabolic activity of the organ, which in turn increased the generation of available ATP. This is a reasonable assertion because the TLM will increase the oxygen available in the preservation solution, and will increase the oxygen partial pressure, and available oxygen at the surface of the organ. Oxygen will then diffuse into the organ and restore the aerobic metabolism of the tissues allowing for efficient production of ATP by oxidative phosphorylation. This outcome may decrease the production of harmful byproducts of anaerobic metabolism and allow for improved recovery when the organ is transplanted and exposed to physiological temperatures and oxygenation. This is an important finding, and laid the foundation for the hypothesis that increased oxygenation results in increased available ATP levels in tissues during CP. However, others have hypothesized that the rat model is not appropriate for the study of large organ preservation due to the relative size difference with human organs<sup>339</sup>. TLM provides oxygenation through diffusion of oxygen into the organ by exposing only the surface of the organ to increased levels of oxygen. This approach will only result in oxygenation of the

tissue near the outer surface of the organ, and will leave the internal aspects of the organ in a potentially harmful hypoxic state.

Elevated ATP:P<sub>i</sub> levels (when compared to static methods of CP like TLM) were observed in all large organs investigated when oxygenated by PSF, and a representative spectrum showing the relative integral areas is shown in **Figure B.4**. There was significant variability in organ viability (as indicated by ATP levels) upon arrival to the lab (**Figure B.5**), and these differences correlate with the WIT noted in the donor medical records. For one organ, the reported WIT did not fit with the observed trend. When the donor records were re-inspected, it was noted that the donor had experienced a 180 minute “hypoxic episode” prior to donation. Although this is not technically a period of WIT, this prolonged hypoxic stress may have resulted in damage to this sensitive organ. This observation may explain why this individual pancreas did not appear to follow the observed trend. <sup>31</sup>P-MRS may provide a “comprehensive picture” of the metabolic capability of an organ prior to transplantation, as it accounts for a large variety of stress factors that an organ experiences during CP.

Furthermore, these results demonstrate that β-ATP:P<sub>i</sub> ratios are a better indicator of oxygenation and metabolic status than total ATP:P<sub>i</sub>. **Figure B.6** clearly shows that most of the kinetic changes in total ATP are due to changes in the β-ATP peak. The total ATP:P<sub>i</sub> trends with β-ATP:P<sub>i</sub> for the duration of the study, but the changes appear to be “muted” when compared to β-ATP:P<sub>i</sub>. It is also observed that the β-ATP peak is more sensitive to oxygenation status, and this peak becomes un-detectibly small almost immediately after oxygenation by PSF is stopped, while the total ATP levels seem to reach a static depressed level without continuous oxygenation by PSF. This finding was unexpected, but may be a residual effect of the generally depressed metabolic state that tissues revert to when undergoing CP. The effect of decreased temperature (hypothermia) on the general metabolic activity of tissues is reasonably well understood, and this is the primary

impetus for employing CP techniques. When examining the process of aerobic metabolism, ATP is first de-phosphorylated to adenosine diphosphate (ADP) and an individual  $P_i$ . At 1.5 T magnetic field, the phosphate peaks of ADP overlap with the  $\alpha$ -ATP and  $\gamma$ -ATP peaks of ATP, and cannot be separately resolved. With the decreased metabolic activity of tissues during CP, the continued process for de-phosphorylation of ADP may be dramatically reduced resulting in a direct trade-off of ATP to ADP and  $P_i$ . This hypothesis would support the findings presented herein, that the  $\beta$ -ATP peak is the first one to disappear as aerobic metabolism progresses with the introduction of oxygen. This would also explain the relatively stable  $\alpha$ -ATP and  $\gamma$ -ATP peaks observed in these studies.

The total ATP: $P_i$  is also shown to decrease during the preservation period, and may reflect the general degeneration of tissues during CP, and could be indicative of irreversible tissue damage. These preliminary findings suggest that  $^{31}\text{P}$ -MRS could be a successful method for assessment of organ quality, and may be able to provide a quantitative measurement of organ viability. It is clear that increasing oxygenation of organs by PSF increases the aerobic metabolism of the tissues, and the  $\beta$ -ATP: $P_i$  ratio can be used as a sensitive indicator of aerobic metabolic activity of organs during CP. These results also confirmed that increased tissue oxygenation using PSF increases the  $\beta$ -ATP: $P_i$  and total ATP: $P_i$ , and furthermore appears to slow down the overall decline in ATP observed during prolonged periods of CP.

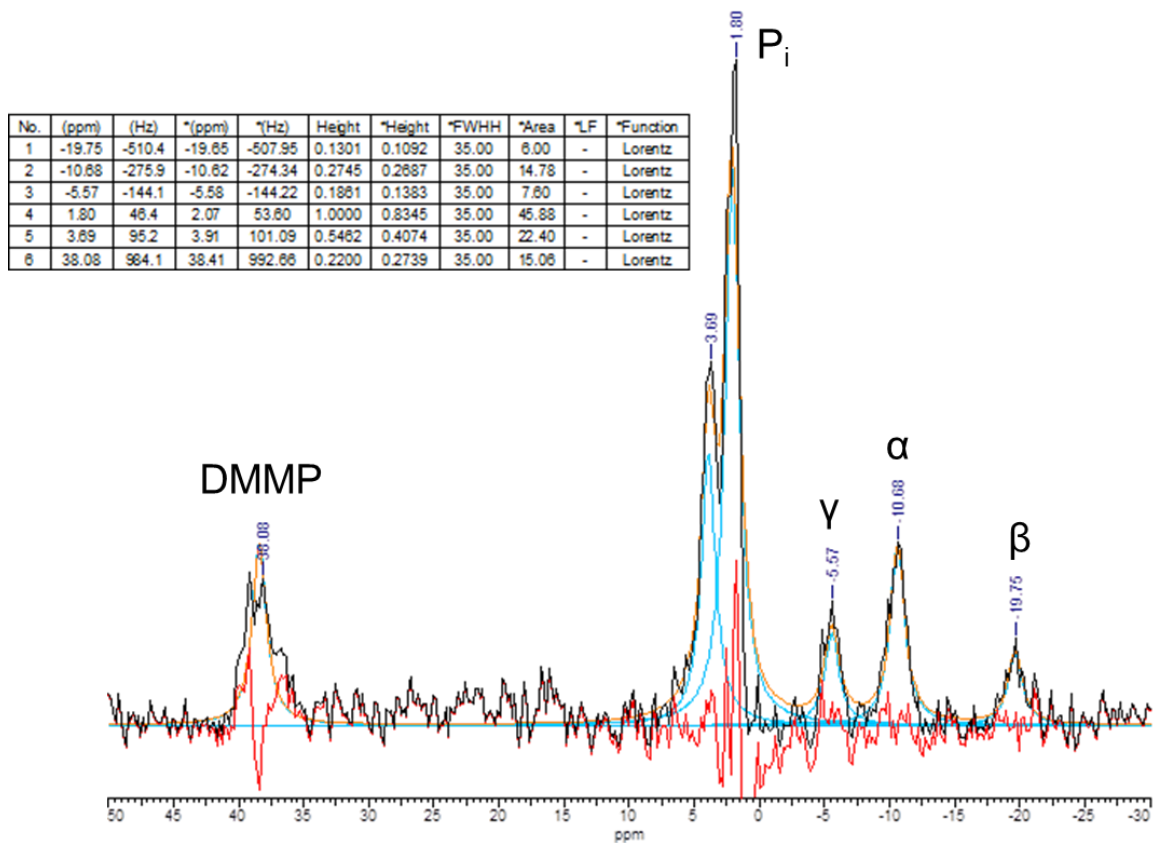


**Figure B.4: Integration analysis of  $^{31}\text{P}$ -MRS spectrum.** Representative  $^{13}\text{P}$ -MRS spectrum from a human pancreas oxygenated by persufflation (PSF) with peak assignment and integration analysis. Dimethyl methylphosphonate (DMMP) standard, phosphomonoester, inorganic phosphate ( $\text{P}_i$ ), and  $\alpha$ ,  $\beta$ , and  $\gamma$  ATP peaks are shown with calculated integration areas. These areas were compared to report the  $\beta$ -ATP: $\text{P}_i$  ratios, and the total ATP: $\text{P}_i$  ratios for these studies.

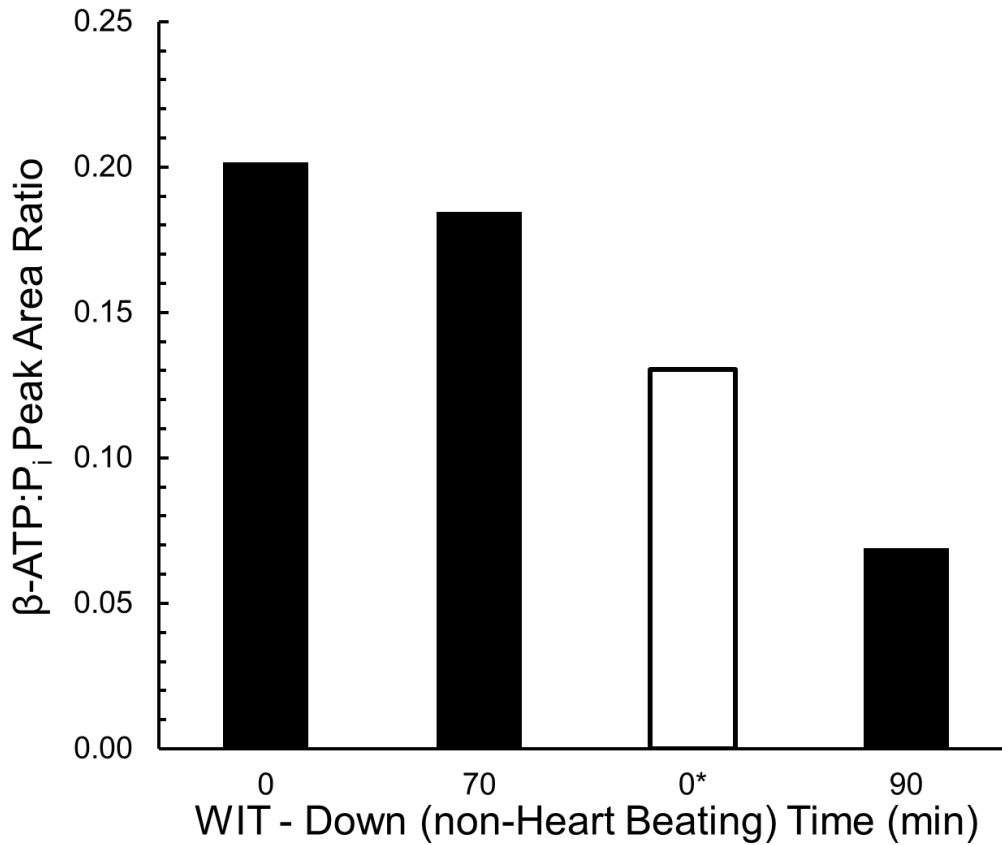


**Figure B.5:  $\beta$ -ATP/ $P_i$  levels in human pancreata.**  $\beta$ -ATP/ $P_i$  observed in 4 individual human research pancreata upon arrival at the lab. Decreased levels are observed in organs that experienced increased stress levels (warm ischemia time, WIT) as indicated in the patient chart. One organ (white bar) arrived with no indicated damage (0\* minutes of WIT), but upon further inspection, the chart indicated that a single 180 minute hypoxic episode occurred prior to procurement. This suggests that the organ was likely damaged during this period of hypoxia and partially recovered prior to procurement. The  $\beta$ -ATP/ $P_i$  measurements were able to resolve this damage that was not indicated by the WIT alone. This method may be able to provide a “snap-shot” indication of organ viability that accounts for the numerous factors and stresses that organs experience during prolonged cold preservation.

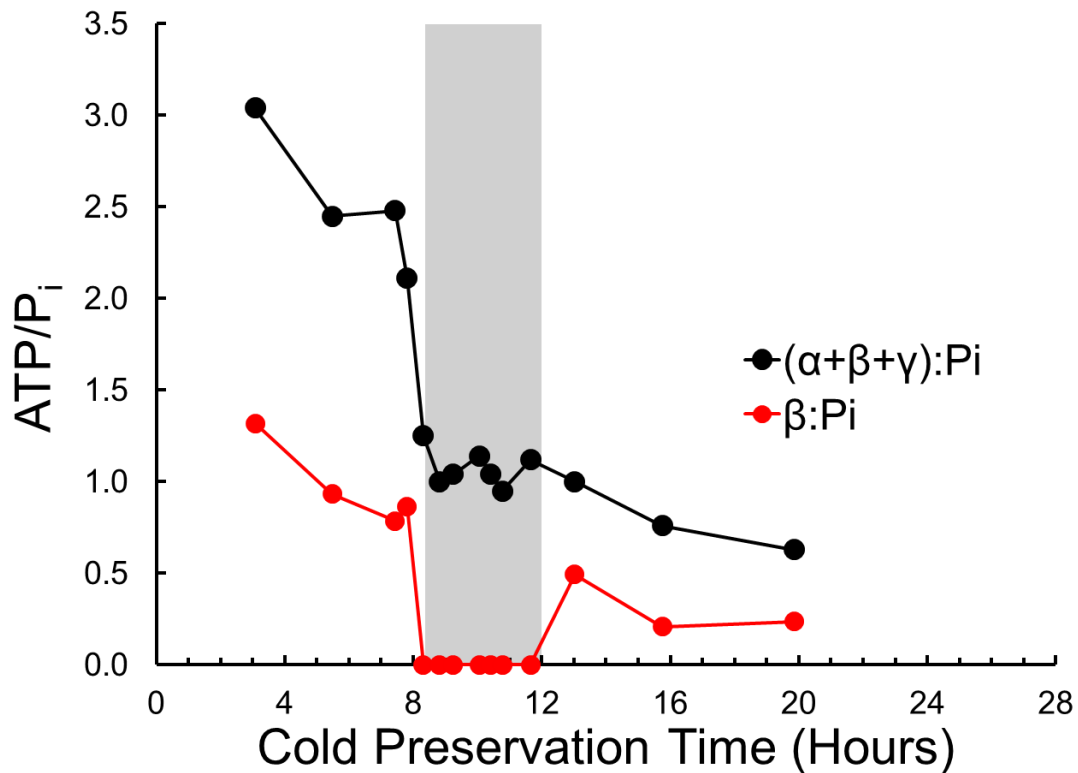


**Figure B.6: Measurements of ATP by  $^{31}\text{P}$ -MRS in human pancreas with PSF.**  $\beta$ -ATP: $P_i$  measurements for one persufflated (PSF) human pancreas. PSF was initiated after 3 hours of cold ischemia time (CIT), and then stopped after 8 hours CIT. A sharp drop in  $\beta$ -ATP was observed, and after 4 hours of measuring little to no  $\beta$ -ATP, PSF was resumed (after 12 hours of CIT) and the levels recovered to about 50% of the maximum, and finally decreased to 25% over the next 12 hours. Total ATP: $P_i$  ( $\alpha+\beta+\gamma$ ) measurements from the same human pancreas are also plotted, and demonstrate that the total ATP levels do not reach zero when oxygenation is stopped, but the  $\beta$ -ATP peak completely disappears to undetectable levels when oxygen is not available.



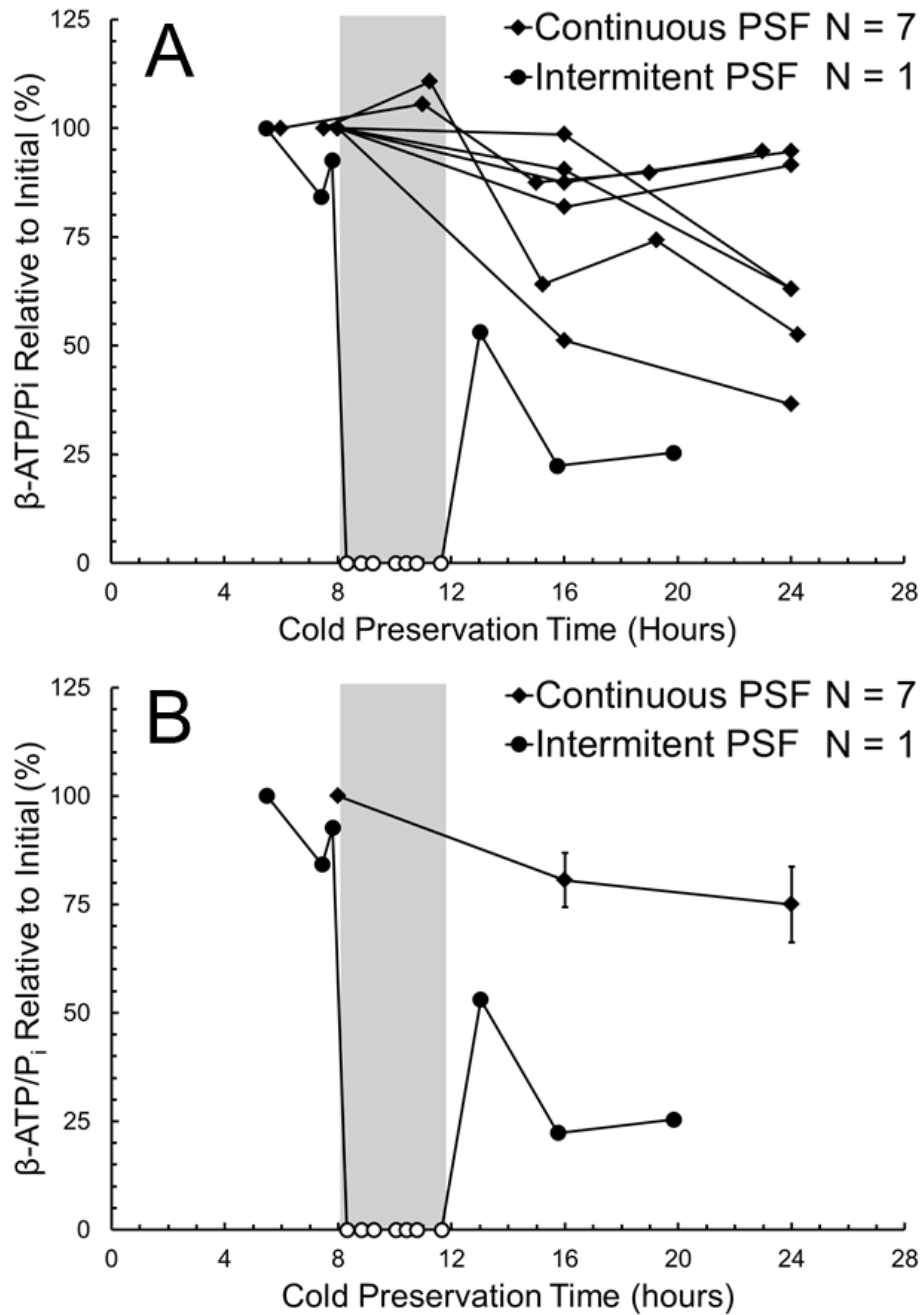


**Figure B.7: PSF maintains ATP in human pancreata.** Charts showing relative  $\beta$ -ATP:Pi levels (normalized to 8 hour time-point) for (A) individual pancreata, and (B) averaged conditions. Results demonstrate that ATP levels were maintained in human pancreata during 24 hours of cold preservation with PSF. Human pancreata were preserved by PSF for 24 hours and examined by  $^{31}\text{P}$ -MRS after 8, 16, and 24 hours. PSF was stopped for one pancreas after 8 hours, and  $\beta$ -ATP:Pi precipitously dropped to undetectable levels. A modest recovery in  $\beta$ -ATP:Pi was observed in that organ when PSF was re-initiated (after 12 hours), but it remained much lower than organs with continuous PSF.

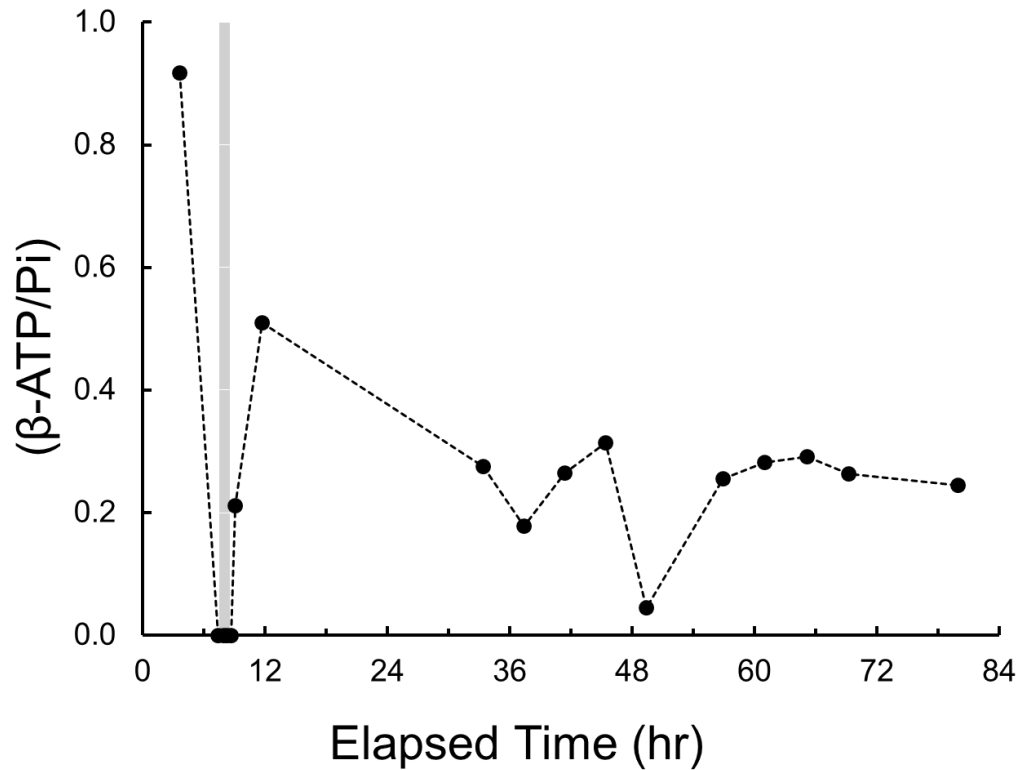


**Figure B.8:  $\beta$ -ATP/ $P_i$  measurements in porcine kidney.**  $\beta$ -ATP/ $P_i$  measurements from a porcine kidney preserved for 80 hours by PSF. As observed with human pancreata, the  $\beta$ -ATP level drops to undetectable levels without adequate oxygenation, and this is observed between 7-9 hours when PSF was inadequate. The PSF was re-established after 9 hours and the  $\beta$ -ATP levels are again observed to increase but do not recover to initial levels. PSF was continued for the remainder of the study, and a gradual decrease in  $\beta$ -ATP/ $P_i$  was observed for the duration of the study.

## **Appendix C USING MRI TO IMPROVE ENZYME DISTRIBUTION**

Sections of this chapter are reproduced in whole, or in part from the following publications with permission:

Scott III WE, **Weegman BP**, Balamurugan AN, Ferrer-Fabrega J, Anazawa T, Karatzas T, Jie T, Hammer BE, Matsumoto S, Avgoustiniatos ES, Maynard K, Sutherland DER, Hering BJ, Papas KK “Magnetic resonance imaging: A tool to monitor and optimize enzyme distribution during porcine pancreas distention for islet isolation” Xenotransplantation, July 2014

License and agreement documentation is included in **Appendix G**.

**Acknowledgements:** The authors would like to thank the Schott Foundation, the Minnesota Lions Diabetes Foundation, the Juvenile Diabetes Research Foundation (JDRF 5-2013-141), Giner Inc., the Schulze Diabetes Institute, and the NIH (P41 EB015894, and S10 RR025031) for supporting this research.

We thank William G. Purvis and Jennifer P. Kitzmann for graphical and editorial assistance and Samuel A. Stein for technical assistance with MRI imaging. This work was supported by the NIH, National Institute of Diabetes and Digestive and Kidney Diseases Grant Numbers R01DK068717 and R44 DK070400, as well as The Carol Olson Memorial Diabetes Research Fund, The Iacocca Foundation, and The Schott Foundation.

The authors acknowledge Kurt Albreck of Donovan Specialties (Osseo, Minn), Denice Dudero, Laurie Macleod, Dr Kristen Maynard, Heather Nelson, William E. Scott III, and Christine Vincent from the Diabetes Institute for Immunology and Transplantation at the UMN.

The research described here was supported in part by grants from US National Institute of Health (R44DK065508-02 - MJT, 1 R44 DK076326-0 & 5 R44DK076326-03- MJT, and R44DK069865 - JW).

## **Magnetic resonance imaging: A tool to monitor and optimize enzyme distribution during porcine pancreas distention for islet isolation**

### ***Summary***

Porcine islet xenotransplantation is emerging as a potential alternative for allogeneic clinical islet transplantation. Optimization of porcine islet isolation in terms of yield and quality is critical for the success and cost effectiveness of this approach. Incomplete pancreas distension and inhomogeneous enzyme distribution have been identified as key factors for limiting viable islet yield per porcine pancreas. The aim of this study was to explore the utility of Magnetic Resonance Imaging (MRI) as a tool to investigate the homogeneity of enzyme delivery in porcine pancreata. Traditional and novel methods for enzyme delivery aimed at optimizing enzyme distribution were examined. Pancreata were procured from Landrace pigs via *en bloc* viscerectomy. The main pancreatic duct was then cannulated with an 18g winged catheter and MRI performed at 1.5 T. Images were collected before and after ductal infusion of chilled MRI contrast agent (gadolinium) in physiological saline. Regions of the distal aspect of the splenic lobe and portions of the connecting lobe and bridge exhibited reduced delivery of solution when traditional methods of distension were utilized. Use of alternative methods of delivery (such as selective re-cannulation and distension of identified problem regions) resolved these issues and MRI was successfully utilized as a guide and assessment tool for improved delivery. Current methods of porcine pancreas distension do not consistently deliver enzyme uniformly or adequately to all regions of the pancreas. Novel methods of enzyme delivery should be investigated and implemented for improved enzyme distribution. MRI serves as a valuable tool to visualize and evaluate the efficacy of current and prospective methods of pancreas distension and enzyme delivery.

## ***Introduction***

Porcine islet xenotransplantation is emerging as an attractive alternative to allogeneic clinical islet transplantation as porcine pancreata may be a source of islets capable of meeting the demand (potentially millions of patients with type 1 diabetes). The possibility of islet isolation from porcine pancreata promises a convenient solution to the limited supply of human pancreata (in the thousands per year in the US) by offering the potential for on demand high quantity and quality islets. Porcine islets have been shown to reverse diabetes in a number of small animal models and to maintain normal glucose levels in diabetic non-human primates for more than 100 days<sup>33,238,281,363</sup>, under the coverage of potent immunosuppression. Clinical translation of porcine islet xenotransplantation will require “clean pigs” maintained in highly specialized and tightly monitored facilities, a costly endeavor<sup>89,319,364</sup>. This high cost, coupled with current difficulties in consistently obtaining high yields of viable islets from even fully mature animals, highlights the need for further optimization of the porcine islet isolation procedure. The successful intraductal infusion of enzyme solution into the pancreas is known to play an important role in obtaining successful islet isolation outcomes and has been highlighted in this study as an area to be targeted for improvement<sup>365–367</sup>.

In this regard, comprehensive knowledge of the anatomy of the porcine pancreatic ductal system is essential for the development of innovative techniques for pancreas preservation and improvements in islet isolation procedures. Due to the complexities of the anatomy of the ductal system and variations between donors<sup>38,69,85,104</sup>, complete distension and homogeneous enzyme distribution remain a challenge despite substantial experience in the field. Failure to consistently obtain high viable islet yields from porcine pancreata with traditional enzyme delivery methods may actually be, in part, due to issues associated with incomplete distention and inhomogeneous enzyme distribution.

Depending on the anatomy and individual variations in the pancreatic ductal system, following the division of the pancreas into its three distinct lobes, significant portions of the organ may not be reachable by the enzyme. In this study we utilized Magnetic Resonance Imaging (MRI) to: 1) investigate the delivery, completeness of distension and homogeneity of enzyme distribution by traditionally used methods of enzyme delivery; and 2) compare two novel strategies for enzyme delivery into porcine pancreata and compare them with the traditional method.

## ***Materials and Methods***

Six female Landrace non-heart beating donor pigs aged between 6 to 24 months with mean weight of  $452 \pm 99$  lb (average  $\pm$  standard deviation, range 248 to 680 lb) were subjected to pancreas resection. All animals were operated on according to the rules and regulations of the Institutional Animal Care and Use Committee of the University of Minnesota.

### **Procurement:**

Animals were heparinized, euthanized by sodium pentobarbital overdose, and, following the cessation of heart rhythm, completely bled out and eviscerated. All intra-abdominal organs were procured *en bloc* onto a procurement table where the pancreas was dissected free of the other organs, as previously described<sup>38</sup>.

### **MRI:**

Following procurement, the pancreata were placed on ice and transported to a 1.5 T magnet (MagneX Scientific, Abingdon, UK) using an Apollo spectrometer (Tecmag, Houston, TX) for MRI. Pancreata were placed into the magnet, as illustrated in **Figure C.1**. Briefly: after division and cannulation, pancreata or separated lobes were placed into the MRI system and baseline images were acquired. A circulating water bath chiller and heat exchanger were used to maintain cold temperatures throughout the infusion and imaging process. Syringes attached to pre-primed lines running into the bore of the magnet were then used to manually infuse each pre-cannulated ductal bed with 5 mM gadolinium contrast solution (Magnevist®, Bayer Healthcare, Berlin, Germany), and post-infusion images were taken to determine the extent of contrast distribution. The dosing of the contrast was selected based on prior experience to maximize the contrast for this magnet. Temperatures were maintained from 4-8 °C with a specially designed water jacket running to a refrigerated water bath. Imaging was performed using a Gradient Echo Imaging sequence with a 90° flip angle, an echo time (TE) of 14 ms and a repetition time (TR) of 20 ms.

Images spanned a field of view of 30 cm x 30 cm at a resolution of 256 x 256 from 5 mm slices, each image had 4 acquisitions averaged to ensure clarity.

*Pancreas Distention:*

Based on the pancreatic ductal anatomy and the different types of ductal networks described in our previous work<sup>38</sup>, the following 3 methods of ductal infusion were investigated twice for each method: **Method 1**, division of the pancreas into its 3 distinct lobes followed by antegrade infusion of the main duct of the splenic lobe, the main duct of the connecting lobe, and the main duct of the duodenal lobe (traditional method); **Method 2**, division of the duodenal lobe from the rest of the pancreas leaving the bridge between connecting and splenic lobes intact followed by antegrade infusion into the pancreatic lobes via cannulation of the main duct of the duodenal lobe, the main duct of the splenic lobe, and the main duct of the connecting lobe ; **Method 3**, cannulation of the main pancreatic duct at the papilla of an in-tact pancreas, and infusion of the total amount of contrast solution. Examples of each of these methods are illustrated in **Figure C.2**. Pancreata were infused with up to a total of 0.6 cc of Lactated Ringer's solution, doped with 5 mM gadolinium contrast agent (Magnevist®, Bayer Healthcare, Berlin, Germany), per gram of pancreas. For **Method 2**, 33% of the combined weight of the splenic and connecting lobes was assigned to the connecting lobe and 67% to the splenic lobe for purposes of contrast solution allocation.



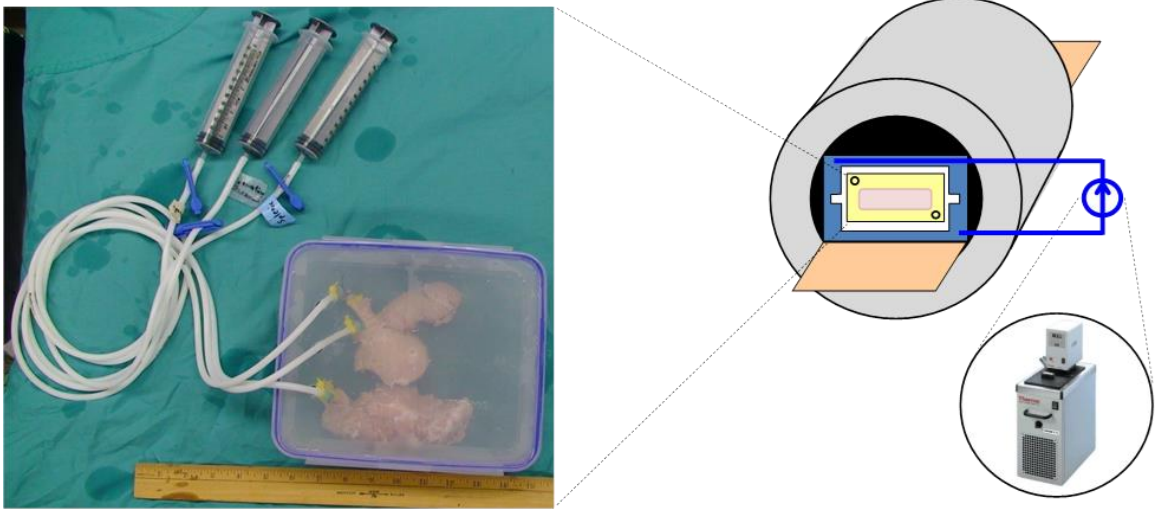


**Figure C.1: Ductal MRI experimental setup.** Illustration of the experimental setup for ductal infusion in a 1.5 T magnet for MRI. (Right Side) After division and cannulation, pancreata or separated lobes were placed into the MRI system and baseline images were acquired. A circulating water bath chiller and heat exchanger were used to maintain cold temperatures throughout the infusion and imaging process. (Left) Syringes attached to pre-primed lines running into the bore of the magnet were then used to manually infuse each lobe or section of the pancreas with the gadolinium contrast solution, and post-infusion images were taken to determine the extent of contrast distribution.

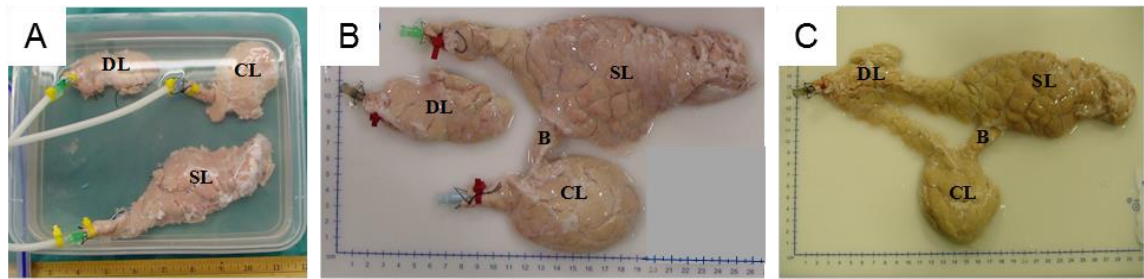


**Figure C.2: Ductal MRI cannulation approaches.** Pictures depicting the different cannulation and infusion methods: (A) Traditional method separating the pancreas into 3 distinct lobes with anterograde infusion of the main ducts (Method 1); (B) Separation of the duodenal lobe with anterograde infusion into divided pancreas via cannulation of the main ducts with the bridge left intact (Method 2); and (C) Cannulation of main pancreatic duct at the papilla and infusion of total amount of contrast (Method 3).

## ***Results***

Six pancreata were investigated for this study. Pancreata were randomly assigned a distention technique with 2 investigated for each of the methods. Using MRI we were able to detect differences in enzyme distribution during distention. In 2 cases where the duodenal lobe was separated from the rest of the pancreas, as is done in **Methods 1 and 2**, we observed reduced or no delivery of contrast solution to regions of the duodenal lobe (**Figure C.3**). Additionally, we observed a lack of delivery of contrast solution to a large portion of the connecting lobe in one case infused using the traditional **Method 1** (**Figure C.4A**). All other cases demonstrated a relatively homogeneous delivery of contrast solution throughout all regions of the pancreas.

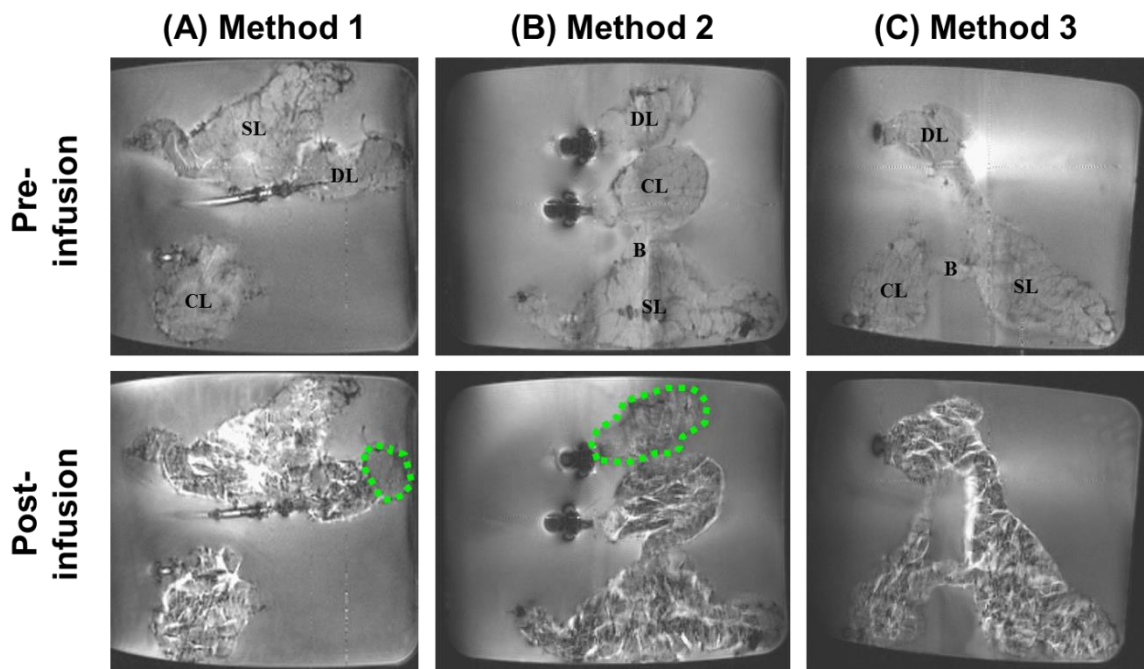


**Figure C.3: Ductal contrast MRI of porcine pancreata lobes.** MRI of pancreata before and after infusion with contrast solution for each of the 3 methods investigated. Areas of the pancreas that were well distended and infused with contrast solution appear as intense white regions in the post-infusion images. When the duodenal lobe was separated, occasionally regions with no delivery or reduced delivery (outlined in green) were observed in the duodenal lobe.

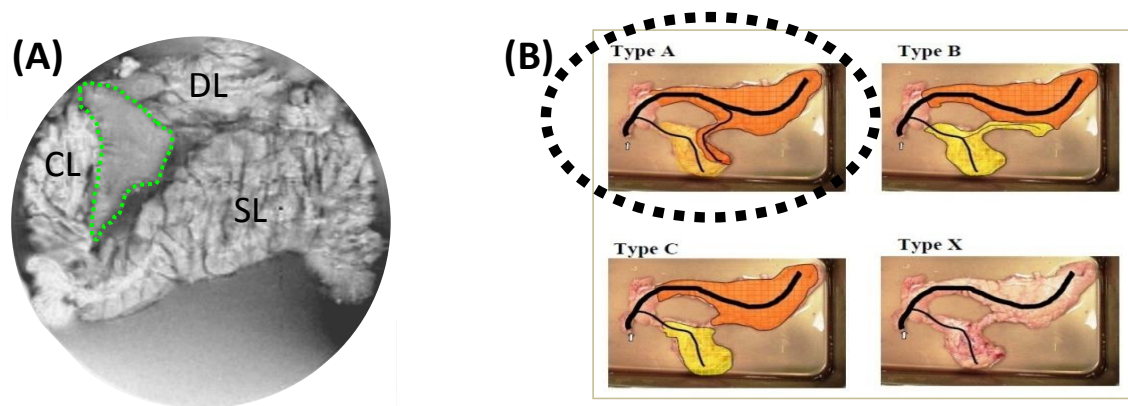


**Figure C.4: MRI detects ductal variants.** (A) MRI of a porcine pancreas with an uncommon variant ductal anatomy infused using Method 1. (B) Illustration of the common types of porcine pancreata ductal anatomy observed by Ferrer-Fabrega et al. in 2008 highlighting type 'A' that is shown by the MRI image. For this pancreas, areas of the connecting lobe outlined in green did not receive any contrast medium (white) during infusion because the ductal system in part of the connecting lobe drains through the bridge and out through the splenic lobe ductal system. Method 1 will not effectively distend this portion of the connecting lobe in these pancreata.

## ***Discussion***

Variations in the anatomy of the pancreatic ductal system may be a major factor affecting successful islet isolation from porcine pancreata. Presently, these variations are not considered prior to distention and this can leave regions within the pancreas with reduced enzyme delivery. Inefficient or limited enzyme delivery is regarded as a major cause of incomplete tissue digestion in some cases, which contributes to reduced islet yields. As such, new techniques must be developed to maximize delivery for all anatomical variants, or the distention should be actively monitored with a tool similar to the one discussed here to ensure optimal and efficient enzyme delivery and distribution. Pancreatic anatomy varies from donor to donor<sup>314</sup> and previous studies<sup>80,315,317</sup> have demonstrated the importance of pig strain on islet isolation outcome. In our study we used Landrace pigs as they are considered to be highly suitable donors for islet isolation and xenotransplantation<sup>316-318</sup> since isolations with this breed can yield large numbers of islets compared to other breeds. A previous study from our laboratory on adult Landrace pig pancreas anatomy<sup>38</sup> suggested that the current methods of enzyme delivery may limit the uniform delivery of enzyme throughout the pancreas when atypical anatomical variations of the ductal network are observed. While visual assessment of pancreatic distention can give some idea of gross delivery, it is difficult to determine or quantitate the extent of delivery within the pancreas since only the superficial aspect can be observed. The MRI method proposed allows for clear visualization of the internal ductal system and can be used to appreciate the efficacy and homogeneity of enzyme delivery throughout and within the entire pancreas.

This study aimed to demonstrate that MRI can be utilized as a tool to evaluate the efficacy of enzyme delivery throughout the pancreatic ductal system, and that it can be used as a cost-effective method to screen and evaluate novel strategies for enzyme infusion with the goal of optimizing enzyme delivery and improve islet isolation outcomes. Three methods of delivery

(**Figure C.2**) including the presently used method (**Method 1**) were investigated, and imaged to evaluate distention efficacy and enzyme delivery. As demonstrated in **Figure C.3**, methods of enzyme delivery that involved removal of the duodenal lobe from the rest of the pancreas can result in reduced or even total lack of delivery to significant portions of the lobe. Additionally, it was demonstrated that for pancreata with an atypical ductal anatomy, severing the bridge prior to enzyme infusion can prevent delivery to significant regions of either the connecting lobe (**Figure C.4B**, Type ‘A’ ductal anatomy) or the splenic lobe (Type ‘B’ anatomy)<sup>69,85,104,309,311,312</sup>. The data presented in this study further suggests that traditional methods of porcine pancreas distention may not facilitate reliable and homogeneous delivery of enzyme throughout the 3 lobes of the pancreas. The most likely cause of the incomplete distention of the pancreatic duct is the severing and mishandling of key ductal networks required for the delivery of the enzyme. One proposed way to avoid disrupting these ductal networks is to avoid segmenting the pancreas prior to distention (**Method 3**). All pancreata investigated with this method exhibited a uniform delivery of contrast medium throughout the organ. Therefore, minimizing the manipulation of the ductal network prior to distention may facilitate optimal distribution of the enzyme.

Prior knowledge of the pancreatic ductal system and the variable anatomy could be used to determine the most effective distention method for each pancreas, and would allow for disqualification of poorly distended pancreata before proceeding with the costly islet isolation process. Further development of this technique may enable prospective and real-time visualization of ductal network distention by MRI. If this could be developed as a prospective tool, it would enable internal visualization to ensure that all regions are adequately infused with digestive enzyme, and could improve the use of targeted local parenchymal enzyme injection to rescue a portion of inadequately distended tissue. Knowing the variable ductal distribution, and avoiding disruption the ductal networks caused by segmenting the pancreas, may make the

distention process more efficient and effective, which may intern improve islet isolation outcomes.

The imaging technique described here for internal visualization of the porcine pancreatic ductal system may also be useful for human pancreata. One major example where MRI could offer value is for cases of pancreas divisum, where there is a lack of a connection between the main and the accessory pancreatic ducts. This condition afflicts 10-22% of all pancreata harvested for islet isolation<sup>368</sup>. It is anticipated that this anatomical variation could affect the distention of significant parts of the pancreas. This may be especially important in clinical islet auto-transplantation<sup>274</sup> for patients with chronic pancreatitis, as pancreas divisum is reported to be associated with chronic pancreatitis<sup>368</sup>. Kin et al. used the traditional technique for distention, and compared isolation outcomes from normal versus visually identified pancreas divisum cases<sup>368</sup>. They observed no visual differences in distention quality, and found no statistical differences in islet yields between the 2 ductal variants, although mean islet yield was lower for pancreas divisum. Application of this imaging tool would enable the direct visualization of enzyme distribution for each of these cases and may offer an explanation for the lower islet yields observed for pancreas divisum. Furthermore, MRI could help detect regions with reduced enzyme delivery surrounding the accessory pancreatic duct due to narrowing. If these regions are not consistently and homogeneously distended, different paths for distention could be tested and optimized to potentially improve human islet isolation. This technique can facilitate the visualization of possible ductal anomalies or narrowing, the recognition of which could make the process of pancreas distention and islet isolation more effective.



## ***Conclusions***

Presently utilized methods for enzyme delivery through ductal distension in pig pancreata are incapable of delivering the enzyme consistently and homogeneously to all pancreatic regions given the variability in porcine pancreas anatomy. Visual assessment of pancreatic distention cannot accurately assess whether enzyme is effectively delivered throughout the entire pancreas. MRI is a valuable tool that can help improve the understanding of the variable pancreatic ductal anatomies, and may help overcome the difficulties associated with incomplete distention and inhomogeneous enzyme distribution for islet isolation. This imaging method can be used to help ensure uniform enzyme distribution in both porcine and human pancreata, and to evaluate and optimize new distention methods that might ensure adequate distention of all regions despite anatomical variations. The presented MRI based method should be further developed into a prospective and quantitative tool for visualization of enzyme distribution during pancreas distention for islet isolation. This would enable anatomy specific modifications to distention protocols for each individual pancreas, and may increase the consistency and success of certain islet isolations.

## Appendix D IMPROVING ISLET SHIPMENT

Sections of this chapter are reproduced in whole, or in part from the following publications with permission:

Rozak PR, **Weegman BP**, Avgoustiniatos ES, Wilson JR, Welch DP, Hering BJ, Papas KK. “Devices and methods for maintenance of temperature and pressure during islet shipment.” *Transplant Proc.* 2008 Mar;40(2):407-10.

**Figure D.3** was added to the published version of this manuscript<sup>93</sup> to improve clarity and provide additional supportive unpublished data. References to this figure and brief sections of text were also added to accommodate this additional data.

License and agreement documentation is included in **Appendix G**.

**Acknowledgements:** The authors would like to thank the Schott Foundation, the Minnesota Lions Diabetes Foundation, the Juvenile Diabetes Research Foundation (JDRF 5-2013-141), Giner Inc., the Schulze Diabetes Institute, and the NIH (P41 EB015894, and S10 RR025031) for supporting this research.

This work was supported by the NIH, National Institute of Diabetes and Digestive and Kidney Diseases Grant Numbers R01DK068717 and R44 DK070400, as well as The Carol Olson Memorial Diabetes Research Fund, The Iacocca Foundation, and The Schott Foundation.

The authors acknowledge Kurt Albreck of Donovan Specialties (Osseo, Minn), Denice Dudero, Laurie Macleod, Dr Kristen Maynard, Heather Nelson, William E. Scott III, and Christine Vincent from the Diabetes Institute for Immunology and Transplantation at the UMN.

The research described here was supported in part by grants from US National Institute of Health (R44DK065508-02 - MJT, 1 R44 DK076326-0 & 5 R44DK076326-03- MJT, and R44DK069865 - JW).

## **Devices and methods for maintenance of temperature and pressure during islet shipment**

### ***Summary***

Exposure to extreme temperatures and pressure fluctuations during shipment by air may have a detrimental impact on islet quality. In this study, we sought to assess the ability of methods and devices to provide better control of the internal environment of islet shipping containers in terms of temperature and pressure. Experimental islet shipping containers were packed with 21 panels of commercially available TCP Phase 22 Phase Change Material (TCP). The containers were then exposed for at least 15 hours to three constant external temperature conditions, namely, -20°C, 4°C, and 40°C, and then evaluated for their ability to maintain an internal temperature close to the desired value of 22°C. Custom-designed pressure regulated gyroscopic shipping containers (PRGSC) placed in a vacuum chamber were exposed to an absolute pressure of 250 mm Hg (substantially lower than that experienced during shipment by air) for 25 minutes to assess their ability to control internal pressure under vacuum. Electronic data loggers were used to monitor internal and external temperatures and pressures under all conditions. Twenty-one TCP panels placed in a single islet shipping container were able to maintain the internal temperature between 17°C and 24°C for a minimum of 15 hours at all three external temperatures. The PRGSC tested were able to maintain a constant internal pressure of 760 mm Hg when exposed to vacuum. Our results demonstrated that the use of containers equipped with TCP and PRGSC exert excellent environmental control over islet shipments by minimizing temperature and eliminating pressure fluctuations.

## ***Introduction***

Islet preparations are sensitive to temperature extremes. Although the effects of pressure changes on islets have not been studied directly, it has been suggested that pressure fluctuations during islet shipment by air may have a negative impact on islet integrity and quality. In addition, some shipping vessels may not be able to withstand pressure fluctuations and thus either deform or break. Frequently, islets are shipped in a Styrofoam container with cooling packs<sup>369</sup>. However, cooling packs may accelerate freezing when islets are shipped to cold climates or during the winter. Overall, cooling temperatures may be detrimental to islet viability and therefore undesirable. Additionally, standard Styrofoam containers alone neither insulate well against temperature extremes (hot/cold) nor regulate internal pressures during shipment. Hence, there is a need to develop methods to control the internal environment of islet shipping containers while they are exposed to extreme external temperatures and pressure fluctuations, with the ultimate goal to make shipment an extension of islet culture.

## ***Materials and Methods***

### ***Temperature Control Investigation***

Experimental container 1 consisted of a corrugated plastic package containing 21 TCP Phase 22 Phase Change Material panels (TCP, Part# FGEL00052, TCP Reliable, Edison, NJ) weighing 6.3 kg, Styrofoam walls 4 inches thick, and plastic bubble wrap to keep the culture vessel in place. Shipping containers were prepared for three separate temperature conditions, -20°C, 4°C, and 40°C. A Ken-more upright freezer (Model# 106.8263511, Sears Holdings Corp., Hoffman Estates, Ill) was used for all -20°C conditions. The freezer temperature oscillated between -20°C and -30°C at an approximate rate of 1 cycle/hour. A Fisher scientific refrigerator (Isotemp Model, Thermo Fisher Scientific, Inc., Waltham, Mass) was used for all 4°C conditions. A Heraeus water-jacketed incubator with 5% CO<sub>2</sub> was used for all 40°C conditions (6000 Model, Thermo Fisher Scientific). The TCP panels were appropriately primed for each temperature. Panels designated for -20°C and 4°C were fully liquified by incubation at 37°C for 6 hours before packaging. Panels designated for 40°C were fully solidified by cooling them at 4°C for 6 hours before packaging. Culture vessels were loaded with 50 mL of distilled deionized water and packed into the shipping containers (one vessel per container). Internal container temperatures were recorded using HOBO electronic temperature loggers (Part# H08-007-02, Onset, Pocasset, Mass) placed next to the culture vessels. The containers were closed and placed in the -20°C freezer, the 4°C refrigerator, or the 40°C incubator. A second set of HOBO electronic temperature loggers were placed outside each of the boxes and recorded the external surface temperatures of each shipping container. The containers were exposed to the experimental temperatures for 15 hours, which is the approximate time of an overnight shipment. After exposure, the containers were removed and the temperature data analyzed.

Experimental container 2 was modeled after a model recently evaluated for standardization of shipments of human research islets by the Islet Cell Resource (ICR) Center Consortium. It consisted of a ThermoSafe EPS Insulated Shipper (Model# 355, Arlington Heights, Ill), 2 ThermoSure Temperature Stabilizer gel packs (TS, Model# 1290, Sebra, Tucson, Ariz) weighing 1.6 kg, and plastic bubble wrap to keep the culture vessel in place. The containers were primed according to the manufacturer's instructions, loaded, and exposed to the above environmental temperatures. Data were recorded in the same manner as for the TCP containing packages. A modified version of experimental container 2 that included 6 TS units was also tested with various pre-shipment preparation techniques. These units were only exposed to -20 °C and 40 °C external conditions, but the TS units were prepared prior to the test to be in the solid phase, the liquid phase, or a slushy phase. Temperature data was collected from these containers for up to 84 hours, and the temperature threshold of  $20 \pm 2$  °C was used. Failure of the temperature regulation for the container was defined as dropping below freezing ( $< 0$  °C), or rising above 40 °C.

A ThermoSafe EPS Insulated Shipper (Model# 413) with Styrofoam walls was packed with plastic bubble wrap, a culture vessel, and a HOBO electronic temperature logger. It was used as a reference container to simulate shipping containers routinely used for distribution of islets in the past. This reference container was exposed to the three experimental temperatures for 8 hours. A second HOBO electronic temperature logger was placed outside the reference container to record external temperatures for each condition. The reference container was also used to record temperatures and pressures during actual islet shipments from the University of Minnesota (UMN) to five investigators around the United States. The data from these shipments are presented in **Figure D.1A**.

*Pressure Control Investigation*

The pressure regulated gyrosopic shipping container (PRGSC, Part# PR-AY-11-0007, Wilson Wolf Manufacturing Corporation, New Brighton, Minn) was designed in a collaboration between the UMN and Wilson Wolf Manufacturing Corporation. The PRGSC was loaded with the same culture vessel used in the temperature investigation and a HOBO absolute pressure logger (Part# HPA0015), sealed, and placed in a custom-designed acrylic vacuum chamber (Donovan Specialties, Osseo, Minn). A second HOBO pressure logger was placed on top of the PRGSC to measure external pressure. The vacuum chamber was sealed and an attached Cole-Parmer vacuum pump (Cat. # K-07061-40, Cole-Parmer Instrument Co., Vernon Hills, Ill) was used to reduce the absolute pressure to 250 mmHg (about 150 mmHg lower than the lowest pressure observed during shipment, as shown in **Figure D.1B**) for 25 minutes. After vacuum exposure, the PRGSC was removed for analysis of the pressure data.

## ***Results***

Internal temperatures and pressures recorded over the course of actual islet shipments with the reference container varied substantially (**Figure D.1**). The variations in temperature depended on several factors such as the climate of the shipping and receiving centers, the season, and the conditions of air transit, ground transit, and warehouse storage. Pressure fluctuations depended on the number of connecting flights used per shipment and the use of pressurized versus nonpressurized flight environments.

When experimental container 1 containing TCP was exposed to temperatures between  $-20^{\circ}\text{C}$  and  $-30^{\circ}\text{C}$  for 15 hours, it maintained an internal temperature between  $21^{\circ}\text{C}$  and  $24^{\circ}\text{C}$  (**Figure D.2A**). In comparison, the internal temperature of experimental container 2 with TS dropped from this range within 2 hours, and reached  $0^{\circ}\text{C}$  after 12 hours of exposure. Experimental container 1 with TCP maintained a stable internal temperature of  $22^{\circ}\text{C}$  for longer than 24 hours when exposed to  $4^{\circ}\text{C}$  (**Figure D.2B**). Experimental container 2 with TS exposed to  $4^{\circ}\text{C}$  was unable to maintain an internal temperature close to  $22^{\circ}\text{C}$ . The temperature fell as low as  $15^{\circ}\text{C}$  before equilibrating at  $17^{\circ}\text{C}$  after 6 hours (**Figure D.2B**). Experimental container 1 containing TCP exposed to  $40^{\circ}\text{C}$  for 15 hours maintained an internal temperature between  $17^{\circ}\text{C}$  and  $22^{\circ}\text{C}$  (**Figure D.2C**). In contrast, experimental container 2 was able to maintain this temperature range for less than 4 hours and the internal temperature was within 3 degrees of the ambient by the end of 15 hours (**Figure D.2C**).

Studies using experimental container 2 with a total of 6 TS units exhibited much better thermal regulation due to the increased mass of thermal regulating material (**Figure D.3**). By increasing the number of TS devices, the time until failure was dramatically increased, and the best performance was achieved when the TS units were prepared allowing for a full phase-transition during shipment. When exposed to  $-20^{\circ}\text{C}$  the solid TS units maintained temperatures above  $0^{\circ}\text{C}$  for up to 30 hours, while the recommended slushy preparation lasted for only 22 hours. The



internal temperature for all three preparations fell outside of the desired temperature threshold in less than 6 hours when exposed to -20 °C, and Experimental container 1 still performed much better. When exposed to 40 °C, the solid prepared TS units maintained temperatures < 40°C for up to 48 hours, and the recommended slushy preparation failed after only 30 hours. The internal temperature of the containers regardless of the TS unit preparation phase fell outside of the desired threshold in less than 12 hours when exposed to 40°C while, as presented above, experimental container 1 was able to maintain the desired temperature for > 24 hours.

During the PRGSC trial, the pressure inside the vacuum chamber was reduced from 760 to 250 mmHg within 1 minute and maintained at that level for over 25 minutes. Despite the large drop in external pressure, the PRGSC maintained a constant internal pressure of 760 mmHg (**Figure D.4**).

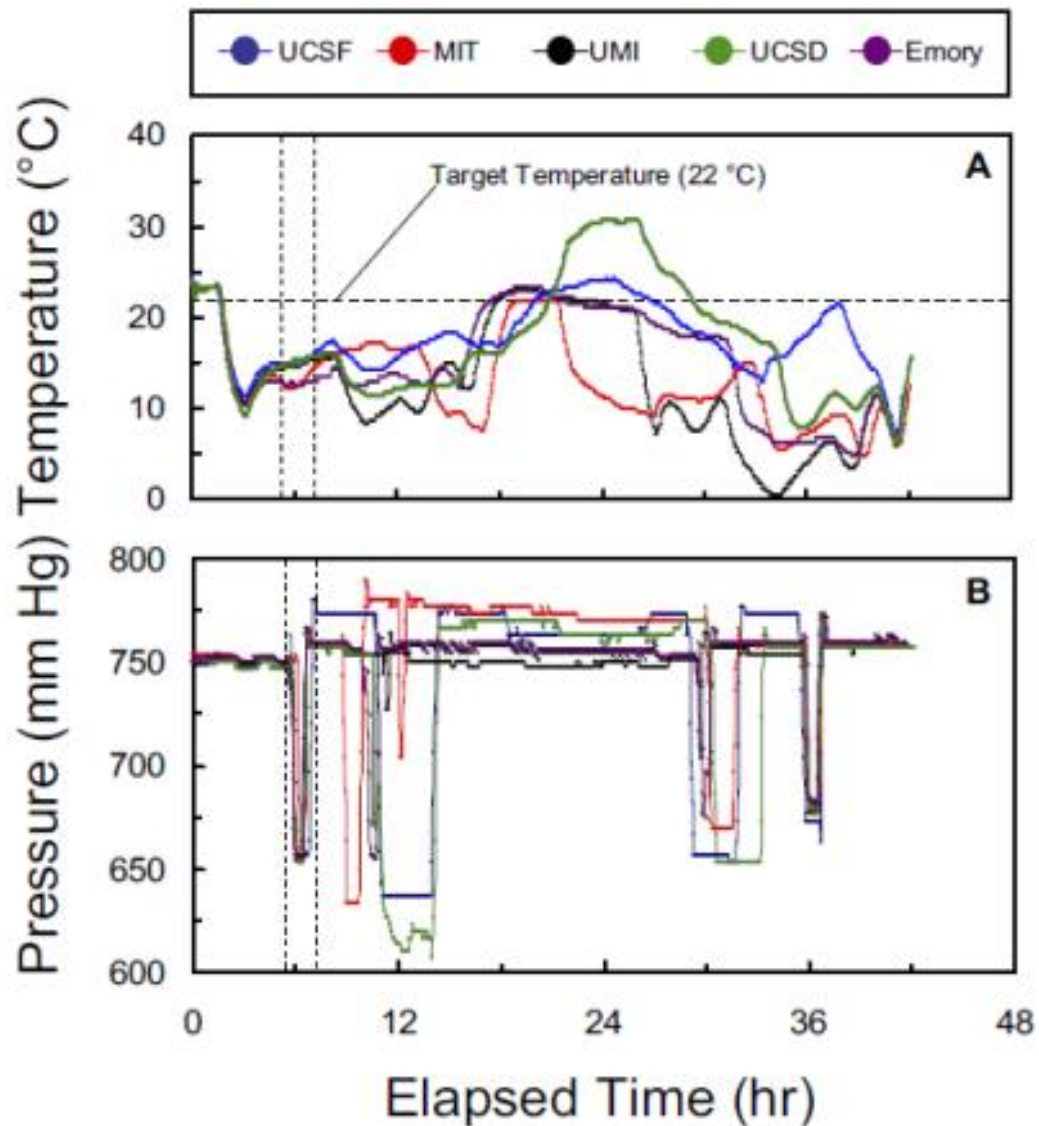


**Figure D.1: Temperature and pressure changes during shipment.** Shipments using the reference container sent to five research centers from the University of Minnesota, Minneapolis, Minnesota, on March 10, 2004. The vertical dashed lines indicate one group of flight departures and arrivals. (A) Temperature data recorded every 4 minutes. The horizontal dashed line indicates target islet vessel temperature (22 °C). (B) Pressure data recorded every 4 minutes.

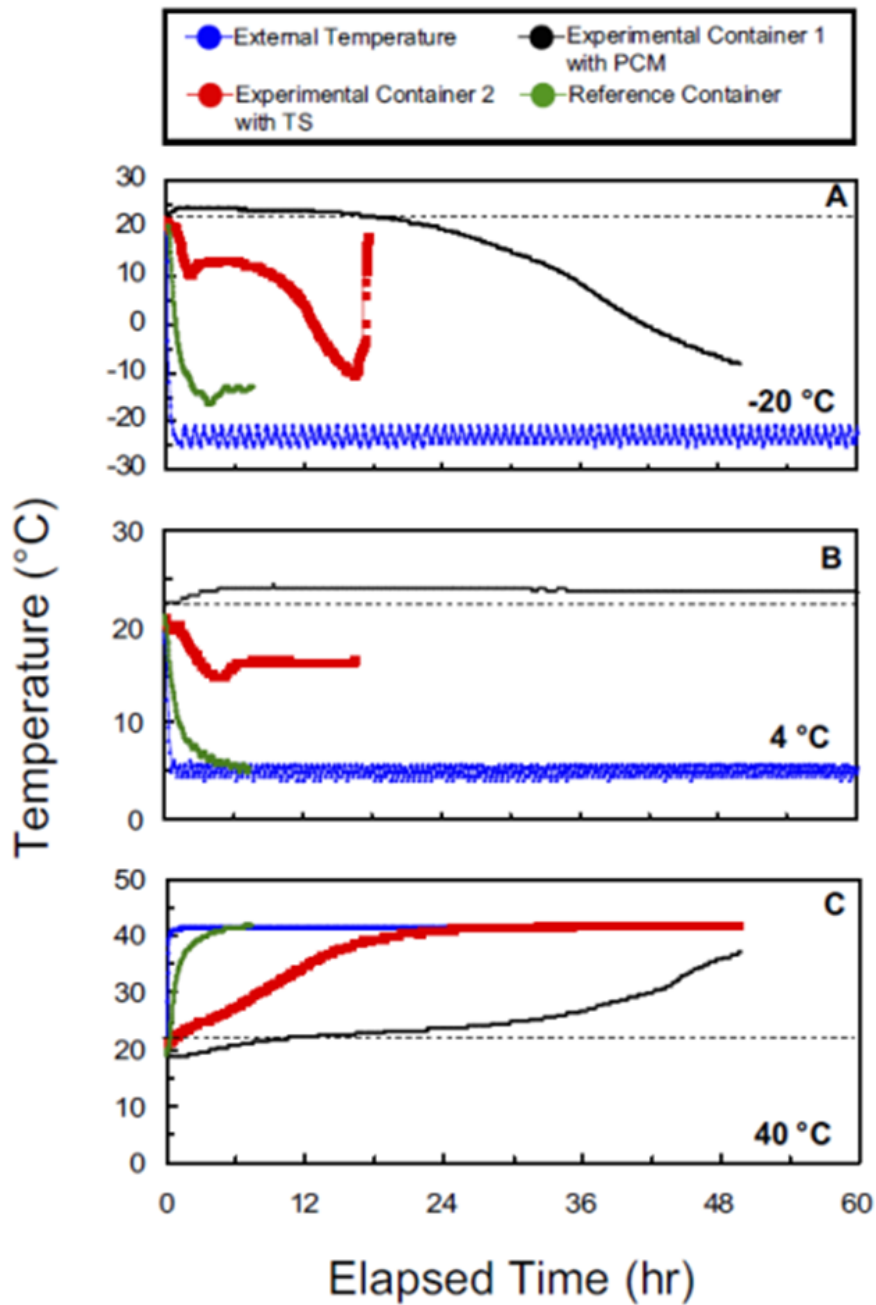


**Figure D.2: Temperature measurements in experimental containers.** Comparison of internal temperatures for various shipping containers plotted over time under exposure to external temperatures of (A) -20°C, (B) 4°C, and (C) 40°C. The horizontal dashed lines indicate the targeted islet vessel temperature (22°C).

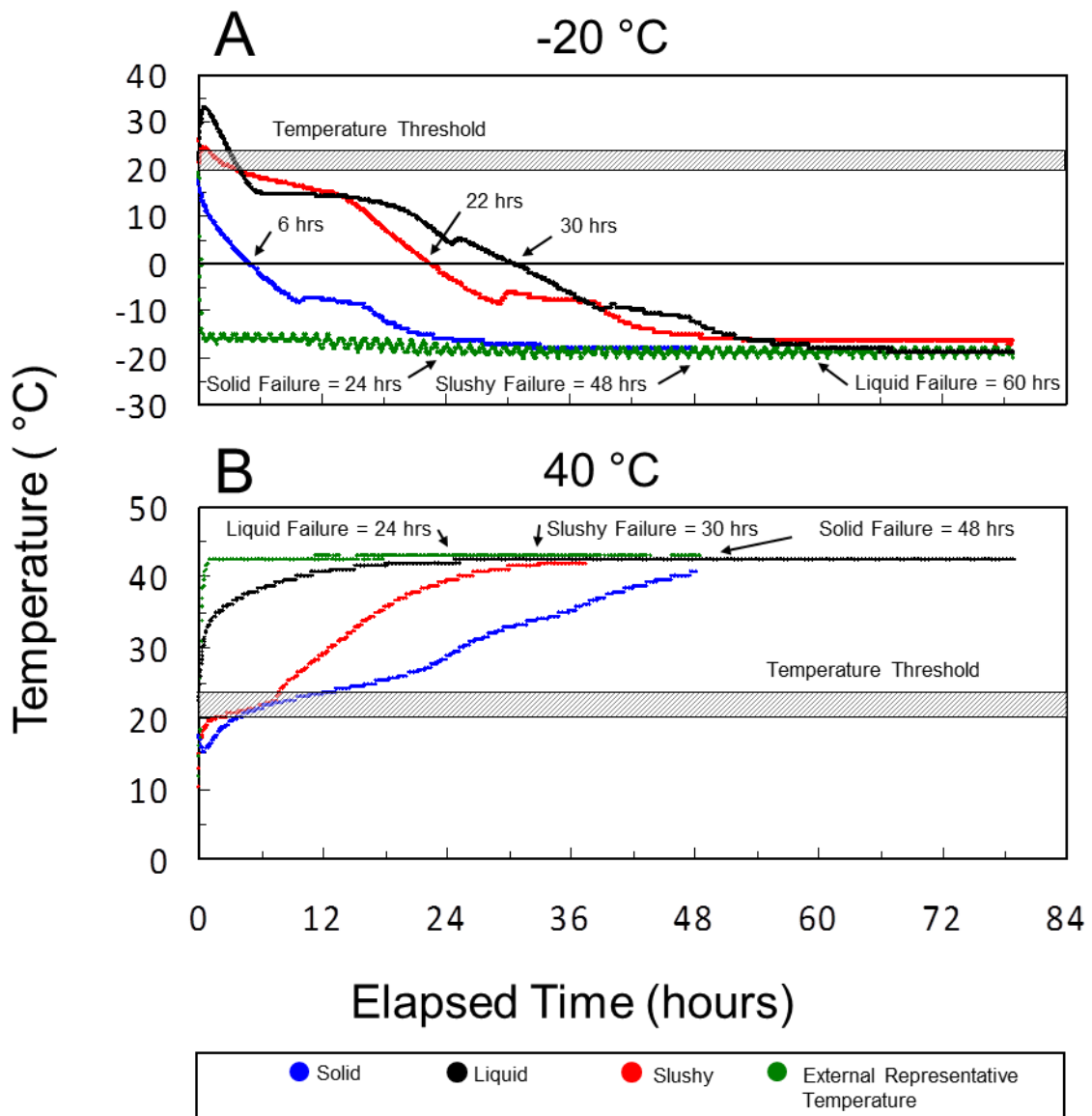


**Figure D.3: Temperature measurements in ICR Shipping containers.** The ICR shipping container contained 6 TS units, and were exposed to  $-20\text{ }^{\circ}\text{C}$  and  $40\text{ }^{\circ}\text{C}$  external environments. The TS units were prepared prior to exposure with three different starting-phase conditions (solid, liquid or slushy), the internal temperatures were monitored, and failure was defined when the internal temperature exceeded  $37\text{ }^{\circ}\text{C}$  or dropped below  $0\text{ }^{\circ}\text{C}$ . This figure was not included in the original published version of this paper<sup>93</sup>, but is included here as supplemental data in the context of this study.

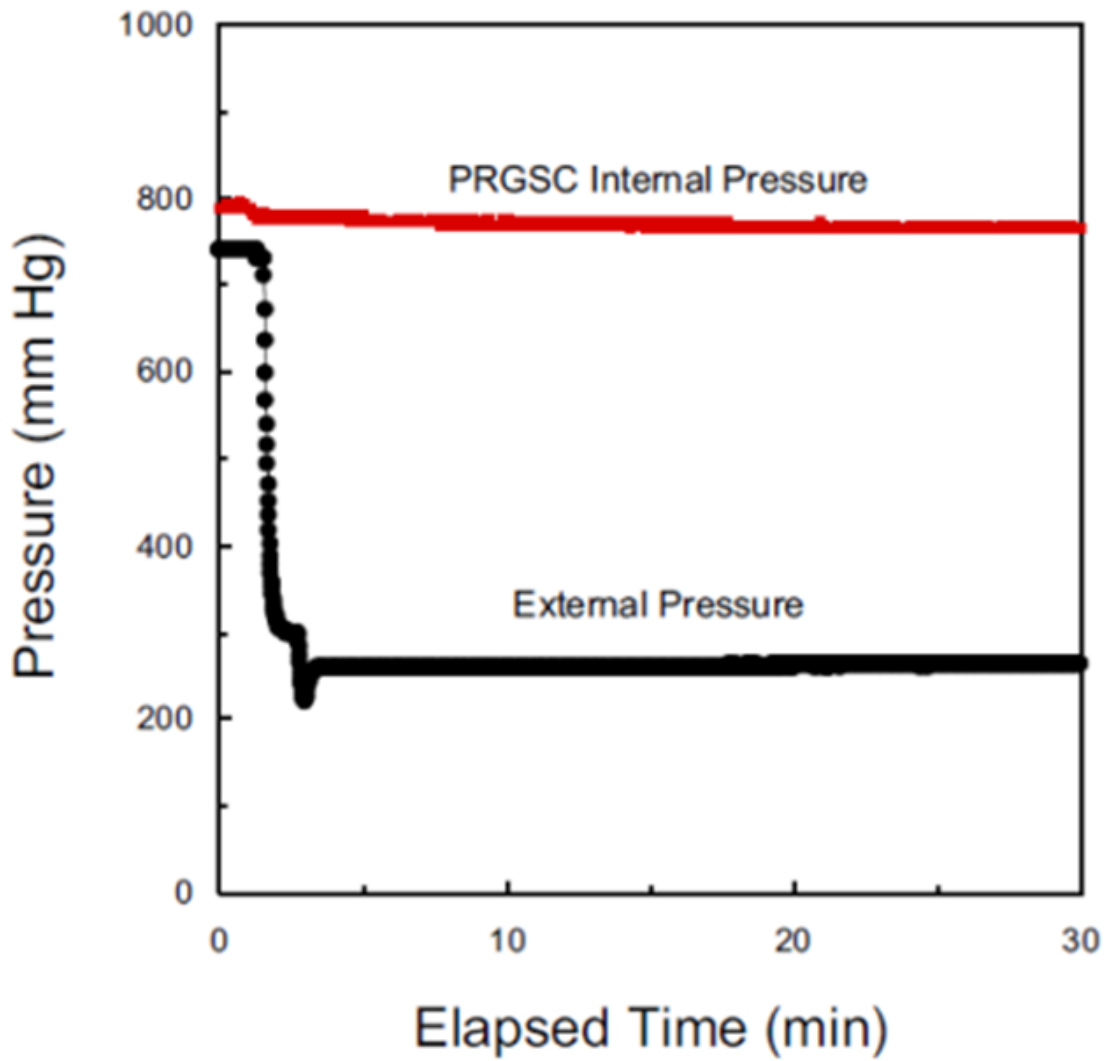


**Figure D.4: PRGSC maintains pressure.** Internal pressure for pressure regulated gyroscopic shipping container (PRGSC) when exposed to 250 mmHg absolute pressure vacuum.

## *Discussion*

Data obtained from actual islet shipments in reference containers during March of 2004 indicated that shipped islets were exposed to temperatures that ranged between 0°C and 32°C (**Figure D.1A**). Additionally, the reference containers experienced pressure drops as much as 200 mmHg during these shipments (**Figure D.1B**). The environmental conditions used in this study simulate conditions that may occur during overnight islet shipments by air. Ground transit on trucks during summer or in warmer climates can result in exposure of shipped islets to external temperatures at least as high as 40°C. At the opposite extreme, nonpressurized flights or warehouses without temperature control during winter can expose shipped islets to subfreezing temperatures. Islet shipments on nonpressurized flights can also experience low pressures (**Figure D.1B**).

More recently adopted packaging, such as experimental container 2 with 2 TS units, is better than previously used Styrofoam reference containers with or without cooling packs, but it is still inadequate for maintaining internal temperature under realistic shipping conditions from various islet isolation centers. During extreme heat exposure, the internal temperature of experimental container 2 came within 3 degrees of the external temperature after 15 hours. Furthermore, when exposed to extreme cold, the internal temperature of experimental container 2 fell below -10°C. It is undesirable for investigators to receive tissue exposed to extreme temperatures; freezing can lead to reduced viability, whereas overheating can lead to increased metabolic demand, nutrient depletion, increased accumulation of toxic metabolic byproducts, and ultimately cell death.

It should be noted that an exact comparison between the two phase-change materials, TS and TCP, was not conducted in this investigation. The number of TS packs used was chosen to simulate test containers evaluated by the ICR Center Consortium. Studies using an increased number of TS packs (**Figure D.3**) demonstrated further improvement in the performance of a shipping container based on this phase-change material. The density, compactness, and pricing of

TS will determine in part the practicality of increasing the number of TS for achieving better temperature control.

The data suggest that the target shipping temperature of  $22 \pm 2^\circ\text{C}$  can be maintained using corrugated plastic shipping containers packed with properly primed TCP. Even when exposed to extreme external temperatures, experimental container 1 with TCP maintained moderate internal temperatures. These stable temperatures approximated the target culture temperatures for human islets 24 hours post-isolation.

Future temperature control studies should focus on simultaneously protecting against both cold and hot temperature extremes. To account for seasonal differences in external temperatures, it has been suggested that liquified packs should be used in the winter and solidified packs in summer. However, this approach of priming the phase-change materials based on season is undesirable because of ambiguity during the spring and fall seasons and, more important, because temperatures can vary significantly across the route of a shipment (e.g., Minneapolis to Miami in January). Two approaches for better addressing this problem have been proposed. The first approach is to prime all packs by bringing them into a slushy (part liquid/part solid) state. However, priming may be poorly controlled with this approach as the fraction of the material in each phase cannot be accurately quantified and reproduced in all laboratory environments and situations in terms of ambient temperature, heat transfer, and timing. The second approach is to liquify a fraction of the packs to protect against cold temperatures and solidify the rest for protection against hot temperatures. The shipping container is then loaded with liquified as well as solidified packs. The fraction of each group could be defined based on the magnitude and duration of the possible temperature gradients in each direction.

The experimental results from the pressure control investigations suggest that the PRGSC can be used to maintain a stable internal pressure during islet shipment. When the external pressure was

reduced to 250 mmHg, a constant atmospheric pressure of 760 mmHg was maintained internally. The PRGSC can reduce the stress upon both the culture vessels and the shipped islets, providing one more measure of protection for islet shipments.

### ***Conclusion***

Based on the results presented in the current manuscript we concluded that, when TCP phase-change material was used in conjunction with the PRGSC for islet shipments, greater environmental control was achieved as pressure variations were eliminated and temperature fluctuations were minimized over long periods of time. This level of environmental control is expected to result in improvements in the quality of shipped islets received by investigators in the United States and worldwide. These improvements are particularly important when shipment of islets for clinical transplantation is implemented on a larger scale.



## Appendix E QMS FOR IMPROVING ISLET PURIFICATION

Sections of this chapter are reproduced in whole, or in part from the following publications with permission:

Manuscripts in Preparation:

**Weegman BP**, Sajja VSK, Suszynski TM, Rizzari MD, Scott 3rd WE, Kitzmann JP, Mueller KR, Hanley TR, Kennedy DJ, Todd PW, Balamurugan AN, Hering BJ, Papas KK, “Improving purified porcine islet viability by continuous quadrupole magnetic sorting (QMS)” To be submitted to Fall 2015

License and agreement documentation is included in **Appendix G**.

**Acknowledgements:** The authors would like to thank the Schott Foundation, the Minnesota Lions Diabetes Foundation, the Juvenile Diabetes Research Foundation (JDRF 5-2013-141), Giner Inc., the Schulze Diabetes Institute, and the NIH (P41 EB015894, and S10 RR025031) for supporting this research.

This work was supported by the NIH, National Institute of Diabetes and Digestive and Kidney Diseases Grant Numbers R01DK068717 and R44 DK070400, as well as The Carol Olson Memorial Diabetes Research Fund, The Iacocca Foundation, and The Schott Foundation.

The authors acknowledge Kurt Albreck of Donovan Specialties (Osseo, Minn), Denice Duderio, Laurie Macleod, Dr Kristen Maynard, Heather Nelson, William E. Scott III, and Christine Vincent from the Diabetes Institute for Immunology and Transplantation at the UMN.

The research described here was supported in part by grants from US National Institute of Health (R44DK065508-02 - MJT,1 R44 DK076326-0 & 5 R44DK076326-03- MJT, and R44DK069865 - JW).

## **Improving purified porcine islet viability by continuous quadrupole magnetic sorting (QMS)**

### ***Summary***

Islet transplantation (ITx) is a minimally invasive alternative to whole pancreas transplant for patients with uncontrolled type 1 diabetes. The islet isolation and purification process requires exposure to extended cold ischemia, warm-enzymatic digestion, mechanical agitation and the use of damaging chemicals for density gradient separation (DG), all of which inflict substantial damage reducing viable islet yield. Quadrupole magnetic separation (QMS) during digestion has been explored as an alternative for islet purification to reduce warm ischemia during isolation, minimize enzyme exposure and eliminate the use of density gradients. We explored the use of QMS for islet purification and compared the viability of QMS and DG purified islets. Porcine pancreata (n=3) were split into 2 parts; the combined connecting/duodenal lobe (CDL) and the splenic lobe (SPL). Islets were preferentially labeled using magnetic micro-particles (MMPs) that lodge within the islet micro-vasculature when infused into the pancreas. This allowed the continuous separation from the exocrine tissue by QMS during the collection phase of the digestion process. An optimized dose of MMPs (4.5  $\mu\text{m}$  diameter) were infused into the splenic artery to label islets within the SPLs, which were then digested using the Ricordi method and then continuously purified by QMS. Unlabeled islets from the paired CDLs were isolated using the same method and purified using DG. Oxygen consumption rate (OCR) normalized to DNA content (OCR/DNA) was used to compare the fractional viability of islets from both groups. Islets purified by QMS exhibited significantly improved viability and better morphology relative to control islets. The mean OCR/DNA of islets purified by QMS was higher than those purified by DG (209 $\pm$ 25 vs. 125 $\pm$ 11 nmol/min/mg DNA; p=0.02 via two-tailed paired student's t test). We conclude that continuous islet purification by QMS can reduce the detrimental effects of

prolonged exposure to toxic enzymes and density gradient solutions and substantially improve islet isolation efficiency and ITx success.

## ***Introduction***

Pancreatic islet transplantation is a promising and cost beneficial treatment for select patients with type 1 diabetes<sup>203,370</sup>, but there are many hurdles to overcome before transitioning to a standard of care. Using the current islet isolation and purification processes, enormous quantities of islets are needed to achieve insulin independence. Because of this large islet dose requirement; patients often require multiple islet infusions from two or more donors<sup>9,202,205</sup>. Islet isolation and pancreas allo-transplantation have similar success rates for maintaining insulin independence five years following transplant, but shortages of suitable donor pancreata limit the application of this encouraging treatment<sup>208</sup>. Some centers have demonstrated success with single donor transplants, and it is clear that a minimum viable islet dose is required to reverse diabetes<sup>208,298</sup>.

Many factors contribute to islet yield and viability including the donor parameters, procurement techniques, organ preservation methods, and especially the isolation process itself. Many islets are never retrieved during isolation<sup>371</sup> or are irreversibly damaged along the way<sup>277,372,373</sup>. The standard isolation processes involves a digestion step to liberate islets from the surrounding parenchyma, and a purification step to separate and purify the islets from the digested exocrine tissue. Other alternative methods are being explored<sup>275,276</sup>, but the standard digestion procedure uses strong proteolytic enzymes that are infused into the pancreatic ductal system to preferentially digest exocrine tissue at 37°C. The digestion process is harmful, and has been shown to damage islets<sup>374,375</sup>, but the purification step also damages islets most likely synergizing with the stresses encountered throughout the islet isolation process. Islets, making up only about 2 % of the total pancreas mass, are purified after digestion to decrease the volume of tissue being transplanted and to eliminate unnecessary and potentially harmful exocrine tissue. The exocrine tissue itself releases endogenous enzymes that may contribute to islet damage and loss in culture<sup>376</sup>. Co-culture of islets with contaminating exocrine tissue has been shown to decrease the overall

viability of the preparation, and this may have lasting effects decreasing the effectiveness of the graft post-transplant. Exocrine contamination may also directly affect graft health post-transplant by hindering vascularization<sup>377</sup> and eliciting damaging inflammation and immunologic responses<sup>378</sup>.

Current purification processes rely on a density gradient technique to separate the less dense islets from the more dense exocrine tissue. This method confounds the damage islets experience during digestion, by prolonging exposure to proteolytic enzymes. Furthermore, islets continue to experience substantial stresses throughout the purification process including extended hypoxia, abrupt temperature changes, mechanical shear stresses, as well as prolonged exposure to reactive oxygen species, hyperosmolar solutions, and pro-inflammatory cytokines<sup>366,379–381</sup>. All of these factors contribute to the overall viability and potency of the islet preparation. The density purification process also involves a collection step where islets are concentrated into pellets which create a very hypoxic environment. This is a paramount concern because islets are known to be especially sensitive to warm and cold ischemia because they lack the ability to cope with hypoxia<sup>291</sup>. Following the collection step, the islets are exposed to the density gradient chemicals (commonly Ficoll<sup>®</sup> or similar), and then centrifuged as a batch process in a COBE 2991 machine to separate the different tissues. The gradient solutions themselves have also been shown to contribute to islet damage and may encourage apoptosis<sup>380–382</sup>. This process can also be difficult to control (especially with human preparations) because of intrinsic inconsistency in exocrine tissue density, and variability in the extent of tissue digestion<sup>366,383,384</sup>.

Many alternative approaches to gradient purification have been explored, but none have proven to be a suitable replacement<sup>366</sup> despite the clear need for improvement. This can be partially attributed to limitations in scale and a lack of large throughput capability that is required for therapeutic islet transplant. Magnetic purification is one suggested method for islet purification,

and could offer significant benefits when compared to other methods. Magnetic separation techniques have been used to purify islets by selective magnetic labeling of the endocrine<sup>383,385</sup>, or the exocrine tissue<sup>386</sup>. Islet yields and transplant outcomes in rats were improved when magnetic micro particles (MMP) were preferentially entrapped within the tortuous microvasculature and purified using magnetic retraction<sup>387</sup>. Furthermore, developments in quadrupole magnetic separation (QMS) technology have shown promise for the large scale batch purification of porcine islets, with no observed detrimental effects on islet function due to magnetic forces or shear stresses<sup>277,388,389</sup>. Suszynski et al. also demonstrate that MPs are well tolerated *in vivo*, with no observed increase in islet cytotoxicity or inflammatory responses in mice<sup>390</sup>.

To further investigate the potential to improve isolated islet quality and viability, this pilot study directly compares density gradient purification and QMS technologies. Three porcine islet isolations were conducted to evaluate potential benefits of QMS. There is a growing interest in porcine islet xenotransplantation as a promising and cost-efficient approach to alleviate the donor shortage<sup>33,112</sup>. Also, porcine donors are a good surrogate model for these purification comparisons due to the similarity in pancreas size to the humans; and the consistency of donor parameters, procurement methods, and isolation parameters. For this study, QMS technology was further adapted for the continuous purification of porcine islets to reduce exposure to damaging digestion components, and eliminate exposure to harmful density gradients. Islet quality was determined by morphology score and viability was determined by oxygen consumption rate normalized to DNA (OCR/DNA)<sup>25-27</sup>, a predictor of islet function<sup>26</sup>. Improving islet quality and viability will improve the potency of transplanted islet preparations and may significantly improve the success of single donor islet transplantation.

## ***Materials and Methods***

### *Experimental design*

This pilot study compares the quality and viability of isolated porcine islets purified by either QMS or continuous density gradients (DG). To control for donor variability, and allow for paired comparisons between techniques, QMS and DG were done on islets from separate lobes of the same pancreas, that were digested using identical parameters. The pancreata were divided into two parts, with the first part composed of the combined connecting and duodenal lobes (CDL), and the second part being composed of the splenic lobe (SPL)<sup>38</sup>. Islets in the SPL were labeled with magnetic micro beads as described below, and islets in the CDL were not labeled. Both lobes were digested simultaneously but in separate digestion chambers and using identical isolation parameters and materials to ensure identical warm and cold ischemia, and similar digestion outcomes. Islets from the CDL were purified using standard DG purification, and labeled islets from the SPL were purified using an islet QMS system. Islet quality based on morphology score, and viability based on oxygen consumption rate normalized to DNA were compared between conditions.

### *Donors, procurement, and labeling*

All procedures involving animals were approved by the Institutional Animal Care and Use Committee (IACUC) and performed at the University of Minnesota. Three adult landrace porcine donors were used for this brief study, and all donors had similar mass ( $257 \pm 3$  Kg) and age ( $36 \pm 0$  months). Procurements were performed using previously described methods<sup>38,50,295</sup>, but briefly described as follows. Porcine donors were chemically sedated with a 100-500 mg dose of telazol, heparinized and then euthanized with a fatal dose of sodium pentobarbital. Following confirmation of death, donors were exsanguinated, eviscerated, and pancreata were dissected from the viscera *en bloc* on the back table. During dissection, the aorta was located and the celiac

trunk (CT) and superior mesenteric artery (SMA) were simultaneously flushed with 3-5 liters of cold organ preservation solution (CPS), and the pancreatic duct was infused with 60 ml of ductal preservation solution. The pancreas was also cooled by applying crushed frozen lactated Ringers solution and irrigation. All pancreata experienced less than 20 minutes of warm ischemia. After complete resection with the vasculature intact, the pancreas was split into the CDL portion, and the SPL portion. The native arterial vasculature was preserved with the SPL for infusion of MMPs. A previously optimized dose of 4.5  $\mu\text{m}$  diameter MMPs (Dynabead M450, Invitrogen, Carlsbad, CA) were suspended in one liter of CPS ( $16 \times 10^8$  MP/L) and infused into the splenic lobe through the CT and SMA using the hand syringe technique described by Rizzari et al in 2010<sup>295</sup>. After bead infusion, a second liter of CPS was flushed into the arteries to rinse out any beads that were not securely lodged in the micro-vessels. Then both portions of the pancreas were submerged in CPS and transported to the isolation facility in an ice-filled cooler. All pancreata in this study experienced less than 250 minutes of cold ischemia before isolation.

### Digestion

Islets were isolated from each lobe by the isolation team at the Schultze Diabetes Institute at the University of Minnesota, in the same manner using the standard enzymatic digestion process<sup>391,392</sup>. The new enzyme mixture described by Balamurugan et al. in 2012 for use with human islet isolation<sup>274</sup>, was used to manually distend the pancreatic lobes from each pancreas. Following distension, the pancreas tissue was cut into 1 cm pieces and placed into a digestion chamber. Both the CDL and SPL from each pancreas were digested separately, using identical isolation parameters. The tissue from the CDLs was collected and purification by density gradients, and tissue from the SPL was continuously purified using QMS.

### Density Gradient Purification



Following the digestion phase, the digested tissue from the CDL of each pancreas was prepared for density gradient purification. The tissue was collected and recombined using the standard method in chilled conical tubes primed with heat inactivated porcine serum serum to reduce the enzyme activity. The tubes were gently centrifuged and all of the tissue pellets were further collected into a single conical. The digested tissue was then separated by continuous density gradients (UW/OptiPrep Axis-Shield, Dundee, UK) using a Cobe 2991 cell separator<sup>392,393</sup>, to attain a pure islet fraction.

#### QMS Purification

After completion of the digestion phase and when periodic sampling indicates that the islets are free, tissue from the SPL of each pancreas was separated by QMS. Rather than collection into conicals, the digested tissue containing MP labeled islets and unlabeled exocrine tissue was directly processed by the QMS system shown in **Figure E.1**. Before the purification process began, the Islet QMS separator (Techshot Inc., Greenville IN)<sup>388</sup> was primed with Hanks' balanced salt solution (HBSS) containing 10% heat inactivated porcine serum, and an infusion bag for flow buffering was prepared containing the same solution. The digested tissue left the chamber, and was directly transferred to the buffer bag. The tissue only remained in the buffer bag for a few moments as it was quickly passed through the QMS system. The QMS inlet flow rate (out of the buffer bag) was matched with the flow rate of tissue leaving the digest chamber to maintain a continuous purification process. The mechanism for the QMS process using this system is described in detail by Kennedy et al. and others<sup>277,388,394</sup>. Briefly, as the tissue flow stream entered the QMS separator column, it is met with a parallel fresh stream of HBSS solution. Labeled islets are pulled by the magnetic force within the column out of the isolation stream and into the fresh solution stream, and then remain within the column. Unlabeled exocrine tissue passes freely through the column and into a waste collection vessel. After all of the tissue

has been processed, the column is removed from the magnet, and the purified islet tissue is gently washed out.

#### Isolation Outcomes and Islet Quality Assessment

After the purified islet fraction is collected from either the COBE bag, or the QMS column, the islets are gently washed with fresh culture medium (supplemented ME199, Mediatech Herndon, VA). Samples were taken for initial quality assessment, and then cultured using the same medium at 37°C with 5% CO<sub>2</sub> for up to 7 days in silicon rubber bottom culture vessels (Wilson Wolf Manufacturing, New Brighton, MN)<sup>91</sup>. Islets from both conditions were cultured at a density of 2000IE/cm<sup>2</sup> or less. Initial samples from both conditions were assessed for quality by comparing islet morphology score<sup>135,365,392,395</sup> and viability by measuring the OCR/DNA as described in literature<sup>26</sup>. These methods are established, but described briefly as follows. Qualitative morphological assessment was made by experienced isolation personnel, where samples of islets were viewed under magnification and scored from 0-2 based on the shape, border, integrity, diameter, and presence of single cells for a total score from 0-10 for each sample. Islets with better gross morphology would have a higher score. Islet viability was determined by measuring the OCR/DNA using a titanium stirred micro-chamber system<sup>25</sup>, and DNA was quantified using the Quant-iT PicoGreen dsDNA kit (Molecular Probes, Eugene, OR).

#### Statistical Methods

Small samples sizes are a limitation of this brief study, nonetheless average values are reported as the mean ± the standard error of the mean. The two tailed un-paired student t test was used to compare OCR/DNA measurements, while the non-parametric Mann-Whitney rank sum test was used to compare islet morphology scores between groups.

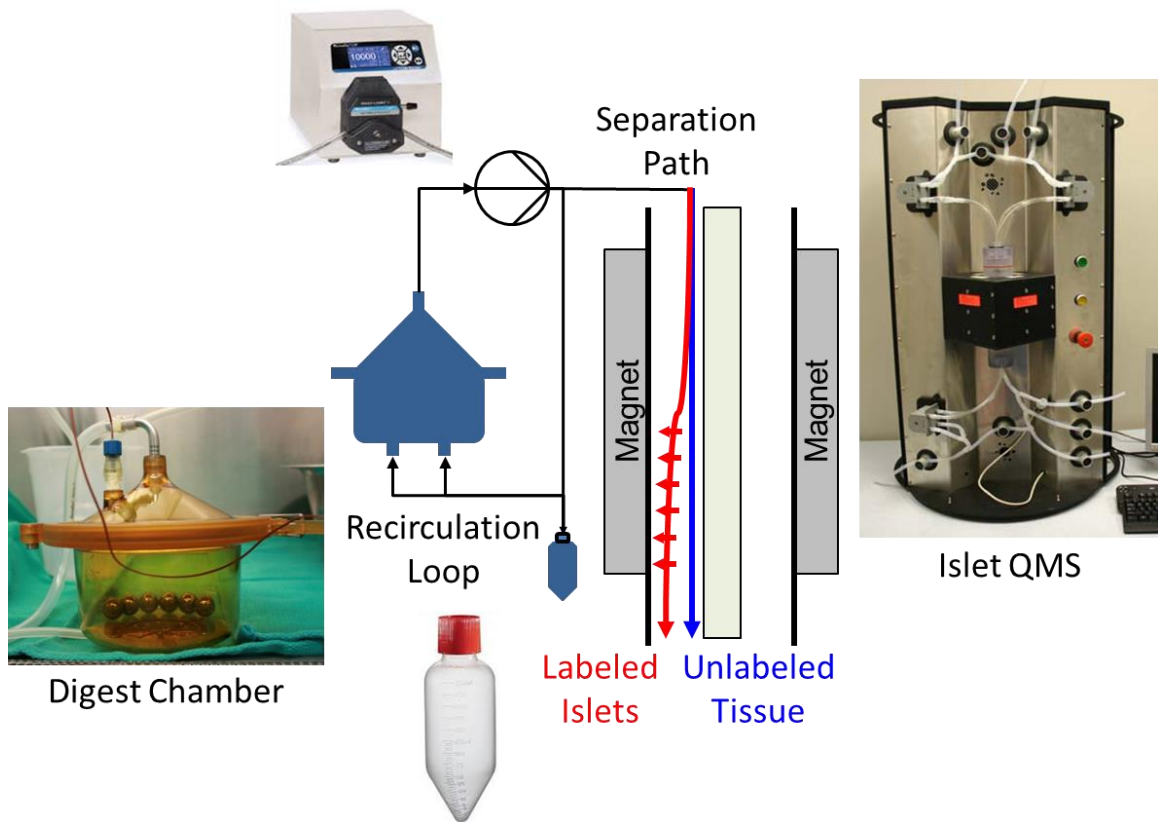


**Figure E.1: Schematic diagram of continuous purification QMS system.** The QMS replaces the collection and purification steps of the islet isolation process with a continuous QMS of labeled islets from the collection stream leaving the digestion chamber. This process streamlines islet preparation, avoids the harmful centrifugation, recombination, and gradient purification steps, and immediately washes and collects the purified islet product.

## ***Results***

To explore the potential of using QMS to improve isolated islet quality and viability, this paired experiment was designed as a pilot study to directly compare this purification method to the traditional method of DG purification. Three porcine pancreata were split into two parts, with the first part (CDL) being isolated and purified by DG, and the second part (SPL) being isolated and purified by continuous islet QMS. Isolated islets were compared for quality as determined by islet morphology score, and viability as determined by OCR/DNA measurements immediately following isolation, and after 7 days of culture.

Porcine islet morphology as reported by the islet score can be a gross indicator of damage that occurs during the digestion and purification process. Islets from porcine donors do not have a robust islet capsule that is often observed surrounding human islets, and this can make them more sensitive to damage associated with the isolation process. Frequently, islets are observed with rough and uneven borders indicating damage to the cells around the islet periphery. **Figure E.2A** shows a plot of average islet morphology scores of islets isolated and then purified using the QMS and DG systems. Islets purified by QMS had an improved average islet score when compared to islets purified using a standard DG system, and **Figure E.2B-C** shows representative micrographs of islets from each condition. Due to the small sample sizes used in this study, the difference in average islet scores is not statistically significant ( $p=0.16$ ), but the differences in gross islet morphology observed in the micrographs can be easily appreciated at the higher magnification shown.

Oxygen consumption rate measurements were taken from samples of islets of each condition to determine the viability. Samples were collected and assessed immediately following isolation, and after 7 days of culture. The OCR/DNA of islets purified by QMS was significantly higher than DG purified islets immediately following isolation with mean values of  $236 \pm 25$ , and  $135 \pm$

11 nmol/min/mg DNA respectively ( $p < 0.03$ ) and marginally higher after 7 days in culture with mean values of  $231 \pm 32$  and  $224 \pm 28$  nmol/min/mg DNA respectively ( $p > 0.8$ ). **Figure E.2D** shows a 67% improvement in islet viability immediately following isolation. This improvement is not as prominent after the 7-day culture period because the DG average viability increased during the culture period. This could be explained by the clearing of dead tissue in the DG condition, which improves the average viability with a loss in total tissue recovery. Comparisons of islet yield and purity were beyond the scope of this small trial because sort parameters were not optimized for these outcomes.

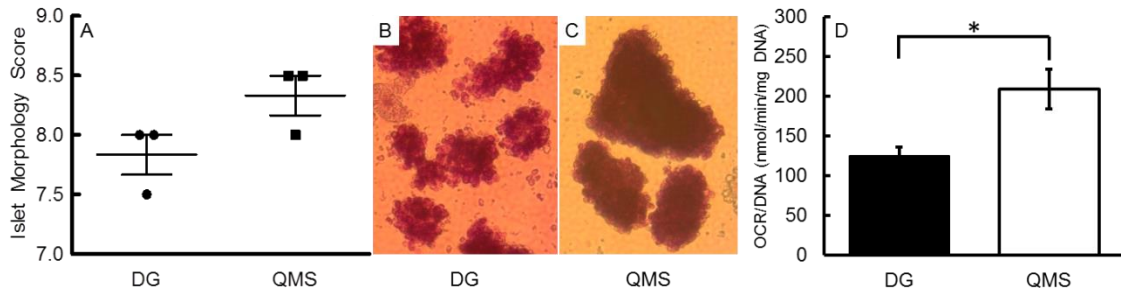


**Figure E.2: Juvenile porcine islet morphology and OCR/DNA.** (A) Islet morphology scores determined immediately following isolation and purification. Islets purified by quadrupole magnetic separation (QMS) show improved morphology scores compared to traditional density gradient purified islets. Higher scores indicate better islet shape, borders, integrity, and diameter along with reduced presence of single cells. The sample size is small so the difference is not significant, however QMS purified islets exhibited a better score for all three islet isolations. (B-C) Representative magnified images of islets stained with dithizone immediately following isolation purified using; (B) density gradients (DG) or; (C) quadrupole magnetic separation (QMS). At higher magnification it is easy to appreciate the improved gross morphology of islets purified by QMS. Islet purified using QMS noticeably exhibit a more robust appearance, with larger sizes, more defined borders and less free single cells. Islets purified using DGs frequently have a more fragmented appearance, with smaller size, and rough borders. (D) Bar graph presenting the measured viability of islets purified using density gradients (DG), or quadrupole magnetic separation (QMS) immediately following isolation-D. QMS purified islets have a significantly higher viability ( $p = 0.03$ ) than DG purified islets immediately after isolation.

## ***Discussion***

Islet allo-transplantation is a promising therapy for the treatment of type 1 diabetes, and islet xeno-transplantation offers the opportunity to alleviate donor shortages, and expand the application of this treatment to a larger patient population. Islet transplantation offers many benefits over other therapies such as whole pancreas transplant, or insulin therapy<sup>68,396</sup>. Despite these benefits, one of the primary barriers to expanding the application of islet transplantation is the frequent need for multiple islet transplants, from 2-3 donors, to maintain insulin independence often in quick succession. This requirement puts further strain on the already stressed organ donation programs, and prevents the growth of this promising treatment. Some centers have encountered success with single-donor transplants<sup>208,298</sup>, but most centers still need multiple donor pancreata to meet the very large total islet dose required for patients to remain insulin independent<sup>9,202,205,396</sup>. Experience in pancreatic surgery suggests that patients can avoid diabetes even when large portions of their pancreas are removed, and research suggests that patients don't become diabetic until a large portion of their islet function fails<sup>397-399</sup>. These experiences suggest that current islet transplant dose requirements have significant room for improvement. There are many factors that contribute to this large dose requirement, but the potency of transplanted islets, and their function in the body post-transplant are of paramount concern. The potency of an islet preparation is affected by a plethora of factors including: donor health, extended exposure to brain death, pancreas condition, organ procurement and preservation methods, and islet isolation and culture methods. This work focuses on improving islet quality and viability which directly affects the therapeutic potency of the islet transplant, and gives islets the best chance of engraftment and survival.

Much attention in the field is given to improving the enzymatic digestion step of the isolation process, but there is also significant damage to islets during the purification step<sup>366,379-381</sup>. Islets

experience very harsh conditions that inflict lasting damage during the mechanical and enzymatic digestion process<sup>374,375</sup>, but the current DG purification method significantly prolongs and exacerbates this damage. This study proposed the use of QMS technology as an alternative method for the purification of liberated islets to significantly improve islet quality and viability. The results presented clearly demonstrate that QMS purified islets have improved morphology, and significantly improved viability immediately following the isolation process. These improvements can be attributed to eliminating the use of harmful DG chemicals<sup>380-382</sup> and the numerous functional benefits of QMS over the traditional DG purification method. During the digestion process, when the tissue within the closed circuit is considered to be adequately digested so that most or all of the islets observed in periodic samples appear to be free from the exocrine tissue, the digestion phase ends, and the collection phase begins. This is commonly called the “switch” point, when closed loop circuit is opened, and the digested tissue is slowly collected. Tissue that is not completely digested remains within the chamber to continue the digestion process. Purification using DG methods then expose islets to extended periods (up to an hour) of warm and cold hypoxia in the digestion solution during the collection, centrifugation (recombination), and COBE processes. When using the continuous islet QMS system, these steps are completely eliminated, and the digested tissue is transferred directly to the QMS system where the islets are almost immediately processed and removed from the harmful digestion solution.

The islet QMS system is a continuous sorting technology previously described in the literature<sup>277,388</sup> where the stream of digested tissue travels through a uniquely designed separation column that is surrounded by a powerful rare-earth magnet. When the tissue stream enters the column, it is met by a cool fresh solution stream that will travel through the column along with the tissue stream in a laminar flow, so that the two streams have minimal mixing. Islets that are



labeled with magnetic beads are quickly but gently “pulled,” by the magnetic forces, out of the digestion stream and into the fresh solution stream. The digestion solution contains many of the harmful enzymes, cytokines, and reactive oxygen species that can damage islets. Using the continuous QMS method within a minute or two after leaving the digestion chamber, the islets are removed from the damaging environment, and washed with a fresh solution stream. Using the current QMS technical parameters (flow rates etc.) the separated islets were pulled to the side wall of the column, and remain within the column for the duration of the purification. During this time, the purified islets were continuously washed with a stream of fresh chilled solution. After the purification process is complete (shortly after completion of the digestion process), the column was sealed, and carefully removed from the QMS system, so that the purified islets could be washed out, and collected for culture and quality assessment.

In this study, QMS purified islet viability as measured by OCR/DNA immediately following isolation showed a 67% improvement over DG purified islets. For cases like auto-islet transplantation, when islets are almost immediately infused following isolation, these results could have profound implications. Auto-islet transplants are routinely done for patients who suffer from chronic pain associated with pancreatitis. The pancreatectomy is done to alleviate pain, and the patient’s own islets are infused to avoid diabetes. Often, the pancreas in these patients is in very poor condition with calcifications and fibrosis, which can significantly reduce the islet yield obtained during isolation. This makes the maintenance of islet dose and potency primary concerns when total islet mass is very limited. To ensure a maximum amount of transplanted islets, sometimes the purification step is avoided, and the total amount of unpurified tissue is infused. Literature suggests that this practice may be detrimental to islet engraftment and function<sup>376–378</sup> due to the large presence of digested exocrine tissue. Some centers will do a purification step using density gradients to decrease the amount of exocrine tissue, and total tissue

volume for transplant. In these cases, when purification is desired, using QMS instead of DG could have a substantial impact on graft function because the purified islets would have increased viability and a better chance of survival post-transplant. **Figure E.3A** illustrates this point by projecting more than two-fold improvement in insulin independence rates. The total OCR transplanted is a reliable benchmark for predicting insulin independence in auto- and allo-islet transplantation<sup>26,96</sup>(and unpublished work), and this metric encompasses both the total amount of tissue transplanted, and the viability of that tissue. More studies focused on the application and optimization of QMS as a potential method for purification of islets for auto-transplant cases are of critical importance.

QMS could have an even greater impact on islet allo-transplant outcomes, because islets are almost always purified using DG methods, and are frequently cultured for 1-2 days following isolation. With significant improvements in viability, the islets will survive better in culture, and this will increase the total number of viable islets available at the time of transplant. **Figure E.3B** predicts a 92% insulin independence rate for islet allografts if islet viability was improved by 67% as observed with QMS purified islets. Future studies comparing the post-culture recovery of human islets purified by QMS and DG would be extremely valuable, and would illuminate the potential of this method for use in allo-transplant applications and may improve the consistency of purification which is problematic at present. QMS purification methods could be a big step toward the success of single-donor islet transplantation.

Furthermore, as the application of porcine islet xeno-transplantation holds much promise for alleviating the donor organ shortage, continuous islet QMS could replace DG purification methods and increase the consistency and viability of isolated islet products. The field of islet xeno-transplantation faces many challenges and islet potency has been determined to be a critical metric for approval of this cellular therapy. Xenogeneic islets will be subject to great scrutiny and

will require extensive characterization and quality control. QMS can eliminate the use of damaging DG chemicals, simplify and streamline the purification process, and improve overall preparation quality and potency.

The results of this pilot study strongly demonstrate that QMS is a promising purification method for improving isolated islet quality and viability. Numerous technical parameters (eg. flow rates) are associated with the QMS system and critical studies with larger scope are required to optimize the process for improving yield and purification efficiency before clinical implementation. Further improvements and adjustments in equipment design and implementation for specific applications (eg. xeno, allo or auto transplants) may be required and may expand the benefits observed in this early study. It should also be noted that the islet labeling methods used for this study were established in literature<sup>387,295</sup>, but in conjunction with QMS equipment and process improvements, additional investigation is required to enhance infusion and labeling for human and porcine islets.

## ***Conclusion***

To conclude, this study establishes that QMS technology adapted for islet separation can be used to significantly improve islet quality and viability immediately post isolation as compared to DG purification. Despite the minimal data set, the results presented suggest that with further optimization, QMS could be a superior method for islet purification. This technology offers great promise for improving the viability of isolated porcine islets, and this application is becoming more relevant as xeno-transplantation is approaching clinical application. QMS technology has the potential for a more-immediate application to improve clinical outcomes for select islet auto-transplantation cases, and nearly all islet allo-transplantation cases, by eliminating the use of DGs, and improving overall islet preparation viability. There are many challenges to overcome for the large-scale implantation of islet transplantation for the treatment of diabetes, but improving isolated islet viability is a major step toward single donor success in allo-transplantation, and implementation of porcine islet products for xeno-transplantation.

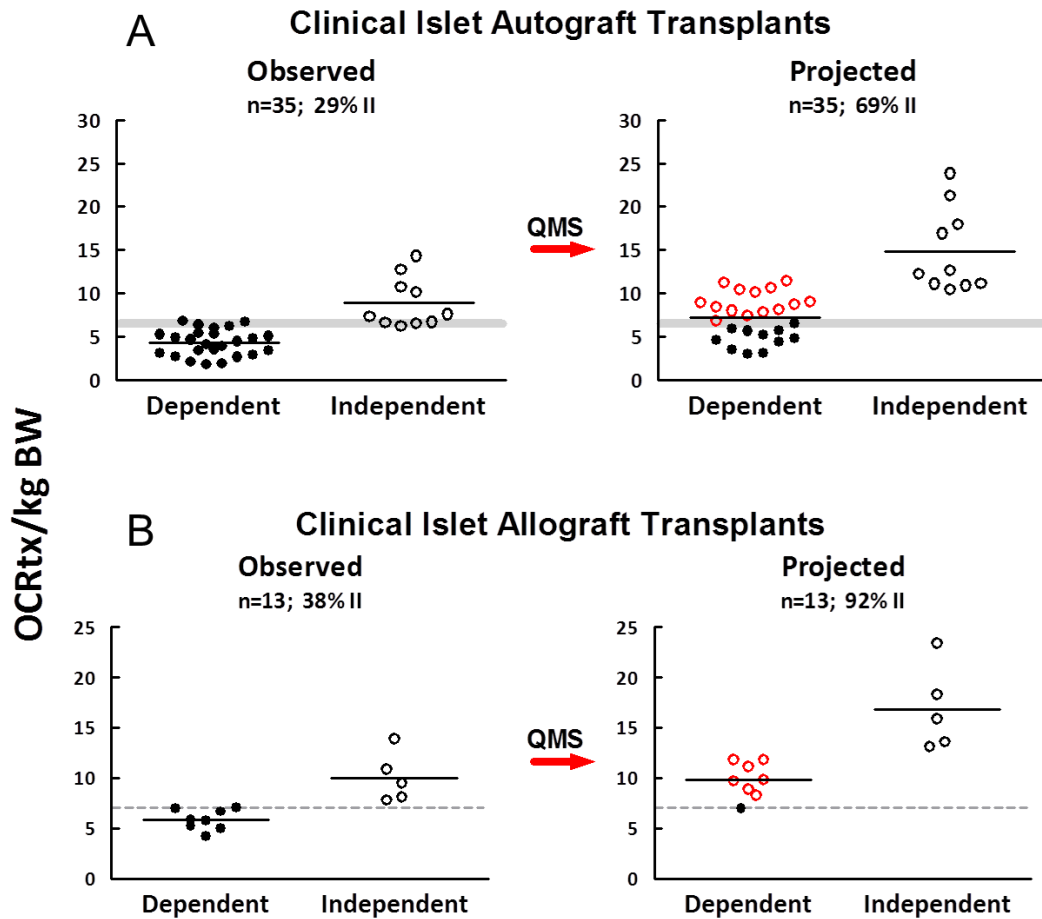


**Figure E.3: Projected transplant outcomes using QMS.** QMS improves isolated islet viability which projects significantly improved insulin independence rates for clinical islet (A) autografts and (B) allografts. When the observed 67% improvement in viability (OCR/DNA) for QMS separated islets is applied to clinical autograft and allograft data, the improvement in viable islet mass (OCRtx/kg BW) causes the majority of patients to overcome the threshold for insulin independents (grey bar, or dashed line). This prediction (based on the limited data-set) suggests an increase in insulin independence rates to 69% and 92% for autografts and allografts respectively.

## Appendix F SUPPLEMENTAL REFERENCE FIGURES

### *Appendix F.1: Organization*

This appendix contains figures and captions providing more details and images on the content from the main chapters and appendices of the Thesis. This appendix is organized into subsections to coincide with the chapters or appendices of the Thesis body. If a section does not have supplemental figures, the heading will be included followed by “None”.

## Appendix F.2: Whole Organ Oxygen Consumption

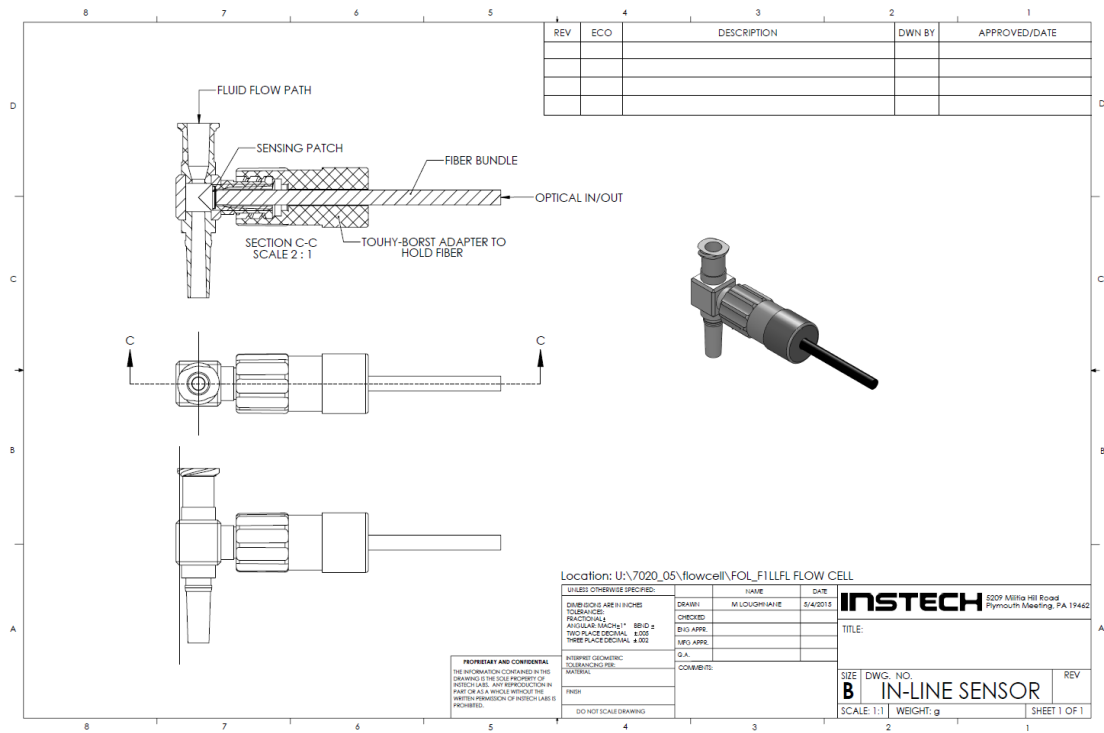


**Figure F.2.1: Flow type fiber optic oxygen sensor.** Specialized fiber optic oxygen sensor designed for whole organ oxygen consumption rate measurements were designed to be reusable, stable, and MR compatible to allow for oxygen measurements in perfusion solutions following calibration.

***Appendix F.3: Improving Pancreas Procurement***

None

***Appendix F.4 Hypothermic Machine Perfusion to improve organ preservation***

None

***Appendix F.5: Juvenile Porcine Islet Culture***

None



## ***Appendix F.6: Nutrient Regulation and SSB Culture***



**Figure F.6.1: Prototype outflow tubes v1.** Picture of various prototype outflow tubes used to prevent the removal of cell-aggregates during perfusion culture in stirred suspension bioreactors. Syringes of various materials and diameters were tested with different “baffle” designs to prevent turbulence in the medium of the outflow tube. All of the tube designs were intended to maintain a volume of medium within the tube that is slowly removed with the linear vertical flow being slower than the settling rate of spheroids in culture. Turbulence was observed with all of these outflow tube designs that prevented proper function and did not prevent removal of aggregates in the perfusion waste stream.



**Figure F.6.2: Prototype outflow tubes v2.** Second series of outflow tube designs tested with cell aggregate cultures in perfusion stirred suspension bioreactors. These designs incorporated more complex geometries to reduce turbulence that was observed within the first series of outflow tubes tested. The most successful tube was a porous “fritted” glass tube that maximized the surface area for medium removal which minimized clogging of the filter. The linear flow velocity through each pore in the filter was much lower than the settling rate which prevented clogging at normal cell/aggregate densities in culture. Some clogging was observed at very-high cell densities ( $\gg 3.0 \times 10^9$  cells/ml), and studies were designed to avoid this upper limit.

## Appendix F.7: $^{19}\text{F}$ -MRS for Oxygen Measurement

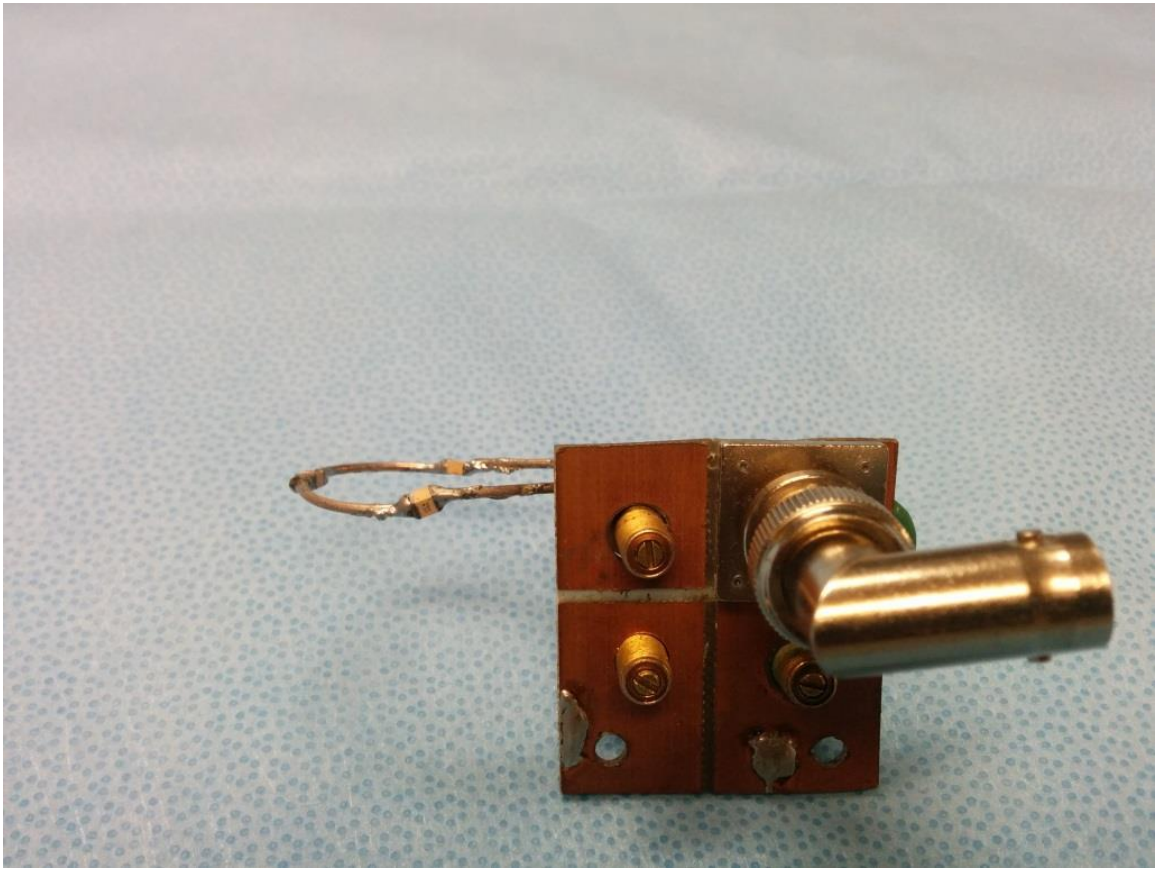


**Figure F.7.1: Surface coil for  $^{19}\text{F}$  –  $^1\text{H}$  *in vitro* studies.** This coil was fabricated for use on *in vitro* studies with relatively small samples. It was constructed with 2 cm x 3 cm oblong single loop surface coil made of silver plated copper wire with three 16 gauge wire segments. The impedance is divided in the circuit by including three ceramic capacitors 4.7, 4.7, 3.6 pf (American technical ceramics) which were equally spaced along the loop. A single variable PTFE capacitor, 0.8 – 20 pF, was used for tuning, and two PTFE variable capacitors, 1.5-40 pF, were used for matching the coil (voltronics). The coil was tuned and matched under sample load prior to each study using a MR safe RF network analyzer.

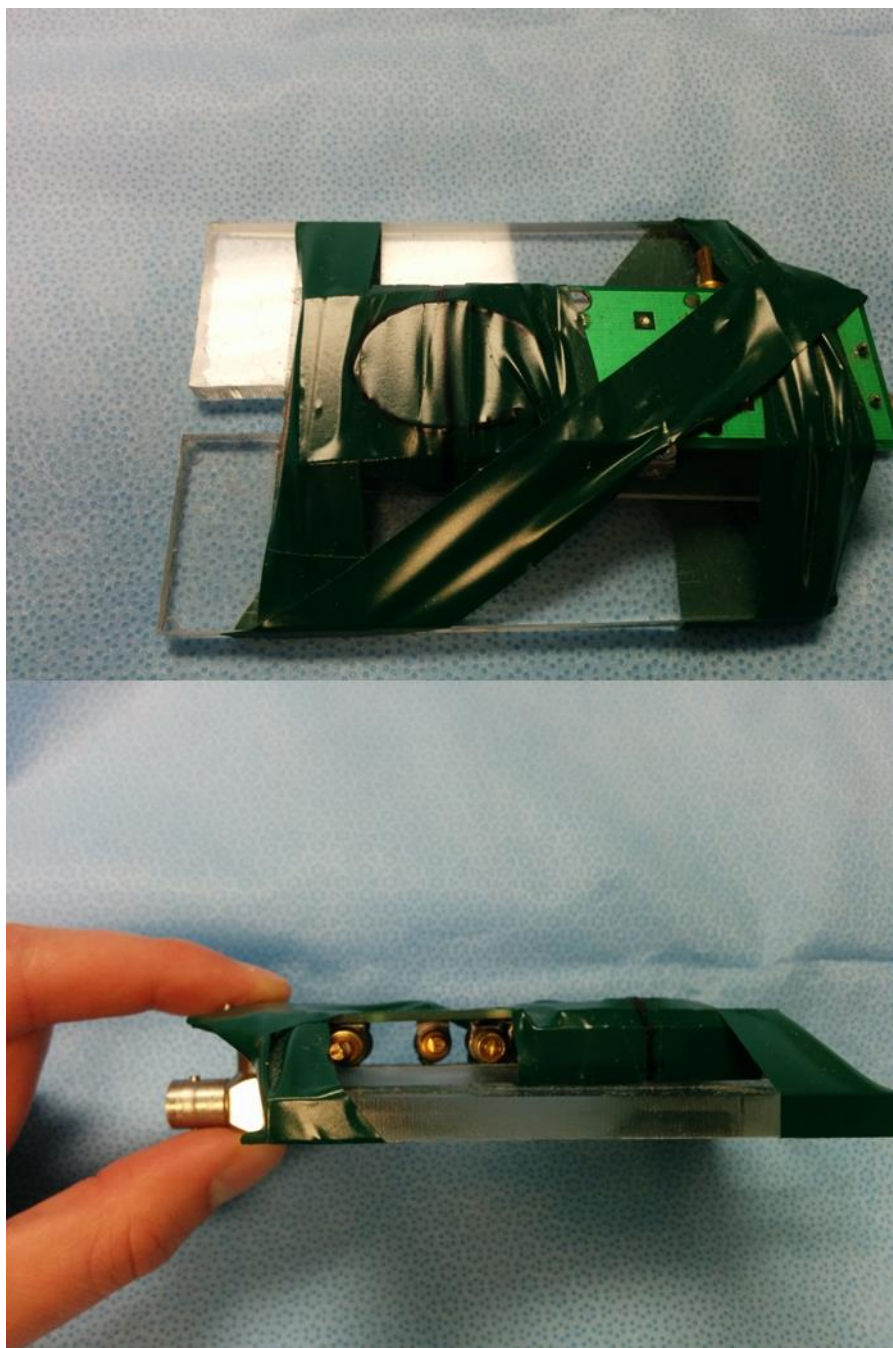


**Figure F.7.2: Surface coil for  $^{19}\text{F}$  –  $^1\text{H}$  *in vivo* studies.** A second coil was fabricated for *in vivo* studies (large samples) with 2 cm x 3 cm oblong single loop surface coil made of silver plated copper wire with three 16 gauge wire segments. The impedance is divided in the circuit by including three 3.9 pF ceramic capacitors (American technical ceramics) which were equally spaced along the loop. A single variable PTFE capacitor, 1 – 19 pF, was used for tuning, and two variable PTFE capacitors, 1.5-40 pF, were used for matching the coil (voltronics). The coil was tuned and matched under sample load prior to each study using a MR safe RF network analyzer.

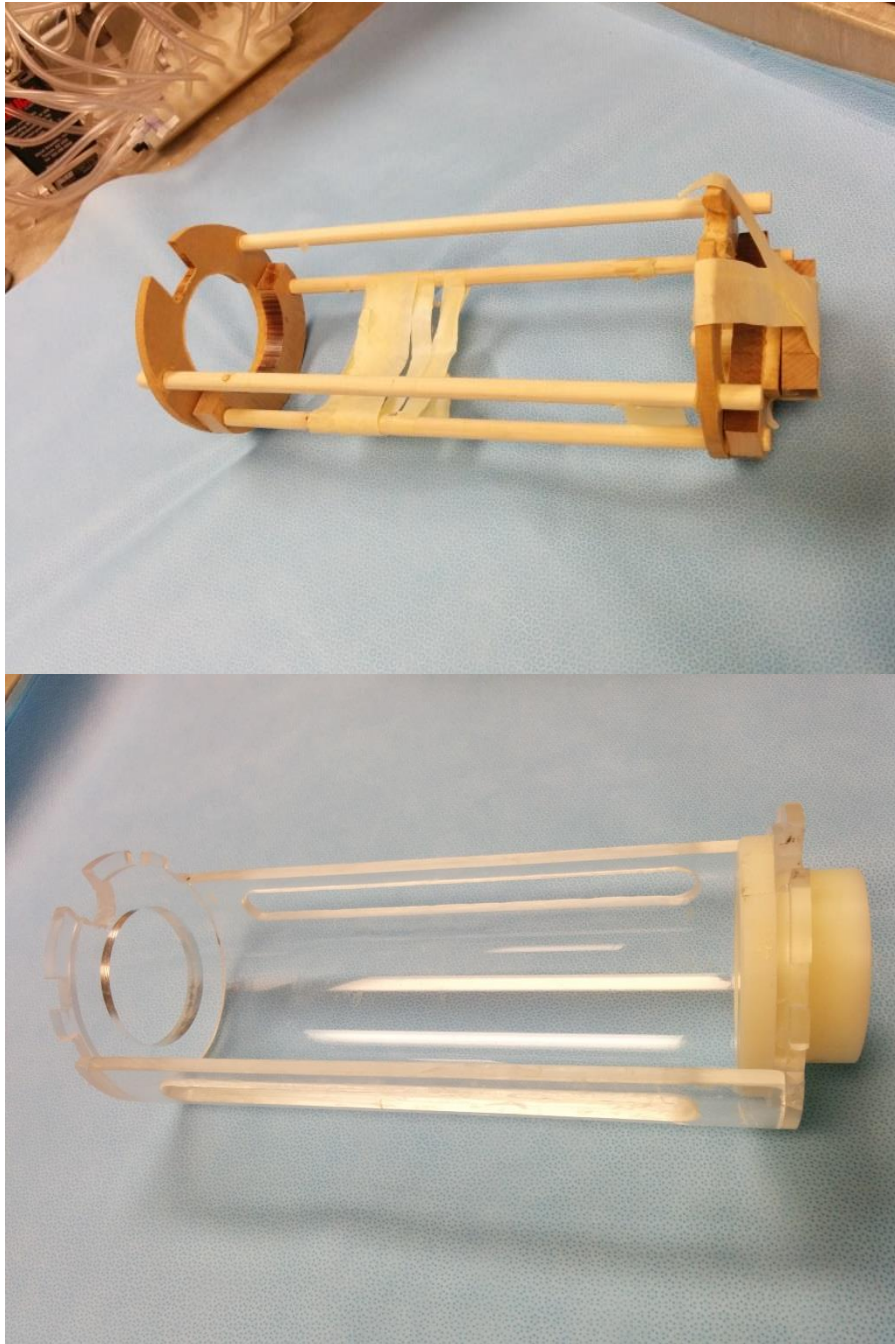


**Figure F.7.3: Rat hammock v1 and v2.** A custom restraint system was designed for rat studies in the 16.4 T MR system. The frame of the first version (v1) was composed of wood (top), and the updated version of the frame (v2) was made of a polycarbonate semi-cylinder and an ABS plastic end for mounting (bottom). The outer diameter of the frame was 11 cm in diameter to coincide with the functional bore diameter of the 16.4 T MR system. Holes were included on either end to allow for un-obstructed cable travel, and strain relief. A notch was also included in the “superior” side of the frame to allow for the anesthesia nose-cone to sit in position.

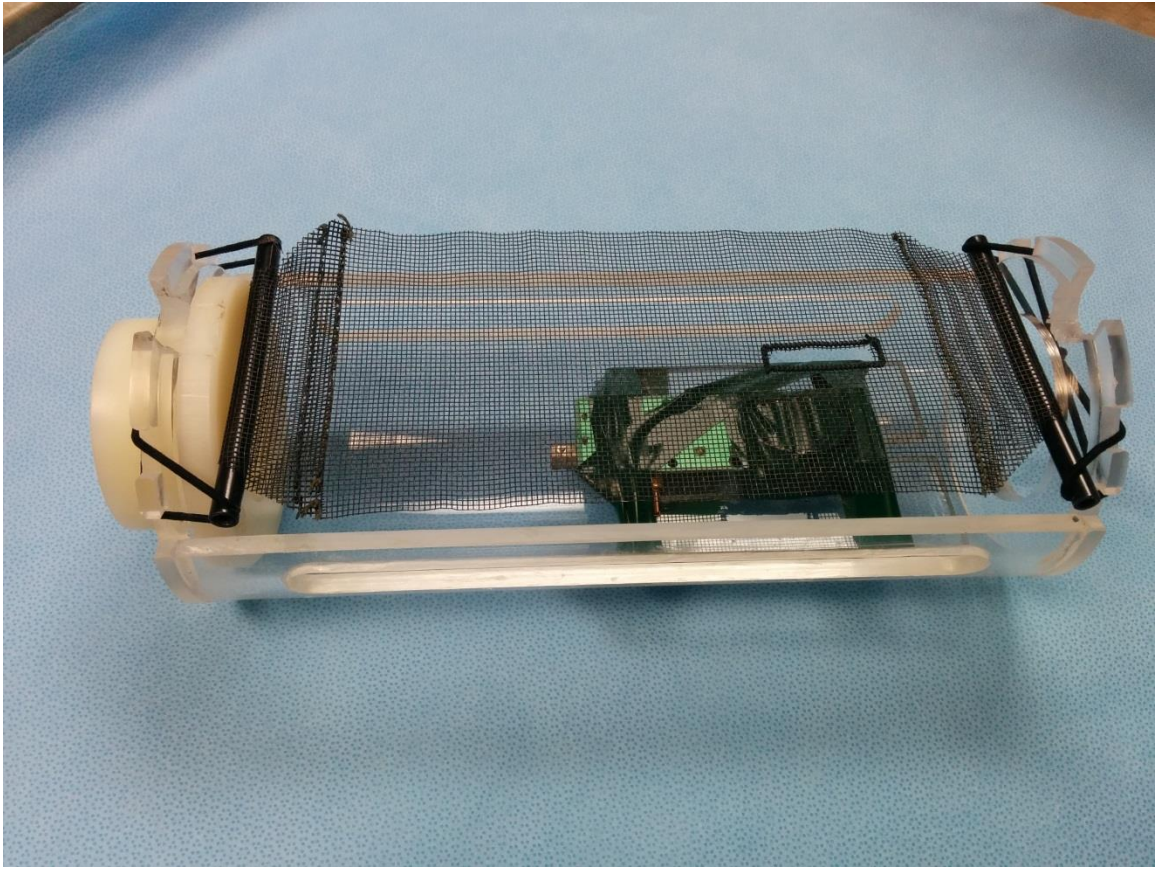


**Figure F.7.4: Rat hammock v2 mock-up.** The updated version of the rat hammock is shown with coil and “hammock” in place. The entire apparatus was attached to the end of a guide to provide a means of centering the animal in the bore of the 16.4 T MR system. The coil rested in the bottom-center of the polycarbonate frame as shown, and coil tuning capacitors were accessed through access slots in the side of the frame. The coil could also be positioned in the axial direction by sliding along the bottom of the frame to align perfectly with the implanted device in the animal. The hammock itself was made from a stitched piece of MR compatible mesh (fiberglass), and was held in-place on the frame with elastic bands.

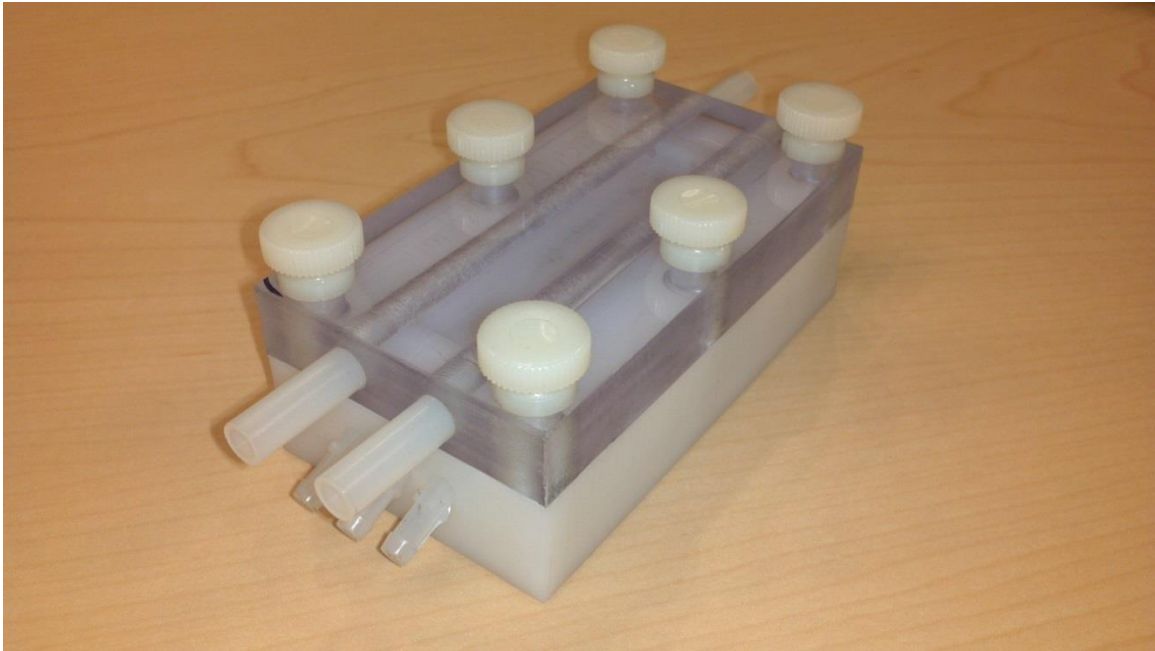


**Figure F.7.5: Perfusion bioreactor picture.** A perfusion bioreactor was designed and comprised a polycarbonate lid with ports for heat-exchanger circulation. The lid was fastened tightly to the main chamber using 6 nylon screws to distribute the force needed to adequately seal against the chamber. A thin 0.5 mm silicon rubber gasket was used at the mating surface to provide a water and air-tight seal. The chamber was made of polyoxymethylene (acetal resin, Delrin) plastic, and a central chamber was machined to accommodate a TheraCyte device. Three access ports were included on each longitudinal end of the chamber to provide access for instrumentation, and for circulating perfusion medium through the central chamber. The approximate external dimensions of the assembly were 3.5" x 1.75" x 1" (L x W x H), and the internal chamber dimensions were approximately 2.5" x 0.75" x 0.125" (L x W x H).

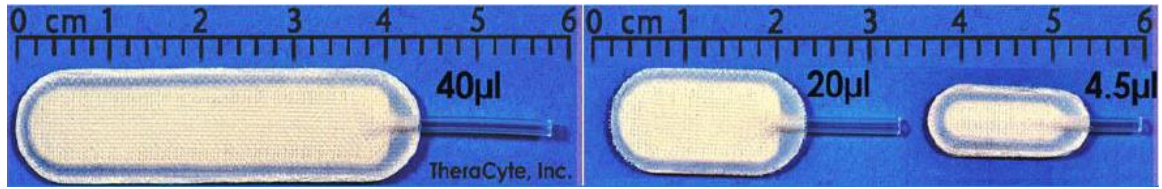


**Figure F.7.6: TheraCyte devices with scale.** Three different sized TheraCyte devices were used for the included studies. The construction of each implant was the same, and only the geometric dimensions were scaled to accommodate different cell-doses.



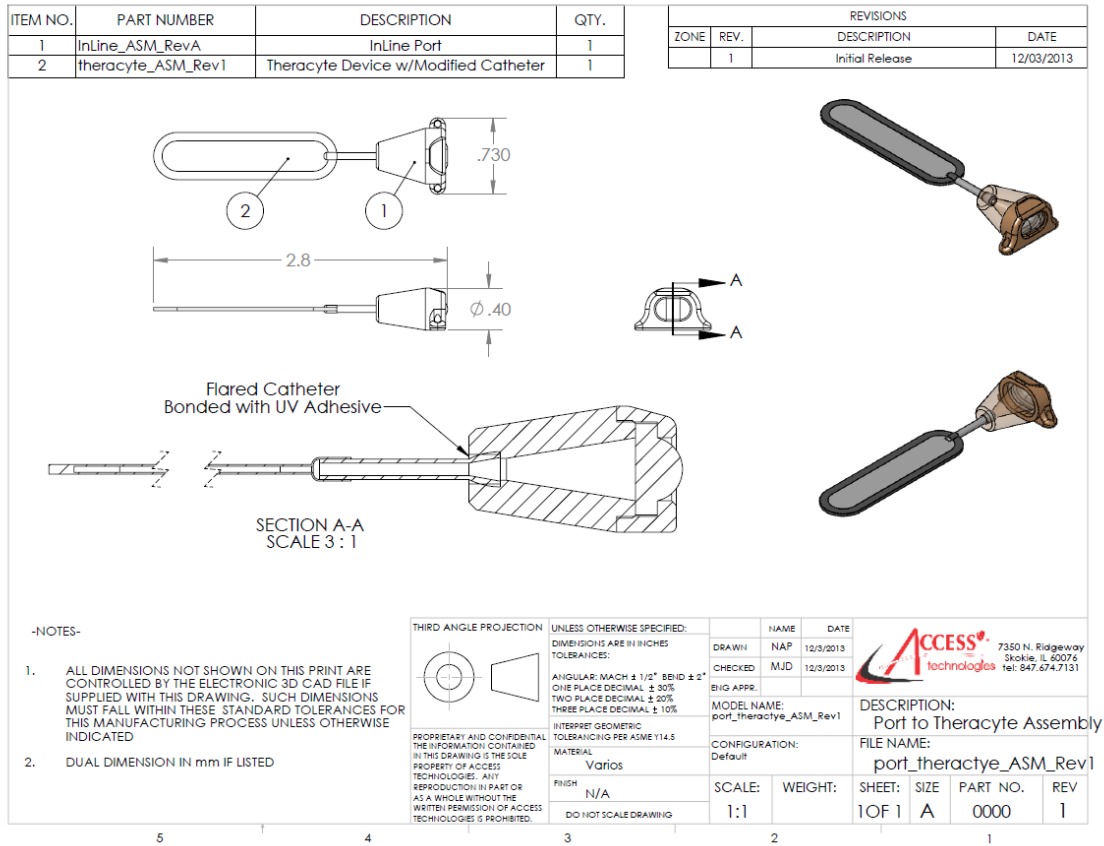


**Figure F.7.7: TheraCyte devices modified for *in vivo* cannulation.** A subcutaneous MR compatible catheter access port (Access Technologies) was attached to the loading port on the TheraCyte devices to allow for cannulation or catheterization of the implanted TheraCyte device. These modified devices were used for studies that required cannulation with a fiber optic oxygen probe. This provided a means of sterile access to the cell compartment of TheraCyte devices, and the fiber optic probe could be inserted using a trocar needle and a catheter.



**Figure F.7.8: TheraCyte with access port.** Image of the prototype modified TheraCyte device with attached access port.

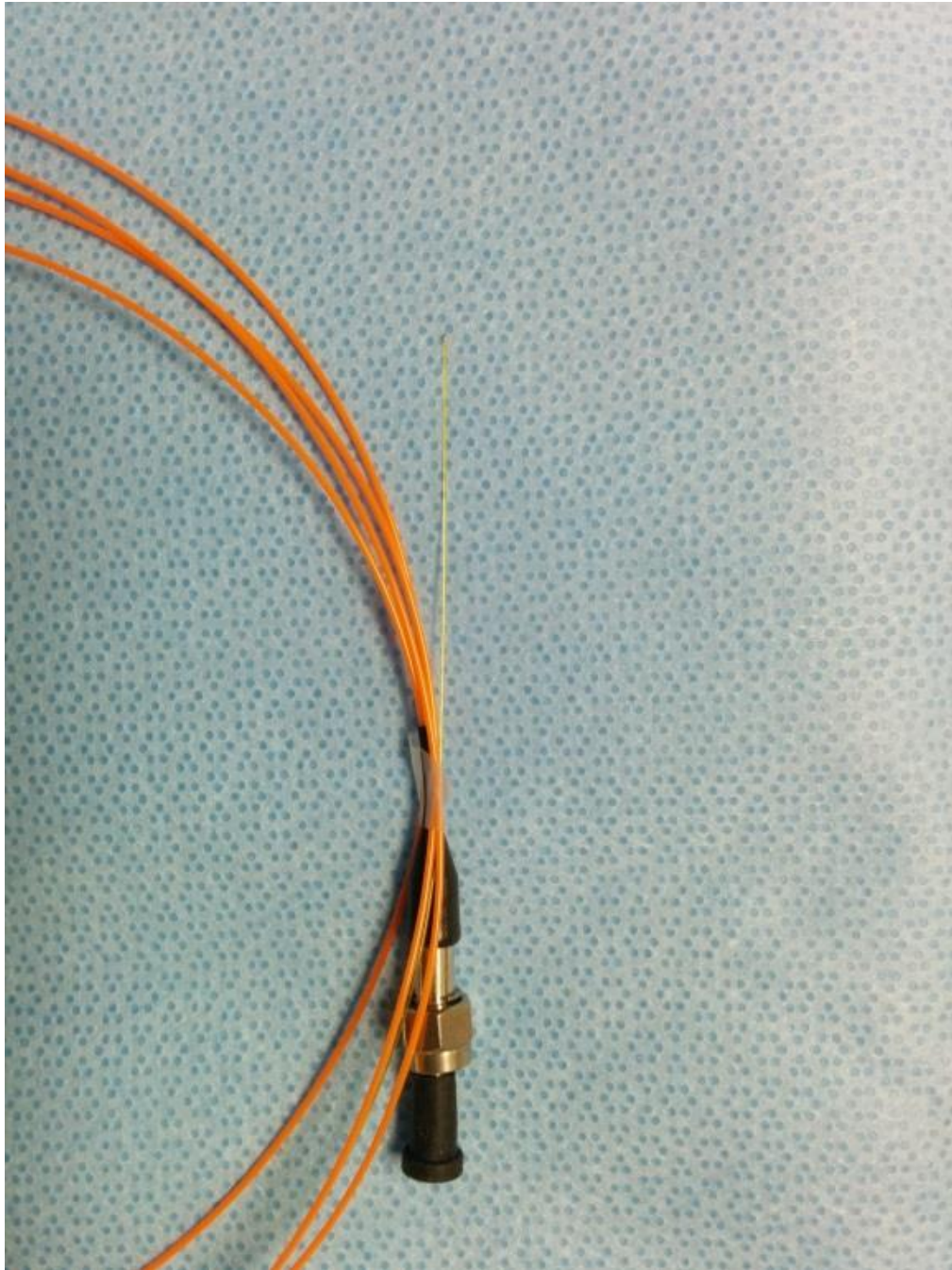


**Figure F.7.9: Fiber optic oxygen probe.** Image of custom designed MR compatible ultra-thin fiber optic oxygen probe (Ocean Optics) built for in vivo validation studies. These probes were designed to be extended in length and with MR compatible materials to avoid RF interference and magnetic induced mechanical stresses. The ultra-thin single fiber tip was 250  $\mu\text{m}$  in diameter to allow for cannulation through the access port of modified TheraCyte devices.

## ***Appendix F.8: Oxygenation of implanted TEGs***

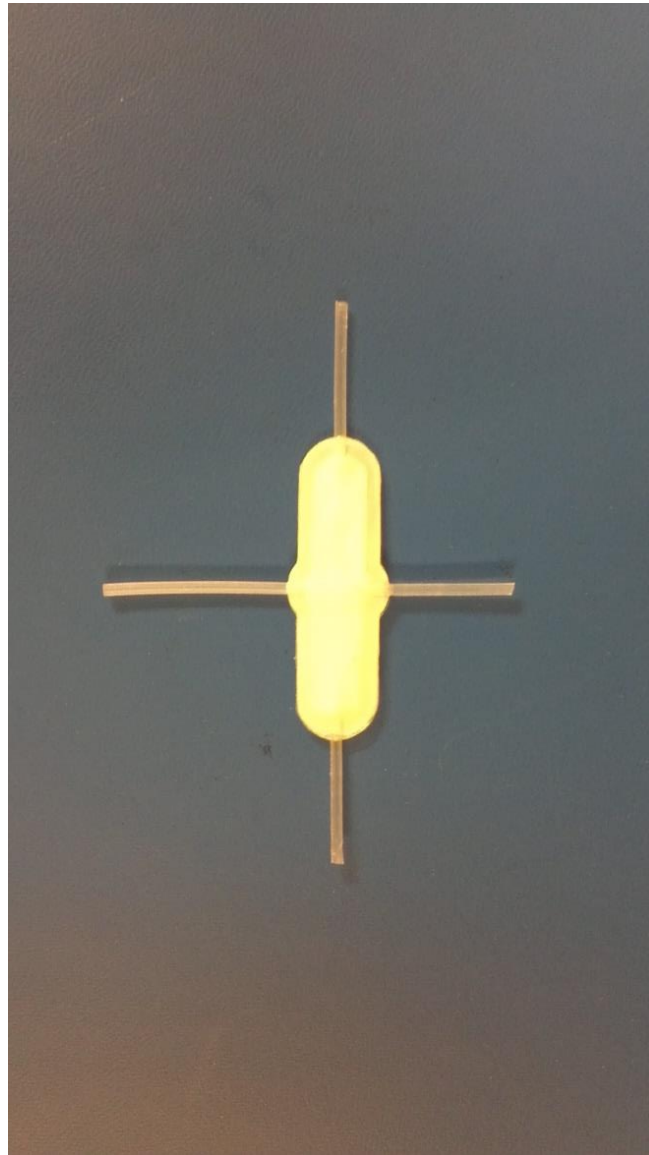


**Figure F.8.1: Picture of three-chamber TheraCyte modified for DSO.** With the assistance of TheraCyte inc. the 40  $\mu$ L TheraCyte devices was modified to include three chambers with 4 access ports. The lateral ports provide access to the top and bottom “cell” chambers, and the two longitudinal ports provide access to the central “oxygen” chamber. This initial concept was further adapted for *in vivo* studies.

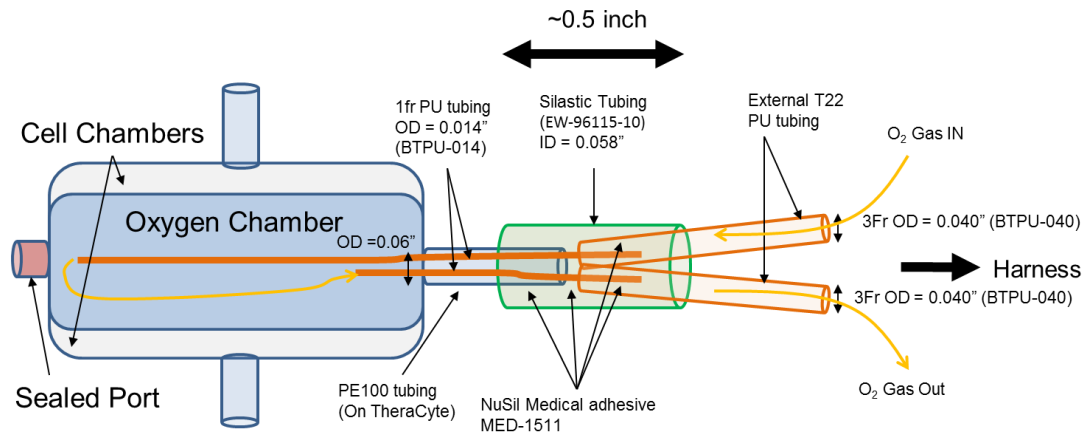


**Figure F.8.2: Illustration of TheraCyte modified for DSO.** The TheraCyte devices was further modified in the lab to accommodate the surgical convenience of locating the gas inlet and outlet on the same side of the device. One lateral port accessing the oxygen chamber was sealed with surgical-grade silicon adhesive. The remaining port was adapted to include two 1 fr polyurethane cannulas which were placed inside the oxygen chamber to facilitate DSO to the central chamber. The inlet cannula extended to the far side of the oxygen chamber, and the outlet cannula only protruded slightly into the chamber. This arrangement ensured adequate oxygen gas filling of the internal oxygen chamber. The 1 fr cannulas were adapted to larger gauge 3 fr polyurethane cannulas to facilitate connection to the harness, and a short section of silicon rubber tubing surrounded the connection points to provide added strain-relief and additional leak protection. All of the gaps in the adapter were sealed with silicon medical adhesive to ensure air-tight seals. All devices were leak-tested prior to ETO sterilization in preparation for implantation in rats. Prior to implantation, the devices were loaded with cells (or islets) in a sterile manner, and the cell chamber access ports were sealed with medical grade silicon adhesive.

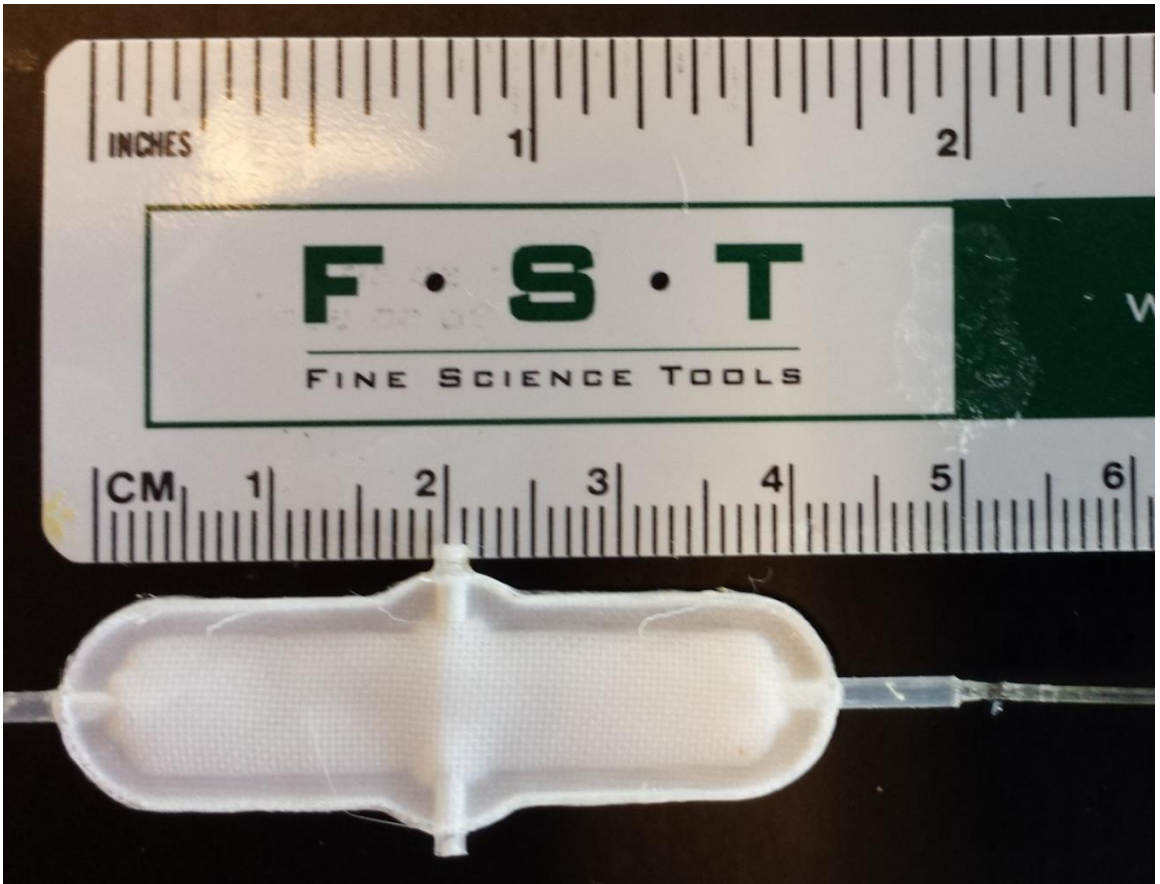
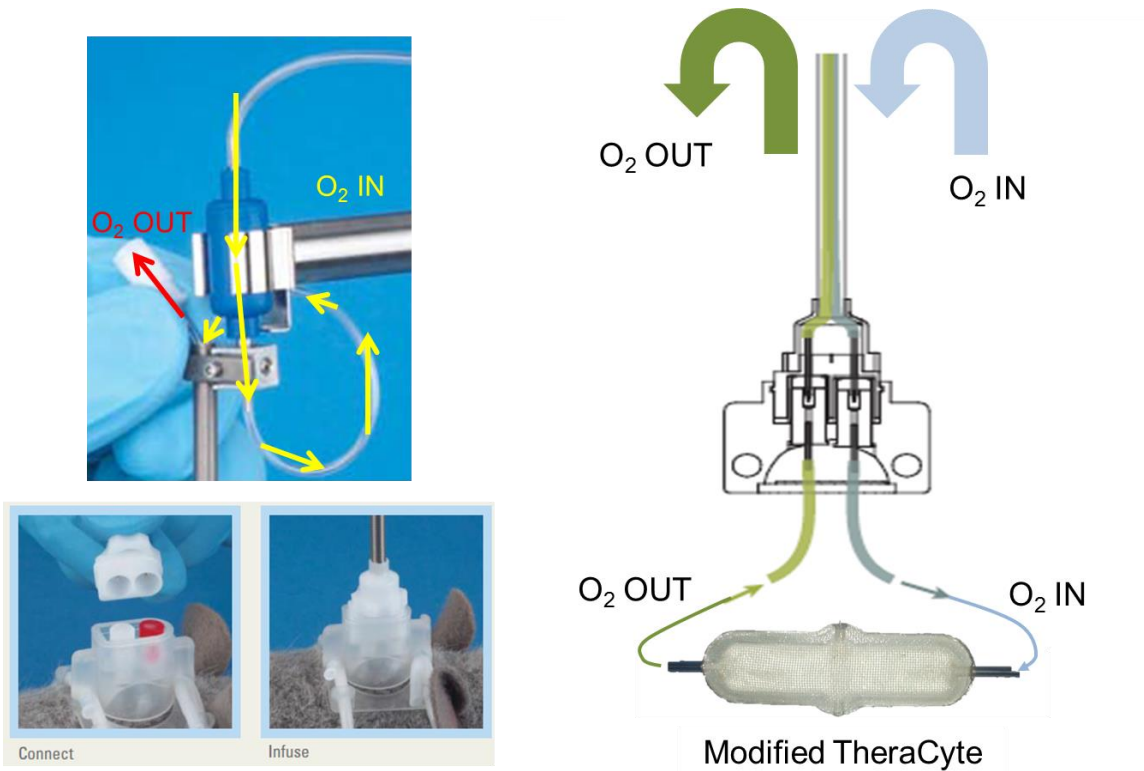
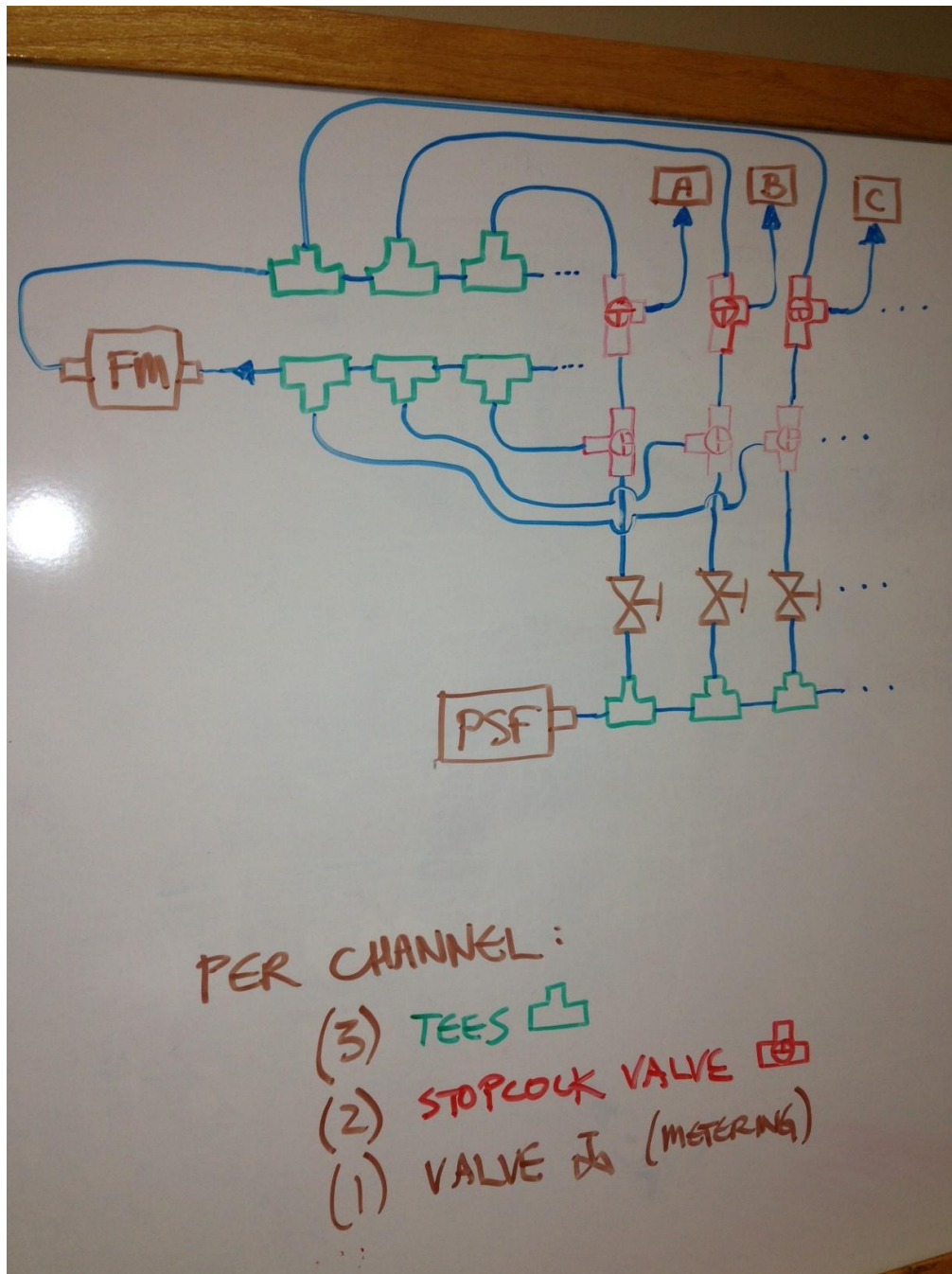


Figure F.8.3: Picture with scale of DSO modified TheraCye device.



**Figure F.8.4: Dual-channel harness and tether apparatus.** Pictures and illustration showing harness location on rats, and dual-channel access with swivel showing oxygen flow into and out of the TheraCyte device modified for DSO. The device shown was further modified to allow for gas inflow and outflow of the same lateral access port.



**Figure F.8.5: DSO manifold schematic diagram.** A DSO manifold was designed in cooperation with Giner Inc. to monitor and regulate oxygen delivery pressure and flow to individual channels (up to 8). The original electrochemical oxygen concentrator (EOC) was modified to deliver a continuous stream of oxygen gas to the manifold, and the manifold was equipped with up to 8 individual channels with needle valves for flow control and a pressure gauge to monitor individual delivery pressure. Three-way valves (stopcocks) were used to re-direct the flow from a single channel at a time through unique flow path that includes a precision ultra-low flow gas flow meter (FM). This approach was employed to avoid individual precision FM for each channel which added exorbitant cost to the manifold construction. When an individual channel was adjusted, the three way valves were oriented to redirect flow through the FM so that the flow and pressure could be controlled and monitored.



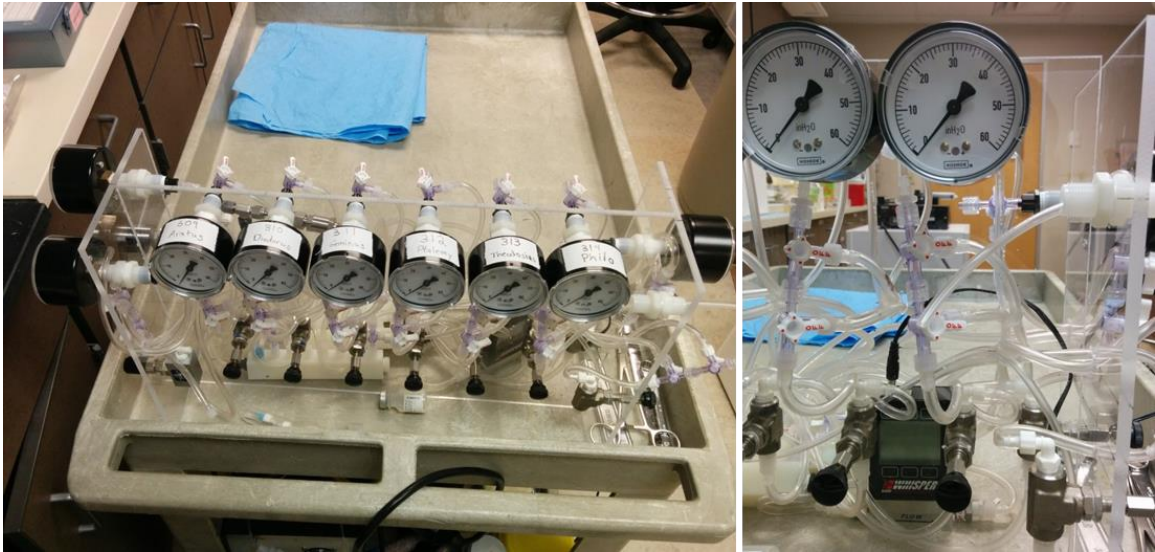


**Figure F.8.6: Pictures of custom assembled DSO manifold.** Individual channels shown on the left, and close-up view of an individual channel with needle valve, three-way valves, and pressure gauge shown on the right. The precision digital mass-air flow meter is also shown on the right (black box). The manifold was connected to the EOC with two independent in-line pressure relief valves to prevent an over-pressure condition that may damage the manifold, implanted device, or animal. The maximum allowable pressure was 3 psi (83 inches of water).

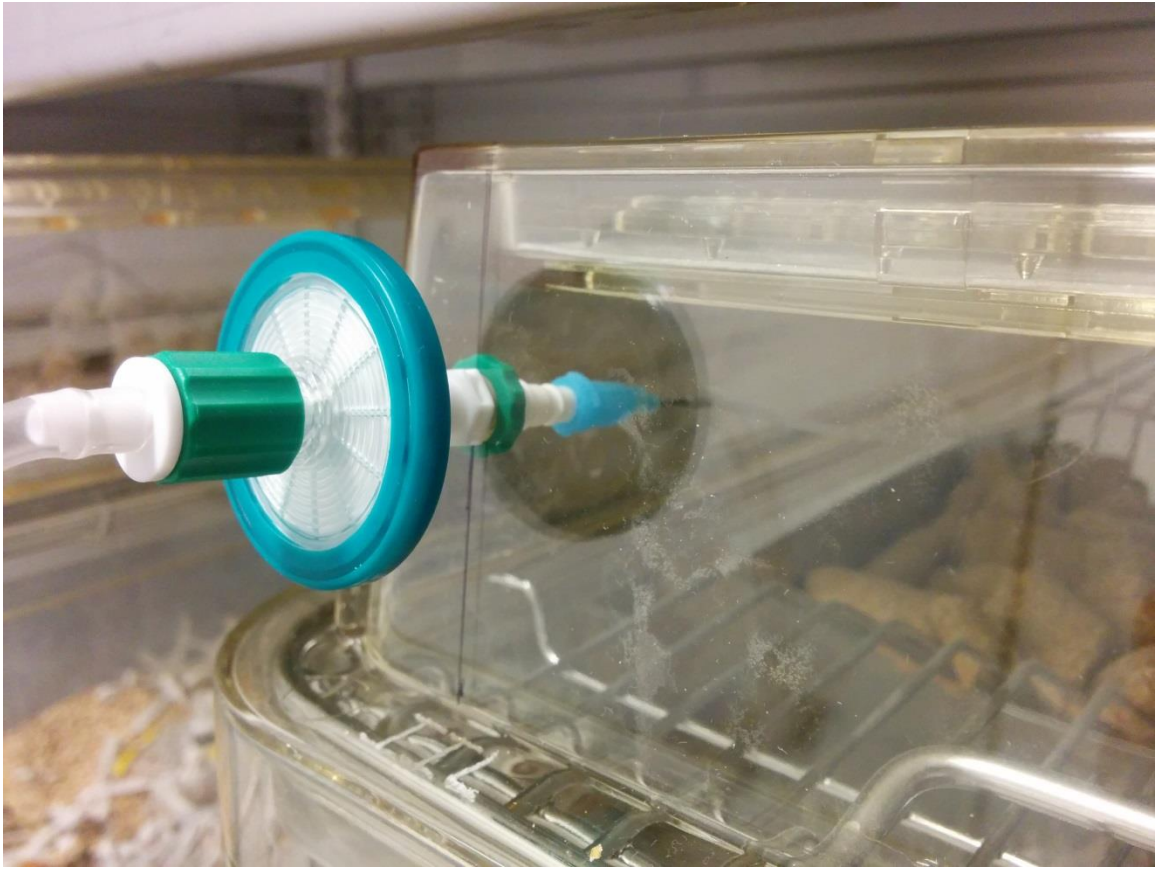


**Figure F.8.7: Animal cage lid modified for DSO.** Each manifold channel was connected to a delivery port on modified cage-lids for each animal in the study. Oxygen gas was delivered from the EOC through the manifold, and to the cage lid through a sterile .22  $\mu\text{m}$  syringe filter.



**Figure F.8.8: Pictures of DSO harness and tether apparatus.** A port was added to each cage lid for animals receiving DSO. The exterior port of the cage lid was connected to the DSO manifold, and the interior port of the cage lid was attached to the tether apparatus (Instech Labs.) The entire cage set-up with counter-balance, tether, and harness apparatus is picture on top, and view from above shows the tether apparatus attached to the dual-channel harness on the animal (animal is illustrated as a toy cow in photo).

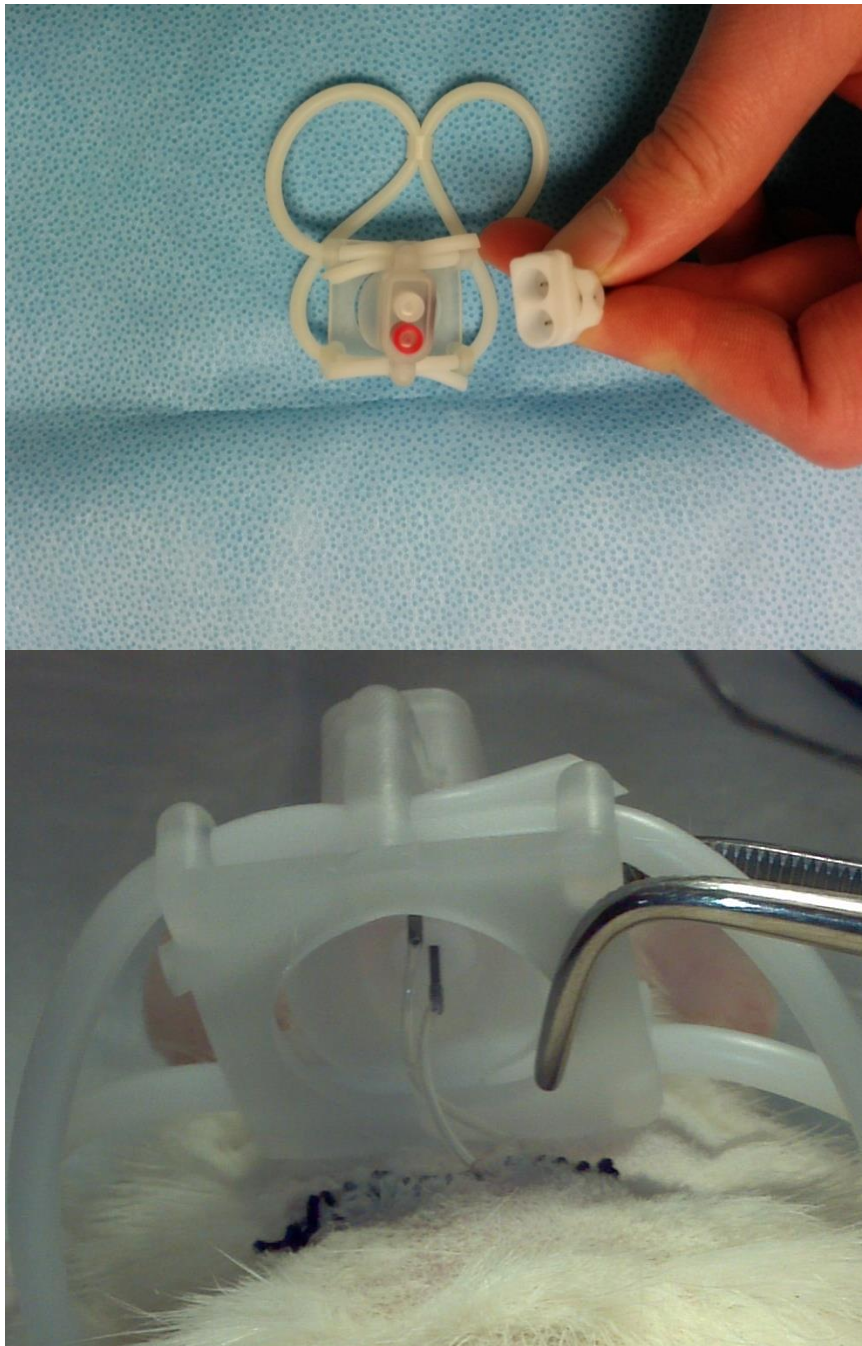


**Figure F.8.9: Dual-channel harness pictures.** The dual-channel harness was attached to the tether connector shown on top, and DSO connections from TheraCyte device were attached to nitinol ports on the underside of the harness. The inlet and outlet cannulas of the modified TheraCyte device protruded through the closed incision and attached to the nitinol ports. The harness was custom manufactured by Instech Labs with nitinol ports to reduce RF interference and improve MR compatibility.

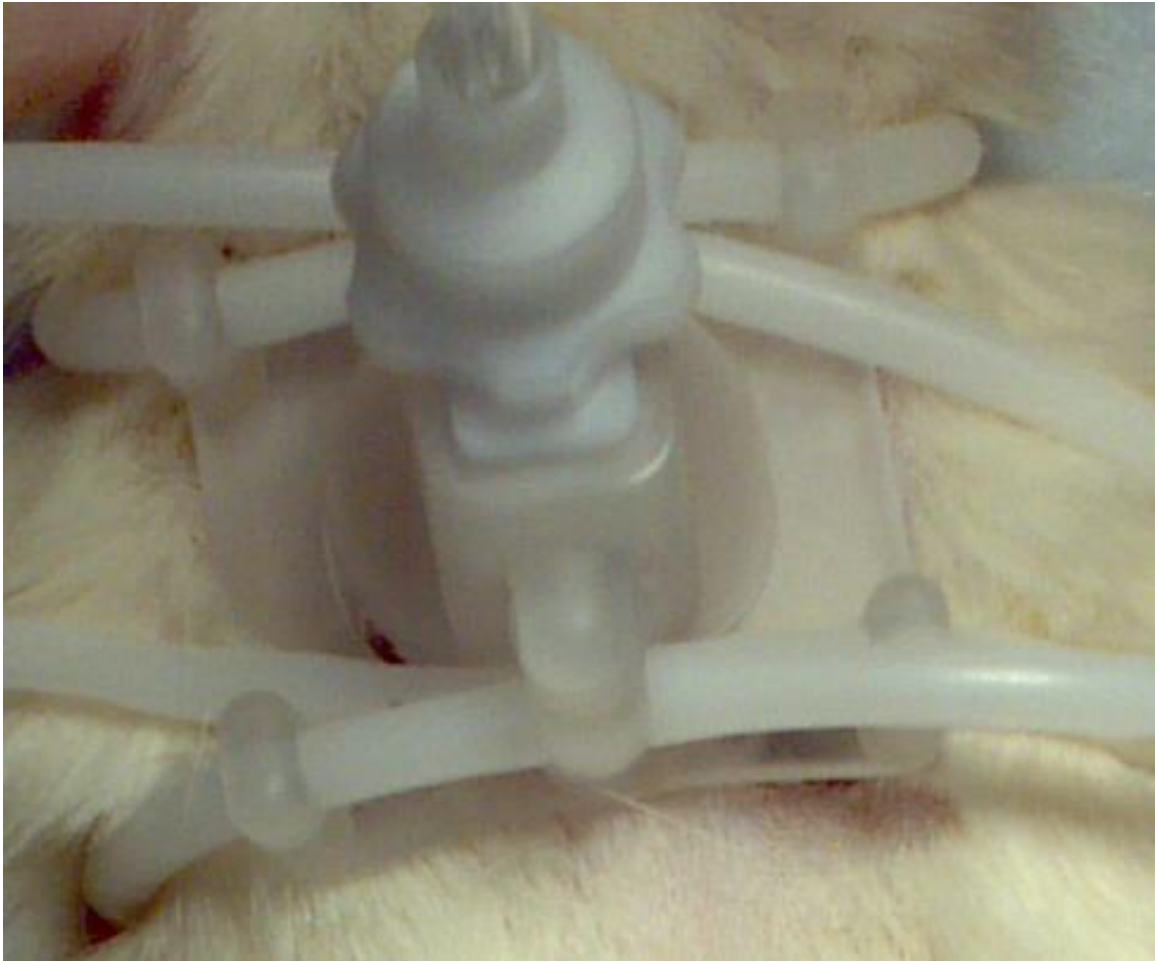


**Figure F.8.10: Dual-channel harness shown in position.** The harness was positioned securely on the dorsal side of the rat and tightened to provide a snug fit so that the harness covered the incision and the protruding cannulas. This arrangement provided protection from the animal and strain-relief for the cannula adapters connecting the cannulas to the TheraCyte device.

## ***Appendix F.A: Porcine Pancreas Anatomy***

None

## *Appendix F.B: Persufflation Improves Pancreas Preservation*

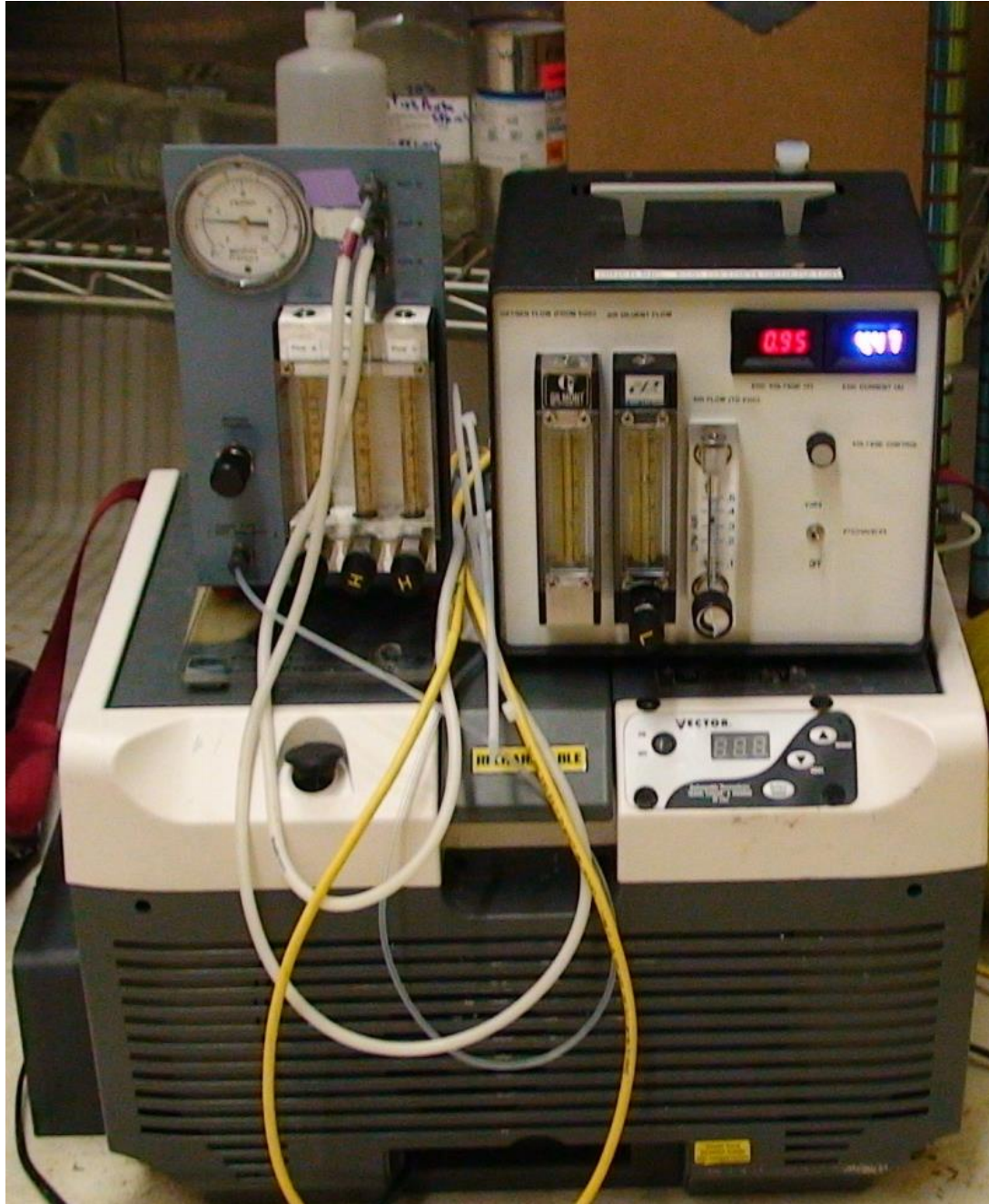


**Figure F.B.1: First pig/human organ persufflation preservation system.** The persufflator (electrochemical oxygen concentrator) was designed by Giner Inc. and was attached to a pressure and flow regulating manifold to deliver humidified gas to the vasculature of a preserved organ. The organ temperature was maintained at hypothermic levels ( $\sim 8\text{ }^{\circ}\text{C}$ ) using a cooler (electric active cooler pictured), or by keeping the entire system inside a “cold room” refrigerator.

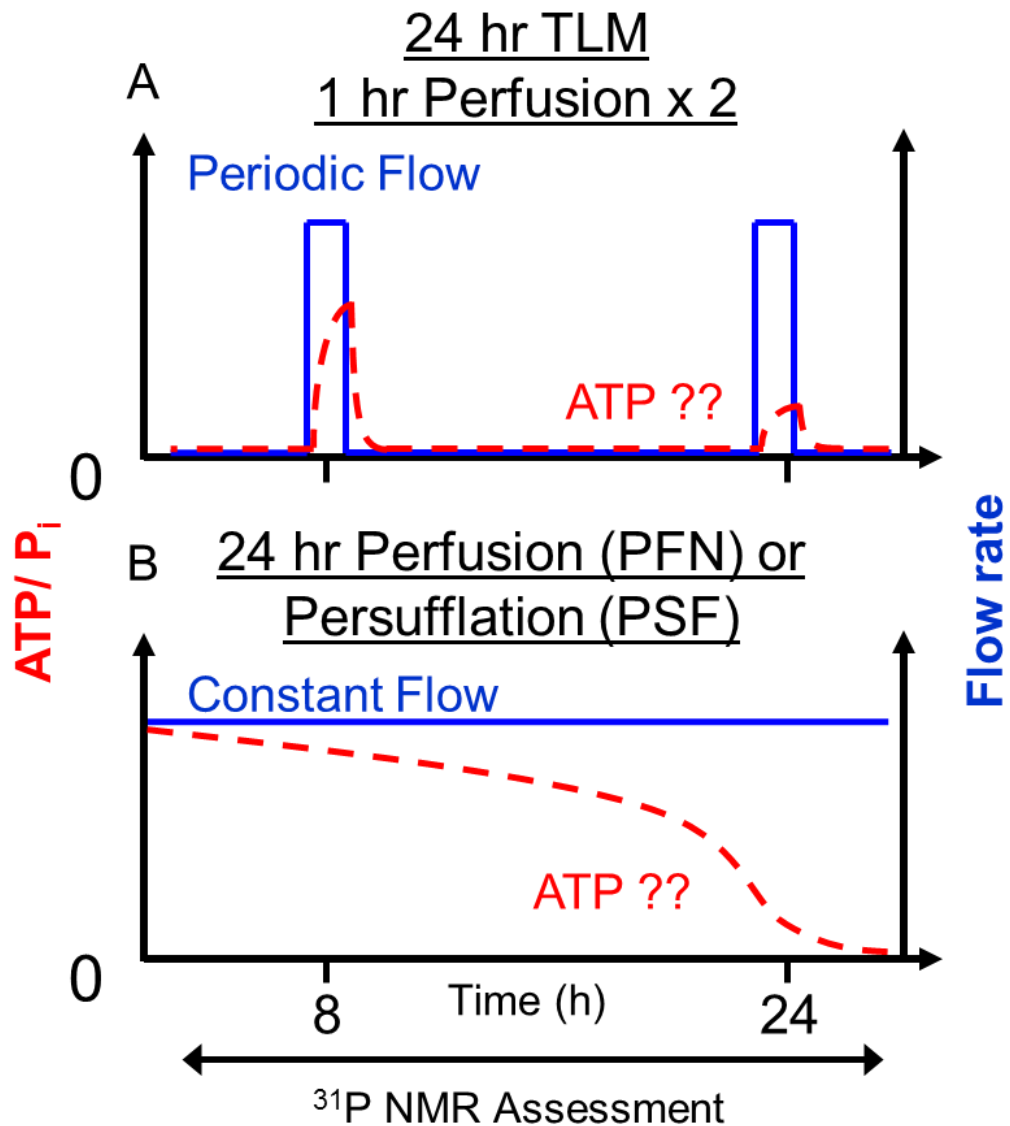


**Figure F.B.2: Illustration of hypothetical ATP levels.** Predicted ATP changes for organs preserved by (A) static cold storage and periodic oxygenation with persufflation and (B) persufflation with constant oxygenation. The ATP levels observed without oxygenation are not detectable, and it is hypothesized that when oxygen is delivered via persufflation the ATP levels will increase to reflect the organ viability at that time. With continuous oxygenation of tissues via persufflation, it is hypothesized that ATP levels will remain at detectable levels, and slowly decrease over time as organ viability decreases during the preservation period.



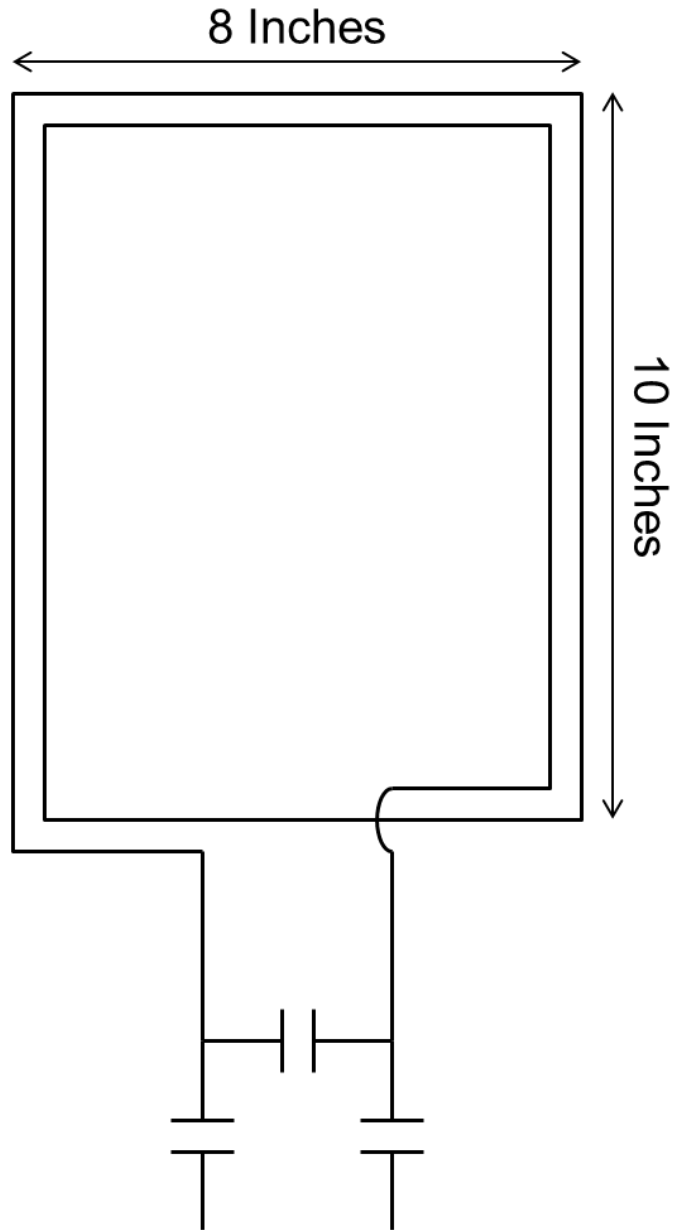


**Figure F.B.3: Two loop Surface coil for  $^{31}\text{P}$ -MRS studies.** Surface coil for measuring ATP with  $^{31}\text{P}$ -MRS at 1.5 T in organs during perfusion or persufflation. The coil was designed to accommodate various organs sizes (pig organs), for convenient placement within the water jacket, and for manual tuning within the MR system. A coil with similar design was used for  $^1\text{H}$ -MRI during the same studies.

## Water Jacket V 3.0

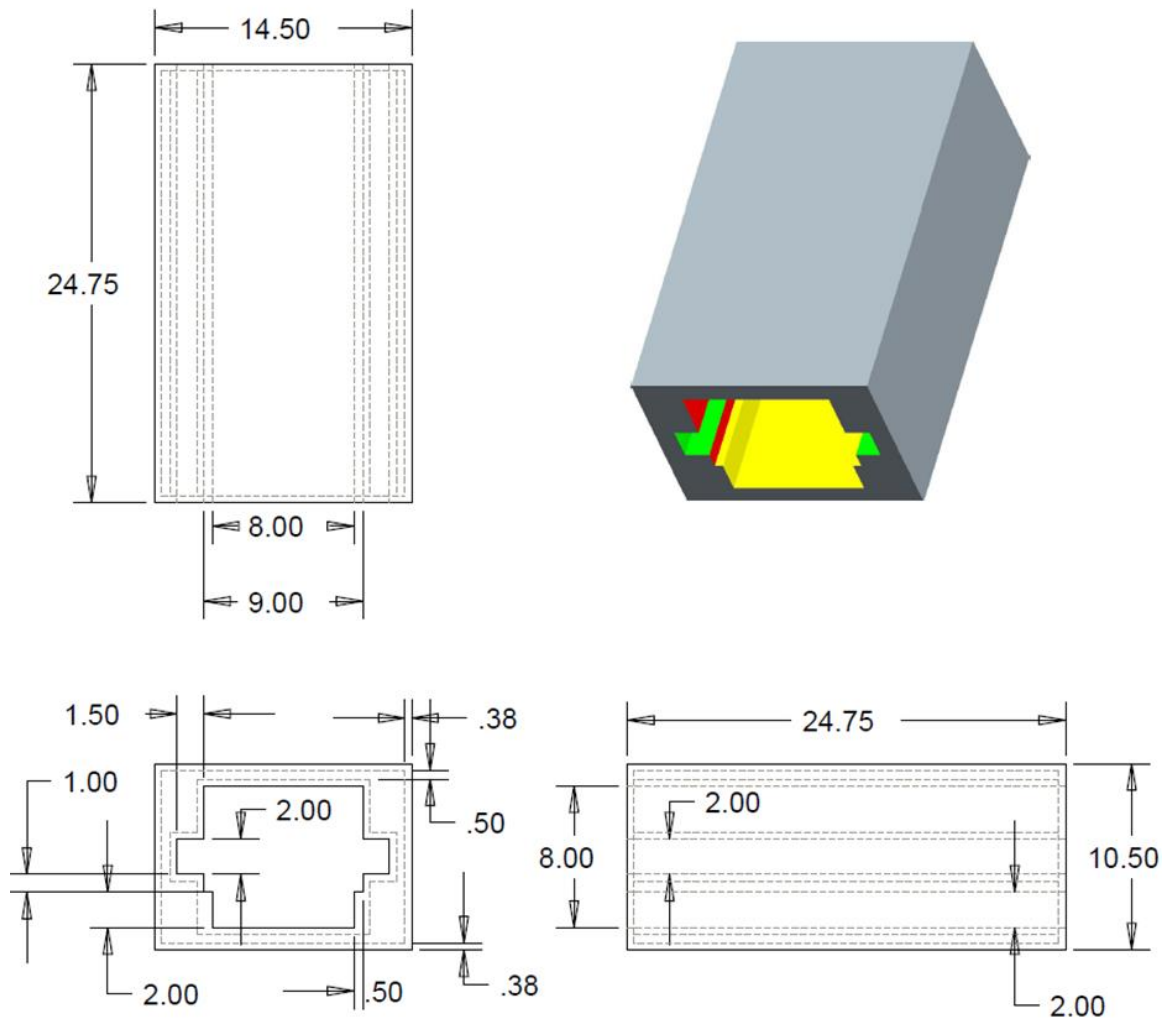


**Figure F.B.4: Water jacket schematic.** Water jacket was used with a circulating water bath for chilling organs and tissues when scanned in the 1.5 T MR system. This was used for scanning organs during long term cold preservation studies, and maintained temperature of the organ and tissues between 4-8°C. The water jacket was designed to accommodate various MR coil designs and an organ container.

### Organ Container V 2.0

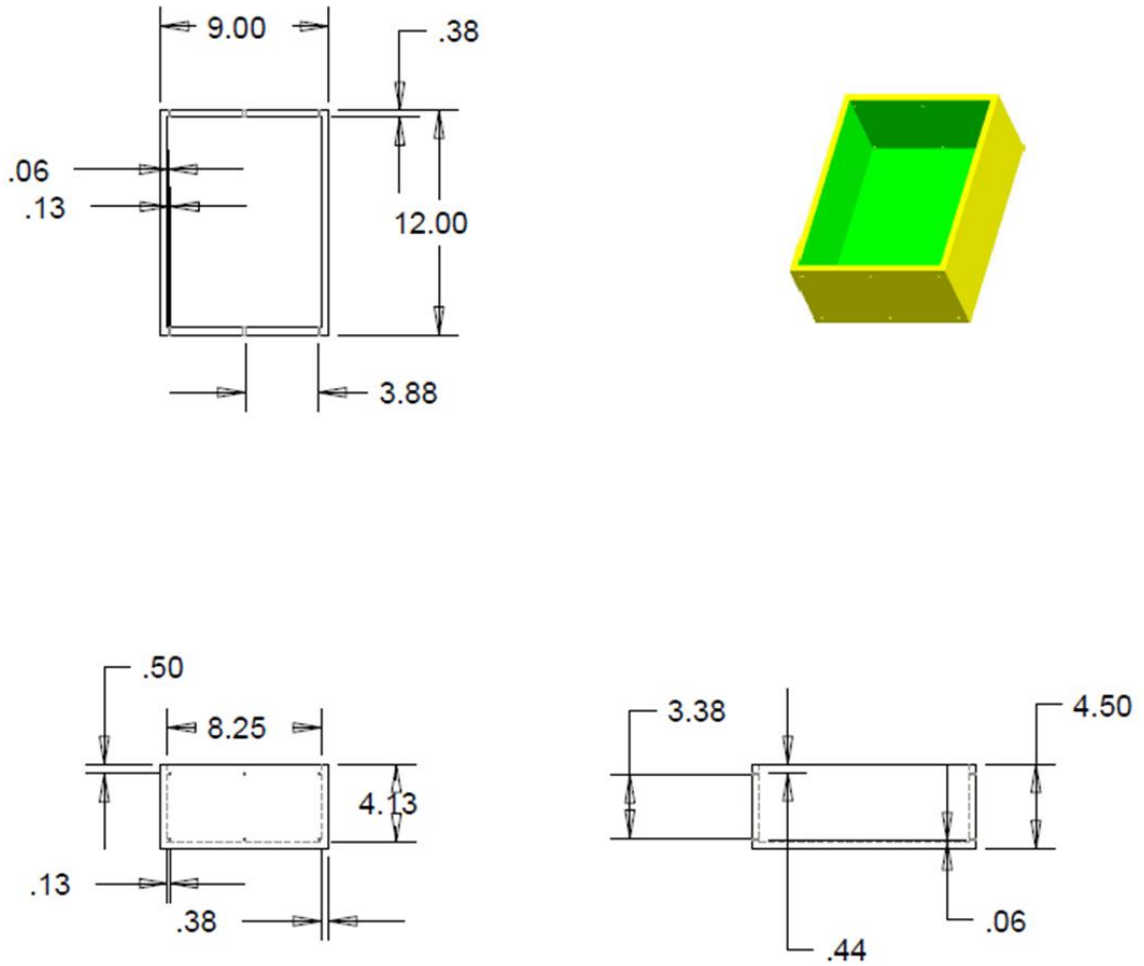


**Figure F.B.5: First-generation PSF organ container schematic.** Container designed to accommodate perfusion or persufflation of preserved organs, and even multiple organs.

# Organ Container Cover V 1.0

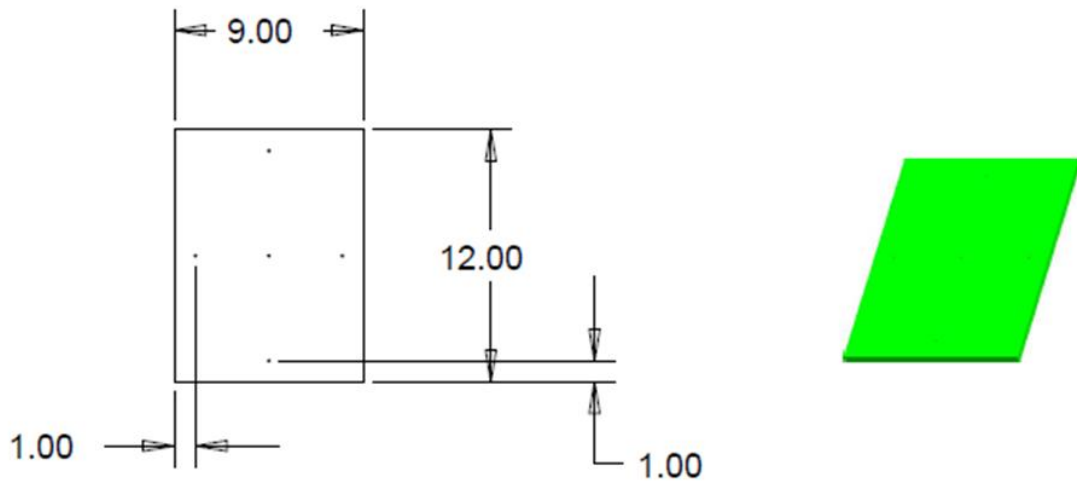


**Figure F.B.6: First-generation organ container lid.** Container lid is equipped with multiple access ports to facilitate organ perfusion or persufflation.

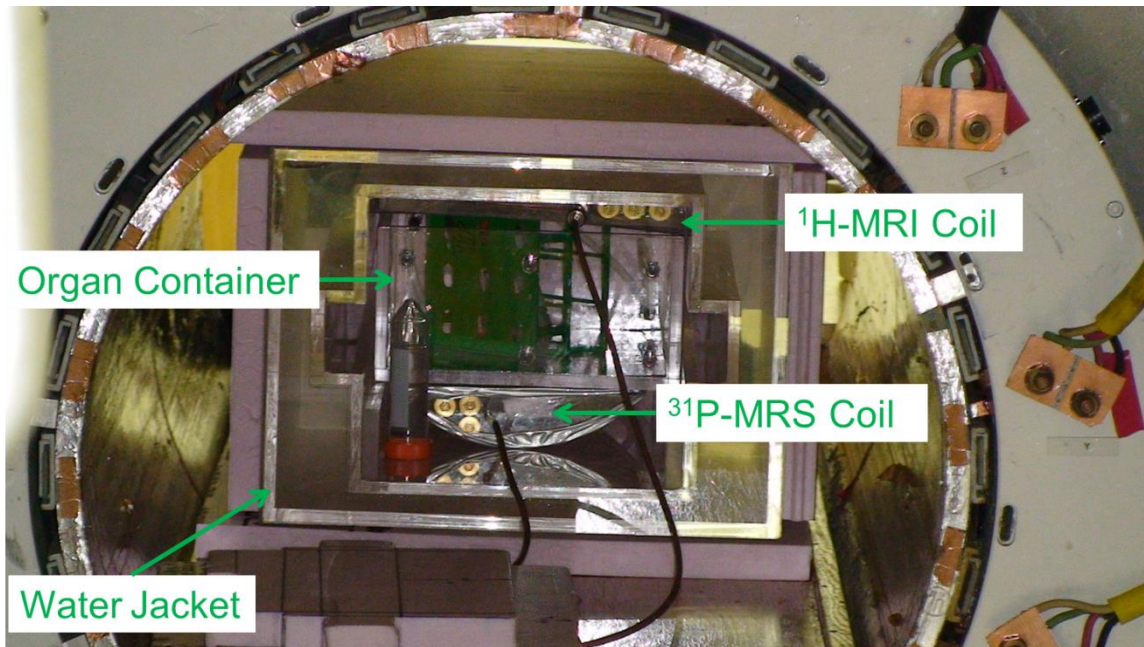


**Figure F.B.7: Picture of  $^{31}\text{P}$ -MRS study experimental set-up.** Experimental set-up showing the water jacket with  $^{31}\text{P}$ -MRS coil (shown on bottom),  $^1\text{H}$ -MRI coil (shown on top) and organ container.

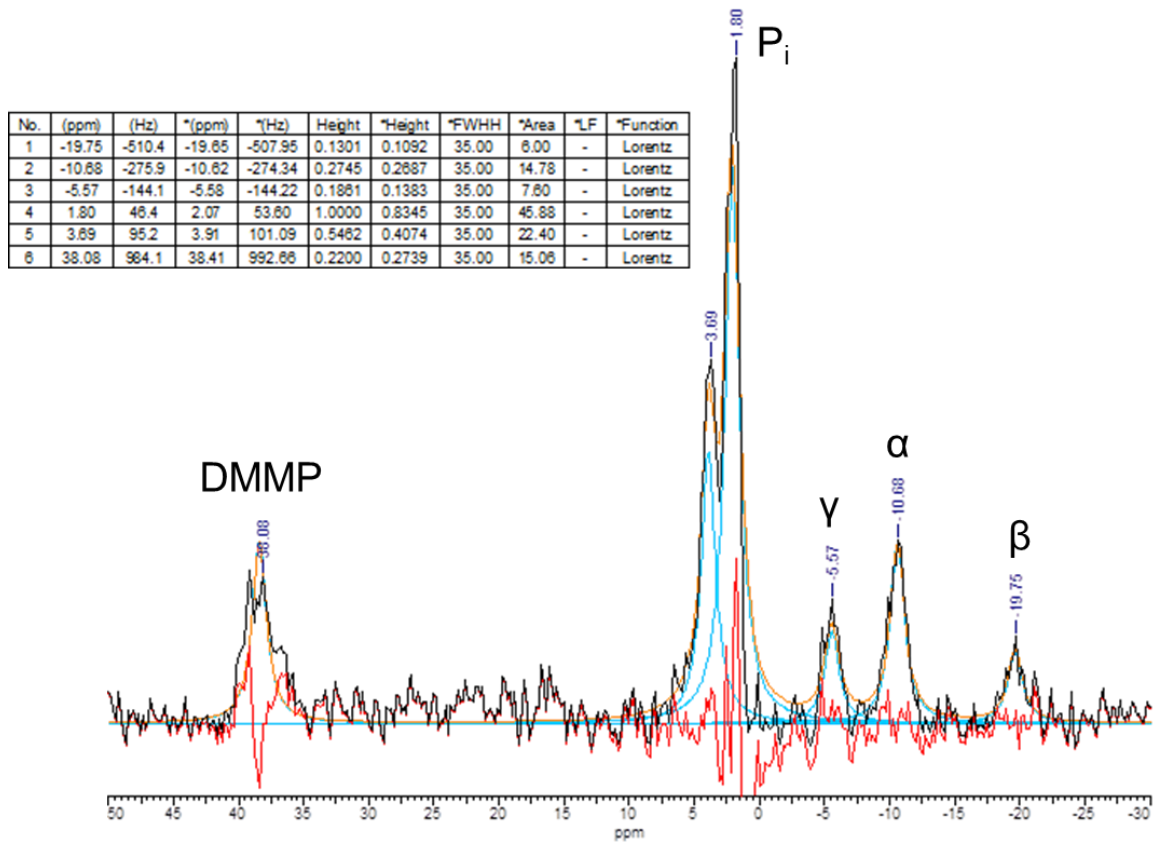


**Figure F.B.8: Integration analysis of  $^{31}\text{P}$ -MRS spectrum.** Representative  $^{13}\text{P}$ -MRS spectrum from a human pancreas oxygenated by persufflation (PSF) with peak assignment and integration analysis. Dimethyl methylphosphonate (DMMP) standard, phosphomonoester, inorganic phosphate ( $\text{P}_i$ ), and  $\alpha$ ,  $\beta$ , and  $\gamma$  ATP peaks are shown with calculated integration areas. These areas were compared to report the  $\beta$ -ATP: $\text{P}_i$  ratios, and the total ATP: $\text{P}_i$  ratios for these studies.

## ***Appendix F.C: Using MRI to Improve Enzyme Distribution***

None

*Appendix F.D: Improving Islet Shipment*



**Figure F.D.1: First generation Wilson Wolf SRM culture devices.** These images illustrate the importance of temperature regulation during islet shipment, and confirm that the culture vessel contents freeze solid when external temperatures are below  $-20\text{ }^{\circ}\text{C}$  for 24 hours.



### The ThermaSure™ Temperature Stabilizing Material:

- Model: SEBRA 1290 ThermaSure™ Temperature Stabilizer
- Mass :~ 530g/unit (n=5)
- Temperature Range: (16°C-20°C)<sup>1</sup>
- Life Span: 3 Years
- Disposal: Standard Waste<sup>1</sup>
- Hazards: Not Skin hazard, should not ingest<sup>1</sup>



### TCP Phase Change Material:

- Model: TCP Phase 22
- Mass: ~ 304g/unit (n=4)
- Temperature Range: (20-22°C)
- Life Span:
- Disposal: Standard Waste
- Hazards: Skin Irritant, should not ingest



**Figure F.D.2: ThermaSure and TCP temperature stabilizing materials.** These two materials were tested for regulating temperature during islet shipment. The ThermaSure (TS) temperature stabilizing material was intended for maintaining temperatures between 16-20 °C and was originally intended for transporting blood products. The TCP Phase Change Material (PCM) was intended for maintaining temperatures between 20-22 °C, and was investigated as an alternative to TS material due to its improved thermal regulatory capacity and because the targeted temperature range coincided well with the standard culture temperature used for human islet cultures (22 °C).

### ThermaSure:

- Stored at RT for 2 hr prior to experiment in liquid phase at RT
- 6 gel packs (3.2 Kg)
- Packed in a cubic arrangement such that the gel packs form 6 sides of a cube.



### Phase Change Material (PCM):

- Warmed in 40°C Incubator until completely in liquid phase
- 21 PCM units (6.4kg)
- Packed in cubic arrangement such that 4 units are on each side of a cube and one unit is beneath the flask.



**Figure F.D.3: Preparation of ThermaSure and TCP materials.** The recommended preparation and loading of temperature stabilizing materials for islet shipment.



ThermoSafe



Red box

**Figure F.D.4: ThermoSafe and Red Box shipping containers.** The ThermoSafe container is the standard container recommended for islet shipment, and the Red Box container was investigated as an alternative container with improved durability and insulation.



**Figure F.D.5: Beverage container for temperature and pressure regulation.** A thermos beverage container was proposed for maintaining temperature and pressure of islets during shipment, but was abandoned due to difficulty with form-factor.



**Figure F.D.6: Pressure regulated gyrosopic shipping container (PRGSC).** A custom-built pressure regulated gyrosopic shipping container was designed and manufactured by Wilson-Wolf Manufacturing for studies to investigate the pressure effects on islets during culture and shipment. This container was designed to work with silicon rubber membrane flasks that function when they are properly oriented (upright), so a gyrosopic mechanism was included in the container to ensure ideal flask orientation during shipment. These devices were tested in a vacuum chamber to simulate the pressure changes experienced during shipment in the cargo-hold of cargo air-shipments.



**Figure F.D.7: PRGSC shown with SRM flask.** The flask was held in position within the gyroscope using a strap and magnetic contacts. The lid created an air-tight seal with the cylinder to maintain normal atmospheric pressures (~760 mmHg) during shipment.

## ***Appendix F.E: QMS for Improving Islet Purification***

None.

Appendix G **COPYRIGHT PERMISSIONS AND LICENSES**  
*Appendix G.1: Permission for Published Manuscripts*





**Note:** Copyright.com supplies permissions but not the copyrighted content itself.



**Step 3: Order Confirmation**

**Thank you for your order!** A confirmation for your order will be sent to your account email address. If you have questions about your order, you can call us at +1.855.239.3415 Toll Free, M-F between 3:00 AM and 6:00 PM (Eastern), or write to us at [info@copyright.com](mailto:info@copyright.com). This is not an invoice.

**Confirmation Number: 11340305**  
**Order Date: 04/15/2015**

If you paid by credit card, your order will be finalized and your card will be charged within 24 hours. If you choose to be invoiced, you can change or cancel your order until the invoice is generated.

**Payment Information**

Bradley Weegman  
 weeg0011@umn.edu  
 +1 (612)6262001  
 Payment Method: invoice

**Billing address:**

2021 Sixth Street SE  
 Center for Magnetic Resonance Research  
 Minneapolis, MN 55455  
 US

**Order Details**

**Transplantation proceedings**

**Order detail ID:** 66740419  
**Order License Id:** 3610380765872  
**ISSN:** 1873-2623  
**Publication Type:** e-Journal  
**Volume:**  
**Issue:**  
**Start page:**  
**Publisher:** ELSEVIER INC.  
**Author/Editor:** Transplantation Society

**Permission Status:** ✔ **Granted**  
**Permission type:** Republish or display content  
**Type of use:** Thesis/Dissertation

<b>Requestor type</b>	Author of requested content
<b>Format</b>	Print, Electronic
<b>Portion</b>	chapter/article
<b>Number of pages in chapter/article</b>	4
<b>Title or numeric reference of the portion(s)</b>	Continuous real-time viability assessment of kidneys based on oxygen consumption
<b>Title of the article or chapter the portion is from</b>	N/A

**Note:** This item will be invoiced or charged separately through CCC's **RightsLink** service. [More info](#)

**\$ 0.00**

**Transplantation proceedings**

**Order detail ID:** 66740423  
**Order License Id:** 3610380768098  
**ISSN:** 0041-1345  
**Publication Type:** Journal  
**Volume:**  
**Issue:**  
**Start page:**  
**Publisher:** ELSEVIER INC.  
**Author/Editor:** TRANSPLANTATION SOCIETY ; INTERNATIONAL SYMPOSIUM ON ORGAN PRESERVATION

**Permission Status:**  **Granted**  
**Permission type:** Republish or display content  
**Type of use:** Thesis/Dissertation

<b>Requestor type</b>	Author of requested content
<b>Format</b>	Print, Electronic
<b>Portion</b>	chapter/article
<b>Number of pages in chapter/article</b>	4
<b>Title or numeric reference of the portion(s)</b>	Devices and methods for maintenance of temperature and pressure during islet shipment
<b>Title of the article or chapter the portion is from</b>	N/A
<b>Editor of portion(s)</b>	N/A
<b>Author of portion(s)</b>	Rozak et al.
<b>Volume of serial or monograph</b>	40
<b>Issue, if republishing an article from a serial</b>	2
<b>Page range of portion</b>	407-410
<b>Publication date of portion</b>	2008 March
<b>Rights for</b>	Main product
<b>Duration of use</b>	Life of current edition
<b>Creation of copies for the disabled</b>	no
<b>With minor editing privileges</b>	yes

**Note:** This item will be invoiced or charged separately through CCC's **RightsLink** service. [More info](#)

**\$ 0.00**

**Transplantation proceedings**

**Order detail ID:** 66740431  
**Order License Id:** 3610380769857  
**ISSN:** 1873-2623  
**Publication Type:** e-Journal  
**Volume:**  
**Issue:**  
**Start page:**  
**Publisher:** ELSEVIER INC.  
**Author/Editor:** Transplantation Society

**Permission Status:**  **Granted**  
**Permission type:** Republish or display content  
**Type of use:** Thesis/Dissertation

<b>Requestor type</b>	Author of requested content
<b>Format</b>	Print, Electronic
<b>Portion</b>	chapter/article
<b>Number of pages in chapter/article</b>	5
<b>Title or numeric reference of the portion(s)</b>	Pancreas oxygen persufflation increases ATP levels as shown by nuclear magnetic resonance
<b>Title of the article or chapter the portion is from</b>	N/A
<b>Editor of portion(s)</b>	N/A
<b>Author of portion(s)</b>	Scott III et al.
<b>Volume of serial or monograph</b>	42
<b>Issue, if republishing an article from a serial</b>	6
<b>Page range of portion</b>	2011-2015
<b>Publication date of portion</b>	2010 Jul-Aug
<b>Rights for</b>	Main product
<b>Duration of use</b>	Life of current edition
<b>Creation of copies for the disabled</b>	no
<b>With minor editing privileges</b>	yes

**Note:** This item will be invoiced or charged separately through CCC's **RightsLink** service. [More info](#) **\$ 0.00**

**Xenotransplantation**

**Order detail ID:** 66740445  
**Order License Id:** 3610380771887  
**ISSN:** 1399-3089  
**Publication Type:** e-Journal  
**Volume:**  
**Issue:**  
**Start page:**  
**Publisher:** BLACKWELL PUBLISHING  
**Author/Editor:** International Xenotransplantation Association

**Permission Status:**  **Granted**

**Permission type:** Republish or display content  
**Type of use:** Republish in a thesis/dissertation

<b>Requestor type</b>	Author of requested content
<b>Format</b>	Print, Electronic
<b>Portion</b>	chapter/article
<b>Number of pages in chapter/article</b>	8
<b>Title or numeric reference of the portion(s)</b>	Temperature profiles of different cooling methods in porcine pancreas procurement
<b>Title of the article or chapter the portion is from</b>	N/A
<b>Editor of portion(s)</b>	N/A
<b>Author of portion(s)</b>	Weegman et al.
<b>Volume of serial or monograph</b>	21
<b>Issue, if republishing an article from a serial</b>	6
<b>Page range of portion</b>	574-581
<b>Publication date of portion</b>	2014 Nov-Dec
<b>Rights for</b>	Main product
<b>Duration of use</b>	Life of current edition
<b>Creation of copies for the disabled</b>	no
<b>With minor editing privileges</b>	yes

**Note:** This item will be invoiced or charged separately through CCC's **RightsLink** service. [More info](#)

**\$ 0.00**

**Xenotransplantation**

**Order detail ID:** 66740464  
**Order License Id:** 3610380773902  
**ISSN:** 1399-3089  
**Publication Type:** e-Journal  
**Volume:**  
**Issue:**  
**Start page:**  
**Publisher:** BLACKWELL PUBLISHING  
**Author/Editor:** International Xenotransplantation Association

**Permission Status:**  **Granted**

**Permission type:** Republish or display content  
**Type of use:** Republish in a thesis/dissertation

<b>Requestor type</b>	Author of requested content
<b>Format</b>	Print, Electronic
<b>Portion</b>	chapter/article
<b>Number of pages in chapter/article</b>	7
<b>Title or numeric reference of the portion(s)</b>	Magnetic resonance imaging: a tool to monitor and optimize enzyme distribution during porcine pancreas distention for islet isolation
<b>Title of the article or chapter the portion is from</b>	N/A
<b>Editor of portion(s)</b>	N/A
<b>Author of portion(s)</b>	Scott III et al.
<b>Volume of serial or monograph</b>	21
<b>Issue, if republishing an article from a serial</b>	5
<b>Page range of portion</b>	473-479
<b>Publication date of portion</b>	2014 Sep-Oct
<b>Rights for</b>	Main product
<b>Duration of use</b>	Life of current edition
<b>Creation of copies for the disabled</b>	no


**Note:** This item will be invoiced or charged separately through CCC's **RightsLink** service. More info

**\$ 0.00**

Special Orders	
<b>Cell medicine : Part B of Cell Transplantation</b>	
<b>Order detail ID:</b>	66740482
<b>Job Ticket:</b>	500996932
<b>ISSN:</b>	2155-1790
<b>Publication Type:</b>	e-Journal
<b>Volume:</b>	
<b>Issue:</b>	
<b>Start page:</b>	
<b>Publisher:</b>	Cognizant Communication Corp
<b>Permission Status:</b>	 <b>Special Order</b>
<b>Special Order Update:</b>	<b>Checking availability</b>
<b>Permission type:</b>	Republish or display content
<b>Type of use:</b>	Republish in a thesis/dissertation
<b>Requestor type</b>	Author of requested content
<b>Format</b>	Print, Electronic
<b>Portion</b>	chapter/article
<b>Title or numeric reference of the portion(s)</b>	Hypothermic Perfusion Preservation of Pancreas for Islet Grafts: Validation Using a Split Lobe Porcine Model
<b>Title of the article or chapter the portion is from</b>	N/A
<b>Editor of portion(s)</b>	N/A
<b>Author of portion(s)</b>	Weegman et al.
<b>Volume of serial or monograph</b>	2
<b>Issue, if republishing an article from a serial</b>	3
<b>Page range of portion</b>	None
<b>Publication date of portion</b>	2012 January
<b>Rights for</b>	Main product
<b>Duration of use</b>	Life of current edition
<b>Creation of copies for the disabled</b>	no
<b>With minor editing privileges</b>	yes
<b>Note:</b> This item will be managed through CCC's <a href="#">RightsLink service</a> . <a href="#">More info</a>	
<b>TBD</b>	

**Transplantation**

**Order detail ID:** 66740494  
**Job Ticket:** 500996933  
**ISSN:** 1534-6080  
**Publication Type:** e-Journal  
**Volume:**  
**Issue:**  
**Start page:**  
**Publisher:** LIPPINCOTT WILLIAMS & WILKINS, INC.  
**Author/Editor:** Transplantation Society

**Permission Status:**  **Special Order**  
**Special Order Update:** Checking availability  
**Permission type:** Republish or display content  
**Type of use:** Thesis/Dissertation

<b>Requestor type</b>	Author of requested content
<b>Format</b>	Print, Electronic
<b>Portion</b>	chapter/article
<b>Title or numeric reference of the portion(s)</b>	Pig pancreas anatomy: implications for pancreas procurement, preservation, and islet isolation
<b>Title of the article or chapter the portion is from</b>	N/A
<b>Editor of portion(s)</b>	N/A
<b>Author of portion(s)</b>	Ferrer et al.
<b>Volume of serial or monograph</b>	86
<b>Issue, if republishing an article from a serial</b>	11
<b>Page range of portion</b>	1503-10
<b>Publication date of portion</b>	2008 Dec 15
<b>Rights for</b>	Main product
<b>Duration of use</b>	Life of current edition
<b>Creation of copies for the disabled</b>	no
<b>With minor editing privileges</b>	yes

**Note:** This item will be managed through CCC's **RightsLink service**. [More info](#)

TBD



---

**Total order items: 7**                      **This is not an invoice.**                      **Order Total: 0.00 USD**  
(Excludes TBD items)



**Confirmation Number: 11340305****Special Rightsholder Terms & Conditions**

The following terms &amp; conditions apply to the specific publication under which they are listed

**Transplantation proceedings****Permission type:** Republish or display content**Type of use:** Thesis/Dissertation**TERMS AND CONDITIONS****The following terms are individual to this publisher:**

None

**Other Terms and Conditions:**

None

**STANDARD TERMS AND CONDITIONS**

1. Description of Service; Defined Terms. This Republication License enables the User to obtain licenses for republication of one or more copyrighted works as described in detail on the relevant Order Confirmation (the "Work(s)"). Copyright Clearance Center, Inc. ("CCC") grants licenses through the Service on behalf of the rightsholder identified on the Order Confirmation (the "Rightsholder"). "Republication", as used herein, generally means the inclusion of a Work, in whole or in part, in a new work or works, also as described on the Order Confirmation. "User", as used herein, means the person or entity making such republication.
2. The terms set forth in the relevant Order Confirmation, and any terms set by the Rightsholder with respect to a particular Work, govern the terms of use of Works in connection with the Service. By using the Service, the person transacting for a republication license on behalf of the User represents and warrants that he/she/it (a) has been duly authorized by the User to accept, and hereby does accept, all such terms and conditions on behalf of User, and (b) shall inform User of all such terms and conditions. In the event such person is a "freelancer" or other third party independent of User and CCC, such party shall be deemed jointly a "User" for purposes of these terms and conditions. In any event, User shall be deemed to have accepted and agreed to all such terms and conditions if User republishes the Work in any fashion.
- 3. Scope of License; Limitations and Obligations.**
- 3.1 All Works and all rights therein, including copyright rights, remain the sole and exclusive property of the Rightsholder. The license created by the exchange of an Order Confirmation (and/or any invoice) and payment by User of the full amount set forth on that document includes only those rights expressly set forth in the Order Confirmation and in these terms and conditions, and conveys no other rights in the Work(s) to User. All rights not expressly granted are hereby reserved.
- 3.2 General Payment Terms: You may pay by credit card or through an account with us payable at the end of the month. If you and we agree that you may establish a standing account with CCC, then the following terms apply: Remit Payment to: Copyright Clearance Center, Dept 001, P.O. Box 843006, Boston, MA 02284-3006. Payments Due: Invoices are payable upon their delivery to you (or upon our notice to you that they are available to you for downloading). After 30 days, outstanding amounts will be subject to a service charge of 1-1/2% per month or, if less, the maximum rate allowed by applicable law. Unless otherwise specifically set forth in the Order Confirmation or in a separate written agreement signed by CCC, invoices are due and payable on "net 30" terms. While User may exercise the rights licensed immediately upon issuance of the Order Confirmation, the license is automatically revoked and is null and void, as if it had never been issued, if complete payment for the license is not received on a timely basis either from User directly or through a payment agent, such as a credit card company.
- 3.3 Unless otherwise provided in the Order Confirmation, any grant of rights to User (i) is "one-time" (including the editions and product family specified in the license), (ii) is non-exclusive and non-transferable and (iii) is subject to any and all limitations and restrictions (such as, but not limited to, limitations on duration of use or circulation) included in the Order Confirmation or invoice and/or in these terms and conditions. Upon completion of the licensed use, User shall either secure a new permission for further use of the Work(s) or immediately cease any new use of the Work(s) and shall render inaccessible (such as by deleting or by removing or severing links or other locators) any further copies of the Work (except for copies printed on paper in accordance with this license and still in User's stock at the end of such period).
- 3.4 In the event that the material for which a republication license is sought includes third party materials (such as photographs, illustrations, graphs, inserts and similar materials) which are identified in such material as having been used by permission, User is responsible for identifying, and seeking separate licenses (under this Service or otherwise) for, any of such third party materials; without a separate license, such third party materials may not be used.
- 3.5 Use of proper copyright notice for a Work is required as a condition of any license granted under the Service. Unless otherwise provided in the Order Confirmation, a proper copyright notice will read substantially as follows:

"Republished with permission of [Rightsholder's name], from [Work's title, author, volume, edition number and year of copyright]; permission conveyed through Copyright Clearance Center, Inc." Such notice must be provided in a reasonably legible font size and must be placed either immediately adjacent to the Work as used (for example, as part of a by-line or footnote but not as a separate electronic link) or in the place where substantially all other credits or notices for the new work containing the republished Work are located. Failure to include the required notice results in loss to the Rightsholder and CCC, and the User shall be liable to pay liquidated damages for each such failure equal to twice the use fee specified in the Order Confirmation, in addition to the use fee itself and any other fees and charges specified.

3.6 User may only make alterations to the Work if and as expressly set forth in the Order Confirmation. No Work may be used in any way that is defamatory, violates the rights of third parties (including such third parties' rights of copyright, privacy, publicity, or other tangible or intangible property), or is otherwise illegal, sexually explicit or obscene. In addition, User may not conjoin a Work with any other material that may result in damage to the reputation of the Rightsholder. User agrees to inform CCC if it becomes aware of any infringement of any rights in a Work and to cooperate with any reasonable request of CCC or the Rightsholder in connection therewith.

4. Indemnity. User hereby indemnifies and agrees to defend the Rightsholder and CCC, and their respective employees and directors, against all claims, liability, damages, costs and expenses, including legal fees and expenses, arising out of any use of a Work beyond the scope of the rights granted herein, or any use of a Work which has been altered in any unauthorized way by User, including claims of defamation or infringement of rights of copyright, publicity, privacy or other tangible or intangible property.

5. Limitation of Liability. UNDER NO CIRCUMSTANCES WILL CCC OR THE RIGHTSHOLDER BE LIABLE FOR ANY DIRECT, INDIRECT, CONSEQUENTIAL OR INCIDENTAL DAMAGES (INCLUDING WITHOUT LIMITATION DAMAGES FOR LOSS OF BUSINESS PROFITS OR INFORMATION, OR FOR BUSINESS INTERRUPTION) ARISING OUT OF THE USE OR INABILITY TO USE A WORK, EVEN IF ONE OF THEM HAS BEEN ADVISED OF THE POSSIBILITY OF SUCH DAMAGES. In any event, the total liability of the Rightsholder and CCC (including their respective employees and directors) shall not exceed the total amount actually paid by User for this license. User assumes full liability for the actions and omissions of its principals, employees, agents, affiliates, successors and assigns.

6. Limited Warranties. THE WORK(S) AND RIGHT(S) ARE PROVIDED "AS IS". CCC HAS THE RIGHT TO GRANT TO USER THE RIGHTS GRANTED IN THE ORDER CONFIRMATION DOCUMENT. CCC AND THE RIGHTSHOLDER DISCLAIM ALL OTHER WARRANTIES RELATING TO THE WORK(S) AND RIGHT(S), EITHER EXPRESS OR IMPLIED, INCLUDING WITHOUT LIMITATION IMPLIED WARRANTIES OF MERCHANTABILITY OR FITNESS FOR A PARTICULAR PURPOSE. ADDITIONAL RIGHTS MAY BE REQUIRED TO USE ILLUSTRATIONS, GRAPHS, PHOTOGRAPHS, ABSTRACTS, INSERTS OR OTHER PORTIONS OF THE WORK (AS OPPOSED TO THE ENTIRE WORK) IN A MANNER CONTEMPLATED BY USER; USER UNDERSTANDS AND AGREES THAT NEITHER CCC NOR THE RIGHTSHOLDER MAY HAVE SUCH ADDITIONAL RIGHTS TO GRANT.

7. Effect of Breach. Any failure by User to pay any amount when due, or any use by User of a Work beyond the scope of the license set forth in the Order Confirmation and/or these terms and conditions, shall be a material breach of the license created by the Order Confirmation and these terms and conditions. Any breach not cured within 30 days of written notice thereof shall result in immediate termination of such license without further notice. Any unauthorized (but licensable) use of a Work that is terminated immediately upon notice thereof may be liquidated by payment of the Rightsholder's ordinary license price therefor; any unauthorized (and unlicensable) use that is not terminated immediately for any reason (including, for example, because materials containing the Work cannot reasonably be recalled) will be subject to all remedies available at law or in equity, but in no event to a payment of less than three times the Rightsholder's ordinary license price for the most closely analogous licensable use plus Rightsholder's and/or CCC's costs and expenses incurred in collecting such payment.

#### 8. Miscellaneous.

8.1 User acknowledges that CCC may, from time to time, make changes or additions to the Service or to these terms and conditions, and CCC reserves the right to send notice to the User by electronic mail or otherwise for the purposes of notifying User of such changes or additions; provided that any such changes or additions shall not apply to permissions already secured and paid for.

8.2 Use of User-related information collected through the Service is governed by CCC's privacy policy, available online here: <http://www.copyright.com/content/cc3/en/tools/footer/privacypolicy.html>.

8.3 The licensing transaction described in the Order Confirmation is personal to User. Therefore, User may not assign or transfer to any other person (whether a natural person or an organization of any kind) the license created by the Order Confirmation and these terms and conditions or any rights granted hereunder; provided, however, that User may assign such license in its entirety on written notice to CCC in the event of a transfer of all or substantially all of User's rights in the new material which includes the Work(s) licensed under this Service.

8.4 No amendment or waiver of any terms is binding unless set forth in writing and signed by the parties. The Rightsholder and CCC hereby object to any terms contained in any writing prepared by the User or its principals, employees, agents or affiliates and purporting to govern or otherwise relate to the licensing transaction described in the Order Confirmation, which terms are in any way inconsistent with any terms set forth in the Order Confirmation and/or in these terms and conditions or CCC's standard operating procedures, whether such writing is prepared prior to, simultaneously with or subsequent to the Order Confirmation, and whether such writing appears on a copy of the Order Confirmation or in a separate instrument.

8.5 The licensing transaction described in the Order Confirmation document shall be governed by and construed under the law of the State of New York, USA, without regard to the principles thereof of conflicts of law. Any case, controversy, suit, action, or proceeding arising out of, in connection with, or related to such licensing transaction

shall be brought, at CCC's sole discretion, in any federal or state court located in the County of New York, State of New York, USA, or in any federal or state court whose geographical jurisdiction covers the location of the Rightsholder set forth in the Order Confirmation. The parties expressly submit to the personal jurisdiction and venue of each such federal or state court. If you have any comments or questions about the Service or Copyright Clearance Center, please contact us at 978-750-8400 or send an e-mail to [info@copyright.com](mailto:info@copyright.com).

v 1.1

**Transplantation proceedings**

**Permission type:** Republish or display content

**Type of use:** Thesis/Dissertation

**TERMS AND CONDITIONS**

**The following terms are individual to this publisher:**

None

**Other Terms and Conditions:**

None

**STANDARD TERMS AND CONDITIONS**

1. Description of Service; Defined Terms. This Republication License enables the User to obtain licenses for republication of one or more copyrighted works as described in detail on the relevant Order Confirmation (the "Work(s)"). Copyright Clearance Center, Inc. ("CCC") grants licenses through the Service on behalf of the rightsholder identified on the Order Confirmation (the "Rightsholder"). "Republication", as used herein, generally means the inclusion of a Work, in whole or in part, in a new work or works, also as described on the Order Confirmation. "User", as used herein, means the person or entity making such republication.

2. The terms set forth in the relevant Order Confirmation, and any terms set by the Rightsholder with respect to a particular Work, govern the terms of use of Works in connection with the Service. By using the Service, the person transacting for a republication license on behalf of the User represents and warrants that he/she/it (a) has been duly authorized by the User to accept, and hereby does accept, all such terms and conditions on behalf of User, and (b) shall inform User of all such terms and conditions. In the event such person is a "freelancer" or other third party independent of User and CCC, such party shall be deemed jointly a "User" for purposes of these terms and conditions. In any event, User shall be deemed to have accepted and agreed to all such terms and conditions if User republishes the Work in any fashion.

**3. Scope of License; Limitations and Obligations.**

3.1 All Works and all rights therein, including copyright rights, remain the sole and exclusive property of the Rightsholder. The license created by the exchange of an Order Confirmation (and/or any invoice) and payment by User of the full amount set forth on that document includes only those rights expressly set forth in the Order Confirmation and in these terms and conditions, and conveys no other rights in the Work(s) to User. All rights not expressly granted are hereby reserved.

3.2 General Payment Terms: You may pay by credit card or through an account with us payable at the end of the month. If you and we agree that you may establish a standing account with CCC, then the following terms apply: Remit Payment to: Copyright Clearance Center, Dept 001, P.O. Box 843006, Boston, MA 02284-3006. Payments Due: Invoices are payable upon their delivery to you (or upon our notice to you that they are available to you for downloading). After 30 days, outstanding amounts will be subject to a service charge of 1-1/2% per month or, if less, the maximum rate allowed by applicable law. Unless otherwise specifically set forth in the Order Confirmation or in a separate written agreement signed by CCC, invoices are due and payable on "net 30" terms. While User may exercise the rights licensed immediately upon issuance of the Order Confirmation, the license is automatically revoked and is null and void, as if it had never been issued, if complete payment for the license is not received on a timely basis either from User directly or through a payment agent, such as a credit card company.

3.3 Unless otherwise provided in the Order Confirmation, any grant of rights to User (i) is "one-time" (including the editions and product family specified in the license), (ii) is non-exclusive and non-transferable and (iii) is subject to any and all limitations and restrictions (such as, but not limited to, limitations on duration of use or circulation) included in the Order Confirmation or invoice and/or in these terms and conditions. Upon completion of the licensed use, User shall either secure a new permission for further use of the Work(s) or immediately cease any new use of the Work(s) and shall render inaccessible (such as by deleting or by removing or severing links or other locators) any further copies of the Work (except for copies printed on paper in accordance with this license and still in User's stock at the end of such period).

3.4 In the event that the material for which a republication license is sought includes third party materials (such as photographs, illustrations, graphs, inserts and similar materials) which are identified in such material as having been used by permission, User is responsible for identifying, and seeking separate licenses (under this Service or otherwise) for, any of such third party materials; without a separate license, such third party materials may not be

used.

3.5 Use of proper copyright notice for a Work is required as a condition of any license granted under the Service. Unless otherwise provided in the Order Confirmation, a proper copyright notice will read substantially as follows: "Republished with permission of [Rightsholder's name], from [Work's title, author, volume, edition number and year of copyright]; permission conveyed through Copyright Clearance Center, Inc." Such notice must be provided in a reasonably legible font size and must be placed either immediately adjacent to the Work as used (for example, as part of a by-line or footnote but not as a separate electronic link) or in the place where substantially all other credits or notices for the new work containing the republished Work are located. Failure to include the required notice results in loss to the Rightsholder and CCC, and the User shall be liable to pay liquidated damages for each such failure equal to twice the use fee specified in the Order Confirmation, in addition to the use fee itself and any other fees and charges specified.

3.6 User may only make alterations to the Work if and as expressly set forth in the Order Confirmation. No Work may be used in any way that is defamatory, violates the rights of third parties (including such third parties' rights of copyright, privacy, publicity, or other tangible or intangible property), or is otherwise illegal, sexually explicit or obscene. In addition, User may not conjoin a Work with any other material that may result in damage to the reputation of the Rightsholder. User agrees to inform CCC if it becomes aware of any infringement of any rights in a Work and to cooperate with any reasonable request of CCC or the Rightsholder in connection therewith.

4. Indemnity. User hereby indemnifies and agrees to defend the Rightsholder and CCC, and their respective employees and directors, against all claims, liability, damages, costs and expenses, including legal fees and expenses, arising out of any use of a Work beyond the scope of the rights granted herein, or any use of a Work which has been altered in any unauthorized way by User, including claims of defamation or infringement of rights of copyright, publicity, privacy or other tangible or intangible property.

5. Limitation of Liability. UNDER NO CIRCUMSTANCES WILL CCC OR THE RIGHTSHOLDER BE LIABLE FOR ANY DIRECT, INDIRECT, CONSEQUENTIAL OR INCIDENTAL DAMAGES (INCLUDING WITHOUT LIMITATION DAMAGES FOR LOSS OF BUSINESS PROFITS OR INFORMATION, OR FOR BUSINESS INTERRUPTION) ARISING OUT OF THE USE OR INABILITY TO USE A WORK, EVEN IF ONE OF THEM HAS BEEN ADVISED OF THE POSSIBILITY OF SUCH DAMAGES. In any event, the total liability of the Rightsholder and CCC (including their respective employees and directors) shall not exceed the total amount actually paid by User for this license. User assumes full liability for the actions and omissions of its principals, employees, agents, affiliates, successors and assigns.

6. Limited Warranties. THE WORK(S) AND RIGHT(S) ARE PROVIDED "AS IS". CCC HAS THE RIGHT TO GRANT TO USER THE RIGHTS GRANTED IN THE ORDER CONFIRMATION DOCUMENT. CCC AND THE RIGHTSHOLDER DISCLAIM ALL OTHER WARRANTIES RELATING TO THE WORK(S) AND RIGHT(S), EITHER EXPRESS OR IMPLIED, INCLUDING WITHOUT LIMITATION IMPLIED WARRANTIES OF MERCHANTABILITY OR FITNESS FOR A PARTICULAR PURPOSE. ADDITIONAL RIGHTS MAY BE REQUIRED TO USE ILLUSTRATIONS, GRAPHS, PHOTOGRAPHS, ABSTRACTS, INSERTS OR OTHER PORTIONS OF THE WORK (AS OPPOSED TO THE ENTIRE WORK) IN A MANNER CONTEMPLATED BY USER; USER UNDERSTANDS AND AGREES THAT NEITHER CCC NOR THE RIGHTSHOLDER MAY HAVE SUCH ADDITIONAL RIGHTS TO GRANT.

7. Effect of Breach. Any failure by User to pay any amount when due, or any use by User of a Work beyond the scope of the license set forth in the Order Confirmation and/or these terms and conditions, shall be a material breach of the license created by the Order Confirmation and these terms and conditions. Any breach not cured within 30 days of written notice thereof shall result in immediate termination of such license without further notice. Any unauthorized (but licensable) use of a Work that is terminated immediately upon notice thereof may be liquidated by payment of the Rightsholder's ordinary license price therefor; any unauthorized (and unlicensable) use that is not terminated immediately for any reason (including, for example, because materials containing the Work cannot reasonably be recalled) will be subject to all remedies available at law or in equity, but in no event to a payment of less than three times the Rightsholder's ordinary license price for the most closely analogous licensable use plus Rightsholder's and/or CCC's costs and expenses incurred in collecting such payment.

#### 8. Miscellaneous.

8.1 User acknowledges that CCC may, from time to time, make changes or additions to the Service or to these terms and conditions, and CCC reserves the right to send notice to the User by electronic mail or otherwise for the purposes of notifying User of such changes or additions; provided that any such changes or additions shall not apply to permissions already secured and paid for.

8.2 Use of User-related information collected through the Service is governed by CCC's privacy policy, available online here: <http://www.copyright.com/content/cc3/en/tools/footer/privacypolicy.html>.

8.3 The licensing transaction described in the Order Confirmation is personal to User. Therefore, User may not assign or transfer to any other person (whether a natural person or an organization of any kind) the license created by the Order Confirmation and these terms and conditions or any rights granted hereunder; provided, however, that User may assign such license in its entirety on written notice to CCC in the event of a transfer of all or substantially all of User's rights in the new material which includes the Work(s) licensed under this Service.

8.4 No amendment or waiver of any terms is binding unless set forth in writing and signed by the parties. The Rightsholder and CCC hereby object to any terms contained in any writing prepared by the User or its principals, employees, agents or affiliates and purporting to govern or otherwise relate to the licensing transaction described in the Order Confirmation, which terms are in any way inconsistent with any terms set forth in the Order Confirmation and/or in these terms and conditions or CCC's standard operating procedures, whether such writing is prepared prior to, simultaneously with or subsequent to the Order Confirmation, and whether such writing appears on a copy of the Order Confirmation or in a separate instrument.

8.5 The licensing transaction described in the Order Confirmation document shall be governed by and construed under the law of the State of New York, USA, without regard to the principles thereof of conflicts of law. Any case, controversy, suit, action, or proceeding arising out of, in connection with, or related to such licensing transaction shall be brought, at CCC's sole discretion, in any federal or state court located in the County of New York, State of New York, USA, or in any federal or state court whose geographical jurisdiction covers the location of the Rightsholder set forth in the Order Confirmation. The parties expressly submit to the personal jurisdiction and venue of each such federal or state court. If you have any comments or questions about the Service or Copyright Clearance Center, please contact us at 978-750-8400 or send an e-mail to [info@copyright.com](mailto:info@copyright.com).

v 1.1

#### Transplantation proceedings

**Permission type:** Republish or display content

**Type of use:** Thesis/Dissertation

#### TERMS AND CONDITIONS

The following terms are individual to this publisher:

None

#### Other Terms and Conditions:

None

#### STANDARD TERMS AND CONDITIONS

1. Description of Service; Defined Terms. This Republication License enables the User to obtain licenses for republication of one or more copyrighted works as described in detail on the relevant Order Confirmation (the "Work(s)"). Copyright Clearance Center, Inc. ("CCC") grants licenses through the Service on behalf of the rightsholder identified on the Order Confirmation (the "Rightsholder"). "Republication", as used herein, generally means the inclusion of a Work, in whole or in part, in a new work or works, also as described on the Order Confirmation. "User", as used herein, means the person or entity making such republication.

2. The terms set forth in the relevant Order Confirmation, and any terms set by the Rightsholder with respect to a particular Work, govern the terms of use of Works in connection with the Service. By using the Service, the person transacting for a republication license on behalf of the User represents and warrants that he/she/it (a) has been duly authorized by the User to accept, and hereby does accept, all such terms and conditions on behalf of User, and (b) shall inform User of all such terms and conditions. In the event such person is a "freelancer" or other third party independent of User and CCC, such party shall be deemed jointly a "User" for purposes of these terms and conditions. In any event, User shall be deemed to have accepted and agreed to all such terms and conditions if User republishes the Work in any fashion.

#### 3. Scope of License; Limitations and Obligations.

3.1 All Works and all rights therein, including copyright rights, remain the sole and exclusive property of the Rightsholder. The license created by the exchange of an Order Confirmation (and/or any invoice) and payment by User of the full amount set forth on that document includes only those rights expressly set forth in the Order Confirmation and in these terms and conditions, and conveys no other rights in the Work(s) to User. All rights not expressly granted are hereby reserved.

3.2 General Payment Terms: You may pay by credit card or through an account with us payable at the end of the month. If you and we agree that you may establish a standing account with CCC, then the following terms apply: Remit Payment to: Copyright Clearance Center, Dept 001, P.O. Box 843006, Boston, MA 02284-3006. Payments Due: Invoices are payable upon their delivery to you (or upon our notice to you that they are available to you for downloading). After 30 days, outstanding amounts will be subject to a service charge of 1-1/2% per month or, if less, the maximum rate allowed by applicable law. Unless otherwise specifically set forth in the Order Confirmation or in a separate written agreement signed by CCC, invoices are due and payable on "net 30" terms. While User may exercise the rights licensed immediately upon issuance of the Order Confirmation, the license is automatically revoked and is null and void, as if it had never been issued, if complete payment for the license is not received on a timely basis either from User directly or through a payment agent, such as a credit card company.

3.3 Unless otherwise provided in the Order Confirmation, any grant of rights to User (i) is "one-time" (including the editions and product family specified in the license), (ii) is non-exclusive and non-transferable and (iii) is subject to any and all limitations and restrictions (such as, but not limited to, limitations on duration of use or circulation) included in the Order Confirmation or invoice and/or in these terms and conditions. Upon completion of the licensed use, User shall either secure a new permission for further use of the Work(s) or immediately cease any new use of the Work(s) and shall render inaccessible (such as by deleting or by removing or severing links or other locators) any further copies of the Work (except for copies printed on paper in accordance with this license and still in User's stock at the end of such period).

3.4 In the event that the material for which a republication license is sought includes third party materials (such as

photographs, illustrations, graphs, inserts and similar materials) which are identified in such material as having been used by permission, User is responsible for identifying, and seeking separate licenses (under this Service or otherwise) for, any of such third party materials; without a separate license, such third party materials may not be used.

3.5 Use of proper copyright notice for a Work is required as a condition of any license granted under the Service. Unless otherwise provided in the Order Confirmation, a proper copyright notice will read substantially as follows: "Republished with permission of [Rightsholder's name], from [Work's title, author, volume, edition number and year of copyright]; permission conveyed through Copyright Clearance Center, Inc." Such notice must be provided in a reasonably legible font size and must be placed either immediately adjacent to the Work as used (for example, as part of a by-line or footnote but not as a separate electronic link) or in the place where substantially all other credits or notices for the new work containing the republished Work are located. Failure to include the required notice results in loss to the Rightsholder and CCC, and the User shall be liable to pay liquidated damages for each such failure equal to twice the use fee specified in the Order Confirmation, in addition to the use fee itself and any other fees and charges specified.

3.6 User may only make alterations to the Work if and as expressly set forth in the Order Confirmation. No Work may be used in any way that is defamatory, violates the rights of third parties (including such third parties' rights of copyright, privacy, publicity, or other tangible or intangible property), or is otherwise illegal, sexually explicit or obscene. In addition, User may not conjoin a Work with any other material that may result in damage to the reputation of the Rightsholder. User agrees to inform CCC if it becomes aware of any infringement of any rights in a Work and to cooperate with any reasonable request of CCC or the Rightsholder in connection therewith.

4. Indemnity. User hereby indemnifies and agrees to defend the Rightsholder and CCC, and their respective employees and directors, against all claims, liability, damages, costs and expenses, including legal fees and expenses, arising out of any use of a Work beyond the scope of the rights granted herein, or any use of a Work which has been altered in any unauthorized way by User, including claims of defamation or infringement of rights of copyright, publicity, privacy or other tangible or intangible property.

5. Limitation of Liability. UNDER NO CIRCUMSTANCES WILL CCC OR THE RIGHTSHOLDER BE LIABLE FOR ANY DIRECT, INDIRECT, CONSEQUENTIAL OR INCIDENTAL DAMAGES (INCLUDING WITHOUT LIMITATION DAMAGES FOR LOSS OF BUSINESS PROFITS OR INFORMATION, OR FOR BUSINESS INTERRUPTION) ARISING OUT OF THE USE OR INABILITY TO USE A WORK, EVEN IF ONE OF THEM HAS BEEN ADVISED OF THE POSSIBILITY OF SUCH DAMAGES. In any event, the total liability of the Rightsholder and CCC (including their respective employees and directors) shall not exceed the total amount actually paid by User for this license. User assumes full liability for the actions and omissions of its principals, employees, agents, affiliates, successors and assigns.

6. Limited Warranties. THE WORK(S) AND RIGHT(S) ARE PROVIDED "AS IS". CCC HAS THE RIGHT TO GRANT TO USER THE RIGHTS GRANTED IN THE ORDER CONFIRMATION DOCUMENT. CCC AND THE RIGHTSHOLDER DISCLAIM ALL OTHER WARRANTIES RELATING TO THE WORK(S) AND RIGHT(S), EITHER EXPRESS OR IMPLIED, INCLUDING WITHOUT LIMITATION IMPLIED WARRANTIES OF MERCHANTABILITY OR FITNESS FOR A PARTICULAR PURPOSE. ADDITIONAL RIGHTS MAY BE REQUIRED TO USE ILLUSTRATIONS, GRAPHS, PHOTOGRAPHS, ABSTRACTS, INSERTS OR OTHER PORTIONS OF THE WORK (AS OPPOSED TO THE ENTIRE WORK) IN A MANNER CONTEMPLATED BY USER; USER UNDERSTANDS AND AGREES THAT NEITHER CCC NOR THE RIGHTSHOLDER MAY HAVE SUCH ADDITIONAL RIGHTS TO GRANT.

7. Effect of Breach. Any failure by User to pay any amount when due, or any use by User of a Work beyond the scope of the license set forth in the Order Confirmation and/or these terms and conditions, shall be a material breach of the license created by the Order Confirmation and these terms and conditions. Any breach not cured within 30 days of written notice thereof shall result in immediate termination of such license without further notice. Any unauthorized (but licensable) use of a Work that is terminated immediately upon notice thereof may be liquidated by payment of the Rightsholder's ordinary license price therefor; any unauthorized (and unlicensable) use that is not terminated immediately for any reason (including, for example, because materials containing the Work cannot reasonably be recalled) will be subject to all remedies available at law or in equity, but in no event to a payment of less than three times the Rightsholder's ordinary license price for the most closely analogous licensable use plus Rightsholder's and/or CCC's costs and expenses incurred in collecting such payment.

#### 8. Miscellaneous.

8.1 User acknowledges that CCC may, from time to time, make changes or additions to the Service or to these terms and conditions, and CCC reserves the right to send notice to the User by electronic mail or otherwise for the purposes of notifying User of such changes or additions; provided that any such changes or additions shall not apply to permissions already secured and paid for.

8.2 Use of User-related information collected through the Service is governed by CCC's privacy policy, available online here: <http://www.copyright.com/content/cc3/en/tools/footer/privacypolicy.html>.

8.3 The licensing transaction described in the Order Confirmation is personal to User. Therefore, User may not assign or transfer to any other person (whether a natural person or an organization of any kind) the license created by the Order Confirmation and these terms and conditions or any rights granted hereunder; provided, however, that User may assign such license in its entirety on written notice to CCC in the event of a transfer of all or substantially all of User's rights in the new material which includes the Work(s) licensed under this Service.

8.4 No amendment or waiver of any terms is binding unless set forth in writing and signed by the parties. The Rightsholder and CCC hereby object to any terms contained in any writing prepared by the User or its principals, employees, agents or affiliates and purporting to govern or otherwise relate to the licensing transaction described in the Order Confirmation, which terms are in any way inconsistent with any terms set forth in the Order Confirmation

and/or in these terms and conditions or CCC's standard operating procedures, whether such writing is prepared prior to, simultaneously with or subsequent to the Order Confirmation, and whether such writing appears on a copy of the Order Confirmation or in a separate instrument.

8.5 The licensing transaction described in the Order Confirmation document shall be governed by and construed under the law of the State of New York, USA, without regard to the principles thereof of conflicts of law. Any case, controversy, suit, action, or proceeding arising out of, in connection with, or related to such licensing transaction shall be brought, at CCC's sole discretion, in any federal or state court located in the County of New York, State of New York, USA, or in any federal or state court whose geographical jurisdiction covers the location of the Rightsholder set forth in the Order Confirmation. The parties expressly submit to the personal jurisdiction and venue of each such federal or state court. If you have any comments or questions about the Service or Copyright Clearance Center, please contact us at 978-750-8400 or send an e-mail to [info@copyright.com](mailto:info@copyright.com).

v 1.1

#### **Xenotransplantation**

**Permission type:** Republish or display content

**Type of use:** Republish in a thesis/dissertation

#### **TERMS AND CONDITIONS**

**The following terms are individual to this publisher:**

#### **TERMS AND CONDITIONS**

This copyrighted material is owned by or exclusively licensed to John Wiley & Sons, Inc. or one of its group companies (each a "Wiley Company") or handled on behalf of a society with which a Wiley Company has exclusive publishing rights in relation to a particular work (collectively "WILEY"). By clicking "accept" in connection with completing this licensing transaction, you agree that the following terms and conditions apply to this transaction (along with the billing and payment terms and conditions established by the Copyright Clearance Center Inc., ("CCC's Billing and Payment terms and conditions"), at the time that you opened your Rightslink account (these are available at any time at <http://myaccount.copyright.com>).

#### **Terms and Conditions**

- The materials you have requested permission to reproduce or reuse (the "Wiley Materials") are protected by copyright.
- You are hereby granted a personal, non-exclusive, non-sub licensable (on a stand-alone basis), non-transferable, worldwide, limited license to reproduce the Wiley Materials for the purpose specified in the licensing process. This license is for a one-time use only and limited to any maximum distribution number specified in the license. The first instance of republication or reuse granted by this license must be completed within two years of the date of the grant of this license (although copies prepared before the end date may be distributed thereafter). The Wiley Materials shall not be used in any other manner or for any other purpose, beyond what is granted in the license. Permission is granted subject to an appropriate acknowledgement given to the author, title of the material/book/journal and the publisher. You shall also duplicate the copyright notice that appears in the Wiley publication in your use of the Wiley Material. Permission is also granted on the understanding that nowhere in the text is a previously published source acknowledged for all or part of this Wiley Material. Any third party content is expressly excluded from this permission.
- With respect to the Wiley Materials, all rights are reserved. Except as expressly granted by the terms of the license, no part of the Wiley Materials may be copied, modified, adapted (except for minor reformatting required by the new Publication), translated, reproduced, transferred or distributed, in any form or by any means, and no derivative works may be made based on the Wiley Materials without the prior permission of the respective copyright owner. You may not alter, remove or suppress in any manner any copyright, trademark or other notices displayed by the Wiley Materials. You may not license, rent, sell, loan, lease, pledge, offer as security, transfer or assign the Wiley Materials on a stand-alone basis, or any of the rights granted to you hereunder to any other person.
- The Wiley Materials and all of the intellectual property rights therein shall at all times remain the exclusive property of John Wiley & Sons Inc, the Wiley Companies, or their respective licensors, and your interest therein is only that of having possession of and the right to reproduce the Wiley Materials pursuant to Section 2 herein during the continuance of this Agreement. You agree that you own no right, title or interest in or to the Wiley Materials or any of the intellectual property rights therein. You shall have no rights hereunder other than the license as provided for above in Section 2. No right, license or interest to any trademark, trade name, service mark or other branding ("Marks") of WILEY or its licensors is granted hereunder, and you agree that you shall not assert any such right, license or interest with respect thereto.
- NEITHER WILEY NOR ITS LICENSORS MAKES ANY WARRANTY OR REPRESENTATION OF ANY KIND TO YOU OR ANY

THIRD PARTY, EXPRESS, IMPLIED OR STATUTORY, WITH RESPECT TO THE MATERIALS OR THE ACCURACY OF ANY INFORMATION CONTAINED IN THE MATERIALS, INCLUDING, WITHOUT LIMITATION, ANY IMPLIED WARRANTY OF MERCHANTABILITY, ACCURACY, SATISFACTORY QUALITY, FITNESS FOR A PARTICULAR PURPOSE, USABILITY, INTEGRATION OR NON-INFRINGEMENT AND ALL SUCH WARRANTIES ARE HEREBY EXCLUDED BY WILEY AND ITS LICENSORS AND WAIVED BY YOU.

- WILEY shall have the right to terminate this Agreement immediately upon breach of this Agreement by you.
- You shall indemnify, defend and hold harmless WILEY, its Licensors and their respective directors, officers, agents and employees, from and against any actual or threatened claims, demands, causes of action or proceedings arising from any breach of this Agreement by you.
- IN NO EVENT SHALL WILEY OR ITS LICENSORS BE LIABLE TO YOU OR ANY OTHER PARTY OR ANY OTHER PERSON OR ENTITY FOR ANY SPECIAL, CONSEQUENTIAL, INCIDENTAL, INDIRECT, EXEMPLARY OR PUNITIVE DAMAGES, HOWEVER CAUSED, ARISING OUT OF OR IN CONNECTION WITH THE DOWNLOADING, PROVISIONING, VIEWING OR USE OF THE MATERIALS REGARDLESS OF THE FORM OF ACTION, WHETHER FOR BREACH OF CONTRACT, BREACH OF WARRANTY, TORT, NEGLIGENCE, INFRINGEMENT OR OTHERWISE (INCLUDING, WITHOUT LIMITATION, DAMAGES BASED ON LOSS OF PROFITS, DATA, FILES, USE, BUSINESS OPPORTUNITY OR CLAIMS OF THIRD PARTIES), AND WHETHER OR NOT THE PARTY HAS BEEN ADVISED OF THE POSSIBILITY OF SUCH DAMAGES. THIS LIMITATION SHALL APPLY NOTWITHSTANDING ANY FAILURE OF ESSENTIAL PURPOSE OF ANY LIMITED REMEDY PROVIDED HEREIN.
- Should any provision of this Agreement be held by a court of competent jurisdiction to be illegal, invalid, or unenforceable, that provision shall be deemed amended to achieve as nearly as possible the same economic effect as the original provision, and the legality, validity and enforceability of the remaining provisions of this Agreement shall not be affected or impaired thereby.
- The failure of either party to enforce any term or condition of this Agreement shall not constitute a waiver of either party's right to enforce each and every term and condition of this Agreement. No breach under this agreement shall be deemed waived or excused by either party unless such waiver or consent is in writing signed by the party granting such waiver or consent. The waiver by or consent of a party to a breach of any provision of this Agreement shall not operate or be construed as a waiver of or consent to any other or subsequent breach by such other party.
- This Agreement may not be assigned (including by operation of law or otherwise) by you without WILEY's prior written consent.
- Any fee required for this permission shall be non-refundable after thirty (30) days from receipt by the CCC.
- These terms and conditions together with CCC's Billing and Payment terms and conditions (which are incorporated herein) form the entire agreement between you and WILEY concerning this licensing transaction and (in the absence of fraud) supersedes all prior agreements and representations of the parties, oral or written. This Agreement may not be amended except in writing signed by both parties. This Agreement shall be binding upon and inure to the benefit of the parties' successors, legal representatives, and authorized assigns.
- In the event of any conflict between your obligations established by these terms and conditions and those established by CCC's Billing and Payment terms and conditions, these terms and conditions shall prevail.
- WILEY expressly reserves all rights not specifically granted in the combination of (i) the license details provided by you and accepted in the course of this licensing transaction, (ii) these terms and conditions and (iii) CCC's Billing and Payment terms and conditions.
- This Agreement will be void if the Type of Use, Format, Circulation, or Requestor Type was misrepresented during the licensing process.
- This Agreement shall be governed by and construed in accordance with the laws of the State of New York, USA, without regards to such state's conflict of law rules. Any legal action, suit or proceeding arising out of or relating to these Terms and Conditions or the breach thereof shall be instituted in a court of competent jurisdiction in New York County in the State of New York in the United States of America and each party hereby consents and submits to the personal jurisdiction of such court, waives any objection to venue in such court and consents to service of process by registered or certified mail, return receipt requested, at the last known address of such party.

**Other terms and conditions:**

**REPUBLICATION IN MAIN PRODUCT, PRODUCT FAMILY, COMPILATIONS OR COLLECTIVE WORKS**

Limitations on reuse of Wiley Materials:

Where the following additional rights have been granted as part of this Agreement, please note that in no instance may the total amount of Wiley Materials used in any Main Product, Compilation or Collective work comprise more than 5% (if figures/tables) or 15% (if full articles/chapters) of the Main Product, Compilation or Collective Work.

**Product Family:** main product AND any product related to the main product



Main Product and related products which are created to supplement or add value to the Main Product, and in which the overall content of the Main Product remains substantially the same with relatively minor additions or variations. Examples include: ancillaries, instructor guides, testing materials, student subject-driven resources, abridgements, and custom editions that are substantially based on a single Main Product.

**Other:** main product AND other compilations or collective works

Main Product and new collective works produced by requestor that do not consist of substantially the same material as an individual Main Product. For example, licensees may wish to acquire rights for use in the Main Product AND for use in separate projects within the same subject discipline as the Main Product. This would include, for example, custom editions or compilations which incorporate chapters from multiple underlying works within or across disciplines.

**All:** main product, AND Product Family AND Other compilations or collective works

This combines the right to republish in the following components: 1) main product, 2) products related to the main product (i.e. Product Family) and 3) other compilations/collective works.

#### **WILEY OPEN ACCESS TERMS AND CONDITIONS**

Wiley Publishes Open Access Articles in fully Open Access Journals and in Subscription journals offering Online Open. Although most of the fully Open Access journals publish open access articles under the terms of the Creative Commons Attribution (CC BY) License only, the subscription journals and a few of the Open Access Journals offer a choice of Creative Commons Licenses: Creative Commons Attribution (CC-BY) license, Creative Commons Attribution Non-Commercial (CC-BY-NC) license and Creative Commons Attribution Non-Commercial-NoDerivs (CC-BY-NC-ND) License. The license type is clearly identified on the article.

Copyright in any research article in a journal published as Open Access under a Creative Commons License is retained by the author(s). Authors grant Wiley a license to publish the article and identify itself as the original publisher. Authors also grant any third party the right to use the article freely as long as its integrity is maintained and its original authors, citation details and publisher are identified as follows: [Title of Article/Author/Journal Title and Volume/Issue. Copyright (c) [year] [copyright owner as specified in the Journal]. Links to the final article on Wiley's website are encouraged where applicable.

#### **The Creative Commons Attribution License**

The Creative Commons Attribution License (CC-BY) allows users to copy, distribute and transmit an article, adapt the article and make commercial use of the article. The CC-BY license permits commercial and non-commercial re-use of an open access article, as long as the author is properly attributed.

The Creative Commons Attribution License does not affect the moral rights of authors, including without limitation the right not to have their work subjected to derogatory treatment. It also does not affect any other rights held by authors or third parties in the article, including without limitation the rights of privacy and publicity. Use of the article must not assert or imply, whether implicitly or explicitly, any connection with, endorsement or sponsorship of such use by the author, publisher or any other party associated with the article.

For any reuse or distribution, users must include the copyright notice and make clear to others that the article is made available under a Creative Commons Attribution license, linking to the relevant Creative Commons web page.

To the fullest extent permitted by applicable law, the article is made available as is and without representation or warranties of any kind whether express, implied, statutory or otherwise and including, without limitation, warranties of title, merchantability, fitness for a particular purpose, non-infringement, absence of defects, accuracy, or the presence or absence of errors.

#### **Creative Commons Attribution Non-Commercial License**

The Creative Commons Attribution Non-Commercial (CC-BY-NC) License permits use, distribution and reproduction in any medium, provided the original work is properly cited and is not used for commercial purposes.(see below)

#### **Creative Commons Attribution-Non-Commercial-NoDerivs License**

The Creative Commons Attribution Non-Commercial-NoDerivs License (CC-BY-NC-ND) permits use, distribution and reproduction in any medium, provided the original work is properly cited, is not used for commercial purposes and no modifications or adaptations are made. (see below)

#### **Use by non-commercial users**

For non-commercial and non-promotional purposes, individual users may access, download, copy, display and redistribute to colleagues Wiley Open Access articles, as well as adapt, translate, text- and data-mine the content subject to the following conditions:

- The authors' moral rights are not compromised. These rights include the right of "paternity" (also known as "attribution" - the right for the author to be identified as such) and "integrity" (the right for the author not to have the work altered in such a way that the author's reputation or integrity may be impugned).
- Where content in the article is identified as belonging to a third party, it is the obligation of the user to ensure that

any reuse complies with the copyright policies of the owner of that content.

- If article content is copied, downloaded or otherwise reused for non-commercial research and education purposes, a link to the appropriate bibliographic citation (authors, journal, article title, volume, issue, page numbers, DOI and the link to the definitive published version on Wiley Online Library) should be maintained. Copyright notices and disclaimers must not be deleted.
- Any translations, for which a prior translation agreement with Wiley has not been agreed, must prominently display the statement: "This is an unofficial translation of an article that appeared in a Wiley publication. The publisher has not endorsed this translation."

#### **Use by commercial "for-profit" organisations**

Use of Wiley Open Access articles for commercial, promotional, or marketing purposes requires further explicit permission from Wiley and will be subject to a fee. Commercial purposes include:

- Copying or downloading of articles, or linking to such articles for further redistribution, sale or licensing;
- Copying, downloading or posting by a site or service that incorporates advertising with such content;
- The inclusion or incorporation of article content in other works or services (other than normal quotations with an appropriate citation) that is then available for sale or licensing, for a fee (for example, a compilation produced for marketing purposes, inclusion in a sales pack)
- Use of article content (other than normal quotations with appropriate citation) by for-profit organisations for promotional purposes
- Linking to article content in e-mails redistributed for promotional, marketing or educational purposes;
- Use for the purposes of monetary reward by means of sale, resale, licence, loan, transfer or other form of commercial exploitation such as marketing products
- Print reprints of Wiley Open Access articles can be purchased from: [corporatesales@wiley.com](mailto:corporatesales@wiley.com)

Further details can be found on Wiley Online Library <http://olabout.wiley.com/WileyCDA/Section/id-410895.html>

#### **Other Terms and Conditions:**

None

#### **STANDARD TERMS AND CONDITIONS**

1. Description of Service; Defined Terms. This Republication License enables the User to obtain licenses for republication of one or more copyrighted works as described in detail on the relevant Order Confirmation (the "Work(s)"). Copyright Clearance Center, Inc. ("CCC") grants licenses through the Service on behalf of the rightsholder identified on the Order Confirmation (the "Rightsholder"). "Republication", as used herein, generally means the inclusion of a Work, in whole or in part, in a new work or works, also as described on the Order Confirmation. "User", as used herein, means the person or entity making such republication.

2. The terms set forth in the relevant Order Confirmation, and any terms set by the Rightsholder with respect to a particular Work, govern the terms of use of Works in connection with the Service. By using the Service, the person transacting for a republication license on behalf of the User represents and warrants that he/she/it (a) has been duly authorized by the User to accept, and hereby does accept, all such terms and conditions on behalf of User, and (b) shall inform User of all such terms and conditions. In the event such person is a "freelancer" or other third party independent of User and CCC, such party shall be deemed jointly a "User" for purposes of these terms and conditions. In any event, User shall be deemed to have accepted and agreed to all such terms and conditions if User republishes the Work in any fashion.

#### **3. Scope of License; Limitations and Obligations.**

3.1 All Works and all rights therein, including copyright rights, remain the sole and exclusive property of the Rightsholder. The license created by the exchange of an Order Confirmation (and/or any invoice) and payment by User of the full amount set forth on that document includes only those rights expressly set forth in the Order Confirmation and in these terms and conditions, and conveys no other rights in the Work(s) to User. All rights not expressly granted are hereby reserved.

3.2 General Payment Terms: You may pay by credit card or through an account with us payable at the end of the month. If you and we agree that you may establish a standing account with CCC, then the following terms apply: Remit Payment to: Copyright Clearance Center, Dept 001, P.O. Box 843006, Boston, MA 02284-3006. Payments Due: Invoices are payable upon their delivery to you (or upon our notice to you that they are available to you for downloading). After 30 days, outstanding amounts will be subject to a service charge of 1-1/2% per month or, if less, the maximum rate allowed by applicable law. Unless otherwise specifically set forth in the Order Confirmation or in a separate written agreement signed by CCC, invoices are due and payable on "net 30" terms. While User may exercise the rights licensed immediately upon issuance of the Order Confirmation, the license is automatically revoked and is null and void, as if it had never been issued, if complete payment for the license is not received on a timely basis either from User directly or through a payment agent, such as a credit card company.

3.3 Unless otherwise provided in the Order Confirmation, any grant of rights to User (i) is "one-time" (including the

editions and product family specified in the license), (ii) is non-exclusive and non-transferable and (iii) is subject to any and all limitations and restrictions (such as, but not limited to, limitations on duration of use or circulation) included in the Order Confirmation or invoice and/or in these terms and conditions. Upon completion of the licensed use, User shall either secure a new permission for further use of the Work(s) or immediately cease any new use of the Work(s) and shall render inaccessible (such as by deleting or by removing or severing links or other locators) any further copies of the Work (except for copies printed on paper in accordance with this license and still in User's stock at the end of such period).

3.4 In the event that the material for which a republication license is sought includes third party materials (such as photographs, illustrations, graphs, inserts and similar materials) which are identified in such material as having been used by permission, User is responsible for identifying, and seeking separate licenses (under this Service or otherwise) for, any of such third party materials; without a separate license, such third party materials may not be used.

3.5 Use of proper copyright notice for a Work is required as a condition of any license granted under the Service. Unless otherwise provided in the Order Confirmation, a proper copyright notice will read substantially as follows: "Republished with permission of [Rightsholder's name], from [Work's title, author, volume, edition number and year of copyright]; permission conveyed through Copyright Clearance Center, Inc." Such notice must be provided in a reasonably legible font size and must be placed either immediately adjacent to the Work as used (for example, as part of a by-line or footnote but not as a separate electronic link) or in the place where substantially all other credits or notices for the new work containing the republished Work are located. Failure to include the required notice results in loss to the Rightsholder and CCC, and the User shall be liable to pay liquidated damages for each such failure equal to twice the use fee specified in the Order Confirmation, in addition to the use fee itself and any other fees and charges specified.

3.6 User may only make alterations to the Work if and as expressly set forth in the Order Confirmation. No Work may be used in any way that is defamatory, violates the rights of third parties (including such third parties' rights of copyright, privacy, publicity, or other tangible or intangible property), or is otherwise illegal, sexually explicit or obscene. In addition, User may not conjoin a Work with any other material that may result in damage to the reputation of the Rightsholder. User agrees to inform CCC if it becomes aware of any infringement of any rights in a Work and to cooperate with any reasonable request of CCC or the Rightsholder in connection therewith.

4. Indemnity. User hereby indemnifies and agrees to defend the Rightsholder and CCC, and their respective employees and directors, against all claims, liability, damages, costs and expenses, including legal fees and expenses, arising out of any use of a Work beyond the scope of the rights granted herein, or any use of a Work which has been altered in any unauthorized way by User, including claims of defamation or infringement of rights of copyright, publicity, privacy or other tangible or intangible property.

5. Limitation of Liability. UNDER NO CIRCUMSTANCES WILL CCC OR THE RIGHTSHOLDER BE LIABLE FOR ANY DIRECT, INDIRECT, CONSEQUENTIAL OR INCIDENTAL DAMAGES (INCLUDING WITHOUT LIMITATION DAMAGES FOR LOSS OF BUSINESS PROFITS OR INFORMATION, OR FOR BUSINESS INTERRUPTION) ARISING OUT OF THE USE OR INABILITY TO USE A WORK, EVEN IF ONE OF THEM HAS BEEN ADVISED OF THE POSSIBILITY OF SUCH DAMAGES. In any event, the total liability of the Rightsholder and CCC (including their respective employees and directors) shall not exceed the total amount actually paid by User for this license. User assumes full liability for the actions and omissions of its principals, employees, agents, affiliates, successors and assigns.

6. Limited Warranties. THE WORK(S) AND RIGHT(S) ARE PROVIDED "AS IS". CCC HAS THE RIGHT TO GRANT TO USER THE RIGHTS GRANTED IN THE ORDER CONFIRMATION DOCUMENT. CCC AND THE RIGHTSHOLDER DISCLAIM ALL OTHER WARRANTIES RELATING TO THE WORK(S) AND RIGHT(S), EITHER EXPRESS OR IMPLIED, INCLUDING WITHOUT LIMITATION IMPLIED WARRANTIES OF MERCHANTABILITY OR FITNESS FOR A PARTICULAR PURPOSE. ADDITIONAL RIGHTS MAY BE REQUIRED TO USE ILLUSTRATIONS, GRAPHS, PHOTOGRAPHS, ABSTRACTS, INSERTS OR OTHER PORTIONS OF THE WORK (AS OPPOSED TO THE ENTIRE WORK) IN A MANNER CONTEMPLATED BY USER; USER UNDERSTANDS AND AGREES THAT NEITHER CCC NOR THE RIGHTSHOLDER MAY HAVE SUCH ADDITIONAL RIGHTS TO GRANT.

7. Effect of Breach. Any failure by User to pay any amount when due, or any use by User of a Work beyond the scope of the license set forth in the Order Confirmation and/or these terms and conditions, shall be a material breach of the license created by the Order Confirmation and these terms and conditions. Any breach not cured within 30 days of written notice thereof shall result in immediate termination of such license without further notice. Any unauthorized (but licensable) use of a Work that is terminated immediately upon notice thereof may be liquidated by payment of the Rightsholder's ordinary license price therefor; any unauthorized (and unlicensable) use that is not terminated immediately for any reason (including, for example, because materials containing the Work cannot reasonably be recalled) will be subject to all remedies available at law or in equity, but in no event to a payment of less than three times the Rightsholder's ordinary license price for the most closely analogous licensable use plus Rightsholder's and/or CCC's costs and expenses incurred in collecting such payment.

#### 8. Miscellaneous.

8.1 User acknowledges that CCC may, from time to time, make changes or additions to the Service or to these terms and conditions, and CCC reserves the right to send notice to the User by electronic mail or otherwise for the purposes of notifying User of such changes or additions; provided that any such changes or additions shall not apply to permissions already secured and paid for.

8.2 Use of User-related information collected through the Service is governed by CCC's privacy policy, available online here: <http://www.copyright.com/content/cc3/en/tools/footer/privacypolicy.html>.

8.3 The licensing transaction described in the Order Confirmation is personal to User. Therefore, User may not assign

or transfer to any other person (whether a natural person or an organization of any kind) the license created by the Order Confirmation and these terms and conditions or any rights granted hereunder; provided, however, that User may assign such license in its entirety on written notice to CCC in the event of a transfer of all or substantially all of User's rights in the new material which includes the Work(s) licensed under this Service.

8.4 No amendment or waiver of any terms is binding unless set forth in writing and signed by the parties. The Rightsholder and CCC hereby object to any terms contained in any writing prepared by the User or its principals, employees, agents or affiliates and purporting to govern or otherwise relate to the licensing transaction described in the Order Confirmation, which terms are in any way inconsistent with any terms set forth in the Order Confirmation and/or in these terms and conditions or CCC's standard operating procedures, whether such writing is prepared prior to, simultaneously with or subsequent to the Order Confirmation, and whether such writing appears on a copy of the Order Confirmation or in a separate instrument.

8.5 The licensing transaction described in the Order Confirmation document shall be governed by and construed under the law of the State of New York, USA, without regard to the principles thereof of conflicts of law. Any case, controversy, suit, action, or proceeding arising out of, in connection with, or related to such licensing transaction shall be brought, at CCC's sole discretion, in any federal or state court located in the County of New York, State of New York, USA, or in any federal or state court whose geographical jurisdiction covers the location of the Rightsholder set forth in the Order Confirmation. The parties expressly submit to the personal jurisdiction and venue of each such federal or state court. If you have any comments or questions about the Service or Copyright Clearance Center, please contact us at 978-750-8400 or send an e-mail to [info@copyright.com](mailto:info@copyright.com).

v 1.1

#### Xenotransplantation

**Permission type:** Republish or display content

**Type of use:** Republish in a thesis/dissertation

#### TERMS AND CONDITIONS

The following terms are individual to this publisher:

#### TERMS AND CONDITIONS

This copyrighted material is owned by or exclusively licensed to John Wiley & Sons, Inc. or one of its group companies (each a "Wiley Company") or handled on behalf of a society with which a Wiley Company has exclusive publishing rights in relation to a particular work (collectively "WILEY"). By clicking "accept" in connection with completing this licensing transaction, you agree that the following terms and conditions apply to this transaction (along with the billing and payment terms and conditions established by the Copyright Clearance Center Inc., ("CCC's Billing and Payment terms and conditions"), at the time that you opened your Rightslink account (these are available at any time at <http://myaccount.copyright.com>).

#### Terms and Conditions

- The materials you have requested permission to reproduce or reuse (the "Wiley Materials") are protected by copyright.
- You are hereby granted a personal, non-exclusive, non-sub licensable (on a stand-alone basis), non-transferable, worldwide, limited license to reproduce the Wiley Materials for the purpose specified in the licensing process. This license is for a one-time use only and limited to any maximum distribution number specified in the license. The first instance of republication or reuse granted by this licence must be completed within two years of the date of the grant of this licence (although copies prepared before the end date may be distributed thereafter). The Wiley Materials shall not be used in any other manner or for any other purpose, beyond what is granted in the license. Permission is granted subject to an appropriate acknowledgement given to the author, title of the material/book /journal and the publisher. You shall also duplicate the copyright notice that appears in the Wiley publication in your use of the Wiley Material. Permission is also granted on the understanding that nowhere in the text is a previously published source acknowledged for all or part of this Wiley Material. Any third party content is expressly excluded from this permission.
- With respect to the Wiley Materials, all rights are reserved. Except as expressly granted by the terms of the license, no part of the Wiley Materials may be copied, modified, adapted (except for minor reformatting required by the new Publication), translated, reproduced, transferred or distributed, in any form or by any means, and no derivative works may be made based on the Wiley Materials without the prior permission of the respective copyright owner. You may not alter, remove or suppress in any manner any copyright, trademark or other notices displayed by the Wiley Materials. You may not license, rent, sell, loan, lease, pledge, offer as security, transfer or assign the Wiley Materials on a stand-alone basis, or any of the rights granted to you hereunder to any other person.
- The Wiley Materials and all of the intellectual property rights therein shall at all times remain the exclusive property

of John Wiley & Sons Inc, the Wiley Companies, or their respective licensors, and your interest therein is only that of having possession of and the right to reproduce the Wiley Materials pursuant to Section 2 herein during the continuance of this Agreement. You agree that you own no right, title or interest in or to the Wiley Materials or any of the intellectual property rights therein. You shall have no rights hereunder other than the license as provided for above in Section 2. No right, license or interest to any trademark, trade name, service mark or other branding ("Marks") of WILEY or its licensors is granted hereunder, and you agree that you shall not assert any such right, license or interest with respect thereto.

- NEITHER WILEY NOR ITS LICENSORS MAKES ANY WARRANTY OR REPRESENTATION OF ANY KIND TO YOU OR ANY THIRD PARTY, EXPRESS, IMPLIED OR STATUTORY, WITH RESPECT TO THE MATERIALS OR THE ACCURACY OF ANY INFORMATION CONTAINED IN THE MATERIALS, INCLUDING, WITHOUT LIMITATION, ANY IMPLIED WARRANTY OF MERCHANTABILITY, ACCURACY, SATISFACTORY QUALITY, FITNESS FOR A PARTICULAR PURPOSE, USABILITY, INTEGRATION OR NON-INFRINGEMENT AND ALL SUCH WARRANTIES ARE HEREBY EXCLUDED BY WILEY AND ITS LICENSORS AND WAIVED BY YOU.
- WILEY shall have the right to terminate this Agreement immediately upon breach of this Agreement by you.
- You shall indemnify, defend and hold harmless WILEY, its Licensors and their respective directors, officers, agents and employees, from and against any actual or threatened claims, demands, causes of action or proceedings arising from any breach of this Agreement by you.
- IN NO EVENT SHALL WILEY OR ITS LICENSORS BE LIABLE TO YOU OR ANY OTHER PARTY OR ANY OTHER PERSON OR ENTITY FOR ANY SPECIAL, CONSEQUENTIAL, INCIDENTAL, INDIRECT, EXEMPLARY OR PUNITIVE DAMAGES, HOWEVER CAUSED, ARISING OUT OF OR IN CONNECTION WITH THE DOWNLOADING, PROVISIONING, VIEWING OR USE OF THE MATERIALS REGARDLESS OF THE FORM OF ACTION, WHETHER FOR BREACH OF CONTRACT, BREACH OF WARRANTY, TORT, NEGLIGENCE, INFRINGEMENT OR OTHERWISE (INCLUDING, WITHOUT LIMITATION, DAMAGES BASED ON LOSS OF PROFITS, DATA, FILES, USE, BUSINESS OPPORTUNITY OR CLAIMS OF THIRD PARTIES), AND WHETHER OR NOT THE PARTY HAS BEEN ADVISED OF THE POSSIBILITY OF SUCH DAMAGES. THIS LIMITATION SHALL APPLY NOTWITHSTANDING ANY FAILURE OF ESSENTIAL PURPOSE OF ANY LIMITED REMEDY PROVIDED HEREIN.
- Should any provision of this Agreement be held by a court of competent jurisdiction to be illegal, invalid, or unenforceable, that provision shall be deemed amended to achieve as nearly as possible the same economic effect as the original provision, and the legality, validity and enforceability of the remaining provisions of this Agreement shall not be affected or impaired thereby.
- The failure of either party to enforce any term or condition of this Agreement shall not constitute a waiver of either party's right to enforce each and every term and condition of this Agreement. No breach under this agreement shall be deemed waived or excused by either party unless such waiver or consent is in writing signed by the party granting such waiver or consent. The waiver by or consent of a party to a breach of any provision of this Agreement shall not operate or be construed as a waiver of or consent to any other or subsequent breach by such other party.
- This Agreement may not be assigned (including by operation of law or otherwise) by you without WILEY's prior written consent.
- Any fee required for this permission shall be non-refundable after thirty (30) days from receipt by the CCC.
- These terms and conditions together with CCC's Billing and Payment terms and conditions (which are incorporated herein) form the entire agreement between you and WILEY concerning this licensing transaction and (in the absence of fraud) supersedes all prior agreements and representations of the parties, oral or written. This Agreement may not be amended except in writing signed by both parties. This Agreement shall be binding upon and inure to the benefit of the parties' successors, legal representatives, and authorized assigns.
- In the event of any conflict between your obligations established by these terms and conditions and those established by CCC's Billing and Payment terms and conditions, these terms and conditions shall prevail.
- WILEY expressly reserves all rights not specifically granted in the combination of (i) the license details provided by you and accepted in the course of this licensing transaction, (ii) these terms and conditions and (iii) CCC's Billing and Payment terms and conditions.
- This Agreement will be void if the Type of Use, Format, Circulation, or Requestor Type was misrepresented during the licensing process.
- This Agreement shall be governed by and construed in accordance with the laws of the State of New York, USA, without regards to such state's conflict of law rules. Any legal action, suit or proceeding arising out of or relating to these Terms and Conditions or the breach thereof shall be instituted in a court of competent jurisdiction in New York County in the State of New York in the United States of America and each party hereby consents and submits to the personal jurisdiction of such court, waives any objection to venue in such court and consents to service of process by registered or certified mail, return receipt requested, at the last known address of such party.

**Other terms and conditions:**

**REPUBLICATION IN MAIN PRODUCT, PRODUCT FAMILY, COMPILATIONS OR COLLECTIVE WORKS**

Limitations on reuse of Wiley Materials:

Where the following additional rights have been granted as part of this Agreement, please note that in no instance may the total amount of Wiley Materials used in any Main Product, Compilation or Collective work comprise more than 5% (if figures/tables) or 15% (if full articles/chapters) of the Main Product, Compilation or Collective Work.

**Product Family:** main product AND any product related to the main product

Main Product and related products which are created to supplement or add value to the Main Product, and in which the overall content of the Main Product remains substantially the same with relatively minor additions or variations. Examples include: ancillaries, instructor guides, testing materials, student subject-driven resources, abridgements, and custom editions that are substantially based on a single Main Product.

**Other:** main product AND other compilations or collective works

Main Product and new collective works produced by requestor that do not consist of substantially the same material as an individual Main Product. For example, licensees may wish to acquire rights for use in the Main Product AND for use in separate projects within the same subject discipline as the Main Product. This would include, for example, custom editions or compilations which incorporate chapters from multiple underlying works within or across disciplines.

**All:** main product, AND Product Family AND Other compilations or collective works

This combines the right to republish in the following components: 1) main product, 2) products related to the main product (i.e. Product Family) and 3) other compilations/collective works.

#### **WILEY OPEN ACCESS TERMS AND CONDITIONS**

Wiley Publishes Open Access Articles in fully Open Access Journals and in Subscription journals offering Online Open. Although most of the fully Open Access journals publish open access articles under the terms of the Creative Commons Attribution (CC BY) License only, the subscription journals and a few of the Open Access Journals offer a choice of Creative Commons Licenses: Creative Commons Attribution (CC-BY) license, Creative Commons Attribution Non-Commercial (CC-BY-NC) license and Creative Commons Attribution Non-Commercial-NoDerivs (CC-BY-NC-ND) License. The license type is clearly identified on the article.

Copyright in any research article in a journal published as Open Access under a Creative Commons License is retained by the author(s). Authors grant Wiley a license to publish the article and identify itself as the original publisher. Authors also grant any third party the right to use the article freely as long as its integrity is maintained and its original authors, citation details and publisher are identified as follows: [Title of Article/Author/Journal Title and Volume/Issue. Copyright (c) [year] [copyright owner as specified in the Journal]. Links to the final article on Wiley's website are encouraged where applicable.

#### **The Creative Commons Attribution License**

The Creative Commons Attribution License (CC-BY) allows users to copy, distribute and transmit an article, adapt the article and make commercial use of the article. The CC-BY license permits commercial and non-commercial re-use of an open access article, as long as the author is properly attributed.

The Creative Commons Attribution License does not affect the moral rights of authors, including without limitation the right not to have their work subjected to derogatory treatment. It also does not affect any other rights held by authors or third parties in the article, including without limitation the rights of privacy and publicity. Use of the article must not assert or imply, whether implicitly or explicitly, any connection with, endorsement or sponsorship of such use by the author, publisher or any other party associated with the article.

For any reuse or distribution, users must include the copyright notice and make clear to others that the article is made available under a Creative Commons Attribution license, linking to the relevant Creative Commons web page.

To the fullest extent permitted by applicable law, the article is made available as is and without representation or warranties of any kind whether express, implied, statutory or otherwise and including, without limitation, warranties of title, merchantability, fitness for a particular purpose, non-infringement, absence of defects, accuracy, or the presence or absence of errors.

#### **Creative Commons Attribution Non-Commercial License**

The Creative Commons Attribution Non-Commercial (CC-BY-NC) License permits use, distribution and reproduction in any medium, provided the original work is properly cited and is not used for commercial purposes.(see below)

#### **Creative Commons Attribution-Non-Commercial-NoDerivs License**

The Creative Commons Attribution Non-Commercial-NoDerivs License (CC-BY-NC-ND) permits use, distribution and reproduction in any medium, provided the original work is properly cited, is not used for commercial purposes and no modifications or adaptations are made. (see below)

#### **Use by non-commercial users**

For non-commercial and non-promotional purposes, individual users may access, download, copy, display and redistribute to colleagues Wiley Open Access articles, as well as adapt, translate, text- and data-mine the content subject to the following conditions:

- The authors' moral rights are not compromised. These rights include the right of "paternity" (also known as "attribution" - the right for the author to be identified as such) and "integrity" (the right for the author not to have the work altered in such a way that the author's reputation or integrity may be impugned).
- Where content in the article is identified as belonging to a third party, it is the obligation of the user to ensure that any reuse complies with the copyright policies of the owner of that content.
- If article content is copied, downloaded or otherwise reused for non-commercial research and education purposes, a link to the appropriate bibliographic citation (authors, journal, article title, volume, issue, page numbers, DOI and the link to the definitive published version on Wiley Online Library) should be maintained. Copyright notices and disclaimers must not be deleted.
- Any translations, for which a prior translation agreement with Wiley has not been agreed, must prominently display the statement: "This is an unofficial translation of an article that appeared in a Wiley publication. The publisher has not endorsed this translation."

#### Use by commercial "for-profit" organisations

Use of Wiley Open Access articles for commercial, promotional, or marketing purposes requires further explicit permission from Wiley and will be subject to a fee. Commercial purposes include:

- Copying or downloading of articles, or linking to such articles for further redistribution, sale or licensing;
- Copying, downloading or posting by a site or service that incorporates advertising with such content;
- The inclusion or incorporation of article content in other works or services (other than normal quotations with an appropriate citation) that is then available for sale or licensing, for a fee (for example, a compilation produced for marketing purposes, inclusion in a sales pack)
- Use of article content (other than normal quotations with appropriate citation) by for-profit organisations for promotional purposes
- Linking to article content in e-mails redistributed for promotional, marketing or educational purposes;
- Use for the purposes of monetary reward by means of sale, resale, licence, loan, transfer or other form of commercial exploitation such as marketing products
- Print reprints of Wiley Open Access articles can be purchased from: [corporatesales@wiley.com](mailto:corporatesales@wiley.com)

Further details can be found on Wiley Online Library <http://olabout.wiley.com/WileyCDA/Section/id-410895.html>

#### Other Terms and Conditions:

None

#### STANDARD TERMS AND CONDITIONS

1. Description of Service; Defined Terms. This Republication License enables the User to obtain licenses for republication of one or more copyrighted works as described in detail on the relevant Order Confirmation (the "Work(s)"). Copyright Clearance Center, Inc. ("CCC") grants licenses through the Service on behalf of the rights holder identified on the Order Confirmation (the "Rights holder"). "Republication", as used herein, generally means the inclusion of a Work, in whole or in part, in a new work or works, also as described on the Order Confirmation. "User", as used herein, means the person or entity making such republication.

2. The terms set forth in the relevant Order Confirmation, and any terms set by the Rights holder with respect to a particular Work, govern the terms of use of Works in connection with the Service. By using the Service, the person transacting for a republication license on behalf of the User represents and warrants that he/she/it (a) has been duly authorized by the User to accept, and hereby does accept, all such terms and conditions on behalf of User, and (b) shall inform User of all such terms and conditions. In the event such person is a "freelancer" or other third party independent of User and CCC, such party shall be deemed jointly a "User" for purposes of these terms and conditions. In any event, User shall be deemed to have accepted and agreed to all such terms and conditions if User republishes the Work in any fashion.

#### 3. Scope of License; Limitations and Obligations.

3.1 All Works and all rights therein, including copyright rights, remain the sole and exclusive property of the Rights holder. The license created by the exchange of an Order Confirmation (and/or any invoice) and payment by User of the full amount set forth on that document includes only those rights expressly set forth in the Order Confirmation and in these terms and conditions, and conveys no other rights in the Work(s) to User. All rights not expressly granted are hereby reserved.

3.2 General Payment Terms: You may pay by credit card or through an account with us payable at the end of the month. If you and we agree that you may establish a standing account with CCC, then the following terms apply: Remit Payment to: Copyright Clearance Center, Dept 001, P.O. Box 843006, Boston, MA 02284-3006. Payments Due: Invoices are payable upon their delivery to you (or upon our notice to you that they are available to you for

downloading). After 30 days, outstanding amounts will be subject to a service charge of 1-1/2% per month or, if less, the maximum rate allowed by applicable law. Unless otherwise specifically set forth in the Order Confirmation or in a separate written agreement signed by CCC, invoices are due and payable on "net 30" terms. While User may exercise the rights licensed immediately upon issuance of the Order Confirmation, the license is automatically revoked and is null and void, as if it had never been issued, if complete payment for the license is not received on a timely basis either from User directly or through a payment agent, such as a credit card company.

3.3 Unless otherwise provided in the Order Confirmation, any grant of rights to User (i) is "one-time" (including the editions and product family specified in the license), (ii) is non-exclusive and non-transferable and (iii) is subject to any and all limitations and restrictions (such as, but not limited to, limitations on duration of use or circulation) included in the Order Confirmation or invoice and/or in these terms and conditions. Upon completion of the licensed use, User shall either secure a new permission for further use of the Work(s) or immediately cease any new use of the Work(s) and shall render inaccessible (such as by deleting or by removing or severing links or other locators) any further copies of the Work (except for copies printed on paper in accordance with this license and still in User's stock at the end of such period).

3.4 In the event that the material for which a republication license is sought includes third party materials (such as photographs, illustrations, graphs, inserts and similar materials) which are identified in such material as having been used by permission, User is responsible for identifying, and seeking separate licenses (under this Service or otherwise) for, any of such third party materials; without a separate license, such third party materials may not be used.

3.5 Use of proper copyright notice for a Work is required as a condition of any license granted under the Service. Unless otherwise provided in the Order Confirmation, a proper copyright notice will read substantially as follows: "Republished with permission of [Rightsholder's name], from [Work's title, author, volume, edition number and year of copyright]; permission conveyed through Copyright Clearance Center, Inc." Such notice must be provided in a reasonably legible font size and must be placed either immediately adjacent to the Work as used (for example, as part of a by-line or footnote but not as a separate electronic link) or in the place where substantially all other credits or notices for the new work containing the republished Work are located. Failure to include the required notice results in loss to the Rightsholder and CCC, and the User shall be liable to pay liquidated damages for each such failure equal to twice the use fee specified in the Order Confirmation, in addition to the use fee itself and any other fees and charges specified.

3.6 User may only make alterations to the Work if and as expressly set forth in the Order Confirmation. No Work may be used in any way that is defamatory, violates the rights of third parties (including such third parties' rights of copyright, privacy, publicity, or other tangible or intangible property), or is otherwise illegal, sexually explicit or obscene. In addition, User may not conjoin a Work with any other material that may result in damage to the reputation of the Rightsholder. User agrees to inform CCC if it becomes aware of any infringement of any rights in a Work and to cooperate with any reasonable request of CCC or the Rightsholder in connection therewith.

4. Indemnity. User hereby indemnifies and agrees to defend the Rightsholder and CCC, and their respective employees and directors, against all claims, liability, damages, costs and expenses, including legal fees and expenses, arising out of any use of a Work beyond the scope of the rights granted herein, or any use of a Work which has been altered in any unauthorized way by User, including claims of defamation or infringement of rights of copyright, publicity, privacy or other tangible or intangible property.

5. Limitation of Liability. UNDER NO CIRCUMSTANCES WILL CCC OR THE RIGHTSHOLDER BE LIABLE FOR ANY DIRECT, INDIRECT, CONSEQUENTIAL OR INCIDENTAL DAMAGES (INCLUDING WITHOUT LIMITATION DAMAGES FOR LOSS OF BUSINESS PROFITS OR INFORMATION, OR FOR BUSINESS INTERRUPTION) ARISING OUT OF THE USE OR INABILITY TO USE A WORK, EVEN IF ONE OF THEM HAS BEEN ADVISED OF THE POSSIBILITY OF SUCH DAMAGES. In any event, the total liability of the Rightsholder and CCC (including their respective employees and directors) shall not exceed the total amount actually paid by User for this license. User assumes full liability for the actions and omissions of its principals, employees, agents, affiliates, successors and assigns.

6. Limited Warranties. THE WORK(S) AND RIGHT(S) ARE PROVIDED "AS IS". CCC HAS THE RIGHT TO GRANT TO USER THE RIGHTS GRANTED IN THE ORDER CONFIRMATION DOCUMENT. CCC AND THE RIGHTSHOLDER DISCLAIM ALL OTHER WARRANTIES RELATING TO THE WORK(S) AND RIGHT(S), EITHER EXPRESS OR IMPLIED, INCLUDING WITHOUT LIMITATION IMPLIED WARRANTIES OF MERCHANTABILITY OR FITNESS FOR A PARTICULAR PURPOSE. ADDITIONAL RIGHTS MAY BE REQUIRED TO USE ILLUSTRATIONS, GRAPHS, PHOTOGRAPHS, ABSTRACTS, INSERTS OR OTHER PORTIONS OF THE WORK (AS OPPOSED TO THE ENTIRE WORK) IN A MANNER CONTEMPLATED BY USER; USER UNDERSTANDS AND AGREES THAT NEITHER CCC NOR THE RIGHTSHOLDER MAY HAVE SUCH ADDITIONAL RIGHTS TO GRANT.

7. Effect of Breach. Any failure by User to pay any amount when due, or any use by User of a Work beyond the scope of the license set forth in the Order Confirmation and/or these terms and conditions, shall be a material breach of the license created by the Order Confirmation and these terms and conditions. Any breach not cured within 30 days of written notice thereof shall result in immediate termination of such license without further notice. Any unauthorized (but licensable) use of a Work that is terminated immediately upon notice thereof may be liquidated by payment of the Rightsholder's ordinary license price therefor; any unauthorized (and unlicensable) use that is not terminated immediately for any reason (including, for example, because materials containing the Work cannot reasonably be recalled) will be subject to all remedies available at law or in equity, but in no event to a payment of less than three times the Rightsholder's ordinary license price for the most closely analogous licensable use plus Rightsholder's and/or CCC's costs and expenses incurred in collecting such payment.

#### 8. Miscellaneous.

8.1 User acknowledges that CCC may, from time to time, make changes or additions to the Service or to these terms



and conditions, and CCC reserves the right to send notice to the User by electronic mail or otherwise for the purposes of notifying User of such changes or additions; provided that any such changes or additions shall not apply to permissions already secured and paid for.

8.2 Use of User-related information collected through the Service is governed by CCC's privacy policy, available online here: <http://www.copyright.com/content/cc3/en/tools/footer/privacypolicy.html>.

8.3 The licensing transaction described in the Order Confirmation is personal to User. Therefore, User may not assign or transfer to any other person (whether a natural person or an organization of any kind) the license created by the Order Confirmation and these terms and conditions or any rights granted hereunder; provided, however, that User may assign such license in its entirety on written notice to CCC in the event of a transfer of all or substantially all of User's rights in the new material which includes the Work(s) licensed under this Service.

8.4 No amendment or waiver of any terms is binding unless set forth in writing and signed by the parties. The Rightsholder and CCC hereby object to any terms contained in any writing prepared by the User or its principals, employees, agents or affiliates and purporting to govern or otherwise relate to the licensing transaction described in the Order Confirmation, which terms are in any way inconsistent with any terms set forth in the Order Confirmation and/or in these terms and conditions or CCC's standard operating procedures, whether such writing is prepared prior to, simultaneously with or subsequent to the Order Confirmation, and whether such writing appears on a copy of the Order Confirmation or in a separate instrument.

8.5 The licensing transaction described in the Order Confirmation document shall be governed by and construed under the law of the State of New York, USA, without regard to the principles thereof of conflicts of law. Any case, controversy, suit, action, or proceeding arising out of, in connection with, or related to such licensing transaction shall be brought, at CCC's sole discretion, in any federal or state court located in the County of New York, State of New York, USA, or in any federal or state court whose geographical jurisdiction covers the location of the Rightsholder set forth in the Order Confirmation. The parties expressly submit to the personal jurisdiction and venue of each such federal or state court. If you have any comments or questions about the Service or Copyright Clearance Center, please contact us at 978-750-8400 or send an e-mail to [info@copyright.com](mailto:info@copyright.com).

v 1.1

**Cell medicine : Part B of Cell Transplantation**

**Permission type:** Republish or display content

**Type of use:** Republish in a thesis/dissertation

**TERMS AND CONDITIONS**

**The following terms are individual to this publisher:**

None

**Other Terms and Conditions:**

None

**STANDARD TERMS AND CONDITIONS**

1. Description of Service; Defined Terms. This Republication License enables the User to obtain licenses for republication of one or more copyrighted works as described in detail on the relevant Order Confirmation (the "Work(s)"). Copyright Clearance Center, Inc. ("CCC") grants licenses through the Service on behalf of the rightsholder identified on the Order Confirmation (the "Rightsholder"). "Republishing", as used herein, generally means the inclusion of a Work, in whole or in part, in a new work or works, also as described on the Order Confirmation. "User", as used herein, means the person or entity making such republication.

2. The terms set forth in the relevant Order Confirmation, and any terms set by the Rightsholder with respect to a particular Work, govern the terms of use of Works in connection with the Service. By using the Service, the person transacting for a republication license on behalf of the User represents and warrants that he/she/it (a) has been duly authorized by the User to accept, and hereby does accept, all such terms and conditions on behalf of User, and (b) shall inform User of all such terms and conditions. In the event such person is a "freelancer" or other third party independent of User and CCC, such party shall be deemed jointly a "User" for purposes of these terms and conditions. In any event, User shall be deemed to have accepted and agreed to all such terms and conditions if User republishes the Work in any fashion.

**3. Scope of License; Limitations and Obligations.**

3.1 All Works and all rights therein, including copyright rights, remain the sole and exclusive property of the Rightsholder. The license created by the exchange of an Order Confirmation (and/or any invoice) and payment by User of the full amount set forth on that document includes only those rights expressly set forth in the Order Confirmation and in these terms and conditions, and conveys no other rights in the Work(s) to User. All rights not expressly granted are hereby reserved.

3.2 General Payment Terms: You may pay by credit card or through an account with us payable at the end of the

month. If you and we agree that you may establish a standing account with CCC, then the following terms apply: Remit Payment to: Copyright Clearance Center, Dept 001, P.O. Box 843006, Boston, MA 02284-3006. Payments Due: Invoices are payable upon their delivery to you (or upon our notice to you that they are available to you for downloading). After 30 days, outstanding amounts will be subject to a service charge of 1-1/2% per month or, if less, the maximum rate allowed by applicable law. Unless otherwise specifically set forth in the Order Confirmation or in a separate written agreement signed by CCC, invoices are due and payable on "net 30" terms. While User may exercise the rights licensed immediately upon issuance of the Order Confirmation, the license is automatically revoked and is null and void, as if it had never been issued, if complete payment for the license is not received on a timely basis either from User directly or through a payment agent, such as a credit card company.

3.3 Unless otherwise provided in the Order Confirmation, any grant of rights to User (i) is "one-time" (including the editions and product family specified in the license), (ii) is non-exclusive and non-transferable and (iii) is subject to any and all limitations and restrictions (such as, but not limited to, limitations on duration of use or circulation) included in the Order Confirmation or invoice and/or in these terms and conditions. Upon completion of the licensed use, User shall either secure a new permission for further use of the Work(s) or immediately cease any new use of the Work(s) and shall render inaccessible (such as by deleting or by removing or severing links or other locators) any further copies of the Work (except for copies printed on paper in accordance with this license and still in User's stock at the end of such period).

3.4 In the event that the material for which a republication license is sought includes third party materials (such as photographs, illustrations, graphs, inserts and similar materials) which are identified in such material as having been used by permission, User is responsible for identifying, and seeking separate licenses (under this Service or otherwise) for, any of such third party materials; without a separate license, such third party materials may not be used.

3.5 Use of proper copyright notice for a Work is required as a condition of any license granted under the Service. Unless otherwise provided in the Order Confirmation, a proper copyright notice will read substantially as follows: "Republished with permission of [Rightsholder's name], from [Work's title, author, volume, edition number and year of copyright]; permission conveyed through Copyright Clearance Center, Inc." Such notice must be provided in a reasonably legible font size and must be placed either immediately adjacent to the Work as used (for example, as part of a by-line or footnote but not as a separate electronic link) or in the place where substantially all other credits or notices for the new work containing the republished Work are located. Failure to include the required notice results in loss to the Rightsholder and CCC, and the User shall be liable to pay liquidated damages for each such failure equal to twice the use fee specified in the Order Confirmation, in addition to the use fee itself and any other fees and charges specified.

3.6 User may only make alterations to the Work if and as expressly set forth in the Order Confirmation. No Work may be used in any way that is defamatory, violates the rights of third parties (including such third parties' rights of copyright, privacy, publicity, or other tangible or intangible property), or is otherwise illegal, sexually explicit or obscene. In addition, User may not conjoin a Work with any other material that may result in damage to the reputation of the Rightsholder. User agrees to inform CCC if it becomes aware of any infringement of any rights in a Work and to cooperate with any reasonable request of CCC or the Rightsholder in connection therewith.

4. Indemnity. User hereby indemnifies and agrees to defend the Rightsholder and CCC, and their respective employees and directors, against all claims, liability, damages, costs and expenses, including legal fees and expenses, arising out of any use of a Work beyond the scope of the rights granted herein, or any use of a Work which has been altered in any unauthorized way by User, including claims of defamation or infringement of rights of copyright, publicity, privacy or other tangible or intangible property.

5. Limitation of Liability. UNDER NO CIRCUMSTANCES WILL CCC OR THE RIGHTSHOLDER BE LIABLE FOR ANY DIRECT, INDIRECT, CONSEQUENTIAL OR INCIDENTAL DAMAGES (INCLUDING WITHOUT LIMITATION DAMAGES FOR LOSS OF BUSINESS PROFITS OR INFORMATION, OR FOR BUSINESS INTERRUPTION) ARISING OUT OF THE USE OR INABILITY TO USE A WORK, EVEN IF ONE OF THEM HAS BEEN ADVISED OF THE POSSIBILITY OF SUCH DAMAGES. In any event, the total liability of the Rightsholder and CCC (including their respective employees and directors) shall not exceed the total amount actually paid by User for this license. User assumes full liability for the actions and omissions of its principals, employees, agents, affiliates, successors and assigns.

6. Limited Warranties. THE WORK(S) AND RIGHT(S) ARE PROVIDED "AS IS". CCC HAS THE RIGHT TO GRANT TO USER THE RIGHTS GRANTED IN THE ORDER CONFIRMATION DOCUMENT. CCC AND THE RIGHTSHOLDER DISCLAIM ALL OTHER WARRANTIES RELATING TO THE WORK(S) AND RIGHT(S), EITHER EXPRESS OR IMPLIED, INCLUDING WITHOUT LIMITATION IMPLIED WARRANTIES OF MERCHANTABILITY OR FITNESS FOR A PARTICULAR PURPOSE. ADDITIONAL RIGHTS MAY BE REQUIRED TO USE ILLUSTRATIONS, GRAPHS, PHOTOGRAPHS, ABSTRACTS, INSERTS OR OTHER PORTIONS OF THE WORK (AS OPPOSED TO THE ENTIRE WORK) IN A MANNER CONTEMPLATED BY USER; USER UNDERSTANDS AND AGREES THAT NEITHER CCC NOR THE RIGHTSHOLDER MAY HAVE SUCH ADDITIONAL RIGHTS TO GRANT.

7. Effect of Breach. Any failure by User to pay any amount when due, or any use by User of a Work beyond the scope of the license set forth in the Order Confirmation and/or these terms and conditions, shall be a material breach of the license created by the Order Confirmation and these terms and conditions. Any breach not cured within 30 days of written notice thereof shall result in immediate termination of such license without further notice. Any unauthorized (but licensable) use of a Work that is terminated immediately upon notice thereof may be liquidated by payment of the Rightsholder's ordinary license price therefor; any unauthorized (and unlicensable) use that is not terminated immediately for any reason (including, for example, because materials containing the Work cannot reasonably be recalled) will be subject to all remedies available at law or in equity, but in no event to a payment of less than three times the Rightsholder's ordinary license price for the most closely analogous licensable use plus Rightsholder's and/or CCC's costs and expenses incurred in collecting such payment.

**8. Miscellaneous.**

8.1 User acknowledges that CCC may, from time to time, make changes or additions to the Service or to these terms and conditions, and CCC reserves the right to send notice to the User by electronic mail or otherwise for the purposes of notifying User of such changes or additions; provided that any such changes or additions shall not apply to permissions already secured and paid for.

8.2 Use of User-related information collected through the Service is governed by CCC's privacy policy, available online here: <http://www.copyright.com/content/cc3/en/tools/footer/privacypolicy.html>.

8.3 The licensing transaction described in the Order Confirmation is personal to User. Therefore, User may not assign or transfer to any other person (whether a natural person or an organization of any kind) the license created by the Order Confirmation and these terms and conditions or any rights granted hereunder; provided, however, that User may assign such license in its entirety on written notice to CCC in the event of a transfer of all or substantially all of User's rights in the new material which includes the Work(s) licensed under this Service.

8.4 No amendment or waiver of any terms is binding unless set forth in writing and signed by the parties. The Rightsholder and CCC hereby object to any terms contained in any writing prepared by the User or its principals, employees, agents or affiliates and purporting to govern or otherwise relate to the licensing transaction described in the Order Confirmation, which terms are in any way inconsistent with any terms set forth in the Order Confirmation and/or in these terms and conditions or CCC's standard operating procedures, whether such writing is prepared prior to, simultaneously with or subsequent to the Order Confirmation, and whether such writing appears on a copy of the Order Confirmation or in a separate instrument.

8.5 The licensing transaction described in the Order Confirmation document shall be governed by and construed under the law of the State of New York, USA, without regard to the principles thereof of conflicts of law. Any case, controversy, suit, action, or proceeding arising out of, in connection with, or related to such licensing transaction shall be brought, at CCC's sole discretion, in any federal or state court located in the County of New York, State of New York, USA, or in any federal or state court whose geographical jurisdiction covers the location of the Rightsholder set forth in the Order Confirmation. The parties expressly submit to the personal jurisdiction and venue of each such federal or state court. If you have any comments or questions about the Service or Copyright Clearance Center, please contact us at 978-750-8400 or send an e-mail to [info@copyright.com](mailto:info@copyright.com).

v 1.1

**Transplantation**

**Permission type:** Republish or display content

**Type of use:** Thesis/Dissertation

**TERMS AND CONDITIONS**

**The following terms are individual to this publisher:**

None

**Other Terms and Conditions:**

None

**STANDARD TERMS AND CONDITIONS**

1. Description of Service; Defined Terms. This Republication License enables the User to obtain licenses for republication of one or more copyrighted works as described in detail on the relevant Order Confirmation (the "Work(s)"). Copyright Clearance Center, Inc. ("CCC") grants licenses through the Service on behalf of the rightsholder identified on the Order Confirmation (the "Rightsholder"). "Republication", as used herein, generally means the inclusion of a Work, in whole or in part, in a new work or works, also as described on the Order Confirmation. "User", as used herein, means the person or entity making such republication.

2. The terms set forth in the relevant Order Confirmation, and any terms set by the Rightsholder with respect to a particular Work, govern the terms of use of Works in connection with the Service. By using the Service, the person transacting for a republication license on behalf of the User represents and warrants that he/she/it (a) has been duly authorized by the User to accept, and hereby does accept, all such terms and conditions on behalf of User, and (b) shall inform User of all such terms and conditions. In the event such person is a "freelancer" or other third party independent of User and CCC, such party shall be deemed jointly a "User" for purposes of these terms and conditions. In any event, User shall be deemed to have accepted and agreed to all such terms and conditions if User republishes the Work in any fashion.

**3. Scope of License; Limitations and Obligations.**

3.1 All Works and all rights therein, including copyright rights, remain the sole and exclusive property of the Rightsholder. The license created by the exchange of an Order Confirmation (and/or any invoice) and payment by User of the full amount set forth on that document includes only those rights expressly set forth in the Order Confirmation and in these terms and conditions, and conveys no other rights in the Work(s) to User. All rights not

expressly granted are hereby reserved.

3.2 General Payment Terms: You may pay by credit card or through an account with us payable at the end of the month. If you and we agree that you may establish a standing account with CCC, then the following terms apply: Remit Payment to: Copyright Clearance Center, Dept 001, P.O. Box 843006, Boston, MA 02284-3006. Payments Due: Invoices are payable upon their delivery to you (or upon our notice to you that they are available to you for downloading). After 30 days, outstanding amounts will be subject to a service charge of 1-1/2% per month or, if less, the maximum rate allowed by applicable law. Unless otherwise specifically set forth in the Order Confirmation or in a separate written agreement signed by CCC, invoices are due and payable on "net 30" terms. While User may exercise the rights licensed immediately upon issuance of the Order Confirmation, the license is automatically revoked and is null and void, as if it had never been issued, if complete payment for the license is not received on a timely basis either from User directly or through a payment agent, such as a credit card company.

3.3 Unless otherwise provided in the Order Confirmation, any grant of rights to User (i) is "one-time" (including the editions and product family specified in the license), (ii) is non-exclusive and non-transferable and (iii) is subject to any and all limitations and restrictions (such as, but not limited to, limitations on duration of use or circulation) included in the Order Confirmation or invoice and/or in these terms and conditions. Upon completion of the licensed use, User shall either secure a new permission for further use of the Work(s) or immediately cease any new use of the Work(s) and shall render inaccessible (such as by deleting or by removing or severing links or other locators) any further copies of the Work (except for copies printed on paper in accordance with this license and still in User's stock at the end of such period).

3.4 In the event that the material for which a republication license is sought includes third party materials (such as photographs, illustrations, graphs, inserts and similar materials) which are identified in such material as having been used by permission, User is responsible for identifying, and seeking separate licenses (under this Service or otherwise) for, any of such third party materials; without a separate license, such third party materials may not be used.

3.5 Use of proper copyright notice for a Work is required as a condition of any license granted under the Service. Unless otherwise provided in the Order Confirmation, a proper copyright notice will read substantially as follows: "Republished with permission of [Rightsholder's name], from [Work's title, author, volume, edition number and year of copyright]; permission conveyed through Copyright Clearance Center, Inc." Such notice must be provided in a reasonably legible font size and must be placed either immediately adjacent to the Work as used (for example, as part of a by-line or footnote but not as a separate electronic link) or in the place where substantially all other credits or notices for the new work containing the republished Work are located. Failure to include the required notice results in loss to the Rightsholder and CCC, and the User shall be liable to pay liquidated damages for each such failure equal to twice the use fee specified in the Order Confirmation, in addition to the use fee itself and any other fees and charges specified.

3.6 User may only make alterations to the Work if and as expressly set forth in the Order Confirmation. No Work may be used in any way that is defamatory, violates the rights of third parties (including such third parties' rights of copyright, privacy, publicity, or other tangible or intangible property), or is otherwise illegal, sexually explicit or obscene. In addition, User may not conjoin a Work with any other material that may result in damage to the reputation of the Rightsholder. User agrees to inform CCC if it becomes aware of any infringement of any rights in a Work and to cooperate with any reasonable request of CCC or the Rightsholder in connection therewith.

4. Indemnity. User hereby indemnifies and agrees to defend the Rightsholder and CCC, and their respective employees and directors, against all claims, liability, damages, costs and expenses, including legal fees and expenses, arising out of any use of a Work beyond the scope of the rights granted herein, or any use of a Work which has been altered in any unauthorized way by User, including claims of defamation or infringement of rights of copyright, publicity, privacy or other tangible or intangible property.

5. Limitation of Liability. UNDER NO CIRCUMSTANCES WILL CCC OR THE RIGHTSHOLDER BE LIABLE FOR ANY DIRECT, INDIRECT, CONSEQUENTIAL OR INCIDENTAL DAMAGES (INCLUDING WITHOUT LIMITATION DAMAGES FOR LOSS OF BUSINESS PROFITS OR INFORMATION, OR FOR BUSINESS INTERRUPTION) ARISING OUT OF THE USE OR INABILITY TO USE A WORK, EVEN IF ONE OF THEM HAS BEEN ADVISED OF THE POSSIBILITY OF SUCH DAMAGES. In any event, the total liability of the Rightsholder and CCC (including their respective employees and directors) shall not exceed the total amount actually paid by User for this license. User assumes full liability for the actions and omissions of its principals, employees, agents, affiliates, successors and assigns.

6. Limited Warranties. THE WORK(S) AND RIGHT(S) ARE PROVIDED "AS IS". CCC HAS THE RIGHT TO GRANT TO USER THE RIGHTS GRANTED IN THE ORDER CONFIRMATION DOCUMENT. CCC AND THE RIGHTSHOLDER DISCLAIM ALL OTHER WARRANTIES RELATING TO THE WORK(S) AND RIGHT(S), EITHER EXPRESS OR IMPLIED, INCLUDING WITHOUT LIMITATION IMPLIED WARRANTIES OF MERCHANTABILITY OR FITNESS FOR A PARTICULAR PURPOSE. ADDITIONAL RIGHTS MAY BE REQUIRED TO USE ILLUSTRATIONS, GRAPHS, PHOTOGRAPHS, ABSTRACTS, INSERTS OR OTHER PORTIONS OF THE WORK (AS OPPOSED TO THE ENTIRE WORK) IN A MANNER CONTEMPLATED BY USER; USER UNDERSTANDS AND AGREES THAT NEITHER CCC NOR THE RIGHTSHOLDER MAY HAVE SUCH ADDITIONAL RIGHTS TO GRANT.

7. Effect of Breach. Any failure by User to pay any amount when due, or any use by User of a Work beyond the scope of the license set forth in the Order Confirmation and/or these terms and conditions, shall be a material breach of the license created by the Order Confirmation and these terms and conditions. Any breach not cured within 30 days of written notice thereof shall result in immediate termination of such license without further notice. Any unauthorized (but licensable) use of a Work that is terminated immediately upon notice thereof may be liquidated by payment of the Rightsholder's ordinary license price therefor; any unauthorized (and unlicensable) use that is not terminated immediately for any reason (including, for example, because materials containing the Work cannot reasonably be recalled) will be subject to all remedies available at law or in equity, but in no event to a payment of

less than three times the Rightsholder's ordinary license price for the most closely analogous licensable use plus Rightsholder's and/or CCC's costs and expenses incurred in collecting such payment.

**8. Miscellaneous.**

8.1 User acknowledges that CCC may, from time to time, make changes or additions to the Service or to these terms and conditions, and CCC reserves the right to send notice to the User by electronic mail or otherwise for the purposes of notifying User of such changes or additions; provided that any such changes or additions shall not apply to permissions already secured and paid for.

8.2 Use of User-related information collected through the Service is governed by CCC's privacy policy, available online here: <http://www.copyright.com/content/cc3/en/tools/footer/privacypolicy.html>.

8.3 The licensing transaction described in the Order Confirmation is personal to User. Therefore, User may not assign or transfer to any other person (whether a natural person or an organization of any kind) the license created by the Order Confirmation and these terms and conditions or any rights granted hereunder; provided, however, that User may assign such license in its entirety on written notice to CCC in the event of a transfer of all or substantially all of User's rights in the new material which includes the Work(s) licensed under this Service.

8.4 No amendment or waiver of any terms is binding unless set forth in writing and signed by the parties. The Rightsholder and CCC hereby object to any terms contained in any writing prepared by the User or its principals, employees, agents or affiliates and purporting to govern or otherwise relate to the licensing transaction described in the Order Confirmation, which terms are in any way inconsistent with any terms set forth in the Order Confirmation and/or in these terms and conditions or CCC's standard operating procedures, whether such writing is prepared prior to, simultaneously with or subsequent to the Order Confirmation, and whether such writing appears on a copy of the Order Confirmation or in a separate instrument.

8.5 The licensing transaction described in the Order Confirmation document shall be governed by and construed under the law of the State of New York, USA, without regard to the principles thereof of conflicts of law. Any case, controversy, suit, action, or proceeding arising out of, in connection with, or related to such licensing transaction shall be brought, at CCC's sole discretion, in any federal or state court located in the County of New York, State of New York, USA, or in any federal or state court whose geographical jurisdiction covers the location of the Rightsholder set forth in the Order Confirmation. The parties expressly submit to the personal jurisdiction and venue of each such federal or state court. If you have any comments or questions about the Service or Copyright Clearance Center, please contact us at 978-750-8400 or send an e-mail to [info@copyright.com](mailto:info@copyright.com).

v 1.1

Close

**Confirmation Number: 11340305**

**Citation Information**

**Order Detail ID:** 66740419

**Transplantation proceedings by Transplantation Society Reproduced with permission of ELSEVIER INC. in the format Thesis/Dissertation via Copyright Clearance Center.**

---

**Order Detail ID:** 66740423

**Transplantation proceedings by TRANSPLANTATION SOCIETY ; INTERNATIONAL SYMPOSIUM ON ORGAN PRESERVATION Reproduced with permission of ELSEVIER INC. in the format Thesis/Dissertation via Copyright Clearance Center.**

---

**Order Detail ID:** 66740431

**Transplantation proceedings by Transplantation Society Reproduced with permission of ELSEVIER INC. in the format Thesis/Dissertation via Copyright Clearance Center.**

---

**Order Detail ID:** 66740445

**Xenotransplantation by International Xenotransplantation Association Reproduced with permission of BLACKWELL PUBLISHING in the format Republish in a thesis/dissertation via Copyright Clearance Center.**

---

**Order Detail ID:** 66740464

**Xenotransplantation by International Xenotransplantation Association Reproduced with permission of BLACKWELL PUBLISHING in the format Republish in a thesis/dissertation via Copyright Clearance Center.**

---

**Order Detail ID:** 66740482

**Cell medicine : Part B of Cell Transplantation by Cognizant Communication Corp. Reproduced with permission of Cognizant Communication Corp in the format Republish in a thesis/dissertation via Copyright Clearance Center.**

---

**Order Detail ID:** 66740494

**Transplantation by Transplantation Society Reproduced with permission of LIPPINCOTT WILLIAMS & WILKINS, INC. in the format Thesis/Dissertation via Copyright Clearance Center.**

---

Close

**Cognizant Communication Corporation LICENSE  
TERMS AND CONDITIONS**

Apr 20, 2015

This is a License Agreement between Bradley P Weegman ("You") and Cognizant Communication Corporation ("Cognizant Communication Corporation") provided by Copyright Clearance Center ("CCC"). The license consists of your order details, the terms and conditions provided by Cognizant Communication Corporation, and the payment terms and conditions.

**All payments must be made in full to CCC. For payment instructions, please see information listed at the bottom of this form.**

License Number	3610791277233
License date	Apr 16, 2015
Licensed content publisher	Cognizant Communication Corporation
Licensed content title	Cell medicine : Part B of Cell Transplantation
Licensed content date	Jan 1, 2010
Type of Use	Thesis/Dissertation
Requestor type	Author of requested content
Format	Print, Electronic
Portion	chapter/article
Title or numeric reference of the portion(s)	Hypothermic Perfusion Preservation of Pancreas for Islet Grafts: Validation Using a Split Lobe Porcine Model
Title of the article or chapter the portion is from	N/A
Editor of portion(s)	N/A
Author of portion(s)	Weegman et al.
Volume of serial or monograph.	2
Issue, if republishing an article from a serial	3
Page range of the portion	None
Publication date of portion	2012 January
Rights for	Main product
Duration of use	Life of current edition
Creation of copies for the disabled	no
With minor editing privileges	yes
For distribution to	Worldwide
In the following language(s)	Original language of publication

With incidental promotional use	no
The lifetime unit quantity of new product	Up to 499
Made available in the following markets	Open Access
Specified additional information	Permission to use this material in Ph.D. Thesis
The requesting person/organization is:	Bradley P Weegman
Order reference number	24083059
Author/Editor	Bradley P Weegman
The standard identifier	N/A
The proposed price	0
Title	Monitoring and improving oxygenation for the preservation and viability assessment of cells, organs, and tissue engineered grafts
Publisher	University of Minnesota
Expected publication date	Jul 2015
Estimated size (pages)	300
Total (may include CCC user fee)	0.00 USD
Terms and Conditions	

## TERMS AND CONDITIONS

**The following terms are individual to this publisher:**

None

### Other Terms and Conditions:

We can grant permission for one-time use of the requested information. Please note that proper reference to the original source of publication is required. This should include listing of the DOI (if any) and publisher reference in addition to volume number and page location. The article(s) and/or figure(s) cannot be used for resale.

## STANDARD TERMS AND CONDITIONS

1. Description of Service; Defined Terms. This Republication License enables the User to obtain licenses for republication of one or more copyrighted works as described in detail on the relevant Order Confirmation (the "Work(s)"). Copyright Clearance Center, Inc. ("CCC") grants licenses through the Service on behalf of the rightsholder identified



on the Order Confirmation (the “Rightsholder”). “Republication”, as used herein, generally means the inclusion of a Work, in whole or in part, in a new work or works, also as described on the Order Confirmation. “User”, as used herein, means the person or entity making such republication.

2. The terms set forth in the relevant Order Confirmation, and any terms set by the Rightsholder with respect to a particular Work, govern the terms of use of Works in connection with the Service. By using the Service, the person transacting for a republication license on behalf of the User represents and warrants that he/she/it (a) has been duly authorized by the User to accept, and hereby does accept, all such terms and conditions on behalf of User, and (b) shall inform User of all such terms and conditions. In the event such person is a “freelancer” or other third party independent of User and CCC, such party shall be deemed jointly a “User” for purposes of these terms and conditions. In any event, User shall be deemed to have accepted and agreed to all such terms and conditions if User republishes the Work in any fashion.

### **3. Scope of License; Limitations and Obligations.**

3.1 All Works and all rights therein, including copyright rights, remain the sole and exclusive property of the Rightsholder. The license created by the exchange of an Order Confirmation (and/or any invoice) and payment by User of the full amount set forth on that document includes only those rights expressly set forth in the Order Confirmation and in these terms and conditions, and conveys no other rights in the Work(s) to User. All rights not expressly granted are hereby reserved.

3.2 General Payment Terms: You may pay by credit card or through an account with us payable at the end of the month. If you and we agree that you may establish a standing account with CCC, then the following terms apply: Remit Payment to: Copyright Clearance Center, Dept 001, P.O. Box 843006, Boston, MA 02284-3006. Payments Due: Invoices are payable upon their delivery to you (or upon our notice to you that they are available to you for downloading). After 30 days, outstanding amounts will be subject to a service charge of 1-1/2% per month or, if less, the maximum rate allowed by applicable law. Unless otherwise specifically set forth in the Order Confirmation or in a separate written agreement signed by CCC, invoices are due and payable on “net 30” terms. While User may exercise the rights licensed immediately upon issuance of the Order Confirmation, the license is automatically revoked and is null and void, as if it had never

been issued, if complete payment for the license is not received on a timely basis either from User directly or through a payment agent, such as a credit card company.

3.3 Unless otherwise provided in the Order Confirmation, any grant of rights to User (i) is “one-time” (including the editions and product family specified in the license), (ii) is non-exclusive and non-transferable and (iii) is subject to any and all limitations and restrictions (such as, but not limited to, limitations on duration of use or circulation) included in the Order Confirmation or invoice and/or in these terms and conditions. Upon completion of the licensed use, User shall either secure a new permission for further use of the Work(s) or immediately cease any new use of the Work(s) and shall render inaccessible (such as by deleting or by removing or severing links or other locators) any further copies of the Work (except for copies printed on paper in accordance with this license and still in User's stock at the end of such period).

3.4 In the event that the material for which a republication license is sought includes third party materials (such as photographs, illustrations, graphs, inserts and similar materials) which are identified in such material as having been used by permission, User is responsible for identifying, and seeking separate licenses (under this Service or otherwise) for, any of such third party materials; without a separate license, such third party materials may not be used.

3.5 Use of proper copyright notice for a Work is required as a condition of any license granted under the Service. Unless otherwise provided in the Order Confirmation, a proper copyright notice will read substantially as follows: “Republished with permission of [Rightsholder’s name], from [Work’s title, author, volume, edition number and year of copyright]; permission conveyed through Copyright Clearance Center, Inc. ” Such notice must be provided in a reasonably legible font size and must be placed either immediately adjacent to the Work as used (for example, as part of a by-line or footnote but not as a separate electronic link) or in the place where substantially all other credits or notices for the new work containing the republished Work are located. Failure to include the required notice results in loss to the Rightsholder and CCC, and the User shall be liable to pay liquidated damages for each such failure equal to twice the use fee specified in the Order Confirmation, in addition to the use fee itself and any other fees and charges specified.

3.6 User may only make alterations to the Work if and as expressly set forth in the Order Confirmation. No Work may be used in any way that is defamatory, violates the rights of third parties (including such third parties' rights of copyright, privacy, publicity, or other tangible or intangible property), or is otherwise illegal, sexually explicit or obscene. In addition, User may not conjoin a Work with any other material that may result in damage to the reputation of the Rightsholder. User agrees to inform CCC if it becomes aware of any infringement of any rights in a Work and to cooperate with any reasonable request of CCC or the Rightsholder in connection therewith.

4. Indemnity. User hereby indemnifies and agrees to defend the Rightsholder and CCC, and their respective employees and directors, against all claims, liability, damages, costs and expenses, including legal fees and expenses, arising out of any use of a Work beyond the scope of the rights granted herein, or any use of a Work which has been altered in any unauthorized way by User, including claims of defamation or infringement of rights of copyright, publicity, privacy or other tangible or intangible property.

5. Limitation of Liability. UNDER NO CIRCUMSTANCES WILL CCC OR THE RIGHTSHOLDER BE LIABLE FOR ANY DIRECT, INDIRECT, CONSEQUENTIAL OR INCIDENTAL DAMAGES (INCLUDING WITHOUT LIMITATION DAMAGES FOR LOSS OF BUSINESS PROFITS OR INFORMATION, OR FOR BUSINESS INTERRUPTION) ARISING OUT OF THE USE OR INABILITY TO USE A WORK, EVEN IF ONE OF THEM HAS BEEN ADVISED OF THE POSSIBILITY OF SUCH DAMAGES. In any event, the total liability of the Rightsholder and CCC (including their respective employees and directors) shall not exceed the total amount actually paid by User for this license. User assumes full liability for the actions and omissions of its principals, employees, agents, affiliates, successors and assigns.

6. Limited Warranties. THE WORK(S) AND RIGHT(S) ARE PROVIDED "AS IS". CCC HAS THE RIGHT TO GRANT TO USER THE RIGHTS GRANTED IN THE ORDER CONFIRMATION DOCUMENT. CCC AND THE RIGHTSHOLDER DISCLAIM ALL OTHER WARRANTIES RELATING TO THE WORK(S) AND RIGHT(S), EITHER EXPRESS OR IMPLIED, INCLUDING WITHOUT LIMITATION IMPLIED WARRANTIES OF MERCHANTABILITY OR FITNESS FOR A PARTICULAR

PURPOSE. ADDITIONAL RIGHTS MAY BE REQUIRED TO USE ILLUSTRATIONS, GRAPHS, PHOTOGRAPHS, ABSTRACTS, INSERTS OR OTHER PORTIONS OF THE WORK (AS OPPOSED TO THE ENTIRE WORK) IN A MANNER CONTEMPLATED BY USER; USER UNDERSTANDS AND AGREES THAT NEITHER CCC NOR THE RIGHTSHOLDER MAY HAVE SUCH ADDITIONAL RIGHTS TO GRANT.

7. Effect of Breach. Any failure by User to pay any amount when due, or any use by User of a Work beyond the scope of the license set forth in the Order Confirmation and/or these terms and conditions, shall be a material breach of the license created by the Order Confirmation and these terms and conditions. Any breach not cured within 30 days of written notice thereof shall result in immediate termination of such license without further notice. Any unauthorized (but licensable) use of a Work that is terminated immediately upon notice thereof may be liquidated by payment of the Rightsholder's ordinary license price therefor; any unauthorized (and unlicensable) use that is not terminated immediately for any reason (including, for example, because materials containing the Work cannot reasonably be recalled) will be subject to all remedies available at law or in equity, but in no event to a payment of less than three times the Rightsholder's ordinary license price for the most closely analogous licensable use plus Rightsholder's and/or CCC's costs and expenses incurred in collecting such payment.

#### **8. Miscellaneous.**

8.1 User acknowledges that CCC may, from time to time, make changes or additions to the Service or to these terms and conditions, and CCC reserves the right to send notice to the User by electronic mail or otherwise for the purposes of notifying User of such changes or additions; provided that any such changes or additions shall not apply to permissions already secured and paid for.

8.2 Use of User-related information collected through the Service is governed by CCC's privacy policy, available online here:  
<http://www.copyright.com/content/cc3/en/tools/footer/privacypolicy.html>.

8.3 The licensing transaction described in the Order Confirmation is personal to User. Therefore, User may not assign or transfer to any other person (whether a natural person or an organization of any kind) the license

created by the Order Confirmation and these terms and conditions or any rights granted hereunder; provided, however, that User may assign such license in its entirety on written notice to CCC in the event of a transfer of all or substantially all of User's rights in the new material which includes the Work(s) licensed under this Service.

8.4 No amendment or waiver of any terms is binding unless set forth in writing and signed by the parties. The Rightsholder and CCC hereby object to any terms contained in any writing prepared by the User or its principals, employees, agents or affiliates and purporting to govern or otherwise relate to the licensing transaction described in the Order Confirmation, which terms are in any way inconsistent with any terms set forth in the Order Confirmation and/or in these terms and conditions or CCC's standard operating procedures, whether such writing is prepared prior to, simultaneously with or subsequent to the Order Confirmation, and whether such writing appears on a copy of the Order Confirmation or in a separate instrument.

8.5 The licensing transaction described in the Order Confirmation document shall be governed by and construed under the law of the State of New York, USA, without regard to the principles thereof of conflicts of law. Any case, controversy, suit, action, or proceeding arising out of, in connection with, or related to such licensing transaction shall be brought, at CCC's sole discretion, in any federal or state court located in the County of New York, State of New York, USA, or in any federal or state court whose geographical jurisdiction covers the location of the Rightsholder set forth in the Order Confirmation. The parties expressly submit to the personal jurisdiction and venue of each such federal or state court. If you have any comments or questions about the Service or Copyright Clearance Center, please contact us at 978-750-8400 or send an e-mail to [info@copyright.com](mailto:info@copyright.com).

v 1.1

Questions? [customercare@copyright.com](mailto:customercare@copyright.com) or +1-855-239-3415 (toll free in the US) or +1-978-646-2777.

**Gratis licenses (referencing \$0 in the Total field) are free. Please retain this printable license for your reference. No payment is required.**

---

---

**Wolters Kluwer Health LICENSE  
TERMS AND CONDITIONS**

Apr 20, 2015

---

This is a License Agreement between Bradley P Weegman ("You") and Wolters Kluwer Health ("Wolters Kluwer Health") provided by Copyright Clearance Center ("CCC"). The license consists of your order details, the terms and conditions provided by Wolters Kluwer Health, and the payment terms and conditions.

**All payments must be made in full to CCC. For payment instructions, please see information listed at the bottom of this form.**

License Number	3613120168993
License date	Apr 20, 2015
Licensed content publisher	Wolters Kluwer Health
Licensed content title	Transplantation
Licensed content date	Jan 1, 1996
Type of Use	Thesis/Dissertation
Requestor type	Author of requested content
Format	Print, Electronic
Portion	chapter/article
Title or numeric reference of the portion(s)	Pig pancreas anatomy: implications for pancreas procurement, preservation, and islet isolation
Title of the article or chapter the portion is from	N/A
Editor of portion(s)	N/A
Author of portion(s)	Ferrer et al.
Volume of serial or monograph.	86
Issue, if republishing an article from a serial	11
Page range of the portion	1503-10
Publication date of portion	2008 Dec 15
Rights for	Main product
Duration of use	Life of current edition
Creation of copies for the disabled	no
With minor editing privileges	yes
For distribution to	Worldwide
In the following language(s)	Original language of publication
With incidental promotional use	no

The lifetime unit quantity of new product	Up to 499
Made available in the following markets	Open Access
Specified additional information	Seeking permission to re-use for Ph.D. Thesis
The requesting person/organization is:	Bradley P Weegman
Order reference number	19077881
Author/Editor	Bradley P Weegman
The standard identifier	N/A
The proposed price	0
Title	Monitoring and improving oxygenation for the preservation and viability assessment of cells, organs, and tissue engineered grafts
Publisher	University of Minnesota
Expected publication date	Jul 2015
Estimated size (pages)	300
Total (may include CCC user fee)	0.00 USD
Terms and Conditions	

## TERMS AND CONDITIONS

### The following terms are individual to this publisher:

None

### Other Terms and Conditions:

Wolters Kluwer Health and its affiliates take no responsibility for the accuracy of the translation from the published English original and are not liable for any errors which may occur. No drug brand/trade name or logo can be included in the same page as the material re-used.

## STANDARD TERMS AND CONDITIONS

1. Description of Service; Defined Terms. This Republication License enables the User to obtain licenses for republication of one or more copyrighted works as described in detail on the relevant Order Confirmation (the "Work(s)"). Copyright Clearance Center, Inc. ("CCC") grants licenses through the Service on behalf of the rightsholder identified on the Order Confirmation (the "Rightsholder"). "Republication", as used herein, generally means the inclusion of a Work, in whole or in part, in a

new work or works, also as described on the Order Confirmation. “User”, as used herein, means the person or entity making such republication.

2. The terms set forth in the relevant Order Confirmation, and any terms set by the Rightsholder with respect to a particular Work, govern the terms of use of Works in connection with the Service. By using the Service, the person transacting for a republication license on behalf of the User represents and warrants that he/she/it (a) has been duly authorized by the User to accept, and hereby does accept, all such terms and conditions on behalf of User, and (b) shall inform User of all such terms and conditions. In the event such person is a “freelancer” or other third party independent of User and CCC, such party shall be deemed jointly a “User” for purposes of these terms and conditions. In any event, User shall be deemed to have accepted and agreed to all such terms and conditions if User republishes the Work in any fashion.

### **3. Scope of License; Limitations and Obligations.**

3.1 All Works and all rights therein, including copyright rights, remain the sole and exclusive property of the Rightsholder. The license created by the exchange of an Order Confirmation (and/or any invoice) and payment by User of the full amount set forth on that document includes only those rights expressly set forth in the Order Confirmation and in these terms and conditions, and conveys no other rights in the Work(s) to User. All rights not expressly granted are hereby reserved.

3.2 General Payment Terms: You may pay by credit card or through an account with us payable at the end of the month. If you and we agree that you may establish a standing account with CCC, then the following terms apply: Remit Payment to: Copyright Clearance Center, Dept 001, P.O. Box 843006, Boston, MA 02284-3006. Payments Due: Invoices are payable upon their delivery to you (or upon our notice to you that they are available to you for downloading). After 30 days, outstanding amounts will be subject to a service charge of 1-1/2% per month or, if less, the maximum rate allowed by applicable law. Unless otherwise specifically set forth in the Order Confirmation or in a separate written agreement signed by CCC, invoices are due and payable on “net 30” terms. While User may exercise the rights licensed immediately upon issuance of the Order Confirmation, the license is automatically revoked and is null and void, as if it had never been issued, if complete payment for the license is not received on a timely basis either from User directly or through a payment agent, such as a credit



card company.

3.3 Unless otherwise provided in the Order Confirmation, any grant of rights to User (i) is “one-time” (including the editions and product family specified in the license), (ii) is non-exclusive and non-transferable and (iii) is subject to any and all limitations and restrictions (such as, but not limited to, limitations on duration of use or circulation) included in the Order Confirmation or invoice and/or in these terms and conditions. Upon completion of the licensed use, User shall either secure a new permission for further use of the Work(s) or immediately cease any new use of the Work(s) and shall render inaccessible (such as by deleting or by removing or severing links or other locators) any further copies of the Work (except for copies printed on paper in accordance with this license and still in User's stock at the end of such period).

3.4 In the event that the material for which a republication license is sought includes third party materials (such as photographs, illustrations, graphs, inserts and similar materials) which are identified in such material as having been used by permission, User is responsible for identifying, and seeking separate licenses (under this Service or otherwise) for, any of such third party materials; without a separate license, such third party materials may not be used.

3.5 Use of proper copyright notice for a Work is required as a condition of any license granted under the Service. Unless otherwise provided in the Order Confirmation, a proper copyright notice will read substantially as follows: “Republished with permission of [Rightsholder’s name], from [Work's title, author, volume, edition number and year of copyright]; permission conveyed through Copyright Clearance Center, Inc. ” Such notice must be provided in a reasonably legible font size and must be placed either immediately adjacent to the Work as used (for example, as part of a by-line or footnote but not as a separate electronic link) or in the place where substantially all other credits or notices for the new work containing the republished Work are located. Failure to include the required notice results in loss to the Rightsholder and CCC, and the User shall be liable to pay liquidated damages for each such failure equal to twice the use fee specified in the Order Confirmation, in addition to the use fee itself and any other fees and charges specified.

3.6 User may only make alterations to the Work if and as expressly set forth in the Order Confirmation. No Work may be used in any way that is

defamatory, violates the rights of third parties (including such third parties' rights of copyright, privacy, publicity, or other tangible or intangible property), or is otherwise illegal, sexually explicit or obscene. In addition, User may not conjoin a Work with any other material that may result in damage to the reputation of the Rightsholder. User agrees to inform CCC if it becomes aware of any infringement of any rights in a Work and to cooperate with any reasonable request of CCC or the Rightsholder in connection therewith.

4. Indemnity. User hereby indemnifies and agrees to defend the Rightsholder and CCC, and their respective employees and directors, against all claims, liability, damages, costs and expenses, including legal fees and expenses, arising out of any use of a Work beyond the scope of the rights granted herein, or any use of a Work which has been altered in any unauthorized way by User, including claims of defamation or infringement of rights of copyright, publicity, privacy or other tangible or intangible property.

5. Limitation of Liability. UNDER NO CIRCUMSTANCES WILL CCC OR THE RIGHTSHOLDER BE LIABLE FOR ANY DIRECT, INDIRECT, CONSEQUENTIAL OR INCIDENTAL DAMAGES (INCLUDING WITHOUT LIMITATION DAMAGES FOR LOSS OF BUSINESS PROFITS OR INFORMATION, OR FOR BUSINESS INTERRUPTION) ARISING OUT OF THE USE OR INABILITY TO USE A WORK, EVEN IF ONE OF THEM HAS BEEN ADVISED OF THE POSSIBILITY OF SUCH DAMAGES. In any event, the total liability of the Rightsholder and CCC (including their respective employees and directors) shall not exceed the total amount actually paid by User for this license. User assumes full liability for the actions and omissions of its principals, employees, agents, affiliates, successors and assigns.

6. Limited Warranties. THE WORK(S) AND RIGHT(S) ARE PROVIDED "AS IS". CCC HAS THE RIGHT TO GRANT TO USER THE RIGHTS GRANTED IN THE ORDER CONFIRMATION DOCUMENT. CCC AND THE RIGHTSHOLDER DISCLAIM ALL OTHER WARRANTIES RELATING TO THE WORK(S) AND RIGHT(S), EITHER EXPRESS OR IMPLIED, INCLUDING WITHOUT LIMITATION IMPLIED WARRANTIES OF MERCHANTABILITY OR FITNESS FOR A PARTICULAR PURPOSE. ADDITIONAL RIGHTS MAY BE REQUIRED TO USE ILLUSTRATIONS, GRAPHS, PHOTOGRAPHS, ABSTRACTS,

INSERTS OR OTHER PORTIONS OF THE WORK (AS OPPOSED TO THE ENTIRE WORK) IN A MANNER CONTEMPLATED BY USER; USER UNDERSTANDS AND AGREES THAT NEITHER CCC NOR THE RIGHTSHOLDER MAY HAVE SUCH ADDITIONAL RIGHTS TO GRANT.

7. Effect of Breach. Any failure by User to pay any amount when due, or any use by User of a Work beyond the scope of the license set forth in the Order Confirmation and/or these terms and conditions, shall be a material breach of the license created by the Order Confirmation and these terms and conditions. Any breach not cured within 30 days of written notice thereof shall result in immediate termination of such license without further notice. Any unauthorized (but licensable) use of a Work that is terminated immediately upon notice thereof may be liquidated by payment of the Rightsholder's ordinary license price therefor; any unauthorized (and unlicensable) use that is not terminated immediately for any reason (including, for example, because materials containing the Work cannot reasonably be recalled) will be subject to all remedies available at law or in equity, but in no event to a payment of less than three times the Rightsholder's ordinary license price for the most closely analogous licensable use plus Rightsholder's and/or CCC's costs and expenses incurred in collecting such payment.

#### **8. Miscellaneous.**

8.1 User acknowledges that CCC may, from time to time, make changes or additions to the Service or to these terms and conditions, and CCC reserves the right to send notice to the User by electronic mail or otherwise for the purposes of notifying User of such changes or additions; provided that any such changes or additions shall not apply to permissions already secured and paid for.

8.2 Use of User-related information collected through the Service is governed by CCC's privacy policy, available online here:  
<http://www.copyright.com/content/cc3/en/tools/footer/privacypolicy.html>.

8.3 The licensing transaction described in the Order Confirmation is personal to User. Therefore, User may not assign or transfer to any other person (whether a natural person or an organization of any kind) the license created by the Order Confirmation and these terms and conditions or any rights granted hereunder; provided, however, that User may assign such

license in its entirety on written notice to CCC in the event of a transfer of all or substantially all of User's rights in the new material which includes the Work(s) licensed under this Service.

8.4 No amendment or waiver of any terms is binding unless set forth in writing and signed by the parties. The Rightsholder and CCC hereby object to any terms contained in any writing prepared by the User or its principals, employees, agents or affiliates and purporting to govern or otherwise relate to the licensing transaction described in the Order Confirmation, which terms are in any way inconsistent with any terms set forth in the Order Confirmation and/or in these terms and conditions or CCC's standard operating procedures, whether such writing is prepared prior to, simultaneously with or subsequent to the Order Confirmation, and whether such writing appears on a copy of the Order Confirmation or in a separate instrument.

8.5 The licensing transaction described in the Order Confirmation document shall be governed by and construed under the law of the State of New York, USA, without regard to the principles thereof of conflicts of law. Any case, controversy, suit, action, or proceeding arising out of, in connection with, or related to such licensing transaction shall be brought, at CCC's sole discretion, in any federal or state court located in the County of New York, State of New York, USA, or in any federal or state court whose geographical jurisdiction covers the location of the Rightsholder set forth in the Order Confirmation. The parties expressly submit to the personal jurisdiction and venue of each such federal or state court. If you have any comments or questions about the Service or Copyright Clearance Center, please contact us at 978-750-8400 or send an e-mail to [info@copyright.com](mailto:info@copyright.com).

v 1.1

Questions? [customercare@copyright.com](mailto:customercare@copyright.com) or +1-855-239-3415 (toll free in the US) or +1-978-646-2777.

**Gratis licenses (referencing \$0 in the Total field) are free. Please retain this printable license for your reference. No payment is required.**

---

---

## *Appendix G.2: Referenced Theses Permissions*

University of Minnesota Mail - How's it going

<https://mail.google.com/mail/u/0/?ui=2&ik=31a82270ad&view=pt&q=fr..>



Bradley Weegman <weeg0011@umn.edu>

---

### **How's it going**

---

**Scott, William Earl** <William.Scott@nuth.nhs.uk>

Thu, Sep 24, 2015 at 4:46  
AM

To: Bradley Weegman <weeg0011@umn.edu>

Dear Brad

I would be happy for you to duplicate portions of my dissertation in your dissertation. Your contributions helped to achieve the goals of this work and I wish you the best of luck.

Sincerely

William E Scott III PhD

## Appendix G.3: Figures Reproduced with Permission

University of Minnesota Mail - Fwd: Permission to use engineering schem... <https://mail.google.com/mail/u/0/?ui=2&ik=31a82270ad&view=pt&search...>



Bradley Weegman <weeg0011@umn.edu>

---

### Fwd: Permission to use engineering schematic - Theracyte modification

---

**Melanie Graham** <graha066@umn.edu>

Tue, May 5, 2015 at 5:06 PM

To: Bradley Weegman <weeg0011@umn.edu>

Brad,  
Permission to use the figure, in writing, plus the attached schematic.  
Enjoy!  
Mel

Begin forwarded message:

---

**From:** Natan Pheil <[npheil@norfolkmedical.com](mailto:npheil@norfolkmedical.com)>  
**Date:** May 5, 2015 at 4:51:22 PM CDT  
**To:** Melanie Graham <[graha066@umn.edu](mailto:graha066@umn.edu)>, Norfolk Medical <[mjdalton@norfolkmedical.com](mailto:mjdalton@norfolkmedical.com)>  
**Subject: Re: Permission to use engineering schematic - Theracyte modification**

Hi Mel,

Just so I'm sure we're talking about the same thing, this is the device, correct?

If so, yes, we give permission for Bradley to use this schematic in his thesis.

Best Regards,  
Natan



Bradley Weegman <weeg0011@umn.edu>

---

## Technical Drawings & More

---

**Mike Loughnane** <mloughnane@instechlabs.com> Mon, May 4, 2015 at 2:01 PM  
To: Bradley Weegman <weeg0011@umn.edu>  
Cc: Paul Loughnane <ploughnane@instechlabs.com>

Brad,

Take a look at the attached drawing to see if you want any changes. Easy to do at this point.

First cut.

You have permission to use this image.

Michael Loughnane

President

Instech Laboratories

800-443-4227

Web: [instechlabs.com](http://instechlabs.com)

**From:** Bradley Weegman [mailto:[weeg0011@umn.edu](mailto:weeg0011@umn.edu)]  
**Sent:** Monday, May 04, 2015 1:41 PM  
**To:** Mike Loughnane; Paul Loughnane  
**Subject:** Technical Drawings & More

[Quoted text hidden]

---

 **IN-LINE SENSOR.PDF**  
161K



Bradley Weegman <weeg0011@umn.edu>

---

## 19-F MRS Oxygen Monitoring Paper for Review

---

Thomas Suszynski <tom.suszynski@gmail.com>

Wed, Oct 7, 2015 at 12:45 PM

To: Bradley Weegman <weeg0011@umn.edu>

Absolutely. Please go ahead and use it.

Sent from my iPhone

On Oct 7, 2015, at 11:52 AM, Bradley Weegman <weeg0011@umn.edu> wrote:

Hi Tom,

Can you reply with permission to use some material from your Thesis in my Thesis. I just need an official email from you granting this permission so I won't run into problems for duplicating images etc.

Thanks,  
BW

On Wed, Jul 29, 2015 at 7:26 AM, Bradley Weegman <weeg0011@umn.edu> wrote:

Tom,

Thanks for the help. The rest of this week I am working on a post-doctoral fellowship grant, and next week I am drafting another manuscript, so I probably won't have a chance to make the changes for a week or so. (I am mostly trying to get them in good enough shape for my thesis. They can be re-tooled as needed prior to publication).

I really appreciate the help and feedback.

Thanks again. Give me a call sometime when you have some :-)

Peace!  
BW